

PART 1: MECHANISTIC INSIGHTS INTO THE PHOTOCHEMISTRY OF
TETRAZOLETHIONES

PART 2: SYNTHESIS OF PHENANTHRIDINE-FUSED QUINAZOLINIMINIUM AND
COMPUTATIONAL INVESTIGATION OF THEIR OPTOELECTRONIC PROPERTIES

by

OLAJIDE E. ALAWODE

B.S., Long Island University, 2005

AN ABSTRACT OF A DISSERTATION

submitted in partial fulfillment of the requirements for the degree

DOCTOR OF PHILOSOPHY

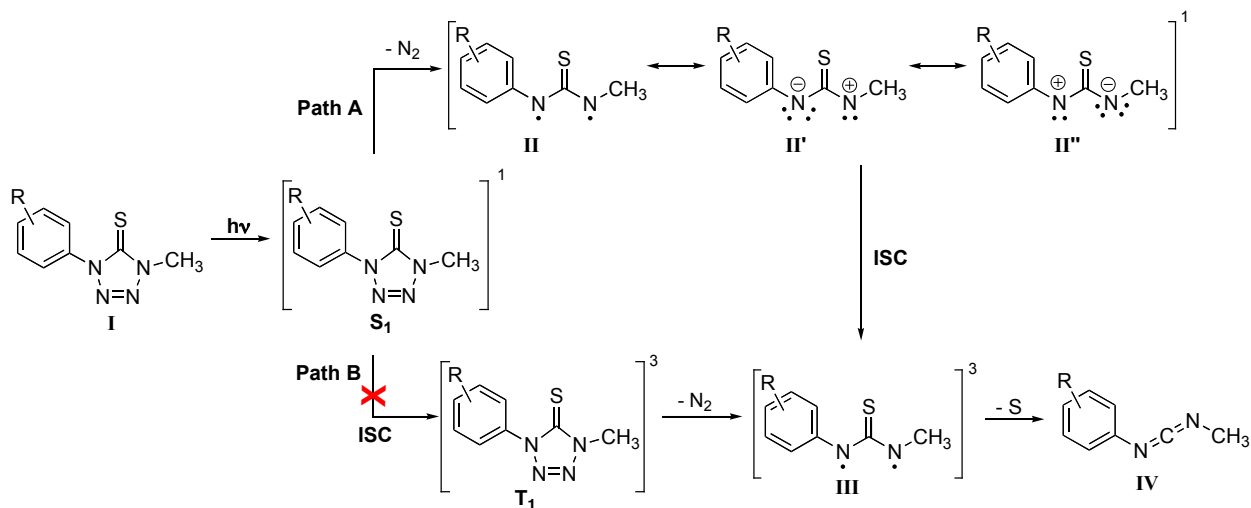
Department of Chemistry
College of Arts and Sciences

KANSAS STATE UNIVERSITY
Manhattan, Kansas

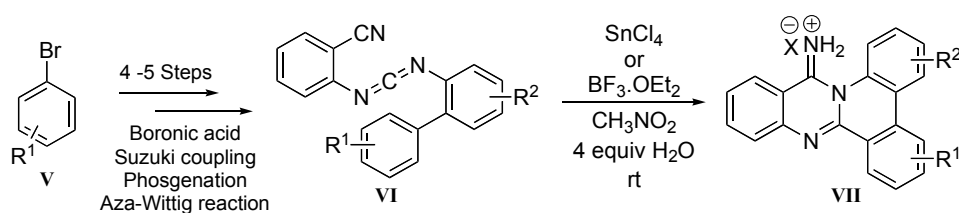
2012

Abstract

Research in our laboratory has focused on designing photoactivated DNA cleaving agents based on tetrazolethione scaffolds. The key step in the activation of these involves conversion of tetrazolethione moiety to carbodiimides upon irradiation. However, the mechanism of this reaction was not previously reported. Therefore, we undertook a study to elucidate the mechanism of photodecomposition of tetrazolethione as to identify reactive intermediates involved, that may interfere or aid with the activity of our synthesized DNA cleaving agents under physiological conditions. In Part 1 of this dissertation, we present mechanistic studies on this photodecomposition. Our results indicate the clean photoconversion of tetrazolethiones **I** to their respective carbodiimides **IV** *via* the expulsion of sulfur and dinitrogen. Photoirradiation in the presence of trapping agent (*e.g.* 1,4-cyclohexadiene) resulted into the formation of their corresponding thioureas. Thus, providing strong evidence for the intermediacy of a 1,3-biradical **III**, which is believed to be in its triplet spin multiplicity. Further investigations (triplet sensitization and quenching experiments) to determine the precursor of the biradical argued against the involvement of a triplet excited state (T_1). We believe that the mechanistic pathway that leads to the formation of a 1,3-triplet biradical **III** is a diradicaloid species **II** – **II''** generated directly from the singlet excited state of tetrazolethiones (S_1) after the expulsion of dinitrogen. Once formed, this diradicaloid species could be envisioned to undergo intersystem crossing to generate the 1,3-triplet biradical **III** which then undergoes desulfurization to form carbodiimides **IV** (Chapter 2).



Bridgehead-nitrogen containing fused heterocycles are regarded as “privileged structure” in biology and have found widespread applications in pharmaceutical industry. These heterocycles have also been evaluated in electroluminescent devices and organic dyes. Part II of the dissertation present new, concise and low cost strategies to a unique class of bridgehead nitrogen-containing fused heterocyclic scaffolds which involves two sequential intramolecular cyclizations from heteroenyne-allenes in the presence of Lewis acids such as SnCl_4 and $\text{BF}_3 \cdot \text{OEt}_2$, and trace water. The starting heteroenyne-allenes **VI** can be prepared from commercially available substrates **V** in 4 – 5 steps following standard protocols (Chapter 3).



Furthermore, we employed density functional theory to gain insights into the optoelectronic properties of select derivatives of phenanthridine-fused quinazoliniminiums (PNQs) **VII** and their free base in order to evaluate their scope in OLED technology. Our results show that the energies of the Highest Occupied Molecular Orbital (HOMO), Lowest Unoccupied Molecular Orbital (LUMO), the HOMO-LUMO energy gaps, the ionization potentials, electron affinities and the reorganization energies can be finely tuned by varying the substituents on these chromophores. In addition, we found that the introduction of an electron donating group (NMe_2) on the PNQs and their free base increases the energies of the HOMOs and decreases the ionization potentials, relative to its unsubstituted derivative, whereas substitution by an electron withdrawing group (NO_2) decreases the energies of the LUMOs and increases the electron affinities which in turn suggests an improvement in their hole and electron creating abilities, respectively (Chapter 4).

PART 1: MECHANISTIC INSIGHTS INTO THE PHOTOCHEMISTRY OF
TETRAZOLETHIONES

PART 2: SYNTHESIS OF PHENANTHRIDINE-FUSED QUINAZOLINIMINIUM AND
COMPUTATIONAL INVESTIGATION OF THEIR OPTOELECTRONIC PROPERTIES

by

OLAJIDE E. ALAWODE

B.S., Long Island University, 2005

A DISSERTATION

submitted in partial fulfillment of the requirements for the degree

DOCTOR OF PHILOSOPHY

Department of Chemistry
College of Arts and Sciences

KANSAS STATE UNIVERSITY
Manhattan, Kansas

2012

Approved by:

Major Professor
Dr. Sundeep Rayat

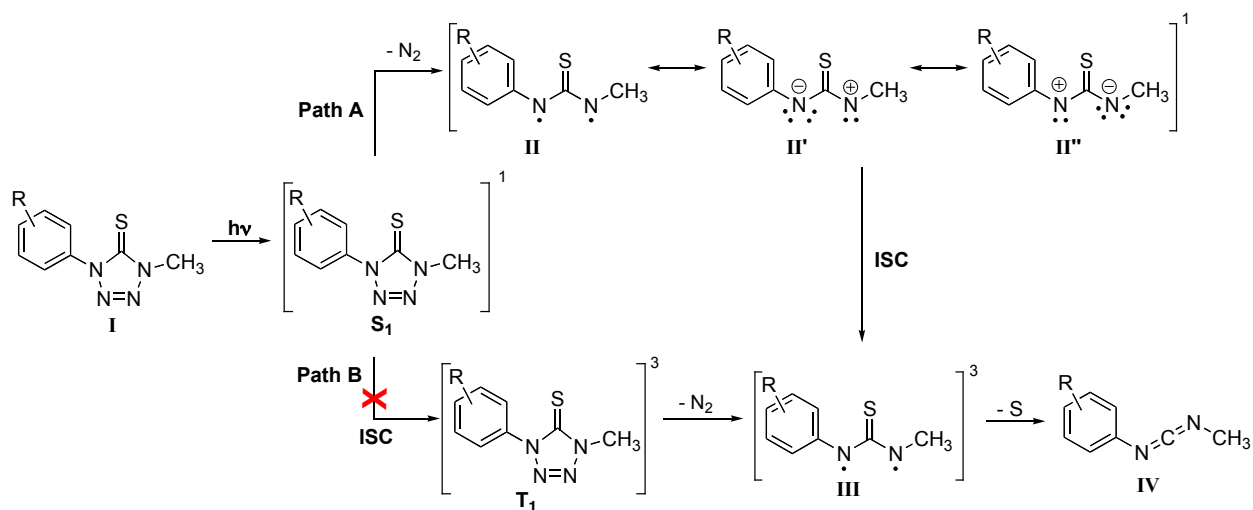
Copyright

OLAJIDE ALWODE

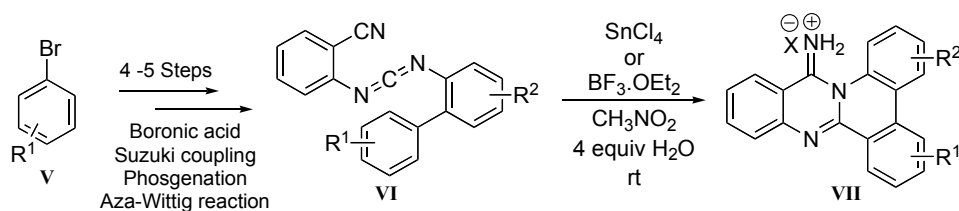
2012

Abstract

Research in our laboratory has focused on designing photoactivated DNA cleaving agents based on tetrazolethione scaffolds. The key step in the activation of these involves conversion of tetrazolethione moiety to carbodiimides upon irradiation. However, the mechanism of this reaction was not previously reported. Therefore, we undertook a study to elucidate the mechanism of photodecomposition of tetrazolethione as to identify reactive intermediates involved, that may interfere or aid with the activity of our synthesized DNA cleaving agents under physiological conditions. In Part 1 of this dissertation, we present mechanistic studies on this photodecomposition. Our results indicate the clean photoconversion of tetrazolethiones **I** to their respective carbodiimides **IV** *via* the expulsion of sulfur and dinitrogen. Photoirradiation in the presence of trapping agent (*e.g.* 1,4-cyclohexadiene) resulted into the formation of their corresponding thioureas. Thus, providing strong evidence for the intermediacy of a 1,3-biradical **III**, which is believed to be in its triplet spin multiplicity. Further investigations (triplet sensitization and quenching experiments) to determine the precursor of the biradical argued against the involvement of a triplet excited state (T_1). We believe that the mechanistic pathway that leads to the formation of a 1,3-triplet biradical **III** is a diradicaloid species **II** – **II''** generated directly from the singlet excited state of tetrazolethiones (S_1) after the expulsion of dinitrogen. Once formed, this diradicaloid species could be envisioned to undergo intersystem crossing to generate the 1,3-triplet biradical **III** which then undergoes desulfurization to form carbodiimides **IV** (Chapter 2).



Bridgehead-nitrogen containing fused heterocycles are regarded as “privileged structure” in biology and have found widespread applications in pharmaceutical industry. These heterocycles have also been evaluated in electroluminescent devices and organic dyes. Part II of the dissertation present new, concise and low cost strategies to a unique class of bridgehead nitrogen-containing fused heterocyclic scaffolds which involves two sequential intramolecular cyclizations from heteroenyne-allenes in the presence of Lewis acids such as SnCl₄ and BF₃.OEt₂, and trace water. The starting heteroenyne-allenes **VI** can be prepared from commercially available substrates **V** in 4 – 5 steps following standard protocols (Chapter 3).



Furthermore, we employed density functional theory to gain insights into the optoelectronic properties of select derivatives of phenanthridine-fused quinazoliniminiums (PNQs) **VII** and their free base in order to evaluate their scope in OLED technology. Our results show that the energies of the Highest Occupied Molecular Orbital (HOMO), Lowest Unoccupied Molecular Orbital (LUMO), the HOMO-LUMO energy gaps, the ionization potentials, electron affinities and the reorganization energies can be finely tuned by varying the substituents on these chromophores. In addition, we found that the introduction of an electron donating group (NMe₂) on the PNQs and their free base increases the energies of the HOMOs and decreases the ionization potentials, relative to its unsubstituted derivative, whereas substitution by an electron withdrawing group (NO₂) decreases the energies of the LUMOs and increases the electron affinities which in turn suggests an improvement in their hole and electron creating abilities, respectively (Chapter 4).

Table of Contents

| | |
|--|------|
| List of Figures | xii |
| List of Tables | xiii |
| List of Abbreviations and Symbols..... | xiv |
| List of Schemes..... | xv |
| Acknowledgments..... | xvi |
| Dedication..... | xvi |
| Preface..... | xvii |
| Chapter 1 - Photochemical Reactions of Tetrazole and its Derivatives..... | 1 |
| 1.1 Introduction..... | 1 |
| 1.2 Photochemical Reactions of Tetrazole Derivatives | 4 |
| 1.2.1 Photolysis of unsubstituted tetrazole | 5 |
| 1.2.2 Photolysis of substituted tetrazole | 5 |
| 1.2.3 Photolysis of tetrazolone derivatives | 8 |
| 1.2.4 Photolysis of imino-dihydro-tetrazoline derivatives..... | 12 |
| 1.2.5 Photolysis of tetrazolethione derivatives | 13 |
| 1.3 Concluding Remarks..... | 14 |
| Reference | 16 |
| Chapter 2 - Synthesis and Mechanistic Insights into the Photodecomposition of Tetrazolethiones | 22 |
| 2.1 Introduction..... | 22 |
| 2.2 Results and Discussion | 27 |
| 2.2.1 Synthesis of tetrazolethiones | 27 |
| 2.2.2 Absorption spectra of tetrazolethiones | 28 |
| 2.2.3 Theoretical investigations of the electronic properties of tetrazolethiones | 30 |
| 2.2.3.1 Molecular geometry | 30 |
| 2.2.3.2 Frontier molecular orbitals..... | 31 |
| 2.2.4.3 Vertical excitation energies..... | 33 |
| 2.2.4 Photochemistry of tetrazolethiones and Mechanistic Studies..... | 36 |
| 2.2.4.1 Photochemical studies using medium pressure Hg lamp..... | 36 |

| | |
|--|----|
| 2.2.4.2 Photochemical studies using Rayonet photochemical reactor | 39 |
| UV Spectral analyses of the irradiated solutions | 39 |
| NMR spectral analyses of the irradiated solutions | 40 |
| 2.2.4.3 Mechanistic considerations | 43 |
| 2.2.4.4 Identifying the precursor to the triplet biradical | 46 |
| 2.2.4.5 Multiphoton excitation experiment..... | 49 |
| 2.3 Summary | 50 |
| 2.4 Computational Methods..... | 51 |
| 2.5 Experimental..... | 51 |
| 2.5.1 Synthesis | 51 |
| 2.5.2 Photochemistry | 52 |
| 2.6 General procedure for synthesis of monosubstituted tetrazolones 83 | 53 |
| 2.6.1 1-Phenyl-1H-tetrazol-5(4H)-one, 83a..... | 53 |
| 2.6.2 1-(3-Methoxyphenyl)-1H-tetrazol-5(4H)-one, 83b | 53 |
| 2.6.3 1-(4-Methoxyphenyl)-1H-tetrazol-5(4H)-one, 83c..... | 53 |
| 2.6.4 1-(3-Chlorophenyl)-1H-tetrazol-5(4H)-one, 83d..... | 53 |
| 2.6.5 1-(4-Nitrophenyl)-1H-tetrazol-5(4H)-one, 83e..... | 54 |
| 2.7 General procedure for synthesis of 1,4-disubstituted tetrazolones 84 | 54 |
| 2.7.1 1-Methyl-4-phenyl-1H-tetrazol-5(4H)-one, 84a..... | 54 |
| 2.7.2 1-Methyl-4-(3-methoxyphenyl)-1H-tetrazol-5(4H)-one, 84b..... | 54 |
| 2.7.3 1-Methyl-4-(4-methoxyphenyl)-1H-tetrazol-5(4H)-one, 84c..... | 54 |
| 2.7.4 1-(3-Chlorophenyl)-4-methyl-1H-tetrazol-5(4H)-one, 84d | 55 |
| 2.7.5 1-(4-Nitrophenyl)-4-methyl-1H-tetrazol-5(4H)-one, 84e..... | 55 |
| 2.8 General procedure for synthesis of tetrazolethiones, 79 | 55 |
| 2.8.1 1-Methyl-4-phenyl-1H-tetrazole-5(4H)-thione, 79a..... | 55 |
| 2.8.2 1-(3-Methoxyphenyl)-4-methyl-1H-tetrazole-5(4H)-thione, 79b..... | 55 |
| 2.8.3 1-(4-Methoxyphenyl)-4-methyl-1H-tetrazole-5(4H)-thione, 79c..... | 56 |
| 2.8.4 1-(3-Chlorophenyl)-4-methyl-1H-tetrazole-5(4H)-thione, 79d..... | 56 |
| 2.8.5 1-(3-Nitrophenyl)-4-methyl-1H-tetrazole-5(4H)-thione, 79e..... | 56 |
| 2.9 General procedure for synthesis of thiourea, 93 | 56 |
| 2.9.1 1-Methyl-3-phenylthiourea, 93a | 57 |

| | | |
|---|--|----|
| 2.9.2 | 1-(3-Methoxyphenyl)-3-methylthiourea, 93b | 57 |
| 2.9.3 | 1-(4-Methoxyphenyl)-3-methylthiourea, 93c | 57 |
| 2.9.4 | 1-(3-Chlorophenyl)-3-methylthiourea, 93d | 57 |
| 2.9.5 | 1-Methyl-3-(4-Nitrophenyl)-thiourea, 93e | 57 |
| 2.10 | General procedure for synthesis of carbodiimides, 80 | 58 |
| 2.10.1 | N-((Methylimino)methylene)aniline, 80a | 58 |
| 2.10.2 | 3-Methoxy-N-((methylimino)methylene)benzenamine, 80b | 58 |
| 2.10.3 | 4-Methoxy-N-((methylimino)methylene)benzenamine, 80c | 58 |
| 2.10.4 | 3-Chloro-N-((methylimino)methylene)benzenamine, 80d | 58 |
| 2.10.5 | N-((methylimino)methylene)-4-nitrobenzenamine, 80e | 59 |
| 2.11 | General photochemical procedures: Medium pressure Hg lamp | 59 |
| 2.11.1 | Photolysis and product identification | 59 |
| 2.11.2 | Carbene trapping experiment | 59 |
| 2.12 | General photochemical procedures: Rayonet reactor | 59 |
| 2.12.1 | UV spectral changes | 59 |
| 2.12.2 | Product identification and Quantitative studies | 59 |
| 2.12.3 | Photolysis of carbodiimides and thioureas | 60 |
| 2.12.4 | Carbene Trapping: Photolysis in the presence of cyclohexene | 60 |
| 2.12.5 | Biradical Trapping: Photolysis in the presence of 1,4-Cyclohexadiene | 60 |
| 2.12.6 | Sensitization experiments | 60 |
| 2.12.7 | Effect of oxygen | 60 |
| 2.12.8 | Triplet quenching experiments | 60 |
| 2.13 | Actinometry and Quantum yield experiments | 61 |
| | References: | 63 |
| Chapter 3 - Synthesis of Phenanthridine-Fused Quinazolininium Salts from Heteroenyne- | | |
| | allenes | 66 |
| 3.1 | Introduction | 66 |
| 3.2 | Retrosynthesis of 2-((4'-methylbiphenylimino)methyleneamino) benzonitrile 109a | 70 |
| 3.3 | Synthesis of 2-((4'-methylbiphenylimino)methyleneamino) benzonitrile (109a) | 71 |
| 3.3.1 | Synthesis of aza-Wittig reagent 119 | 71 |
| 3.3.2 | Synthesis of 2-amino-4'-methylbiphenyl (124a) | 71 |

| | | |
|--------|---|----|
| 3.3.3 | Synthesis of 4'-methyl-2-biphenyl isocyanate (118a) and attempts towards the synthesis of 2-((4'-methylbiphenylimino)methyleneamino) benzonitrile (109a)..... | 72 |
| 3.4 | Synthesis of 4'-methyl-phenanthridine- <i>N</i> -quinazoliniminium salt (111a)..... | 74 |
| 3.4.1 | Attempts towards the synthesis of 4'-methyl-phenanthridine- <i>N</i> -quinazoliniminium salt 111a..... | 74 |
| 3.4.2 | Mechanistic investigations for the formation PNQs 111..... | 79 |
| 3.4.3 | Scope of cascade cyclization reaction..... | 82 |
| 3.5 | Conclusion..... | 86 |
| 3.6 | Experimental..... | 86 |
| 3.7 | Synthesis of Boronic Acids..... | 86 |
| 3.7.1 | General procedure for synthesis of arylboronic acids 122..... | 86 |
| 3.7.2 | General Procedure A..... | 86 |
| 3.7.3 | General Procedure B..... | 87 |
| 3.7.4 | <i>p</i> -Tolylboronic acid 122a..... | 87 |
| 3.7.5 | 4-Chlorophenylboronic acid 122b..... | 87 |
| 3.7.6 | 4-Fluorophenylboronic acid 122c..... | 87 |
| 3.7.7 | 4-Methoxyphenylboronic acid 122d..... | 87 |
| 3.7.8 | 3-Fluorophenylboronic acid 122e..... | 88 |
| 3.7.9 | 3-Methylphenyl boronic acid 122f..... | 88 |
| 3.7.10 | 3-Methoxyphenylboronic acid 122g..... | 88 |
| 3.7.11 | 3-(Trifluoromethyl)phenyl boronic acid 122h..... | 88 |
| 3.8 | Synthesis of <i>n</i> -Tetrabutylammonium tribromide and 2-bromo-4-methoxyaniline..... | 88 |
| 3.8.1 | Synthesis of <i>n</i> -Tetrabutylammonium tribromide..... | 88 |
| 3.8.2 | Synthesis of 2-Bromo-4-methoxyaniline 121j..... | 88 |
| 3.9 | Synthesis of 2-Aminobiphenyls 124..... | 89 |
| 3.9.1 | General procedure for synthesis of 2-Aminobiphenyls 124..... | 89 |
| 3.9.2 | 2-Amino-4'-methylbiphenyl 124a..... | 89 |
| 3.9.3 | 2-Amino-4'-chlorobiphenyl 124b..... | 89 |
| 3.9.4 | 2-Amino-4'-fluorobiphenyl 124c..... | 90 |
| 3.9.5 | 2-Amino-4'-methoxybiphenyl 124d..... | 90 |
| 3.9.6 | 2-Amino-3'-fluorobiphenyl 124e..... | 90 |

| | | |
|---------|--|----|
| 3.9.7 | 2-Amino-3'-methylbiphenyl 124f..... | 91 |
| 3.9.8 | 2-Amino-3'-methoxybiphenyl 124g..... | 91 |
| 3.9.9 | 2-Amino-3'-trifluoromethylbiphenyl 124h..... | 91 |
| 3.9.10 | 2-Amino-4-methylbiphenyl 124i..... | 91 |
| 3.9.11 | 2-Amino-4-methoxybiphenyl 124j..... | 92 |
| 3.9.12 | 2-Amino-3'-methoxy-4-methyl-biphenyl 124k..... | 92 |
| 3.10 | Synthesis of Biphenyl Isocyanates 118..... | 92 |
| 3.10.1 | General Procedure A..... | 92 |
| 3.10.2 | 4'-Methyl-2-biphenyl Isocyanate 118a..... | 93 |
| 3.10.3 | 3'-Methoxy-2-biphenyl Isocyanate 118g..... | 93 |
| 3.10.4 | 3'-Trifluoromethyl-2-biphenyl Isocyanate 118h..... | 93 |
| 3.10.5 | General Procedure B..... | 94 |
| 3.10.6 | 4'-Methyl-2-biphenyl Isocyanate 118a..... | 94 |
| 3.10.7 | 4'-Chloro-2-biphenyl Isocyanate 118b..... | 94 |
| 3.10.8 | 4'-Fluoro-2-biphenyl Isocyanate 118c..... | 94 |
| 3.10.9 | 4'-Methoxy-2-biphenyl Isocyanate 118d..... | 94 |
| 3.10.10 | 3'-Fluoro-2-biphenyl Isocyanate 118e..... | 94 |
| 3.10.11 | 3'-Methyl-2-biphenyl Isocyanate 118f..... | 94 |
| 3.10.12 | 3'-Methoxy-2-biphenyl Isocyanate 118g..... | 94 |
| 3.10.13 | 3'-Trifluoromethyl-2-biphenyl Isocyanate 118h..... | 95 |
| 3.10.14 | 5-Methyl-2-biphenyl Isocyanate 118i..... | 95 |
| 3.10.15 | 5-Methoxy-2-biphenyl Isocyanate 118j..... | 95 |
| 3.10.16 | 3'-Methoxy-5-Methyl-2-biphenyl Isocyanate 118k..... | 95 |
| 3.11 | Synthesis of aza-Wittig reagent, Iminophosphorane 119..... | 95 |
| 3.12 | Synthesis of 2-((biphenylimino)methyleneamino) benzonitrile..... | 95 |
| 3.12.1 | General Procedure for synthesis of 2-((biphenylimino)methyleneamino) benzonitrile 109..... | 95 |
| 3.12.2 | Synthesis of 2-((4'-methylbiphenylimino)methyleneamino) benzonitrile 109a..... | 96 |
| 3.12.3 | Synthesis of 2-((4'-chlorobiphenylimino)methyleneamino) benzonitrile 109b..... | 96 |
| 3.12.4 | Synthesis of 2-((4'-fluorobiphenylimino)methyleneamino) benzonitrile 109c..... | 96 |

| | | |
|---------|---|-----|
| 3.12.5 | Synthesis of 2-((4'-methoxybiphenylimino)methyleneamino) benzonitrile 109d. | 97 |
| 3.12.6 | Synthesis of 2-((3'-Fluorobiphenylimino)methyleneamino) benzonitrile 109e | 97 |
| 3.12.7 | Synthesis of 2-((3'-methylbiphenylimino)methyleneamino) benzonitrile 109f | 97 |
| 3.12.8 | Synthesis of 2-((3'-methoxybiphenylimino)methyleneamino) benzonitrile 109g. | 98 |
| 3.12.9 | Synthesis of 2-((3'-trifluoromethylbiphenylimino)methyleneamino) benzonitrile 109h | 98 |
| 3.12.10 | Synthesis of 2-((5-methylbiphenylimino)methyleneamino) benzonitrile 109i | 99 |
| 3.12.11 | Synthesis of 2-((5-methoxybiphenylimino)methyleneamino) benzonitrile 109j | 99 |
| 3.12.12 | Synthesis of 2-((3'-methoxyl-5-methylbiphenylimino)methyleneamino) benzonitrile 109k | 99 |
| 3.13 | Synthesis of 2-halo-3-biphenyl quinazoliniminiums halide salts | 100 |
| 3.13.1 | General procedure for Lewis acids mediated intramolecular cyclization 110 | 100 |
| 3.13.2 | 2-Bromo-3-(4'-methylbiphenyl) quinazolin-4(3H)-iminium bromide 110a | 100 |
| 3.13.3 | 2-Chloro-3-(4'-methylbiphenyl) quinazolin-4(3H)-iminium chloride 110a' | 100 |
| 3.14 | Synthesis of Phenanthridine fused quinazoliniminiums (PNQs) | 101 |
| 3.14.1 | General procedure for Lewis acids mediated cascade cyclization of 111 | 101 |
| 3.14.2 | Synthesis of 4'-methyl-phenanthridine-N-quinazoliniminiums hydrochloride salt 111a' | 101 |
| 3.14.3 | Synthesis of 4'-methyl-phenanthridine-N- quinazoliniminiums tetrafluoroborate Salt 111a'' | 101 |
| 3.14.4 | Synthesis of 3'-fluoro-phenanthridine-N-quinazoliniminiums tetrafluoroborate salt 111e'' | 102 |
| 3.14.5 | Synthesis of 3'-methyl-phenanthridine-N-quinazoliniminiums hydrochloride salt 111f' | 102 |
| 3.14.6 | Synthesis of 3'-methoxyl-phenanthridine-N-quinazoliniminiums tetrafluoroborate salt 111g'' | 102 |
| 3.14.7 | Synthesis of 5-methyl-phenanthridine-N-quinazoliniminiums hydrochloride salt 111i' | 103 |
| 3.14.8 | Synthesis of 5-methyl-3'-methoxy-phenanthridine-N- quinazoliniminiums tetrafluoroborate salt 111k | 103 |

| | |
|--|-----|
| 3.15 Formation of 1-(2-cyanophenyl)-3-(biphenyl-2-yl) urea 126..... | 103 |
| 3.15.1 1-(2-cyanophenyl)-3-(5-methoxybiphenyl-2-yl) urea 126j | 103 |
| References:..... | 105 |
| Chapter 4 - Theoretical Studies on the Optoelectronic Properties of Phenanthridine fused | |
| Quinazoliniminiums | 111 |
| 4.1 Introduction..... | 111 |
| 4.2 Computational Methods..... | 115 |
| 4.3 Results and Discussion | 115 |
| 4.3.1 Frontier Molecular Orbitals | 115 |
| 4.3.2 Ionization potentials and Electron affinities | 119 |
| 4.4 Conclusion | 121 |
| Reference: | 122 |
| Appendix..... | 125 |
| Appendix A - Absorption spectra, TDDFT data, NMR spectra of synthesized compounds and reaction mixtures during photochemical experiments..... | 126 |
| Appendix B - NMR Spectra for 2-bromo-4-methoxyaniline, substituted biphenyl amines, biphenyl isocyanates, 2-((biphenylimino)methyleneamino)benzotrile, 2-halo-3- biphenyl quinazoliniminium halides and phenanthridine-fused quinazoliniminium salts | 163 |

List of Figures

| | |
|---|----|
| Figure 1.1: Structure of <i>1H</i> -tetrazole 1 (top) and its <i>1H</i> - and <i>2H</i> - tautomeric forms (bottom). ^{1,2} .. | 1 |
| Figure 1.2: Various coordination modes of tetrazole ligands with Y= N, C. ^{19,21,24,25} | 2 |
| Figure 1.3: (a) Triangular [Mn ₃ (μ -OH)] motif and (b) two-dimensional [Ag ₂ (5-methyltetrazolate)] ⁺ motif. ²⁴⁻²⁶ | 2 |
| Figure 1.4: Structures of tetrazole-based insecticides (2 and 3) and herbicides (4 and 5) currently used in agriculture. ^{6,29,31} | 3 |
| Figure 1.5: Examples of tetrazole-based therapeutic agents. ^{6,7,41} | 4 |
| Figure 1.6: Common ring fragmentation patterns observed for tetrazole and its derivatives in solution or cryogenic matrix. | 5 |
| Figure 1.7: Stabilization of pyrimidinones 48 by alcohols. ³⁵ | 11 |
| Figure 2.1: Jablonski diagram illustrating the single photon activation of the photosensitizer leading to cellular damage through type I and type II reactions in PDT, ET = energy transfer. ¹ | 23 |
| Figure 2.2: Jablonski diagram illustrating the two photon activation of the photosensitizers and subsequent cellular damage through type I and type II reactions in PDT, ET = energy transfer. ¹ | 24 |
| Figure 2.3: Absorption spectra of 79a (left), 79b (right) and 79c (center bottom) in cyclohexane (red), THF (green) and acetonitrile (blue). | 28 |
| Figure 2.4: B3LYP/6-311+G* optimized structures showing bond lengths and the dihedral angle (in red) between the tetrazolethione ring and the aryl rings. | 31 |
| Figure 2.5: Resonance structures of 79a' – c' | 32 |
| Figure 2.6: Experimental absorption spectra of 79a in cyclohexane, tetrahydrofuran and acetonitrile, and the vertical excitation calculated with TDDFT/6-311+G* | 33 |
| Figure 2.7: Excited State (root = 8) for 1-methyl-4-(4-chlorophenyl)-1 <i>H</i> -tetrazol-5(4 <i>H</i>)-thione 86f optimized at CIS/6-31+G* | 37 |
| Figure 2.8: EI-MS/MS of the peak with m/z = 273. | 39 |
| Figure 2.9: Changes in UV absorption spectra of 79a in acetonitrile induced by irradiation at 254 (left) and 313 nm (right), arrows indicate the direction of spectral change upon irradiation. | 40 |

| | |
|---|-----|
| Figure 2.10: Changes in UV absorption spectra of 79b in acetonitrile induced by irradiation at 254 (left) and 313 nm (right), arrows indicate the direction of spectral change upon irradiation. | 40 |
| Figure 2.11: ¹ H NMR spectra overlay taken at 0 min (bottom) and 20 min (top) during UV-irradiation of 79a in acetonitrile- <i>d</i> ₃ | 41 |
| Figure 2.12: Plot showing the steady formation of thioureas 93a (left) and 93b (right) with increase in the concentration of 1,4-CHD during irradiation of 79a and 79b in acetonitrile, respectively. | 45 |
| Figure 2.13: Plots showing modest quenching of carbodiimides 80a (left) and 80b (right) during the photolysis of tetrazolethione 79a,b in the presence of biphenyl. | 48 |
| Figure 2.14: UV spectral changes of tetrazolethione 79a in acetonitrile induced by single photon excitation (top, irradiation time 20 sec) and multiphoton excitation (bottom, irradiation time 30 min). | 50 |
| Figure 3.1: 4(3 <i>H</i>)-Quinazolinones 98 and some biologically active natural products containing this scaffold. ^{3,5,6,7} | 66 |
| Figure 3.2: 4(3 <i>H</i>)-quinazolinimine ring structure 102 and synthetic compounds containing this scaffold 104 – 106. ^{14,15,16} | 67 |
| Figure 3.3: Quinazoliniminium ring structure in a rigid framework of fused heterocyclic rings. | 68 |
| Figure 3.4: Phenanthridine core and biologically relevant benzo[<i>c</i>]phenanthridine natural products. ^{22,26,27,29} | 69 |
| Figure 3.5: Phenanthridine-fused quinazolinimines (PNQs) 111. Highlighted within the red and the blue box are quinazolinimine and phenanthridine moieties, respectively. | 70 |
| Figure 3.6: ORTEP diagram of 110a' | 77 |
| Figure 3.7: ORTEP diagram of <i>N</i> -heterocycle 111a'' ('' indicates a BF ₄ ⁻ counter ion). | 78 |
| Figure 4.1: Basic schematic of multilayer OLED device. | 111 |
| Figure 4.2: Schematic of energy level diagram for a multilayer OLED. | 112 |
| Figure 4.3: Chemical structure of small molecules and polymeric materials used in the fabrication of OLEDs. ^{4,8} | 113 |
| Figure 4.4: Bridgehead-nitrogen containing chromophores proposed for use in OLEDs. ¹³⁻¹⁵ ... | 113 |
| Figure 4.5: Chemical structure of some polymeric materials used in OLEDs. ^{21,22} | 114 |

| | |
|--|-----|
| Figure 4.6: Structure of phenanthridine-fused quinazolininiums 148 _n -X,Y and their free base 149 _n -X,Y | 115 |
| Figure 4.7: Selected FMOs of 148H and 148 ₃ -NO ₂ | 116 |
| Figure 4.8:FMOs of 149H | 117 |
| Figure 4.9: Selected FMOs of 149 _n -NO ₂ | 118 |
| Figure A.1: Experimental absorption spectra of 79b in cyclohexane, tetrahydrofuran and acetonitrile. The vertical excitations calculated at TDDFT/6-311+G* are shown as stick spectra. | 127 |
| Figure A.2: Experimental absorption spectra of 79c in cyclohexane, tetrahydrofuran and acetonitrile. The vertical excitations calculated at TDDFT/6-311+G* are shown as stick spectra. | 128 |
| Figure A.3: ¹ H and ¹³ C NMR of 83b | 131 |
| Figure A.4: ¹ H and ¹³ C NMR of 84b | 132 |
| Figure A.5: ¹ H and ¹³ C NMR of 79b | 133 |
| Figure A.6: ¹ H and ¹³ C NMR of 83c | 134 |
| Figure A.7: ¹ H and ¹³ C NMR of 84c | 135 |
| Figure A.8: ¹ H and ¹³ C NMR of 79c | 136 |
| Figure A.9: ¹ H and ¹³ C NMR of 93a | 137 |
| Figure A.10: ¹ H NMR of 93b | 138 |
| Figure A.11: ¹ H and ¹³ C NMR of 93c | 139 |
| Figure A.12: ¹ H and ¹³ C NMR of 93d | 140 |
| Figure A.13: ¹ H NMR of 93e | 141 |
| Figure A.14: ¹ H and ¹³ C NMR of 80a | 142 |
| Figure A.15: ¹ H and ¹³ C NMR of 80b | 143 |
| Figure A.16: ¹ H and ¹³ C NMR of 80c | 144 |
| Figure A.17: ¹ H and ¹³ C NMR of 80d | 145 |
| Figure A.18: ¹ H and ¹³ C NMR of 80e | 146 |
| Figure A.19: ¹ H NMR spectra of 79b in acetonitrile- <i>d</i> ₃ taken at 0 (bottom), 10 (middle) and 20 (top) min of UV-irradiation at 254 nm, respectively. | 147 |
| Figure A.20: ¹ H NMR spectra of 79c in acetonitrile- <i>d</i> ₃ taken at 0 (bottom), 15 (middle) and 30 (top) min of UV-irradiation at 254 nm, respectively. | 148 |

| | |
|---|-----|
| Figure A.21: ^1H NMR spectra of 79d in acetonitril- d_3 taken at 0 (bottom), 15 (middle) and 30 (top) min of UV-irradiation at 254 nm, respectively. | 149 |
| Figure A.22: ^1H NMR spectra of 79e in acetonitrile- d_3 taken at 0 (bottom), 15 (middle) and 30 (top) minute of UV-irradiation at 254 nm, respectively. | 150 |
| Figure A.23: ^1H NMR spectra of 79a in methanol- d_4 taken at 0 (bottom), 10 (middle) and 20 (top) min of UV-irradiation at 254 nm, respectively. | 151 |
| Figure A.24: ^1H NMR spectra of 79b in methanol- d_4 taken at 0 (bottom), 10 (middle) and 20 (top) min UV-irradiation in 254 nm, respectively. | 152 |
| Figure A.25: ^1H NMR spectra of 79a in benzene- d_6 taken at 0 (bottom) and 20 (top) min of UV-irradiation at 254 nm, respectively..... | 153 |
| Figure A.26: ^1H NMR spectra of 79b in benzene- d_6 taken at 0 (bottom) and 20 (top) min of UV-irradiation at 254 nm, respectively..... | 154 |
| Figure A.27: ^1H NMR spectra of 79a in acetonitrile- d_3 taken at 0 (bottom) and 60 (top) min of UV-irradiation at 300 nm at 300 nm, respectively. | 155 |
| Figure A.28: ^1H NMR spectra of 79b in acetonitrile- d_3 taken at 0 (bottom) and 60 (top) min of UV-irradiation at 300 nm, respectively. | 156 |
| Figure A.29: ^1H NMR spectra of 79a in methanol- d_4 taken at 0 (bottom) and 60 (top) min of UV-irradiation at 300 nm, respectively..... | 157 |
| Figure A.30: ^1H NMR spectra of 79b in methanol- d_4 taken at 0 (bottom), 30 (middle) and 60 (top) min of UV-irradiation at 300 nm, respectively. | 158 |
| Figure A.31: ^1H NMR spectra of 79a in benzene- d_6 taken at 0 (bottom) and 60 (top) minutes of UV-irradiation at 300 nm, respectively. | 159 |
| Figure A.32: ^1H NMR spectra of 79b in benzene- d_6 taken at 0 (bottom) and 60 (top) min of UV-irradiation at 300 nm, respectively..... | 160 |
| Figure A.33: ^1H NMR spectra of 79a and 1,4-CHD in acetonitrile- d_6 taken at 0 (bottom) and 60 (top) min of UV-irradiation at 300 nm, respectively. | 161 |
| Figure A.34: ^1H NMR spectra of 79b and 1,4-CHD in acetonitrile- d_6 taken at 0 (bottom) and 60 (top) min of UV-irradiation at 300 nm, respectively. | 162 |
| Figure B.1: ^1H and ^{13}C NMR of 121j | 164 |
| Figure B.2: ^1H and ^{13}C NMR of 124a | 165 |
| Figure B.3: ^1H and ^{13}C NMR of 124b | 166 |

| | |
|--|-----|
| Figure B.4: ^1H and ^{13}C NMR of 124c | 167 |
| Figure B.5: ^1H and ^{13}C NMR of 124d | 168 |
| Figure B.6: ^1H and ^{13}C NMR of 124e | 169 |
| Figure B.7: ^1H and ^{13}C NMR of 124f | 170 |
| Figure B.8: ^1H and ^{13}C NMR of 124g | 171 |
| Figure B.9: ^1H and ^{13}C NMR of 124h | 172 |
| Figure B.10: ^1H and ^{13}C NMR of 124i | 173 |
| Figure B.11: ^1H and ^{13}C NMR of 124j | 174 |
| Figure B.12: ^1H and ^{13}C NMR of 124k | 175 |
| Figure B.13: ^1H and ^{13}C NMR of 115a | 176 |
| Figure B.14: ^1H and ^{13}C NMR of 115g | 177 |
| Figure B.15: ^1H and ^{13}C NMR of 115h | 178 |
| Figure B.16: ^1H and ^{13}C NMR of 119 | 179 |
| Figure B.17: ^1H and ^{13}C NMR of 109a | 180 |
| Figure B.18: ^1H and ^{13}C NMR of 109b | 181 |
| Figure B.19: ^1H and ^{13}C NMR of 109c | 182 |
| Figure B.20: ^1H and ^{13}C NMR of 109d | 183 |
| Figure B.21: ^1H and ^{13}C NMR of 109e | 184 |
| Figure B.22: ^1H and ^{13}C NMR of 109f | 185 |
| Figure B.23: ^1H and ^{13}C NMR of 109g | 186 |
| Figure B.24: ^1H and ^{13}C NMR of 109h | 187 |
| Figure B.25: ^1H and ^{13}C NMR of 109i | 188 |
| Figure B.26: ^1H and ^{13}C NMR of 109j | 189 |
| Figure B.27: ^1H and ^{13}C NMR of 109k | 190 |
| Figure B.28: ^1H and ^{13}C NMR of 110a | 191 |
| Figure B.29: ^1H and ^{13}C NMR of 110a' | 192 |
| Figure B.30: ^1H and ^{13}C NMR of 111a' | 193 |
| Figure B.31: ^1H and ^{13}C NMR of 111a'' | 194 |
| Figure B.32: ^1H and ^{13}C NMR of 111e'' | 195 |
| Figure B.33: ^1H and ^{13}C NMR of 111f' | 196 |
| Figure B.34: ^1H and ^{13}C NMR of 111g'' | 197 |

| | |
|--|-----|
| Figure B.35: ^1H and ^{13}C NMR of 111i' | 198 |
| Figure B.36: ^1H and ^{13}C NMR of 111k'' | 199 |
| Figure B.37: ^1H and ^{13}C NMR of 126j | 200 |
| Figure B.38: ^1H and ^{13}C NMR of 127a | 201 |

List of Tables

| | |
|--|-----|
| Table 2.1: Energies (λ (E)) and molar absorptivities ($\log \epsilon$) for bands observed in the absorption spectra of 79a – c in cyclohexane, THF and acetonitrile..... | 29 |
| Table 2.2: Frontier molecular orbitals for B3LYP/6-311+G* optimized geometries of 79a – c in acetonitrile..... | 32 |
| Table 2.3: TDDFT/6-311+G* vertical excitation energies (E (λ) / eV (nm)), oscillator strengths (f), MO character and transition type of 79a in cyclohexane, tetrahydrofuran and acetonitrile..... | 34 |
| Table 2.4: Amounts of tetrazolethione 79a,b remaining and photoproduct 80a,b produced after irradiation in acetonitrile- d_3 and respective quantum yields (Φ)..... | 42 |
| Table 2.5: Amounts of tetrazolethiones remaining and photoproducts produced in acetonitrile- d_3 | 48 |
| Table 3.1: Antiproliferative activity of 2-Halo-3-aryl-4(3 <i>H</i>)- quinazolininium halides 106 in L1210 and SK-BR-3 tumor cells <i>in vitro</i> | 67 |
| Table 3.2: Lewis acid and reaction conditions screened for intramolecular cyclization of 109a. 75 | 75 |
| Table 3.3: Optimization of reaction conditions for the synthesis of PNQ 111a',a'' | 79 |
| Table 3.4: Mechanistic study to investigate possible conversion of 110 to <i>N</i> -heterocyclic PNQ 111..... | 80 |
| Table 3.5: Scope of the reaction with cascade cyclization of cyano-ene-carbodiimide 109 to <i>N</i> -heterocyclic PNQs 111. | 84 |
| Table 4.1: HOMOs, LUMOs energies and energy gaps (ΔE) calculated for PNQs 148 and its free base 149. | 119 |
| Table 4.2: Calculated Ionization Potentials (IP), Electron affinities (EA), Extraction Potentials (EP) and reorganization energies for 148 _n -X and 148 _n -Y..... | 120 |
| Table 4.3: Calculated Ionization Potentials (IP), Electron affinities (EA), Extraction Potentials (EP) and reorganization energies for 149 _n -X and 149 _n -Y..... | 120 |
| Table A.1: TDDFT/6-311+G* vertical excitation energies (E (λ) / eV (nm)), oscillator strengths (f), MO character and transition type of 79b in cyclohexane, tetrahydrofuran and acetonitrile..... | 129 |

Table A.2: TDDFT/6-311+G* vertical excitation energies (E (λ) / eV (nm)), oscillator strengths (f), MO character and transition type of **79c** in cyclohexane, tetrahydrofuran and acetonitrile
..... 130

List of Abbreviations and Symbols

| | |
|---------------------------------------|---|
| 1,4-CHD | 1,4-Cyclohexadiene |
| a | Adiabatic excitation |
| ATR | Attenuated total reflectance |
| BBr₃ | Boron trichloride |
| BF₃.OEt₂ | Boron trifluoride etherate |
| C₂Cl₆ | Hexachloroethane |
| CD₃CN | Acetonitrile- <i>d</i> ₃ |
| CDCl₃ | Chloroform- <i>d</i> |
| CF₃SO₃Ag | Silver trifluoromethanesulfonate |
| CH₂Cl₂ | Methylene Chloride |
| CH₃NO₂ | Nitromethane |
| CT | Charge transfers |
| DFT | Density functional theory |
| DMAP | 4-Dimethylaminopyridine |
| DMS | Dimethyl sulfate |
| DMSO-<i>d</i>₆ | Dimethyl sulfoxide- <i>d</i> ₆ |
| E | energy |
| EA | Electron affinities |
| EDG | Electron donating group |
| EEP | Electron extraction potential |
| EML | Emissive layer |
| ESI MS | Electrospray ionization mass spectrometry |
| ET | Energy transfer |
| E_T | Triplet excited energy |
| Et₃N | Triethyl amine |
| ETL | Electron-transport layer |
| EtOAc | Ethylacetate |
| eV | electron volt |
| EWG | Electron Withdrawing group |

| | |
|--|--|
| FeBr₃ | Iron(III) bromide |
| FMOs | Frontier molecular orbitals |
| FT-IR/IR | Fourier transform infrared spectroscopy/Infrared |
| HEP | Hole extraction potentials |
| HMPA | Hexmethylphosphoramide |
| HOMO | Highly occupied molecular orbitals |
| HPLC | high-pressure liquid chromatography |
| HRMS | High resolution mass spectrometry |
| HTL | Hole-transport layer |
| Hz | Hertz |
| hν | Light/Light source/ Photon energy |
| IC | Internal conversion |
| IP | Ionization potentials |
| ISC | Intersystem crossing |
| <i>J</i> | Coupling constant |
| K₂CO₃ | Potassium carbonate |
| LEDs | Light-emitting diodes |
| LUMO | Lowest occupied molecular orbitals |
| M | molecule |
| MeOH | Methanol |
| MgSO₄ | Magnesium Sulfate |
| mHz | mega hertz |
| MS/MS | Tandem mass spectrometry |
| <i>n</i>-BuLi | <i>n</i> -Butyllithium |
| NaSO₄ | Sodium sulfate |
| NH₄Cl | Ammonium chloride |
| NIR | Near infrared |
| OLEDs | Organic light-emitting diodes |
| Pd(PPh₃)₂Cl₂ | Bis(triphenylphosphine)palladium(II) dichloride |
| PDT | Photodynamic therapy |
| PLEDs | Polymer light-emitter diodes |

| | |
|----------------------------------|--|
| PNQs | Phenanthridine- <i>N</i> -quinazolinimines |
| PPh₃ | Triphenylphosphine |
| ROS | Reactive oxygen species |
| S₀ | Singlet ground state |
| S₁ | Singlet excited state |
| SnCl₄ | Tin tetrachloride |
| SPE | Singlet photon excitation |
| <i>t</i>-Bu | <i>tetra</i> -Butyl |
| T₁ | Triplet excited state |
| TBABr | Tetrabutylammonium bromide |
| TDDFT | Time-dependent density functional theory |
| THF | Tetrahydrofuran |
| TiCl₄ | Titanium tetrachloride |
| TMSA | Trimethylsilyl azide |
| TMSBr | Trimethylsilyl bromide |
| TMSCl | Trimethylsilyl chloride |
| TMSI | Trimethylsilyl iodine |
| TMSOTf | Trimethylsilyl trifluoromethanesulfonate |
| TPE | Two-photon excitation |
| v | Vertical excitation |
| ΔE | Change in energy |
| λ(nm) | Wavelength (nanometer <i>i.e</i> x 10 ⁻⁹) |
| λ_{hole/electron} | Reorganization energies for hole injection and electron transfer |

List of Schemes

| | |
|--|----|
| Scheme 1.1: Photodecomposition pathways of matrix-isolated unsubstituted tetrazole 13. ^{1,45} | 5 |
| Scheme 1.2: Photodecomposition pathways for UV-irradiated alkyloxy-1-phenyl-1 <i>H</i> -tetrazole 19 in argon matrix. ^{12b,46} | 6 |
| Scheme 1.3: Photodecomposition pathways for the allyloxy tetrazoles 25 in solution. ³⁷ | 7 |
| Scheme 1.4: Photodecomposition route of 1,4,5-substituted alkylidenedihydropyridotetrazoles 34 in solution. ⁴⁸ | 8 |
| Scheme 1.5: Photoproducts formed during UV irradiation of 38 in solution and cryogenic matrix. ^{49,50} | 9 |
| Scheme 1.6: Photoconversion of 41 to alkenyl-diaziridinone 42 and its hydrolyzed derivatives 43 in solution. ⁵¹ | 9 |
| Scheme 1.7: Photodecomposition pathway of series of alkyl- phenyltetrazolones 44 in solution. ⁵² | 10 |
| Scheme 1.8: Photocleavage of 4-allyl-1-phenyltetrazolones 44 in solution. ^{35,53} | 10 |
| Scheme 1.9: Photodecomposition pathways of allyl phenyltetrazolone 44a and 44c in solid matrix. ^{36,54} | 12 |
| Scheme 1.10: Photoproducts generated during irradiation of 55 in solution. ^{55,56} | 13 |
| Scheme 1.11: Photodecomposition products of dialkyltetrazolethiones 62 in solution. ⁵¹ | 13 |
| Scheme 1.12: Photoproducts and fragmentation pathways resulting from irradiation of 1-methyl-1 <i>H</i> -tetrazole-5(4 <i>H</i>)-thione 65 in argon matrix. ¹⁷ | 14 |
| Scheme 2.1: TPE generation of reactive enediyne 73 and subsequent cycloaromatization. ¹⁸ | 25 |
| Scheme 2.2: Mechanism of action of the proposed enynyl-1 <i>H</i> -tetrazole-5(4 <i>H</i>)-thiones 76 upon light activation. | 26 |
| Scheme 2.3: Model tetrazolethione compounds 79 employed for photodecomposition studies discussed in this Chapter | 27 |
| Scheme 2.4: Synthesis of tetrazolethiones 79a–e. ^{23,24} | 27 |
| Scheme 2.5: Photoproducts formed during irradiation of tetrazolethiones 79b,d in solution with medium pressure Hg lamp. | 37 |
| Scheme 2.6: Proposed carbene addition products possible during photochemical trapping experiments of 87b in various alkenes. | 38 |

| | |
|--|----|
| Scheme 2.7: Photoconversion of tetrazolethiones 79 into their respective carbodiimides 80 in solution using Rayonet reactor..... | 41 |
| Scheme 2.8: Proposed photodecomposition pathways of tetrazolethione ring systems..... | 43 |
| Scheme 2.9: Proposed cyclopropane adduct 88a,b expected during the reaction of 79 with cyclohexene in case of the presence of a carbene intermediate..... | 44 |
| Scheme 2.10: Trapping experiment to provide support for the involvement of 1,3-biradical intermediate 92 in the photodecomposition of tetrazolethiones 79..... | 45 |
| Scheme 2.11: Possible pathways for the formation of 1,3-triplet biradical 92..... | 47 |
| Scheme 2.12: Enynyl-1 <i>H</i> -tetrazole-5(4 <i>H</i>)-thiones 76 based photoactivated DNA cleavage agents that generate two different types of biradicals in one pot cellular damage..... | 51 |
| Scheme 3.1: Formation of 2-halo-3-aryl-4(3 <i>H</i>)-quinazoliniminium halides 106 from heteroenyne-allenes. ¹⁹ | 68 |
| Scheme 3.2: Cyclization reaction of heteroenyne-allenes 109 to produce series of phenanthridine fused quinazoliniminiums 111..... | 69 |
| Scheme 3.3: Retrosynthetic route showing precursors for the synthesis of heteroenyne-allenes 109a..... | 71 |
| Scheme 3.4: Retrosynthetic route for the preparation of 4'-methyl-2-biphenyl isocyanate 118a..... | 71 |
| Scheme 3.5: Preparation of aza-Wittig reagent 119..... | 71 |
| Scheme 3.6: Synthesis of 2-amino-4'-methylbiphenyl (124a). ^{34,35,36} | 72 |
| Scheme 3.7: Synthesis of 4'-methyl-2-biphenyl isocyanate (118a)..... | 72 |
| Scheme 3.8: Unsuccessful attempt to form 109a <i>via</i> aza-Wittig reaction (Route A)..... | 73 |
| Scheme 3.9: Unsuccessful attempted to form 109a involving the coupling of isocyanate with anthranilonitrile (Route B) (Dashed arrow indicate planned reaction that was not attempted)..... | 73 |
| Scheme 3.10: Successful synthesis of heteroenyne-allene 109a via route A..... | 74 |
| Scheme 3.11: Formation of 2-bromo-3-(4'-methylbiphenyl)-quinazolin-4(3 <i>H</i>)iminium bromide (110a) from 109a with TMSBr..... | 74 |
| Scheme 3.12: Synthesis of 2-chloro-3-(4'-methylbiphenyl)-quinazolin-4(3 <i>H</i>)iminium chloride (110a') and compound 127a' (' indicates a Cl ⁻ counter ion)..... | 75 |

| | |
|--|-----|
| Scheme 3.13: Possible reaction mechanism for the formation of 110a, a' (MX = TMSBr, TMSCl, SnCl ₄)..... | 76 |
| Scheme 3.14: Formation of 1-(2-cyanophenyl)-3-(4'-methylbiphenyl) urea 126a from 109a in TMSCl/HMPA..... | 77 |
| Scheme 3.15: Synthesis of ring-fused <i>N</i> -heterocyclic PNQ 111a',a'' (X=Cl ⁻ or BF ₄ ⁻ indicated by ' or '' , respectively)..... | 79 |
| Scheme 3.16: Treatment of 110a, a' with Lewis acids..... | 80 |
| Scheme 3.17: Plausible mechanism for SnCl ₄ /BF ₃ .OEt ₂ promoted cascade reaction to produce ring-fused PNQ 111a..... | 82 |
| Scheme 3.18: Synthesis of a series of PNQs 109a – k..... | 83 |
| Scheme 3.19: Resonance structure of substituents (Y = Cl, F and OCH ₃)..... | 84 |
| Scheme 4.1: Resonance structure of 148 ₃ -NO ₂ | 116 |
| Scheme 4.2: Resonance structures of 149-H..... | 117 |
| Scheme 4.3: Resonance structures of 149 _n -NO ₂ '..... | 118 |

Acknowledgments

This accomplishment would not be possible without the incredible love and encouragement of my family.

Thank you mom, Iyabo for your love, prayers and tireless scarifies which has made all of this possible. You were my advocate when I had not voice, you battled lives challenges with immense determination and you've won, you were my inspiration when I needed one, thanks Ma. You are my hero and my guiding angel, I love you mommy!!!! I would like to express my deepest appreciation to my true friend and the love of my life, Safiyyah. Through the good times and the very challenging ones you have been caring and loving beyond grasp, thank you for being supportive and always looking out for my best interest. You challenge me to be better and most of all you always give me a reason to laugh, I love you my African queen!!!!!!

Also, I would like to thank my siblings, Adesola, Adenike, Olarenwaju and Adeyemi Jr. for your enduring love and encouragement. Thank you guys for encouraging my dreams and aspirations, having my back and most of all for always cheering me to greater accomplishments. I would like to thank my other family, Jannett, Danion and Kadian for embracing me with tremendous love and kindness, thank you for making me part of the family. You are all the aligning center to my world and I deeply appreciate your support, love and counsel.

Furthermore, I would like to thank my research adviser Dr. Sundeep Rayat who has offered invaluable support and guidance during my graduate study. Also, my appreciation goes to members of the supervisory committee; Dr. Eric Maatta, Dr. Stefan Bossmann, Dr. Thomas Roche, Dr. Jean-Pierre H. Perchellet and Dr. Amit Chakrabarti for their time, invaluable expertise and guidance. I gratefully acknowledge a fellowship from the KSU NSF GK-12 program during my 2010-2011 academic year.

Special thanks to the entire chemistry department faculty and staff especially Dr. Leila Maurmann for taking the time to teach me how to interpret 2D NMRs, Dr. John Desper for his quick analysis of my crystal structures and Jim Hogdson for designing unique glassware needed. And special thank you to Dr. Itzik Ben-Itzhak for laser time for the multiphoton experience. I would also like to extend a special thanks to all my graduate friends and past group members especially Dr. Gundugola for his valuable advices.

Dedication

Dedicated to my incredible mother Iyabo, my queen and lovely wife Safiyyah;
two brilliant individuals whom I have learned from to approach life with honor, humility and
optimism.

Preface

Research carried out at Kansas State University for this dissertation led to the following publications in peer-reviewed scientific journals:

Alawode, O. E.; Robinson, C.; Rayat, S. “Clean photodecomposition of 1-methyl-4-phenyl-1H-tetrazole-5(4H)-thiones to carbodiimides proceeds via a biradical” *J. Org. Chem.* **2011**, *76*, 216.

Rayat, S.; Chhabra, R; **Alawode, O.;** Gundugola, A. S. “Electronic properties of 1-methyl-4-phenyl-1H-tetrazole-5(4H)-thiones: An experimental and theoretical study” *J. Mol. Struct.* **2009**, *933*, 38.

Rayat, S.; **Alawode, O.;** Desper, J. “Intermolecular interactions in the crystal structures of substituted tetrazolones” *CrystEngComm.* **2009**, *13*, 1892.

Chapter 1 - Photochemical Reactions of Tetrazole and its Derivatives

1.1 Introduction

Tetrazole (CN₄H₂) **1** is a five-membered unsaturated heterocyclic ring consisting of one carbon and four nitrogen atoms (Figure 1.1, top). The nitrogen content of this molecule is rated at 80% of its total weight.^{1,2} These ring systems exhibit annular tautomerism, and co-exist in *1H*- and *2H*- tautomeric forms (Figure 1.1, bottom).^{2,3,4} There are no known reports of the presence of these heterocyclic scaffolds in natural products, but several tetrazole containing compounds and their derivatives have been synthetically prepared and are known to be relatively stable under different reaction conditions and in the presence of various chemical reagents.¹ These synthetic compounds have attracted considerable attention due to their widely growing applications in many fields, such as chemical,⁵ agricultural⁶ and pharmaceutical industry.⁷

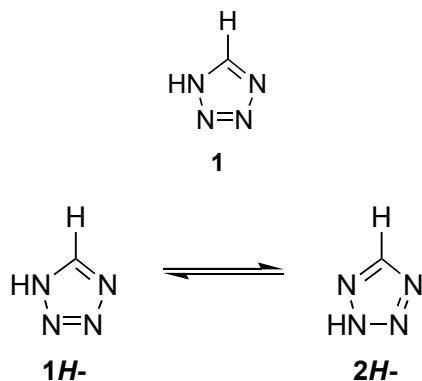


Figure 1.1: Structure of *1H*-tetrazole **1** (top) and its *1H*- and *2H*- tautomeric forms (bottom).^{1,2}

In chemical industry, tetrazole and its derivatives are employed in the protection of metal surfaces as corrosion inhibitors,^{5,8,9} and as additives in anti-wear and friction reduction oils.¹⁰ Also, these scaffolds are used as stabilizers in photography and photoimaging.^{1,11,12} The high nitrogen content of tetrazoles makes them excellent sources of environmentally friendly high-energy materials for specialty explosives and pyrotechnics.^{4,13,14} As a result of this property, they

have also found applications as propellants in rockets,^{1,15} and as gas generating agents for airbags.^{1,16,17}

Furthermore, the tetrazolyl heterocycles have demonstrated applications in coordination chemistry due to their wide range of binding patterns with metal ions.^{16,18} These heterocycles can act as monodentate (N), bidentate (N, N) and/or bridging ligands to form stable complexes with several transition metal ions through coordinate bonding (Figure 1.2).^{19,20,21} As a result, the tetrazole ring systems have been used in designing polymers and building interesting molecular architectures with a variety of different metal ions and co-ligands.^{21,22,23} Two examples of metal-organic frameworks are shown below. Figure 1.3 (left) depicts the crystal structure of two independent Mn ions (Mn^{+1} and Mn^{+2}) coordinated to three equivalent bridged tetrazoles and two water molecules.^{24,25} Also, two-dimensional motif of tetradentate 5-methyltetrazole coordinated to Ag (2^+ , 1^+) is shown in Figure 1.3 (right), that further demonstrates the versatility in the coordination properties of tetrazolylic ligand.²⁶ These compounds have exhibited interesting optical and magnetic properties in material science and have potential applications as mesoporous hydrogen storage material in supramolecular chemistry.^{3,21,24,25}

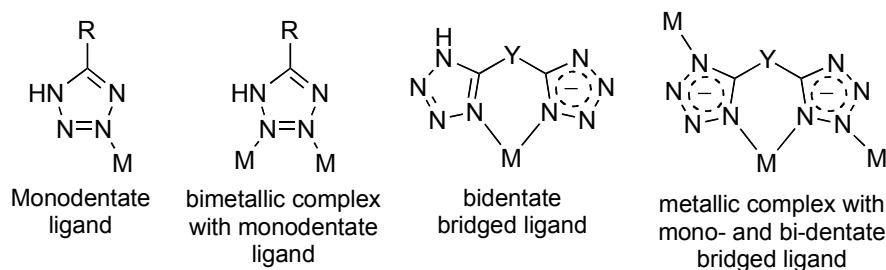


Figure 1.2: Various coordination modes of tetrazole ligands with Y= N, C.^{19,21,24,25}

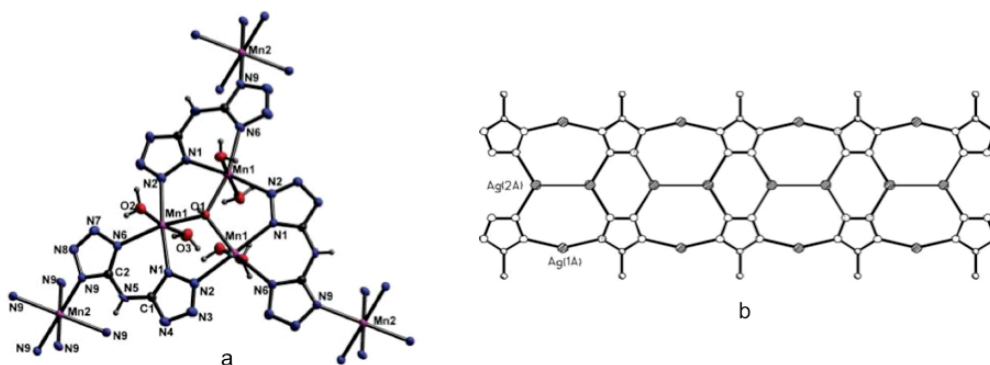


Figure 1.3: (a) Triangular $[Mn_3(\mu-OH)]$ motif and (b) two-dimensional $[Ag_2(5\text{-methyltetrazolate})]^+$ motif.²⁴⁻²⁶

The chelating properties of the tetrazole ring system have been successfully utilized in analytical chemistry for the removal of heavy metal ions from liquids, and biological fluids.^{8,27} Furthermore, tetrazoles have been successfully used as derivatising agents for benzyl alcohols to corresponding ethers prior to hydrogenolysis.²⁸ The electron-withdrawing properties of these heterocycles aid in weakening the C-O bond and thus, making the carbon atom more susceptible to nucleophilic attack.

In agriculture, tetrazole moieties are well known for their efficient fungicidal and insecticidal properties that make them excellent candidates for pest management in agriculture (Figure 1.4).^{6,29,30} For example, tetrazole-based compounds **2** and **3** were found to show selective and excellent insecticidal activity against different species of insects;^{6,31} and compounds **4** and **5** both exhibit herbicidal properties and act by inhibiting the plant cell division cycle and chlorophyll biosynthesis, respectively.⁶

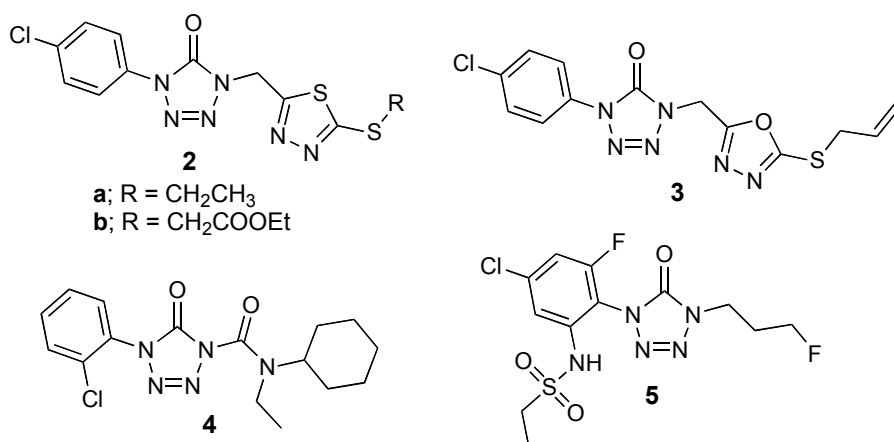


Figure 1.4: Structures of tetrazole-based insecticides (**2** and **3**) and herbicides (**4** and **5**) currently used in agriculture.^{6,29,31}

These nitrogen rich five-membered rings have also demonstrated excellent applications in medicinal chemistry.^{32,33} It is well known that tetrazolic fragment (-CN₄H) exhibits physical characteristics and abnormally high acidity similar to that of carboxylic acid moiety (-CO₂H) in biologically active molecules.^{7,34,35} Thus, these are allosteric with the carboxylic acid groups. Furthermore, tetrazole moieties exhibit superior metabolic stability at physiological pH and increased bioavailability than that of the -CO₂H group.⁷ Therefore, tetrazoles are being employed

as synthetic surrogates of the carboxylic acid moiety in modern drug design.^{19,36,37,38} Tetrazole derivatives have found applications in pharmaceuticals as *cis*-peptide linkers^{39,40} and lipophilic spacers.^{41,42} Tetrazoles containing compounds have also been reported to possess anesthetic, antihypertensive, anti-allergic, antiviral, antibacterial, antibiotic and anti-inflammatory properties.^{6,7,43,44} For instance alfentanil **6** is used for short time anesthesia,⁶ benzodiazepine analogues **7** and **8**, are employed in the treatment of cardiac arrhythmias and Meniere's disease (an inner ear disorder),^{38d,e} and losartan **9** is used as anti-hypertensive drug (Figure 1.5).⁷ Furthermore, *N*-(α -aminoalkyl)tetrazoles (**10** – **12**) have been proposed to exhibit potential applications in the prevention and treatment of diseases associated with the formation of advanced glycation end products (AGEs) and advanced lipoxidation end products (ALEs) because of their protein synthesis inhibitory properties.^{38c}

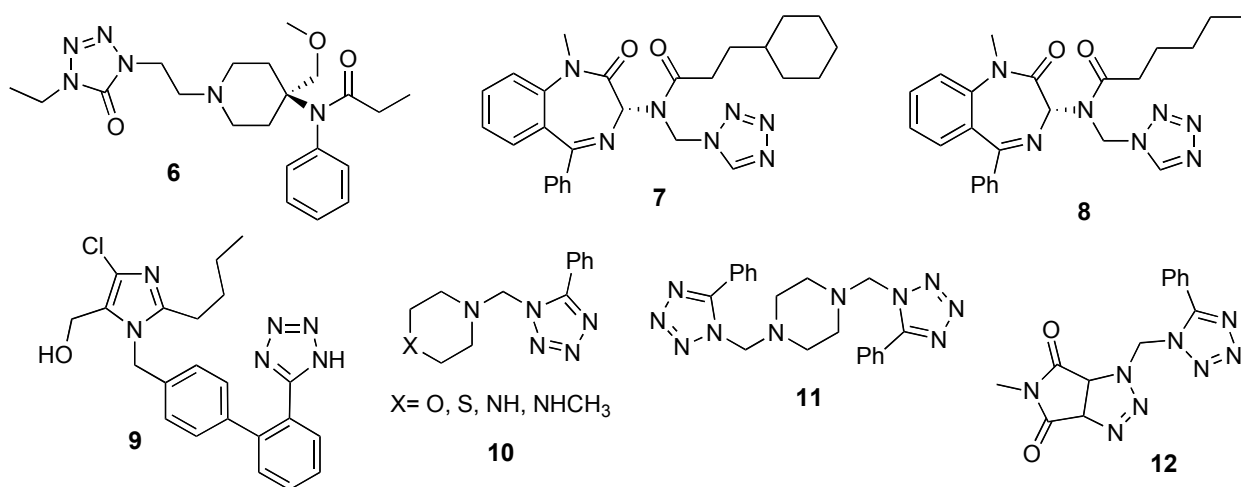


Figure 1.5: Examples of tetrazole-based therapeutic agents.^{6,7,41}

1.2 Photochemical Reactions of Tetrazole Derivatives

The tetrazolylic ring systems are known to exhibit very strong photochemical reactivity. In the past three decades, there have been a number of reports on the photochemistry of tetrazoles and their derivatives, studied in solution as well as in the gas phase and based on the range of tetrazolyl scaffolds investigated, several decomposition patterns have been established

that depend upon the reaction conditions (*e.g.* cryogenic inert matrix or solution), solvent polarity and nature of the substituents present on the tetrazolyl ring.

Figure 1.6 shows general structure of tetrazole derivatives **I** – **III** that are discussed in this chapter. The common fragmentation pathway in all derivatives of tetrazoles **I** – **III** involves the rapid photorelease of molecular nitrogen (N_2) from the ring (referred to as *a*) that further results in the formation of a variety of products depending on the nature of the substituents present on the heterocycle. The second most prevalent pathway in tetrazoles is the ring cleavage through a 1,3-dipolar cycloreversion (referred to as *b*) to generate the corresponding photoproducts. This pathway is not observed in annulated derivatives of tetrazoles **II**, most likely, because of the strain in the putative photoproduct. In case of tetrazole derivatives **III** with $X = S$, an additional pathway is observed that involves simultaneous loss of molecular nitrogen and sulfur (indicated by *a* and *c*) (Figure 1.6).

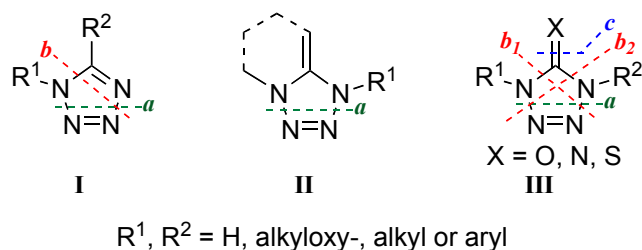
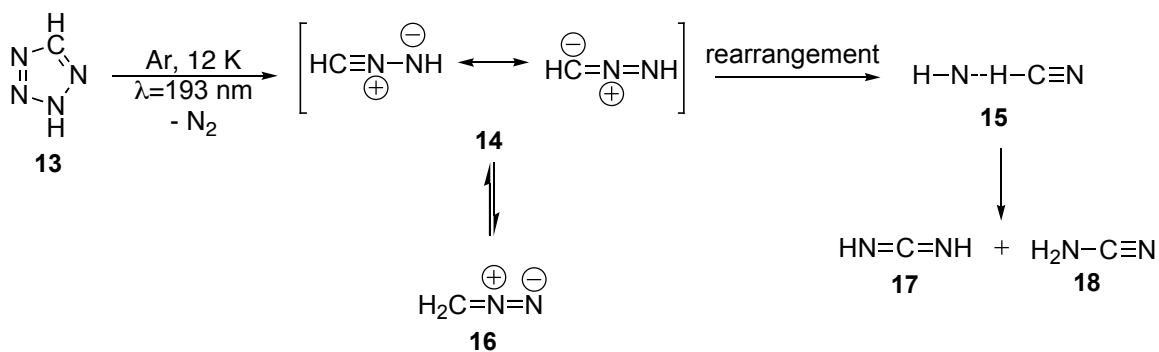


Figure 1.6: Common ring fragmentation patterns observed for tetrazole and its derivatives in solution or cryogenic matrix.

1.2.1 Photolysis of unsubstituted tetrazole

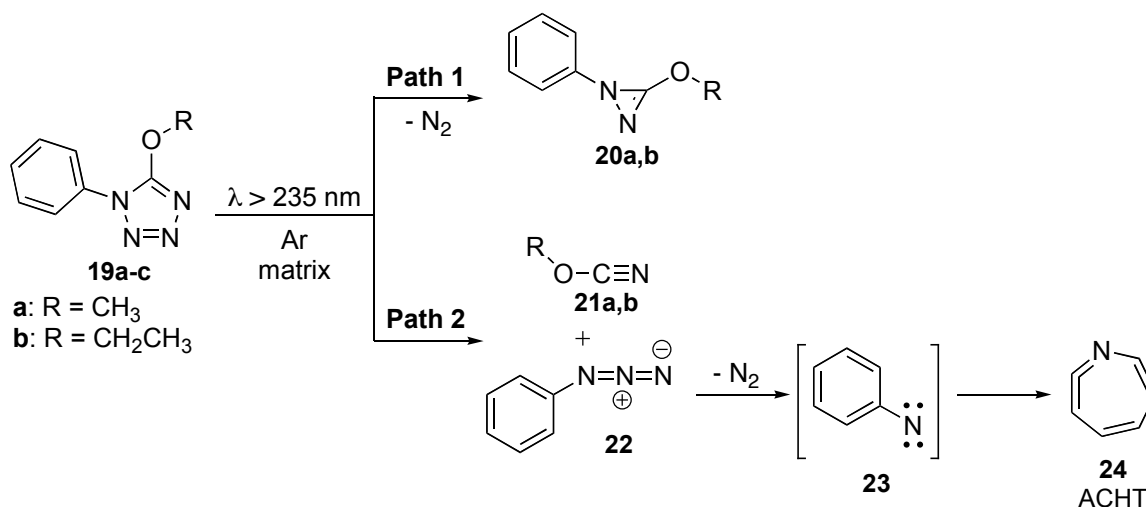
Maier and co-workers described the photochemistry of unsubstituted tetrazole in cryogenic argon matrix.^{1,45} Using IR spectroscopic analysis these researchers were able to identify the reactive intermediates and the mixture of photoproducts generated. The results revealed that the immediate release of N_2 led to the formation of resonance stabilized nitrilimine intermediate **14** that tautomerized to afford diazomethane **16** as a photoproduct. The authors reported that nitrilimine **14** also underwent rearrangement to produce $HCN \cdots NH$ complex **15** that decomposed further to give tautomers, carbodiimide **17** and cyanamide **18** (Scheme 1.1).



Scheme 1.1: Photodecomposition pathways of matrix-isolated unsubstituted tetrazole **13**.^{1,45}

1.2.2 Photolysis of substituted tetrazole

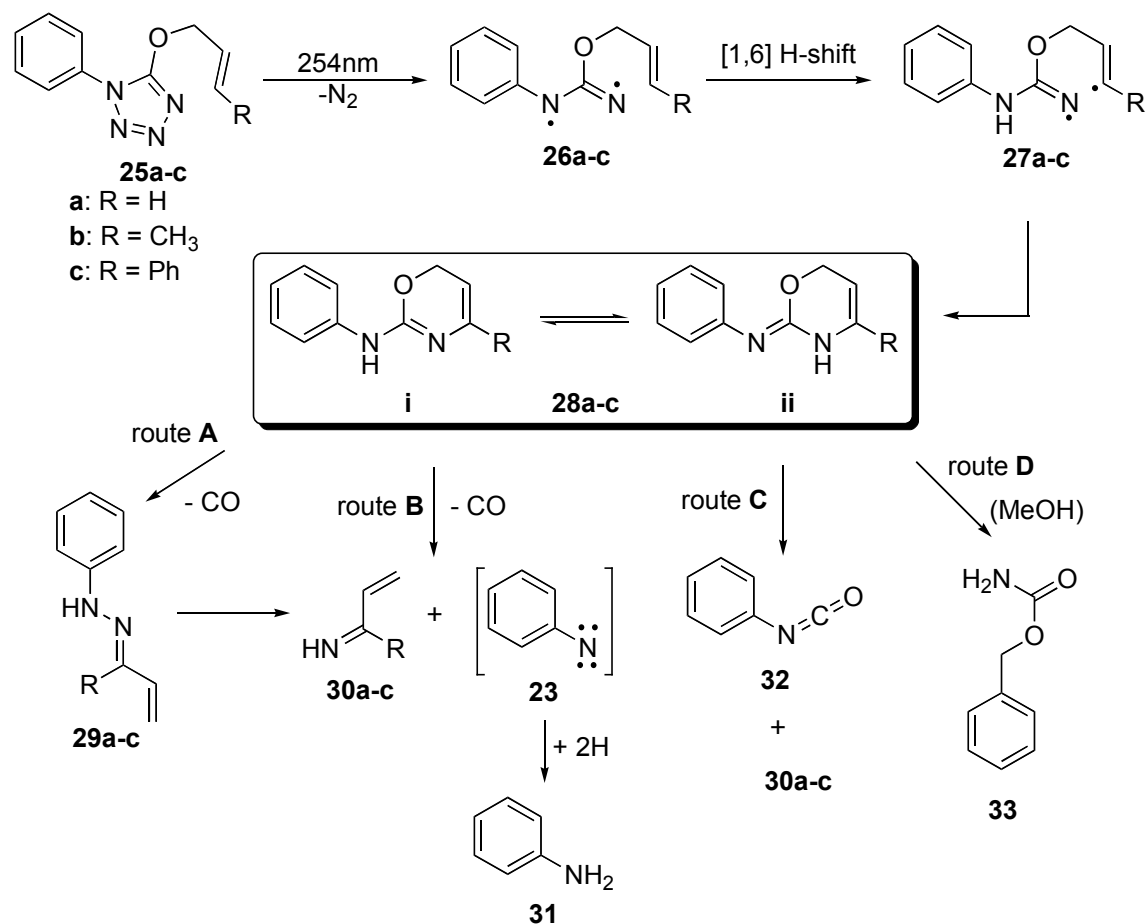
Fausto and Gómez-Zavaglia described the photochemistry of several substituted tetrazole derivatives using matrix isolated FT-IR spectroscopy and high-level DFT-based quantum mechanical calculations.^{12b,46} The UV-induced photochemistry of alkoxy-1-phenyl-1*H*-tetrazoles **19** in argon matrix resulted in two different fragmentation pathways of the ring system. The first pathway involved the production of antiaromatic alkoxy-1-phenyl-1*H*-diazirene **20** *via* the loss of molecular nitrogen from compound **19**. The second pathway involved the ring cleavage that led to the formation of alkyloxycyanate **21** and phenylazide (**22**) as the primary photoproducts *via* 1,3-dipolar cycloreversion. Subsequent loss of nitrogen from **22** resulted into the formation of 1-aza-1,2,4,6-cycloheptatetraene (AHT) (**24**), possibly through a singlet phenylnitrene (**23**) (Scheme 1.2).^{12b,46} The photoproducts obtained were analyzed and identified by IR spectroscopy, and the interpretation of the experimental data was extensively supported by DFT calculations performed at B3LYP/6-311++G(d,p) level of theory.



Scheme 1.2: Photodecomposition pathways for UV-irradiated alkyloxy-1-phenyl-1*H*-tetrazole **19** in argon matrix.^{12b,46}

Cristiano and coworkers investigated the photochemistry of various 1-allyloxy-4-phenyl-1*H*-tetrazoles **25** in methanol, acetonitrile and cyclohexane solutions with a low-pressure mercury lamp ($\lambda = 254 \text{ nm}$).³⁷ The photolysis of these ether compounds resulted in the loss of nitrogen from the tetrazolyl ring to produce triplet 1,3-biradicals **26**, which underwent a [1,6] H-shift followed by cyclization to afford two tautomeric *N*-phenyl-1,3-oxazines **28i-ii** as the primary photoproducts (Scheme 1.3).³⁷ Due to the photosensitive nature of generated oxazines, prolonged irradiation resulted in secondary photoreactions that are discussed below.

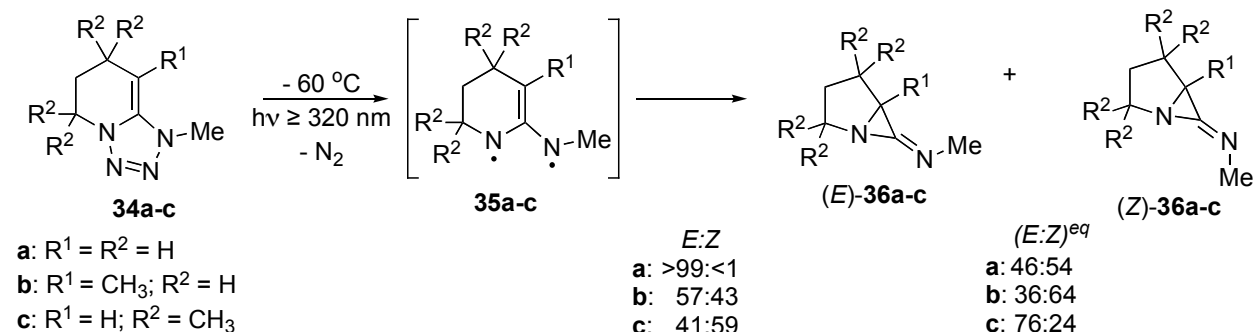
The photodecomposition of oxazines **28** followed three pathways in all the solvents (methanol, acetonitrile and cyclohexane), however an additional fourth pathway was observed in methanol. The route **A** produced phenyl vinyl hydrazine **29** after the photorelease of carbon monoxide (CO) from **28i**, and continuous exposure of **29** to UV-irradiation led to the formation of photoproduct **30** and phenyl nitrene **22** that subsequently decomposed to aniline **31**. Similarly, route **B** released CO through a concerted mechanism that transformed **28i** to **30** and **22**; which eventually decomposed to **31**. The route **C** produced phenyl isocyanate **32** and photoproduct **30** from tautomer **28ii**. In methanolic solution, the formation of benzyl carbamate **33** was also observed via route **D** (Scheme 1.3).³⁷



Scheme 1.3: Photodecomposition pathways for the allyloxy tetrazoles **25** in solution.³⁷

Furthermore, Quast and coworkers also investigated the photochemistry of a series of annulated tetrazole derivatives in solution⁴⁷ e.g. 1,4,5-substituted alkylidenedihydropyridotetrazoles **34**. These researchers irradiated diluted, degassed solutions of **34a** in toluene-*d*₈ at low temperature (-60 °C) with the filtered focused medium pressure mercury lamp ($\lambda \geq 320$ nm).⁴⁸ The photodecomposition was diastereoselective involving the release of molecular nitrogen to form the triplet diazatriethylene biradical intermediate **35a** followed by ring closure to give the annulated (*E*)-iminoaziridines **36a** (99%) with an exocyclic CN double bond. However, at room temperature rapid (*E*) \rightleftharpoons (*Z*) equilibration was observed after several days (Scheme 1.4).⁴⁸ In the case of **34b**, the photochemical reaction performed in toluene-*d*₈ at -60 °C with $\lambda \geq 320$ nm similarly resulted in the formation of compound **36b** via the biradical intermediate **35b**. However, the results indicated poor diastereoselectivity with almost equal amounts of *E* and *Z*

(*E/Z*, 57:43). Again *E/Z* ratio changed after sample equilibrated at room temperature (Scheme 1.4).⁴⁸



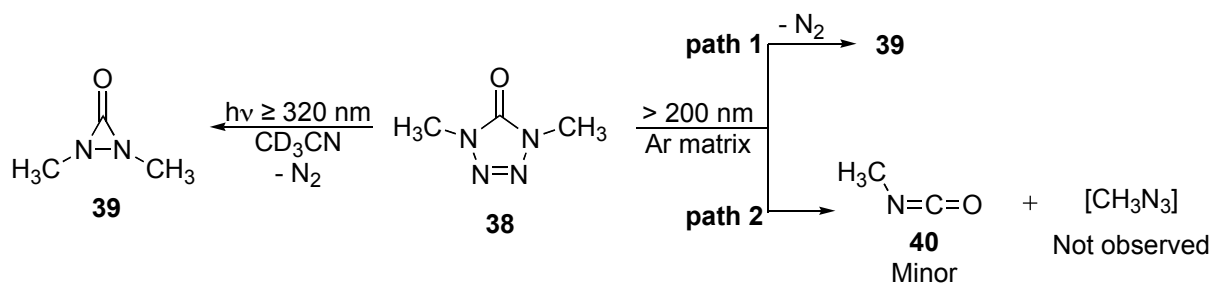
Scheme 1.4: Photodecomposition route of 1,4,5-substituted alkylidenedihydro-tetrazoles **34** in solution.⁴⁸

Similarly, the photolysis ($\lambda \geq 320\text{ nm}$) of degassed toluene-*d*₈ solution of geminal tetramethylalkylidenedihydro-tetrazole **34c** at -60 °C resulted into a mixture of diastereomers with (*Z*)-iminoaziridine **36c** as the major product (59%). During equilibration at room temperature for several days, diastereomerization to (*E*)-iminoaziridine **36c** was observed (Scheme 1.4). The difference in the diastereoselectivities observed in case of **34a** and **34b,c** was attributed to the geometric feature of the C=C-N-Me moiety which remained conserved when R¹ = H, to give exclusively the *E*-conformer (**34a**). However, the steric effect caused by the presence of methyl group (R¹ = CH₃) at the C=C bond in **34b** or geminal methyls in **34c** (R² = CH₃) resulted in the (*E*) → (*Z*) diastereomerization of the biradical intermediates **35b,c** before ring closure that afforded a mixture of *E* and *Z*-**36b,c**.⁴⁸

1.2.3 Photolysis of tetrazolone derivatives

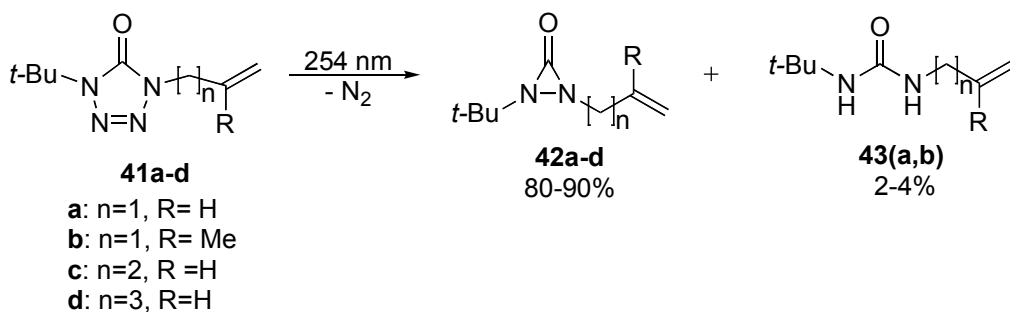
In 1975, Quast and Bieber reported that photolysis ($\lambda \geq 320\text{ nm}$) of 1,4-dimethyl-1,4-dihydro-5*H*-tetrazol-5-one (**38**) in acetonitrile-*d*₃ produced a single photoproduct, the 1,4-dimethyldiaziridinones (**39**), following the loss of molecular nitrogen (Scheme 1.6, left).⁴⁹ Several years later, Quast and Dunkin revisited the photochemistry of **38** in cryogenic matrix and the results indicated the formation of **39** as the major photoproduct, plus a minor photoproduct methyl isocyanate **40**. The photodecomposition pathway that led to the formation of compound

40 was thought to involve a different pathway involving 1,3-dipolar cycloreversion (Scheme 1.5, right).⁵⁰ However, there was no evidence of the second photoproduct of this latter pathway, the methylazide, which was probably due to the sensitivity of the photoproduct to undergo secondary reactions in matrix at prolonged irradiation times.



Scheme 1.5: Photoproducts formed during UV irradiation of **38** in solution and cryogenic matrix.^{49,50}

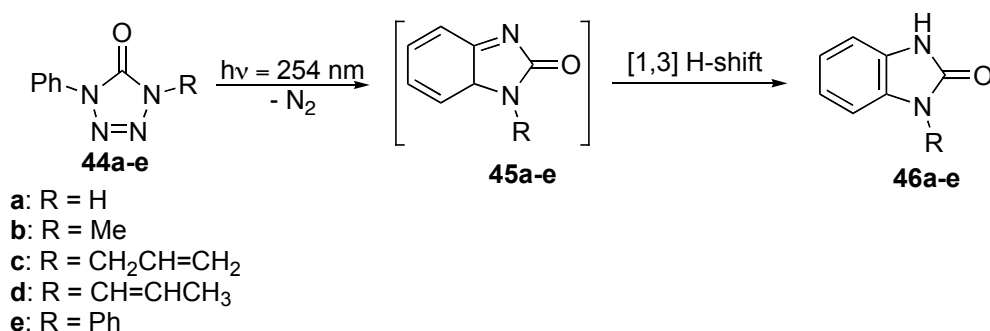
These researchers also investigated the UV-induced photochemistry ($\lambda = 254 \text{ nm}$) of a series of alkenyldihydrotriazolones **41a-d** in acetonitrile-*d*₃, cyclohexane-*d*₁₂ and methylcyclohexane-*d*₁₄ solutions.⁵¹ The photolysis of all derivatives of **41** afforded alkenyldiaziridinones **42** as the primary photoproduct in all the solvents *via* the loss of molecular nitrogen. However, irradiation of **41a,b** in acetonitrile-*d*₃ also resulted in the formation of a byproduct **43a,b** which was identified as the hydrolyzed form of **42a,b** (Scheme 1.6).



Scheme 1.6: Photoconversion of **41** to alkenyl-diaziridinone **42** and its hydrolyzed derivatives **43** in solution.⁵¹

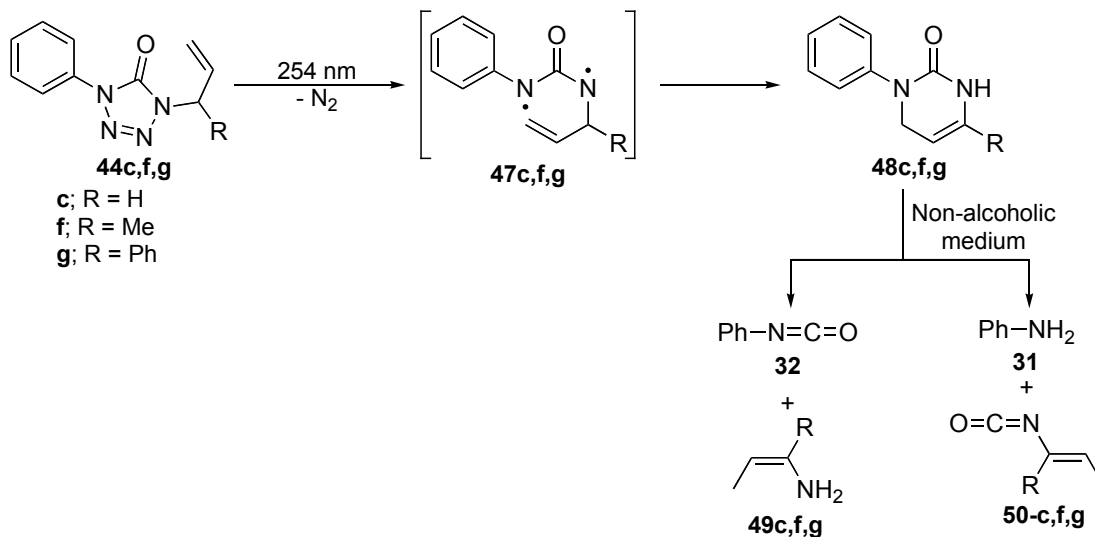
Furthermore, it has been shown that modification of the substituents on the triazolone ring could lead to the formation of different photoproducts through the common

photodecomposition pathway involving the loss of molecular nitrogen. For example, Quast and Nahr reported that the UV irradiation of a series of phenyl, alkyl phenyl, allylphenyl and diphenyl tetrazolones **44** in acetonitrile, methanol and 2-propanol solutions at 20 °C with 254 nm light (15 W Hg lamp) yielded primarily benzimidazolones **46a–e** in quantitative yields *via* a intermediate **45** formed by the release of molecular nitrogen (Scheme 1.7).⁵²



Scheme 1.7: Photodecomposition pathway of series of alkyl-phenyltetrazolones **44** in solution.⁵²

Recently, Cristiano and coworkers re-examined the photochemistry of a series of 4-allyltetrazolones in various solvents *e.g.* acetonitrile, cyclohexane, carbon tetrachloride, methanol, 1-hexanol and 1-propanol.^{35,53} They showed that photolysis of 4-allyl-tetrazolones **44c,f,g** (254 nm; 16W low pressure Hg lamp; 25 °C) in all the solvents led to the formation of intermediate **47c,f,g** after the photorelease of molecular nitrogen, that rapidly underwent ring closure and a [1,2] H-shift to produce pyrimidinones **48c,f,g** as the sole primary photoproduct (Scheme 1.8). When the photochemistry was carried out in acetonitrile, cyclohexane and carbon tetrachloride, the primary photoproduct **48** was unstable and underwent secondary photoreactions to afford aniline **31**, aminoalkene **49**, phenyl and allyl isocyanates **32** and **50**, respectively.^{35,53}



Scheme 1.8: Photocleavage of 4-allyl-1-phenyltetrazolones **44** in solution.^{35,53}

The authors attributed this disparity to different experimental conditions employed. The photostability exhibited by **48** in alcoholic medium was attributed to efficient solvation, which entailed hydrogen bonding with the solvent (Figure 1.7).³⁵ This solvent caging was also believed to be responsible for absence of any secondary photoreactions from **48**.

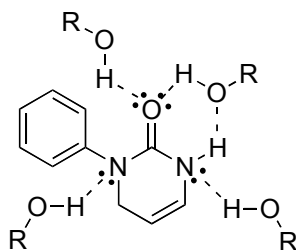
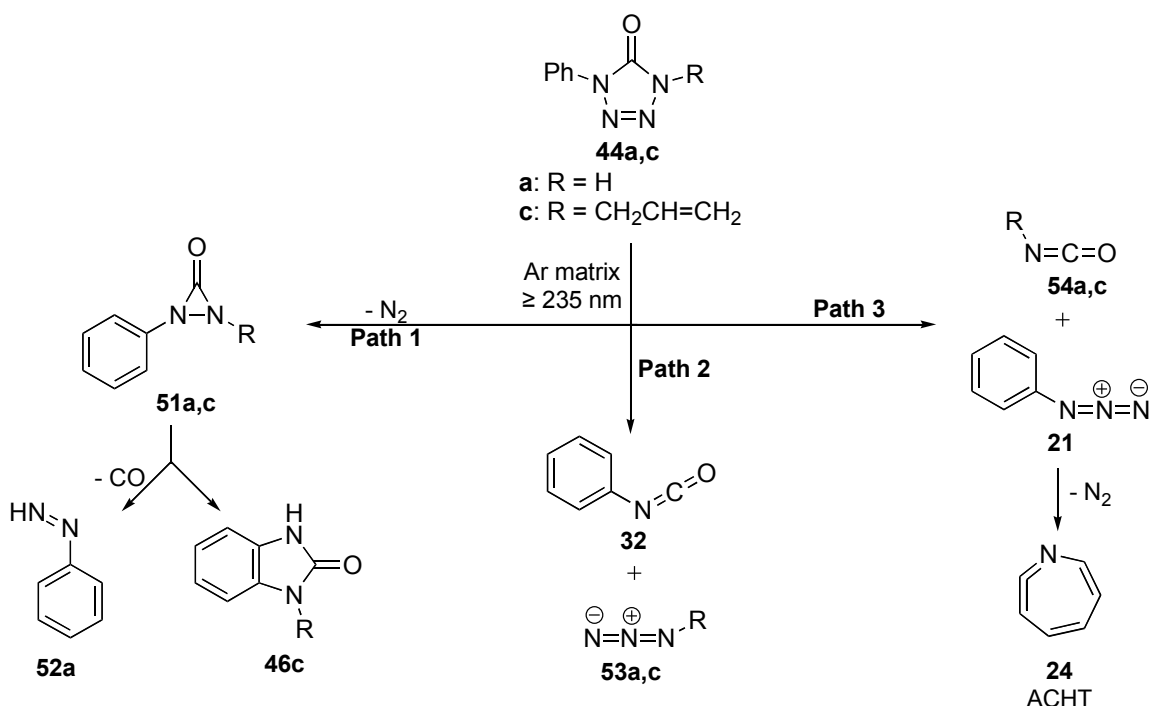


Figure 1.7: Stabilization of pyrimidinones **48** by alcohols.³⁵

Note that this study reported the formation of different photoproducts contrary to what was observed by Quast above (Scheme 1.7).

Furthermore, the photochemistry of **44a,c** has also been investigated with FT-IR matrix-isolation spectroscopy ($\lambda \geq 235$ nm) and the results revealed the formation of diverse array of photoproducts *via* three different photodecomposition pathways.^{36,54} Path **1** involved the elimination of molecular nitrogen which afforded the substituted aryldiaziridinones **52a,c**. The latter underwent further decomposition to produce **53a** *via* the loss of carbon monoxide, and

rearrangement to produce 1-allyl-1*H*-benzimidazol-2(3*H*)-one **46c** as secondary photoproducts. Note that **46c** was also observed in solution by Quast (Scheme 1.7). Path **2** followed a retro 1,3-dipolar cycloaddition pathway that produced phenyl isocyanates **32** and allyl azide **53**, and path **3** involved a different retro 1,3-dipolar cycloreversion of the tetrazolyl moiety to generate allyl isocyanates **54a,c** and phenyl azide **21**. The latter decomposed further to produce 1-aza-1,2,4,6-cycloheptatetraene (AHT) **24** (Scheme 1.9).^{36,54}

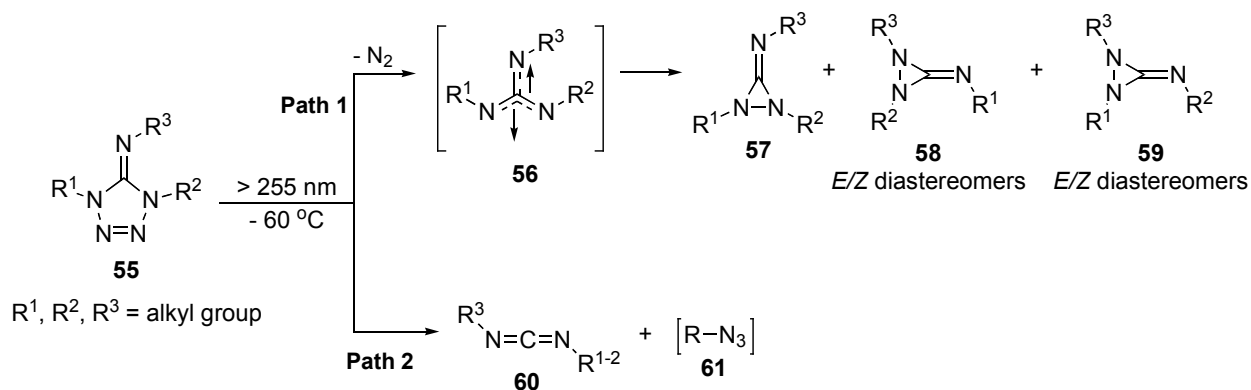


Scheme 1.9: Photodecomposition pathways of allyl phenyltetrazolone **44a** and **44c** in solid matrix.^{36,54}

1.2.4 Photolysis of imino-dihydropyridazine derivatives

Quast and coworkers also contributed to the studies involving the UV-induced photochemistry of a number of iminodihydropyridazines both in solution and in cryogenic matrix.^{50,55} In the course of their investigation, the authors observed that photolysis of iminotetrazolines both in solution (> 255 nm) and argon matrix (> 200 nm) produced similar results.⁵⁰ Two decomposition pathways were observed. Once again, path **1** involved the initial photorelease of molecular nitrogen that resulted in the formation of singlet

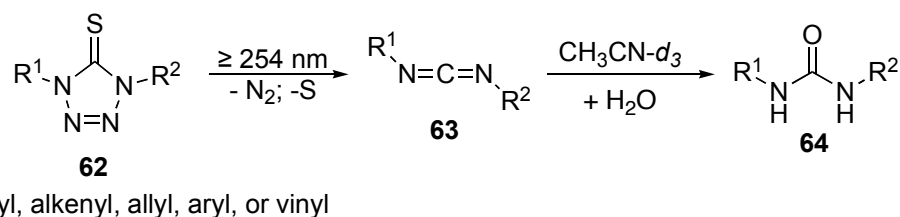
triazamethylenemethane biradicals **56**,^{55,56} which subsequently produced mixtures of iminodiaziridines **57** – **59** as the major photoproducts, and path 2 involved a photochemical 1,3-dipolar cycloreversion that yielded small amounts of alkylcarbodiimides **50**. The second product of this latter pathway was alkyl azide **61** which was highly photolabile and was undetected (Scheme 1.10).⁵⁵



Scheme 1.10: Photoproducts generated during irradiation of **55** in solution.^{55,56}

1.2.5 Photolysis of tetrazolethione derivatives

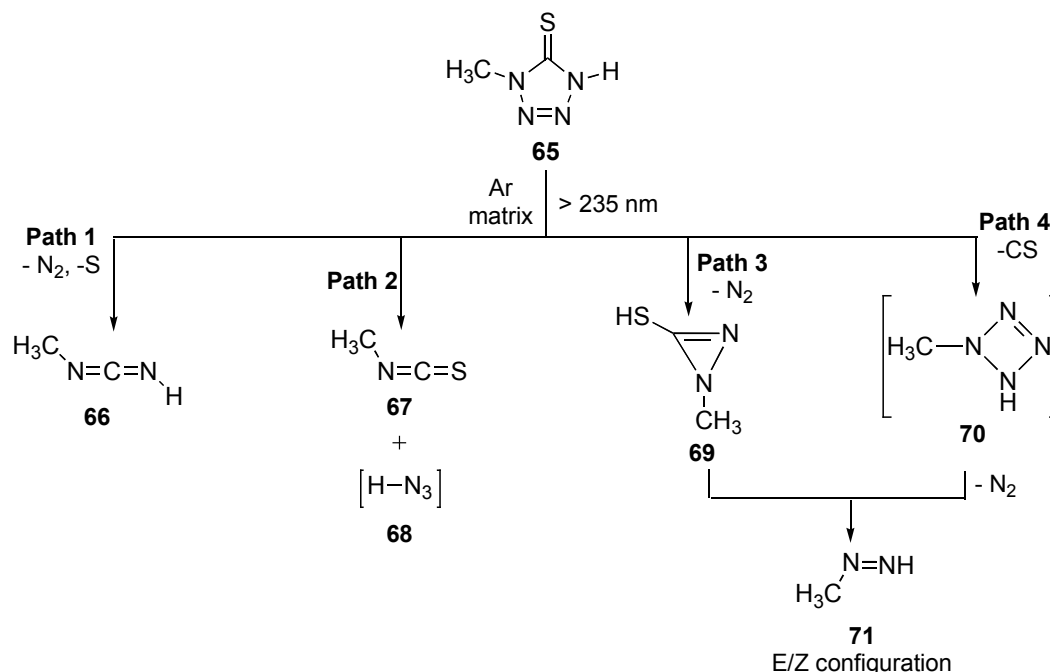
Quast and coworkers investigated the photochemistry (≥ 254 nm) of a series of 1,4-dialkyl tetrazolethiones **62** in acetonitrile-*d*₃, dichloromethane, methanol-*d*₄ and methylcyclohexane-*d*₁₄ solutions.^{1,51} The photolysis of **62** resulted in the simultaneous loss of molecular nitrogen and sulfur to produce the dialkyl carbodiimides **63**, in 50-80% yield. There was no evidence of any alternative photoproduct(s). The formed photoproduct **63** was unstable in acetonitrile because it was subsequently converted to the corresponding ureas **64** by reaction with trace amount of water present in solution (Scheme 1.11).



Scheme 1.11: Photodecomposition products of dialkyltetrazolethiones **62** in solution.⁵¹

In a later publication, the same authors described the UV-induced photochemistry (> 200 nm) of alkyl phenyltetrazolethione and dialkyl tetrazolethione in nitrogen matrix.⁵⁰ And, the researchers reported the formation of corresponding carbodiimides similar to the solution studies.

Recently, Cristiano and coworkers reported the matrix-isolated photochemistry of 1-methyl-1*H*-tetrazole-5(4*H*)-thione (**65**).¹⁷ Under these reaction conditions, the UV-irradiation (> 235 nm) resulted in the formation of a variety of photoproducts via different decomposition pathways all involving the cleavage of the tetrazolethione ring. The proposed photodecomposition pathways involves (i) simultaneous elimination of molecular nitrogen and sulfur to generate *N*-methyl carbodiimide **66**, (ii) ring cleavage involving 1,3-dipolar cycloreversion to produce methyl isothiocyanate **67** and possibly, the azide **68**, (iii) photo-elimination of N₂ that result in the formation of two different conformers of 1-methyl-1*H*-diazirine-3-thiol **69** that further decomposed to afford *E* and *Z* conformers of methyl diazene **71**, and (iv) the direct fragmentation of **65** may have yielded **70** through the elimination of carbon monosulfide, that subsequently decomposed to **71** (Scheme 1.12).¹⁷ The results of this study are slightly different from previous report by Dunkin and Quast (Scheme 1.11). This can be attributed to the presence of hydrogen on the N1 of **65** that is expected to allow the formation secondary photoproducts with relative ease, especially **71**. The authors believe that the different photolysis conditions employed in the two studies (> 200 nm and > 235 nm), could have also influenced the reaction pathways.



Scheme 1.12: Photoproducts and fragmentation pathways resulting from irradiation of 1-methyl-1*H*-tetrazole-5(4*H*)-thione **65** in argon matrix.¹⁷

1.3 Concluding Remarks

In contrast to the 5-oxo derivatives of tetrazoles, the photochemistry of 5-thio derivatives, *i.e.* the tetrazolethiones has not received much attention. No information is available on the nature of reactive intermediates involved or their photochemical quantum yields. Considering the vast applications of tetrazolethiones in industry, agriculture and medicinal chemistry, the understanding of their mechanism of photodecomposition is critical for designing compounds with improved performance/properties. We were interested in tetrazolethione photochemistry because of our interest in using these scaffolds for designing photoactivated DNA cleaving prodrugs.

Chapter 2 of this dissertation will begin with a brief overview of the photoactivated DNA cleaving agents based on tetrazolethione scaffolds that our laboratory is interested, in and will focus on the:

- Synthesis of tetrazolethiones.
- Study of the molecular and electronic properties of tetrazolethiones by theoretical methods.

- Study of photoreactivity of tetrazolethiones and characterization of their photoproducts.
- Study of the mechanism of photodecomposition of these ring systems.

Reference

- ¹ Frija, L. M.; Ismael, A.; Cristiano, M. L., Photochemical transformations of tetrazole derivatives: applications in organic synthesis. *Molecules* **2010**, *15* (5), 3757-74.
- ² Pinto, R. M.; Dias, A. A.; Costa, M. L., Electronic structure and thermal decomposition of 5-aminotetrazole studied by UV photoelectron spectroscopy and theoretical calculations. *Chemical Physics* **2011**, *381* (1-3), 49-58.
- ³ Pagacz-Kostrzewa, M.; Reva, I. D.; Bronisz, R.; Giuliano, B. M.; Fausto, R.; Wierzejewska, M., Conformational behavior and tautomer selective photochemistry in low temperature matrices: the case of 5-(1H-tetrazol-1-yl)-1,2,4-triazole. *J Phys Chem A* **2011**, *115* (22), 5693-707.
- ⁴ Benson, F. R., The chemistry of the tetrazoles. *Chem Rev* **1947**, *41* (1), 1-61.
- ⁵ Lee, J.-W.; Kang, M.-C.; Kim, J. J., Characterization of 5-Aminotetrazole as a Corrosion Inhibitor in Copper Chemical Mechanical Polishing. *J. Electrochem. Soc.* **2005**, *152* (12), C827-C831.
- ⁶ Brase, S.; Friedrich, A.; Gartner, M.; Schroder, T., Cycloaddition Reaction of Azides Including Bioconjugation. *Top. Heterocycl. Chem.* **2008**, *12*, 45-115.
- ⁷ Herr, R. J., 5-Substituted-1H-tetrazoles as carboxylic acid isosteres: medicinal chemistry and synthetic methods. *Bioorg. Med. Chem.* **2002**, *10* (11), 3379-3393.
- ⁸ Popova, E. A.; Trifonov, R. E.; Ostrovskii, V. A., Advances in the synthesis of tetrazoles coordinated to metal ions. *ARKIVOC* **2012**, *i*, 45-65.
- ⁹ (a) Zucchi, F.; TrabANELLI, G.; Fonsati, M., Tetrazole derivatives as corrosion inhibitors for copper in chloride solutions. *Corrosion Science* **1996**, *38* (11), 2019-2029; (b) El-Sayed M.; Erasmus, R. M.; Comins, J. D., Inhibition of copper corrosion in acidic chloride pickling solutions by 5-(3-aminophenyl)-tetrazole as a corrosion inhibitor. *Corrosion Science* **2008**, *50* (12), 3439-3445.
- ¹⁰ Li, J.; Ren, T.; Liu, H.; Wang, D.; Liu, W., The tribological study of a tetrazole derivative as additive in liquid paraffin. *Wear* **2000**, *246* (1-2), 130-133.
- ¹¹ (a) Baumann, H.; Dwars, U.; Strehmel, B.; Simpson, C. D.; Savariar-Hauck, C.; Hauck, G., Imageable elements with components having 1H-tetrazole groups. U.S. Pat. Appl. Publ. (2009), US 20090142695 A1 20090604; (b) Tani, T., On photographic stabilizers and antifoggants. Part IV. Sensitization caused by thiolic antifoggants. *Photographic Science and Engineering* **1978**, *22* (4), 179-88; (c) Jursic, B. S.; LeBlanc, B. W., Preparation of tetrazoles from organic nitriles and sodium azide in micellar media. *J Heterocyclic Chem* **1998**, *35* (2), 405-408; (c) Roh, J.; Artamonova, T. V.; Vavrova, K.; Koldobskii, G. I.; Hrabalek, A., Practical Synthesis of 5-Substituted Tetrazoles under Microwave Irradiation. *Synthesis* **2009**, *13* (2175-2178), 2175.
- ¹² (a) Eachus, R. S.; Muentner, A. A.; Pawlik, T. D.; Lenhard, J. R., An EPR study of two-electron sensitization by fragmentable electron donors. *J Phys Chem B* **2005**, *109* (20), 10126-36; (b) Lv, F.; Liu, Y.; Zou, J.; Zhang, D.; Yao, Z., Synthesis of the novel photographic DIAR couplers. *Dyes and Pigments* **2005**, *68* (2-3), 211-216; (c) Modarresi-Alam, A. R.; Narsrollahzadeh, M., Synthesis of 5-Arylamino-1H (2H)-tetrazoles and 5-Amino-1-aryl-1H-tetrazoles from Secondary Arylcyanamides in Glacial Acetic Acid: A simple and Efficient Method. *Turk. J. Chem.* **2009**, *33*, 267-280; (d) Frija, L. M.; Reva, I. D.; Gomez-Zavaglia, A.; Cristiano, M. L.; Fausto, R.,

Photochemistry and vibrational spectra of matrix-isolated 5-ethoxy-1-phenyl-1H-tetrazole. *J Phys Chem A* **2007**, *111* (15), 2879-88.

¹³ (a) Hammerl, A.; Holl, G.; Klapötke, T. M.; Mayer, P.; Noth, H.; Piotrowski, H.; Warchhold, M. Salts of 5,5'-Azotetrazolate *Eur. J. Inorg. Chem.* **2002**, *4*, 834; (b) Geith, J.; Klapötke, T. M.; Weigand, J.; Holl, G. Calculation of the Detonation Velocities and Detonation Pressures of Dinitrobiuret (DNB) and Diaminotetrazolium Nitrate (HDAT-NO₃). *Propellants, Explos., Pyrotech.* **2004**, *29* (1), 3; (c) Henry, R. A., *USA Patent 3.096,312 (1963)*; *Chem. Abstr.* **1980**, *92*, 8480.

¹⁴ (a) Brown, M., *US Patent 3,338,915 (1967)*; *Chem. Abstr.* **1968**, 87299; (b) Tarver, C. M.; Goodale, T. C.; Shaw, R.; Cowperthwaite, M., *Off Nav. Res. (Tech Rep) ACR (US), ACR-221, Proc. Symp. Int. Detonation 6th 1967*, *231*, 1967; (c) Morisson, H., Chemistry of tetrazole derivative explosives. *Util. Elem. Pyrotechniques Explos. Syst. Spatiaux, Colloq. Int.* **1969**, 111-20.

¹⁵ (a) Lesnikovich, A. I.; Ivashkevich, O. A.; Levchik, S. V.; Balabanovich, A. I.; Gaponik, P. N.; Kulak, A. A. Thermal decomposition of aminotetrazoles. *Thermochim. Acta* **2002**, *388* (1-2), 233-251; (b) Gomez-Zavaglia, A.; Reva, I. D.; Frija, L.; Cristiano, M. L.; Fausto, R., Molecular structure, vibrational spectra and photochemistry of 2-methyl-2H-tetrazol-5-amine in solid argon. *J Phys Chem A* **2005**, *109* (35), 7967-76.

¹⁶ Klapötke, T. M.; Mayer, P.; Schulz, A.; Weigand, J. J. 1,4-Bis-[1-Methyltetrazol-5-yl]-1,4-Dimethyl-2-Tetrazene: A Stable, Highly Energetic Hexamer of Diazomethane (CH₂N₂)₆. *Propellants, Explos., Pyrotech.* **2004**, *29* (6), 325.

¹⁷ Wood, J. C.; Wood, E. H., Metal oxide-free aminotetrazole-based gas-generating propellants for inflation of vehicle airbags. U.S. (2001), US 6328830 B1 20011211.

¹⁸ (a) Stassen, A. F.; Kooijman, H.; Spek, A. L.; Haasnoot, J. G.; Reedijk, J., Synthesis, spectroscopy, magnetism, and X-ray structures of hexakis(1-(2-chloroethyl)-tetrazole-N₄)copper(II) salts. *J. Chem. Crystallogr.* **2001**, *31*, 307-314; (b) Wu, T.; Yi, B.-Y.; Li, D., Two Novel Nanoporous Supramolecular Architectures Based on Copper(I) Coordination Polymers with Uniform (8, 3) and (8210) Nets: In Situ Formation of Tetrazolate Ligands. *Inorg. Chem* **2005**, *44* (12), 4130-4132.

¹⁹ Bond, A. D.; Fleming, A.; Kelleher, F.; McGinley, J.; Prajapati, V., Reactions of 14-bis(tetrazole)benzenes: formation of long chain alkyl halides. *Tetrahedron* **2006**, *62* (41), 9577-9581.

²⁰ (a) Chen, Q.-Y.; Li, Y.; Zheng, F.-K.; Zou, W.-Q.; Wu, M.-F.; Guo, G.-C.; Wu, A.-Q.; Huang, J.-S., A 3D-diamond-like tetrazole-based Zn(II) coordination polymer: Crystal structure, nonlinear optical effect and luminescent property. *Inorganic Chemistry Communications* **2008**, *11* (9), 969-971; (b) Slyvka, Y.; Pokhodylo, N.; Savka, R.; Mazej, Z.; Goresnik, E.; Mys'kiv, M., Copper(I) complexes with 5-(allylthio)-1H-tetrazoles: synthesis and crystal structure of [Cu₂(C₁₀H₁₀N₄S)₂(H₂O)₂](BF₄)₂ and [Cu₂(C₁₀H₉CIN₄S)₂(H₂O)₂](BF₄)₂·C₂H₅OH π -compounds (C₁₀H₁₀N₄S and C₁₀H₉CIN₄S - 5-(allylthio)-1-phenyl- and 5-(allylthio)-1-(4-chlorophenyl)-1H-tetrazole). *Chem. Met. Alloys* **2010**, (3), 201-297.

²¹ Zhao, H.; Qu, Z. R.; Ye, H. Y.; Xiong, R. G., In situ hydrothermal synthesis of tetrazole coordination polymers with interesting physical properties. *Chem Soc Rev* **2008**, *37* (1), 84-100.

²² (a) Tong, X.-L.; Wang, D.-Z.; Hu, R.-L.; Song, W.-C.; Tao, Y.; Bu, X.-H., Zinc and Cadmium Coordination Polymers with Bis(tetrazole) Ligands Bearing Flexible Spacers: Synthesis, Crystal Structures, and Properties. *Cryst Growth Des* **2009**, *9* (5), 2280-2286; (b) Liu, P.-P.; Cheng, A.-

- L.; Yue, Q.; Liu, N.; Sun, W.-W.; Gao, E.-Q., Cobalt(II) Coordination Networks Dependent upon the Spacer Length of Flexible Bis(tetrazole) Ligands. *Cryst. Growth Des.* **2008**, *8* (5), 1668-1674; (c) Toa, Y.; Li, J.-R.; Chang, Z.; Bu, X.-H., ZnII and HgII Complexes with 2,3-Substituted-5,6-di(1H-tetrazol-5-yl)pyrazine Ligands: Roles of Substituting Groups and Synthetic Conditions on the Formation of Complexes. *Cryst. Growth Des.* **2010**, *10* (2), 564-574.
- ²³ Song, W. C.; Li, J. R.; Song, P. C.; Tao, Y.; Yu, Q.; Tong, X. L.; Bu, X. H., Tuning the framework topologies of Co(II)-doped Zn(II)-tetrazole-benzoate coordination polymers by ligand modifications: structures and spectral studies. *Inorg Chem* **2009**, *48* (8), 3792-9.
- ²⁴ Liu, N.; Yue, Q.; Wang, Y. Q.; Cheng, A. L.; Gao, E. Q., Coordination compounds of bis(5-tetrazolyl)amine with manganese(II), zinc(II) and cadmium(II): synthesis, structure and magnetic properties. *Dalton Trans* **2008**, (34), 4621-9.
- ²⁵ Sun, L.; Ma, L.; Cai, J.-B.; Liang, L.; Deng, H., Novel tetrazole-based metal-organic frameworks constructed from in situ synthesize bifunction ligands: synthesis, structure and luminescent properties. *CrystEngComm* **2012**, *14*, 890-898.
- ²⁶ Zhang, X.-M.; Zhao, Y.-F.; Wu, H.-S.; Batten, S. R.; Ng, S. W., Synthesis and structures of metal tetrazole coordination polymers. *Dalton Trans* **2006**, 3170-3178.
- ²⁷ (a) Jimenez-Sandoval, O.; Cea-Olivares, R.; Hernandez-Ortega, S.; Silaghi-Dumitrescu, I., Structural studies of tetrazoles. Crystal and molecular structure and ab initio calculations of 1-phenyl-1H-tetrazole-5-thiolate, as its [diaqua(18-crown-6)sodium] salt: An anionic tetrazole free of direct metal interactions. *Heteroatom Chem* **1997**, *8* (4), 351-359; (b) Moore, D. S.; Robinson, S. D., Catenated Nitrogen Ligands Part II.1 Transition Metal Derivatives of Triazoles, Tetrazoles, Pentazoles, and Hexazine. *Advance in Inorganic Chemistry* **1988**, *32*, 171-239.
- ²⁸ Araujo, N. C. P.; Brigas, A. F.; Cristiano, M. L. S.; Frija, L. M. T.; Guimaraes, E. M. O.; Loureiro, R. M. S., Heteroaromatic benzyl ethers as intermediates for palladium-catalysed transfer hydrogenolysis of benzyl alcohols. *J. Mol. Cat. A: Chem.* **2004**, *215*, 113-120.
- ²⁹ (a) Luo, Y.-P.; Yang, G.-F., Discovery of a new insecticide lead by optimizing a target-diverse scaffold: Tetrazolinone derivatives. *Bioorg. Med. Chem.* **2007**, *15* (4), 1716-1724; (b) Bekircan, O.; Bektas, H., Synthesis of new bis-1,2,4-triazole derivatives. *Molecules* **2006**, *11* (6), 469-77.
- ³⁰ Zhao, P. S.; Jian, F. F.; Xiao, H. L.; Hou, Y. X., A novel synthesis and crystal structure of 2,3-substituted-1,4-2H-tetrazolthione. *Bull. Korean Chem. Soc.* **2004**, *25* (12), 1935-1936.
- ³¹ May, B. C. H.; Abell, A. D., α -Methylene tetrazole-based peptidomimetics: synthesis and inhibition of HIV protease. *J. Chem. Soc., Perkin Trans. 1* **2002**, 172-178.
- ³² (a) Bradbury, R. H.; Allott, C. P.; Dennis, M.; Girdwood, J. A.; Kenny, P. W.; Major, J. S.; Oldham, A. A.; Ratcliffe, A. H.; Rivett, J. E.; Roberts, D. A.; et al., New nonpeptide angiotensin II receptor antagonists. 3. Synthesis, biological properties, and structure-activity relationships of 2-alkyl-4-(biphenylmethoxy)pyridine derivatives. *J Med Chem* **1993**, *36* (9), 1245-54; (b) Carini, D. J.; Duncia, J. V.; Aldrich, P. E.; Chiu, A. T.; Johnson, A. L.; Pierce, M. E.; Price, W. A.; Santella, J. B., 3rd; Wells, G. J.; Wexler, R. R.; et al., Nonpeptide angiotensin II receptor antagonists: the discovery of a series of N-(biphenylmethyl)imidazoles as potent, orally active antihypertensives. *J Med Chem* **1991**, *34* (8), 2525-47.
- ³³ Gutmann, B.; Roduit, J.-P.; Roberge, D.; Kappe, C. O., Synthesis of 5-Substituted 1H-Tetrazole from Nitriles and Hydrazoic Acid by Using a Safe and Scalable High-Temperature Microreactor Approach. *Angew. Chem. Int. Ed.* **2010**, *49* (39), 7101-7105.
- ³⁴ McKie, A. H.; Friedland, S.; Hof, F., Tetrazoles are potent anion recognition elements that emulate the disfavored anti conformations of carboxylic acids. *Org Lett* **2008**, *10* (20), 4653-5.

- ³⁵ Frija, L. M.; Khmelinskii, I. V.; Cristiano, M. L., Mechanistic investigations into the photochemistry of 4-allyl-tetrazolones in solution: a new approach to the synthesis of 3,4-dihydro-pyrimidinones. *J Org Chem* **2006**, *71* (9), 3583-91.
- ³⁶ Frija, L. M.; Reva, I. D.; Gomez-Zavaglia, A.; Cristiano, M. L.; Fausto, R., UV-induced photochemistry of matrix-isolated 1-phenyl-4-allyl-tetrazolone. *Photochem Photobiol Sci* **2007**, *6* (11), 1170-6.
- ³⁷ Frija, L. M.; Khmelinskii, I. V.; Serpa, C.; Reva, I. D.; Fausto, R.; Cristiano, M. L., Photochemistry of 5-allyloxy-tetrazoles: steady-state and laser flash photolysis study. *Org Biomol Chem* **2008**, *6* (6), 1046-55.
- ³⁸ (a) Pinter, T.; Jana, S.; Courtemanche, R. J.; Hof, F., Recognition properties of carboxylic acid bioisosteres: anion binding by tetrazoles, aryl sulfonamides, and acyl sulfonamides on a calix[4]arene scaffold. *J Org Chem* **2011**, *76* (10), 3733-41; (b) Katritzky, A. R.; El-Gendy Bel, D.; Draghici, B.; Hall, C. D.; Steel, P. J., NMR study of the tautomeric behavior of N-(alpha-aminoalkyl)tetrazoles. *J Org Chem* **2010**, *75* (19), 6468-76. (c) Miyata, T.; Kurokawa, K. PCT Int. Appl. WO 2005051930, 2005; (d) Siegl, P. K. S.; Goldberg, A. I.; Goldberg, M. R.; Chang, P. I. PCT Int. Appl. WO 9749690, 1997. (e) Siegl, P. K. S.; Goldberg, A. I.; Goldberg, M. R.; Chang, P. I. U. S. Patent 5817658, 1998.
- ³⁹ (a) Zabrocki, J.; Smith, G. D.; Dunbar, J. B.; Iijima, H.; Marshall, G. R., Conformational mimicry. 1. 1,5-Disubstituted tetrazole ring as a surrogate for the cis amide bond. *J. Am. Chem. Soc.* **1988**, *110* (17), 5875-5880; (b) Zabrocki, J.; Dunbar, J. B.; Iijima, H.; Marshall, K. W., Toth, M. V.; Marshall, G. R., Conformational mimicry. 3. Synthesis and incorporation of 1,5-disubstituted dipeptide analogs into peptides with preservation of chiral integrity: bradykinin. *J. Org. Chem.* **1992**, *57* (1), 202-209.
- ⁴⁰ Yu, K. L.; Johnson, R. L., Synthesis and chemical properties of tetrazole peptide analogs. *J. Org. Chem.* **1987**, *52* (10), 2051-2059.
- ⁴¹ (a) Himo, F.; Demko, Z. P.; Noodleman, L.; Sharpless, K. B., Mechanisms of tetrazole formation by addition of azide to nitriles. *J Am Chem Soc* **2002**, *124* (41), 12210-6; (b) Himo, F.; Demko, Z. P.; Noodleman, L.; Sharpless, K. B., Why is tetrazole formation by addition of azide to organic nitriles catalyzed by zinc(II) salts? *J Am Chem Soc* **2003**, *125* (33), 9983-7.
- ⁴² (a) Huang, H. C.; Reitz, D. B.; Chamberlain, T. S.; Olins, G. M.; Corpus, V. M.; McMahon, E. G.; Palomo, M. A.; Koepke, J. P.; Smits, G. J.; McGraw, D. E.; Blaine, E. H.; Manning, R. E., Synthesis and structure-activity relationships of nonpeptide, potent triazolone-based angiotensin II receptor antagonists. *J. Med. Chem.* **1993**, *36* (15), 2172-81; (b) Das, B.; Reddy, C. R.; Kumar, C. R.; Krishnaiah, M.; Narender, R., A simple, advantageous synthesis of 5-substituted 1H-tetrazoles. *Synlett* **2010**, *3*, 391-394.
- ⁴³ Raman, K.; Parmar, S. S.; Singh, S. P., Synthesis of 1-(5-phenyl-2H-tetrazol-2-ylacetyl)-4-substituted thiosemicarbazides as possible antiinflammatory agents. *J. Heterocyclic Chem.* **1980**, *17* (5), 1137-1139.
- ⁴⁴ (a) Koyama, M.; Ohtani, N.; Kai, F.; Moriguchi, I.; Inouye, S., Synthesis and quantitative structure-activity relationship analysis of N-triiodoallyl- and N-iodopropargylazoles. New antifungal agents. *J Med Chem* **1987**, *30* (3), 552-62; (b) Maxwell, J. R.; Wasdahl, D. A.; Wolfson, A. C.; Stenberg, V. I., Synthesis of 5-aryl-2H-tetrazoles, 5-aryl-2H-tetrazole-2-acetic acids, and [(4-phenyl-5-aryl-4H-1,2,4-triazol-3-yl)thio]acetic acids as possible superoxide scavengers and antiinflammatory agents. *J. Med. Chem.* **1984**, *27* (12), 1565-1570.

-
- ⁴⁵ Maier, G.; Eckwert, J.; Bothur, A.; Reisenaur, H. P.; Schmidt, C., Photochemical Fragmentation of Unsubstituted Tetrazole, 1,2,3-Triazole, and 1,2,4-Triazole: First Matrix-Spectroscopic Identification of Nitrilimine HCNH. *Liebigs Annalen* **1996**, (7), 1041-1053.
- ⁴⁶ Gomez-Zavaglia, A.; Reva, I. D.; Frija, I.; Cristiano, M. L. S.; Fausto, R., Infrared spectrum and UV-Induce photochemistry of matrix-isolated 5-methoxy-1-phenyl-1H-tetrazole. *J. Photochem. Photobiol. A* **2006**, 180 (1-2), 175-183.
- ⁴⁷ (a) Quast, H.; Schmitt, E., Aziridine Imines. *Angew. Chem. Int. Ed.* **1970**, 9 (5), 381-382; (b) Quast, H.; Aldenkortt, S.; Schafer, P.; Schmitt, E.; Wurthwein, E.-U., Synthesis and thermal reorganisations of iminoaziridines. Ab initio calculations of their transition states, of diazatriethylenemethanes, and some cyclic members of the C₂H₄N₂ potential-energy hypersurface. *Liebigs Annalen* **1995**, (12), 2171-2188.
- ⁴⁸ Quast, H.; Fuss, A.; Nudling, W., Photoextrusion of Molecular Nitrogen from Annulated 5-Alkylidene-4,5-dihydro-1H-tetrazoles: Annulated Iminoaziridines and the First Triplet Diazatriethylenemethane. *Eur. J. Inorg. Chem.* **1998**, (2), 317-327.
- ⁴⁹ Quast, H.; Bieber, L., Aziridinimines, Diaziridinimines, Diaziridinones, and Carbodiimides by Photolysis of 2-Tetrazolines. *Angew. Chem. Int. Ed.* **1975**, 14 (6), 428-429.
- ⁵⁰ Dunkin, I. R.; Shields, C. J.; Quast, H., The photochemistry of 1,4-dihydro-5H-tetrazole derivatives isolated in low-temperature matrices. *Tetrahedron* **1989**, 45 (1), 259-268.
- ⁵¹ Quast, H.; U., N., Photochemische Stickstoff-Eliminierung aus 1-Alkenyl-4-alkyl-1,4-dihydro-5H-tetrazol-5-onen und -thionen. Diaziridinone und Carbodiimide mit Alkenylsubstituenten. *Chemische Berichte* **1983**, 116 (10), 3427-3437.
- ⁵² Quast, H.; U., N., Photochemische Stickstoff-Eliminierung aus 1,4-Dihydro-1-phenyl-5H-tetrazol-5-onen und -thionen. Benzimidazolone und Carbodiimide. *Chemische Berichte* **1985**, 118 (2), 526-540.
- ⁵³ Frija, L. M. T.; Khmelinskii, I. V.; Cristiano, M. L., Novel efficient synthesis of 3,4-dihydro-6-substituted-3-phenylpyrimidin-2(1H)-ones. *Tetrahedron Lett.* **2005**, 46 (39), 6757-6760.
- ⁵⁴ Gomez-Zavaglia, A.; Reva, I. D.; Frija, I.; Cristiano, M. L.; Fausto, R., Photochemistry of 1-phenyl-tetrazolone isolated in solid argon. *J. Photochem. Photobiol. A* **2006**, 179 (243-235), 243.
- ⁵⁵ Quast, H.; Nudling, W.; Klemm, G.; Kirschfeld, A.; Neuhaus, P.; Sander, W.; Hrovat, D. A.; Borden, W. T., A perimidine-derived non-Kekule triplet diradical. *J. Org. Chem.* **2008**, 73 (13), 4956-61.
- ⁵⁶ Quast, H.; Bieber, L., Iminodiaziridines by Regio- and Stereoselective Cyclization of Diastereomeric Singlet Triazatriethylenemethane Diradicals Generated Through Photolysis of 5-Imino-4,5-dihydro-1H-tetrazoles. *J. Org. Chem.* **2008**, 73 (10), 3738-3744.

Chapter 2 - Synthesis and Mechanistic Insights into the Photodecomposition of Tetrazolethiones

2.1 Introduction

The concept of treatment using light has been known for thousands of years. For example, ancient Egyptians, Indian and Chinese civilizations used light to treat various diseases such as psoriasis, rickets, vitiligo and skin diseases.^{1,2,3} However, it was only in the last century that Niels and Finsen developed phototherapy that involved the use of light in a clinical setting for therapeutic purposes.^{1,2} Finsen described the successful treatment of smallpox pustules and cutaneous tuberculosis by exposing infected patients to red and ultraviolet light.^{1,2}

In 1900, research contribution from Oscar Raab revealed that the combination of acridine red and light induced cytotoxic effects on infusoria (*Paramecium caudatum*),⁴ and several investigations following this discovery subsequently led to the development of Photodynamic therapy or PDT.^{1,2} Today PDT is described as a treatment method that employs a combination of drug (a photosensitizer, usually a porphyrin-based compound) and visible light in the presence of oxygen to kill tumor/cancerous cells.^{5,6} In general, the biochemical mechanism of action in PDT involves irradiation of the sensitizing agent with light, that results in the activation of the sensitizer from a ground state (S_0) to an excited singlet state (S_1) followed by intersystem crossing (ISC) to its excited triplet state (T_1) (Figure 2.1). As the triplet excited state of the sensitizer returns to the ground state, it releases energy that can be used for two pathways: Type I and Type II reactions.^{1,2,3,5} The former involves the direct reaction of the triplet excited sensitizer with cellular membrane or biomolecules to produce radicals that interact with oxygen to form reactive oxygen species (ROS; O_2^{\bullet}). The latter cause localized destruction of the tumor cells. Alternatively, the triplet excited sensitizer can transfer its energy directly to the ground state molecular oxygen (3O_2), subsequently forming the cytotoxic singlet oxygen (1O_2), that causes oxidations of biomolecules resulting in cell death (Figure 2.1).^{1,7} Note that the singlet electronic excited state of molecular oxygen is 94KJ/mole, and therefore for the type II reactions to be thermodynamically favorable the sensitizer's triplet excited state must be $\geq 94KJ/mole$.^{7b}

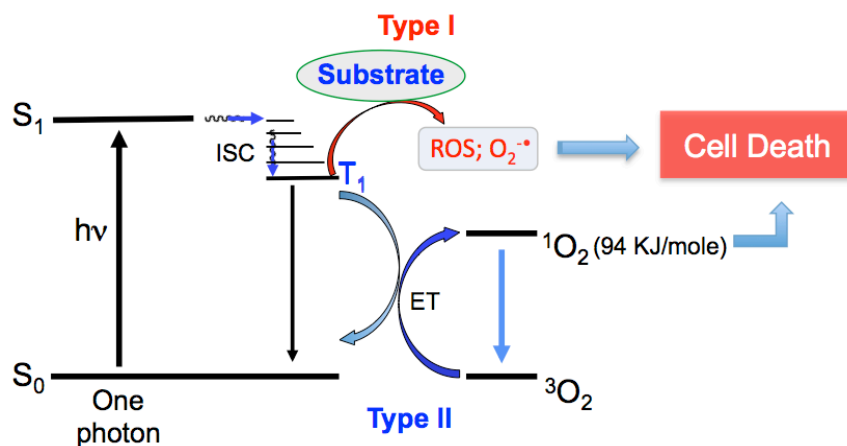


Figure 2.1: Jablonski diagram illustrating the single photon activation of the photosensitizer leading to cellular damage through type I and type II reactions in PDT, ET = energy transfer.¹

Porphyrins have been widely used as photosensitizers (drugs) for PDT due to their high singlet oxygen quantum yields and high tendency to accumulate in tumor cells.⁸ There are three generations of porphyrin based photosensitizers currently known. The first generation PDT sensitizers include Photofrin which is a mixture of hematoporphyrin derived oligomers. However, Photofrin has several limitations such as poor photon absorption at wavelengths used in PDT (> 650 nm), and its administration as a mixture of compounds. Furthermore, it exhibits non-specific biodistribution and prolonged accumulation in healthy tissues that results in sensitivity of the patient to light.⁹

With the discovery of second generation photosensitizers with improved absorption at larger wavelengths ($> 650 - 800$ nm), an increase in singlet oxygen quantum yield was achieved, which also meant that reduced amount of the drug could be used for PDT. In addition, these new sensitizers are administered as a single compound thus resulting in short photosensitivity of the patients.¹⁰ Recently, third generation photosensitizers have also been reported with selective targeting anchors to increase the drug concentration within the tumor site.

Since its advent, PDT has been used in the treatment of several benign and malignant cancers, age-related macular degeneration, antibiotic-resistant biofilms and wound infections as well as an adjuvant treatment for disseminated diseases. This technique is gaining considerable advancement clinically, because it is minimally invasive with reduced toxicity.

Traditionally, single photon excitation (SPE) is employed for the activation of photosensitizer in PDT (Figure 2.1). However, this method suffers from a number of drawbacks,

particularly, the limited penetration of light (3-10 millimeters) into larger tumors due to optical scattering and absorption by blood and tissue. As a result, PDT is most effective for the treatment of superficial conditions such as skin cancer or the lining of internal organs or cavities. Furthermore, the light that is used for SPE is cytotoxic and mutagenic (because the light source that is used produces broadband radiation), and it is also non-localized, so significant absorption occurs along the path of the beam.

Therefore, the two photon excitation (TPE) of photosensitizers is receiving considerable attention as an alternative to SPE. This process involves simultaneous absorption of two photons of near-infrared (NIR) light from a pulsed laser (750-1000 nm) such that sum of their energy is equal to the first excited state of the photosensitizer (S_1), (*i.e.* $h\nu_1 + h\nu_1$ is equal to $h\nu$ in Figure 2.2). Once S_1 is produced, the cellular damage occurs as discussed above and also shown below (Figure 2.2).¹¹ TPE provides spatial and precision activation of the sensitizers due to the use of laser as a light source that allows deeper penetration in living tissues than traditional SPE. In addition, the use of NIR wavelengths enables treatment in the tissue transparent window.¹² Furthermore, this technique allows reduced light scattering, localized absorption and a minimal risk of laser hyperthermia.^{13,14} Despite these benefits, TPE-PDT has been dwarfed by the lack of suitable photosensitizers as the majority of the currently used sensitizers are based on porphyrins that exhibit low two-photon absorption cross-sections (δ).

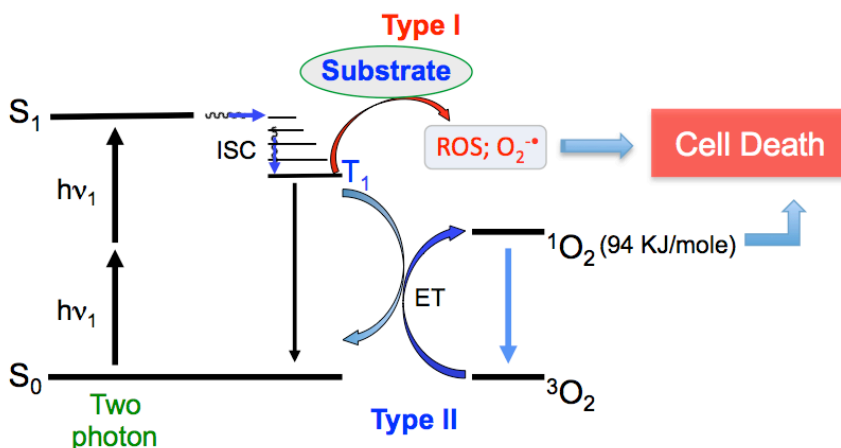
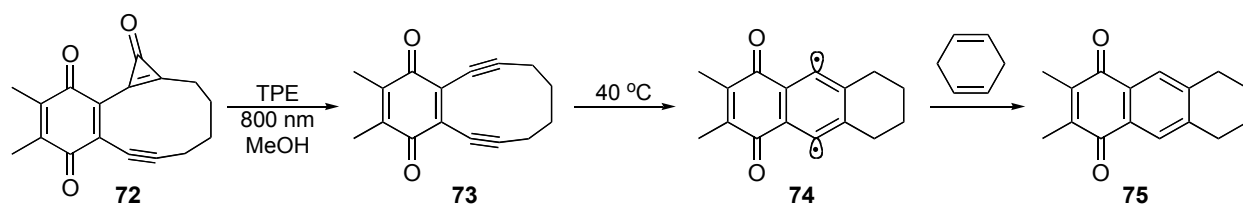


Figure 2.2: Jablonski diagram illustrating the two photon activation of the photosensitizers and subsequent cellular damage through type I and type II reactions in PDT, ET = energy transfer.¹

Some of the proposed approaches to address this drawback include the chemical modification of the existing photosensitizers.¹⁵ For instance, modified photosensitizers in which two-photon absorbing dyes have been covalently attached to the porphyrin-core (photosensitizers) have been put forth to enhance the efficiency of TPE in PDT. These dyes funnel energy to the photosensitizers via the Forster Resonance Energy Transfer (FRET).^{12,13,16} However, the protocols to synthesize these compounds often involve tedious and complicated steps with less fruitful results. Another method involved the design of conjugated porphyrin dimers (or oligomers) in order to improve their two photon absorption cross-sections.¹⁷ Although, this method demonstrates promising potential in TPE-PDT, it has some limitations such as poor singlet oxygen quantum yields. Note that one of the prerequisite for an efficient photosensitizer is its ability to produce singlet oxygen in high quantum yields. In order to achieve this goal (and as noted above) the triplet excited energy of the photosensitizer must be higher than singlet excited state of the molecular oxygen (>94KJ/mole) (Figures 2.1 and 2.2). In many porphyrin oligomers that have been developed for use in TPE-PDT, the triplet state energy is close to 94KJ/mole and therefore, the quantum yield of singlet oxygen in these systems is compromised.

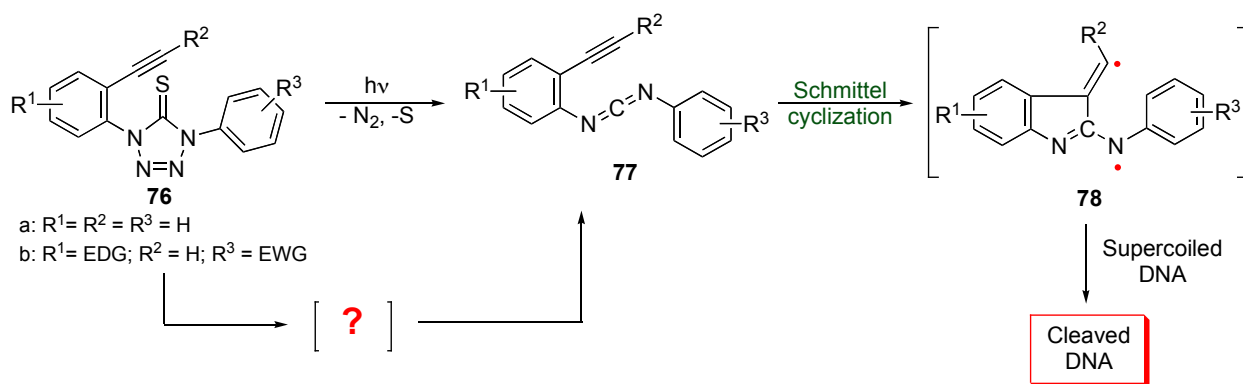
One way to alleviate the problem of low singlet oxygen quantum yields in TPE-PDT, will be to choose a method of photodestruction in PDT that does not involve the generation of singlet oxygen and one such method may involve photodamage *via* biradicals. Recently, Popik showed that photoirradiation of *p*-quinoid cyclopropanone-containing enediyne precursor **72** with TPE generated a highly reactive enediyne **73** that was thermally triggered to undergo Bergman cyclization (cycloaromatization), which resulted in the formation of biradicals **74**.¹⁸ The latter abstracts hydrogen from appropriate hydrogen donor as shown below to form **75**.¹⁹ At first glance, this method seems ideal for causing damage through TPE-PDT where **74** could be used to abstract hydrogen atoms from the sugar phosphate backbone of the DNA leading to cell death. However this also has limitations. For example, sensitive and tedious synthetic routes are required for the preparation of the enediyne precursor **72**. Furthermore, the cyclopropanone moieties have poor stability under physiological conditions and the thermal cycloaromatization to produce biradicals requires elevated temperatures (40 °C), which is not feasible under biological conditions. Thus, there is a need to construct a new class of compound that are easy of

synthesize, are stable under physiological conditions and can spontaneously undergo biradical formation upon irradiation which induces DNA cleavage.



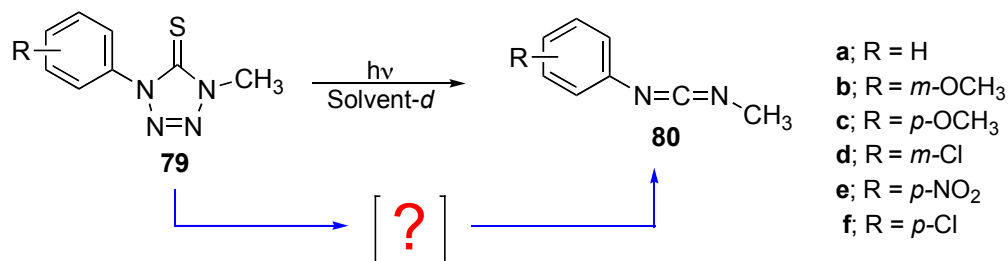
Scheme 2.1: TPE generation of reactive enediyne **73** and subsequent cycloaromatization.¹⁸

As a result, we have designed enynyl-1*H*-tetrazole-5(4*H*)-thiones **76** as photoactivated DNA cleaving agents for use in PDT. We hypothesized that upon light activation (multiphoton excitation), **76** would undergo two sequential photochemical steps in one pot, involving the decomposition of the tetrazolethione ring system to produce enyne-carbodiimides **77** with the simultaneous loss of molecular nitrogen and sulfur, followed by the Schmittel cyclization of compound **77** to generate the biradical **78**. The generated biradical **78** would induce DNA cleavage through H-atom abstraction. Work in our laboratory has already revealed that derivatives of **76** do have the ability to abstract hydrogen atom from the sugar-phosphate backbone of KS⁺ Bluescript super coiled DNA upon light activation through single photon excitation at 350 nm, causing single and double stranded breaks and thus, supporting our hypothesis.²⁰ Future work in the group is targeted toward studying the DNA cleavage by **76** at 800 nm through multiphoton excitation.



Scheme 2.2: Mechanism of action of the proposed enynyl-1*H*-tetrazole-5(4*H*)-thiones **76** upon light activation.

At the time, we began our studies on the DNA cleaving abilities of enynyl-1*H*-tetrazole-5(4*H*)-thiones **76**, the biradical forming Schmittel cyclization of enyne-carbodiimides was well studied in literature,^{21,22} but the mechanism of photodecomposition of tetrazolethiones ring system to carbodiimide was not known. Therefore, it was critical to elucidate the mechanism of this first photochemical step that involved the decomposition of tetrazolethiones (in compound **76**) to carbodiimides (in compound **77**), and identify any reactive intermediates, or other photoproduct(s) that may interfere with the activation of our proposed prodrug **76** *in vivo* (Scheme 2.2). To achieve this task, model tetrazolethiones **79** were synthesized and their photophysical and photochemical properties were extensively investigated with single photon excitation. As mentioned in Chapter 1, tetrazole and its derivatives have a wide range of applications and therefore, the elucidation of tetrazolethione photodecomposition mechanism would not only provide better understanding of the mode of action of our proposed prodrug **76**, but would also aid in the design of new tetrazolethione-based compounds with enhanced performance for application in industry and medicine.



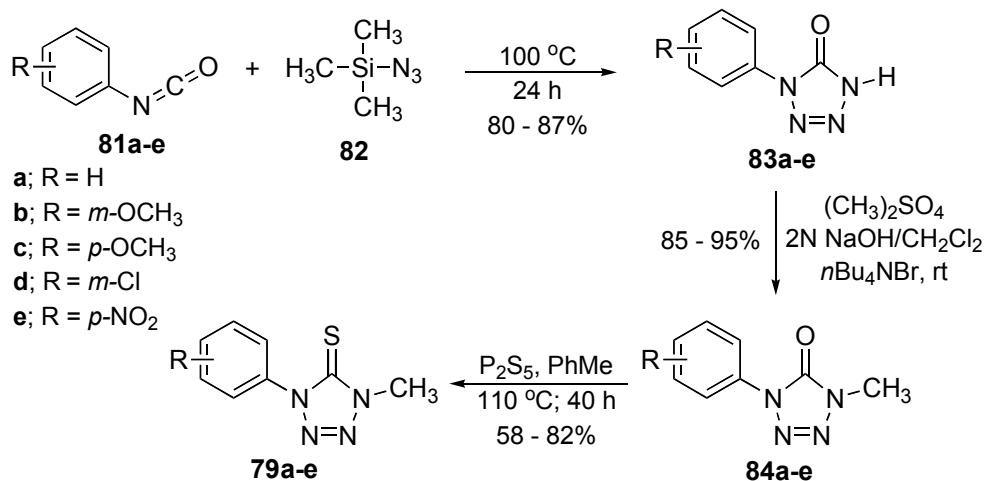
Scheme 2.3: Model tetrazolethione compounds **79** employed for photodecomposition studies discussed in this Chapter.

This chapter begins with a study of the electronic, structural and photophysical properties of a series of model tetrazolethiones **79**, through a combination of experimental and quantum mechanical methods. This is followed by the discussion of their photochemistry and mechanistic investigations at 254 and 300 nm (single photon excitation). Since our ultimate goal is to be able to induce the chemistry outlined in Scheme 2.2 with multiphoton excitation, we also investigated the photochemical decomposition of tetrazolethiones **79** at 800nm and the preliminary investigations are presented.

2.2 Results and Discussion

2.2.1 Synthesis of tetrazolethiones

The tetrazolethione compounds were all synthesized from commercially available aryl isocyanates. Briefly, the reaction of aryl isocyanates **81** with neat trimethylsilyl azide **82** furnished the 1,3 dipolar cyclized products, the corresponding aryl-1*H*-tetrazol-5(4*H*)-ones **83**. Subsequent, methylation employing dimethyl sulfate in sodium hydroxide and a phase transfer catalyst, *n*-Bu₄NBr, resulted into the formation of 1,4-disubstituted tetrazolones **84**. The treatment of disubstituted tetrazolones with phosphorus pentasulfide afforded the desired 1-aryl-4-methyl-1*H*-tetrazole-5(4*H*)-thiones **79** (Scheme 2.4).^{23,24}



Scheme 2.4: Synthesis of tetrazolethiones **79a-e**.^{23,24}

2.2.2 Absorption spectra of tetrazolethiones

The absorption spectra of tetrazolethiones **79a – e** were recorded in cyclohexane, tetrahydrofuran (THF) and acetonitrile.^{23c} All the five compounds displayed similar absorption characteristics. Herein, we will discuss the data on **79a – c**. These compounds exhibited four distinct absorption bands λ_1 , λ_2 , λ_3 and λ_4 in cyclohexane and acetonitrile, however λ_4 was not observed in THF because of solvent inference (Figure 2.3). The corresponding values of the energies and molar absorptivities for the bands observed for **79a – c** in three solvents are shown in Table 2.1.

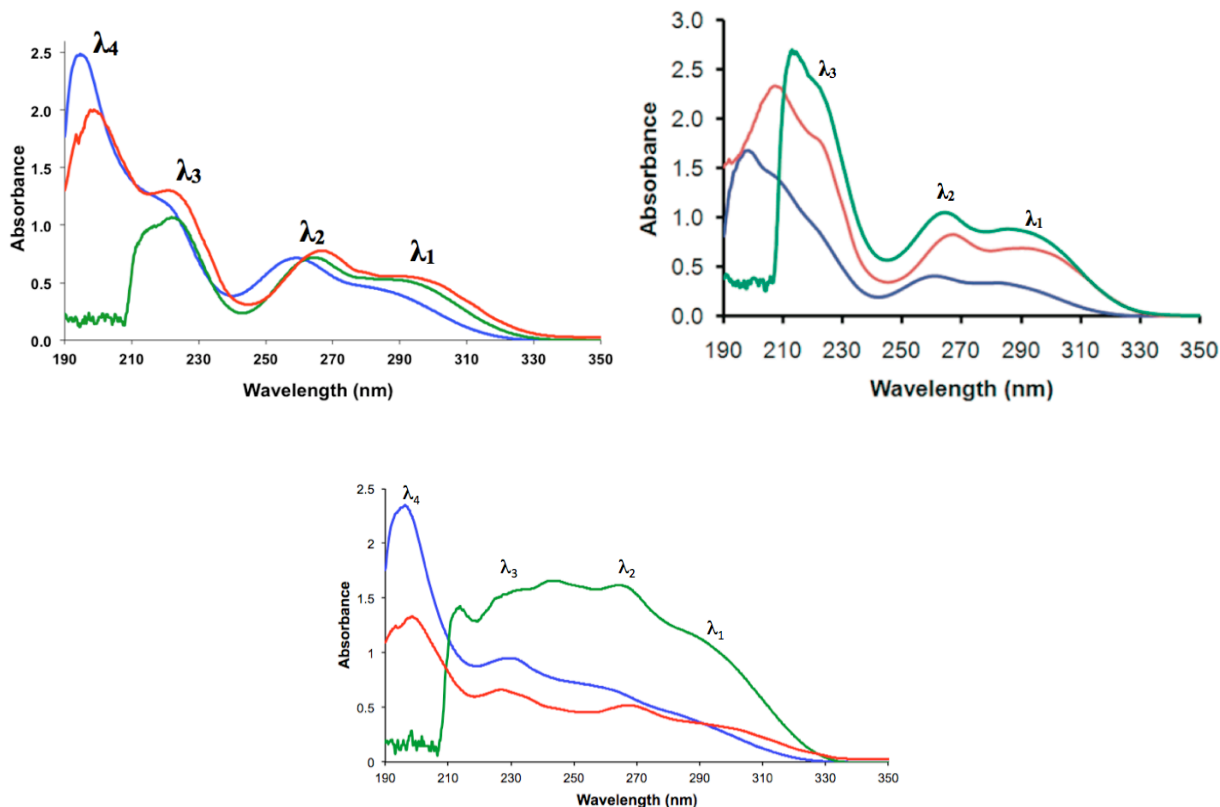


Figure 2.3: Absorption spectra of **79a** (left), **79b** (right) and **79c** (center bottom) in cyclohexane (red), THF (green) and acetonitrile (blue).

λ_1 and λ_2 bands for tetrazolethione **79a–c** both underwent slight blue shifts as the polarity of the solvent increased from cyclohexane \rightarrow THF \rightarrow acetonitrile. However, λ_3 of **79a–c** remained practically unchanged from cyclohexane \rightarrow THF \rightarrow acetonitrile. λ_4 showed a slight blue shift from cyclohexane to acetonitrile for **79b**, but was unchanged for **79a,c** with increasing polarity from cyclohexane to acetonitrile (Table 2.1). Overall, the absorption spectra of **79a–c** showed no dependence on the polarity of the solvents.

Furthermore, changes in the absorption bands were observed upon varying the substituent from moderate electron donor *e.g.* $-\text{C}_6\text{H}_5$ (**79a**) to a strong electron donor *e.g.* $-\text{C}_6\text{H}_4\text{OCH}_3$ (**79b**, **c**), as well as upon changing the position of the methoxy group on the aromatic ring attached to the tetrazolethione rings from *meta*- (**79b**) and *para*- (**79c**). When λ_1 of **79a** was compared to **79b**, the absorption band remained unchanged in cyclohexane, while a slight blue shift was observed in THF (5 nm) and slight red shift in acetonitrile (5 nm). Comparing **79a** to **79c** indicated a slight blue shift in cyclohexane (5 nm) and THF (8 nm), whereas there was no

noticeable change in acetonitrile. λ_2 bands for **79a – c** remain unchanged in spite of the change in substituents and their position on the aromatic ring. Similarly, λ_3 was unaffected from **79a** to **79b** in all the solvents, whereas a slight red shift of 6 nm, 6 nm, 13 nm was observed when comparing **79a** to **79c** in cyclohexane, THF and acetonitrile, respectively. λ_4 band of **79a – c** remain unaffected in acetonitrile whereas in cyclohexane the band produced a red shift when comparing **79a** to both **79b** (14 nm) and **79c** (6 nm). From these studies only a modest effect on the absorption spectra of tetrazolethione compounds was observed upon changing the substituents and their position on the aromatic ring.

Table 2.1: Energies (λ (E)) and molar absorptivities ($\log \epsilon$) for bands observed in the absorption spectra of **79a – c** in cyclohexane, THF and acetonitrile.

| | Cyclohexane | | THF | | Acetonitrile | |
|-------------|----------------------------|------------------------------|----------------------------|------------------------------|----------------------------|------------------------------|
| | λ (E) ^a | $\log \epsilon$ ^b | λ (E) ^a | $\log \epsilon$ ^b | λ (E) ^a | $\log \epsilon$ ^b |
| 79a | | | | | | |
| λ_1 | 291.0 (4.26) | 3.82 | 290.0 (4.27) | 3.79 | 276.1 (4.49) | 3.79 |
| λ_2 | 267.0 (4.65) | 3.97 | 264.1 (4.69) | 3.94 | 259.4 (4.78) | 3.95 |
| λ_3 | 221.0 (5.63) | 4.02 | 222.0 (5.58) | 4.03 | 217.0 (5.84) | 4.12 |
| λ_4 | 193.0 (6.42) | 4.06 | | | 195.0 (6.36) | 4.42 |
| 79b | | | | | | |
| λ_1 | 290.0 (4.27) | 3.82 | 285.0 (4.35) | 3.97 | 281.0 (4.41) | 3.82 |
| λ_2 | 266.0 (4.66) | 3.89 | 264.0 (4.69) | 4.03 | 260.0 (4.77) | 3.90 |
| λ_3 | 222.0 (5.58) | 4.31 | 223.0 (5.55) | 4.40 | 221.0 (5.61) | 4.34 |
| λ_4 | 207.0 (5.98) | 4.27 | | | 196.0 (6.32) | 4.15 |
| 79c | | | | | | |
| λ_1 | 286.0 (4.34) | 3.81 | 282.3 (4.39) | 3.77 | 277.4 (4.47) | 3.86 |
| λ_2 | 267.5 (4.63) | 3.96 | 264.1 (4.69) | 3.89 | 254.2 (4.99) | 4.03 |
| λ_3 | 227.0 (5.46) | 4.03 | 228.0 (5.44) | 4.03 | 230.0 (5.40) | 4.08 |
| λ_4 | 199.0 (6.23) | 4.31 | | | 197.0 (6.29) | 4.46 |

^a In nm (eV), ^b In M⁻¹ cm⁻¹

2.2.3 Theoretical investigations of the electronic properties of tetrazolethiones

All compounds **79a** – **e** displayed similar electronic properties. Herein, we discuss only compounds **79a** – **c**.

2.2.3.1 Molecular geometry

To gain insight into the electronic properties of tetrazolethiones **79a** – **c**, quantum mechanical calculations were performed at the density functional level of theory (DFT) employing B3LYP functional and using standard 6-311+G* basis set. The optimized geometries of **79a** – **c** and their corresponding bond lengths are shown in Figure 2.6. The molecules display C_1 symmetry and calculated showed that the dihedral angle between the phenyl substituent and tetrazolethione rings ranged between 41.1° to 47.0° . The calculated gas phase dipole moment for **79a** – **c** were 1.1, 0.96 and 2.1D, respectively.

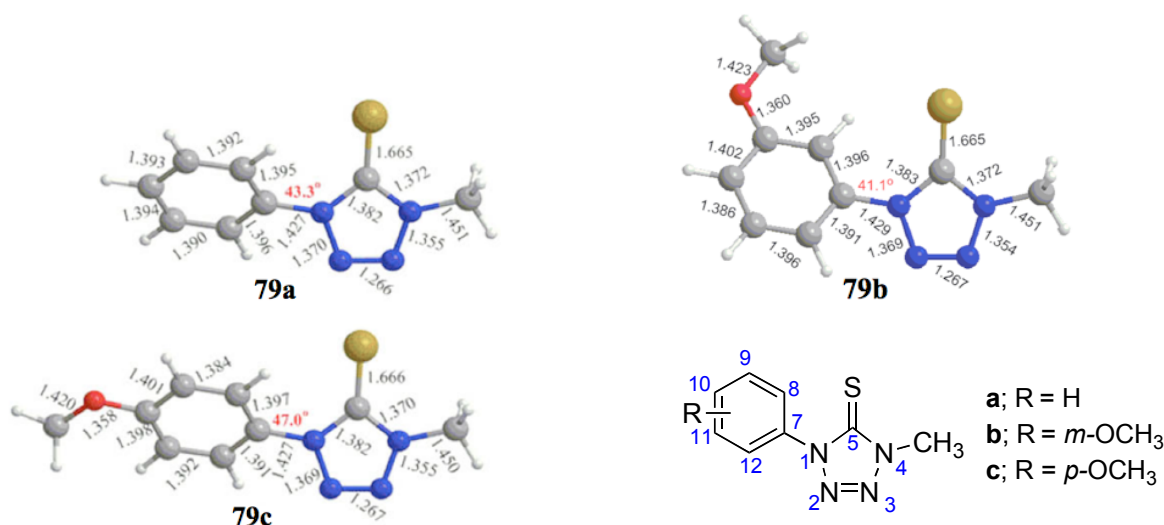


Figure 2.4: B3LYP/6-311+G* optimized structures showing bond lengths and the dihedral angle (in red) between the tetrazolethione ring and the aryl rings.

2.2.3.2 Frontier molecular orbitals

The electronic structure of **79a** – **c** was analyzed in cyclohexane, THF and acetonitrile, and similar results were obtained in three solvents. The isodensity plots of the frontier molecular orbitals that includes HOMO (Highest Occupied Molecular Orbital) and LUMO (Lowest Unoccupied Molecular Orbital) obtained at B3LYP/6-311+G* level of theory in acetonitrile indicated that these molecular orbitals exhibit π -type symmetry (Table 2.2). The HOMO-3 for

79a – c and HOMO-2 of **79a** are exclusively localized over the aromatic ring; whereas the HOMO-2 of **79b, c** is delocalized over the entire molecule. The HOMO-1 is predominantly localized on the tetrazolethione ring and has major contribution from the C₅–S₁₃ π bond. The HOMOs of **79a – c** are delocalized over the entire molecule showing some bonding contributions from the aromatic ring. All the HOMOs display significant contribution from C₅–S₁₃ π bond.

The LUMOs exhibit a bonding character at the N₁–C₇, C₈–C₉ and C₁₁–C₁₂ bonds that supports the resonance structures of **79a' – c'** (Figure 2.5). The LUMO+1 of **79a – c** is mostly localized over the tetrazolethione ring, while the LUMO+2 is a π^* orbital exclusively localized over the aromatic ring. LUMO+3 of **79a – c** is delocalized over the entire molecule. Overall, the molecular orbitals were unaffected by change in the solvent or the substituents and their position. This in turn means that the photoreactivity of tetrazolethione based compounds may not be affected by changing the solvent or the substituent.

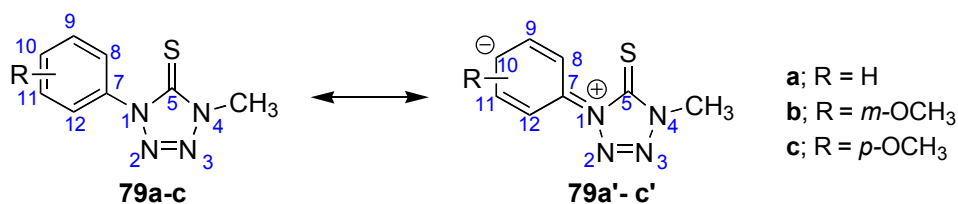
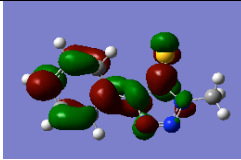
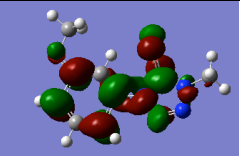
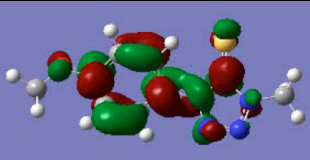
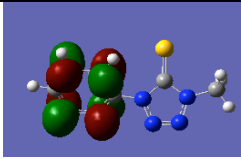
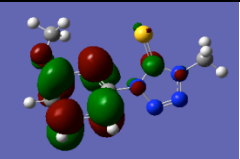
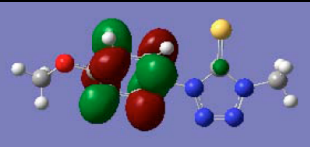
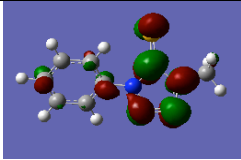
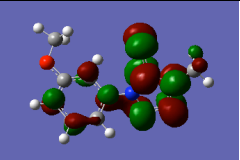

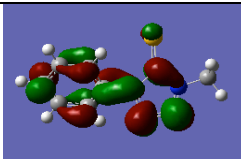
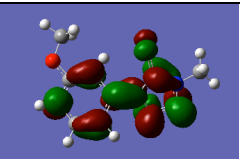
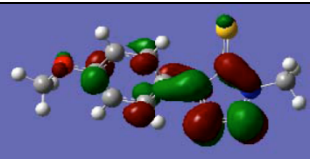
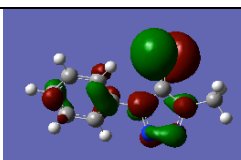
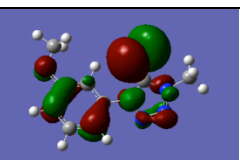
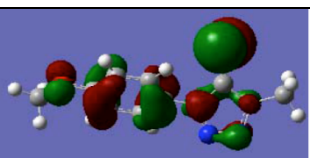
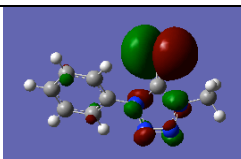
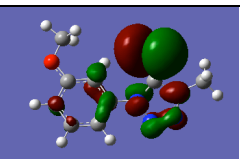
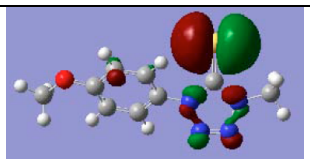
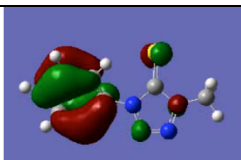
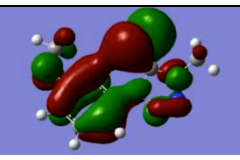
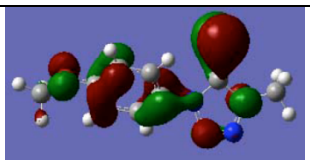
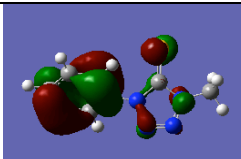
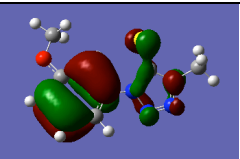
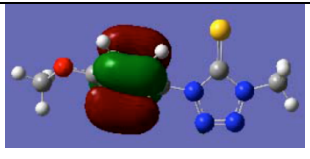


Figure 2.5: Resonance structures of **79a' – c'**.

Table 2.2: Frontier molecular orbitals for B3LYP/6-311+G* optimized geometries of **79a** – **c** in acetonitrile.

| | 79a | 79b | 79c |
|--------|---|---|---|
| LUMO+3 |  |  |  |
| LUMO+2 |  |  |  |
| LUMO+1 |  |  |  |
| LUMO |  |  |  |
| HOMO |  |  |  |
| HOMO-1 |  |  |  |
| HOMO-2 |  |  |  |
| HOMO-3 |  |  |  |

2.2.4.3 Vertical excitation energies

In order to determine the nature of the electronic transitions that give rise to bands in the UV spectra of **79a** – **c**, time-dependent density functional calculations (TDDFT) were carried out and thirty low lying singlet excited states were calculated. Figure 2.6 show the absorption spectra of **79a** in three solvents). The calculated TDDFT vertical excitations energies are shown as stick spectra (see Figure A.1 – A.2 for **79b,c** in all the three solvents. Note that TDDFT predicted excitations matches well with the experimentally obtained absorption spectra.

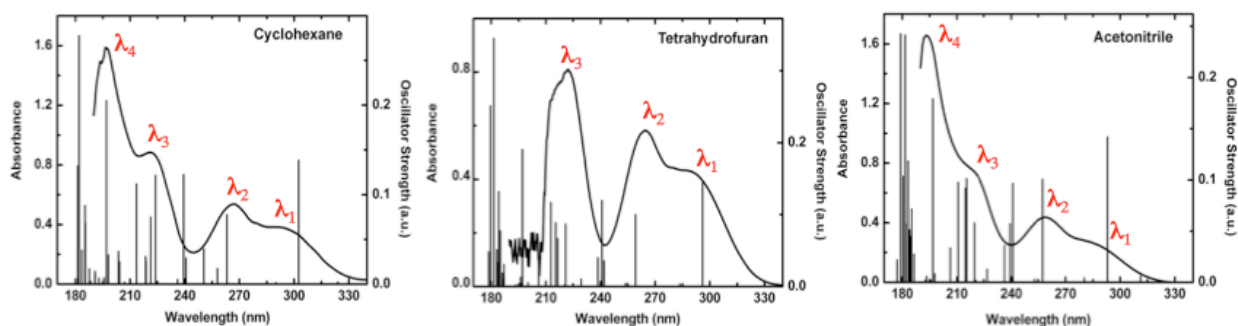


Figure 2.6: Experimental absorption spectra of **79a** in cyclohexane, tetrahydrofuran and acetonitrile, and the vertical excitation calculated with TDDFT/6-311+G*

The vertical excitation energies, corresponding wavelengths, oscillator strengths, molecular orbitals (MO) character and the transition type for the most intense transitions calculated at TDDFT/6-311+G* in cyclohexane, THF and acetonitrile for **79a** are provided in Table 2.3. The analysis of TDDFT wave function of **79a** indicated that λ_1 experimentally observed at 4.26, 4.27 and 4.49 eV in cyclohexane, THF and acetonitrile (Table 2.1), corresponds to a transition from HOMO-1 or HOMO to the LUMO and is calculated at 4.10 eV, 4.19 eV and 4.23 eV in three solvents (Table 2.3). λ_2 experimentally found at 4.65, 4.69 and 4.78 eV in cyclohexane, THF and acetonitrile, is comprised of one to three excited states consisting of transitions from HOMO-3 \rightarrow LUMO, HOMO-2 \rightarrow LUMO, HOMO-1 \rightarrow LUMO+1/LUMO+2, HOMO \rightarrow LUMO+1/LUMO+2; it was calculated at 4.71, 4.96 and 5.05 eV in the three solvents, respectively. λ_3 was predicted at 5.51, 5.74 and 5.76 eV (Table 2.3) and observed at 5.63, 5.58 and 5.84 eV in cyclohexane, THF and acetonitrile (Table 2.1).

Table 2.3: TDDFT/6-311+G* vertical excitation energies ($E(\lambda)$ / eV (nm)), oscillator strengths (f), MO character and transition type of **79a** in cyclohexane, tetrahydrofuran and acetonitrile.

| State | $E(\lambda)$ | f | MO Character | Type | |
|-----------------|--------------|--------------|--------------|----------------------------------|------------------------------|
| Cyclohexane | | | | | |
| λ_1 | 2 | 4.10 (302.5) | 0.138 | H-1→L; H→L | $\pi \rightarrow \pi^*$ / CT |
| λ_2 | 4 | 4.71 (263.2) | 0.078 | H-1→L+1; H→L+1; H→L+2 | $\pi \rightarrow \pi^*$ / CT |
| λ_3 | 8 | 5.18 (239.3) | 0.122 | H-2→L | $\pi \rightarrow \pi^*$ / CT |
| | 10 | 5.53 (224.0) | 0.122 | H-1→L+3; H→L+3 | $\pi \rightarrow \pi^*$ / CT |
| | 14 | 5.81 (213.5) | 0.112 | H-2→L+1 | $\pi \rightarrow \pi^*$ / CT |
| λ_4 | 19 | 6.29 (197.0) | 0.205 | H-3→L+2 | $\pi \rightarrow \pi^*$ |
| | 29 | 6.82 (182.0) | 0.277 | H-3→L+2; H-2→L+3 | $\pi \rightarrow \pi^*$ |
| | 30 | 6.84 (181.2) | 0.132 | H-3→L+2; H-2→L+3 | $\pi \rightarrow \pi^*$ |
| Tetrahydrofuran | | | | | |
| λ_1 | 2 | 4.19 (296.0) | 0.144 | H-1→L; H→L | $\pi \rightarrow \pi^*$ / CT |
| λ_2 | 4 | 4.78 (259.2) | 0.100 | H-1→L+1; H→L+1; H→L+2 | $\pi \rightarrow \pi^*$ / CT |
| | 7 | 5.15 (241.0) | 0.120 | H-3→L; H-2→L | $\pi \rightarrow \pi^*$ / CT |
| λ_3 | 10 | 5.62 (220.8) | 0.087 | H-2→L+1 | $\pi \rightarrow \pi^*$ / CT |
| | 13 | 5.76 (215.4) | 0.088 | H-2→L+1; H-3→L+1 | $\pi \rightarrow \pi^*$ / CT |
| | 14 | 5.83 (212.7) | 0.117 | H-2→L+1; H-3→L+1 | $\pi \rightarrow \pi^*$ / CT |
| λ_4^a | 17 | 6.29 (197.1) | 0.190 | H-3→L+2; H-2→L+2; H-2→L+3 | $\pi \rightarrow \pi^*$ |
| | 25 | 6.74 (184.0) | 0.132 | H-3→L+3 | $\pi \rightarrow \pi^*$ |
| | 28 | 6.83 (181.4) | 0.345 | H-3→L+2; H-2→L+3 | $\pi \rightarrow \pi^*$ |
| | 29 | 6.90 (180.0) | 0.251 | H-3→L+3; H-2→L+2 | $\pi \rightarrow \pi^*$ |
| Acetonitrile | | | | | |
| λ_1 | 2 | 4.23 (293.0) | 0.142 | H-1→L; H→L | $\pi \rightarrow \pi^*$ / CT |
| λ_2 | 4 | 4.82 (257.4) | 0.101 | H-1→L+1; H→L+1 | $\pi \rightarrow \pi^*$ |
| | 6 | 5.14 (241.0) | 0.097 | H-3→L; H-2→L | $\pi \rightarrow \pi^*$ / CT |
| | 7 | 5.18 (239.4) | 0.057 | H-2→L; H-1→L+2; H→L+2 | $\pi \rightarrow \pi^*$ / CT |
| λ_3 | 12 | 5.75 (215.3) | 0.101 | H-3→L+1; H-2→L+1; H-1→L+3; H→L+3 | $\pi \rightarrow \pi^*$ / CT |
| | 13 | 5.78 (214.6) | 0.092 | H-3→L+1; H-2→L+1 | $\pi \rightarrow \pi^*$ / CT |
| λ_4 | 17 | 6.30 (196.8) | 0.179 | H-3→L+2; H-3→L+3; H-2→L+2 | $\pi \rightarrow \pi^*$ |
| | 27 | 6.83 (181.5) | 0.242 | H-3→L+3; H-2→L+3 | $\pi \rightarrow \pi^*$ |
| | 29 | 6.92 (179.0) | 0.243 | H-3→L+3 | $\pi \rightarrow \pi^*$ |

^a experimentally not observed

Similarly, this band is formed by two to three excited states comprising of transitions from several MOs of similar energy that included HOMO-3 \rightarrow LUMO+1, HOMO-2 \rightarrow LUMO/LUMO+1, HOMO-1 \rightarrow LUMO+3 and HOMO \rightarrow LUMO+3.

λ_4 appears experimentally at 6.42 and 6.63 eV in cyclohexane and acetonitrile and was calculated at 6.65, 6.69 and 6.68 eV, consisting of transitions from HOMO-3 \rightarrow LUMO+2/LUMO+3 and HOMO-2 \rightarrow LUMO+2/LUMO+3. Similarly, the calculated values of absorption bands for **79b,c** in all the three solvent are shown in Tables A.1 and A.2. As discussed for **79a** their UV bands are composed of several excited states consisting of transitions between several molecular orbital of similar energy.

Furthermore, the analysis of the MOs indicate that all bands observed in the UV spectra of **79a-c** are of $\pi \rightarrow \pi^*$ in nature. Some degree of intramolecular charge transfer from the heterocyclic ring to the phenyl ring was exhibited in λ_1 . Note that both HOMO-1 and HOMO are mostly localized on the tetrazolethione ring, whereas LUMO is delocalized over the entire molecule and has bonding characteristics at the N₁-C₇, C₈-C₉ and C₁₁-C₁₂ bonds. Likewise, λ_2 and λ_3 correspond to a $\pi \rightarrow \pi^*$ transition, the latter is also associated with some degree of charge transfer within the molecule. λ_4 is a $\pi \rightarrow \pi^*$ transition predominantly localized on the phenyl ring.

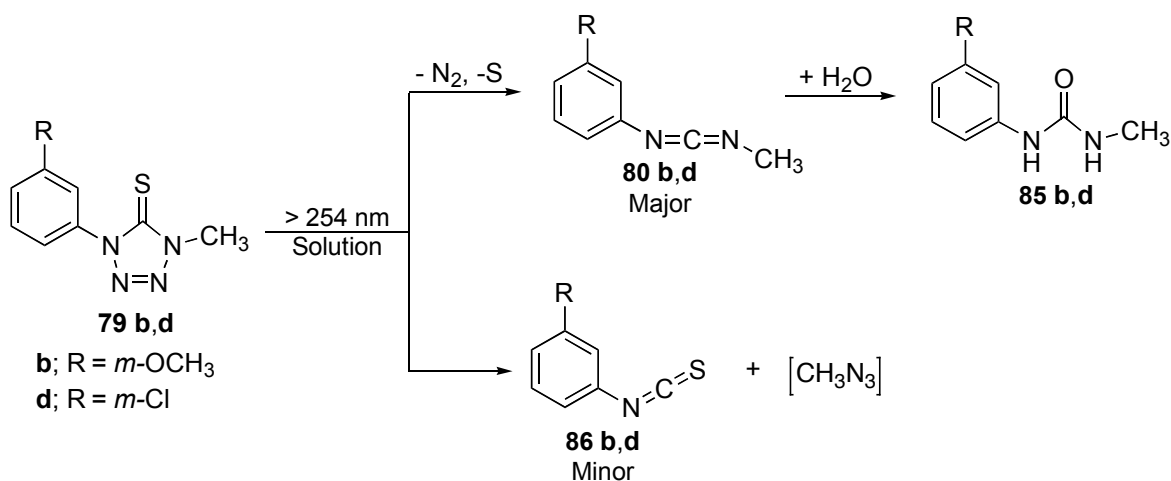
The experimental and calculated transitions both strongly indicated that solvent polarity only has negligible effect on the photophysical properties of tetrazolethione-based compounds. Also, there was no significant effect on the electronic properties of the tetrazolethione derivatives when the substituents or their position on the aromatic ring was changed.

2.2.4 Photochemistry of tetrazolethiones and Mechanistic Studies

The photochemistry of the tetrazolethiones **79** was studied in (i) photochemical reactor vessel with double walled quartz immersion well using a Ace-Hanovia medium pressure mercury lamp producing radiation predominantly at 254 nm and emitting minor photon energy at 265, 297, 303 and 360 nm, and in (ii) Rayonet photochemical reactor (Rayonet RMR- 600) equipped with eight interchangeable lamps emitting radiation at 254 and 300 nm.

2.2.4.1 Photochemical studies using medium pressure Hg lamp

The photochemistry of tetrazolethiones **79b** and **79d** in tetrahydrofuran and acetonitrile solutions was investigated using medium pressure Hg lamp. The analysis of the irradiated samples was carried out by GCMS, which indicated the formation of corresponding carbodiimides **80**, ureas **85** and isocyanates **86** (Scheme 2.5). Based on the work on tetrazolethiones in literature,^{25,26,27} we concluded that the initial photorelease of molecular nitrogen and sulfur from **79b,d** produced the corresponding carbodiimide **80b,d** as the major photoproduct, which immediately underwent hydrolysis with trace amount of water present in the solvent to form the respective ureas **85b,d**. The formation of corresponding isothiocyanates **86b,d** occurred through a retro 1,3-dipolar cycloaddition (Scheme 2.5). However, there was no evidence of the azide photoproduct (CH_3N_3) of this latter pathway possibly due to further decomposition upon its formation. All attempts towards isolating carbodiimides **80b,d** for NMR spectroscopic characterization were unsuccessful.



Scheme 2.5: Photoproducts formed during irradiation of tetrazolethiones **79b,d** in solution with medium pressure Hg lamp.

We performed geometry optimizations on a related derivative, 1-methyl-4-(4-chlorophenyl)-1*H*-tetrazol-5(4*H*)-thione **79f** at the Restricted Hartree-Fock (RHF) level of theory using the 6-311+G** basis set. Subsequently, Configuration Interaction Singles method (CIS/6-311+G*) was employed to obtain the excited state using the ground state geometry at RHF/6-311+G**. Our computational result predicted a substantial lengthening of the C=S bond in the

excited state (4.117 Å) (Figure 2.7). Thus, suggesting the possible involvement of a heterocyclic carbene in the photodecomposition of tetrazolethiones that would subsequently lose nitrogen to afford carbodiimide as the major photoproduct.

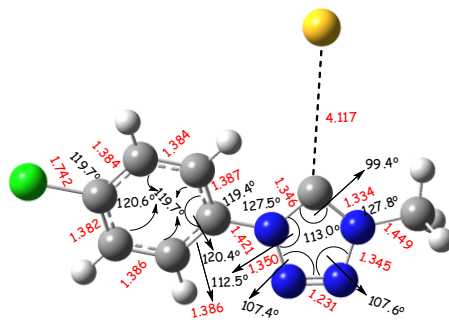
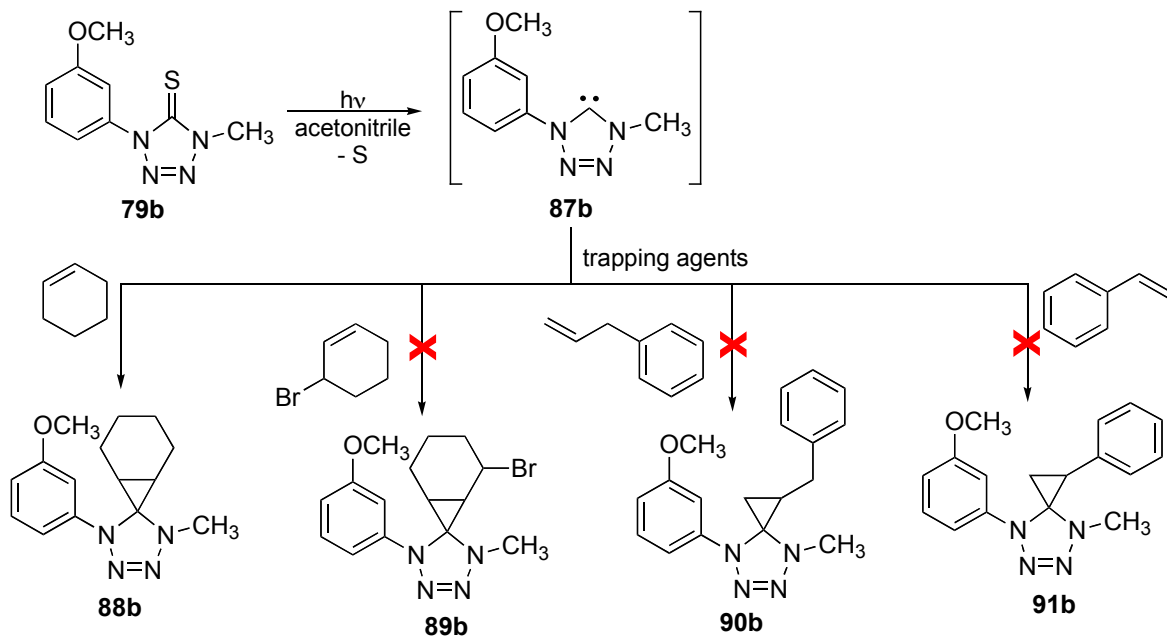


Figure 2.7: Excited State (root = 8) for 1-methyl-4-(4-chlorophenyl)-1H-tetrazol-5(4H)-thione **86f** optimized at CIS/6-31+G*.

Based on the computational result obtained above, we experimentally explored the involvement of a heterocyclic carbene in the photodecomposition of tetrazolethiones by carrying out carbene trapping experiments. The photoirradiation of **79b** in acetonitrile was carried out in the presence of various alkenes such as cyclohexene, 3-bromocyclohexene, allylbenzene and styrene. Hypothetically, if a heterocyclic carbene intermediate **87b** was involved, then photolysis in the presence of these trapping agents would result in the formation of carbene addition products *e.g.* **88b** – **91b** (Scheme 2.6).



Scheme 2.6: Proposed carbene addition products possible during photochemical trapping experiments of **87b** in various alkenes.

The electrospray ionization mass spectrometric analysis of the irradiated solution of **79b** in the presence of cyclohexene showed a $[M + H]^+$ at $m/z = 273.0$ which suggested the formation of the cyclopropane adduct **88b**. The ESI-MS/MS spectrum of the peak at 273.0 is shown in Figure 2.8. The fragmentation pattern was consistent with the structure of trapped carbene product **88b**. However, all the attempts to isolate **88b** through flash column chromatography, preparative thin-layer chromatography and HPLC were met with failure. This may possibly be due to the instability of the cyclopropane ring in the adduct **88b** resulting into its decomposition during isolation. We were also not successful in obtaining any spectroscopic evidence for the formation of **89b – d**, in case of trapping reactions with other alkenes. This prompted us to believe that the photodecomposition pathway involving heterocyclic carbene may only be a minor pathway.

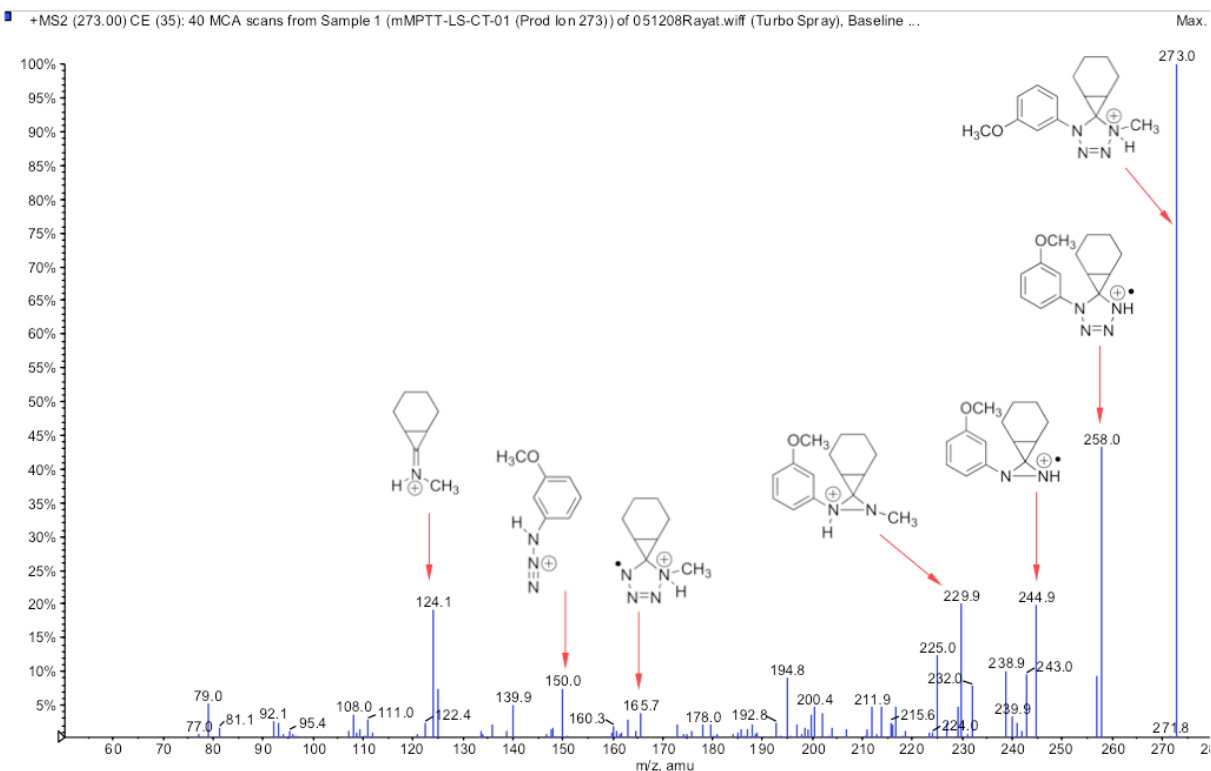


Figure 2.8: EI-MS/MS of the peak with m/z = 273.

2.2.4.2 Photochemical studies using Rayonet photochemical reactor

UV Spectral analyses of the irradiated solutions

The photolyses of argon-saturated acetonitrile solutions of **79a,b** were carried out in a Rayonet reactor equipped with 254 and 313 nm lamps in a quartz cuvette, and the progress of the photoreaction was monitored by UV-Vis spectroscopy. The UV spectral changes of **79a,b** upon irradiation at 254 nm are shown in Figures 2.9 (left) and 2.10 (left). Similarly, the UV spectral changes upon exposing **79a,b** to 313 nm light (obtained by using broadband 300 nm lamp with a chromate filter) is also shown in Figures 2.9 (right) and 2.10 (right), and were found to be identical to that observed at 254 nm, however the photoreaction proceeded much slower. The reason could be attributed to the low molar absorptivity of **79a,b** at the region of irradiation (313 nm).

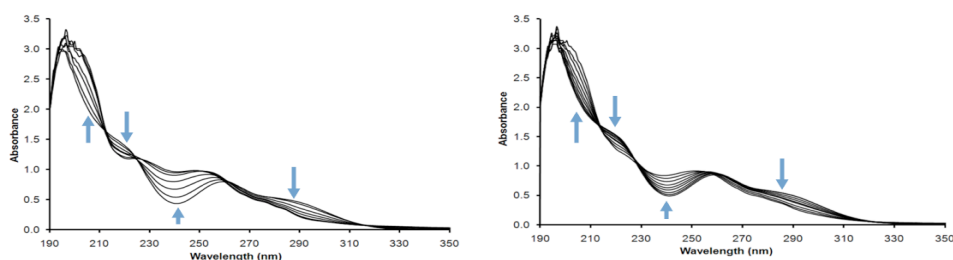


Figure 2.9: Changes in UV absorption spectra of **79a** in acetonitrile induced by irradiation at 254 (left) and 313 nm (right), arrows indicate the direction of spectral change upon irradiation.

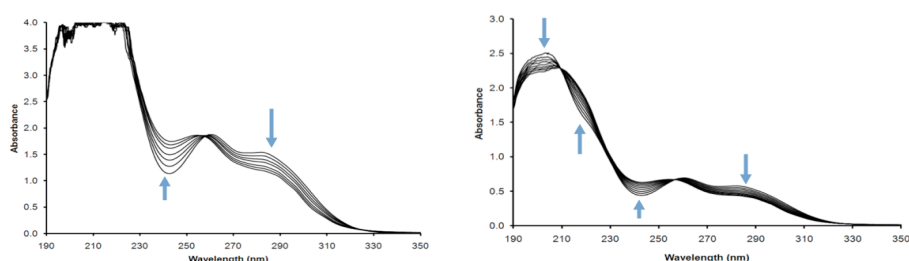


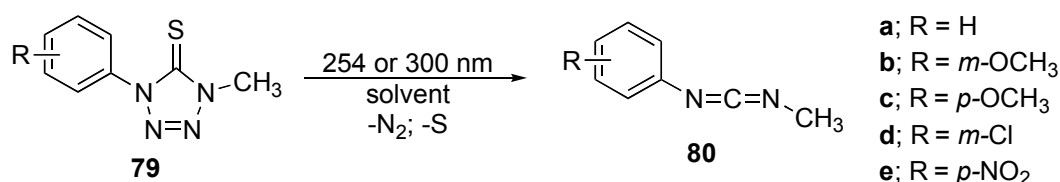
Figure 2.10: Changes in UV absorption spectra of **79b** in acetonitrile induced by irradiation at 254 (left) and 313 nm (right), arrows indicate the direction of spectral change upon irradiation.

Overall, the UV spectra exhibited well-defined isosbestic points in each case **79a,b** suggesting the formation of a single photoproduct. This observation was noteworthy as most tetrazolyl derivatives in literature (Chapter 1) often produce several products upon exposure to UV light.^{25,26,27,28}

NMR spectral analyses of the irradiated solutions

The argon-saturated solutions of tetrazolethione **79a – e** in acetonitrile- d_3 , and of **79a,b** in benzene- d_6 , and methanol- d_4 were irradiated at 254 and 300 nm for different time intervals in a quartz NMR tube, and the ^1H NMR spectra were recorded after each irradiation. The chemical shift values for the obtained photoproduct coincided with those of the independently synthesized carbodiimides **80**. Thus, indicating that photodecomposition of tetrazolethiones **79** involves photorelease of nitrogen and sulfur to form carbodiimides **80** (Scheme 2.7). The ^1H NMR spectra of **79a** obtained at 0 and 20 min of irradiation in acetonitrile- d_3 is shown in Figure 2.11. The peak corresponding to the methyl (3.89 ppm) group of compound **79a** decreased in intensity

while new peak corresponding to the chemical shift value of methyl group of the carbodiimide **80a** emerged (3.14 ppm) and grew quickly with prolonged irradiation (Figure 2.11). This result complied with the UV-Vis spectroscopic studies (Figure 2.9), and corroborated with the previous reports by Quast.^{25,26,27} Similarly, the irradiation of **79b – e** in acetonitrile-*d*₃ and of **79a,b** in benzene-*d*₆, and methanol-*d*₄ produced carbodiimides **80a – e** as indicated by ¹H NMR spectroscopy (Figure A.19 – A.26). Note that the photochemistry of tetrazolethiones **79a,b** at 254 nm proceeded much slower in benzene-*d*₆ because of the competition for UV light between the tetrazolethione substrates and the solvent, (See Figure A.31 – A.32).



Scheme 2.7: Photoconversion of tetrazolethiones **79** into their respective carbodiimides **80** in solution using Rayonet reactor.

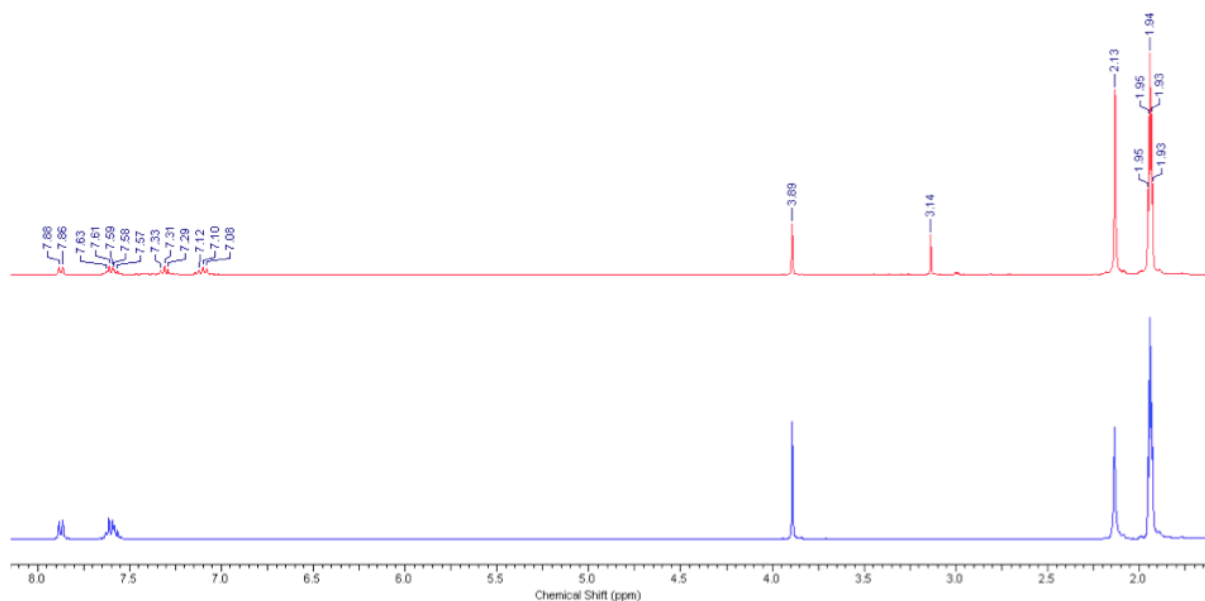


Figure 2.11: ¹H NMR spectra overlay taken at 0 min (bottom) and 20 min (top) during UV-irradiation of **79a** in acetonitrile-*d*₃.

Furthermore, photolysis of tetrazolethiones **79a,b** was also studied at 300 nm in acetonitrile-*d*₃, benzene-*d*₆, and methanol-*d*₄ solutions and it resulted in the formation of their

respective carbodiimides **79a,b** (Figure A.27 – A.32 in Appendix A). The rate of photoconversion at 300 nm was noticeably slower compared to irradiation at 254 nm, most likely due to reasons noted above.

Since only the formation of carbodiimides was observed in all the solvents this clearly shows that solvent polarity does not influence the photoreactivity of the tetrazolethione derivatives. The hydrolysis of compounds **80a,b** to corresponding ureas was not observed with rayonet reactor contrary to irradiation with medium pressure Hg lamp (Scheme 2.5), most likely because of the small amount of solvent used.

Quantification of the photoreaction was carried out by NMR spectroscopy for **79a,b** using 1,4-dioxane as an internal standard. The amounts of carbodiimide formed and the starting material remaining after irradiation for 15 min and 60 min at 254 and 300 nm, respectively are shown in Table 2.4.

Table 2.4: Amounts of tetrazolethione **79a,b** remaining and photoproduct **80a,b** produced after irradiation in acetonitrile-*d*₃ and respective quantum yields (Φ).

| | λ (nm) | Irradiation time (min) | | Unreacted 79a,b ^a | Yield of 80a,b . ^a [%] | Φ |
|------------|-------------------|---------------------------|-----------|--|---|--------|
| 79a | 254 | 15 | Ar-purged | 57 | 44 | 0.045 |
| | 300 | 60 | Ar-purged | > 95 | trace | |
| 79b | 254 | 15 | Ar-purged | 60 | 42 | 0.031 |
| | 300 | 60 | Ar-purged | > 95 | trace | |

^a Amounts calculated using 1,4-dioxane as an internal standard (average of three irradiated samples) with the standard deviation in the range 0.4-2% range.

Note that the exposure of argon purged tetrazolethiones **79a,b** to UV light at 254 nm afforded the corresponding carbodiimides **80a,b** in 42 – 44% yield, while 57 – 60% of the substrate remained unreacted after irradiation (Table 2.4). There was trace amount of other photoproduct(s) formed which were not identified because the yield was $\leq 1\%$. Only trace amounts of corresponding carbodiimides **80a,b** were observed after 60 min of photolysis at 300 nm (Table 2.4), while most of the substrate remained unreacted.

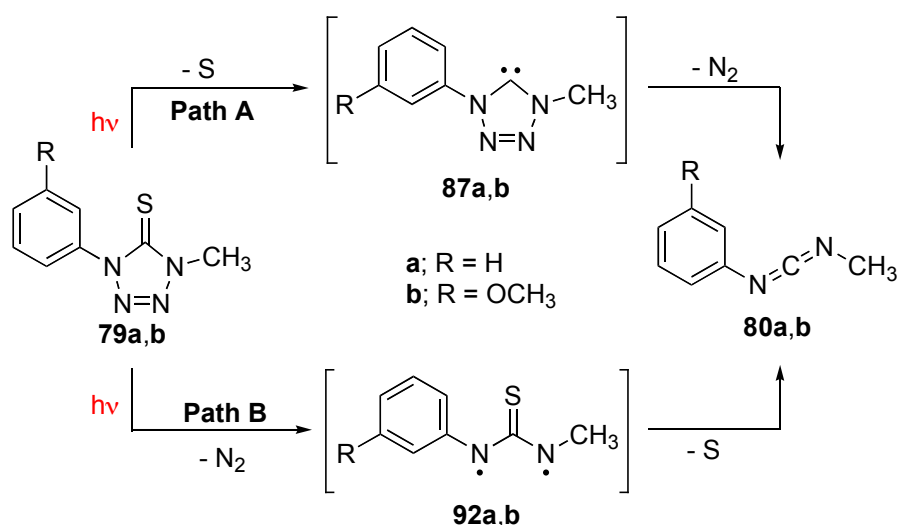
In order to rule out the possibility of secondary photoreactions from carbodiimide, and to verify its photostability, synthetically obtained carbodiimides **80a,b** were subjected to prolonged

irradiation at 254 nm for 120 min. The results revealed no signs of further decomposition and thus, indicating that carbodiimides once formed were photostable.

Furthermore, azoxybenzene actinometer²⁹ was used to calculate the quantum yields for the formation of the carbodiimides at 254 nm (Table 2.4). The low quantum yields suggested that these heterocyclic ring systems might be involved in some radiationless decay or fluorescence mechanisms. Overall, the photochemical decomposition of tetrazolethiones showed modest dependency on the nature of the substituents present on the aromatic ring attached to the tetrazolethione ring.

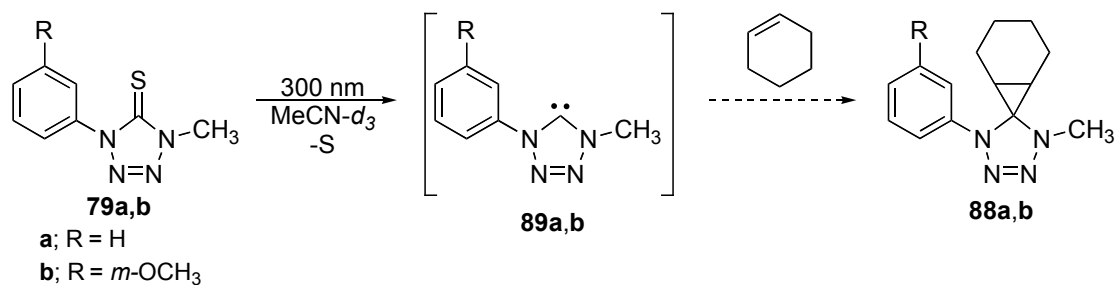
2.2.4.3 Mechanistic considerations

The photochemical formation of carbodiimides **80** from tetrazolethiones **79** involved the loss of molecular nitrogen and sulfur. In order to adeptly study the photodecomposition mechanism, two possible pathways must be considered. Path **A** involves the initial desulfurization of the heterocyclic ring to generate a carbene **87** that subsequently, would lose nitrogen to afford the observed photoproduct **80**. Whereas, path **B** would involve the initial photorelease of molecular nitrogen to produce a biradical **92** followed by desulfurization to form the observed photoproduct **80** (Scheme 2.8).



Scheme 2.8: Proposed photodecomposition pathways of tetrazolethione ring systems.

In order to determine the involvement of a heterocyclic carbene **87**, the photolyses were performed in acetonitrile- d_3 with excess cyclohexene (5-10 equiv., see experimental procedure for detailed reaction conditions). If the photodecomposition of tetrazolethiones **79a,b** involved the intermediacy of **87a,b**, the presence of a trapping agent would completely or partly obstruct the formation of photoproduct **80a,b** and form the typical carbene addition product **88a,b** (Scheme 2.9). However, the NMR spectroscopic and the mass spectrometry analyses of the reaction mixture did not provide any evidence for the formation of trapped product **88a,b**.

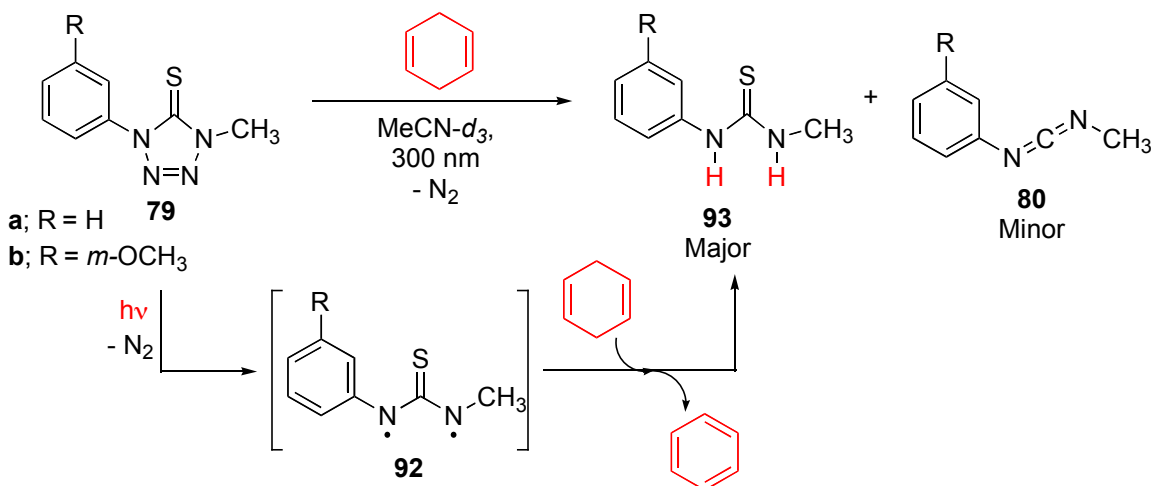


Scheme 2.9: Proposed cyclopropane adduct **88a,b** expected during the reaction of **79** with cyclohexene in case of the presence of a carbene intermediate.

Our above result employing a Rayonet photochemical reactor equipped with 300 nm lamp was not consistent with our earlier studies that hinted at the probability of a carbene intermediate. Recall that during the irradiation of tetrazolethiones **79b** with medium pressure Hg lamp, we observed the formation of the trapped carbene product **88b** that was identified by ESI-MS/MS spectrometry (Scheme 2.6 and Figure 2.8). It is plausible that the cyclopropane adduct **88b** in case of **79b** in the previous study was formed as a result of thermal reaction as the temperature generated by the lamp could reach up to 600 – 800 °C.³⁰

Subsequently, mechanistic studies to explore if biradical intermediate **92** is involved in the formation of carbodiimides were conducted. The photoirradiation of tetrazolethiones **79a,b** was carried out in acetonitrile- d_3 in the presence of a hydrogen atom donor, 1,4-cyclohexadiene (1,4-CHD) at 300 nm (Figure A.33 – A.34 in Appendix A). We hypothesized that if the photofragmentation that produced carbodiimide involves the intermediacy of a biradical **92**, the photolysis of tetrazolethiones **79** in the presence of 1,4-CHD would consequently produce the reduced product, thiourea **93**. Indeed, the ¹H NMR spectral analysis of the irradiated samples indicated the formation of thioureas **93a,b** as the major products along with trace amounts of

carbodiimides **80a,b** (Scheme 2.10) (Figure A.33–34; appendix A). Again, **93a,b** were identified by comparing their ^1H NMR spectra with that of independently synthesized samples.



Scheme 2.10: Trapping experiment to provide support for the involvement of 1,3-biradical intermediate **92** in the photodecomposition of tetrazolethiones **79**.

Furthermore, the results indicated that the amount of thiourea produced was directly proportional to the concentration of 1,4-CHD used (Figure 2.12). Thus, clearly confirming that the mechanism of photodecomposition of tetrazolethione scaffolds **79** involves the formation of 1,3-biradical intermediate **92**.

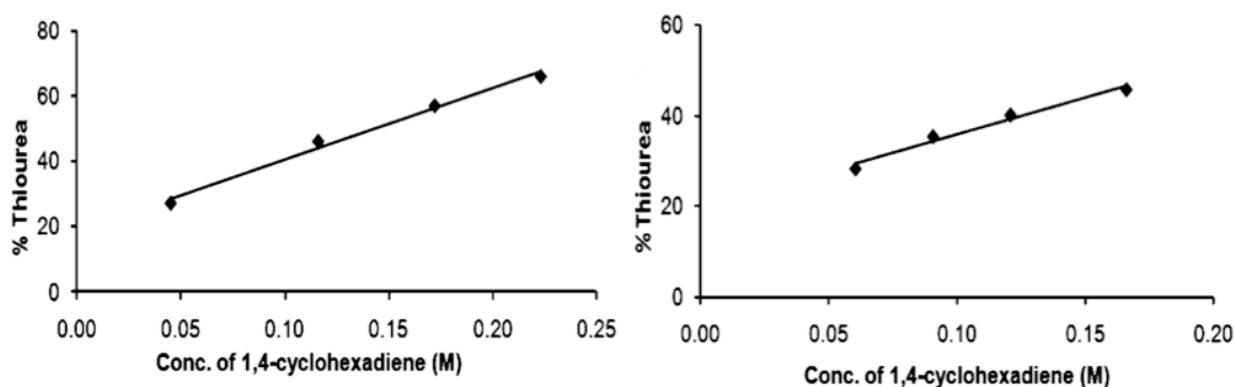


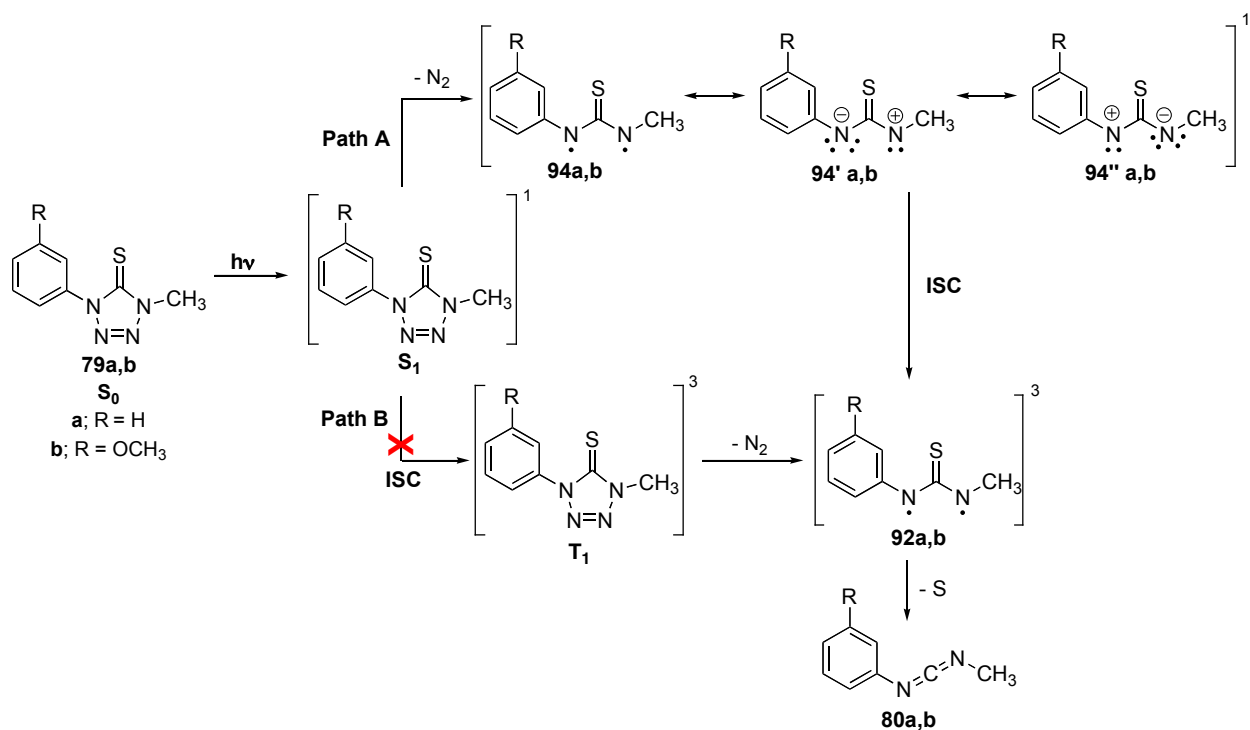
Figure 2.12: Plot showing the steady formation of thioureas **93a** (left) and **93b** (right) with increase in the concentration of 1,4-CHD during irradiation of **79a** and **79b** in acetonitrile, respectively.

While the biradical trapping experiment strongly revealed the intermediacy of 1,3 biradicals, it does not provide definitive evidence as to whether the biradical exist in its triplet or singlet spin multiplicity. Since the singlet biradicals have a short lifetime ($\sim 10^{-13} - 10^{-11}$ s)^{31,32} it is highly likely that the trapped reactive species was the triplet biradical because only those have a lifetime long enough that allows reaction with external trapping agents.³³ Moreover, desulfurization from a triplet biradical to afford corresponding carbodiimide **87** would yield a ground state triplet sulfur atom (3P)³⁴ that is energetically more favorable than desulfurization from a singlet biradical, which will lead to the formation of an excited state singlet sulfur atom (1D). The lost sulfur atom becomes S₈ as this is the most common allotrope of sulfur.³⁵ This argument is further supported by the yellow coloration of the reaction mixture produced after photolysis, which is also suggestive of S₈ formation.

Also, an irradiation experiment to study the photodecomposition of thiourea under extended exposure to UV light was preformed. There was no photochemical reaction observed, which inferred that thiourea does not undergo further fragmentation or desulfurization to carbodiimide once formed.

2.2.4.4 *Identifying the precursor to the triplet biradical*

The photodecomposition mechanism of tetrazolethiones **79a,b** that led to the formation of 1,3-triplet biradicals **92a,b** could possibly involve two pathways: Path A involves the initial excitation of the **79** from its ground state (S₀) to the first excited singlet state (S₁). The latter could lose molecular nitrogen to generate excited singlet diradicaloid species **94**, which would subsequently undergo intersystem crossing (ISC) to form the 1,3-triplet biradical **92** and the loss of sulfur from latter will afford the observed carbodiimide **80a,b**. Path B would involve intersystem crossing from S₁ to the first excited triplet state (T₁) of tetrazolethione followed by the loss of nitrogen to afford the 1,3-triplet biradical **92**, which would lose sulfur to produce the desired carbodiimide **80a,b** (Scheme 2.11).



Scheme 2.11: Possible pathways for the formation of 1,3-triplet biradical **92**.

In order to investigate the involvement of a triplet excited state in the photodecomposition of the tetrazolethiones **79**, we carried out indirect irradiation, *i.e.* triplet sensitization experiments. An indirect irradiation excites the triplet sensitizer from its ground state S_0 to its excited singlet state S_1 , which rapidly undergo intersystem crossing to its excited triplet state T_1 . As the sensitizer relaxes to the ground state it undergoes a triplet-triplet energy transfer with an acceptor molecule (photosensitization), which in our case would be the surrounding tetrazolethiones in solution. Therefore, if the mechanism involves a triplet excited state, increase in the yields of the carbodiimides **80**, is expected.

The irradiation of argon-purged solutions of **79a,b** in acetonitrile- d_3 was carried out at 300 nm in the presence of triplet sensitizers of varying energies such as benzophenone ($E_T = 69$ kcal/mol), acetophenone ($E_T = 74$ kcal/mol), and acetone ($E_T = 77$ kcal/mol).³⁶ However, ^1H NMR spectroscopic analysis of the irradiated samples after 60 minutes did not indicate the formation of carbodiimide **80a,b**. We also attempted the sensitization experiment with varying the amounts of the sensitizers and at different irradiation wavelength (350 nm) but the results were unproductive.

In order to rule out the possibility of high lying triplet state, triplet quenching experiments were performed at 300 nm. Similar to previous experiments, tetrazolethiones **79a, b** were photolyzed in the presence of triplet quenchers such as *trans*-1,3-pentadiene, 1,3-cyclohexadiene and biphenyl. The quenching experiments were expected to thwart any triplet photochemical process and result in lower yields of the photoproduct, *i.e.* carbodiimide **80a,b**.

However, photolysis of **79** with *trans*-1,3-pentadiene and 1,3-cyclohexadiene as quenchers showed formation of corresponding thioureas and an increase in the yield of carbodiimides. The thioureas were formed by hydrogen atom abstraction from the dienes similar to 1,4-CHD discussed above (Scheme 2.10). Perhaps, the explanation for the increased carbodiimide yields may involve the formation of exciplex, which influenced the photoreactivity either by aiding the rapid photorelease of nitrogen or sulfur.

The photolysis in the presence of biphenyl as a quencher indicated only a slight decrease in the formation of carbodiimides **80a,b** with increasing concentration of biphenyl (Figure 2.13). This modest decrease in yields of the photoproduct can be attributed to a slight competitive absorption between the tetrazolethione and the quencher at irradiating wavelength *i.e.* at 300 nm.

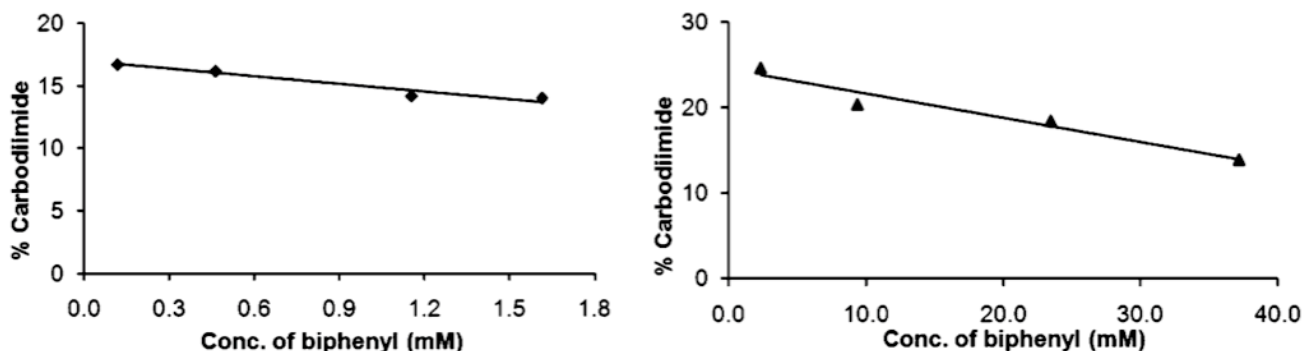


Figure 2.13: Plots showing modest quenching of carbodiimides **80a** (left) and **80b** (right) during the photolysis of tetrazolethione **79a,b** in the presence of biphenyl.

The inability to detect any photoproducts during the triplet sensitization and the slight inhibition of carbodiimide formation observed in the triplet quenching experiments, does not provide a strong support for the photochemistry from a triplet excited state. Also, the photochemical studies of tetrazolethiones **79a,b** (Table 2.5) in oxygen-saturated solutions

showed negligible oxygen effect on product yields, hence further excluding the involvement of a triplet excited state (Compare Tables 2.4 and 2.5).

Table 2.5: Amounts of tetrazolethiones remaining and photoproducts produced in acetonitrile- d_3 .

| | λ (nm) | Irradiation time (min) | | Unreacted 79a,b ^a | Yield of 80a,b ^a [%] |
|------------|-------------------|---------------------------|----------------------|-------------------------------------|---|
| 79a | 254 | 15 | O ₂ -satd | 55 | 47 |
| | 300 | 60 | O ₂ -satd | > 95 | trace |
| 79b | 254 | 15 | O ₂ -satd | 57 | 45 |
| | 300 | 60 | O ₂ -satd | > 95 | trace |

^a Amounts calculated using 1,4-dioxane as an internal standard (average of three irradiated samples) with the standard deviation in the range 0.4-2% range.

Therefore, the above experiments suggest that photocleavage of these heterocyclic rings probably follows path A involving the singlet excited state, followed by rapid loss of nitrogen to the diradicaloid species and subsequent, intersystem crossing to 1,3-triplet diradical.

2.2.4.5 Multiphoton excitation experiment

Our results above indicate that tetrazolethiones **79** can be cleanly converted into carbodiimides **80** employing single photon excitation at 254 nm or 300 nm *via* the intermediacy of a 1,3-triplet biradical. Next, we examined if we could reproduce this chemistry at 800 nm through a multiphoton excitation process. Irradiation of tetrazolethione **79a** in acetonitrile at 800 nm with Ti-Sapphire laser (~800 nm) was carried out to investigate (*i*) if multiphoton irradiation could be used for the fragmentation of tetrazolethione ring systems and (*ii*) if multiphoton excitation follows similar photochemical pathways as that observed with single-photon excitation (254 nm). The photolysis of argon-purged solution of **79a** in acetonitrile at 800 nm was carried out and the UV spectrum was recorded. Note that the UV spectral changes observed at 30 min of irradiation at 800 nm (Figure 2.14, bottom) were similar to that observed at 20 sec of irradiation at 254 nm (Figure 2.14; top). Thus, indicating that tetrazolethione most likely follows the same decomposition pathway at 800 nm as that observed at 254 nm.

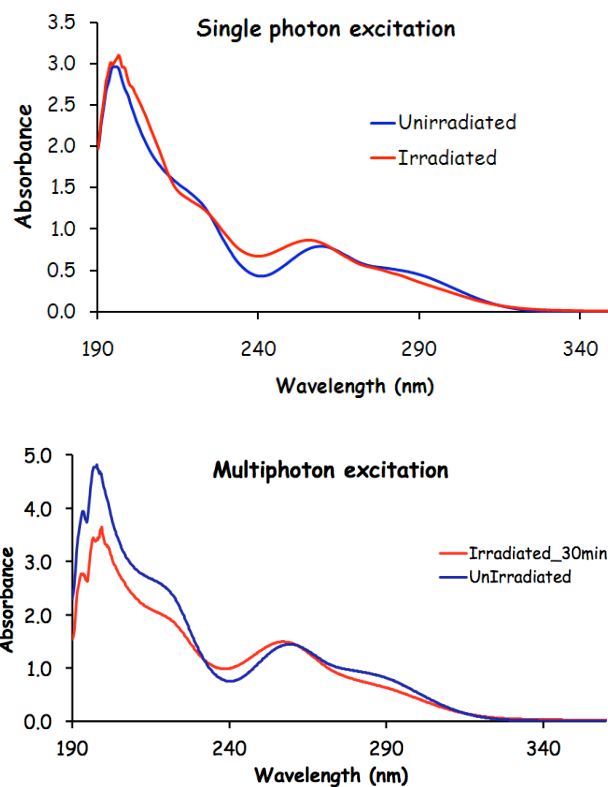


Figure 2.14: UV spectral changes of tetrazolethione **79a** in acetonitrile induced by single photon excitation (top, irradiation time 20 sec) and multiphoton excitation (bottom, irradiation time 30 min).

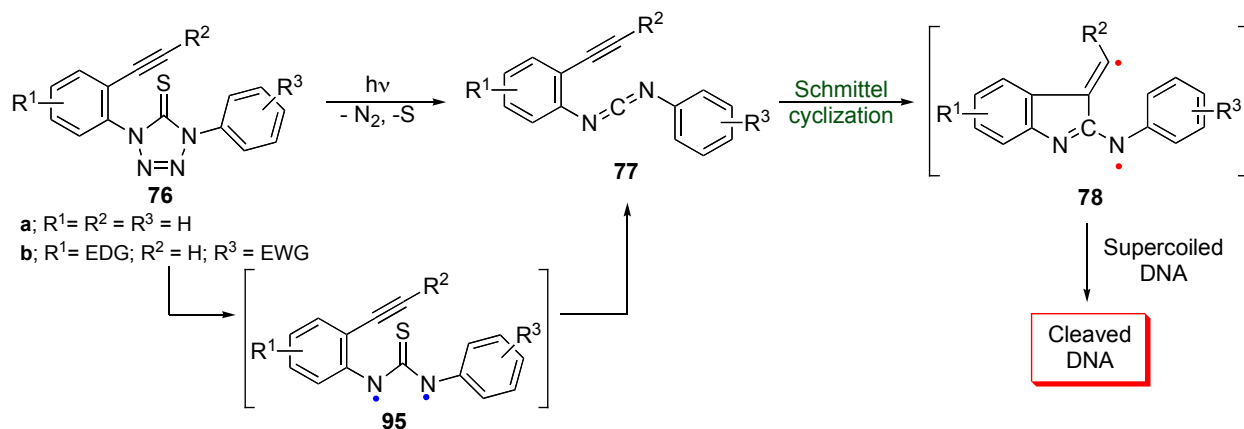
2.3 Summary

A number of model tetrazolethiones were successfully synthesized. UV-Vis absorption spectra of these compounds were recorded and quantum mechanical calculations were employed to determine the nature of the electronic transitions that gave rise to these bands. Our results clearly showed that solvent polarity and substituents have negligible effect on the UV characteristics of these compounds and hence, their photophysical properties.

Photochemical studies indicated a clean conversion of a series of tetrazolethione heterocycles to their respective photostable carbodiimides. Between the two proposed photodecomposition pathways, there was no evidence for the intermediacy of a heterocyclic carbene, wherein desulfurization occurs prior to loss of dinitrogen. Similar to the tetrazolone derivatives the photochemistry of tetrazolethione occurs via a 1,3-biradical intermediate, which was concluded to be in its triplet spin multiplicity.

The photosensitization and triplet-quenching experiments to identify the nature of the precursor that led to the biradical provided no conclusive evidence of a triplet excited state. The most feasible precursor that could lead to the formation of a 1,3- triplet biradical was concluded to be the diradicaloid species generated directly from the singlet excited state of tetrazolethione ring systems after the elimination of molecular nitrogen. Subsequently, these diradicaloid species could be envisioned to undergo intersystem crossing to generate the triplet biradical which would undergo desulfurization to form corresponding carbodiimides. The multiphoton irradiation of the tetrazolethiones suggested the formation of similar photoproducts, *i.e.* carbodiimides.

Our results indicate that the photochemical conversion of the tetrazolethiones to carbodiimides is clean and thus, perfectly suited for use in the designing of photoactivated DNA cleaving agents such as enynyl-1*H*-tetrazole-5(4*H*)-thiones **76**. Furthermore, the intermediate 1,3-triplet biradicals **95** are also expected to cause DNA damage through hydrogen atom abstraction (Scheme 2.12). To our knowledge, this is the first reported case where photochemical reaction involves the formation of two different types of biradicals that can be exploited for DNA damage.



Scheme 2.12: Enynyl-1*H*-tetrazole-5(4*H*)-thiones **76** based photoactivated DNA cleavage agents that generate two different types of biradicals in one pot cellular damage.

2.4 Computational Methods

All calculations were carried out with Gaussian 03 package of programs. B3LYP functional in conjunction with 6-311+G* basis set was used. B3LYP combines Becke's three-

parameter exchange functional with the correlation functional of Lee, Yang, and Parr. All the geometry optimizations were followed by vibrational analyses to ensure the positive sign of all eigenvalues of the Hessian matrix and to confirm that the stationary point found was a true minimum on the potential energy surface. Vertical excitation energies were computed using time-dependent density functional theory (TDDFT) at optimized geometries. The solvent effects on the ground state geometries and excitation energies were considered using the integral equation formalism of the polarized continuum model (IEFPCM). The molecular orbitals were visualized using Gauss View.

2.5 Experimental

2.5.1 Synthesis

All reactions were carried out under an atmosphere of argon in glassware, which had been oven-dried. Thin layer chromatography was carried out on 250 μm silica gel plates with UV 254 fluorescent indicator and UV-light was used as a visualizing agent. Standard column chromatography was performed using 63–200 μm silica gel. ^1H and ^{13}C NMR spectra were recorded at ambient temperature on 400 MHz spectrometers. The carrier frequencies were 399.74 MHz (^1H) and 100.53 MHz (^{13}C) respectively. The number of scans used were 64 for ^1H NMR spectra and for ^{13}C , those ranged from 3-5 K depending on the sample concentration. Both ^1H and ^{13}C spectra were recorded with longer relaxation time (10 s). The data is listed as follows: chemical shifts in parts per million, coupling constants in Hertz, multiplicity (s = singlet, d = doublet, t = triplet, q = quartet, m = multiplet) and integration values. The infrared spectroscopic frequencies are reported in cm^{-1} .

Low-resolution mass spectra (LRMS) were obtained on a mass spectrometer equipped with an electrospray ion source (ESI) operated in positive ion mode and connected to a triple quadrupole mass analyzer. Collision-induced dissociation of mass selected ions was performed using nitrogen as a target gas at collision energy of 25 eV. High resolution mass spectra (HRMS) were acquired on a quadrupole/time-of-flight mass spectrometer. The samples were prepared in methanol/acetonitrile (containing 0.1% formic acid in some cases) and were introduced by continuous infusion into the electrospray ionization (ESI) source at a rate of 30 $\mu\text{L}/\text{min}$. TOF

scans were carried out in positive ionization mode. In most cases, both $[M + H]^+$ and $[M + Na]^+$ ions were detectable for each species.

2.5.2 Photochemistry

All irradiations were carried out either in Ace-photochemical vessel with a 254 nm Ace-Hanovia medium pressure mercury lamp or in a Rayonet reactor (Rayonet RMR- 600) equipped with 254 nm and broadband 300 nm UV lamps. Monochromatic 313 nm was obtained by using broad band 300 nm UV lamps and by filtering the radiation through a solution of 0.002 M K_2CrO_4 in 5% Na_2CO_3 . All the quantitative analyses of the photolyzed reaction mixtures were performed by NMR spectroscopy with 1,4-dioxane as an internal standard. These experiments were carried out on a 500 MHz NMR spectrometer equipped with a 3 mm triple resonance inverse detection pulse field gradient probe operating at 499.848 MHz for 1H . The spectra were an accumulation of 64 individual scans. The photoproducts were assigned by comparison of their chemical shift values to that of authentic samples.

NOTE: Trimethylsilyl azide, aryl isocyanate and dimethyl sulfate are hazardous and highly toxic compounds. Adequate precaution should be taken when handling these compounds.

2.6 General procedure for synthesis of monosubstituted tetrazolones 83

Trimethylsilyl azide (TMSA) (1.5 mmol) was added to a round-bottom flask containing the corresponding aryl isocyanate (1.0 mmol), and then the resulting mixture was refluxed at 100 °C for 24 h. After the reaction mixture was cooled to room temperature, the excess TMSA was removed under reduced pressure. The solid was recrystallized from ethyl acetate-hexane to afford the desired monosubstituted tetrazolone.

2.6.1 1-Phenyl-1H-tetrazol-5(4H)-one, 83a

The general procedure was followed using phenylisocyanate (6.30 mmol), which afforded **83a** as a white solid (0.868 g, 85%); $R_f = 0.29$ (70:30 hexane/ EtOAc). 1H NMR (DMSO- d_6 , 400 MHz): δ 7.42 (t, $J = 7.51$ Hz, 1H), 7.56 (t, $J = 7.60$ Hz, 2H), 7.85 (d, $J = 7.68$ Hz, 2H); ^{13}C NMR (DMSO- d_6 , 100 MHz): δ 119.5, 127.5, 129.4, 134.1, 150.2.

2.6.2 *1-(3-Methoxyphenyl)-1H-tetrazol-5(4H)-one, 83b*

The general procedure was followed using 3-methoxyphenylisocyanate (3.35 mmol), which afforded **83b** as a pale white solid (0.522 g, 81% yield); $R_f = 0.12$ (7:3 hexane/EtOAc); m.p. 151–153 °C; ^1H NMR (DMSO- d_6 , 400 MHz): δ 3.80 (s, 3H), 6.98 (d, $J = 4$ Hz, 1H), 7.41–7.47 (m, 3H); ^{13}C NMR (DMSO- d_6 , 100 MHz): δ 55.4, 105.0, 111.3, 113.0, 130.4, 135.2, 150.1, 159.7. IR (KBr pellet) ν_{max} 3178, 3092, 3019, 2833, 2773, 1709, 1602, 1591, 1501, 1361, 1264, 1155, 1071, 977, 864, 733, 622, 591 cm^{-1} . LRMS (ESI): m/z calculated for $\text{C}_8\text{H}_9\text{N}_4\text{O}_2$ (M^+) 193.0720, found 193.0727.

2.6.3 *1-(4-Methoxyphenyl)-1H-tetrazol-5(4H)-one, 83c*

The general procedure was followed using 4-methoxyphenylisocyanate (10.06 mmol), which afforded **83c** as a pale white solid (1.12 g, 87% yield); $R_f = 0.42$ (7:3 hexane/EtOAc); m.p. 177–179 °C; ^1H NMR (DMSO- d_6 , 400 MHz): δ 3.81 (s, 3H), 7.10 (d, $J = 8.98$ Hz, 2H), 7.71 (d, $J = 9.17$ Hz, 2H); ^{13}C NMR (DMSO- d_6 , 100 MHz): δ 55.5, 114.5, 122.0, 127.1, 150.5, 158.5.

2.6.4 *1-(3-Chlorophenyl)-1H-tetrazol-5(4H)-one, 83d*

The general procedure was followed using 3-chlorophenylisocyanate (13.1 mmol) which afforded **83d** as a white solid (2.33 g, 90% yield); $R_f = 0.22$ (7:3 hexane/EtOAc); ^1H NMR (DMSO- d_6 , 400 MHz): δ 7.46 (d, $J = 8.4$ Hz, 1H), 7.57 (t, $J = 8$ Hz), 7.83 (dd, $J_1 = 0.8$ Hz, $J_2 = 8$ Hz, 1H), 7.95 (s, 1H); ^{13}C NMR (DMSO- d_6 , 100 MHz): δ 117.6, 118.6, 127.2, 131.3, 133.7, 135.5, 150.4.

2.6.5 *1-(4-Nitrophenyl)-1H-tetrazol-5(4H)-one, 83e*

The general procedure was followed using 4-nitrophenylisocyanate (9.14 mmol) which afforded **83d** as a yellow solid (1.53 g, 81% yield); ^1H NMR (400 MHz, DMSO): δ 8.21 (d, $J = 8.1$ Hz, 2H), 8.41 (d, $J = 8.2$ Hz, 2H); ^{13}C NMR (100 MHz, DMSOC): δ 119.1, 125.3, 139.2, 145.4, 150.0.

2.7 General procedure for synthesis of 1,4-disubstituted tetrazolones **84**

To a mixture of monosubstituted tetrazolone, tetrabutylammonium bromide (TBABr), 20% NaOH in methylene chloride was added to a solution of dimethyl sulfate (DMS) in

methylene chloride. The resulting mixture was stirred at room temperature for approximately 3 h (or monitored with TLC until completion). After the completion of the reaction, the organic layer was separated and washed (3x) with water to remove any excess TBABr then dried over Na₂SO₄. The filtrate was concentrated under reduced pressure and dried under vacuum to afford the desired product. The synthesis of compound **84e** has been reported from previous work carried out in our lab.

2.7.1 *1-Methyl-4-phenyl-1H-tetrazol-5(4H)-one, 84a*

The general procedure was followed using 1-phenyl-1*H*-tetrazol-5(4*H*)-one (3.08 mmol) to produce **84a** as a crystalline colorless solid (0.52 g, 95%); $R_f = 0.81$ (40:60 hexane/EtOAc); ¹H NMR (DMSO-*d*₆, 400 MHz): δ 3.62 (s, 3H), 7.44 (t, $J = 7.40$ Hz, 1H), 7.58 (t, $J = 7.03$ Hz, 2H), 7.85 (d, $J = 8.27$ Hz, 2H); ¹³C NMR (DMSO-*d*₆, 100 MHz): δ 31.2, 119.4, 127.7, 129.5, 134.2, 148.8. HRMS (ESI): m/z calculated for C₈H₈N₄ONa (M+Na⁺) 199.0596, found 199.0602.

2.7.2 *1-Methyl-4-(3-methoxyphenyl)-1H-tetrazol-5(4H)-one, 84b*

The general procedure was followed using 1-(3-Methoxyphenyl)-1*H*-tetrazol-5(4*H*)-one (2.60 mmol) to produce **84b** as a white crystalline solid (0.482 g, 90% yield); $R_f = 0.37$ (7:3 hexane/EtOAc); m.p. 79–81 °C; ¹H NMR (CDCl₃, 400 MHz): δ 3.70 (s, 3H), 3.86 (s, 3H), 6.89–6.92 (m, 1H), 7.39 (t, $J = 8.4$ Hz, 1H), 7.52–7.56 (m, 2H); ¹³C NMR (CDCl₃, 100 MHz): δ 31.6, 55.7, 104.7, 111.4, 113.9, 130.4, 135.8, 149.4, 160.4. IR (KBr pellet) ν_{\max} 3118, 3091, 3012, 2966, 2840, 1729, 1608, 1588, 1502, 1387, 1461, 1299, 1231, 1142, 1042, 866, 782, 727 cm⁻¹. LRMS (ESI): m/z calculated for C₉H₁₁N₄O₂⁺ (M⁺) 207.0877, found 207.0878.

2.7.3 *1-Methyl-4-(4-methoxyphenyl)-1H-tetrazol-5(4H)-one, 84c*

The general procedure was followed using 1-(4-methoxyphenyl)-1*H*-tetrazol-5(4*H*)-one (2.08 mmol) to produce **84c** as a crystalline colorless solid (0.30 g, 91% yield); $R_f = 0.51$ (4:6 hexane/EtOAc); m.p. 119–120 °C; ¹H NMR (CDCl₃, 400 MHz): δ 3.70 (s, 3H), 3.86 (s, 3H), 7.01 (d, $J = 9.17$ Hz, 2H), 7.80 (d, $J = 9.17$ Hz, 2H); ¹³C NMR (CDCl₃, 100 MHz): δ 31.6, 55.7, 114.7, 121.6, 128.0, 149.6, 159.2. IR (KBr pellet) ν_{\max} 3088, 3011, 2975, 2945, 2847, 1721, 1618, 1519, 1424, 1357, 1252, 1155, 1048, 1028, 824, 744, 729, 574, 511 cm⁻¹. LRMS (ESI): m/z calculated for C₉H₁₀N₄O₂Na⁺ (M+Na⁺) 229.0702, found 229.0712.

2.7.4 1-(3-Chlorophenyl)-4-methyl-1H-tetrazol-5(4H)-one, 84d

The general procedure was followed using 1-(3-chlorophenyl)-1H-tetrazol-5(4H)-one (2.54 mmol) to produce **84d** as a pale white solid (0.51 g, 96% yield); $R_f = 0.35$ (7:3 hexane/EtOAc); $^1\text{H NMR}$ (CDCl_3 , 400 MHz): δ 3.70 (s, 3H), 3.86 (s, 3H), 7.32 (d, $J = 7.8$ Hz, 1H), 7.42 (t, $J = 7.6$ Hz, 1H), 7.80 (dd, $J_1 = 7.8$ Hz, $J_2 = 1.94$ Hz, 1H), 8.00 (s, 1H); $^{13}\text{C NMR}$ (CDCl_3 , 100 MHz): δ 31.7, 117.0, 119.2, 127.9, 130.7, 135.4, 135.7, 149.1.

2.7.5 1-(4-Nitrophenyl)-4-methyl-1H-tetrazol-5(4H)-one, 84e

The general procedure was followed using 1-(4-nitrophenyl)-1H-tetrazol-5(4H)-one (2.41 mmol) to produce **84e** as a yellow solid (0.45 g, 85% yield); $^1\text{H NMR}$ (400 MHz, DMSO): δ 3.67 (s, 3H, CH_3), 8.20 (d, $J = 8.2$ Hz, 2H), 8.46 (d, $J = 8.1$ Hz, 2H); $^{13}\text{C NMR}$ (100 MHz, DMSO): δ 31.1, 119.0, 125.1, 139.3, 145.6, 148.8.

2.8 General procedure for synthesis of tetrazolethiones, 79

Phosphorus pentasulfide (P_2S_5) was added to a solution of disubstituted tetrazolone in dry toluene and the resulting reaction mixture was reflux at 110°C until the starting material disappeared, as indicated by TLC. After cooling, the reaction mixture was filtered, dried over Na_2SO_4 and concentrated under reduced pressure. Purification by column chromatography afforded the product.

2.8.1 1-Methyl-4-phenyl-1H-tetrazole-5(4H)-thione, 79a

The general procedure was followed by using 1-methyl-4-phenyl-1H-tetrazol-5(4H)-one (22.7 mmol) and purification by column chromatography (SiO_2 , 88:12 hexane/EtOAc) produced **86a** as a yellow solid (2.3 g, 53%); $R_f = 0.77$ (4:6 hexane/EtOAc); $^1\text{H NMR}$ (400 MHz, DMSO- d_6): δ 3.91 (s, 3H), 7.68-7.55 (m, 3H), 7.87 (d, $J = 7.14$ Hz, 2H); $^{13}\text{C NMR}$ (100 MHz, DMSO- d_6): δ 34.7, 124.3, 129.3, 129.8, 134.4, 163.2. HRMS (ESI): m/z calculated for $\text{C}_8\text{H}_9\text{N}_4\text{S}$ (M^+) 193.0548, found 193.0545.

2.8.2 1-(3-Methoxyphenyl)-4-methyl-1H-tetrazole-5(4H)-thione, 79b

The general procedure was followed by using 1-(3-methoxyphenyl)-4-methyl-1H-tetrazol-5(4H)-one (2.4 mmol) and purification by column chromatography (SiO₂, 93:7 hexane/EtOAc) produced **79b** as a white solid (0.42 g, 78% yield): $R_f = 0.64$ (70:30 hexane/EtOAc); m.p. 52–54°C; ¹H NMR (400 MHz, CD₃CN): δ 3.85 (s, 3H), 3.89 (s, 3H), 7.10–7.13 (m, 1H), 7.43–7.46 (m, 1H), 7.49–7.51 (m, 1H), 7.53 (s, 1H); ¹³C NMR (100 MHz, CD₃CN): δ 35.5, 56.4, 111.0, 116.2, 117.2, 131.2, 137.0, 161.0, 165.0. IR (ZnSe ATR crystal): 1600, 1590, 1492, 1440, 1356, 1324, 1238, 1195, 1160, 1065, 1022, 865, 839, 782, 681 cm⁻¹. HRMS (ESI): m/z calculated for C₉H₁₁N₄OS⁺ (M⁺) 223.0654, found 223.0648; calculated for C₉H₁₀N₄OSNa (M+Na⁺) 245.0473, found 245.0468.

2.8.3 1-(4-Methoxyphenyl)-4-methyl-1H-tetrazole-5(4H)-thione, 79c

The general procedure was followed by using 1-methyl-4-(4-methoxyphenyl)-1H-tetrazol-5(4H)-one (1.46 mmol) and purification by column chromatography (SiO₂, 90:10 hexane/EtOAc) produced **79c** as a white crystalline solid (0.24 g, 75% yield): $R_f = 0.62$ (6:4 hexane/EtOAc); m.p. 134–135°C; ¹H NMR (200 MHz, CDCl₃): δ 3.88 (s, 3H), 3.98 (s, 3H), 7.05 (d, $J = 9.16$ Hz, 2H), 7.82 (d, $J = 9.16$ Hz, 2H); ¹³C NMR (100 MHz, CDCl₃): δ 35.2, 55.8, 114.6, 125.7, 127.8, 160.5, 163.9. IR (KBr pellet) ν_{\max} 3076, 2998, 2965, 2926, 2840, 1612, 1591, 1514, 1446, 1369, 1326, 1302, 1256, 1191, 1114, 1080, 1041, 1028, 825, 742, 561, 543 cm⁻¹; HRMS (ESI): m/z calculated for C₉H₁₁N₄OS⁺ (M⁺) 223.0654, found 223.0645.

2.8.4 1-(3-Chlorophenyl)-4-methyl-1H-tetrazole-5(4H)-thione, 79d

The general procedure was followed by using 1-methyl-4-(3-chlorophenyl)-1H-tetrazol-5(4H)-one (1.90 mmol) and purification by column chromatography (SiO₂, 96:4 hexane/EtOAc) produced **79d** as a white solid (0.28 g, 65% yield): $R_f = 0.61$ (7:3 hexane:EtOAc); ¹H NMR (200 MHz, CDCl₃): δ 3.88, 7.55–7.60 (m, 2H), 7.87–7.90 (m, 2H), 8.03 (s, 1H); ¹³C NMR (100 MHz, CDCl₃): δ 35.5, 123.4, 124.8, 130.6, 131.8, 135.1, 137.0, 165.0.

2.8.5 1-(3-Nitrophenyl)-4-methyl-1H-tetrazole-5(4H)-thione, 79e

The general procedure was followed by using 1-methyl-4-(4-nitrophenyl)-1H-tetrazol-5(4H)-one (3.17 mmol) and purification by column chromatography (SiO₂, 96:4 hexane/EtOAc) produced **79e** as a white solid (0.28 g, 65% yield): $R_f = 0.61$ (7:3 hexane:EtOAc); ¹H NMR (400 MHz,

DMSO): δ 3.91 (s, 3H, CH₃), 8.35 (d, J = 9.4 Hz, 2H), 8.50 (d, J = 8 Hz, 2H); ¹³C NMR (100 MHz, DMSO): δ 34.9, 124.7, 125.0, 139.4, 147.4, 163.1.

2.9 General procedure for synthesis of procedure for synthesis of thiourea, 93

To a stirring solution of aromatic amine **96** (16.10 mmol) in methanol (50 mL) was added a commercially obtained methyl isothiocyanate (17.70 mmol), and the reaction mixture was refluxed at 65 °C for 24-30 h. After complete consumption of the starting material the mixture was concentrated under reduced pressure and the crude compound was recrystallized in ethanol to produce the corresponding arylthioureas **93**.

2.9.1 1-Methyl-3-phenylthiourea, 93a

Compound **93a** was prepared from aniline **96a** (16.1 mmol) using the general procedure. White solid (2.46 g, 92% yield); R_f = 0.29 (60:40 hexane/ EtOAc); m.p. 110-112 °C; ¹H NMR (400 MHz, CD₃CN): δ 2.97 (d, J = 8 Hz, 3H), 6.56 (s, 1H), 7.22-7.29 (m, 3H), 7.37-7.41 (m, 1H), 8.12 (s, 1H). ¹³C NMR (100 MHz, CD₃CN): δ 32.1, 126.0, 127.0, 130.4, 138.7, 182.8. IR (ZnSe ATR crystal) 3259, 3155, 2989, 2937, 1515, 1490, 1287, 1246, 1210, 1026, 1001, 723, 689, 640, 602 cm⁻¹. HRMS (ESI): m/z calculated for C₈H₁₁N₂S⁺ (M⁺) 167.0643, found 167.0637; calculated for C₈H₁₀N₂SNa⁺ (M+Na⁺) 189.0462, found 189.0457.

2.9.2 1-(3-Methoxyphenyl)-3-methylthiourea, 93b

Compound **93b** was prepared from 3-methoxyaniline **96b** (8.12 mmol) using the general procedure. White solid (1.46 g, 92% yield); R_f = 0.15 (70:30 hexane/EtOAc); m.p. 98- 100 °C. ¹H NMR (400 MHz, CD₃CN): δ 2.97 (d, J = 8 Hz, 3H), 3.78 (s, 3H), 6.62 (s, 1H), 6.78-6.88 (m, 3H), 7.29 (t, 1H), 8.06 (s, 1H). ¹³C NMR (100 MHz, CD₃CN): δ 32.2, 56.1, 111.4, 112.5, 117.7, 131.3, 139.7, 161.5, 182.7. HRMS (ESI): m/z calculated for C₉H₁₃N₂OS⁺ (M⁺) 197.0749, found 197.0743; calculated for C₉H₁₂N₂OSNa⁺ (M+Na⁺) 219.0568, found 219.0563.

2.9.3 *1-(4-Methoxyphenyl)-3-methylthiourea, 93c*

Compound **93c** was prepared from 4-methoxyaniline **96c** (12.18 mmol) using the general procedure. Crystalline lavender solid (2.08 g, 87% yield); $R_f = 0.46$ (3:7 hexane/EtOAc); ^1H NMR (400 MHz, CD_3CN): δ 2.94 (d, $J = 4.4$ Hz, 3H), 3.79 (s, 3H), 6.36 (br s, 1H), 6.94 (d, $J = 8.8$ Hz, 2H), 7.16 (d, $J = 8.8$ Hz, 2H), 7.96 (br s, 1H); ^{13}C NMR (100 MHz, CD_3CN): δ 32.1, 56.2, 115.6, 128.6, 159.3, 183.4.

2.9.4 *1-(3-Chlorophenyl)-3-methylthiourea, 93d*

Compound **93d** was prepared from 3-chloroaniline **96d** (19.60 mmol) using the general procedure. Brown crystalline colorless solid (3.26 g, 84% yield); $R_f = 0.20$ (3:7 hexane/EtOAc); ^1H NMR (400 MHz, CD_3CN): δ 2.98 (d, $J = 4.4$ Hz, 3H), 6.73 (br s, 1H), 7.18-7.23 (m, 2H), 7.16 (t, $J = 8$ Hz, 1H), 7.44 (br s, 1H), 8.34 (br s, 1H); ^{13}C NMR (100 MHz, CD_3CN): δ 32.0, 123.7, 125.2, 126.3, 131.5, 134.9, 140.5, 182.6.

2.9.5 *1-Methyl-3-(4-Nitrophenyl)-thiourea, 93e*

Compound **93e** was prepared from 3-nitroaniline **96e** (10.86 mmol) using the general procedure. Brownish yellow solid (1.81 g, 79% yield); $R_f = 0.17$ (6:4 hexane/EtOAc); ^1H NMR (400 MHz, CD_3CN): δ 3.03 (d, $J = 4.4$ Hz, 1H), 6.92 (s, 1H), 7.72 (d, $J = 7.6$ Hz, 2H), 8.16 (d, $J = 9.2$ Hz, 2H), 8.48 (s, 1H).

2.10 General procedure for synthesis of carbodiimides, **80**

Mercuric oxide (18.1 mmol) was added to a solution of arylthiourea (6.0 mmol) in $\text{CH}_2\text{Cl}_2:\text{H}_2\text{O}$ (4:1, 30 mL), and the reaction mixture was stirred at room temperature for 30 min. After completion the mixture was filtered through Celite, washed with ample amount of CH_2Cl_2 and the filtrate was concentrated under reduced pressure. Purification of the crude compound by a short silica gel flash column chromatography afforded the corresponding carbodiimides.

2.10.1 *N-((Methylimino)methylene)aniline, 80a*

Compound **80a** was prepared from 1-methyl-3-phenylthiourea (**93a**) (6.0 mmol) using the general procedure. Purification using 5% EtOAc/hexanes afforded a yellow oil (0.10 g, 12% yield); $R_f = 0.83$ (7:3 hexane/EtOAc); ^1H NMR (400 MHz, CD_3CN): δ 3.14 (s, 3H), 7.09-7.14

(m, 3H), 7.29-7.33 (t, 2H); ^{13}C NMR (100 MHz, CD_3CN): δ 32.8, 124.4, 125.6, 130.5, 137.0, 142.0. IR (ZnSe ATR crystal) 3059, 3024, 2935, 2879, 2121, 2026, 1592, 1499, 1406, 1282, 1156, 1070, 891cm^{-1} . HRMS (ESI): m/z calculated for $\text{C}_8\text{H}_9\text{N}_2^+$ (M^+) 133.0766, found 133.0760.

2.10.2 3-Methoxy-*N*-((methylimino)methylene)benzenamine, **80b**

Compound **80b** was prepared from 1-(3-methoxyphenyl)-3-methylthiourea (**93b**) (5.1 mmol) using the general procedure. Purification using a 5% EtOAc/hexanes afforded a yellow oil (0.35 g, 42% yield); $R_f = 0.71$ (70:30 hexane/EtOAc); ^1H NMR (400 MHz, CD_3CN): δ 3.14 (s, 3H), 3.76 (s, 3H), 6.63 - 6.70 (m, 3H), 7.20 (t, 1H); ^{13}C NMR (100 MHz, CD_3CN): δ 32.8, 56.0, 109.9, 111.3, 116.7, 131.1, 136.7, 143.2, 161.6. IR (ZnSe ATR crystal) 2937, 2834, 2123, 1594, 1581, 1493, 1464, 1421, 1281, 1243, 1127, 1038, 945, 840, 769, 684 589cm^{-1} . HRMS (ESI): m/z calculated for $\text{C}_9\text{H}_{11}\text{N}_2\text{O}^+$ (M^+) 163.0871, found 163.0866.

2.10.3 4-Methoxy-*N*-((methylimino)methylene)benzenamine, **80c**

Compound **80c** was prepared from 1-(4-methoxyphenyl)-3-methylthiourea (**93c**) (6.11 mmol) using the general procedure. Purification using a 5% EtOAc/hexanes afforded pure 4-methoxy-*N*-((methylimino)methylene)benzenamine **80c** as a pale yellow oil (0.35 g, 42% yield); $R_f = 0.71$ (6:4, hexane/EtOAc); ^1H NMR (400 MHz, CD_3CN): δ 3.10 (s, 3H), 3.75 (s, 3H), 6.86 (d, $J = 12\text{Hz}$, 2H), 7.02 (d, $J = 8\text{Hz}$, 2H); ^{13}C NMR (100 MHz, CD_3CN): δ 33.3, 56.5, 116.0, 125.7, 134.5, 138.5, 158.3.

2.10.4 3-Chloro-*N*-((methylimino)methylene)benzenamine, **80d**

Compound **80d** was prepared from 1-(4-methoxyphenyl)-3-methylthiourea (**93d**) (2.17 mmol) using the general procedure. Purification using 1% EtOAc/hexanes afforded pure 3-chloro-*N*-((methylimino)methylene)benzenamine **80d** as a yellow oil (0.35 g, 42% yield); $R_f = 0.80$ (7:3 hexane/EtOAc); ^1H NMR (400 MHz, CD_3CN): δ 3.16 (s, 3H), 7.01 (d, $J = 8\text{Hz}$, 1H), 7.12 (s, 2H) 7.27 (t, $J = 8\text{Hz}$, 1H); ^{13}C NMR (100 MHz, CD_3CN): δ 32.7, 122.9, 124.4, 125.4, 131.7, 135.3, 143.9.

2.10.5 *N*-((methylimino)methylene)-4-nitrobenzenamine, **80e**

Compound **80e** was prepared from 1-methyl-3-(4-nitrophenyl)-thiourea (**93e**) (3.55 mmol) using the general procedure. Purification using 4% EtOAc/hexanes afforded pure *N*-((methylimino)methylene)-4-nitrobenzenamine **80e** as a yellow oil (0.11 g, 26% yield); $R_f = 0.65$ (6:4, hexane/EtOAc); $^1\text{H NMR}$ (400 MHz, CD_3CN): δ 3.23 (s, 3H), 7.21 (d, $J = 8\text{Hz}$, 2H), 8.15 (d, $J = 8\text{Hz}$, 2H); $^{13}\text{C NMR}$ (100 MHz, CD_3CN): δ 32.5, 124.9, 126.1, 132.3, 145.1, 150.2.

2.11 General photochemical procedures: Medium pressure Hg lamp

2.11.1 Photolysis and product identification

An argon purged solution of 1-(3-methoxyphenyl)-4-methyl-1*H*-tetrazol-5(4*H*)-one **79b,d** (0.22 mmol) in acetonitrile (125 mL) was irradiated for 60 min at 254 nm in Ace-photochemical vessel using a 100W medium-pressure mercury lamp. GCMS analysis of aliquot of irradiated sample was carried out. The sample was concentrated under reduced pressure and purified with flash column chromatograph to afford the corresponding urea.

2.11.2 Carbene trapping experiment

1-(3-Methoxyphenyl)-4-methyl-1*H*-tetrazol-5(4*H*)-one (0.05g, 0.22 mmol) **79b** in acetonitrile (125-130 mL) containing 10 equivalent of carbene trapping agents (cyclohexene, 3-bromocyclohexene, allylbenzene and styrene) was irradiated with medium-pressure mercury lamp (100W; 254 nm) for 60 min in Ace-photochemical vessel. Aliquots of irradiated samples was analyzed by GCMS.

2.12 General photochemical procedures: Rayonet reactor

2.12.1 UV spectral changes

An argon-purged solution of **79a** (0.07 mM) and **79b** (0.13 mM) in acetonitrile was irradiated in a quartz cuvette at 254 nm. In the case of **79a**, a UV spectrum was obtained after each irradiation at 0, 20, 40, 60, 120, 200, 300, and 420s, whereas in the case of **79b**, a UV spectrum was obtained after each irradiation at 0, 20, 40, 60, 80, 120, and 150s, respectively. Similarly, the irradiation of an argon-purged solution of **79a** (0.2 mM) and **79b** (0.075 mM) in

acetonitrile was carried out in a quartz cuvette at 313 nm, and a UV spectrum was obtained after irradiation at different time intervals (at 0, 1, 5, 10, 15, 20, 30, 40, and 50 min for **79a** and 0, 5, 10, 15, 20, 25, 30, 35 and 40 min for **79b**).

2.12.2 Product identification and Quantitative studies

Irradiation of argon-purged solution of **79a,b** (4.63 mM; 0.65 mL) in acetonitrile- d_3 was carried out at 254 and 300 nm in a quartz NMR tube and ^1H NMR spectrum was recorded after photolysis at every 5 min time interval for 15 and 60 min respectively.

2.12.3 Photolysis of carbodiimides and thioureas

Photolysis of compound **79a – b** (4.70 mM) in an argon-purged acetonitrile- d_3 was conducted in a quartz NMR tube at 254 for 90 min. Similarly, an argon-purged solution of **93a – b** (4.70 mM; 0.7 mL) in acetonitrile- d_3 was irradiated in a quartz NMR tube at 254 for 120 min, and a NMR spectrum was obtained.

2.12.4 Carbene Trapping: Photolysis in the presence of cyclohexene

An argon-purged solution of **79a – b** (4.55mM; 0.7 mL) in acetonitrile- d_3 containing 10 equiv. of cyclohexene was photolyzed at 254 and 300 nm in a quartz NMR tube for 30 and 60 min, respectively, and a NMR spectrum was obtained. For the ESI-MS/MS experiments, 8mL of 1.5 mM tetrazolethione **79a – b** solution was irradiated at 254 and 300 nm. The samples were concentrated using rotary evaporator and crude was analyzed.

2.12.5 Biradical Trapping: Photolysis in the presence of 1,4-Cyclohexadiene

Four separate solutions of **79a – b** (4.63 mM; 0.7 mL) in acetonitrile- d_3 containing varying amounts of 1,4-CHD (10-50 equiv.) were taken in quartz NMR tubes. The mixture in each tube was purged with argon for 15 min and irradiated with broadband 300 nm UV lamp for 60 min, and the ^1H NMR spectrum was recorded.

2.12.6 Sensitization experiments

The photolysis of three separate argon purged solutions of **79a – b** (4.63 mM; 0.7 mL) in acetonitrile- d_3 containing varying amounts (1–20 equiv.) of benzophenone, acetophenone, and

acetone, respectively, was performed with broadband 300 nm UV lamp. Subsequently, the ^1H NMR spectrum was recorded after 60 min.

2.12.7 Effect of oxygen

An oxygen-purged solution of **79a – b** (0.65 mL) in acetonitrile- d_3 (approximately in the range 4.63 mM) was irradiated in a quartz NMR tube at 254 and 300 nm for 15 min and 60 min, respectively and NMR spectrum was recorded.

2.12.8 Triplet quenching experiments

A solution of **79a – b** (4.02 – 4.64 mM) in acetonitrile- d_3 containing *trans*-1,3-pentadiene and 1,3-cyclohexadiene (10 equiv) respectively, was photolyzed at 300 nm in a quartz NMR tube for 60 min and the ^1H NMR spectrum was recorded. For the biphenyl experiment, four separate solutions of **79a – b** in acetonitrile- d_3 (4.63 mM; 0.7 mL) containing varying amounts of biphenyl (0-15 equiv) was purged with argon for 15 min and irradiated with broad band 300 nm UV lamp for 60 min, and NMR spectrum was obtained.

2.13 Actinometry and Quantum yield experiments

A 5.04 mM solution of azoxybenzene in 95% ethanol and a 0.1 M solution of KOH in 95% ethanol were prepared. The azoxybenzene solution was irradiated every 60 sec for 10 min in a quartz cuvette at 254 nm (no purging with Ar required), and 0.1 mL of the irradiated solution was mixed with 1 mL of 0.1 M KOH solution followed by the addition of 23.9 mL of 95% ethanol in a 25 mL volumetric flask. A UV spectrum was subsequently recorded, and the incident light intensity was calculated, as described by Bunce et al., using the equations below:

$$P = (A/\epsilon) = (\text{moles of X})(\text{dilution factor}) \quad \text{Equation 2.1}$$

$$\text{Extent of reaction} = \{[\text{product concentration}]/[\text{initial concentration}]\} * 100 \quad \text{Equation 2.2}$$

$$I_0 = -\{A_0 * \ln(1 - (P/A_0))\} / \Phi_r t \quad \text{Equation 2.3}$$

Where, P = concentration of product formed at time t ; A = absorbance; A_0 = absorbance at initial concentration; ϵ = molar absorptivity of azoxybenzene (= 7600); Φ_r = photosensitivity of azoxybenzene (~0.02); t = irradiation time; I_0 = incident light intensity.

An argon-purged solution of 0.25 mM **79a** and 0.27 mM **79b** in acetonitrile was irradiated every 5sec for 25 sec (approximately <10% conversions) and the UV spectra were recorded after each irradiation. The progress of the reaction was linear and the photoconversion was analyzed at 5-10% completion. The quantum yields (Φ ; in mol/L/s) were calculated using the equations below:

$$\text{Extent of reaction} = \{(A_t - A_o) / A_o\} * 100 \quad \text{Equation 2.4}$$

$$P_{cd} = (\text{Extent of reaction}/100) * [\text{initial concentration of sample}] \quad \text{Equation 2.5}$$

$$\text{Slope} = (P_{cd} / \text{irradiation time}) \quad \text{Equation 2.6}$$

$$\Phi = \text{slope} / I_o \quad \text{Equation 2.7}$$

Where, A_o = absorbance at initial concentration; A_t = absorbance at irradiated time t ; P_{cd} = concentration of product (carbodiimide) formed; t = irradiation time; slope can also be obtained by plotting P_{cd} vs t ; I_o = incident light intensity.

References:

- ¹ Dolmans, D. E.; Fukumura, D.; Jain, R. K., Photodynamic therapy for cancer. *Nature reviews. Cancer* **2003**, *3* (5), 380-7.
- ² Ackroyd, R.; Kelty, C.; Brown, N.; Reed, M., The history of photodetection and photodynamic therapy. *Photochemistry and photobiology* **2001**, *74* (5), 656-69.
- ³ Spikes, J. D., *Primary Photoprocesses in Biology and Medicine*. Plenum Press: New York, 1985.
- ⁴ Allison, R. R.; Downie, G. H.; Cuenca, R.; Hu, X.-H.; Childs, C. J.-H.; Sibata, C. H., Photosensitizers in clinical PDT. *Photodiagnosis and Photodynamic Therapy* **2004**, *1* (1), 27-42.
- ⁵ Luksiene, Z., Photodynamic therapy: mechanism of action and ways to improve the efficiency of treatment. *Medicina (Kaunas)* **2003**, *39* (12), 1137-50.
- ⁶ Vrouenraets, M. B.; Visser, G. W.; Snow, G. B.; van Dongen, G. A., Basic principles, applications in oncology and improved selectivity of photodynamic therapy. *Anticancer research* **2003**, *23* (1B), 505-22.
- ⁷ (a) Allison, R. R.; Downie, G. H.; Cuenca, R.; Hu, X.-H.; Childs, C. J.-H.; Sibata, C. H., Photosensitizers in clinical PDT. *Photodiagnosis and Photodynamic Therapy* **2004**, *1* (1), 27-42. (b) Francis, W.; Helman, P. W.; Ross, A. B., Rate constants for the decay and reactions of the lowest electronically excited singlet state of molecular oxygen in solution. An expanded and revised compilation. *Journal of Physical and Chemical Reference Data*, **1995**, *24*(2), 663-1021.
- ⁸ Bonnett, R., Photosensitizers of the porphyrin and phthalocyanine series for photodynamic therapy. *Chem. Soc. Rev.*, **1995**, *24*, 19-33.
- ⁹ (a) Macdonald, I. J.; Dougherty, T. J., *Basic principles of photodynamic therapy. J. Porphyrins and Phthalocyanines.*, **2001**, *5*, 109-129; (b) Wöhrle, D.; Hirth, A.; T. Bogdahn-Rai, T.; Schnurpfeil, G.; Shopova, M., Photodynamic therapy of cancer: Second and third generations of photosensitizers., *Russian Chemical Bulletin.*, **1998**, *47*(5), 807-816.
- ¹⁰ Hopper, C., Photodynamic therapy: a clinical reality in the treatment of cancer. *Lancet Oncology*, **2000**, *1*, 212-219.
- ¹¹ (a) Oar, M. A.; Serin, J. M.; Dichtel, W. R.; Fréchet, J. M. J., Photosensitization of Singlet Oxygen via Two-Photon-Excited Fluorescence Resonance Energy Transfer in a Water-Soluble Dendrimer. *Chemistry of Materials*, **2005**, *17*(9), 2267-2275.; (b) Nielsen, C. B.; Johnsen, M.; Arnbjerg, J.; Pittelkow, M.; McIlroy, S. P.; Ogilby, P. R.; Jorgensen, M., Synthesis and characterization of water-soluble phenylene-vinylene-based singlet oxygen sensitizers for two-photon excitation. *The Journal of organic chemistry* **2005**, *70* (18), 7065-79.
- ¹² Kim, S.; Ohulchanskyy, T. Y.; Pudavar, H. E.; Pandey, R. K.; Prasad, P. N., Organically modified silica nanoparticles co-encapsulating photosensitizing drug and aggregation-enhanced two-photon absorbing fluorescent dye aggregates for two-photon photodynamic therapy. *Journal of the American Chemical Society* **2007**, *129* (9), 2669-75.
- ¹³ Pawlicki, M.; Collins, H. A.; Denning, R. G.; Anderson, H. L., Two-photon absorption and the design of two-photon dyes. *Angew. Chem. Int. Ed.* **2009**, *48*(18), 3244-3266.
- ¹⁴ Fisher, W. G.; Partridge Jr., W. P.; Dees C.; Wachter, E. A., Simultaneous two-photon activation of type-i photodynamic therapy agents. *Photochemistry and Photobiology*, **1997**, *66*(2), 141-155.

-
- ¹⁵ (a) Frederiksen, P. K.; McIlroy, S. P.; Nielsen, C. B.; Nikolajsen, L.; Skovsen, E.; Jorgensen, M.; Mikkelsen, K. V.; Ogilby, P. R., Two-photon photosensitized production of singlet oxygen in water. *Journal of the American Chemical Society* **2005**, *127* (1), 255-69.; (b) Dy, J.; Ogawa, K.; Kamada, K.; Ohta, K.; Yoshiaki Kobuke, Y., Stepwise elongation effect on the two-photon absorption of self-assembled butadiyne porphyrins., *Chem. Commun.*, **2008**, 3411-3413.
- ¹⁶ Dichtel, W. R.; Serin, J. M.; Edder, C.; Frechet, J. M.; Matuszewski, M.; Tan, L. S.; Ohulchansky, T. Y.; Prasad, P. N., Singlet oxygen generation via two-photon excited FRET. *Journal of the American Chemical Society* **2004**, *126* (17), 5380-1.
- ¹⁷ (a) Drobizhev, M.; Stepanenko, Y.; Dzenis, Y.; Karotki, A.; Rebane, A.; Taylor, P. N.; Anderson, H. L., Understanding strong two-photon absorption in pi-conjugated porphyrin dimers via double-resonance enhancement in a three-level model. *Journal of the American Chemical Society* **2004**, *126* (47), 15352-3.;(b) Hazel A. Collins, H. A.; Khurana, M.; Eduardo H. Moriyama, E. H.; Mariampillai, A.; Dahlstedt, E.; Balaz, M.; Kuimova, M. K.; Drobizhev, M.; Yang, V. X. D.; Phillips, D.; Rebane, A.; Wilson, B. C.; Anderson, H. L., Blood-vessel closure using photosensitizers engineered for two-photon excitation. *Nature photonics*, **2008**, *2*(7), 420-424.
- ¹⁸ Poloukhine, A.; Popik, V. V., Two-photon photochemical generation of reactive enediyne. *The Journal of organic chemistry* **2006**, *71* (19), 7417-21.
- ¹⁹ (a) Pandithavidana, D. R.; Poloukhine, A.; Popik, V. V., Photochemical generation and reversible cycloaromatization of a nine-membered ring cyclic enediyne. *Journal of the American Chemical Society* **2009**, *131* (1), 351-6.; (b) Kuzmin, A. V.; Popik, V. V., Dual reactivity of a photochemically-generated cyclic enyne-allene. *Chem. Commun.*, **2009**, 5707-5709.
- ²⁰ Gudugola dissertation
- ²¹ Schmittel, M.; Mahajan, A. A.; Bucher, G., Photochemical myers-saito and C2-C6 cyclizations of enyne-allenes: direct detection of intermediates in solution. *Journal of the American Chemical Society* **2005**, *127* (15), 5324-5.
- ²² Schmittel, M.; Rodriguez, D.; Steffen, J.-P., A Highly Efficient Triplet Analogue of a Thermal Biradical Cyclization—The Photochemical C2–C6 Cyclization of Enyne-Heteroallenes. *Angew. Chem. Int. Ed.* **2000**, *39* (12), 2152-2155.
- ²³ (a) Alawode, O. E.; Robinson, C.; Rayat, S., Clean photodecomposition of 1-methyl-4-phenyl-1*H*-tetrazole-5(4*H*)-thiones to carbodiimides proceeds via a biradical. *The Journal of organic chemistry* **2011**, *76* (1), 216-22.; (b) Rayat, S.; Chhabra, R.; Alawode, O.; Gundugalo, A. S., Electronic properties of 1-methyl-4-phenyl-1*H*-tetrazole-5(4*H*)-thiones: An experimental and theoretical study. *J. Mol. Struct.* **2009**, *933* (1-3), 38-45.
- ²⁴ Tsuge, O.; Urano, S.; Oe, K., Reaction of trimethylsilyl azide with heterocumulenes. *J. Org. Chem.* **1980**, *45* (25), 5130-5136.
- ²⁵ Quast, H.; U., N., Photochemische Stickstoff-Eliminierung aus 1-Alkenyl-4-alkyl-1,4-dihydro-5*H*-tetrazol-5-onen und -thionen. Diaziridinone und Carbodiimide mit Alkenylsubstituenten. *Chemische Berichte* **1983**, *116* (10), 3427-3437.
- ²⁶ Dunkin, I. R.; Shields, C. J.; Quast, H., The photochemistry of 1,4-dihydro-5*H*-tetrazole derivatives isolated in low-temperature matrices. *Tetrahedron* **1989**, *45* (1), 259-268.
- ²⁷ Gomez-Zavaglia, A.; Reva, I. D.; Frija, L.; Cristiano, M. L.; Fausto, R., Molecular structure, vibrational spectra and photochemistry of 5-mercapto-1-methyltetrazole. *J. Mol. Struct.* **2006**, *786* (2-3), 182-192.

-
- ²⁸ Frija, L. M.; Ismael, A.; Cristiano, M. L., Photochemical transformations of tetrazole derivatives: applications in organic synthesis. *Molecules* **2010**, *15* (5), 3757-74.
- ²⁹ Bunce, N. J.; Lamarre, J.; Vaish, S. P., Photorearrangement of azoxybenzene to 2-hydroxyazobenzene: a convenient chemical actinometer. *Photochem. Photobiol.* **1984**, *39* (4), 531-533.
- ³⁰ General operating instructions for Ace photochemical U.V. power supplies and mercury vapor lamps. http://www.aceglass.com/dpro/attachment_files.php?id=119 (accessed 01/30/2012)
- ³¹ (a) Smith, M. B.; March, J., *Advanced Organic Chemistry: Reactions, Mechanism, and Structure*. 5th ed.; Wiley-Interscience: New York, **2001**.; (b) Hoyle, C. E.; Clark, S. C.; Viswanathan, K.; Jonsson, S., Laser flash photolysis of bismaleimides. *Photochem. Photobiol. Sci.* **2003**, *2*, 1074-1079.
- ³² Casey, C. P.; Boggs, R. A., Nonstereospecific formation of olefins in the Norrish type II photochemical cleavage of ketones from the singlet excited state. Evidence for a singlet diradical intermediate. *J. Am. Chem. Soc.* **1972**, *94* (18), 6457-6463.
- ³³ Bucher, G.; Mahajan, A. A.; Schmittel, M. Photochemical C²-C⁶ Cyclization of Enyne-Allenenes: Detection of a Fulvene Triplet Diradical in the Laser Flash Photolysis, *J. Org. Chem.* **2008**, *73*(22), 8815-8828.
- ³⁴ Breckenridge, W. H.; Taube, H., Some Reactions of Ground-State (3P) and Electronically Excited (1D) Sulfur Atoms. *J. Chem. Phys.* **1970**, *53*, 1750.
- ³⁵ Greenwood, N. N.; Earnshaw, A. *Chemistry of the Elements*, 2nd ed; Butterworth-Heinemann: Oxford, 1997.
- ³⁶ Murov, S. L.; Carmichael, I.; Hug, G. L., *Handbook of Photochemistry*, 2nd ed., Marcel Dekker, New York, 1993.

Chapter 3 - Synthesis of Phenanthridine-Fused Quinazolininium Salts from Heteroenyne-allenes

3.1 Introduction

An important class of *N*-heterocyclic moieties that appears in significant number of natural products are 4(3*H*)-quinazolinones **97** and their derivatives which demonstrate a wide range of pharmacological activities.^{1,2,3,4} Examples of natural products containing this scaffold are chrysogine **98** isolated from *Penicillium chrysogenum* and febrifugine **99** obtained from Chinese plant *Dichrofebrifuga*, both of which exhibit potent antimalarial activity,³ luotonine A **100** extracted from the Chinese plant *Peganum nigellastrum* acts as a Topoisomerase I inhibitor,^{3,5} and rutaecarpine **101** isolated from *Evodia rutaecarpa* is used extensively in Chinese medicine for headaches, and for the treatment of cholera and hypertension (Figure 3.1).^{3,6,7} In addition, many compounds containing quinazolinone scaffold possess a vast range of other biological activities such as antimicrobial, antibacterial, antifungal, antiviral, antidepressant, anti-inflammatory and diuretics.^{1,3,8,9,10} These are also known to act on central nervous system as stimulants, psychotropics, hypnotics and antianxiety drug.^{1,3,4,11,12} Therefore, quinazolinones and their derivatives are interesting structural scaffolds that are capable of interacting with multiple biological receptors and are thus, considered as privileged structures in drug discovery.¹

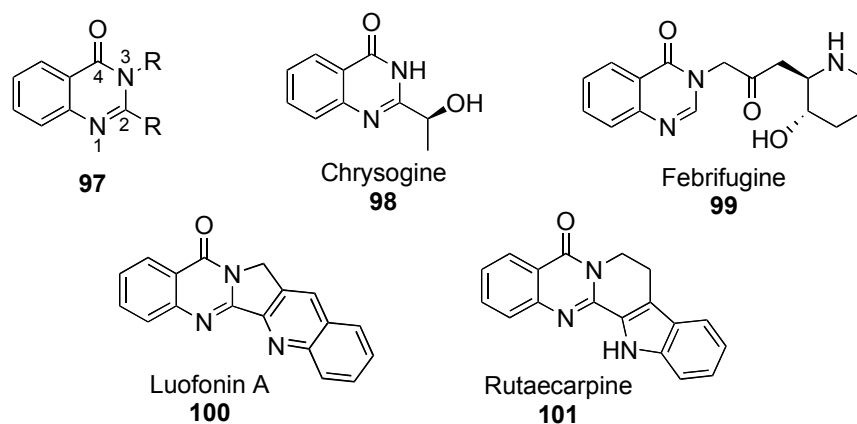


Figure 3.1: 4(3*H*)-Quinazolinones **98** and some biologically active natural products containing this scaffold.^{3,5,6,7}

4(3*H*)-Quinazolinimine **102** is a related heterocyclic scaffold that has not received as much attention in biology.^{10,13} For instance, heterocycles **103** – **105** containing this scaffold are known to exhibit cholinesterase inhibitory activity, and therefore, have been proposed for use in the treatment of Alzheimer's disease (Figure 3.2).^{14,15} Recently, our laboratory reported the antiproliferative activity of 2-halo-3-aryl-4(3*H*)-quinazoliniminium halides against leukemia (L1210) and breast cancer cell lines (SK-BR-3) and select data is shown in Table 3.1.¹⁶

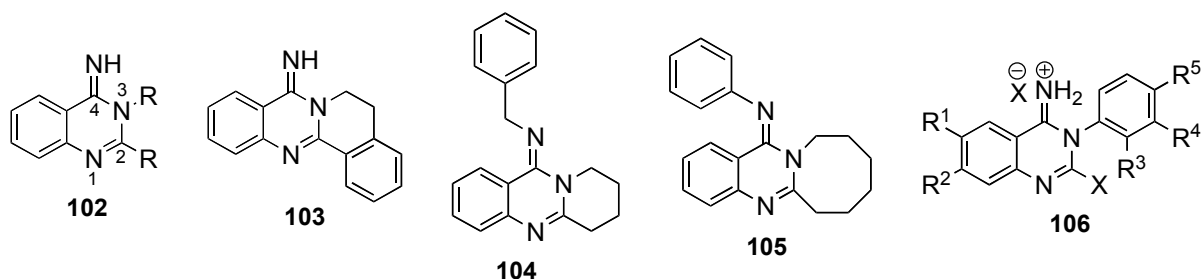


Figure 3.2: 4(3*H*)-quinazolinimine ring structure **102** and synthetic compounds containing this scaffold **104** – **106**.^{14,15,16}

Table 3.1: Antiproliferative activity of 2-Halo-3-aryl-4(3*H*)-quinazoliniminium halides **106** in L1210 and SK-BR-3 tumor cells *in vitro*.

| Compd. | X | R ¹ | R ² | R ³ | R ⁴ | R ⁵ | IC ₅₀ (μM) ^a in L1210 Cells ^b | IC ₅₀ (μM) ^a in SK-BR-3 Cells ^b |
|--------------|----|-----------------|-----------------|------------------|----------------|----------------|--|--|
| 106a | Cl | H | H | H | H | H | 3.4±0.3 | 3.5±0.3 |
| 106b | I | H | H | H | H | H | 3.6±0.2 | |
| 106c | Cl | H | H | OCH ₃ | H | H | 0.9±0.1 | 1.0±0.1 |
| 106d | Cl | H | H | Cl | H | H | 5.9±0.5 | 8.4±0.3 |
| 106e | Cl | CH ₃ | H | H | H | H | 4.8±0.2 | |
| 106f | Cl | H | CH ₃ | H | H | H | 5.3±0.2 | |
| Daunorubicin | | | | | | | 10.3 ± 0.2 nM | |
| Mitoxantrone | | | | | | | 0.6 ± 0.1 nM | |

^a mean standard derivation (n=3), ^b IC₅₀ reported at day 4

When compared to the known anticancer drugs such as daunorubicin and mitoxantrone, the 2-halo-3-aryl-4(3*H*)-quinazoliniminium halides **106** showed mediocre activity (Table 3.1), however, our results suggested that careful modification of the quinazoliniminium scaffold may provide more potent analogs. Since rigidification is an important tactic used in medicinal chemistry to increase efficacy and decrease side effects,^{17,18} one way to enhance the antiproliferative activity of quinazolinimines may be by increasing the structural rigidity through the construction of ring-fused quinazoliniminium scaffolds such as **107** (Figure 3.3).

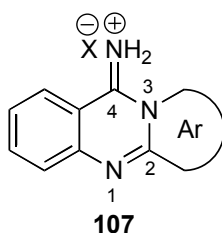
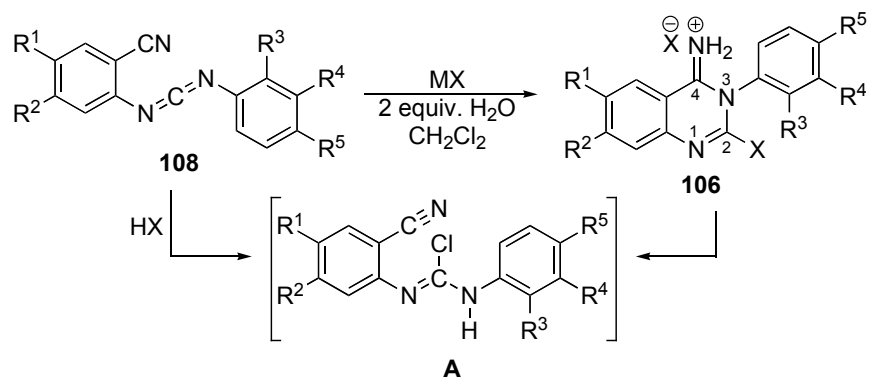


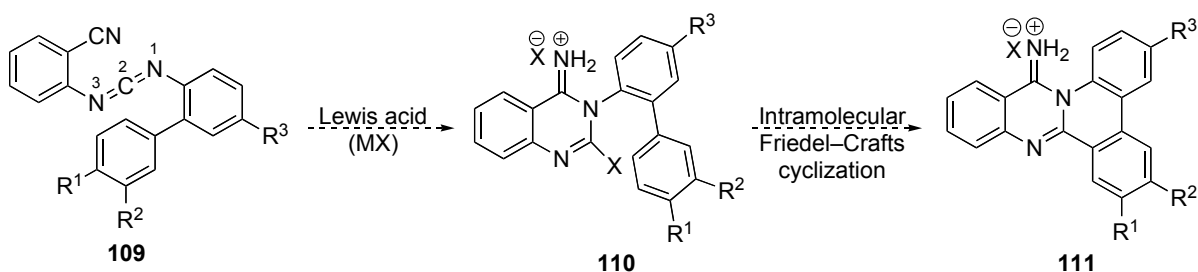
Figure 3.3: Quinazoliniminium ring structure in a rigid framework of fused heterocyclic rings.

Previously, we synthesized the 2-halo-3-aryl-4(3*H*)-quinazoliniminium halides **106** through the intramolecular cyclization of heteroenyne-allenes **108** in the presence of a hydrogen halide generated *in situ* from a Lewis acid and trace water (Scheme 3.1).¹⁹ The reaction is believed to involve the intermediacy of *N'*-(2-cyanophenyl)-*N*-phenylcarbamidic halides **A**. We envisaged that the presence of a halogen atom at C2 of the quinazoliniminiums **106** may provide the possibility to exploit this functionality into further chemistry, specifically, in an intramolecular Friedel-Crafts type reaction involving C2 and the aryl substituent at N3 to construct a rigid molecular framework of fused heterocyclic rings of the type shown in **107**.



Scheme 3.1: Formation of 2-halo-3-aryl-4(3*H*)-quinazoliniminium halides **106** from heteroenyne-allenes.¹⁹

Therefore, through a careful choice of the aryl group on the N1 of the heteroenyne-allenes *e.g.* a biphenyl, such as in **109**, we planned to construct a series of phenanthridine fused quinazoliniminiums **111** through cascade/tandem cyclization *via* 2-halo-3-biphenyl-4(3*H*)-quinazoliniminium halides **110** (Scheme 3.2).



Scheme 3.2: Cyclization reaction of heteroenyne-allenes **109** to produce series of phenanthridine fused quinazoliniminiums **111**.

Note that the phenanthridine cores **112** and **113** and their derivatives, especially the benzo[*c*]phenanthridine alkaloids have attracted considerable attention in medicinal chemistry,^{20,21,22} because of their antitumor, antimicrobial, antifungal, antimalarial and antiviral properties (Figure 3.4).^{23,24,25,26} For example, the natural product nitidine **114** exhibits antimalarial activity,^{23,27} lycorine **115** displays antiviral properties,^{22,28} whereas chelerythrine **116** and NK109 **117** both demonstrate potent antitumor activity.^{23,29,30} Furthermore, molecules containing these core motifs have also been reported to exhibit applications in material science especially in optoelectronic devices.^{31,32,33}

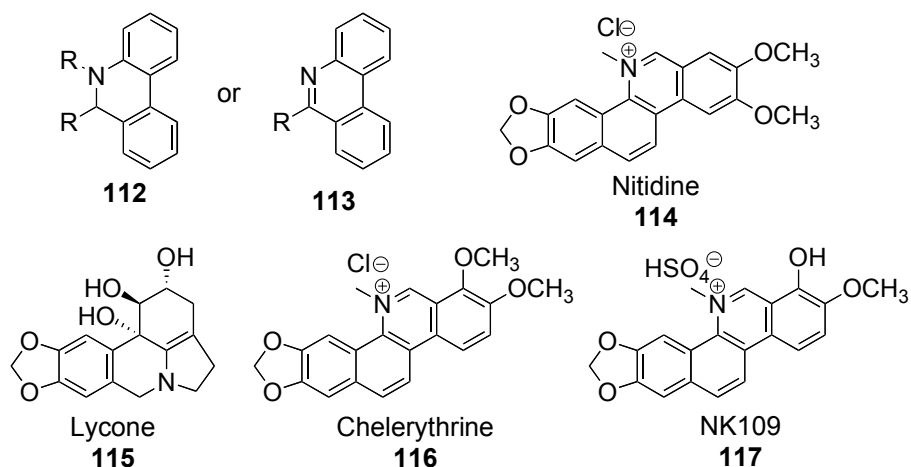


Figure 3.4: Phenanthridine core and biologically relevant benzo[*c*]phenanthridine natural products.^{22,26,27,29}

Since phenanthridine serves as a core structure in many drugs or drug-like molecules^{20,23} and a quinazolinimine moiety is also biologically active,¹⁶ we believe that the combination of these two heterocyclic cores in one molecule *e.g.* **111**, would increase the number of potential targets and therefore, produce more potent analogs (Figure 3.5). While a number of synthetic methods for the preparation of phenanthridine and quinazolinimine derivatives already exist, the phenanthridine-fused quinazolinimine (PNQ) molecular framework has not been previously constructed or reported.

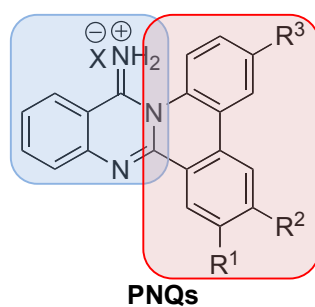


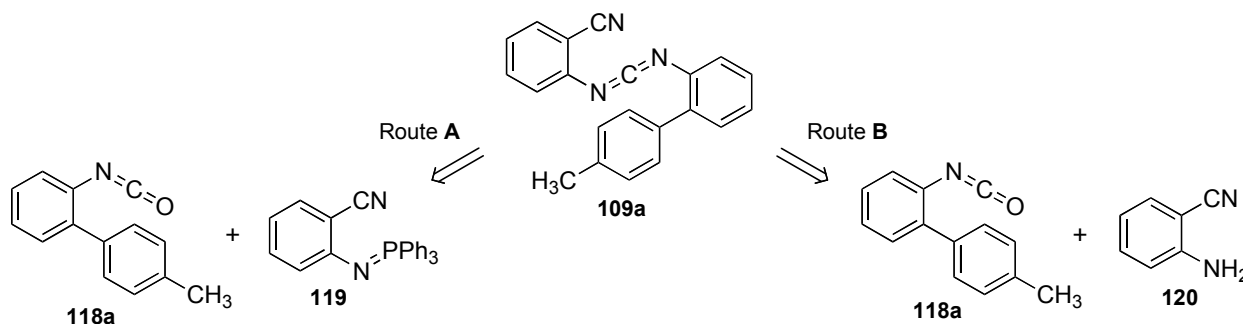
Figure 3.5: Phenanthridine-fused quinazolinimines (PNQs) **111**. Highlighted within the red and the blue box are quinazolinimine and phenanthridine moieties, respectively.

This chapter describes our work on the development of a quick, versatile and practical protocol for the synthesis of a series of novel phenanthridine-fused quinazolinimines (PNQs) **111**

from heteroenyne-allenes **109** via two sequential intramolecular cyclizations (also called cascade/tandem cyclization reaction, Scheme 3.2). Our initial investigations focused on streamlining the synthesis of the simplest derivative of the heteroenyne-allenes **109**, the 2-((4'-methylbiphenylimino)methyleneamino) benzonitrile (**109a**) ($R^1 = \text{CH}_3$; $R^2 = R^3 = \text{H}$) and finding the best reaction conditions for its cyclization to the corresponding PNQ **111a** ($R^1 = \text{CH}_3$; $R^2 = R^3 = \text{H}$). Note that the characterization of the cyclized product **111a** by NMR spectroscopy was not expected to be trivial because of the presence of heteroatoms and aromatic protons. We hoped that the presence of a methyl group on the biphenyl of **111a** and its relative position on the ring would aid in the identification of the cyclized product by NMR spectroscopy. The optimized reaction conditions from this initial study were then employed to obtain a series of heteroenyne allenes **109b** – **k** and corresponding PNQ derivatives **111b** – **k**, decorated with different electron donating and electron withdrawing substituents.

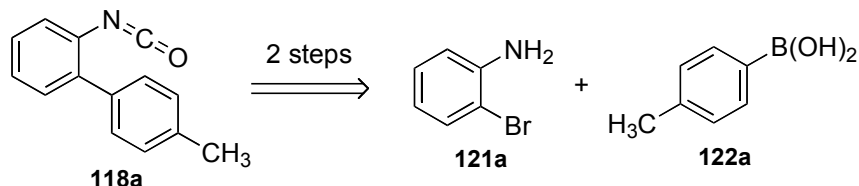
3.2 Retrosynthesis of 2-((4'-methylbiphenylimino)methyleneamino) benzonitrile **109a**

The ability to successfully synthesize heteroenyne-allene, 2-((4'-methylbiphenylimino)methyleneamino) benzonitrile **109a** was vital to the construction of the PNQ **111a**. We envisioned two possible routes (route **A** and **B**) to obtain this critical precursor that involved (1) the aza-Wittig-reaction of 4'-methyl-2-biphenyl isocyanate (**118a**) with iminophosphorane **119** to directly form the desired isocyanate **109a** or (2) the reaction of the isocyanate **118a** with anthranilonitrile (**120**) to afford the substituted urea followed by dehydration to the desired **109a** (Scheme 3.3).



Scheme 3.3: Retrosynthetic route showing precursors for the synthesis of heteroenyne-allenes **109a**.

The required isocyanates **118a** for routes **A** and **B** above would be obtained in two steps involving the Suzuki coupling of 2-bromoaniline (**121a**) with *p*-tolylboronic acid (**122a**) to produce the 2-aminobiphenyl followed by phosgenation reaction (Scheme 3.4).

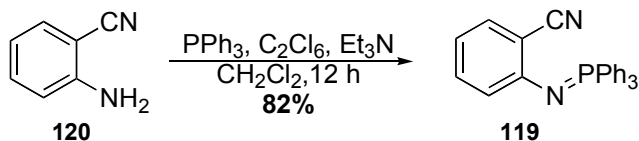


Scheme 3.4: Retrosynthetic route for the preparation of 4'-methyl-2-biphenyl isocyanate **118a**.

3.3 Synthesis of 2-((4'-methylbiphenylimino)methyleneamino) benzonitrile (**109a**)

3.3.1 Synthesis of aza-Wittig reagent **119**

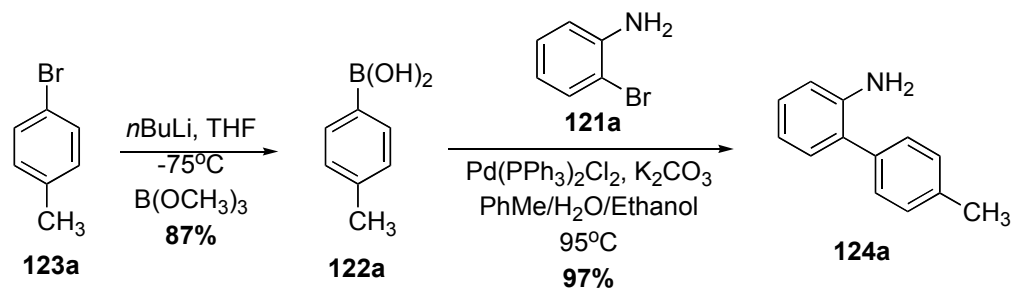
The reaction of anthranilonitrile (**120**) with triphenylphosphine in the presence of triethylamine and hexachloroethane in dry methylene chloride at room temperature gave the desired iminophosphorane **119** in good yields (Scheme 3.5).⁷



Scheme 3.5: Preparation of aza-Wittig reagent **119**.

3.3.2 Synthesis of 2-amino-4'-methylbiphenyl (**124a**)

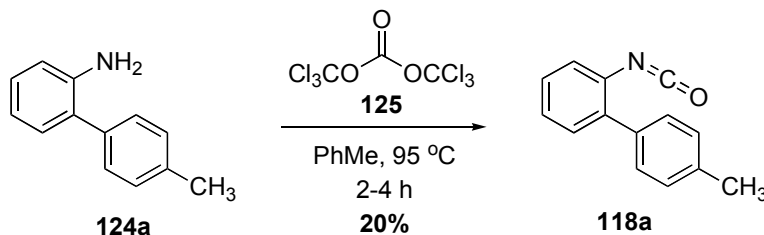
4-Bromotoluene (**123a**) was treated with *n*-butyllithium at -78 °C followed by reaction with trimethyl borate to provide the *p*-tolylboronic acid (**122a**).^{34,35} The latter was then coupled with 2-bromoaniline (**121a**) using Pd(PPh₃)₂Cl₂ catalyst under Suzuki reaction conditions to afford **124a** in excellent yields (Scheme 3.6).³⁶



Scheme 3.6: Synthesis of 2-amino-4'-methylbiphenyl (**124a**).^{34,35,36}

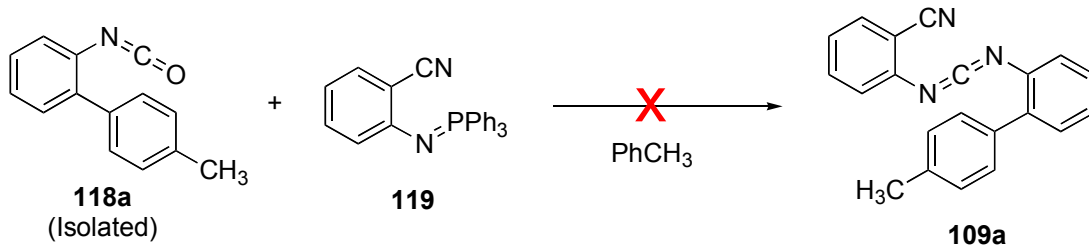
3.3.3 Synthesis of 4'-methyl-2-biphenyl isocyanate (**118a**) and attempts towards the synthesis of 2-((4'-methylbiphenylimino)methyleneamino) benzonitrile (**109a**)

Treatment of a toluene solution of **124a** with triphosgene (**125**) afforded a viscous oily residue,^{37,38} which was purified on a short silica gel column (Scheme 3.7). The IR analysis of the isolated product showed a strong peak at 2249 cm^{-1} corresponding to a NCO stretch. The formation of 4'-methyl-2-biphenyl isocyanate (**118a**) was further confirmed by NMR spectroscopy.



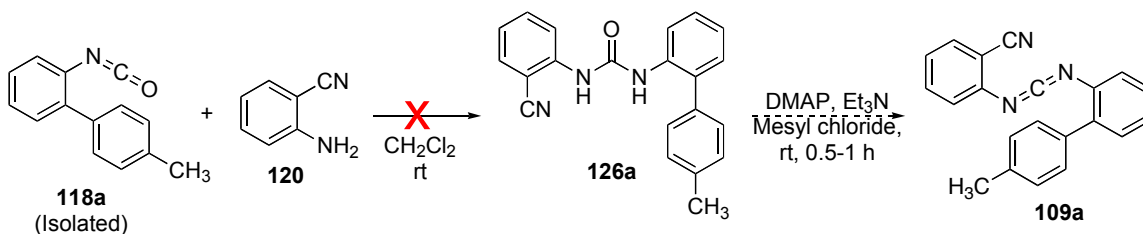
Scheme 3.7: Synthesis of 4'-methyl-2-biphenyl isocyanate (**118a**).

Next, we attempted the reaction of the obtained **118a** with the iminophosphorane **119** in dry toluene, to produce the desired 2-((4'-methylbiphenylimino)methyleneamino) benzonitrile (**109a**), however we were unsuccessful (Scheme 3.8).^{7,9a,39} Further attempts to synthesize the latter *via* the modification of the reaction condition by varying relative ratios of the reactants, at different temperatures or reaction times were similarly unsuccessful.



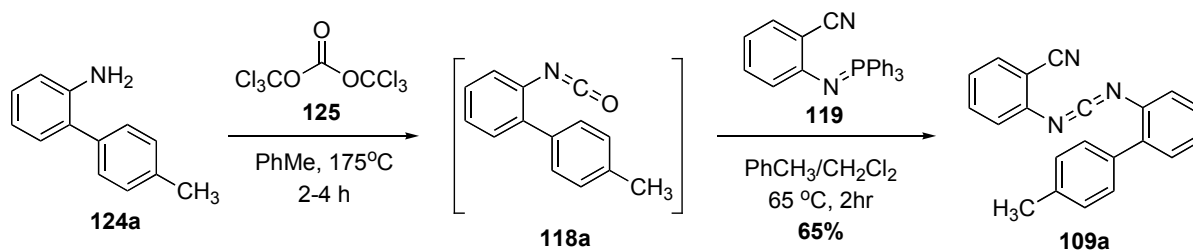
Scheme 3.8: Unsuccessful attempt to form **109a** via aza-Wittig reaction (Route A).

We also attempted to obtain **109a** through route **B** outlined in Scheme 3.3 that involved the reaction of the isolated isocyanate **118a** with anthranilonitrile (**120**) followed by its dehydration as shown in Scheme 3.9.⁴⁰ However, we failed to form the required urea **126a** in the first step. The inability to react **118a** with iminophosphorane **119** (Scheme 3.8) or anthranilonitrile **120** (Scheme 3.9) to form heteroenyne-allene **109a** or urea **126a**, respectively, prompted us to question the stability of the isolated **118a** as the latter are notorious for their instability and high reactivity. For instance, isocyanates are known to undergo spontaneous di- or trimerization after isolation, especially at temperature below 30 °C.^{41,42,43} To avoid these problems, in most literature investigation, the isocyanates have been freshly generated and used *in situ* for the next synthetic step.^{44,45} We also came across reports that indicated that polymerization of isocyanates can be reversed under high temperature.^{41a,46}



Scheme 3.9: Unsuccessful attempted to form **109a** involving the coupling of isocyanate with anthranilonitrile (Route **B**) (Dashed arrow indicate planned reaction that was not attempted).

Therefore, modified reaction conditions were employed during our next attempt that involved preparation of isocyanate **118a** at a much higher temperature (175 °C) and subsequently, reacting it with iminophosphorane **119** *in situ* (Scheme 3.10). To our delight, under these conditions the reaction afforded the much desired heteroenyne-allene **109a** in good yields.

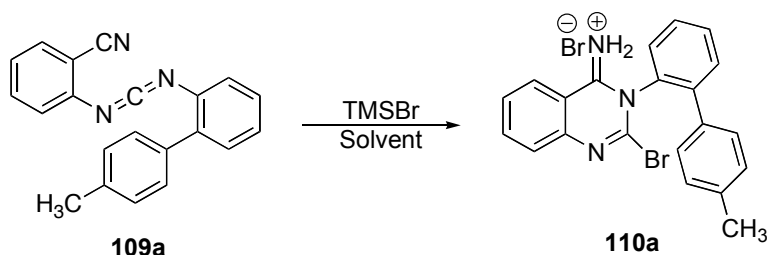


Scheme 3.10: Successful synthesis of heteroenyne-allene **109a** via route **A**.

3.4 Synthesis of 4'-methyl-phenanthridine-*N*-quinazoliniminium salt (**111a**)

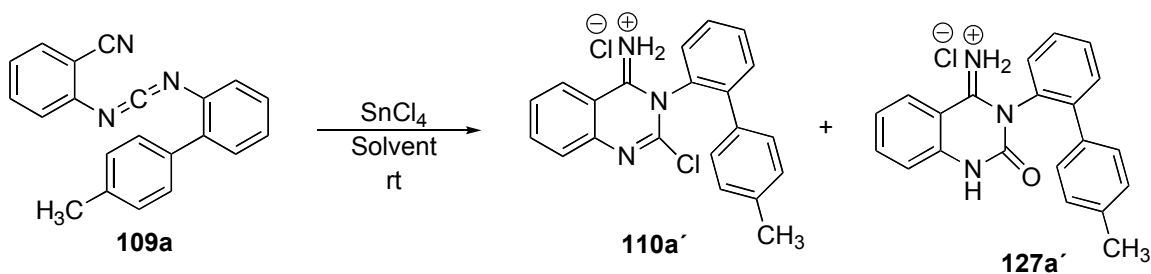
3.4.1 Attempts towards the synthesis of 4'-methyl-phenanthridine-*N*-quinazoliniminium salt **111a**

Our initial studies were aimed at screening a variety of Lewis acids that can promote cascade cyclization of heteroenyne-allene **109a** to the *N*-fused heterocycle **111a** in order to establish optimal reaction conditions. The influence of temperature and different solvents was also studied and the results are summarized in Table 3.2. In the presence of TMSBr, 2-bromo-3-(4'-methylbiphenyl-2-yl)-quinazolin-4(3*H*)iminium bromide (**110a**) was obtained when the reaction was performed either in CH₂Cl₂ or in 1,2-dichloroethane (Scheme 3.11; Table 3.1, entries 1 – 3). Note that conducting the reaction for longer time and at slightly elevated temperature (55 °C) for 72 h still led to the formation of **110a** (Table 3.1, entry 2).



Scheme 3.11: Formation of 2-bromo-3-(4'-methylbiphenyl-2-yl)-quinazolin-4(3*H*)iminium bromide (**110a**) from **109a** with TMSBr.

Similarly, the reaction carried out in the presence of TMSCl (Table 3.1, entry 4) afforded the corresponding chloride salt, 2-chloro-3-(4'-methylbiphenyl)-quinazolin-4(3*H*)iminium chloride **110a'**. However, reaction in the presence of TMSI and FeBr₃ resulted in the formation of a complex mixture of products that was not characterized (Table 3.1, entries 5 – 6). SnCl₄ was found to produce a mixture of **110a'** plus 3,4-dihydro-4-imino-3-(biaryl-2-yl)-quinazolin-2(1*H*)-one (**127a'**) (Scheme 3.12; Table 3.1, entry 7). The nucleophilic substitution of the chlorine atom at C2 of **110a'** by water likely resulted in the formation of **127a'**.



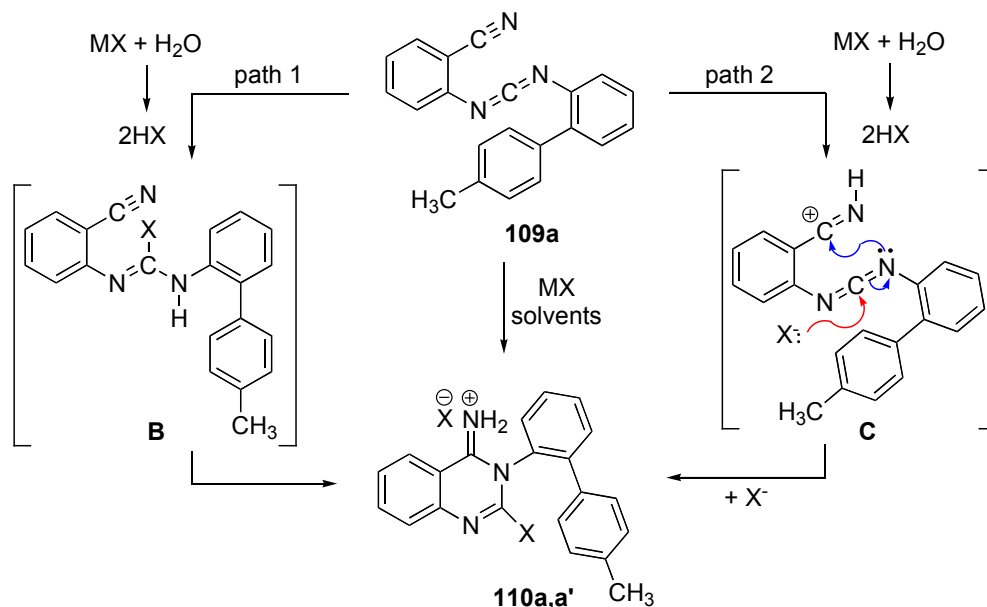
Scheme 3.12: Synthesis of 2-chloro-3-(4'-methylbiphenyl)-quinazolin-4(3*H*)iminium chloride (**110a'**) and compound **127a'** (' indicates a Cl⁻ counter ion).

Table 3.2: Lewis acid and reaction conditions screened for intramolecular cyclization of **109a**.

| Entry | Lewis acids ^a | Solvent | X ⁻ | Time [h] | Product (s) | Yield [%] |
|-----------|---------------------------------------|--------------------------------------|-----------------------|-----------------|----------------------|-----------|
| 1 | TMSBr | CH ₂ Cl ₂ | Br | 48 | 110a | 72 |
| 2 | TMSBr | CH ₂ Cl ₂ | Br | 72 ^b | 110a | 40 |
| 3 | TMSBr | ClCH ₂ CH ₂ Cl | Br | 48 | 110a | 42 |
| 4 | TMSCl | ClCH ₂ CH ₂ Cl | Cl | 47 | 110a' | 82 |
| 5 | TMSI | ClCH ₂ CH ₂ Cl | - | 36 | None ^c | - |
| 6 | FeBr ₃ | ClCH ₂ CH ₂ Cl | - | 48 | None ^c | - |
| 7 | SnCl ₄ | ClCH ₂ CH ₂ Cl | Cl | 48 | 110a' + 127a' | - |
| 8 | TMSCl | HMPA | - | 20 | 126a' | - |
| 9 | TMSCl | CH ₃ NO ₂ | Cl | 5 | 110a' | 76 |
| 10 | TiCl ₄ | CH ₃ NO ₂ | Cl | 10 | 110a' | 45 |
| 11 | CF ₃ SO ₄ Ag | CH ₃ NO ₂ | - | 36 | None ^c | - |
| 12 | BBr ₃ | CH ₃ NO ₂ | - | 12 | None ^c | - |
| 13 | BF₃.OEt₂ | CH₃NO₂ | BF₄ | 12 | 111 | 10 |

^a 3.0 equiv. was used, ^b refluxed at 55 °C, ^c complex mixture of products

The two possible mechanisms for the formation 2-halo-3-(4'-methylbiphenyl-2-yl)-quinazolin-4(3*H*)iminium halide salts (**110a,a'**) in the above reactions are shown in Scheme 3.14. Path **1** involves the initial formation of hydrogen halide HX (HCl/HBr) from the reaction of Lewis acid with the trace amounts of water in the solvent used. The addition reaction of HX to the heteroenyne-allene **109a** would furnish intermediate **B**, which would subsequently undergo cyclization to give compounds **110a,a'**. Another possible pathway, path **2**, may involve protonation of the nitrile group by the HX generated in the reaction to produce intermediate **C** followed by the attack of the halide ion at the heteroenyne-allene moiety and ring closure to form **110a,a'** (Scheme 3.14). The latter were initially characterized by two-dimensional NMR spectroscopy. Eventually, we were also able to obtain a crystal structure of **110a'**, which further supported the structural assignment (Figure 3.6).



Scheme 3.13: Possible reaction mechanism for the formation of **110a, a'** (MX = TMSBr, TMSCl, SnCl₄).

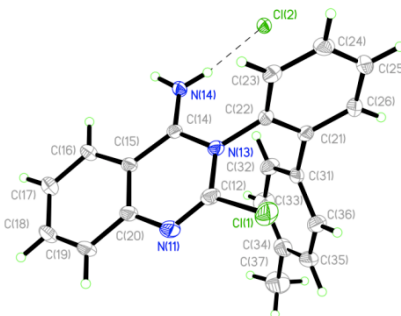
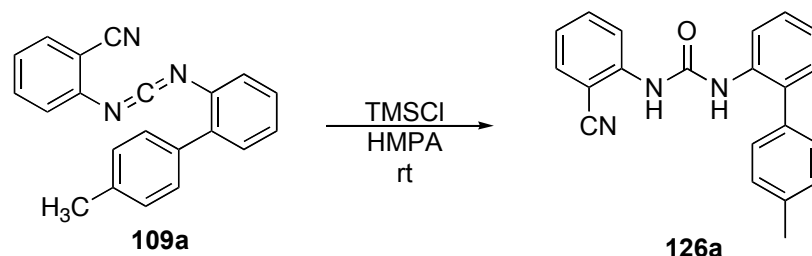


Figure 3.6: ORTEP diagram of **110a'**.

The failure to obtain the desired **111a, a'** above prompted us to revisit the reaction conditions and we noticed that in the above reactions, 2-halo-3-(4'-methylbiphenyl-2-yl)-quinazolin-4(3*H*)iminium halide salts (**110a, a'**) precipitated out of the solution (Table 3.2 entries 1 – 4, 7). Since this compound was expected to be an intermediate in the synthesis of PNQs (Scheme 3.2), we envisioned that the insolubility of **110a, a'** in the solvents used, may be preventing its Friedel Crafts intramolecular cyclization to the desired **111a, a'**. Hence, to increase the solubility of **110a, a'**, we decided to use more polar solvents, *e.g.* HMPA and nitromethane.

However, the reaction of **109a** in HMPA with TMSCl gave the hydrolyzed product **126a** (Scheme 3.13; Table 3.1, entry 8).



Scheme 3.14: Formation of 1-(2-cyanophenyl)-3-(4'-methylbiphenyl) urea **126a** from **109a** in TMSCl/HMPA.

A series of Lewis acids were screened in nitromethane. This solvent is also known to improve the acidity of the Lewis acids probably by solvation of the cationic intermediate.^{47,48} Unfortunately, when carbodiimide **109a** dissolved in nitromethane was reacted with TMSCl and the result still indicated the formation of the undesired product **110a'** (Table 3.2, entry 9). It is worth mentioning that the use of nitromethane as solvent showed a noticeable influence on the reaction rate resulting into reduced reaction times to form **110a'**, most likely, through the stabilization of the charged transition states/intermediates involved in the reaction (compare entries 4 and 9). Similar outcome was obtained when the reaction was performed in the presence of TiCl_4 where **110a'** was isolated (Table 3.2, entry 10). Reactions carried out in the presence of $\text{CF}_3\text{SO}_4\text{Ag}$ and BBr_3 both resulted in the formation of complex mixture of products that were not characterized (Table 3.2, entries 11 – 12). To our delight, the reaction of **109a** in with $\text{BF}_3 \cdot \text{OEt}_2$ in nitromethane furnished the desired PNQ **111a''**, albeit, in very low yield (10%) (Table 3.2, entry 13). The structure of **111a''** was first confirmed by a series of two-dimensional NMR spectroscopic experiments and finally, by single crystal X-ray analysis (Figure 3.7).

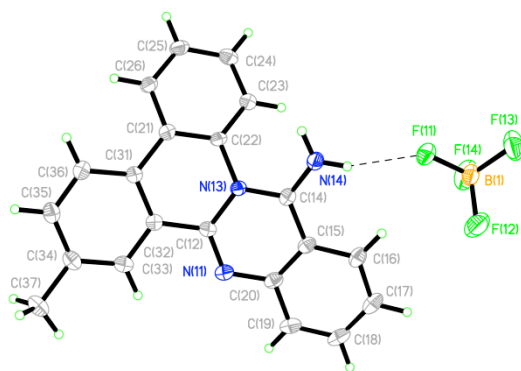
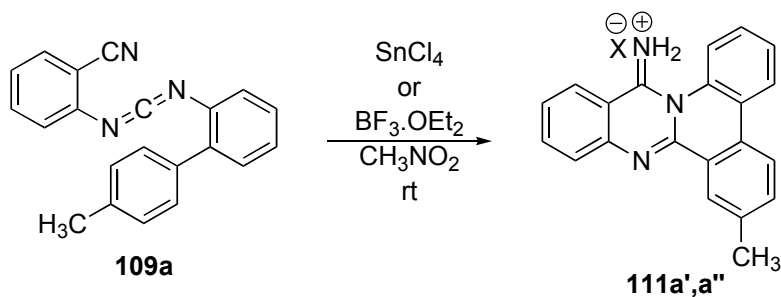


Figure 3.7: ORTEP diagram of *N*-heterocycle **111a''** ('' indicates a BF_4^- counter ion).

Our future efforts were focused on increasing the yield of **111a''** and determining the optimized reaction conditions. The general reaction is shown in Scheme 3.15 and results are summarized in Table 3.3. The reactions performed using different equivalents of $\text{BF}_3 \cdot \text{OEt}_2$ in reagent grade CH_3NO_2 ($\leq 0.05\%$ H_2O),⁴⁹ all afforded the desired cascade cyclized PNQ **111a''**, however in very low yields (Table 3.3, entries 1 – 3). We also investigated the reaction in the presence of a more powerful Lewis acid combination ($\text{BF}_3 \cdot \text{OEt}_2/\text{TMSOTf}$); but the results were not encouraging (Table 3.3, entry 4).

We noticed that, when the reaction was performed in dry and high-purity CH_3NO_2 ($\leq 0.005\%$ H_2O),⁵⁰ no product was observed even after extended reaction time (Table 3.3, entry 5), probably because trace amounts of water was necessary for the generation of required hydrogen halide and for the reaction to occur (Schemes 3.14 and 3.2).^{50,51} This premise was validated by adding 4 equivalents of water to the reaction mixture, which gave the expected product **111a''** with improved yields (27%) (Table 3.3, entry 6).



Scheme 3.15: Synthesis of ring-fused *N*-heterocyclic PNQ **111a',a''** (X= Cl^- or BF_4^- indicated by ' or '' , respectively).

Table 3.3: Optimization of reaction conditions for the synthesis of PNQ **111a'**,**a''**.

| Entry | Lewis acids | Equiv. | H ₂ O (equiv.) | X ⁻ | Time [h] | Yield [%] |
|-------|--|--------|------------------------------|-----------------|-------------|--------------|
| 1 | BF ₃ .OEt ₂ | 1.5 | trace | BF ₄ | 120 | 15 |
| 2 | BF ₃ .OEt ₂ | 3 | trace | BF ₄ | 12 | 10 |
| 3 | BF ₃ .OEt ₂ | 5 | trace | BF ₄ | 48 | 21 |
| 4 | BF ₃ .OEt ₂ /TMSOTf | 3:3 | trace | - | 48 | 15 |
| 5 | BF ₃ .OEt ₂ ^a | 3 | - | BF ₄ | 72 | None |
| 6 | BF ₃ .OEt ₂ | 3 | 4 | BF ₄ | 48 | 27 |
| 7 | BF ₃ .OEt ₂ | 4 | 4 | BF ₄ | 30 | 39 |
| 8 | SnCl ₄ | 4 | 4 | Cl | 24 | 44 |

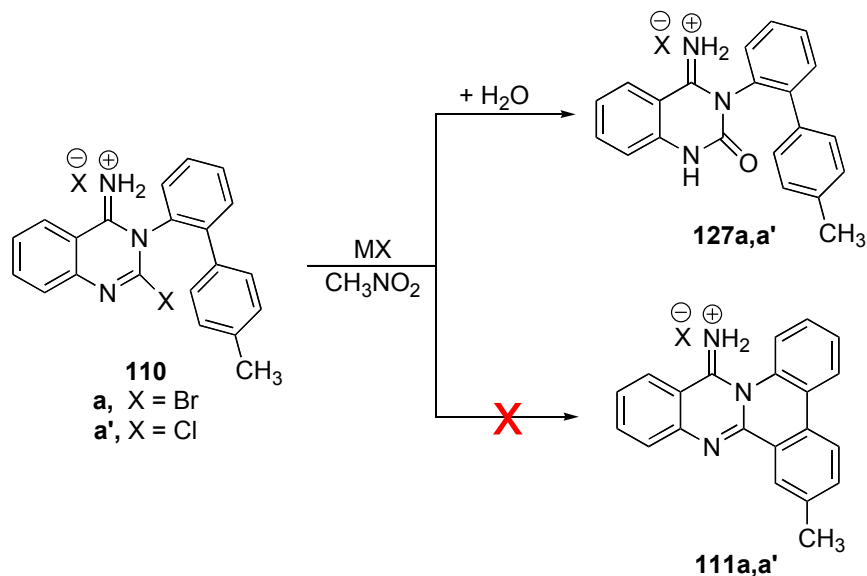
^a high-purity nitromethane was used.

A further increase in the yields of **111a''** (39%) was observed when the reaction was performed using slightly higher equivalents of BF₃.OEt₂ and 4 equivalents of water (Table 3.3, entry 7). Furthermore, we found that, SnCl₄ in the presence of 4 equivalents of water can also promote the formation of **111a'** (' indicates Cl⁻ counter ion) in marginally higher yields (44%) when compared to BF₃.OEt₂ (39%) (Table 3.3, entry 8).

3.4.2 Mechanistic investigations for the formation PNQs 111

As shown in Scheme 3.2, we expected 2-halo-3-(biphenyl-2-yl)-quinazolin-4(3*H*)iminium halides **110** to be intermediates during the cascade cyclization of heteroenyne-allenes **109** to PNQs **111**. To provide evidence in support of this hypothesis, we treated **110a** and **110a'** with stoichiometric amounts (5 equiv.) of two different Lewis acids (TMSBr or BF₃.OEt₂) under various reaction conditions. The results are summarized in Scheme 3.16 and Table 3.4. The reaction of **110a** at room temperature in the presence of TMSBr for prolonged reaction time failed and the unreacted starting material was recovered (Table 3.4, entry 1). However, the treatment of **110a** with TMSBr at elevated temperature yielded compound **127a** with no trace of the desired **111a** (Table 3.4, entry 2). The starting compound was recovered

when the reaction of **110a'** was conducted in the presence of TMSBr (Table 3.4, entry 3). Further reaction of **110a'** carried out in the presence of BF₃.OEt₂ alone or BF₃.OEt₂/water (Table 3.5, entries 4 and 5 respectively) led to the formation of **127a'**. We believe that the direct nucleophilic attack of a water molecule on **110a,a'** resulted in the formation of **127a,a'**.



Scheme 3.16: Treatment of **110a, a'** with Lewis acids.

Table 3.4: Mechanistic study to investigate possible conversion of **110** to *N*-heterocyclic PNQ **111**

| Entry | 110 | Lewis acids ^a | Solvent | Time [h] | Products | Yield [%] |
|-------|------------|--|---------------------------------|-----------------|-------------------|-----------|
| 1 | a | TMSBr | CH ₃ NO ₂ | 96 | None ^b | - |
| 2 | a | TMSBr | CH ₃ NO ₂ | 72 ^c | 127a | 10 |
| 3 | a' | TMSBr | CH ₃ NO ₂ | 48 | None ^b | - |
| 4 | a' | BF ₃ .OEt ₂ | CH ₃ NO ₂ | 48 | 127a' | 23 |
| 5 | a' | BF ₃ .OEt ₂ ^d | CH ₃ NO ₂ | 72 | 127a' | 29 |

^a 5 equiv. were used, ^b reactant was recovered ^c refluxed at 95 °C, ^d 4 equiv. H₂O

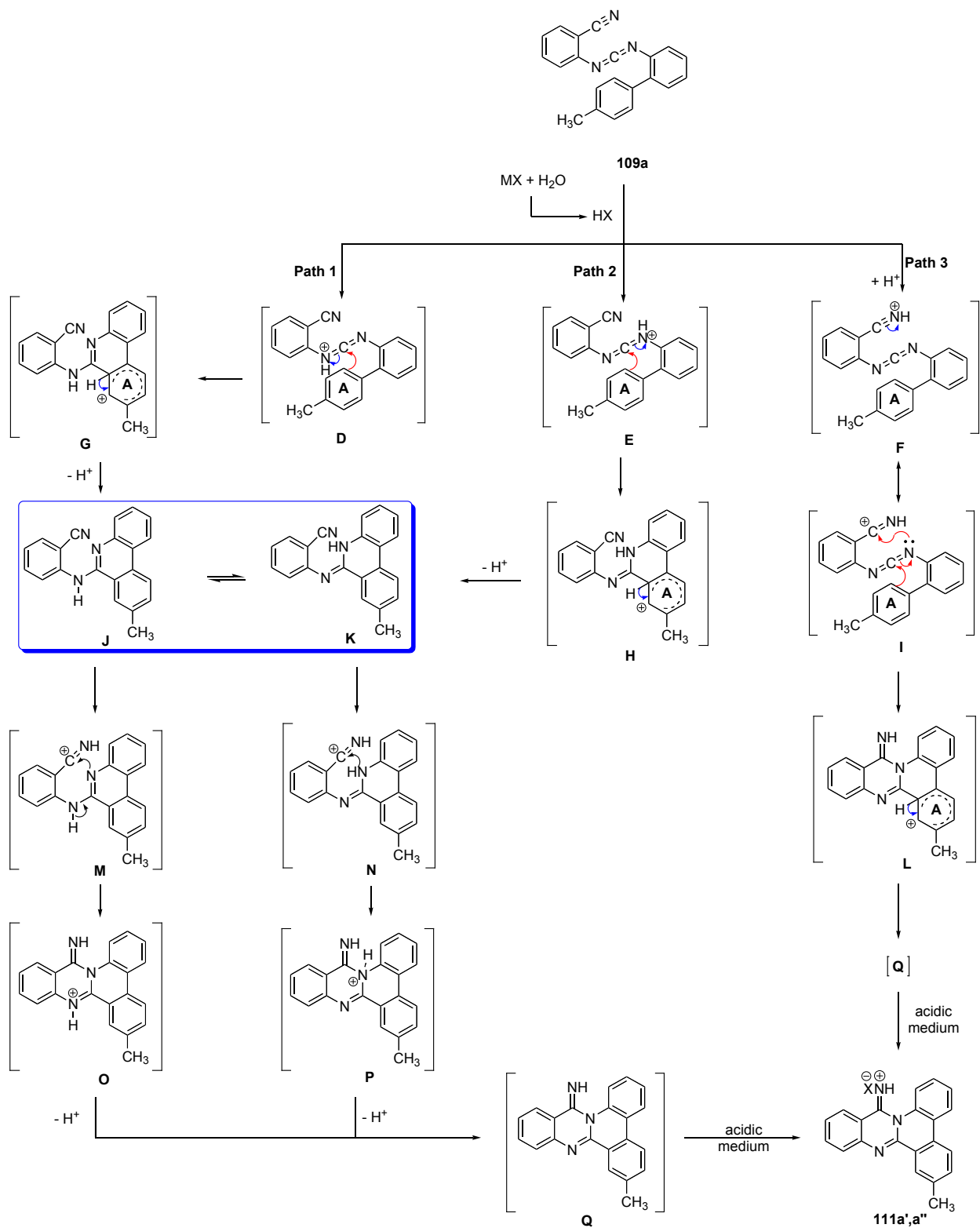
The failure to convert 2-halo-3-(biphenyl-2-yl)-quinazolin-4(3*H*)iminium halides **110a, a'** to the desired **111a, a'** evidently implies that the formation of **PNQs** does not proceed *via*

110a, a'. The three possible reaction mechanisms for the formation of **111** are shown in Scheme 3.17. In Path **1**, the heteroenyne-allene **109a** is protonated by trace amounts of acid generated *in situ* at N3 to give intermediate **D** which subsequently undergo electrophilic aromatic substitution to form a non-aromatic cyclohexadienyl cation intermediate **G**; also known as arenium ion. The removal of the proton from the latter would restore aromaticity and result in the formation of compound **J** that may tautomerize to compound **K**. Protonation of the cyano group in these tautomers would generate **M** and **N**, followed by nucleophilic attack from the nitrogen to generate intermediates **O** and **P**, respectively; which would subsequently, undergo loss of a proton to form the imine **Q**. The acidic medium of the reaction mixture will result in the formation of PNQ salt **111a', a''**.

Path **2** involves the protonation of the N1 of the heteroenyne-allenes **109** by the trace acid generated *in situ* to form intermediate **E**. Similarly, the latter would undergo electrophilic aromatic substitution to produce arenium ion, intermediate **H**; and the lose of proton from **H** would generate compound **K** that may tautomerize to compound **J** and result in the formation of **111a** as discussed above.

Path **3** involves the initial protonation of the cyano group of the heteroenyne-allenes **109a** by trace amounts of acid generated *in situ* to afford intermediate **F**, which will be in resonance with species **I**. This is followed by the nucleophilic attack at the electron deficient carbon by the N1 of heteroenyne-allenes that in turn activates the carbodiimide carbon towards nucleophilic attack from the biphenyl ring to produce arenium ion, intermediate **L**. Subsequently, the removal of the proton from the latter would yield imine **Q** followed by protonation to the desired ring-fused *N*-heterocycle PNQs **111**.

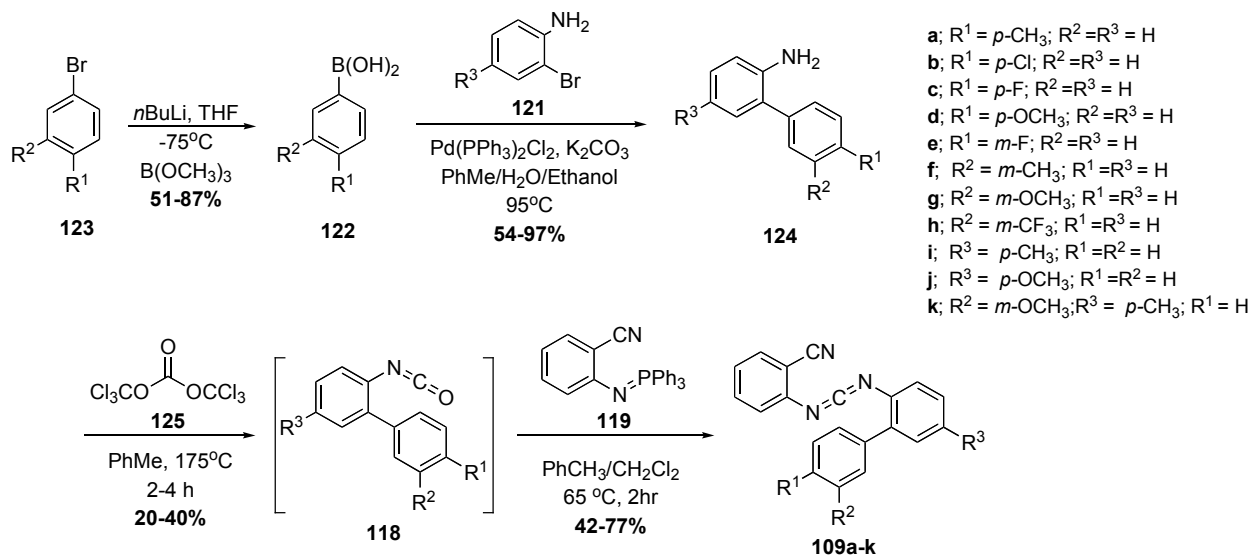
Note that the intermediates **J** and **K** formed during the proposed mechanistic pathways **1** and **2**, contain phenanthridine moieties that are known to be very stable. The stability of these rings would make it highly difficult for these to attack the carbon atom of protonated nitrile group, such as in intermediates **M** and/or **N** as that would involve destruction of the aromaticity in the phenanthridine moiety. To the best of our knowledge, we did not observe the formation of side products corresponding to **J** and/or **K**. Therefore, we strongly believe that the formation of PNQs **111** involve path 3.



Scheme 3.17: Plausible mechanism for $\text{SnCl}_4/\text{BF}_3 \cdot \text{OEt}_2$ promoted cascade reaction to produce ring-fused PNQ **111a**.

3.4.3 Scope of cascade cyclization reaction

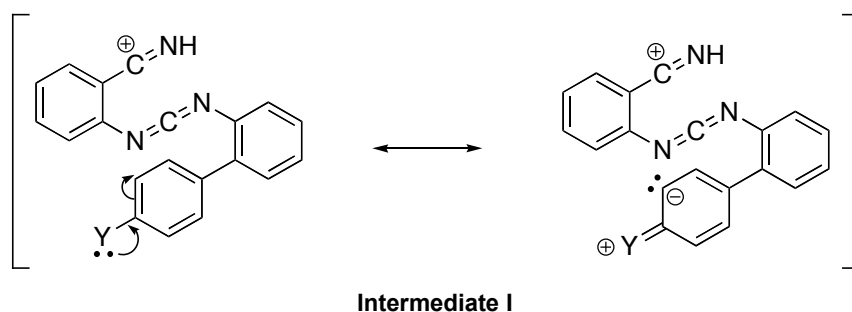
With the optimal reaction conditions in hand, the scope of this protocol was further explored with variously substituted heteroenyne-allenes **109b – k**. These were prepared as shown in Scheme 3.18. Briefly, substituted arylbromides **123** were converted to corresponding arylboronic acids **122** by lithiation followed by treatment with trimethyl borate (note that **122f** was purchased). **122** were subjected to Suzuki coupling with 2-bromoanilines **121a – c** to obtain biphenyl amines **124b – k**. Treatment of the latter with triphosgene generated the isocyanate **118b – k**, which was not isolated and reacted with iminophosphorane **119** *in situ* to yield the desired compounds **109b – k**.



Scheme 3.18: Synthesis of a series of PNQs **109a – k**.

As discussed above that the cascade cyclization of **109a** proceeded smoothly in the presence of SnCl₄ to afford **111a'** in moderate yields (Table 3.5, entry 1). However, when heteroenyne-allenes **109b – d** were reacted with SnCl₄ or BF₃.OEt₂, their cyclization to corresponding **111b – d** did not occur (Table 3.5, entries 2 – 7). It is conceivable that the fluoro, chloro and methoxy substituents destabilize the biphenyl ring towards electrophilic aromatic substitution because these substituents are *ortho/para* directing in electrophilic aromatic substitution.⁵² If the mechanism of cyclization involves path 3 as discussed above (Scheme 3.17), then intermediate **I** for **111b – d** is shown in Scheme 3.19. Note that the C-C bond formation to form the expected PNQs in **111b – d** need to occur *meta* to these substituents which

is difficult. Unfortunately, all the reactions of compound **109d** performed in the presence of SnCl₄ or BF₃.OEt₂ hydrolyzed the heteroenyne-allenes and produced the corresponding urea (**126d**) (Table 3.5, entries 6 – 7). In this case, the strong electron withdrawing inductive effect of the methoxy substituent appears to activate the heteroenyne-allene carbon toward nucleophilic attack by water to produce the corresponding urea.



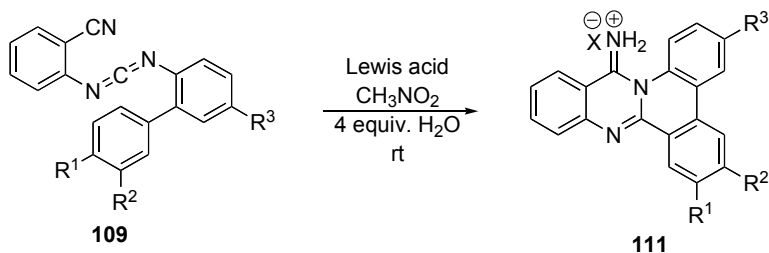
Scheme 3.19: Resonance structure of substituents (Y = Cl, F and OCH₃).

Initial reaction of **109e** with SnCl₄ led to the formation of trace amounts of product **111e'**, and when the same reaction was performed under prolonged reaction time the compound decomposed (Table 3.5, entry 8). Interestingly, when substrate **109e** was reacted with BF₃.OEt₂ the result gave the cascade *N*-heterocycle product **111e''** in moderate yields in less reaction time (Table 3.5, entry 9) compared to **111e'**. Furthermore, the reaction of SnCl₄ with compound **109f** afforded the desired *N*-heterocycle **111f'** in very good yield (Table 3.5, entry 10).

The reaction of **109g** in the presence of SnCl₄ resulted into the formation of mixture of products with trace amount of **111g'** (Table 3.4, entry 11). When the reaction was carried out using BF₃.OEt₂ and without adding any water, the ring-fused *N*-heterocyclic compound **111g''** was obtained in good yields (Table 3.4, entry 12). Reaction conducted in the presence of BF₃.OEt₂ and water only led to the formation of urea, the hydrolyzed form of **109g** (**126g**).⁵³

When R² was a CF₃ group, the reaction did not afford the desired products (Table 3.5, entries 13 – 14). Note that the strong electron withdrawing nature of the CF₃ is known to deactivate an aromatic ring toward electrophilic aromatic substitution and this effect is most pronounced at *ortho* and *para* positions. Unfortunately, the CF₃ in **109h** is located *para* to the position where C-C bond formation will have to occur, and thus, no **111h''** was observed.⁵²

Table 3.5: Scope of the reaction with cascade cyclization of cyano-ene-carbodiimide **109** to *N*-heterocyclic PNQs **111**.



| Entry | Compd. | Lewis acids | X ⁻ | Time [h] | R ¹ | R ² | R ³ | Yield [%] |
|-------|------------|--|-----------------|----------------|------------------|------------------|------------------|-----------------------------------|
| | 109 | | | | | | | |
| 1 | a | SnCl ₄ | Cl | 24 | CH ₃ | H | H | 111a' ; 44 |
| 2 | b | SnCl ₄ | - | - | Cl | H | H | None |
| 3 | b | BF ₃ .OEt ₂ | - | - | Cl | H | H | None |
| 4 | c | SnCl ₄ | - | - | F | H | H | None |
| 5 | c | BF ₃ .OEt ₂ | - | - | F | H | H | None |
| 6 | d | SnCl ₄ | - | - | OCH ₃ | H | H | None ^a |
| 7 | d | BF ₃ .OEt ₂ | - | - | OCH ₃ | H | H | None ^a |
| 8 | e | SnCl ₄ | Cl | 2 ^b | H | F | H | 111e' ; trace ^c |
| 9 | e | BF ₃ .OEt ₂ | BF ₄ | 5 | H | F | H | 111e'' ; 45 |
| 10 | f | SnCl ₄ | Cl | 30 | H | CH ₃ | H | 111f' ; 81 |
| 11 | g | SnCl ₄ | Cl | 6 | H | OCH ₃ | H | 111g' ; trace ^c |
| 12 | g | BF ₃ .OEt ₂ ^d | BF ₄ | 40 | H | OCH ₃ | H | 111g'' ; 51 |
| 13 | h | SnCl ₄ | - | - | H | CF ₃ | H | None |
| 14 | h | BF ₃ .OEt ₂ | - | - | H | CF ₃ | H | None |
| 15 | i | SnCl ₄ | Cl | 24 | H | H | CH ₃ | 111i' ; 79 |
| 16 | j | SnCl ₄ | - | - | H | H | OCH ₃ | None ^a |
| 17 | j | BF ₃ .OEt ₂ | - | - | H | H | OCH ₃ | None ^a |
| 18 | k | BF ₃ .OEt ₂ | BF ₄ | 12 | H | OCH ₃ | CH ₃ | 111k' ; 37 ^d |

^a hydrolyzed to the corresponding urea, ^b compound decomposed at prolonged reaction times, ^c mixture of products with trace amount of product observed, ^d no water was needed

Compound **111i'** was prepared in very good yield by reacting **109i** with SnCl₄ (Table 3.5, entry 15). The reaction of **109j** in the presence both SnCl₄ and BF₃.OEt₂ in water failed to yield the desired product but instead resulted in the formation of the hydrolyzed **126j** (Table 3.5, entries 16 – 17). The inability to produce the desired **111j** was probably due to the activation of carbon of the heteroenyne-allene **109j** via the inductive effect of the methoxy substituent towards nucleophilic attack. The reaction of **109k** with BF₃.OEt₂ in the presence of water produced the hydrolyzed product **126k**, however, the reaction in the absence of water afforded the ring-fused compound **111k''** in modest yields (Table 3.5, entry 18).⁵³

3.5 Conclusion

In summary, we have developed a concise, facile and a versatile protocol for the construction of a novel class of phenanthridine-fused quinazolinimines **111** from heteroenyne-allene **109** *via* SnCl₄/BF₃.OEt₂ mediated cascade intramolecular cyclization. The reaction conditions are compatible with most of the tested functional groups and effectively afforded the desired product **111** in moderate to excellent yields. Since the electrophilic aromatic substitution is a critical step in the formation of these N-fused heterocycles, the cyclization outcome is strongly dependent on the electronic nature of the substituents and their positioning on the biphenyl ring. Furthermore, this method can provide a new and useful strategy for designing quinazoline precursors. The investigation of the biological relevance of these novel nitrogen fused heterocycles compounds is in progress.

3.6 Experimental

Thin layer chromatography was carried out on 250 μm silica gel plates with a fluorescent indicator and UV-light was used as a visualizing agent. Standard column chromatography was performed using 63–200 μm silica gel. ¹H and ¹³C NMR spectra were recorded at ambient temperature using 400 MHz spectrometers. The carrier frequencies were 399.74 MHz (¹H) and 100.53 MHz (¹³C). The data were recorded as follows: chemical shifts in parts per million, coupling constants in Hertz, multiplicity (s = singlet, d = doublet, t = triplet, q = quartet, m = multiplet) and the number of integrate protons. The infrared spectroscopy frequencies are

reported in cm^{-1} . Low-resolution mass spectra (LRMS) were obtained on a mass spectrometer equipped with an electrospray ion source (ESI) operated in positive ion mode and connected to a triple quadrupole mass analyzer. High resolution mass spectra (HRMS) were acquired on a quadrupole/time-of-flight mass spectrometer. TOF scans were carried out in positive ionization mode. In most cases, both $[\text{M} + \text{H}]^+$ ions were detectable for each species.

3.7 Synthesis of Boronic Acids

3.7.1 General procedure for synthesis of arylboronic acids 122

3.7.2 General Procedure A

n-Butyllithium (2.5 M in hexane, 11 mmol) was added dropwise to a stirring solution of aryl bromide (10 mmol) in dry THF:toluene (1:2) at $-78\text{ }^{\circ}\text{C}$ under argon. The reaction mixture was stirred at $-78\text{ }^{\circ}\text{C}$ for a 1.5 h, and trimethyl borate (12 mmol) was added dropwise. The solution was stirred for an additional 1 h after which the reaction mixture was allowed to warm to room temperature and quenched with saturated NH_4Cl . The aqueous and organic layers were separated, and the aqueous layer was extracted with CH_2Cl_2 (3x30 mL). The organic layers were combined, dried (Na_2SO_4), filtered and concentrated under reduce pressure to give the crude solid. The obtained solid was recrystallized from acetonitrile to afford the corresponding arylboronic acids, which were characterized with proton NMR spectroscopy and the data was in agreement with that reported in literature.

3.7.3 General Procedure B

n-Butyllithium (2.5 M in hexane, 12 mmol) was added dropwise to a stirring solution of aryl bromide (10 mmol) in dry THF at $-78\text{ }^{\circ}\text{C}$ under argon. The solution was slightly warmed up to about $-20\text{ }^{\circ}\text{C}$ to allow thorough mixing of the lithium salts, then re-cooled to $-78\text{ }^{\circ}\text{C}$ and stirred further for a 1.5 h. Trimethyl borate (12.5 mmol) was added dropwise, after which the solution was stirred for an additional 1 h. Following this, the reaction mixture was warmed to room temperature and quenched with 2N HCl. The aqueous and organic layers were separated, and the aqueous layer was extracted with ethyl acetate (3x20 mL). The organic layers were combined, dried (MgSO_4), filtered and concentrated under reduce pressure to give a pale white solid. The obtained solid was recrystallized from ethyl acetate-hexane to afford the corresponding

arylboronic acids, which were characterized with proton NMR spectroscopy and the data was in agreement with that reported in literature.

3.7.4 *p*-Tolylboronic acid 122a

This compound was prepared by following general procedure B from 4-bromotoluene (29.20 mmol, 3.60 mL), in THF (50 mL). White solid (3.45 g, 87% yield). ^1H NMR (400MHz, CDCl_3): δ 2.46 (s, 3H), 7.32 (d, $J = 7.6\text{Hz}$, 2H), 8.14(d, $J = 8\text{Hz}$, 2H).

3.7.5 4-Chlorophenylboronic acid 122b

This compound was prepared by following general procedure A from 1-bromo-4-chlorobenzene (26.12 mmol, 5.00 g) in THF:PhCH₃ (20:40 mL). White solid (2.95 g, 72% yield). ^1H NMR (400MHz, DMSO- d_6): δ 7.43 (d, $J = 8$, 2H), 7.84 (d, $J = 8.4$, 2H).

3.7.6 4-Fluorophenylboronic acid 122c

This compound was prepared by following general procedure A from 1-bromo-4-fluorobenzene (34.29 mmol, 3.77 mL) in dry THF:PhCH₃ (25:50 mL). White solid (3.04 g, 63% yield). ^1H NMR (400MHz, DMSO- d_6): δ 7.17 (t, $J = 8$, 2H), 7.91 (t, $J = 6.6$, 2H).

3.7.7 4-Methoxyphenylboronic acid 122d

This compound was prepared by following general procedure B using 4-bromoanisole (26.73 mmol, 3.45 mL) in THF (50 mL). White solid (2.09 g, 51% yield). ^1H NMR (400MHz, CDCl_3): δ 3.90 (s, 3H), 7.03 (d, $J = 8.4\text{Hz}$, 2H), 8.14(d, $J = 8.8\text{Hz}$, 2H).

3.7.8 3-Fluorophenylboronic acid 122e

This compound was prepared by following general procedure A using 1-bromo-3-fluorobenzene (28.57 mmol, 3.19 mL) in dry THF:PhCH₃ (20:40 mL). White solid (2.79g, 70% yield). ^1H NMR (400MHz, DMSO- d_6): δ 7.20 (dt, $J_1 = 2.4\text{Hz}$, $J_2 = 8.8\text{Hz}$, 1H), 7.36-7.41 (m, 1H), 7.52 (dd, $J_1 = 2.4\text{ Hz}$, $J_2 = 10$, 1H), 7.61 (d, $J = 7.2\text{ Hz}$, 1H), 8.20 (br s, 2H).

3.7.9 3-Methylphenyl boronic acid 122f

Purchased from Sigma-Aldrich

3.7.10 3-Methoxyphenylboronic acid 122g

This compound was prepared by following general procedure B from 3-bromoanisole (21.40 mmol, 2.70 mL) in THF (30 mL). White solid (2.5 g, 78% yield). ^1H NMR (400MHz, DMSO- d_6): δ 3.74 (s, 3H), 6.93-6.97 (m, 1H), 7.25 (t, J = 8 Hz, 1H), 7.35-7.30 (m, 2H), 8.06 (br s, 2H).

3.7.11 3-(Trifluoromethyl)phenyl boronic acid 122h

This compound was prepared by following general procedure B from 3-bromo-(trifluoromethyl) benzene (8.90 mmol, 1.20 mL) in THF (30 mL). White solid (1.36g, 80% yield). ^1H NMR (400MHz, CDCl_3): δ 7.69 (t, J = 8Hz, 1H), 7.89 (d, J = 7.6Hz, 1H), 8.42-8.45 (m, 2H).

3.8 Synthesis of *n*-Tetrabutylammonium tribromide and 2-bromo-4-methoxyaniline

2-Bromoaniline (**121ä**) and 2-bromo-4methylaniline (**121i**) were commercially obtained from Aldrich. *n*-Tetrabutylammonium tribromide was initial prepared as indicated below, then reacted with 4-methoxyaniline to afford 2-bromo-4-methoxyaniline (procedure shown below).

3.8.1 Synthesis of *n*-Tetrabutylammonium tribromide

2.4 mL of bromine (7.44g, 46.98 mmol) was added via syringe to a stirring solution of *n*-tetrabutylammonium bromide (15.1 g, 47 mmol) dissolved in 100 mL methylene chloride. The color of the solution turned orange. The reaction mixture was allowed to stir for an additional 30 minute, and then poured into a flask containing 300 mL ether that caused the product to crystallize. The product was filtered and dried *in vacuum*, to afford an orange crystalline solid (22.12 g, 98%). m.p = 70–73 °C (lit. m.p = 72-76 °C)

3.8.2 Synthesis of 2-Bromo-4-methoxyaniline 121j

n-Tetrabutylammonium tribromide prepared above (9.68g, 20.1 mmol) was added in one portion into a round bottom flask containing *p*-anisidine (2.47 g, 20.1 mmol) dissolved in methanol (40 mL) and CH_2Cl_2 (80 mL). The reaction mixture was stirred at 25 °C for 35 minutes, then diluted with 100 mL of saturated aqueous Na_2SO_3 and 100 mL of CH_2Cl_2 . Using separatory funnel, the organic layer was collected then washed with water (2 x 100 mL) and

brine (100 mL). The organic layer was dried over MgSO₄, filtered through a plug of silica and concentrated under reduced pressure. The crude compound was purified by silica gel column chromatography (95:5, hexane/EtOAc) to produce **121c** as a brown oil (1.47g, 36%). $R_f = 0.58$ (8:2, hexane/EtOAc); IR (ZnSe ATR crystal; neat, cm⁻¹): 3435, 3358, 2831, 1598, 1573, 1493, 1272, 1227, 1210, 1024, 837, 806. ¹H NMR (400 MHz, CDCl₃): δ 3.74-3.79 (m, 5H), 6.73-6.74 (m, 2H), 7.02 (dd, $J_1 = 0.4$ Hz, $J_2 = 2.4$ Hz); ¹³C NMR (100 MHz, CDCl₃): δ 56.1, 109.8, 115.2, 116.8, 117.7, 138.1, 152.9.

3.9 Synthesis of 2-Aminobiphenyls 124

3.9.1 General procedure for synthesis of 2-Aminobiphenyls 124

In a 100 mL round bottom flask, 2-bromoaniline (8.72 mmol), phenylboronic acids (11.34 mmol), K₂CO₃ (34.88 mmol) and Pd(PPh₃)₂Cl₂ (0.69 mmol) were dissolved in toluene (30 mL), water (20 mL) and ethanol (10 mL); then stirred for 18 – 24 h at 95 °C. After cooling, the reaction mixture was diluted with 100 mL of saturated aqueous NH₄Cl and extracted with 100 mL of CH₂Cl₂ (3x). The combine organic layers were dried over Na₂SO₃, filtered and concentrated under reduced pressure. The crude product was purified by silica gel column chromatography to give the corresponding products.

3.9.2 2-Amino-4'-methylbiphenyl 124a

The general procedure was followed by reacting 4-methylphenylboronic acid **122a** (11.34 mmol) with 2-bromoaniline **121ä** (8.72 mmol). Purification by column chromatography on silica gel using a gradient eluent of 5% EtOAc in hexane afforded **124a** as a clear oil (1.55 g, 97%), $R_f = 0.47$ (8:2, hexane/EtOAc). IR (ZnSe ATR crystal; neat, cm⁻¹): 3460, 3376, 3021, 2918, 1612, 1514, 1487, 1448, 1293, 1004, 818; ¹H NMR (400MHz, CDCl₃): δ 2.46 (s, 3H), 3.80 (s, 2H), 6.81 (dd, $J_1 = 7.6$ Hz, $J_2 = 0.8$ Hz, 1H), 6.87 (dt, $J_1 = 7.6$ Hz, $J_2 = 1.2$ Hz, 1H), 7.17-7.22 (m, 2H), 7.31 (d, $J = 8$ Hz, 2H), 7.40-7.42 (m, 2H); ¹³C NMR (100 MHz, CDCl₃): δ 21.4, 115.7, 118.8, 127.7, 128.5, 129.1, 129.7, 130.6, 136.7, 137.0, 143.7.

3.9.3 2-Amino-4'-chlorobiphenyl 124b

The general procedure was followed by reacting 4-chlorophenylboronic acid **122b** (12.09 mmol) with 2-bromoaniline **121ä** (9.30 mmol). Purification by column chromatography on silica

gel using a gradient eluent of 6% EtOAc in hexane afforded **124b** as a waxy pale white solid (1.48 g, 78%), $R_f = 0.50$ (9:1, hexane/EtOAc). IR (ZnSe ATR crystal; neat, cm^{-1}): 3480, 3382, 1611, 1478, 1451, 1291, 1087, 1002, 823, 743; ^1H NMR (400MHz, CDCl_3): δ 3.74 (s, 3H), 6.78 (dd, $J_1 = 8\text{Hz}$, $J_2 = 1.2\text{Hz}$, 1H), 6.85 (dt, $J_1 = 7.6\text{Hz}$, $J_2 = 1.2\text{Hz}$, 1H), 7.12 (dd, $J_1 = 7.6\text{Hz}$, $J_2 = 1.6\text{Hz}$, 1H), 7.17-7.21 (m, 1H), 7.42-7.44 (m, 4H); ^{13}C NMR (100 MHz, CDCl_3): δ 21.4, 115.9, 118.9, 126.5, 129.0, 129.2, 130.5, 130.6, 133.3, 138.1, 143.61.

3.9.4 2-Amino-4'-fluorobiphenyl **124c**

The general procedure was followed by reacting 4-fluorophenylboronic acid **122c** (12.56 mmol) with 2-bromoaniline **121ä** (10.46 mmol). Purification by column chromatography on silica gel using a gradient eluent of 5% EtOAc in hexane afforded **124c** as a waxy pale white solid (1.58 g, 81%), $R_f = 0.47$ (9:1, hexane/EtOAc). IR (ZnSe ATR crystal; neat, cm^{-1}): 3466, 3378, 2993, 1613, 1509, 1484, 1449, 1291, 1211, 1155, 831, 807, 747; ^1H NMR (400MHz, CDCl_3): δ 3.73 (s, 2H), 6.79 (dd, $J_1 = 8\text{Hz}$, $J_2 = 1.2\text{ Hz}$, 1H), 6.85 (dt, $J_1 = 8\text{Hz}$, $J_2 = 4\text{Hz}$, 1H), 7.11-7.21 (m, 4H), 7.42-7.46 (m, 2H); ^{13}C NMR (100 MHz, CDCl_3): δ 115.8, 115.9 (d, $J_{\text{CF}} = 21\text{Hz}$), 118.9, 126.8, 128.8, 130.8 (d, $J_{\text{CF}} = 33\text{Hz}$), 130.9, 135.6 (d, $J_{\text{CF}} = 3\text{Hz}$), 143.7, 162.22 ($J_{\text{CF}} = 246\text{Hz}$).

3.9.5 2-Amino-4'-methoxybiphenyl **124d**

The general procedure was followed by reacting 4-methoxyphenylboronic acid **122d** (9.90 mmol) with 2-bromoaniline **121ä** (7.07 mmol). Purification by column chromatography on silica gel using a gradient eluent of 6% EtOAc in hexane afforded **124d** as a brown oil (1.16 g, 82%), $R_f = 0.55$ (8:2, hexane/EtOAc). IR (ZnSe ATR crystal; neat, cm^{-1}): 3444, 3369, 2957, 1610, 1512, 1487, 1451, 1289, 1238, 1175, 1029, 828, 747; ^1H NMR (400MHz, CDCl_3): δ 3.76 (s, 2H), 3.87 (s, 3H), 6.78 (dd, $J_1 = 8\text{Hz}$, $J_2 = 0.8\text{Hz}$, 1H), 6.83 (dt, $J_1 = 7.6\text{Hz}$, $J_2 = 1.2\text{Hz}$, 1H), 6.98-7.02 (m, 2H), 7.12-7.18 (m, 2H), 7.39-7.42 (m, 2H); ^{13}C NMR (100 MHz, CDCl_3): δ 55.5, 114.4, 115.7, 118.8, 127.5, 128.37, 130.4, 130.7, 131.9, 143.8, 158.9.

3.9.6 2-Amino-3'-fluorobiphenyl **124e**

The general procedure was followed by reacting 3-fluorophenylboronic acid **122e** (15.12 mmol) with 2-bromoaniline **121ä** (11.63 mmol). Purification by column chromatography on silica gel using a gradient eluent of 4% EtOAc in hexane afforded **124e** as a light yellow oil

(1.72 g, 79%), $R_f = 0.44$ (9:1, hexane/EtOAc). IR (ZnSe ATR crystal; neat, cm^{-1}): 3451, 3360, 3035, 1732, 1611, 1582, 1475, 1423, 1291, 1266, 1180, 1155, 879, 747; ^1H NMR (400MHz, CDCl_3): δ 3.75 (br s, 2H), 6.76 (dd, $J_1 = 7.6\text{Hz}$, $J_2 = 1\text{Hz}$, 1H), 6.82 (dt, $J_1 = 7.2\text{Hz}$, $J_2 = 1\text{Hz}$, 1H), 7.03 (ddt, $J_1 = 8.4\text{Hz}$, $J_2 = 2.8\text{Hz}$, $J_3 = 0.8\text{Hz}$, 1H), 7.14 (dd, $J_1 = 7.6\text{Hz}$, $J_2 = 1.6\text{Hz}$, 1H), 7.13-7.19 (m, 2H), 7.23-7.25 (m, 1H), 7.37-7.43 (m, 1H); ^{13}C NMR (100 MHz, CDCl_3): δ 114 (d, $J_{\text{CF}} = 21\text{Hz}$), 115.95, 116.25 (d, $J_{\text{CF}} = 20\text{Hz}$), 119, 125 (d, $J_{\text{CF}} = 3\text{Hz}$), 126 (d, $J_{\text{CF}} = 2\text{Hz}$), 129.13, 130.50 (d, $J_{\text{CF}} = 9\text{Hz}$), 130.51, 142 (d, $J_{\text{CF}} = 7\text{Hz}$), 144, 163 (d, $J_{\text{CF}} = 246\text{Hz}$).

3.9.7 2-Amino-3'-methylbiphenyl 124f

The general procedure was followed by reacting commercially obtained 3-methylphenylboronic acid (13.95 mmol) with 2-bromoaniline **121a** (11.63 mmol). Purification by column chromatography on silica gel using a gradient eluent of 5% EtOAc in hexane afforded **124f** as a light beige oil (1.75 g, 82%), $R_f = 0.35$ (9.5:0.5, hexane/EtOAc). IR (ZnSe ATR crystal; neat, cm^{-1}): 3452, 3371, 3026, 1611, 1478, 1447, 1294, 1156, 869, 787, 742; ^1H NMR (400MHz, CDCl_3): δ 2.46 (s, 3H), 3.78 (s, 2H), 6.80 (dd, $J_1 = 0.8\text{Hz}$, $J_2 = 8\text{Hz}$, 1H), 6.87 (dt, $J_1 = 7.6\text{Hz}$, $J_2 = 0.8\text{Hz}$, 1H), 7.17-7.22 (m, 3H), 7.29-7.32 (m, 2H), 7.39 (t, $J = 7.6\text{Hz}$, 1H); ^{13}C NMR (100 MHz, CDCl_3): δ 21.7, 115.7, 118.7, 126.2, 127.9, 128.1, 128.5, 128.9, 130.0, 130.6, 138.6, 139.6, 143.7.

3.9.8 2-Amino-3'-methoxybiphenyl 124g

The general procedure was followed by reacting 3-methoxyphenylboronic acid **122g** (8.09 mmol) with 2-bromoaniline **121a** (6.22 mmol). Purification by column chromatography on silica gel using a gradient eluent of 6% EtOAc in hexane afforded **124g** as a brown oil (1.11 g, 89%), $R_f = 0.38$ (8:2, hexane/EtOAc). IR (ZnSe ATR crystal; neat, cm^{-1}): 3467, 3371, 2956, 2833, 1601, 1498, 1477, 1454, 1418, 1290, 1208, 1175, 1036, 1016, 745; ^1H NMR (400MHz, CDCl_3): δ 3.82-3.85 (s, 5H), 6.78 (dd, $J_1 = 8\text{Hz}$, $J_2 = 0.8\text{Hz}$, 1H), 6.84 (dt, $J_1 = 7.6\text{Hz}$, $J_2 = 1.2\text{Hz}$, 1H), 6.92 (dd, $J_1 = 8\text{Hz}$, $J_2 = 0.8\text{Hz}$, 1H), 7.01-7.03 (m, 1H), 7.07 (td, $J_1 = 7.6\text{Hz}$, $J_2 = 1.2\text{Hz}$, 1H), 7.15-7.20 (m, 2H), 7.38 ($J = 8\text{Hz}$, 1H); ^{13}C NMR (100 MHz, CDCl_3): δ 55.5, 113.1, 114.6, 115.8, 118.7, 121.6, 127.6, 128.7, 130.0, 130.5, 141.1, 143.7, 160.1.

3.9.9 2-Amino-3'-trifluoromethylbiphenyl 124h

The general procedure was followed by reacting 3-(trifluoromethyl)phenyl boronic acid **122h** (14.11 mmol) with 2-bromoaniline **121ä** (10.85 mmol). Purification by column chromatography on silica gel using a gradient eluent of 4% EtOAc in hexane afforded **124h** as a light brown oil (1.52 g, 59%), $R_f = 0.42$ (8.2 hexane/EtOAc). IR (ZnSe ATR crystal; neat, cm^{-1}): 3465, 3376, 3037, 1615, 1500, 1483, 1425, 1331, 1257, 1159, 1117, 1072, 805, 744; ^1H NMR (400MHz, CDCl_3): δ 3.74 (s, 2H), 6.81 (dd, $J_1 = 8\text{Hz}$, $J_2 = 0.8\text{Hz}$, 1H), 6.87 (dt, $J_1 = 7.6\text{Hz}$, $J_2 = 1.2\text{Hz}$, 1H), 7.14 (dd, $J_1 = 7.6\text{Hz}$, $J_2 = 1.6\text{Hz}$, 1H), 7.20-7.24 (m, 1H), 7.56-7.64 (m, 2H), 7.68 (d, 7.6Hz, 1H), 7.76 (s, 1H). ^{13}C NMR (100 MHz, CDCl_3): δ 116, 119, 124.2 (q, $J_{\text{CF}} = 4\text{Hz}$), 124.3 (q, $J_{\text{CF}} = 271\text{Hz}$), 126.1 (t, $J_{\text{CF}} = 4\text{Hz}$), 126.2, 129, 130, 131, 131.4 (q, $J_{\text{CF}} = 32\text{Hz}$), 132.7 (d, $J_{\text{CF}} = 2\text{Hz}$), 141, 144.

3.9.10 2-Amino-4-methylbiphenyl 124i

The general procedure was followed by reacting 2-bromo-4-methylaniline **121i** (10.75 mmol) with commercially obtained phenylboronic acid (11.82 mmol). Purification by column chromatography on silica gel using a gradient eluent of 6% EtOAc in hexane afforded **124i** as a light yellow solid (1.61 g, 82%), $R_f = 0.48$ (8:2, hexane/EtOAc). IR (ZnSe ATR crystal; neat, cm^{-1}): 3419, 3345, 2970, 1617, 1502, 1487, 1440, 1244, 818, 765, 734; ^1H NMR (400MHz, CDCl_3): δ 2.32 (s, 3H), 3.66 (s, 2H), 6.72 (d, $J = 8\text{Hz}$, 1H), 7.00-7.03 (m, 2H), 7.35-7.39 (m, 1H), 7.45-7.51 (m, 4H); ^{13}C NMR (100 MHz, CDCl_3): δ 20.6, 116.0, 127.3, 127.9, 128.0, 128.9, 129.2, 129.3, 131.2, 139.9, 141.2.

3.9.11 2-Amino-4-methoxybiphenyl 124j

The general procedure was followed by reacting 2-bromo-4-methoxyaniline **121j** (9.90 mmol) with commercially obtained phenylboronic acid (10.89 mmol). Purification by column chromatography on silica gel using a gradient eluent of 7% EtOAc in hexane afforded **124j** as a brown oil (1.74 g, 88%), $R_f = 0.44$ (8:2, hexane/EtOAc). IR (ZnSe ATR crystal; neat, cm^{-1}): 3436, 3356, 2933, 2830, 1731, 1601, 1498, 1486, 1414, 1270, 1205, 1038, 809, 755; ^1H NMR (400MHz, CDCl_3): δ 4.43 (s, 2H), 3.80 (s, 3H), 6.74-6.82 (m, 3H), 7.36-7.40 (m, 1H), 7.45-7.51 (m, 4H); ^{13}C NMR (100 MHz, CDCl_3): δ 56.0, 114.6, 115.9, 117.1, 127.4, 128.9, 129.0, 129.2, 137.3, 139.7, 152.9.

3.9.12 2-Amino-3'-methoxy-4-methyl-biphenyl 124k

The general procedure was followed by reacting commercially obtained 2-bromo-4-methylaniline **121j** (10.75 mmol) with 3-methoxyphenylboronic acid **122g** (12.90 mmol). Purification by column chromatography on silica gel using a gradient eluent of 5% EtOAc in hexane afforded 2-amino-3'-methoxy-4-methyl-biphenyl **124k** as a brown oil (1.47 g, 54%), $R_f = 0.53$ (8:2, hexane/EtOAc). IR (ZnSe ATR crystal; neat, cm^{-1}): ^1H NMR (400MHz, CDCl_3): δ 2.42 (s, 3H), 3.69 (s, 2H), 3.87 (s, 3H), 6.71- 6.73 (m, 1H), 6.91-6.94 (m, 1H), 7.00-7.04 (m, 3H), 7.06-7.09 (m, 1H), 7.38 (t, $J = 8\text{Hz}$, 1H); ^{13}C NMR (100 MHz, CDCl_3): δ 20.5, 55.4, 113.0, 114.6, 115.9, 121.5, 127.6, 127.8, 129.2, 129.9, 130.9, 141.1, 141.2, 160.0.

3.10 Synthesis of Biphenyl Isocyanates 118

CAUTION: *Toxic gases (phosgene and hydrogen chloride) maybe released, therefore this reaction should be carried out under a well-ventilated hood.*

3.10.1 General Procedure A

To a stirring solution of 2-amino biphenyl (2.50 mmol) in dry toluene was added triphosgene at room temperature and the reaction mixture was reflux at 105-110 $^{\circ}\text{C}$ for 12-18 h. After cooling, the reaction mixture was concentrated under vacuum and the corresponding biphenyl isocyanates was obtain after purification by column chromatography.

3.10.2 4'-Methyl-2-biphenyl Isocyanate 118a

This compound was synthesized according to the general procedure A from 2-amino-4'-methyl biphenyl **124a** (5.46 mmol). The crude reaction mixture was purified by a quick flash column chromatography on silica gel using a gradient eluent of 15% CH_2Cl_2 in hexane to afford **118a** as a white solid (0.99 g, 86%). $R_f = 0.78$ (1:1, hexane/ CH_2Cl_2); IR (ZnSe ATR crystal; neat, cm^{-1}): 3025, 2920, 2249 (NCO), 1783, 1600, 1502, 1464, 1250, 1184, 1090, 1042, 1008, 819, 753; ^1H NMR (400MHz, CDCl_3): δ 2.32 (s, 3H), 7.06-7.09 (m, 1H), 7.12-7.15 (m, 1H), 7.16-7.19 (m, 3H), 7.21-7.25 (m, 3H); ^{13}C NMR (100 MHz, CDCl_3): δ 21.5, 124.4, 125.7, 126.1, 128.4, 129.1, 129.5, 130.8, 131.33, 135.5, 137.7, 138.0.

3.10.3 3'-Methoxy-2-biphenyl Isocyanate 118g

This compound was synthesized according to the general procedure A from 2-amino-3'-methoxy biphenyl **124g** (2.50 mmol). The crude reaction mixture was purified by a quick flash column chromatography on silica gel using a gradient eluent of 35% CH₂Cl₂ in hexane to afford **118g** as a clear oil (0.32 g, 86%). $R_f = 0.65$ (1:1, hexane/CH₂Cl₂); IR (ZnSe ATR crystal; neat, cm⁻¹): 2960, 2249 (NCO), 1581, 1509, 1464, 1414, 1257, 1209, 1093, 1038, 1019, 863, 792, 753; ¹H NMR (400MHz, CDCl₃): δ 3.85 (s, 3H), 6.95-6.97 (m, 2H), 6.99-7.01 (m, 1H), 7.15-7.18 (m, 1H), 7.22-7.39 (m, 5H); ¹³C NMR (100 MHz, CDCl₃): δ 55.5, 113.8, 114.8, 121.6, 124.5, 125.6, 126.1, 128.7, 129.8, 130.6, 131.4, 137.6, 139.7, 159.8.

3.10.4 3'-Trifluoromethyl-2-biphenyl Isocyanate 118h

This compound was synthesized according to the general procedure A by reacting 0.43 g 2-amino-3'-trifluoromethyl biphenyl **115h** (1.80 mmol). The crude reaction mixture was purified by a quick flash column chromatography on silica gel using a gradient eluent of 20% CH₂Cl₂ in hexane to afford 3'-trifluoromethyl-2-biphenyl isocyanate **118d** as a yellowish brown oil (0.21 g, 46%). IR (ZnSe ATR crystal; neat, cm⁻¹): 3025, 2919, 2263 (NCO), 1603, 1494, 1334, 1245, 1166, 1127, 1073, 1029, 804, 757; ¹H NMR (400MHz, CDCl₃): δ 7.24 (d, $J = 8\text{Hz}$, 1H), 7.28-7.32 (m, 1H), 7.35-7.40 (m, 3H), 7.58-7.62 (m, 1H), 7.65-7.71 (M, 2H); ¹³C NMR (100 MHz, CDCl₃): δ . 124.1 (q, $J_{\text{CF}} = 271\text{Hz}$), 124.5, 124.9 (q, $J_{\text{CF}} = 3.7\text{Hz}$), 126.1 (q, $J_{\text{CF}} = 3.7\text{Hz}$), 126.3, 126.4, 129.0 (d $J_{\text{CF}} = 52\text{Hz}$), 129.2, 129.4, 130.7, 131.1 (q, $J_{\text{CF}} = 32\text{Hz}$), 131.3, 132.6 (d, $J_{\text{CF}} = 1.5\text{Hz}$), 135.8, 139.1.

CAUTION: *Toxic gases (phosgene and hydrogen chloride) maybe released, therefore this reaction should be carried out under a well-ventilated hood.*

3.10.5 General Procedure B

Triphosgene **125** (0.40 mmol) was added to a stirring solution of 2-amino biphenyl (1.00 mmol) in dry toluene at 25 °C, resulting in the formation of precipitate and then the reaction mixture was slowly brought to reflux at 175 °C under argon for 2-4 h. Aliquot of the cooled, crude reaction mixture was removed to confirm the formation of corresponding isocyanates using IR

absorption (strong NCO peak at 2250-2290 cm^{-1}). The crude biphenyl Isocyanates were used immediately in the next reaction step without further purification.

3.10.6 4'-Methyl-2-biphenyl Isocyanate 118a

This compound was synthesized according to the general procedure B by reacting 1.00 g 2-amino-4'-methyl biphenyl (**115a**) (5.46 mmol). $R_f = 0.61$ (1:1, hexane/ CH_2Cl_2); IR (ZnSe ATR crystal; NCO, cm^{-1}): 2249.

3.10.7 4'-Chloro-2-biphenyl Isocyanate 118b

This compound was synthesized according to the general procedure B from 2-amino-4'-chloro biphenyl (**124b**) (4.91 mmol). $R_f = 0.88$ (7:3, hexane/ CH_2Cl_2); IR (ZnSe ATR crystal; NCO, cm^{-1}): 2260.

3.10.8 4'-Fluoro-2-biphenyl Isocyanate 118c

This compound was synthesized according to the general procedure B from 2-amino-4'-fluoro biphenyl **124c** (4.01 mmol). $R_f = 0.82$ (7:3, hexane/ CH_2Cl_2); IR (ZnSe ATR crystal; NCO, cm^{-1}): 2252.

3.10.9 4'-Methoxy-2-biphenyl Isocyanate 118d

This compound was synthesized according to the general procedure B from 2-amino-4'-methoxy biphenyl (**124d**) (5.02 mmol). $R_f = 0.76$ (1:1, hexane/ CH_2Cl_2); IR (ZnSe ATR crystal; NCO, cm^{-1}): 2253.

3.10.10 3'-Fluoro-2-biphenyl Isocyanate 118e

This compound was synthesized according to the general procedure B from 2-amino-3'-fluoro biphenyl (**124e**) (5.34 mmol). $R_f = 0.78$ (7:3, hexane/ CH_2Cl_2); IR (ZnSe ATR crystal; NCO, cm^{-1}): 2251.

3.10.11 3'-Methyl-2-biphenyl Isocyanate 118f

This compound was synthesized according to the general procedure B from 2-amino-3'-methyl biphenyl (**124f**) (5.46 mmol). $R_f = 0.93$ (7:3, hexane/ CH_2Cl_2); IR (ZnSe ATR crystal; NCO, cm^{-1}): 2248.

3.10.12 *3'-Methoxy-2-biphenyl Isocyanate 118g*

This compound was synthesized according to the general procedure B from 2-amino-3'-methoxy biphenyl (**124g**) (5.17 mmol). $R_f = 0.61$ (1:1, hexane/CH₂Cl₂); IR (ZnSe ATR crystal; NCO, cm⁻¹): 2255.

3.10.13 *3'-Trifluoromethyl-2-biphenyl Isocyanate 118h*

This compound was synthesized according to the general procedure B from 2-amino-3'-trifluoromethyl biphenyl (**124h**) (3.16 mmol). $R_f = 0.78$ (1:1, hexane/CH₂Cl₂); IR (ZnSe ATR crystal; NCO, cm⁻¹): 2254.

3.10.14 *5-Methyl-2-biphenyl Isocyanate 118i*

This compound was synthesized according to the general procedure B from 2-amino-4'-methyl biphenyl (**124i**) (5.46 mmol). $R_f = 0.75$ (7:3, hexane/CH₂Cl₂); IR (ZnSe ATR crystal; NCO, cm⁻¹): 2260.

3.10.15 *5-Methoxy-2-biphenyl Isocyanate 118j*

This compound was synthesized according to the general procedure B from 2-amino-4-methoxy biphenyl (**124j**) (5.52 mmol). $R_f = 0.64$ (7:3, hexane/CH₂Cl₂); IR (ZnSe ATR crystal; NCO, cm⁻¹): 2260.

3.10.16 *3'-Methoxy-5-Methyl-2-biphenyl Isocyanate 118k*

This compound was synthesized according to the general procedure B from 2-amino-4-methyl-3'-methoxy biphenyl (**124k**) (4.22 mmol). $R_f = 0.64$ (7:3, hexane/CH₂Cl₂); IR (ZnSe ATR crystal; NCO, cm⁻¹): 2255.

3.11 Synthesis of aza-Wittig reagent, Iminophosphorane 119

To a solution of anthranilonitrile **118** (12.70 mmol, 1.50 g), PPh₃ (19.10 mmol, 5.01 g), C₂Cl₆ (19.10 mmol, 4.52 g) in dry CH₂Cl₂ (60 mL) cooled to 0 °C was added dropwise Et₃N (63.5 mmol, 6.43 g), causing the solution to quickly turn yellow. The reaction mixture was stirred for 20 h, filtered through short plug of celite and then washed with 100 mL of EtOAc. The filtrate was concentrated under reduced pressure resulting in a yellow solid, which was

recrystallized from CH₂Cl₂-MeOH (1:5) to afford the iminophosphorane **119** as a white solid (3.97 g, 82%). $R_f = 0.48$ (7:3, hexane/EtOAc). IR (ZnSe ATR crystal; neat, cm⁻¹): 2209, 1587, 1470, 1445, 1436, 1346, 1283, 1154, 1107, 1043, 996, 754; ¹H NMR (400MHz, CDCl₃): δ 6.42 (d, $J = 8.4$ Hz, 1H), 6.61 (t, $J = 7.2$ Hz, 1H), 6.98-7.03 (m, 1H), 7.43-7.58 (m, 10H), 7.79-7.85 (m, 6H). ¹³C NMR (100 MHz, CDCl₃): δ 107.9 (d, $J = 24.9$ Hz), 116.8, 120.8, 121.3 (d, $J = 10$ Hz), 129.0 (d, $J = 12.4$ Hz), 129.6, 130.6, 132.3 (d, $J = 3$ Hz), 132.7, 132.8 (d, $J = 10.2$ Hz), 133.6 (d, $J = 2$ Hz), 155.5.

3.12 Synthesis of 2-((biphenylimino)methyleneamino) benzonitrile

3.12.1 General Procedure for synthesis of 2-((biphenylimino)methyleneamino)

benzonitrile 109

A solution of iminophosphorane (5 mmol) in dry CH₂Cl₂ (15 mL) was added slowly to a stirring solution of corresponding freshly prepared isocyanates (5 mmol) in toluene (15 mL), and then the resulting reaction mixture was stirred and heated at 65 °C under argon for 2-4 h. The reaction mixture was concentrated under reduced pressure, and the crude product was purified by a quick flash column chromatography on silica gel using a EtOAc/hexane gradient elution to afford the corresponding 2-((biphenylimino)methyleneamino) benzonitrile **109**.

3.12.2 Synthesis of 2-((4'-methylbiphenylimino)methyleneamino) benzonitrile 109a

The compound was synthesized from crude 4'-methyl-2-biphenyl isocyanate **118a** (5.46 mmol) using general procedure described above. Purification by flash column chromatography on silica gel using a gradient eluent of 7% EtOAc afforded **109a** as a viscous yellow oil (1.09 g, 65%), $R_f = 0.48$ (8:2, hexane/EtOAc). IR (ZnSe ATR crystal; neat, cm⁻¹): 2226, 2138, 2106, 1592, 1570, 1514, 1476, 1441, 1210, 1160, 1103, 1041, 818, 752; ¹H NMR (400MHz, CDCl₃): δ 2.27 (s, 3H), 6.82 (d, $J = 8$ Hz, 1H), 7.01-7.15 (m, 3H), 7.23-7.26 (m, 1H), 7.29-7.34 (m, 5H), 7.35-7.39 (m, 1H), 7.51 (dt, $J_1 = 8$ Hz, $J_2 = 1.2$ Hz, 1H); ¹³C NMR (100MHz, CDCl₃): δ 21.4, 107.7, 116.9, 124.9, 125.1, 125.7, 126.6, 128.5, 129.2, 129.3, 130.5, 130.8, 133.2, 133.5, 133.8, 135.7, 137.8, 137.9, 142.8. HRMS (ESI): m/z calculated for C₂₁H₁₆N₃ (M⁺) 310.1339, found 310.1324.

3.12.3 Synthesis of 2-((4'-chlorobiphenylimino)methyleneamino) benzonitrile 109b

The compound was synthesized from crude 4'-chloro-2-biphenyl isocyanate **118b** (4.67 mmol) using general procedure described above. Purification by flash column chromatography on silica gel using a gradient eluent of 7% EtOAc afforded **109b** as a viscous yellow oil (0.75 g, 49%), $R_f = 0.49$ (9:1, hexane/EtOAc). IR (ZnSe ATR crystal; neat, cm^{-1}): 2223, 2138, 2106, 1592, 1570, 1476, 1441, 1210, 1103, 1041, 818, 752; ^1H NMR (400MHz, CDCl_3): δ 6.93 (d, $J = 8\text{Hz}$, 1H), 7.19 (dt, $J_1 = 7.6\text{Hz}$, $J_2 = 0.8\text{Hz}$, 1H), 7.27-7.38 (m, 6H), 7.40-7.43 (m, 2H), 7.43-7.48 (m, 1H), 7.58 (dd, $J_1 = 8\text{Hz}$, $J_2 = 1.6\text{Hz}$, 1H); ^{13}C NMR (100MHz, CDCl_3): δ 107.9, 116.8, 125.1, 125.3, 126.0, 126.7, 128.8, 129.1, 130.7, 130.5, 130.9, 133.5, 133.8, 133.9, 134.1, 136.4, 137.1, 142.4. HRMS (ESI): m/z calculated for $\text{C}_{20}\text{H}_{12}\text{N}_3\text{ClNa}$ (M^+) 352.0612; 354.0589, found 352.0628; 354.0586.

3.12.4 Synthesis of 2-((4'-fluorobiphenylimino)methyleneamino) benzonitrile 109c

The compound was synthesized from crude 4'-fluoro-2-biphenyl isocyanate **118c** (3.81 mmol) using general procedure described above. Purification by flash column chromatography on silica gel using a gradient eluent of 6% EtOAc afforded **109c** as a viscous yellow oil (0.67 g, 67%), $R_f = 0.41$ (9:1, hexane/EtOAc). IR (ZnSe ATR crystal; neat, cm^{-1}): 2225, 2139, 2107, 1733, 1592, 1569, 1509, 1477, 1443, 1211, 1158, 1042, 835, 752; ^1H NMR (400MHz, CDCl_3): δ 6.95 (dd, $J_1 = 8\text{Hz}$, $J_2 = 0.8\text{Hz}$, 1H), 7.04-7.09 (m, 2H), 7.18 (dt, $J_1 = 7.6\text{Hz}$, $J_2 = 1.2\text{Hz}$, 1H), 7.28-7.33 (m, 2H), 7.34-7.38 (m, 2H), 7.43-7.47 (m, 3H), 7.56 (dd, $J_1 = 8\text{Hz}$, $J_2 = 0.8\text{Hz}$, 1H); ^{13}C NMR (100MHz, CDCl_3): δ 108.0, 115.5 (d, $J_{\text{CF}} = 21.3\text{Hz}$), 116.8, 125.1 (d, $J_{\text{CF}} = 11.7\text{Hz}$), 126.0, 126.7, 128.9, 130.9, 131.3 (d, $J_{\text{CF}} = 8.1\text{Hz}$), 133.6 (d, $J_{\text{CF}} = 26.3\text{Hz}$), 136.7, 142.6, 162.7 (d, $J_{\text{CF}} = 246\text{Hz}$). HRMS (FAB): m/z calculated for $\text{C}_{20}\text{H}_{13}\text{N}_3\text{F}$ (M^+) 314.1094, found 314.1081.

3.12.5 Synthesis of 2-((4'-methoxybiphenylimino)methyleneamino) benzonitrile 109d

The compound was synthesized from crude 4'-methoxy-2-biphenyl isocyanate **118d** (5.02 mmol) using general procedure described above. Purification by flash column chromatography on silica gel using a gradient eluent of 8% EtOAc afforded **109d** as a viscous yellow oil (1.06 g, 65%), $R_f = 0.51$ (8:2, hexane/EtOAc). IR (ZnSe ATR crystal; neat, cm^{-1}): 2136, 1732, 1592, 1570, 1513, 1477, 1422, 1242, 1210, 1176, 1103, 1032, 828, 757; ^1H NMR (400MHz, CDCl_3): δ 3.78 (s, 3H), 6.88-6.92 (m, 4H), 7.17 (dt, $J_1 = 7.6\text{Hz}$, $J_2 = 0.8\text{Hz}$, 1H), 7.28-

7.31 (m, 1H), 7.34-7.37 (m, 3H), 7.39-7.45 (m, 3H), 7.56 (d, $J = 8\text{Hz}$, 1H); ^{13}C NMR (100MHz, CDCl_3): δ 55.4, 107.7, 114.0, 116.9, 124.9, 124.9, 125.1, 125.8, 126.7, 128.4, 130.6, 130.7, 130.8, 130.9, 133.3, 133.6, 133.9, 137.7, 142.9, 159.4. HRMS (ESI): m/z calculated for $\text{C}_{21}\text{H}_{16}\text{N}_3\text{O}$ (M^+) 326.1288, found 326.1285.

3.12.6 Synthesis of 2-((3'-Fluorobiphenylimino)methyleneamino) benzonitrile 109e

The compound was synthesized from crude 3'-fluoro-2-biphenyl isocyanate **118e** (5.34 mmol) using general procedure described above. Purification by flash column chromatography on silica gel using a gradient eluent of 5% EtOAc afforded **109e** as a clear oil (1.04 g, 62%), $R_f = 0.43$ (9:1, hexane/EtOAc). IR (ZnSe ATR crystal; neat, cm^{-1}): 2225, 2135, 2109, 1591, 1570, 1473, 1443, 1256, 1212, 1181, 1157, 1104, 882, 753; ^1H NMR (400MHz, CDCl_3): δ 6.95-7.00 (m, 2H), 7.14-7.20 (m, 2H), 7.24-7.38 (m, 6H), 7.42-7.46 (m, 1H), 7.55 (dd, $J_1 = 8\text{Hz}$, $J_2 = 1.6\text{Hz}$, 1H); ^{13}C NMR (100MHz, CDCl_3): δ 108.0, 114.8 (d, $J_{\text{CF}} = 21.2\text{Hz}$), 116.5, 116.8 (d, $J_{\text{CF}} = 8.8\text{Hz}$), 125.2 (d, $J_{\text{CF}} = 4.4\text{Hz}$), 125.4 (d, $J_{\text{CF}} = 3\text{Hz}$), 126.1, 126.7, 129.2, 130.1 (d, $J_{\text{CF}} = 8.8\text{Hz}$), 130.4, 130.7, 133.6 (d, $J_{\text{CF}} = 32.9\text{Hz}$), 133.9, 136.3 (d, $J_{\text{CF}} = 2.2\text{Hz}$), 140.8 (d, $J_{\text{CF}} = 7.3\text{Hz}$), 142.4, 162.7 (d, $J_{\text{CF}} = 245.3\text{Hz}$). HRMS (ESI): m/z calculated for $\text{C}_{20}\text{H}_{13}\text{N}_2\text{F}$ (M^+) 314.1094, found 314.1117.

3.12.7 Synthesis of 2-((3'-methylbiphenylimino)methyleneamino) benzonitrile 109f

The compound was synthesized from crude 3'-methyl-2-biphenyl isocyanate **118f** (5.46 mmol) using general procedure described above. Purification by flash column chromatography on silica gel using a gradient eluent of 4% EtOAc afforded **109f** as a clear oil (1.22 g, 73%), $R_f = 0.45$ (9:1, hexane/EtOAc). IR (ZnSe ATR crystal; neat, cm^{-1}): 2225, 2136, 2111, 1592, 1569, 1474, 1442, 1256, 1212, 1104, 906, 793, 752, 730; ^1H NMR (400MHz, CDCl_3): δ 2.31 (s, 3H), 6.84 (dd, $J_1 = 8.8\text{Hz}$, $J_2 = 0.8\text{Hz}$, 1H), 7.15 (dt, $J_1 = 7.6\text{Hz}$, $J_2 = 0.8\text{Hz}$, 1H), 7.24-7.35 (m, 8H), 7.37-7.41 (m, 1H), 7.53 (dd, $J_1 = 7.6\text{Hz}$, $J_2 = 1.2\text{Hz}$, 1H); ^{13}C NMR (100MHz, CDCl_3): δ 21.6, 107.8, 116.9, 124.9, 125.2, 125.7, 126.5, 128.6, 128.7, 130.2, 130.9, 133.3, 133.6, 133.8, 138.2, 138.3, 138.6, 143.0. HRMS (ESI): m/z calculated for $\text{C}_{21}\text{H}_{16}\text{N}_3$ (M^+) 310.1344, found 310.1369.

3.12.8 Synthesis of 2-((3'-methoxybiphenylimino)methyleneamino) benzonitrile 109g

The compound was synthesized from crude 3'-methoxy-2-biphenyl isocyanate **118g** (4.91 mmol) using general procedure described above. Purification by flash column chromatography on silica gel using a gradient eluent of 5% EtOAc afforded **109g** as a viscous yellow oil (0.78g, 49%), $R_f = 0.36$ (8:2, hexane/EtOAc). IR (ZnSe ATR crystal; neat, cm^{-1}): 2146, 2112, 1592, 1521, 1443, 1259, 1209, 1108, 1020, 872, 756; ^1H NMR (400MHz, CDCl_3): δ 3.78 (s, 3H), 6.81 (dd, $J_1 = 8.4\text{Hz}$, $J_2 = 1.2\text{Hz}$, 1H), 6.88 (dd, $J_1 = 8.4\text{Hz}$, $J_2 = 0.8\text{Hz}$, 1H), 6.98-6.99 (m, 1H), 7.02-7.05 (m, 1H), 7.15 (td, $J_1 = 7.6\text{Hz}$, $J_2 = 0.8\text{Hz}$, 1H), 7.25-7.43 (m, 6H), 7.54 (dd, $J_1 = 7.6\text{Hz}$, $J_2 = 1.6\text{Hz}$, 1H); ^{13}C NMR (100MHz, CDCl_3): δ 55.4, 107.8, 113.5, 115.1, 116.8, 121.9, 124.9, 125.2, 125.7, 126.6, 128.8, 129.6, 130.0, 130.7, 133.3, 133.6, 133.8, 137.9, 140.0, 142.8, 159.6. HRMS (ESI): m/z calculated for $\text{C}_{21}\text{H}_{16}\text{N}_3\text{O}$ (M^+) 326.1293, found.

3.12.9 Synthesis of 2-((3'-trifluoromethylbiphenylimino)methyleneamino) benzonitrile 109h

The compound was synthesized from crude 3'-trifluoromethyl-2-biphenyl isocyanate **118h** (3.16 mmol) using general procedure described above. Purification by flash column chromatography on silica gel using a gradient eluent of 4% EtOAc afforded **109h** as a viscous yellow oil (0.48 g, 42%), $R_f = 0.45$ (9:1, hexane/EtOAc). IR (ZnSe ATR crystal; neat, cm^{-1}): 2221, 2143, 2113, 1593, 1570, 1478, 1333, 1247, 1163, 1121, 1073, 805, 756; ^1H NMR (400MHz, CDCl_3): δ 6.97 (dd, $J_1 = 8.4\text{Hz}$, $J_2 = 0.8\text{Hz}$, 1H), 7.29 (dt, $J_1 = 7.6\text{Hz}$, $J_2 = 1.2\text{Hz}$, 1H), 7.30-7.34 (m, 1H), 7.35-7.47 (m, 4H), 7.52-7.59 (m, 3H), 7.70-7.74 (m, 2H); ^{13}C NMR (100MHz, CDCl_3): δ 108.0, 116.8, 124.2 (q, $J_{\text{CF}} = 271\text{Hz}$), 124.7 (q, $J_{\text{CF}} = 3.6\text{Hz}$), 125.1, 125.4, 126.2, 126.3 (t, $J_{\text{CF}} = 3.7\text{Hz}$), 126.8, 129.0, 129.5, 130.5, 130.8, 130.9 (q, $J_{\text{CF}} = 32\text{Hz}$), 133.1, 133.5, 133.9, 133.9, 136.0, 139.4, 142.2. HRMS (ESI): m/z calculated for $\text{C}_{21}\text{H}_{16}\text{N}_3\text{F}_3$ (M^+) 364.1062, found 364.1093.

3.12.10 Synthesis of 2-((5-methylbiphenylimino)methyleneamino) benzonitrile 109i

The compound was synthesized from crude 4-methyl-2-biphenyl isocyanate **118i** (5.47 mmol) using general procedure described above. Purification by flash column chromatography

on silica gel using a gradient eluent of 4% EtOAc afforded **109i** as a clear viscous oil (1.23 g, 73%), $R_f = 0.45$ (9:1, hexane/EtOAc). IR (ZnSe ATR crystal; neat, cm^{-1}): 2225, 2131, 2113, 1593, 1570, 1481, 1271, 1213, 1112, 908, 815, 757; ^1H NMR (400MHz, CDCl_3): δ 2.38 (s, 3H), 6.85 (d, $J = 8\text{Hz}$, 1H), 7.09-7.16 (m, 3H), 7.22-7.29 (m, 2H), 7.33-7.40 (m, 3H), 7.43-7.46 (m, 2H), 7.51 (dd, $J_1 = 7.6\text{Hz}$, $J_2 = 2\text{Hz}$, 1H); ^{13}C NMR (100MHz, CDCl_3): δ 21.2, 107.7, 116.9, 124.8, 125.1, 125.7, 127.8, 128.5, 129.4, 129.5, 130.3, 130.9, 131.5, 133.3, 133.6, 136.6, 137.6, 138.8, 143.2. HRMS (ESI): m/z calculated for $\text{C}_{21}\text{H}_{16}\text{N}_3$ (M^+) 310.1344, found 310.1349.

3.12.11 Synthesis of 2-((5-methoxybiphenylimino)methyleneamino) benzonitrile 109j

The compound was synthesized from crude 4-methoxy-2-biphenyl isocyanate **118j** (5.52 mmol) using general procedure described above. Purification by flash column chromatography on silica gel using a gradient eluent of 4% EtOAc afforded **109j** as a clear viscous oil (1.38 g, 77%), $R_f = 0.52$ (8:2, hexane/EtOAc). IR (ZnSe ATR crystal; neat, cm^{-1}): 2225, 2127, 2113, 1594, 1567, 1477, 1443, 1400, 1298, 1207, 1173, 1030, 813, 757; ^1H NMR (400MHz, CDCl_3): δ 3.83 (s, 3H), 6.85-6.90 (m, 3H), 7.12 (dt, $J_1 = 8\text{Hz}$, $J_2 = 1.2\text{Hz}$, 1H), 7.25-7.29 (m, 2H), 7.33-7.41 (m, 3H), 7.44-7.46 (m, 2H), 7.51 (dd, $J_1 = 8\text{Hz}$, $J_2 = 1.4\text{Hz}$, 1H); ^{13}C NMR (100MHz, CDCl_3): δ 55.8, 107.7, 114.3, 115.9, 116.9, 124.7, 125.0, 126.2, 127.1, 128.0, 128.6, 129.4, 130.4, 133.3, 133.6, 138.6, 139.1, 143.5, 158.1. IHRMS (ESI): m/z calculated for $\text{C}_{21}\text{H}_{16}\text{N}_3\text{O}$ (M^+) 326.1293, found 326.1306.

3.12.12 Synthesis of 2-((3'-methoxyl-5-methylbiphenylimino)methyleneamino) benzonitrile 109k

The compound was synthesized from crude 3'-methoxyl-5-methyl-2-biphenyl isocyanate **118k** (5.47 mmol) using general procedure described above. Purification by flash column chromatography on silica gel using a gradient eluent of 6% EtOAc afforded **109k** as a viscous pale yellow oil (1.11 g, 78%), $R_f = 0.45$ (9:1, hexane/EtOAc). IR (ZnSe ATR crystal; neat, cm^{-1}): 2226, 2128, 2114, 1593, 1570, 1477, 1429, 1259, 1215, 1161, 1111, 1050, 1032, 820, 757; ^1H NMR (400MHz, CDCl_3): δ 2.39 (s, 3H), 3.79 (s, 3H), 6.80 (dd, $J_1 = 8.4\text{Hz}$, $J_2 = 2.2\text{Hz}$, 1H), 6.88 (d, $J = 8.4\text{Hz}$, 1H), 6.97-6.98 (m, 1H), 7.02 (dd, $J_1 = 7.2\text{Hz}$, $J_2 = 0.8\text{Hz}$, 1H), 7.13-7.18 (m, 3H), 7.22-7.25 (m, 1H), 7.28 (d, $J = 5.2\text{Hz}$, 1H), 7.40 (dt, $J_1 = 8\text{Hz}$, $J_2 = 1.6\text{Hz}$, 1H), 7.53 (dd, $J_1 = 7.6\text{Hz}$, $J_2 = 1.2\text{Hz}$, 1H); ^{13}C NMR (100MHz, CDCl_3): δ 21.2, 55.4, 107.7,

113.5, 115.0, 116.9, 121.9, 124.8, 125.1, 125.6, 129.4, 129.6, 130.4, 130.9, 131.3, 133.2, 133.6, 136.5, 137.6, 140.0, 143.1, 159.6. HRMS (ESI): m/z calculated for $C_{22}H_{18}N_3O$ (M^+) 340.1450, found 340.1456.

3.13 Synthesis of 2-halo-3-biphenyl quinazoliniminiums halide salts

3.13.1 General procedure for Lewis acids mediated intramolecular cyclization 110

Lewis acids were added dropwise to a stirring solution of 2-((biphenylimino)methyleneamino) benzonitrile (0.08 g, 0.26 mmol) in the indicated organic solvent (3 mL) at the specified temperature. The reaction mixture was monitored by TLC, after complete consumption of the starting material and the resulting precipitates was filtered and washed with hexane- CH_2Cl_2 to quench the acid. The precipitates are dried under vacuum to afford the corresponding 2-halo-3-biphenyl quinazoliniminiums halide salts.

3.13.2 2-Bromo-3-(4'-methylbiphenyl) quinazolin-4(3H)-iminium bromide 110a

The compound was obtained from the reaction of **109a** with TMSBr (2.82 mmol) following the general procedure. The solvent used were CH_2Cl_2 or $ClCH_2CH_2Cl$ as indicated on Table 3.2. Pale yellow solid (0.077 g, 82%) was obtained. $R_f = 0.49$ (9.5:0.5, $CH_2Cl_2/MeOH$). 1H NMR (400MHz, CH_3OH-d_4): δ 2.24 (s, 3H), 7.12 (d, $J = 8.2Hz$, 2H), 7.19-7.22 (m, 2H), 7.69-7.88 (m, 6H), 8.11 (dt, $J_1 = 7.2Hz$, $J_2 = 1.2Hz$, 1H), 8.42 (d, $J_1 = 8.8Hz$, $J_2 = 1.2Hz$, 1H); ^{13}C NMR (100MHz, CH_3OH-d_4): δ 21.2, 114.4, 126.6, 129.1, 129.5, 130.1, 130.6, 131.4, 131.7, 134.1, 134.8, 135.7, 136.1, 139.5, 140.2, 141.7, 147.4, 160.3. LRMS (ESI): m/z calculated for $C_{21}H_{17}BrN_3^+$ (M^+) 390.06, found 390.1 and 390.9.

3.13.3 2-Chloro-3-(4'-methylbiphenyl) quinazolin-4(3H)-iminium chloride 110a'

Following the general procedure, TMSCl, $SnCl_4$ or $TiCl_4$ (3 equiv) was added dropwise to a stirring solution of 2-((4'-methylbiphenylimino)methyleneamino)benzonitrile (**109a**) (0.15 g, 0.04 mmol) in the specified organic solvent (2-3 mL). White solid (0.077 g, 82%) was obtained. $R_f = 0.49$ (9.5:0.5, $CH_2Cl_2/MeOH$). 1H NMR (400MHz, CH_3OH-d_4): δ 2.24 (s, 3H), 7.12 (d, $J = 8Hz$, 2H), 7.17 (d, $J = 8Hz$, 2H), 7.69-7.87 (m, 6H), 8.09-8.14 (m, 1H), 8.43 (d, $J_1 = 8.4Hz$, $J_2 =$

0.8Hz, 1H); ^{13}C NMR (100MHz, $\text{CH}_3\text{OH}-d_4$): δ 21.2, 114.2, 126.7, 129.0, 129.5, 129.8, 130.6, 131.3, 131.7, 134.0, 134.1, 134.8, 139.6, 140.3, 141.7, 144.1, 147.0, 160.9, 129.5, 129.8, 130.6, 131.3, 131.7, 134.0, 134.1, 134.8, 139.6, 140.3, 141.7, 144.1, 147.0, 160.9. HRMS (ESI): m/z calculated for $\text{C}_{21}\text{H}_{17}\text{ClN}_3^+$ (M^+) 346.1, found 346.1.

3.14 Synthesis of Phenanthridine fused quinazoliniminiums (PNQs)

3.14.1 General procedure for Lewis acids mediated cascade cyclization of 111

To a stirring solution of 2-((biphenylimino)methyleneamino) benzonitrile **109** (0.50 mmol) in nitromethane (3 mL) was added either SnCl_4 or $\text{BF}_3\cdot\text{OEt}_2$ dropwise at 25 °C. In many reactions water (4 equiv.) was also needed as specified. The reaction mixture was stirred for an additional 2-48 h. The product precipitated out of the solution. Upon completion of the reaction, the precipitates were filtered and washed with hexane- CH_2Cl_2 , and then dried under vacuum to afford the corresponding ring-fused phenanthridine *N*-quinazoliniminiums salt.

3.14.2 Synthesis of 4'-methyl-phenanthridine-*N*-quinazoliniminiums hydrochloride salt 111a'

The compound was obtained following general procedure by reacting **109a** (0.24 mmol) with SnCl_4 (0.97 mmol) and water (4 equiv.) to afford a pale green solid (0.08 g, 44%). R_f = 0.4 (9.5:0.5, $\text{CH}_2\text{Cl}_2/\text{MeOH}$). IR (ZnSe ATR crystal; neat, cm^{-1}): 3257, 3151, 1635, 1598, 1566, 1497, 1369, 1309, 1242, 1184, 1008, 821, 754; ^1H NMR (400MHz, $\text{DMSO}-d_6$): δ 2.54 (s, 3H), 7.62-7.70 (m, 2H), 7.75 (d, J = 8.4Hz, 1H), 7.81 (dt, J_1 = 0.8Hz, J_2 = 7.6Hz, 1H), 8.01 (d, J = 8Hz, 1H), 8.12 (dt, J_1 = 8.4Hz, J_2 = 1.2Hz, 1H), 8.42 (dd, J_1 = 8.4Hz, J_2 = 1.6Hz, 1H), 8.45 (d, J = 8.4Hz, 1H), 8.51 (d, J_1 = 1.6Hz, J_2 = 7.6Hz, 1H), 8.59 (s, 1H), 8.73 (d, J = 8Hz, 1H), 11.01 (br s, 1H), 11.34 (br s, 1H); ^{13}C NMR (100MHz, $\text{DMSO}-d_6$): 21.1, 114.8, 121.2, 123.0, 124.6, 124.9, 125.6, 125.9, 127.1, 127.3, 127.9, 128.2, 128.6, 128.7, 130.6, 134.6, 136.9, 139.5, 144.4, 144.5, 158.2. HRMS (ESI): m/z calculated for $\text{C}_{21}\text{H}_{16}\text{N}_3\text{O}$ (M^+) 310.1, found 310.0.

3.14.3 Synthesis of 4'-methyl-phenanthridine-N-quinazoliniminiums tetrafluoroborate salt 111a''

The compound was obtained following general procedure by reacting **109a** (0.69 mmol) with BF₃.OEt₂ (2.77 mmol) and water (4 equiv.) to afford a pale green solid (0.19 g, 70%). R_f = 0.51 (9.5:0.5, CH₂Cl₂/MeOH). IR (ZnSe ATR crystal; neat, cm⁻¹): 3366, 3218, 1660, 1594, 1566, 1474, 1345, 1085, 1053, 1011, 828, 764; ¹H NMR (400MHz, DMSO-*d*₆): δ 2.54 (s, 3H), 7.63-7.71 (m, 2H), 7.77 (d, *J* = 8Hz, 1H), 7.82 (t, *J* = 8Hz, 1H), 8.02 (d, *J* = 8.4Hz, 1H), 8.13 (t, *J* = 7.6Hz, 1H), 8.43 (d, *J* = 8.4Hz, 1H), 8.47 (d, *J* = 8Hz, 1H), 8.53 (d, *J* = 8.4Hz, 1H), 8.60-8.63 (m, 2H), 11.04 (br s, 2H); ¹³C NMR (100MHz, DMSO-*d*₆): 21.4, 115.4, 121.8, 123.6, 125.3, 125.5, 126.2, 126.3, 127.8, 128.0, 128.6, 128.8, 129.2, 129.3, 131.2, 135.3, 137.6, 140.1, 145.1, 145.1, 158.8. HRMS (ESI): *m/z* calculated for C₂₁H₁₆N₃ (M⁺) 310.1339, found 310.1331.

3.14.4 Synthesis of 3'-fluoro-phenanthridine-N-quinazoliniminiums tetrafluoroborate salt 111e''

The compound was obtained following general procedure by reacting **109e** (0.77 mmol) with BF₃.OEt₂ (3.08 mmol) and water (4 equiv.) to afford a green solid (0.14 g, 45%). R_f = 0.7 (9.5:0.5; CH₂Cl₂/MeOH). IR (ZnSe ATR crystal; neat, cm⁻¹): 3222, 1685, 1591, 1565, 1475, 1354, 1302, 1201, 1085, 1053, 992, 877, 764. ¹H NMR (400MHz, DMSO-*d*₆): δ 7.61-7.65 (m, 1H), 7.70-7.33 (m, 2H), 7.82 (t, *J* = 7.2Hz, 1H), 7.98 (d, *J* = 8Hz, 1H), 8.12 (t, *J* = 7.6Hz, 1H), 8.44-8.48 (m, 2H), 8.56-8.61 (m, 2H), 8.82-8.86 (m, 1H), 11.09 (br s, 2H); ¹³C NMR (100MHz, DMSO-*d*₆): 109.5 (d, *J*_{CF} = 24.2Hz), 114.7, 117.5 (d, *J*_{CF} = 22.7Hz), 121.3, 122.5 (d, *J*_{CF} = 2Hz), 123.8 (d, *J*_{CF} = 2Hz), 125.7, 127.3, 128.0, 128.7, 129.7, 130.9 (d, *J*_{CF} = 10.3Hz), 131.3, 133.3 (d, *J*_{CF} = 9.5Hz), 137.0, 144.0, 144.4, 158.3, 165.4 (d, *J*_{CF} = 250Hz). HRMS (ESI): *m/z* calculated for C₂₀H₁₃N₃F (M⁺) 314.1094, found 314.1078.

3.14.5 Synthesis of 3'-methyl-phenanthridine-N-quinazoliniminiums hydrochloride salt 111f'

The compound was obtained following general procedure by reacting **109f** (0.65 mmol) with SnCl₄ (2.59 mmol) and water (4 equiv.) to afford a green solid (0.18 g, 82%). R_f = 0.43 (9.5:0.5, CH₂Cl₂/MeOH). IR (ZnSe ATR crystal; neat, cm⁻¹): 3210, 1674, 1638, 1610, 1560, 1485, 1363, 1263, 1181, 812, 761; ¹H NMR (400MHz, DMSO-*d*₆): δ 2.58 (s, 3H), 7.58 (t, *J* =

8.4Hz, 1H), 7.6-7.72 (m, 2H), 7.77-7.81 (m, 1H), 7.96 (d, $J = 8\text{Hz}$, 1H), 8.09-8.13 (m, 1H), 8.39 (s, 1H), 8.43 (dd, $J_1 = 7.6\text{Hz}$, $J_2 = 2\text{Hz}$, 1H), 8.55 (dd, $J_1 = 7.6\text{Hz}$, $J_2 = 1.6\text{Hz}$, 1H), 8.66 (t, $J = 7.6\text{Hz}$, 2H), 10.99 (br s, 1H), 11.19 (br s, 1H). ^{13}C NMR (100MHz, DMSO- d_6): 21.5, 114.7, 121.3, 123.0, 123.2, 124.6, 125.1, 125.8, 127.3, 127.5, 127.7, 128.7, 128.9, 130.5, 130.7, 131.0, 136.9, 144.2, 144.6, 158.2. HRMS (ESI): m/z calculated for $\text{C}_{21}\text{H}_{16}\text{N}_3$ (M^+) 310.1344, found 310.1334.

3.14.6 Synthesis of 3'-methoxyl-phenanthridine-*N*-quinazoliniminiums

tetrafluoroborate salt 111g''

The compound was obtained following general procedure by reacting **109g** (1.14 mmol) with $\text{BF}_3\cdot\text{OEt}_2$ (4.55 mmol) to afford a green solid (0.24 g, 51%). $R_f = 0.37$ (9.5:0.5, $\text{CH}_2\text{Cl}_2/\text{MeOH}$). IR (ZnSe ATR crystal; neat, cm^{-1}): 3104, 1680, 1597, 1565, 1506, 1474, 1352, 1314, 1297, 1233, 1170, 1052, 1014, 874, 768; ^1H NMR (400MHz, DMSO- d_6): δ 4.02 (s, 3H), 7.32 (dd, $J_1 = 8.8\text{Hz}$, $J_2 = 2.8\text{Hz}$, 1H), 7.67-7.77 (m, 3H), 7.91 (d, $J = 7.6\text{Hz}$, 1H), 7.96 (ds, $J = 2.4\text{Hz}$, 1H), 8.05-8.09 (m, 1H), 8.42-8.45 (m, 1H), 8.55 (d, $J = 8\text{Hz}$, 1H), 8.60-8.62 (m, 1H), 8.65 (d, 9.2Hz, 1H), 11.05 (br s, 2H); ^{13}C NMR (100MHz, DMSO- d_6): 55.2, 106.1, 114.4, 117.6, 118.6, 121.4, 124.6, 125.7, 127.2, 127.5, 128.7, 129.2, 129.7, 131.2, 132.7, 137.0, 144.6, 144.9, 158.2, 163.6. HRMS (ESI): m/z calculated for $\text{C}_{21}\text{H}_{16}\text{N}_3\text{O}$ (M^+) 326.1288, found 326.1286.

3.14.7 Synthesis of 5-methyl-phenanthridine-*N*-quinazoliniminiums hydrochloride salt

111i'

The compound was obtained following general procedure by reacting **109i** (0.03 mmol) with SnCl_4 (1.29 mmol) and water (4 equiv.) to afford a pale green solid (0.08 g, 79%). $R_f = 0.44$ (9.5:0.5, $\text{CH}_2\text{Cl}_2/\text{MeOH}$). IR (ZnSe ATR crystal; neat, cm^{-1}): 3188, 1674, 1634, 1608, 1564, 1541, 1484, 1365, 1264, 1172, 829, 781, 767, 753; ^1H NMR (400MHz, DMSO- d_6): δ 2.52 (s, 3H), 7.48 (d, $J = 8.8\text{Hz}$, 1H), 7.74 (t, $J = 7.6\text{Hz}$, 1H), 7.79 (t, $J = 8.4\text{Hz}$, 1H), 7.90 (t, $J = 7.2\text{Hz}$, 1H), 7.96 (d, $J = 8\text{Hz}$, 1H), 8.10 (t, $J = 7.2\text{Hz}$, 1H), 8.29 (d, $J = 8.4\text{Hz}$, 1H), 8.36 (s, 1H), 8.53 (d, $J = 8\text{Hz}$, 1H), 8.75 (t, $J = 7.6\text{Hz}$, 1H), 10.94 (br s, 1H), 11.33 (br s, 1H); ^{13}C NMR (100MHz, DMSO- d_6): 20.7, 114.7, 121.0, 122.9, 124.4, 125.0, 125.6, 125.9, 127.3, 127.4, 127.9, 128.6, 129.4, 129.7, 130.6, 133.4, 136.8, 138.5, 144.4, 144.5, 157.9. HRMS (ESI): m/z calculated for $\text{C}_{21}\text{H}_{17}\text{N}_3\text{Cl}$ (M^+) 346.1111, found 346.1101.

3.14.8 Synthesis of 5-methyl-3'-methoxy-phenanthridine-N-quinazoliniminiums tetrafluoroborate salt 111k

The compound was obtained following general procedure by reacting **109k** (0.86 mmol) with $\text{BF}_3 \cdot \text{OEt}_2$ (3.42 mmol) to afford a pale green solid (0.14 g, 37%). $R_f = 0.31$ (9.5:0.5, $\text{CH}_2\text{Cl}_2/\text{MeOH}$). IR (ZnSe ATR crystal; neat, cm^{-1}): 3201, 1658, 1600, 1566, 1473, 1411, 1364, 1301, 1235, 1192, 1097, 1051, 1006, 836, 767; ^1H NMR (400MHz, $\text{DMSO}-d_6$): δ 2.54 (s, 3H), 4.05 (s, 3H), 7.34 (dd, $J_1 = 8.8\text{Hz}$, $J_2 = 2.8\text{Hz}$, 1H), 7.50 (dd, $J_1 = 8.8\text{Hz}$, $J_2 = 1.2\text{Hz}$, 1H), 7.76 (t, $J_1 = 7.4\text{Hz}$, $J_2 = 1.2\text{Hz}$, 1H), 7.93 (d, $J = 7.6\text{Hz}$, 1H), 7.98 (ds, $J = 2.4\text{Hz}$, 1H), 8.08 (dt, $J_1 = 7.4\text{Hz}$, $J_2 = 1.2\text{Hz}$, 1H), 8.31 (d, $J = 8.4\text{Hz}$, 1H), 8.46 (s, 1H), 8.56 (d, $J = 8\text{Hz}$, 1H), 8.71 (d, $J = 8.8\text{Hz}$, 1H); ^{13}C NMR (100MHz, $\text{DMSO}-d_6$): 20.6, 56.1, 105.9, 114.2, 117.5, 118.6, 124.4, 125.3, 125.5, 127.1, 127.3, 128.8, 129.7, 129.8, 132.7, 136.8, 138.5, 144.5, 144.8, 157.9, 163.5. HRMS (ESI): m/z calculated for $\text{C}_{22}\text{H}_{18}\text{N}_3\text{O}$ (M^+) 340.1450, found 340.1449.

3.15 Formation of 1-(2-cyanophenyl)-3-(biphenyl-2-yl) urea 126

3.15.1 1-(2-cyanophenyl)-3-(5-methoxybiphenyl-2-yl) urea 126j

Compound **126j** was obtained from the reaction of SnCl_4 with **109j** (0.04 mmol) following the general procedure earlier stated in Section 3.15.1. The reaction yielded a white solid (0.11g, 88%). ^1H NMR (400MHz, $\text{DMSO}-d_6$): δ 3.79 (s, 3H), 6.84 (d, $J = 3.2\text{ Hz}$, 1H), 6.96 (dd, $J_1 = 8.8\text{ Hz}$, $J_2 = 3.2\text{ Hz}$, 1H), 7.14 (dt, $J_1 = 8\text{ Hz}$, $J_2 = 1.2\text{ Hz}$, 1H), 7.37-7.50 (m, 5H), 7.53 (d, $J = 8.8\text{ Hz}$, 1H), 7.57-7.62 (m, 1H), 7.70 (dd, $J_1 = 8\text{ Hz}$, $J_2 = 1.4\text{ Hz}$, 1H), 8.01 (d, $J = 8.4\text{ Hz}$, 1H), 8.34 (s, 1H), 8.80 (s, 1H); ^{13}C NMR (100MHz, $\text{DMSO}-d_6$): 55.3, 101.6, 113.4, 114.9, 117.0, 121.3, 122.7, 127.3, 127.4, 127.6, 128.6, 128.9, 133.1, 133.8, 136.5, 138.7, 142.2, 153.1, 156.3.

References:

- ¹ Horton, D. A.; Bourne, G. T.; Smythe, M. L., The combinatorial synthesis of bicyclic privileged structures or privileged substructures. *Chemical reviews* **2003**, *103* (3), 893-930.
- ² Michael, J. P., Quinoline, quinazoline and acridone alkaloids. *Natural product reports* **2001**, *18* (5), 543-59.
- ³ Witt, A.; Bergman, J., Recent Developments in the Field of Quinazoline Chemistry. *Curr. Org. Chem.* **2003**, *7* (7), 659.
- ⁴ Xu, W.; Jin, Y.; Liu, H.; Jiang, Y.; Fu, H., Copper-catalyzed domino synthesis of quinazolinones via Ullmann-type coupling and aerobic oxidative C-H amidation. *Organic letters* **2011**, *13* (6), 1274-7.
- ⁵ (a) Ma, Z.-Z.; Hano, Y.; Nomura, T.; Chen, Y.-J., Two New Pyrroloquinazolinoquinoline Alkaloids from *Peganum nigellastrum*. *Heterocycles* **1997**, *1997* (46), 541; (b) Cinelli, M. A.; Morrell, A.; Dexheimer, T. S.; Scher, E. S.; Pommier, Y.; Cushman, M., Design, synthesis, and biological evaluation of 14-substituted aramathecins as topoisomerase I inhibitors. *Journal of medicinal chemistry* **2008**, *51* (15), 4609-19.
- ⁶ Zhou, J.; Fang, J., One-pot synthesis of quinazolinones via iridium-catalyzed hydrogen transfers. *The Journal of organic chemistry* **2011**, *76* (19), 7730-6.
- ⁷ Zeng, F.; Alper, H., One-step synthesis of quinazolino[3,2-a]quinazolinones via palladium-catalyzed domino addition/carboxamidation reactions. *Organic letters* **2010**, *12* (16), 3642-4.
- ⁸ (a) Liverton, N. J.; Armstrong, D. J.; Claremon, D. A.; Remy, D. C.; Baldwin, J. J.; Lynch, R. J.; Zhang, G.; Gould, R. J., Nonpeptide glycoprotein IIb/IIIa inhibitors: substituted quinazolinones and quinazolinones as potent fibrinogen receptor antagonists. *Bioorganic & medicinal chemistry letters* **1998**, *8* (5), 483-6; (b) Pendergast, W.; Johnson, J. V.; Dickerson, S. H.; Dev, I. K.; Duch, D. S.; Ferone, R.; Hall, W. R.; Humphreys, J.; Kelly, J. M.; Wilson, D. C., Benzoquinazoline inhibitors of thymidylate synthase: enzyme inhibitory activity and cytotoxicity of some 3-amino- and 3-methylbenzo[f]quinazolin-1(2H)-ones. *Journal of medicinal chemistry* **1993**, *36* (16), 2279-91.
- ⁹ (a) Zeng, F.; Alper, H., Tandem palladium-catalyzed addition/cyclocarbonylation: an efficient synthesis of 2-heteroquinazolin-4(3H)-ones. *Organic letters* **2010**, *12* (6), 1188-91; (b) Alagarsamy, V.; Dhanabal, K.; Parthiban, P.; Anjana, G.; Deepa, G.; Murugesan, B.; Rajkumar, S.; Beevi, A. J., Synthesis and pharmacological investigation of novel 3-(3-methylphenyl)-2-substituted amino-3H-quinazolin-4-ones as analgesic and anti-inflammatory agents. *The Journal of pharmacy and pharmacology* **2007**, *59* (5), 669-77.
- ¹⁰ (a) Mhaske, S. B.; Argade, N. P., The Chemistry of recently isolated naturally occurring quinazolinone alkaloids. *Tetrahedron* **2006**, *62* (42), 9787-9826; (b) Connolly, D. J.; Cusack, D.; O'Sullivan, T. P.; Guiry, P. J., Synthesis of quinazolinones and quinazoline. *Tetrahedron* **2005**, *61* (43), 10153-10202.
- ¹¹ Sharma, M.; Pandey, S.; Chauhan, K.; Sharma, D.; Kumar, B.; Chauhan, P. M., Cyanuric Chloride Catalyzed Mild Protocol for Synthesis of Biologically Active Dihydro/Spiro Quinazolinones and Quinazolinone-glycoconjugates. *The Journal of organic chemistry* **2012**, *77* (2), 929-37.
- ¹² Xu, W.; Fu, H., Amino acids as the nitrogen-containing motifs in copper-catalyzed domino synthesis of N-heterocycles. *The Journal of organic chemistry* **2011**, *76* (10), 3846-52.

¹³ Wang, Y.; Wang, H.; Peng, J.; Zhu, Q., Palladium-catalyzed intramolecular C(sp²)-H amidination by isonitrile insertion provides direct access to 4-aminoquinazolines from N-arylamidines. *Organic letters* **2011**, *13* (17), 4604-7.

¹⁴ (a) Decker, M.; Kraus, B.; Heilmann, J., Design, synthesis and pharmacological evaluation of hybrid molecules out of quinazolinimines and lipoic acid lead to highly potent and selective butyrylcholinesterase inhibitors with antioxidant properties. *Bioorganic & medicinal chemistry* **2008**, *16* (8), 4252-61; (b) Decker, M., Homobivalent quinazolinimines as novel nanomolar inhibitors of cholinesterases with dirigible selectivity toward butyrylcholinesterase. *Journal of medicinal chemistry* **2006**, *49* (18), 5411-3.

¹⁵ Decker, M.; Krauth, F.; Lehmann, J., Novel tricyclic quinazolinimines and related tetracyclic nitrogen bridgehead compounds as cholinesterase inhibitors with selectivity towards butyrylcholinesterase. *Bioorganic & medicinal chemistry* **2006**, *14* (6), 1966-77.

¹⁶ Perchellet, J. P.; Waters, A. M.; Perchellet, E. M.; Naganaboina, V. K.; Chandra, K. L.; Desper, J.; Rayat, S., Bioactivity of synthetic 2-halo-3-aryl-4(3H)-quinazoliniminium halides in L1210 leukemia and SK-BR-3 mammary tumor cells in vitro. *Anticancer research* **2011**, *31* (6), 2083-93.

¹⁷ (a) Hoveyda, H. R.; Marsault, E.; Gagnon, R.; Mathieu, A. P.; Vezina, M.; Landry, A.; Wang, Z.; Benakli, K.; Beaubien, S.; Saint-Louis, C.; Brassard, M.; Pinault, J. F.; Ouellet, L.; Bhat, S.; Ramaseshan, M.; Peng, X.; Foucher, L.; Beauchemin, S.; Bherer, P.; Veber, D. F.; Peterson, M. L.; Fraser, G. L., Optimization of the potency and pharmacokinetic properties of a macrocyclic ghrelin receptor agonist (Part I): Development of ulimorelin (TZP-101) from hit to clinic. *Journal of medicinal chemistry* **2011**, *54* (24), 8305-20; (b) Smith, V. C.; Cleghorn, L. A.; Woodland, A.; Spinks, D.; Hallyburton, I.; Collie, I. T.; Mok, N. Y.; Norval, S.; Brenk, R.; Fairlamb, A. H.; Frearson, J. A.; Read, K. D.; Gilbert, I. H.; Wyatt, P. G., Optimisation of the anti-Trypanosoma brucei activity of the opioid agonist U50488. *ChemMedChem* **2011**, *6* (10), 1832-40.

¹⁸ (a) White, M. C.; Burke, M. D.; Peleg, S.; Brem, H.; Posner, G. H., Conformationally restricted hybrid analogues of the hormone 1 alpha,25-dihydroxyvitamin D(3): design, synthesis, and biological evaluation. *Bioorganic & medicinal chemistry* **2001**, *9* (7), 1691-9; (b) Altmann, K. H.; Bold, G.; Caravatti, G.; Florsheimer, A.; Guagnano, V.; Wartmann, M., Synthesis and biological evaluation of highly potent analogues of epothilones B and D. *Bioorganic & medicinal chemistry letters* **2000**, *10* (24), 2765-8.

¹⁹ Naganaboina, V. K.; Chandra, K. L.; Desper, J.; Rayat, S., An easy entry into 2-halo-3-aryl-4(3H)-quinazoliniminium halides from heteroenyne-allenes. *Organic letters* **2011**, *13* (14), 3718-21.

²⁰ Krane, B. D.; Fagbule, M. O.; Shamma, M.; Gozler, B., The Benzophenanthridine Alkaloids. *J. Nat. Prod.* **1984**, *47* (1), 1-43.

²¹ Youn, S. W.; Bihn, J. H., Trifluoroacetic acid-mediated facile construction of 6-substituted phenanthridines. *Tetrahedron letters* **2009**, *50* (32), 4598-4601.

²² Donaldson, L. R.; Wallace, S.; Haigh, D.; Patton, E. E.; Hulme, A. N., Rapid synthesis and zebrafish evaluation of a phenanthridine-based small molecule library. *Organic & biomolecular chemistry* **2011**, *9* (7), 2233-9.

²³ (a) Ishikawa, T., Benzo[c]phenanthridine bases and their antituberculosis activity. *Medicinal research reviews* **2001**, *21* (1), 61-72; (b) Nakanishi, T.; Masuda, A.; Suwa, M.; Akiyama, Y.; Hoshino-Abe, N.; Suzuki, M., Synthesis of derivatives of NK109, 7-OH benzo[c]phenanthridine

alkaloid, and evaluation of their cytotoxicities and reduction-resistant properties. *Bioorganic & medicinal chemistry letters* **2000**, *10* (20), 2321-3.

²⁴ (a) Candito, D. A.; Lautens, M., Palladium-Catalyzed Domino Direct Arylation/N-Arylation: Convenient Synthesis of Phenanthridines. *Angew. Chem. Int. Ed.* **2009**, *48* (36), 6713-6716; (b) Buden, M. E.; Dorn, V. B.; Gamba, M.; Pierini, A. B.; Rossi, R. A., Electron-transfer-mediated synthesis of phenanthridines by intramolecular arylation of anions from N-(ortho-halobenzyl)arylamines: regiochemical and mechanistic analysis. *The Journal of organic chemistry* **2010**, *75* (7), 2206-18.

²⁵ (a) Linsenmeier, A. M.; Williams, C. M.; Brase, S., Synthesis of phenanthridine derivatives via photolysis. *The Journal of organic chemistry* **2011**, *76* (21), 9127-32; (b) Bernardo, P. H.; Wan, K. F.; Sivaraman, T.; Xu, J.; Moore, F. K.; Hung, A. W.; Mok, H. Y.; Yu, V. C.; Chai, C. L., Structure-activity relationship studies of phenanthridine-based Bcl-XL inhibitors. *Journal of medicinal chemistry* **2008**, *51* (21), 6699-710.

²⁶ (a) Blanchot, M.; Candito, D. A.; Larnaud, F.; Lautens, M., Formal synthesis of nitidine and NK109 via palladium-catalyzed domino direct arylation/N-arylation of aryl triflates. *Organic letters* **2011**, *13* (6), 1486-9; (b) Peng, J.; Chen, T.; Chen, C.; Li, B., Palladium-catalyzed intramolecular C-H activation/C-C bond formation: a straightforward synthesis of phenanthridines. *The Journal of organic chemistry* **2011**, *76* (22), 9507-13.

²⁷ (a) Gakunju, D. M. N.; Mberu, E. K.; Dossaji, S. F.; Gray, A. I.; Waigh, R. D.; Waterman, P. G.; Watkins, W. M., Potent Antimalarial Activity of the Alkaloid Nitidine, Isolated from a Kenyan Herbal Remedy. *Antimicrobial Agents and Chemotherapy* **1995**, *39* (12), 2606-2609; (b) Li, D.; Zhao, B.; Sim, S.-P.; Li, T.-K.; Liu, A.; Liu, L. F.; LaVoie, E. J., 8,9-Methylenedioxybenzo[i]phenanthridines: Topoisomerase I-Targeting activity and cytotoxicity. *Bioorganic & medicinal chemistry* **2003**, *11* (17), 3795-3805.

²⁸ (a) Pettit, G. R.; Gaddamidi, V.; Herald, D. L.; Singh, S. B.; Cragg, G. M.; Schmidt, J. M.; Boettner, F. E.; Williams, M.; Sagawa, Y., Antineoplastic agents, 120. *Pancreaticum littorale*. *Journal of natural products* **1986**, *49* (6), 995-1002; (b) Lewis, J. R., Amaryllidaceae and Sceletium alkaloids. *Natural product reports* **1994**, *11* (3), 329-32.

²⁹ (a) Nakanishi, T.; Suzuki, M., Revision of the structure of fagaridine based on the comparison of UV and NMR data of synthetic compounds. *Journal of natural products* **1998**, *61* (10), 1263-7; (b) Nakanishi, T.; Suzuki, M.; Mashiba, A.; Ishikawa, K.; Yokotsuka, T., Synthesis of NK109, an Anticancer Benzo[c]phenanthridine Alkaloid. *J. Org. Chem.* **1998**, *63* (13), 4235-4239.

³⁰ Chan, S. L.; Lee, M. C.; Tan, K. O.; Yang, L. K.; Lee, A. S.; Flotow, H.; Fu, N. Y.; Butler, M. S.; Soejarto, D. D.; Buss, A. D.; Yu, V. C., Identification of chelerythrine as an inhibitor of BclXL function. *The Journal of biological chemistry* **2003**, *278* (23), 20453-6.

³¹ (a) Amendola, V.; Fabbri, L.; Gianelli, L.; Maggi, C.; Mangano, C.; Pallavicini, P.; Zema, M., Electrochemical assembling/disassembling of helicates with hysteresis. *Inorganic chemistry* **2001**, *40* (14), 3579-87; (b) Bondarev, S. L.; Knyukshto, V. N.; Tikhomirov, S. A.; Pyrko, A. N., Picosecond dynamics of singlet excited states of oxotetrahydrobenzo[c]phenanthridine in protic and aprotic solvents. *Opt Spectrosc+* **2006**, *100* (3), 386-393.

³² (a) Zhang, J.; Lakowicz, J. R., Enhanced luminescence of phenyl-phenanthridine dye on aggregated small silver nanoparticles. *The journal of physical chemistry. B* **2005**, *109* (18), 8701-6; (b) Denny, W. A., Acridine derivatives as chemotherapeutic agents. *Current medicinal chemistry* **2002**, *9* (18), 1655-65.

-
- ³³ Stevens, N.; O'Connor, N.; Vishwasrao, H.; Samaroo, D.; Kandel, E. R.; Akins, D. L.; Drain, C. M.; Turro, N. J., Two color RNA intercalating probe for cell imaging applications. *Journal of the American Chemical Society* **2008**, *130* (23), 7182-3.
- ³⁴ (a) Lloyd, D. G.; Hughes, R. B.; Zisterer, D. M.; Williams, D. C.; Fattorusso, C.; Catalanotti, B.; Campiani, G.; Meegan, M. J., Benzoxepin-derived estrogen receptor modulators: a novel molecular scaffold for the estrogen receptor. *Journal of medicinal chemistry* **2004**, *47* (23), 5612-5; (b) Li, W.; Nelson, D. P.; Jensen, M. S.; Hoerrner, R. S.; Cai, D.; Larsen, R. D.; Reider, P. J., An improved protocol for the preparation of 3-pyridyl- and some arylboronic acids. *The Journal of organic chemistry* **2002**, *67* (15), 5394-7.
- ³⁵ (a) Fukuda, T.; Sudo, E.-I.; Shimokawa, K.; Iwao, M., Palladium-catalyzed cross-coupling of N-benzenesulfonyl-3,4-dibromopyrrole and its application to the total syntheses of lamellarins O, P, Q, and R. *Tetrahedron* **2008**, *64* (2), 328-338; (b) Tang, S.; Liu, M.; Gu, C.; Zhao, Y.; Lu, P.; Lu, D.; Liu, L.; Shen, F.; Yang, B.; Ma, Y., Synthesis and electrochemical properties of peripheral carbazole functional Ter(9,9-spirobifluorene)s. *The Journal of organic chemistry* **2008**, *73* (11), 4212-8.
- ³⁶ Stokes, B. J.; Jovanovic, B.; Dong, H.; Richert, K. J.; Riell, R. D.; Driver, T. G., Rh(2)(II)-catalyzed synthesis of carbazoles from biaryl azides. *The Journal of organic chemistry* **2009**, *74* (8), 3225-8.
- ³⁷ (a) Ashimori, A.; Bachand, B.; Calter, M. A.; Govek, S. P.; Overman, L. E.; Poon, D. J., Catalytic Asymmetric Synthesis of Quaternary Carbon Centers. Exploratory Studies of Intramolecular Heck Reactions of (Z)- α,β -Unsaturated Anilides and Mechanistic Investigations of Asymmetric Heck Reactions Proceeding via Neutral Intermediates. *Journal of the American Chemical Society* **1998**, *120* (26), 6488-6499; (b) Yanada, R.; Obika, S.; Kobayashi, Y.; Inokuma, T.; Oyama, M.; Yanada, K.; Takemoto, Y., Stereoselective Synthesis of 3-Alkylideneoxindoles using Tandem Indium-Mediated Carbometallation and Palladium-Catalyzed Cross-Coupling Reactions. *Adv. Synth. Catal.* **2005**, *347* (11-13), 1632-1642.
- ³⁸ (a) Cantagrel, G.; de Carne-Caravalet, B.; Meyer, C.; Cossy, J., Iron trichloride-promoted cyclization of o-alkynylaryl isocyanates: synthesis of 3-(chloromethylene)oxindoles. *Organic letters* **2009**, *11* (19), 4262-5; (b) Charalambides, Y. C.; Moratti, S. C., Comparison of Base-Promoted and Self-Catalyzed Conditions in the Synthesis of Isocyanates from Amines Using Triphosgene. *Synth. Commun.* **2007**, *37* (6), 1037-1044.
- ³⁹ Alajarin, M.; Molina, P.; Sanchez-Andrada, P., Preparation and Intramolecular Cyclization of Bis(carbodiimides). Synthesis and X-ray Structure of 1,3-Diazetidene-2,4-diimine Derivatives. *J. Org. Chem.* **1999**, *64* (4), 1121-1130.
- ⁴⁰ Jonckers, T. H.; van Miert, S.; Cimanga, K.; Bailly, C.; Colson, P.; De Pauw-Gillet, M. C.; van den Heuvel, H.; Claeys, M.; Lemiere, F.; Esmans, E. L.; Rozenski, J.; Quirijnen, L.; Maes, L.; Dommissie, R.; Lemiere, G. L.; Vlietinck, A.; Pieters, L., Synthesis, cytotoxicity, and antiparasitic activity of new neocryptolepine derivatives. *Journal of medicinal chemistry* **2002**, *45* (16), 3497-508.
- ⁴¹ (a) Wegener, G.; Brandt, M.; Duda, L.; Hofmann, J.; Kleszczewski, B.; Koch, D.; Kumpf, R.-J.; Orzesek, H.; Pirkl, H.-G.; Six, C.; Steinlein, C.; Weisbeck, M., Trends in industrial catalysis in the polyurethane industry. *Applied Catalysis A: General* **2001**, *221* (1-2), 303-335; (b) Hassner, A., *The Chemistry of Heterocyclic Compounds, Small Ring Heterocycles*. Wiley-Interscience: 1983; Vol. 42, p 524.

- ⁴² (a) Brown, C. J., The crystal structure of the phenyl isocyanate dimer. *J. Chem. Soc.* **1955**, 2931; (b) Buckles, R. E. M., L. A., A Kinetic Study of the Dimerization of Phenyl Isocyanate. *J. Am. Chem. Soc.*, **1966**, *88* (15), 3582-3586.
- ⁴³ Saunders, J. H. S., R. J., The Chemistry of the Organic Isocyanates. *Chem. Rev.*, **1948**, *43* (2), 203-218.
- ⁴⁴ (a) Nishikawa, T.; Urabe, D.; Tomita, M.; Tsujimoto, T.; Iwabuchi, T.; Isobe, M., One-pot transformation of trichloroacetamide into readily deprotectable carbamates. *Organic letters* **2006**, *8* (15), 3263-5; (b) Mukai, C.; Yoshida, T.; Sorimachi, M.; Odani, A., Co₂(CO)₈-catalyzed intramolecular hetero-Pauson-Khand reaction of alkynecarbodiimide: synthesis of (+/-)-physostigmine. *Organic letters* **2006**, *8* (1), 83-6.
- ⁴⁵ Dube, P.; Nathel, N. F.; Vetelino, M.; Couturier, M.; Aboussafy, C. L.; Pichette, S.; Jorgensen, M. L.; Hardink, M., Carbonyldiimidazole-mediated Lossen rearrangement. *Organic letters* **2009**, *11* (24), 5622-5.
- ⁴⁶ Arnold, R. G.; Nelson, J.; Verbanc, J. J., Recent Advances In Isocyanate Chemistry. *Chem. Rev.*, **1957**, *57* (1), 47-76.
- ⁴⁷ a) Kinoshita, H.; Ingham, O. J.; Ong, W. W.; Beeler, A. B.; Porco, J. A., Jr., Tandem processes identified from reaction screening: nucleophilic addition to aryl N-phosphinylimines employing La(III)-TFAA activation. *Journal of the American Chemical Society* **2010**, *132* (18), 6412-8; (b) Kiyooka, S.-I.; Fujiyama, R.; Uddin, K.; Goh, K.; Nagano, Y.; Fujio, M.; Tsuno, Y., The first N,N'-ditosyl-substituted cyclic boron cation, stabilized by neighboring-group participation by two sulfonyl groups, and the alternative, stabilized by polar solvents. *Tetrahedron letters* **2005**, *46* (2), 209-212.
- ⁴⁸ (a) Horino, Y.; Nakashima, Y.; Hashimoto, K.; Kuroda, S., Gold-Catalyzed Stereoselective Synthesis of Di- or Trisubstituted Olefins Possessing a 1,4-Diene Framework via Intramolecular Allylation of Alkynes. *Synlett* **2010**, *19*, 2879-2882; (b) Matveev, S. V.; Matveev, A. G.; Matrosov, E. I.; Shcherbakov, B. K.; Polikarpov, Y. M.; Kabachnik, M. I., Synthesis and acid-base properties of phosphorylated diazacycloalkanes and their cyclic analogs. *Russian Chemical Bulletin* **1994**, *43* (11), 1895-1901.
- ⁴⁹ Information obtained from the chemical properties of nitromethane on the bottle and also available at http://www.sigmaaldrich.com/catalog/ProductDetail.do?lang=en&N4=360554%7CSIAL&N5=SEARCH_CONCAT_PNO%7CBRAND_KEY&F=SPEC webpage accessed on 02/10/2012.
- ⁵⁰ DeHaan, F. P.; Delker, G. L.; Covey, W. C.; Ahn, J.; Anisman, M. S.; Brehm, E. C.; Chang, J.; Chicz, R. M.; Cowan, R. L., Electrophilic aromatic substitution. 8. A kinetic study of the Friedel-Crafts benzylation reaction in nitromethane, nitrobenzene, and sulfolane. Substituent effects in Friedel-Crafts benzylation. *Journal of the American Chemical Society* **1984**, *106* (23), 7038-7046.
- ⁵¹ Ohta, K.; Koketsu, E.; Nagase, Y.; Takahashi, N.; Watanabe, H.; Yoshimatsu, M., Lewis acid-catalyzed propargylic etherification and sulfanylation from alcohols in MeNO-HO. *Chemical & pharmaceutical bulletin* **2011**, *59* (9), 1133-40.
- ⁵² Graham Solomons, T. W.; Fryhle, C., *Organic Chemistry*. 9th ed.; Wiley: 2007; p 650.
- ⁵³ This reaction was carried out in reagent grade CH₃NO₂ (≤ 0.05% H₂O) and appears that the trace amount of water presence in the nitromethane was sufficient to for the cascade cyclization reaction without the need for additional water

Chapter 4 - Theoretical Studies on the Optoelectronic Properties of Phenanthridine fused Quinazoliniminiums

4.1 Introduction

There is a growing research interest in the development of more efficient and high performance Organic Light-Emitting Diodes (OLEDs) due to their applications in the development of new electroluminescent components for organic materials.^{1,2} OLEDs have several advantages over conventional LEDs such as greater contrast, superior brightness, broader emission. These are also low weight and offer low-cost display.³ Most importantly, the photophysical properties of organic LED molecules can be manipulated by chemical modification to produce materials with tailored optoelectronic properties.⁴ Thus, OLEDs have revolutionized display technologies and are already in use in mobile phones, car radios, digital cameras and personal computers etc.⁵

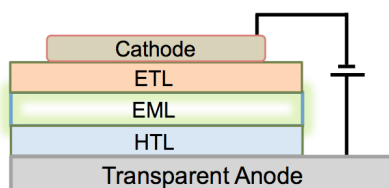


Figure 4.1: Basic schematic of multilayer OLED device.

OLEDs consist of an electron-transport layer (ETL), emissive layer (EML), hole-transport layer (HTL) sandwiched between two electrodes. The cathode is metallic and anode is usually made of indium tin oxide (Figure 4.1).^{6,7} The mechanism of electroluminescence is well established and involves the injection of electrons from the low work function metallic cathode into the LUMO (Lowest Unoccupied Molecular Orbital) of the electron-transport layer (ETL) and simultaneous, injection of holes (extraction of electrons) into the HOMO (Highest Occupied Molecular Orbital) of the hole-transport layer (HTL) at the anode under an applied current (Figure 4.2). The electron-hole pairs migrate and recombine in the emissive layer (EML) to form excitons, which relax to the ground state by emitting light.^{7,8,9,10} The energy difference (band gap) between the HOMO and LUMO levels (HOMO-LUMO gap) of EML determines the color

of light emitted and influences the charge transport and injection, which in turn determines the efficiency of OLEDs.

It is believed that for an efficient hole-injection from the anode, the HOMO level of HTL should be in 5 – 6 eV range, whereas for an efficient electron injection from the cathode, the LUMO energy level of ETL must be in the range 2–3 eV.¹⁰ A band gap of 0.5 eV or smaller is desired in the EML for high performance in electroluminescent applications, which is a considerable challenge.¹¹

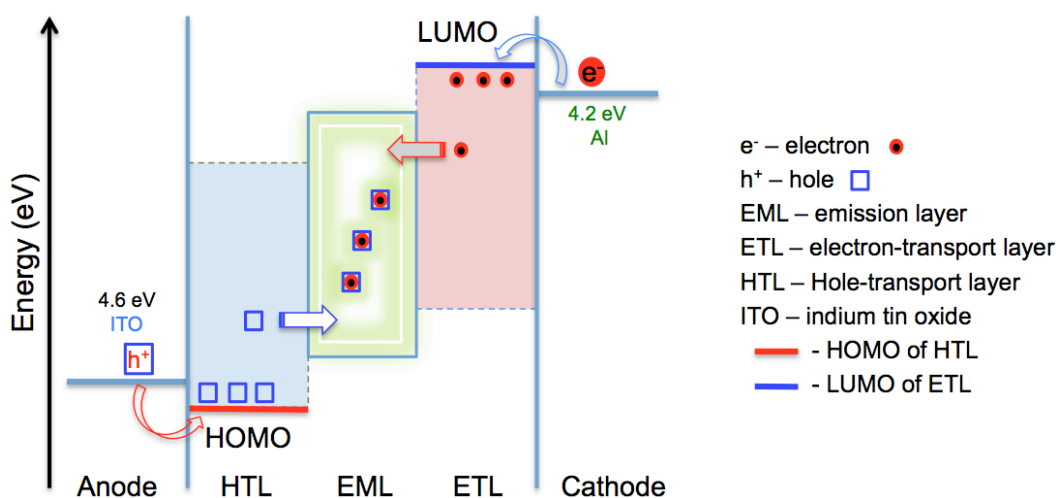


Figure 4.2: Schematic of energy level diagram for a multilayer OLED.

There are two types of organic materials (chromophores) commonly used for OLEDs. Those that are based on small molecules and polymers, both of which have demonstrated significant advantages in OLED technology, and have also contributed to the basic understanding of current electroluminescent materials.^{8,9} Some examples of small compounds commonly used as hole transporters are shown in Figure 4.3 that includes 4,4',4''-tris(3-methylphenylphenylamino) triphenylamine (MT-DATA) (**128**) *N,N'*-diphenyl-*N,N'*-(3-methylphenyl)-1,1'-biphenyl-4,4'-diamine (TPD) (**129**) and its analog 1,4-bis(1-naphthylphenylamino) biphenyl (NPB) (**130**). Tris(8-hydroxyquinolato)aluminum (Alq₃) (**131**) and 2-(4-biphenyl)-5-(4-*tert*-butylphenyl)-1,3,4-oxadiazole (PBD) (**132**), both are normally used as electron transporters.^{8,9} **131** is also a widely used emitter.^{4,8}

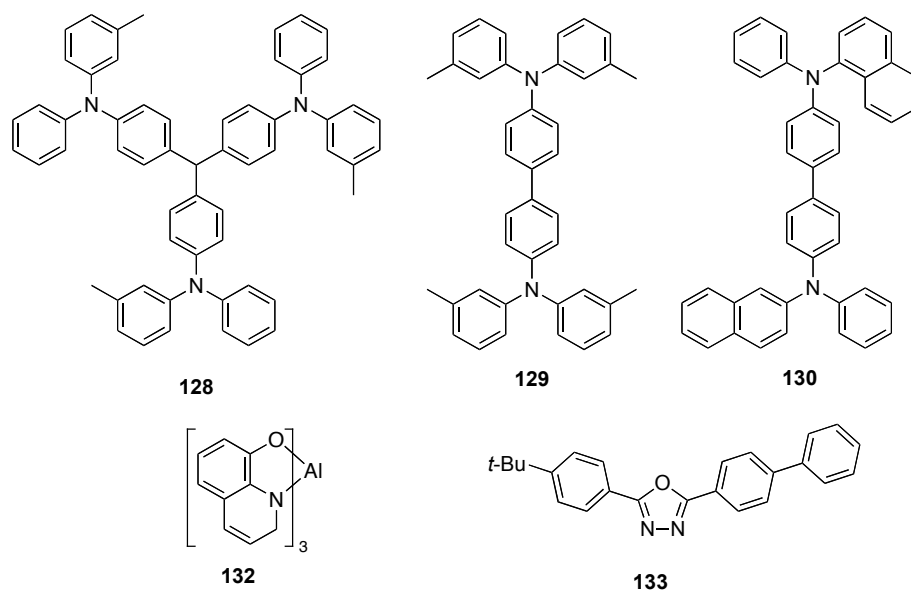


Figure 4.3: Chemical structure of small molecules and polymeric materials used in the fabrication of OLEDs.^{4,8}

Recently, bridgehead-nitrogen containing fused heterocyclic molecules have attracted interest as highly efficient chromophores for the development of OLEDs (Figure 4.4). For instance, imidazole[1,5-*a*]pyridines¹² (**136**) and pyrrolo[1,2-*b*]pyridines¹³ (**137**) both emit intense blue light whereas pyrrolo[1,2-*b*]cinnolines (**138**) as well as benzo[*f*]pyridazines[6,1-*a*]isoindole-5,10-diones (**139**) both emit green light.¹³ Similarly, indolizino[3,4,5-*ab*]isoindoles (**140**) chromophores are excellent light-emitting compounds that emit different colors ranging from blue to green.^{14,15} The presence of N-atom at the ring fusion is known to impart unique photophysical properties to these compounds,^{16,17} such as excellent luminescence and easily tunable emission colors for device fabrication.¹⁸ Furthermore, these small organic molecules exhibit considerable advantages such as broad emission spectra, and easy fabrication into multilayer devices.¹⁴

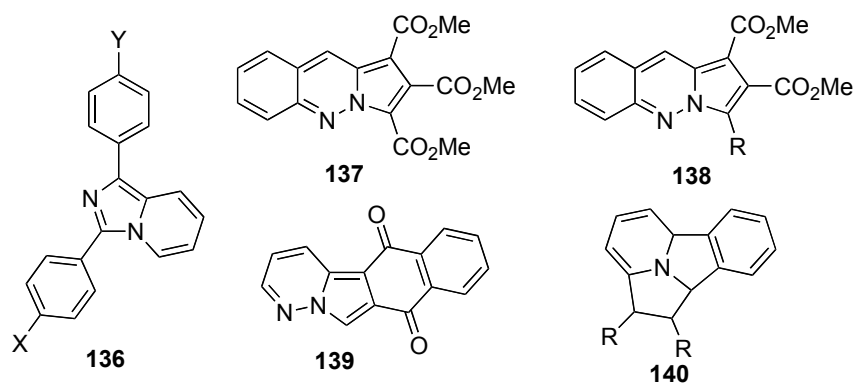


Figure 4.4: Bridgehead-nitrogen containing chromophores proposed for use in OLEDs.¹³⁻¹⁵

Polymeric materials used for the fabrication of OLEDs are usually conjugated in order to increase conductance. These polymer LEDs (PLEDs) are lightweight and flexible, therefore, can easily be employed for image display technology.^{19,20} Poly(9,9-dioctylfluorene) (**141**) and its analog, the poly(9,9-dioctylfluorene-co-benzothiadiazole) (**142**), and poly(9,9-dioctylfluorene-co-*N*-(4-butylphenyl)diphenylamine) (**143**), poly(*p*-phenylenevinylene) (**144**), poly(ethylene dioxathiophene) (**145**), poly(*N*-vinylcarbazole) (**146**) and poly(styrene sulfonic acid) (**147**) are interesting examples of electroluminescent polymers used in PLED displays (Figure 4.5).^{21,22}

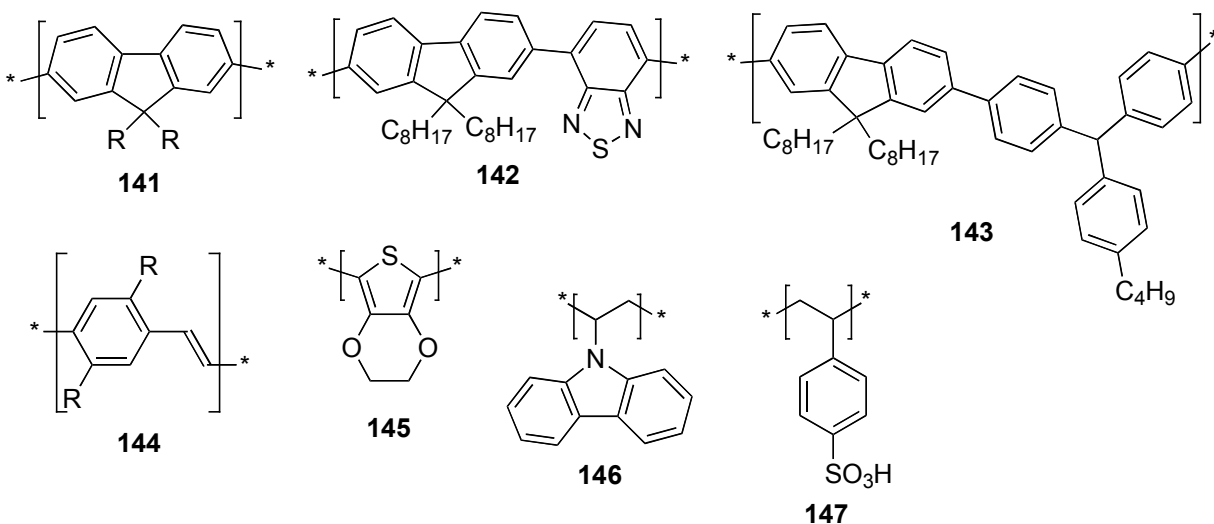


Figure 4.5: Chemical structure of some polymeric materials used in OLEDs.^{21,22}

Although, many chromophores based on small molecules or polymers have been designed for potential OLEDs, only a few to date have been particularly successful in these

applications. There are many drawbacks of the existing OLED molecules.^{23,24,25} For instance, current OLEDs are composed of multilayers of hole transporting layer, an emissive layer, an electron transporting layer sandwiched between two electrodes (Figure 2.1). The fabrication of very thin OLEDs with one or two layers is still a major challenge as only a limited number of molecules are available to date that can function as an emitter as well as either a hole- or electron-transport material.^{26,27,28} In addition, chromophores that offer the possibility of tuning emission color and HOMO-LUMO energy levels without compromising the fluorescence are scarce. Therefore, more compounds with finer properties are needed that overcome these aforementioned limitations and to broaden the range of available properties²⁹ so as to obtain improved performance.

We evaluated derivatives of phenanthridine-fused quinazoliniminiums, PNQs (**148_n-X** and **148_n-Y**) and their free base (**149_n-X** and **149_n-Y**) for potential applications in OLED technology. Note that “X” refers to the presence of an electron donating group (EDG) *e.g.* NMe₂ while “Y” refers to the presence of an electron withdrawing groups (EWG) *e.g.* Cl, NO₂, and the subscript “n” refers to their position on the chromophore. The substitution at C3, C6 and C12 was considered on A, B and C rings respectively, therefore “n” was equal to 3, 6, 12 (Figure 4.6). We believed that due to the presence of a bridgehead nitrogen atom, analogous to the OLED molecules shown in Figure 4.4, these would exhibit optical properties desired for application in electroluminescent devices. Since computational methods have provided indispensable tools in gaining insight into the optoelectronic properties of organic compounds and subsequently, guiding experimental research, we decided to use density functional theory to identify lead structures with promise in organic materials and the results are presented and discussed.

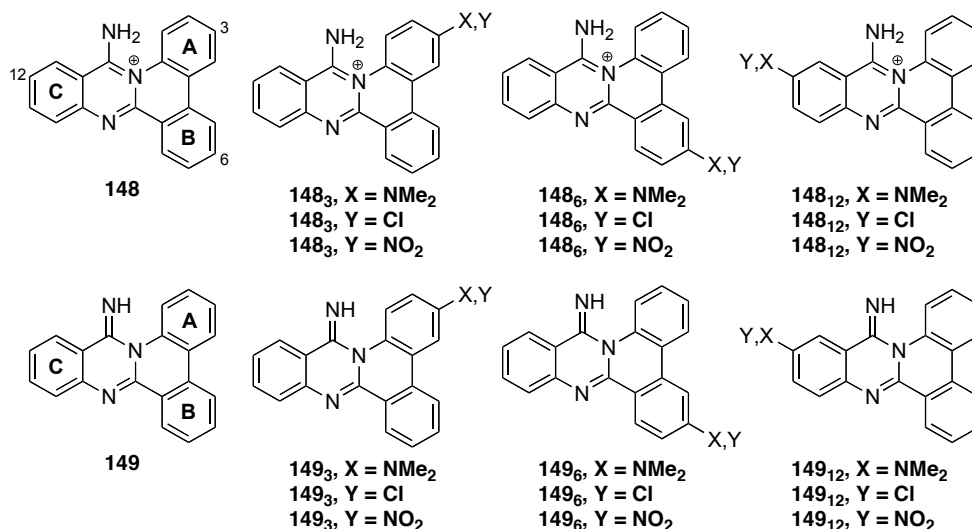


Figure 4.6: Structure of phenanthridine-fused quinazoliniminiums **148_n-X,Y** and their free base **149_n-X,Y**.

4.2 Computational Methods

All calculations have been performed using the Gaussian 09 package of program. The geometry optimizations employed B3LYP functional in conjunction with 6-311+G* basis set. All geometry optimizations were followed by vibrational analyses to confirm that each structure corresponded to a stationary point on the potential energy surface. Vertical excitation energies were computed using Time Dependent Density Functional Theory (TDDFT) at the optimized geometries. The molecular orbitals were visualized using Gaussview. The vertical and adiabatic Ionization Potentials (IP) and Electron Affinities (EA), Hole Extraction Potentials (HEP), Electron Extraction Potentials (EEP), reorganization energies for hole (λ_{hole}) and electron ($\lambda_{\text{electron}}$) were calculated using the equations below, and as described by Rang and Fang.³⁰ M refers to **148_n-X,Y** or **149_n-X,Y**.

$$\text{IP (v)} = E^+ (\text{M}) - E (\text{M}) \quad \text{Equation 4.1}$$

$$\text{IP (a)} = E^+ (\text{M}^+) - E (\text{M}) \quad \text{Equation 4.2}$$

$$\text{EA (v)} = E (\text{M}) - E^- (\text{M}) \quad \text{Equation 4.3}$$

$$\text{EA (a)} = E (\text{M}) - E^- (\text{M}^-) \quad \text{Equation 4.4}$$

$$\text{HEP} = E^+ (\text{M}^+) - E (\text{M}^+) \quad \text{Equation 4.5}$$

$$EEP = E(M^+) - E^-(M^+) \quad \text{Equation 4.6}$$

$$\lambda_{\text{hole}} = IP(v) - HEP \quad \text{Equation 4.7}$$

$$\lambda_{\text{electron}} = EEP - EA(v) \quad \text{Equation 4.8}$$

4.3 Results and Discussion

4.3.1 Frontier Molecular Orbitals

In order to determine the optoelectronic properties of PNQs **148_n-X, Y** and **149_n-X,Y**, the HOMOs, LUMOs and their corresponding energy gaps were examined for the optimized geometries at B3LYP /6-311+G*. The isodensity plots of the Frontier Molecular Orbitals (FMOs) for **148_n-X, Y** all exhibit π -type characteristics. The FMOs of the unsubstituted **148-H** are shown in Figure 4.7 (top). In general, the HOMO exhibits a bonding character whereas the LUMO display an antibonding character. The HOMO orbital is delocalized over the entire molecule, while the LUMO orbital is mainly localized over the quinazoliniminium moiety. The FMOs of all other the derivatives of **148_n-X** and **148_n-Y** considered in this study demonstrate similar characteristics as that of **148-H**, with the exception of **148₃-NO₂** in which the LUMOs exhibit a bonding character at the N-C₁₆, C₁-C₂, C₃-N and C₄-C₁₇, bonds (Figure 4.7, bottom right) and supports the resonance structure **148₃-NO₂'** (Scheme 4.1).

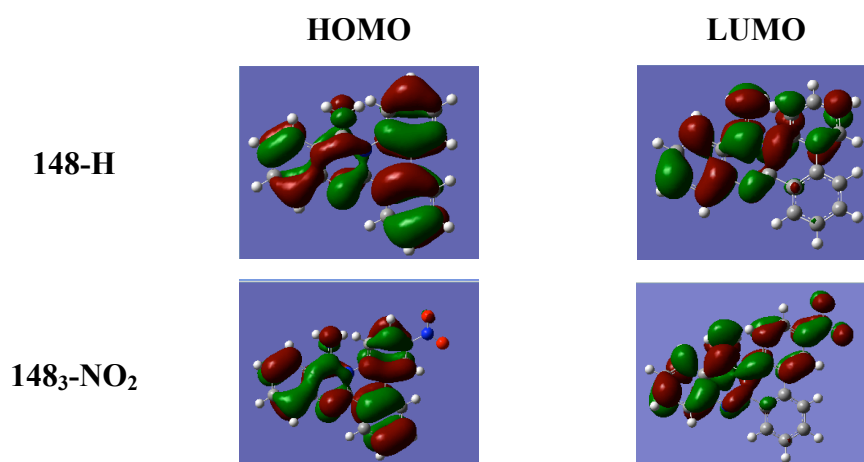
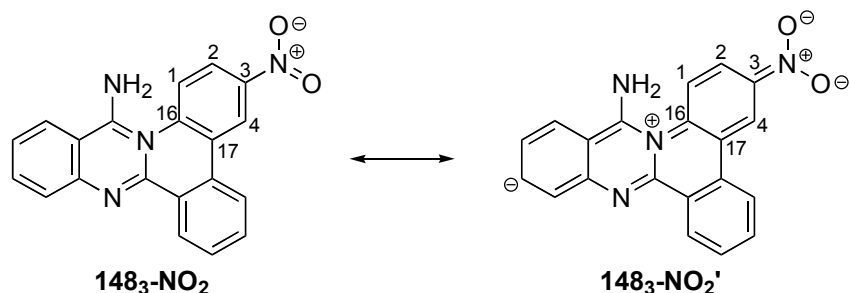


Figure 4.7: Selected FMOs of **148H** and **148₃-NO₂**



Scheme 4.1: Resonance structure of **148₃-NO₂**.

The FMOs of the unsubstituted free base PNQ **149-H** is shown below (Figure 4.8). Similar to **148-H**, the HOMO and LUMO exhibit a bonding and antibonding characteristics, respectively and are delocalized over the entire molecule. The LUMOs exhibit a bonding character at the C₅-C₁₈, C₇-C₈, C₉-C₁₉, N-C₂₀, C₁₅-N, C₁₀-C₁₁ and C₁₃-C₁₄ bonds that supports the resonance structures **149-H'** and **149-H''** (Scheme 4.2).

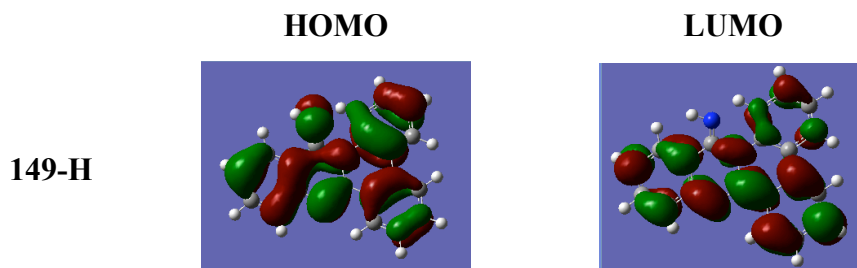
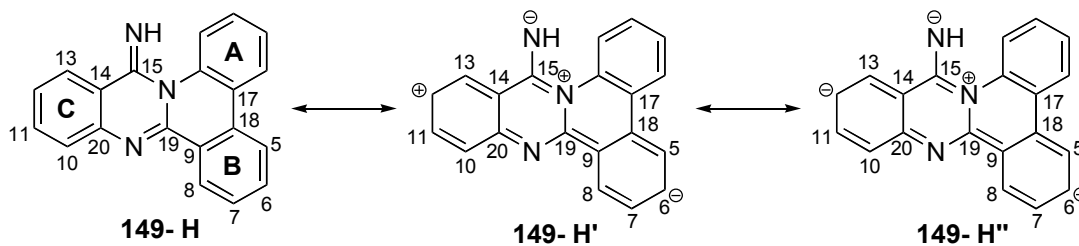


Figure 4.8:FMOs of **149H**.



Scheme 4.2: Resonance structures of **149-H**.

The FMOs of all other derivatives of PNQs **149_n-X** and **149_n-Y** considered in this study demonstrate similar characteristics as that of **149-H**, except the LUMO of **149₃-NO₂**, **149₆-NO₂** and **149₁₂-NO₂**, which is exclusively localized on the A, B and C rings of the PNQ scaffold,

respectively (Figure 4.9), indicating significant contributions from the corresponding resonance structures $149_3\text{-NO}_2'$, $149_6\text{-NO}_2'$ and $149_{12}\text{-NO}_2'$ (Scheme 4.3).

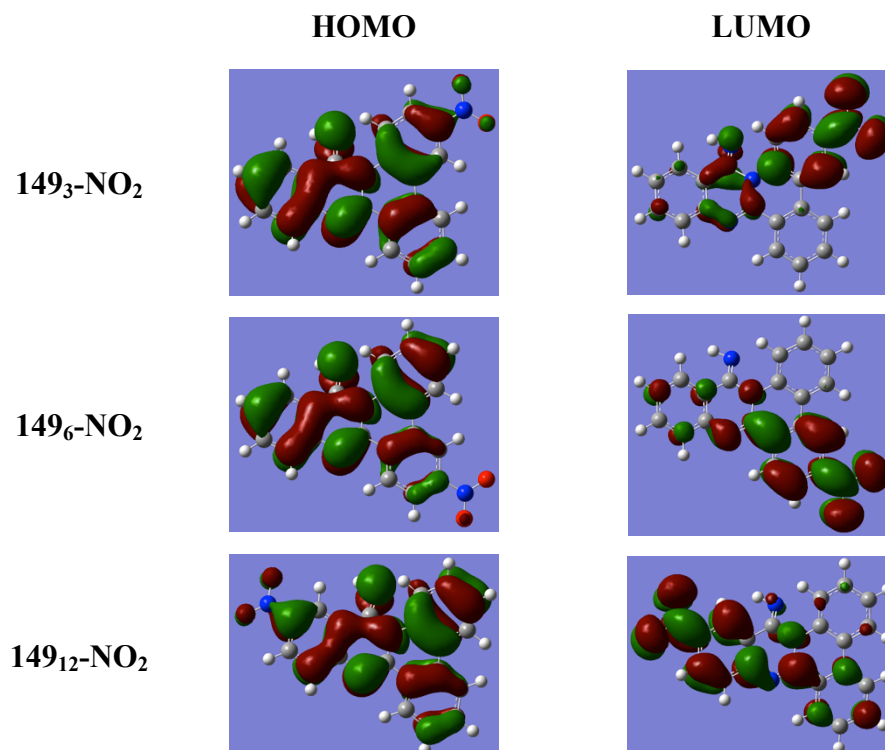
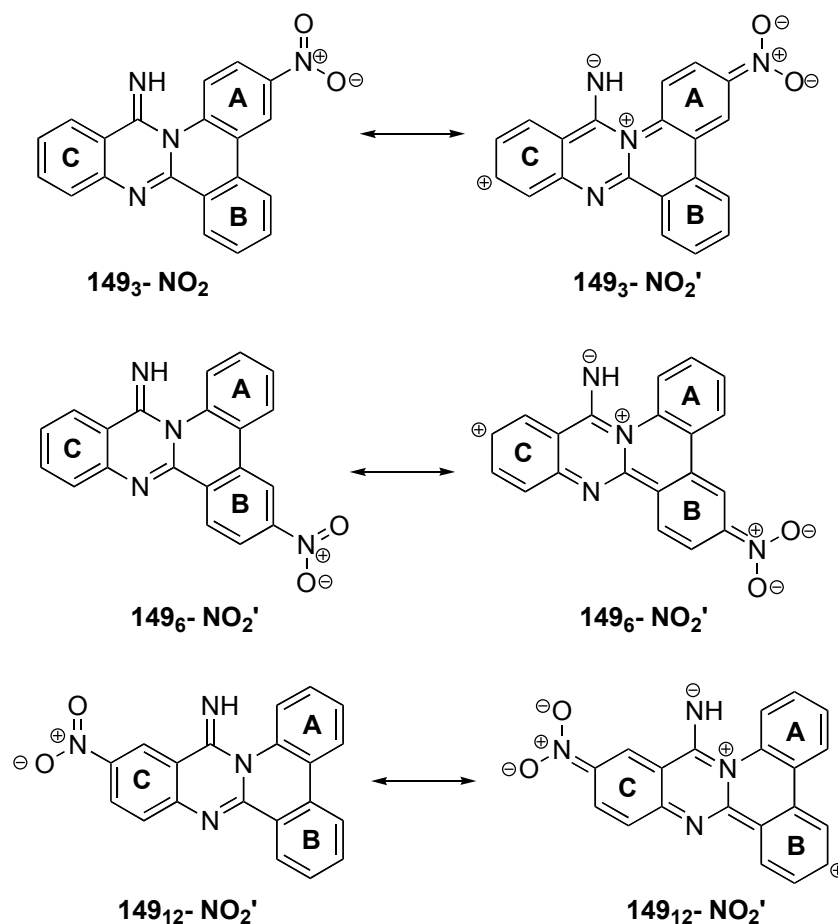


Figure 4.9: Selected FMOs of 149_n-NO_2 .



Scheme 4.3: Resonance structures of **149_n-NO₂'**.

The HOMO, and LUMO energies and corresponding gaps (ΔE_{H-L}) are listed in Table 4.1. Our results revealed that the HOMO energies increase with the incorporation of EDG (NMe₂) on PNQs **148** and their free bases **149**, suggesting an improved hole creating ability, while the LUMO energies decrease upon substitution with EWG (Cl, NO₂) implying an improved electron accepting ability (Figure 4.2). Overall, the HOMO-LUMO energy gaps are influenced by the nature of the substituent and its position, which indicates the tunability in the electronic properties of these PNQs chromophores. Furthermore, the HOMO (~5-6 eV) and LUMO energies (~2-3 eV) of the free base PNQs **149** are in the range desired for efficient hole and electron injection in OLEDs devices.¹⁰

Table 4.1: HOMOs, LUMOs energies and energy gaps (ΔE) calculated for PNQs **148** and its free base **149**.

| X, Y | 148 | | | 149 | | |
|----------------------------|----------------------|----------------------|--------------------------|----------------------|----------------------|--------------------------|
| | -HOMO [eV] | -LUMO [eV] | ΔE_{H-L} [eV] | -HOMO [eV] | -LUMO [eV] | ΔE_{H-L} [eV] |
| -H | 9.57 | 5.93 | 3.64 | 5.80 | 1.89 | 3.91 |
| Substitution at C3 | | | | | | |
| NMe ₂ | 8.53 | 5.54 | 2.99 | 5.23 | 1.74 | 3.49 |
| Cl | 9.67 | 6.03 | 3.65 | 5.92 | 2.04 | 3.88 |
| NO ₂ | 9.93 | 6.40 | 3.54 | 6.26 | 2.87 | 3.39 |
| Substitution at C6 | | | | | | |
| NMe ₂ | 8.36 | 5.56 | 2.80 | 5.38 | 1.52 | 3.86 |
| Cl | 9.58 | 6.01 | 3.57 | 5.92 | 2.06 | 3.87 |
| NO ₂ | 9.99 | 6.24 | 3.75 | 6.19 | 3.16 | 3.03 |
| Substitution at C12 | | | | | | |
| NMe ₂ | 8.52 | 5.58 | 2.94 | 5.17 | 1.60 | 3.57 |
| Cl | 9.60 | 6.08 | 3.51 | 5.91 | 2.05 | 3.86 |
| NO ₂ | 9.92 | 6.40 | 3.52 | 6.30 | 3.01 | 3.29 |

4.3.2 Ionization potentials and Electron affinities

Since the performance of OLED devices depend on the injection and mobility of holes and electrons as well as the charge balance, we evaluated the energy barrier for the injection of holes and electrons by investigating the ionization potentials (IP) and electron affinities (EA) of PNQs **148** and their free bases **149**. The rate of charge transfer and balance was estimated by calculating reorganization energies (λ). Table 4.2 shows a list of the calculated vertical (v) and adiabatic (a) IP and EA as well as the hole extraction potentials (HEP), electron extraction potentials (EEP), reorganization energies for hole injection (λ_{hole}) and electron transfer ($\lambda_{\text{electron}}$) for **148_n-X** and **148_n-Y**.

Our results reveal that IP for **148₃-NMe₂** are lower (9.92 eV) than **148-H** (10.93 eV), which indicates that the presence of EDG (NMe₂) improves the hole creating ability of the chromophore. In case of **148₃-NO₂**, EA values (5.07 eV) are higher than **148-H** (4.51 eV), thus demonstrating that incorporation of a strong EWG increases the electron accepting abilities of the chromophore. Similar results were obtained for other derivatives of **148** (**148₆-X**, **148₆-Y**, **148₁₂-X**, **148₁₂-Y**).

Table 4.2: Calculated Ionization Potentials (IP), Electron affinities (EA), Extraction Potentials (EP) and reorganization energies for **148_n-X** and **148_n-Y**.

| Structure | IP (v) | IP (a) | HEP | EA (v) | EA (a) | EEP | λ_{hole} | $\lambda_{\text{electron}}$ |
|-------------------------------------|--------|--------|-------|--------|--------|------|-------------------------|-----------------------------|
| 148-H | 10.93 | 10.84 | 10.74 | 4.51 | 4.81 | 5.13 | 0.19 | 0.62 |
| 148 ₃ -NMe ₂ | 9.92 | 9.83 | 9.71 | 4.18 | 4.48 | 4.81 | 0.21 | 0.64 |
| 148 ₃ -Cl | 10.99 | 10.90 | 10.81 | 4.63 | 4.92 | 5.24 | 0.18 | 0.61 |
| 148 ₃ -NO ₂ | 11.27 | 11.16 | 11.06 | 5.07 | 5.29 | 5.55 | 0.21 | 0.48 |
| 148 ₆ -NMe ₂ | 9.68 | 9.61 | 9.54 | 4.20 | 4.52 | 4.87 | 0.14 | 0.66 |
| 148 ₆ -Cl | 10.90 | 10.80 | 10.69 | 4.60 | 4.90 | 5.23 | 0.20 | 0.63 |
| 148 ₆ -NO ₂ | 11.32 | 11.21 | 11.11 | 4.89 | 5.12 | 5.45 | 0.21 | 0.56 |
| 148 ₁₂ -NMe ₂ | 9.85 | 9.74 | 9.61 | 4.23 | 4.53 | 4.84 | 0.24 | 0.61 |
| 148 ₁₂ -Cl | 10.91 | 10.81 | 10.70 | 4.69 | 4.99 | 5.31 | 0.21 | 0.62 |
| 148 ₁₂ -NO ₂ | 11.27 | 11.17 | 11.06 | 5.03 | 5.28 | 5.58 | 0.21 | 0.54 |

We also calculated the IP and EA for free bases of PNQs **149**. Analogous to **148**, the presence of EDG in case of **149₃-NMe₂**, **149₆-NMe₂**, **149₁₂-NMe₂** decreases the IPs relative to **149-H** (6.52 eV, 6.63 eV, 6.48 eV Vs 7.15 eV), while the incorporation of EWG such as in **149₃-NO₂**, **149₆-NO₂**, **149₁₂-NO₂** increases the EAs (1.40 eV, 1.69 eV, 1.61 eV Vs 0.77 eV)

confirming an improvement in the hole creating and electron accepting abilities relative to the unsubstituted free base **149-H**, respectively.

Table 4.3: Calculated Ionization Potentials (IP), Electron affinities (EA), Extraction Potentials (EP) and reorganization energies for **149_n-X** and **149_n-Y**.

| Structure | IP (v) | IP (a) | HEP | EA (v) | EA (a) | EEP | λ_{hole} | $\lambda_{\text{electron}}$ |
|-----------------------------------|--------|--------|------|--------|--------|------|-------------------------|-----------------------------|
| 2-H | 7.15 | 7.05 | 6.95 | 0.56 | 0.77 | 0.99 | 0.21 | 0.43 |
| 2 ₃ -NMe ₂ | 6.52 | 6.36 | 6.23 | 0.45 | 0.68 | 0.93 | 0.29 | 0.48 |
| 2 ₃ -Cl | 7.24 | 7.14 | 7.04 | 0.74 | 0.94 | 1.16 | 0.21 | 0.42 |
| 2 ₃ -NO ₂ | 7.59 | 7.46 | 7.33 | 1.40 | 1.59 | 1.78 | 0.25 | 0.38 |
| 2 ₆ -NMe ₂ | 6.63 | 6.52 | 6.42 | 0.27 | 0.58 | 0.86 | 0.20 | 0.59 |
| 2 ₆ -Cl | 7.25 | 7.15 | 7.03 | 0.75 | 0.96 | 1.17 | 0.23 | 0.42 |
| 2 ₆ -NO ₂ | 7.53 | 7.42 | 7.31 | 1.69 | 1.95 | 2.20 | 0.22 | 0.52 |
| 2 ₁₂ -NMe ₂ | 6.48 | 6.29 | 6.12 | 0.32 | 0.63 | 0.91 | 0.36 | 0.59 |
| 2 ₁₂ -Cl | 7.23 | 7.12 | 7.00 | 0.74 | 0.95 | 1.16 | 0.23 | 0.42 |
| 2 ₁₂ -NO ₂ | 7.61 | 7.52 | 7.43 | 1.61 | 1.80 | 1.97 | 0.18 | 0.36 |

In order to gain insight into the mobility of the hole injection and electron transport for these PNQs chromophores we calculated the reorganization energies (λ) using equations 4.7 and 4.8.³⁰ The calculated hole injection (λ_{hole}) and the electron acceptance ($\lambda_{\text{electron}}$) values for PNQs **148_n-X,-Y** and its free base **149_n-X,-Y** are listed on Tables 4.2 and 4.3, respectively. Note that lower the λ values, the bigger the charge-transport rate. Our results revealed that for all the PNQs considered in this study, the λ_{hole} values are smaller than their respective $\lambda_{\text{electron}}$ values, suggesting that PNQs can serve as a better hole transporting organic molecules than the electron transporting organic molecules.

4.4 Conclusion

These studies show that the optoelectronics properties of the PNQ derivatives **148_n-X,Y** and their free bases **149_n-X,Y** such as HOMOs, LUMOs and energy gaps can be fine tuned by varying the nature and positions of the substituents. The HOMO and LUMO levels of the free base derivatives, **149_n-X,Y** are in the range desired for applications in organic materials (~5 – 6 eV and 2 – 3 eV, respectively). The presence of electron donating group on these ring systems increases the energies of the HOMOs while the presence of electron withdrawing group decrease energies of the LUMOs. And, similarly the ionization potentials decreases and electron affinities increase upon incorporation of electron donating group and electron withdrawing group, which indicates an improvement in the hole creating and electron accepting capabilities, respectively. The results of the reorganization energy (λ) suggest that PNQs and their free bases can serve as efficient hole transporting materials in OLEDs.

Reference:

- ¹ (a) Kraft, A.; Grimsdale, A. C.; Holmes, A.B.; Electroluminescent Conjugated Polymers—Seeing Polymers in a New Light, *Angew. Chem., Int. Ed.* **1998**, *37*, 402; (b) Braun, D.; Heeger, A. Visible light emission from semiconducting polymer diodes; *J. Appl. Phys. Lett.* **1991**, *58*, 1982.
- ² (a) Shirota, Y.; Organic materials for electronic and optoelectronic devices; *J. Mater. Chem.* **2000**, *10*, 1.; (b) Zou, L. Y.; Ren, A. M.; Feng, J. K.; Liu, Y. L.; Ran, X. Q.; Sun, C. C.; Theoretical Study on Photophysical Properties of Multifunctional Electroluminescent Molecules with Different π -Conjugated Bridges; *J. Phys. Chem. A.*, **2008**, *112*, 12172.
- ³ Bardsley, J. N.; International OLED technology roadmap; *IEEE Journal of Selected Topics in Quantum Electronics*; **2004**, *10* (1): 3–9.
- ⁴ Khan, R. U. A.; Hunziker, C.; Guenter, P.; Perspectives on organic light-emitting diodes for display applications. *J. Mater. Sci.: Mater. Electron* **2006**, *17*, (6), 467-474.
- ⁵ (a) Dimitrakopoulou, C. D.; Malenfant, P. R. L.; Organic Thin Film Transistors for Large Area Electronics; *Adv. Mater.* **2002**, *14*, 99; (b) Peumans, P.; Yakimov, A.; Forrest, S. R.; Small molecular weight organic thin-film photodetectors and solar cells; *J. Appl. Phys.* **2003**, *93*, 3693.
- ⁶ (a) Baldo, M. A.; O'Brien, D. F.; You, Y.; Shoustikov, A.; Sibley, S.; Thompson, M. E.; Forrest, S. R.; Highly efficient phosphorescent emission from organic electroluminescent devices; *Nature*, **1998**, *395*, 151; (b) Koech, P. K.; Polikarpov, E.; Rainbolt, J. E., Cosimbescu, L.; Swensen, J. S.; Von Ruden, A. L.; Padmaperuma, A. B.; Synthesis and Application of Pyridine-Based Ambipolar Hosts: Control of Charge Balance in Organic Light-Emitting Devices by Chemical Structure Modification; *Org. Lett.* **2010**, *12*(23), 5534-37.
- ⁷ Huang, Q.; Evmenenko, G. A.; Dutta, P.; Lee P.; Armstrong, N. R.; Marks, T. J.; Covalently Bound Hole-Injecting Nanostructures. Systematics of Molecular Architecture, Thickness, Saturation, and Electron-Blocking Characteristics on Organic Light-Emitting Diode Luminance, Turn-on Voltage, and Quantum Efficiency; *J. Am. Chem. Soc.* **2005**, *127*, 10227-242.
- ⁸ Veinot, J. G. C.; Marks, T. J.; Toward the Ideal Organic Light-Emitting Diode. The Versatility and Utility of Interfacial Tailoring by Cross-Linked Siloxane Interlayers; *Acc. Chem. Res.* **2005**, *38*, 632-643
- ⁹ (a) Kido, J.; Okamoto Y.; Organo lanthanide metal complexes for electroluminescent materials; *Chem. Rev.* **2002**, *102*, 2357-68.
- ¹⁰ Geffroy, B.; Le Roy, P.; Prat, C.; Organic light-emitting diode (OLED) technology: materials, devices and display technologies; *Polym Int.* **2006**, *55*, 572-582.
- ¹¹ Perepichka D. F.; Bryce, M. R.; Molecules with exceptionally small HOMO-LUMO gaps. *Angew. Chem. Int. Ed.* **2005**, *44*, 5370-5373
- ¹² Shibahara, F.; Sugiura, R.; Yamaguchi, E.; Kitagawa, A.; Murai, T.; Synthesis of Fluorescent 1,3-Diarylated Imidazo[1,5-*a*]pyridines: Oxidative Condensation–Cyclization of Aryl-2-Pyridylmethylamines and Aldehydes with Elemental Sulfur as an Oxidant; *J. Org. Chem.*, **2009**, *74* (9), 3566–3568.
- ¹³ Mitsumori, T.; Bendikov, M.; Sedó, J.; Wudl, F.; Synthesis and Properties of Novel Highly Fluorescent Pyrrolopyridazine Derivatives; *Chem. Mater.* **2003**, *15*, 3759
- ¹⁴ Mitsumori, T.; Bendikov, M.; Dautel, O.; Wudl, F.; Shioya, T.; Sato, H.; Sato, Y.; Synthesis and Properties of Highly Fluorescent Indolizino[3,4,5-*ab*]isoindoles; *J. Am. Chem. Soc.* **2004**, *126*, 16793-803.

- ¹⁵ Shen, Y.-M.; Grampp, G.; Leesakul, N.; Hu, H.-W.; Xu, J.-H. Synthesis and Emitting Properties of the Blue-Light Fluorophores Indolizino[3,4,5-*ab*]isoindole Derivatives; *Eur. J. Org. Chem.* **2007**, 3718-26.
- ¹⁶ Shibahara, F.; Kitagawa, A.; Yamaguchi, E.; Murai, T., Synthesis of 2-Azaindolizines by Using an Iodine-Mediated Oxidative Desulfurization Promoted Cyclization of N-2-Pyridylmethyl Thioamides and an Investigation of Their Photophysical Properties. *Org. Lett.* **2006**, 8, (24), 5621-5624.
- ¹⁷ Shibahara, F.; Sugiura, R.; Yamaguchi, E.; Kitagawa, A.; Murai, T., Synthesis of fluorescent 1,3-diarylated imidazo[1,5-*a*]pyridines: Oxidative condensation-cyclization of aryl-2-pyridylmethylamines and aldehydes with elemental sulfur as an oxidant. *J. Org. Chem.* **2009**, 74, (9), 3566-3568.
- ¹⁸ Shen, W.-J.; Dodda, R.; Wu, C.-C.; Wu, F.-I.; Liu, T.-H.; Chen, H.-H.; Chen, C. H.; Shu, C.-F., Spirobifluorene-Linked Bisanthracene: An Efficient Blue Emitter with Pronounced Thermal Stability. *Chem. Mater.* **2004**, 16, (5), 930-934.
- ¹⁹ Hebner, T. R.; Wu, C. C.; Marcy, D.; Lu, M. H.; Sturm, J. C.; Ink-jet printing of doped polymers for organic light emitting devices; *Appl. Phys. Lett.* **1998**, 72 (5): 519; (b) Bharathan, J.; Yang, Y.; Polymer electroluminescent devices processed by inkjet printing: I. Polymer light-emitting logo; *Appl. Phys. Lett.* **1998**, 72 (21): 2660.
- ²⁰ Gustafsson, G.; Cao, Y.; Treacy, G. M.; Klavetter, F.; Colaneri, N.; Heeger, A. J.; Flexible light-emitting diodes made from soluble conducting polymers; *Nature*, **1992**, 357 (6378): 477
- ²¹ (a) Kulkarni, A.P.; Tonzola, C.J.; Babel, A.; Jenekhe, S.A.; Electron Transport Materials for Organic Light-Emitting Diodes; *Chem. Mater.* **2004**, 16, 4556-73; (b) Levermore, P.A.; Jin, R.; Wang, X.; de Mello, J.C.; Bradley, D. D. C.; Organic Light-Emitting Diodes Based on Poly(9,9-dioctylfluorene-*co*-bithiophene) (F8T2); *Adv. Funct. Mater.* **2009**, 19, 950.
- ²² (a) Huang, Y.-S.; Westenhoff, S.; Avilov, I.; Sreearunothai, P.; Hodgkiss, J.M.; Deleener, C.; Friend, R.H.; Beljonneu, D.; Electronic structures of interfacial states formed at polymeric semiconductor heterojunctions; *Nature material*, **2008**, 7, 483; (b) Huang, Q.; Evmenenko, G.A.; Dutta, P.; Lee, P.; Armstrong, N.R.; Marks, T.J.; Covalently Bound Hole-Injecting Nanostructures. Systematics of Molecular Architecture, Thickness, Saturation, and Electron-Blocking Characteristics on Organic Light-Emitting Diode Luminance, Turn-on Voltage, and Quantum Efficiency; *J. Am. Chem. Soc.* **2005**, 127, 10227-42.
- ²³ Kim, H.; Byun, Y.; Das, R. R.; Choi, B.-K.; Ahn, P.-S., Small molecule based and solution processed highly efficient red electrophosphorescent organic light emitting devices. *Appl. Phys. Lett.* **2007**, 91, (9), 093512/1-093512/3.
- ²⁴ Justel, T.; Nikol, H.; Ronda, C., New developments in the field of luminescent materials for lighting and displays. *Angew. Chem., Int. Ed.* **1998**, 37, (22), 3084-3103.
- ²⁵ Sheats, J. R.; Antoniadis, H.; Hueschen, M.; Leonard, W.; Miller, J.; Moon, R.; Roitman, D.; Stocking, A., Organic electroluminescent devices. *Science (Washington, D. C.)* **1996**, 273, (5277), 884-888.
- ²⁶ (a) Zheng, M.; Bai, F.; Li, Y.; Yu, G.; Zhu, D., Synthesis and characterization of a high-efficiency light-emitting alternating copolymer. *J. Polym. Sci., Part A: Polym. Chem.* **1999**, 37, (14), 2587-2594.; (b) Peng, Z.; Bao, Z.; Galvin, M. E., Oxadiazole-containing conjugated polymers for light-emitting diodes. *Adv. Mater. (Weinheim, Ger.)* **1998**, 10, (9), 680-684.
- ²⁷ (a) Grice, A. W.; Tajbakhsh, A.; Burn, P. L.; Bradley, D. D. C., A blue-emitting triazole-based conjugated polymer. *Adv. Mater. (Weinheim, Ger.)* **1997**, 9, (15), 1174-1178.; (b) Schulz, B.;

Kaminorz, Y.; Brehmer, L., New aromatic poly(1,3,4-oxadiazole)s for light emitting diodes. *Synth. Met.* **1997**, 84, (1-3), 449-450.

²⁸ (a) Hanack, M.; Segura, J. L.; Spreitzer, H., New LEDs based on soluble poly(2,6-naphthylenevinylene). *Adv. Mater. (Weinheim, Ger.)* **1996**, 8, (8), 663-666.; (b) Kido, J.; Harada, G.; Nagai, K., Electroluminescent poly(arylene ether) containing both hole-transporting and electron-transporting units. *Chem. Lett.* **1996**, (2), 161-2.; (c) Greenham, N. C.; Moratti, S. C.; Bradley, D. D. C.; Friend, R. H.; Holmes, A. B., Efficient light-emitting diodes based on polymers with high electron affinities. *Nature (London)* **1993**, 365, (6447), 628-30.

²⁹ Mitsumori, T.; Campos, L. M.; Garcia-Garibay, M. A.; Wudl, F.; Sato, H.; Sato, Y., Synthesis, properties, and LED performance of highly luminescent metal complexes containing indolizino[3,4,5-ab]isoindoles. *J. Mater. Chem.* **2009**, 19, (32), 5826-5836.

³⁰ Ran, X.-Q.; Feng, J.-K.; Ren, A.-M.; Li, W.-C.; Zou, L.-Y.; Sun, C.-C.; Theoretical Study on Photophysical Properties of Ambipolar Spirobifluorene Derivatives as Efficient Blue-Light-Emitting Materials; *J. Phys. Chem A.* **2009**, 113, 7933-39.

Appendix

**Appendix A - Absorption spectra, TDDFT data, NMR spectra of
synthesized compounds and reaction mixtures during
photochemical experiments**

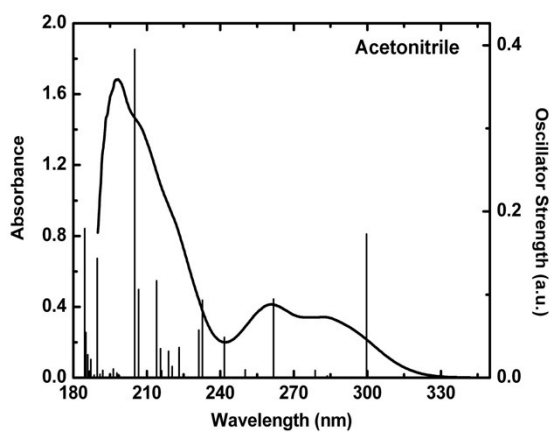
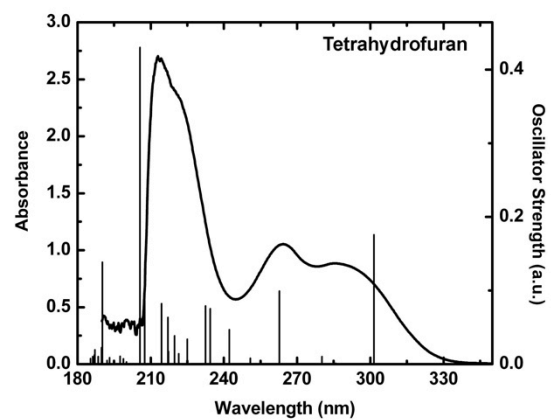
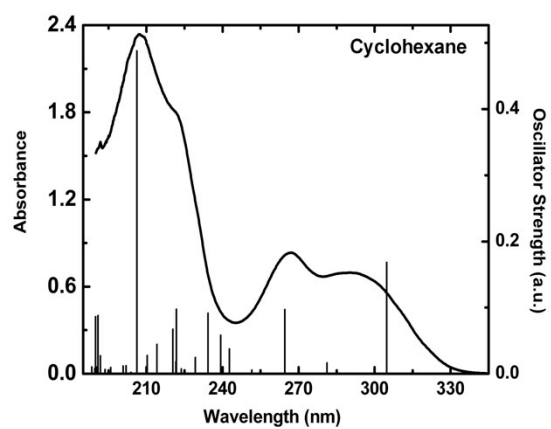


Figure A.1: Experimental absorption spectra of 79b in cyclohexane, tetrahydrofuran and acetonitrile. The vertical excitations calculated at TDDFT/6-311+G* are shown as stick spectra.

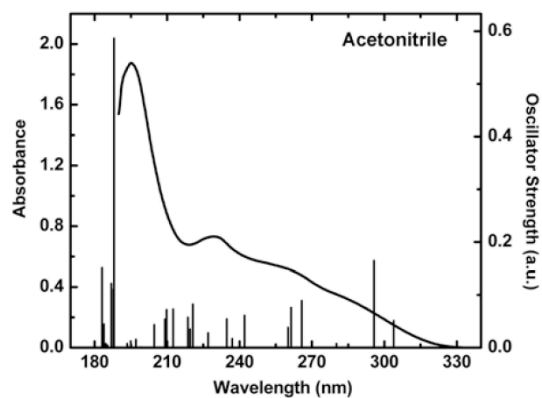
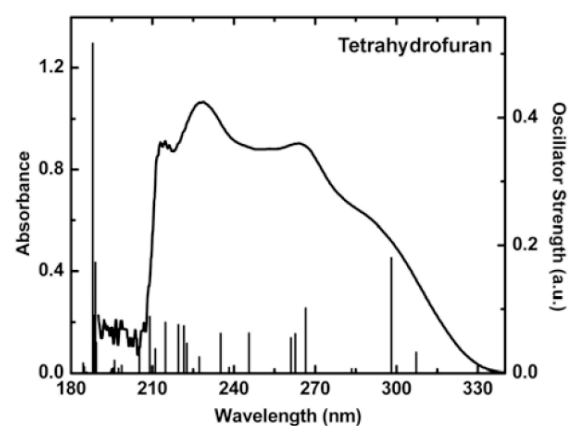
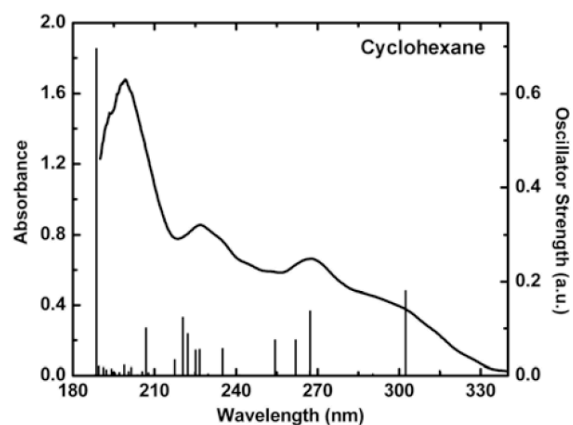


Figure A.2: Experimental absorption spectra of 79c in cyclohexane, tetrahydrofuran and acetonitrile. The vertical excitations calculated at TDDFT/6-311+G* are shown as stick spectra.

Table A.1: TDDFT/6-311+G* vertical excitation energies ($E(\lambda)$ / eV (nm)), oscillator strengths (f), MO character and transition type of 79b in cyclohexane, tetrahydrofuran and acetonitrile.

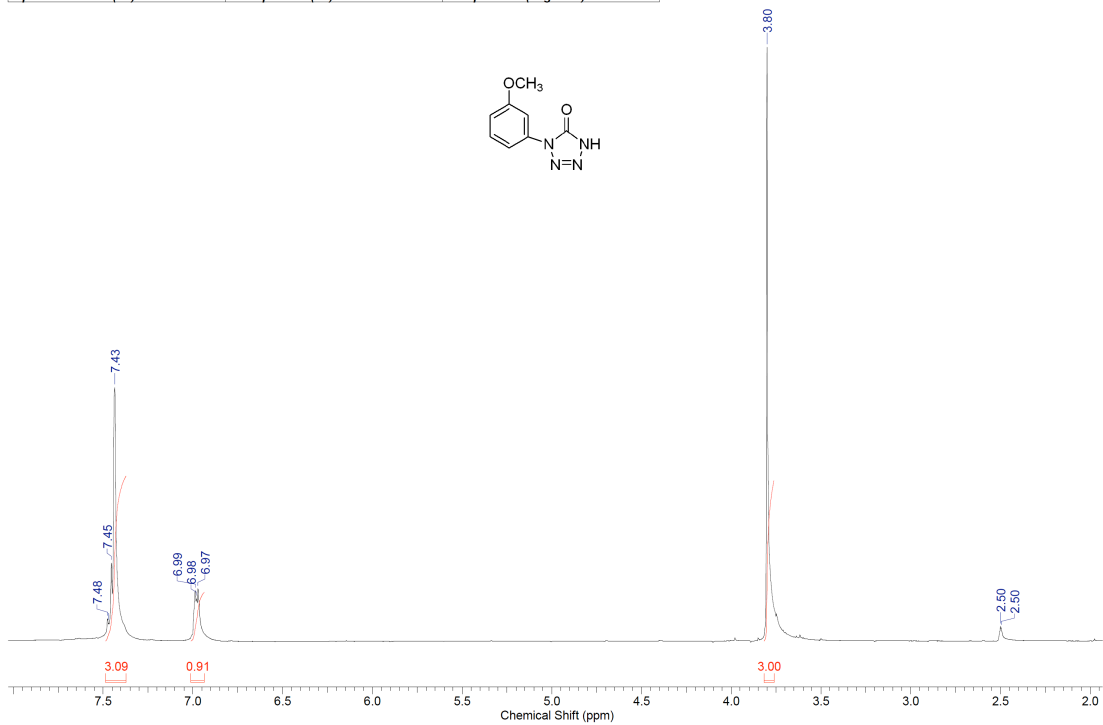
| State | $E(\lambda)$ | f | MO Character | Type | |
|-----------------|--------------|--------------|--------------|--------------------------------|------------------------------|
| Cyclohexane | | | | | |
| λ_1 | 2 | 4.07(304.8) | 0.168 | H-1→L; H→L | $\pi \rightarrow \pi^*$ / CT |
| λ_2 | 5 | 4.67 (264.5) | 0.097 | H→L+1; H-1→L+1 | $\pi \rightarrow \pi^*$ |
| λ_3 | 8 | 5.18 (239.3) | 0.058 | H-1→L+2 | $\pi \rightarrow \pi^*$ |
| | 9 | 5.29 (234.3) | 0.091 | H-3→L; H→L+2; H-1→L+2; H-1→L+3 | $\pi \rightarrow \pi^*$ / CT |
| | 12 | 5.58 (221.8) | 0.098 | H-3→L+1; H-1→L+2; H-2→L+2 | $\pi \rightarrow \pi^*$ |
| λ_4 | 17 | 6.01 (206.2) | 0.488 | H-2→L+3 | $\pi \rightarrow \pi^*$ |
| Tetrahydrofuran | | | | | |
| λ_1 | 2 | 4.11 (301.5) | 0.175 | H-1→L; H→L | $\pi \rightarrow \pi^*$ / CT |
| λ_2 | 5 | 4.72 (262.7) | 0.099 | H→L+1; H-1→L+1 | $\pi \rightarrow \pi^*$ |
| λ_3 | 8 | 5.29 (234.4) | 0.075 | H-1→L+2; H-1→L+3; H→L+2 | $\pi \rightarrow \pi^*$ |
| | 9 | 5.33 (232.5) | 0.079 | H-3→L; H-1→L+2; H→L+2 | $\pi \rightarrow \pi^*$ / CT |
| λ_4^a | 17 | 6.03 (206.0) | 0.430 | H-2→L+3 | $\pi \rightarrow \pi^*$ |
| Acetonitrile | | | | | |
| λ_1 | 2 | 4.14 (300.0) | 0.173 | H-1→L; H→L | $\pi \rightarrow \pi^*$ / CT |
| λ_2 | 5 | 4.74 (261.7) | 0.094 | H→L+1; H-1→L+1 | $\pi \rightarrow \pi^*$ |
| λ_3 | 8 | 5.33 (232.6) | 0.093 | H-1→L+2; H-1→L+3; H→L+2 | $\pi \rightarrow \pi^*$ |
| | 9 | 5.36 (231.2) | 0.057 | H-3→L; H-1→L+2; H→L+2 | $\pi \rightarrow \pi^*$ / CT |
| λ_4 | 17 | 6.05 (205.0) | 0.395 | H-2→L+3 | $\pi \rightarrow \pi^*$ |

^a experimentally not observed

Table A.2: TDDFT/6-311+G* vertical excitation energies ($E(\lambda)$ / eV (nm)), oscillator strengths (f), MO character and transition type of **79c** in cyclohexane, tetrahydrofuran and acetonitrile

| State | | $E(\lambda)$ | f | MO Character | Type |
|-----------------|----|--------------|-------|-----------------------|------------------------------|
| Cyclohexane | | | | | |
| λ_1 | 2 | 4.10 (302.4) | 0.180 | H-1→L; H→L | $\pi \rightarrow \pi^*$ / CT |
| λ_2 | 4 | 4.64 (267.3) | 0.137 | H-2→L; H-1→L+1; H→L+1 | $\pi \rightarrow \pi^*$ / CT |
| | 6 | 4.73 (261.9) | 0.075 | H-2→L; H-1→L+2; H→L+1 | $\pi \rightarrow \pi^*$ / CT |
| | 7 | 4.87 (254.3) | 0.075 | H-1→L+2 | $\pi \rightarrow \pi^*$ / CT |
| λ_3 | 11 | 5.47 (226.6) | 0.054 | H→L+3 | $\pi \rightarrow \pi^*$ / CT |
| | 12 | 5.51 (225.1) | 0.053 | H-3→L; H-2→L+2 | $\pi \rightarrow \pi^*$ / CT |
| | 13 | 5.58 (222.2) | 0.088 | H→L+3 | $\pi \rightarrow \pi^*$ |
| λ_4 | 29 | 6.57 (188.7) | 0.695 | H-3→L+2 | $\pi \rightarrow \pi^*$ |
| Tetrahydrofuran | | | | | |
| λ_1 | 2 | 4.16 (298.1) | 0.180 | H-1→L; H→L | $\pi \rightarrow \pi^*$ / CT |
| λ_2 | 4 | 4.65 (266.5) | 0.101 | H-2→L; H→L+1 | $\pi \rightarrow \pi^*$ / CT |
| | 5 | 4.72 (262.7) | 0.610 | H→L+1; H→L+2 | $\pi \rightarrow \pi^*$ / CT |
| | 6 | 4.75 (261.0) | 0.055 | H-2→L; H→L+1; H→L+2 | $\pi \rightarrow \pi^*$ / CT |
| λ_3 | 12 | 5.59 (221.6) | 0.073 | H-1→L+3; H→L+3 | $\pi \rightarrow \pi^*$ / CT |
| | 13 | 5.65 (219.6) | 0.075 | H→L+3 | $\pi \rightarrow \pi^*$ |
| | 16 | 5.93 (209.0) | 0.088 | H-3→L+1 | $\pi \rightarrow \pi^*$ / CT |
| λ_4^a | 27 | 6.59 (188.0) | 0.516 | H-3→L+2 | $\pi \rightarrow \pi^*$ |
| Acetonitrile | | | | | |
| λ_1 | 2 | 4.19 (296.0) | 0.165 | H-1→L; H→L | $\pi \rightarrow \pi^*$ / CT |
| λ_2 | 4 | 4.66 (266.0) | 0.089 | H-2→L; H→L+15 | $\pi \rightarrow \pi^*$ / CT |
| | 5 | 4.74 (261.4) | 0.076 | H→L+1; H→L+2 | $\pi \rightarrow \pi^*$ / CT |
| λ_3 | 11 | 5.62 (220.6) | 0.082 | H-1→L+3; H→L+3 | $\pi \rightarrow \pi^*$ / CT |
| | 13 | 5.67 (218.6) | 0.058 | H→L+3 | $\pi \rightarrow \pi^*$ |
| | 15 | 5.91 (210.0) | 0.072 | H-3→L+1 | $\pi \rightarrow \pi^*$ / CT |
| λ_4 | 24 | 6.59 (188.0) | 0.586 | H-3→L+2 | $\pi \rightarrow \pi^*$ |

| | | | | | | | |
|------------------------|---|------------------|------------|------------------------|----------------|----------------------|------------|
| Acquisition Time (sec) | 2.0487 | Comment | Std proton | Date | Apr 2 2012 | Date Stamp | Apr 2 2012 |
| File Name | G:\UNTITLED FOLDER\ID-MMP\TETRAZOLONE-H | Frequency (MHz) | 399.72 | Nucleus | ¹ H | Number of Transients | 8 |
| Original Points Count | 13102 | Points Count | 16384 | Pulse Sequence | s2pul | Receiver Gain | 38.00 |
| Spectrum Offset (Hz) | 2411.5708 | Sweep Width (Hz) | 6395.40 | Temperature (degree C) | 25.000 | Solvent | DMSO-d6 |



| | | | | | | | |
|------------------------|---|----------------------|------------|------------------|-----------------|------------------------|------------|
| Acquisition Time (sec) | 1.3005 | Comment | Std proton | Date | Apr 2 2012 | Date Stamp | Apr 2 2012 |
| File Name | G:\UNTITLED FOLDER\ID-MMP\TETRAZOLONE-C13 | Frequency (MHz) | 100.62 | Nucleus | ¹³ C | Number of Transients | 1500 |
| Original Points Count | 31375 | Points Count | 32768 | Pulse Sequence | s2pul | Receiver Gain | 30.00 |
| Solvent | DMSO-d6 | Spectrum Offset (Hz) | 10489.9258 | Sweep Width (Hz) | 24125.45 | Temperature (degree C) | 25.000 |

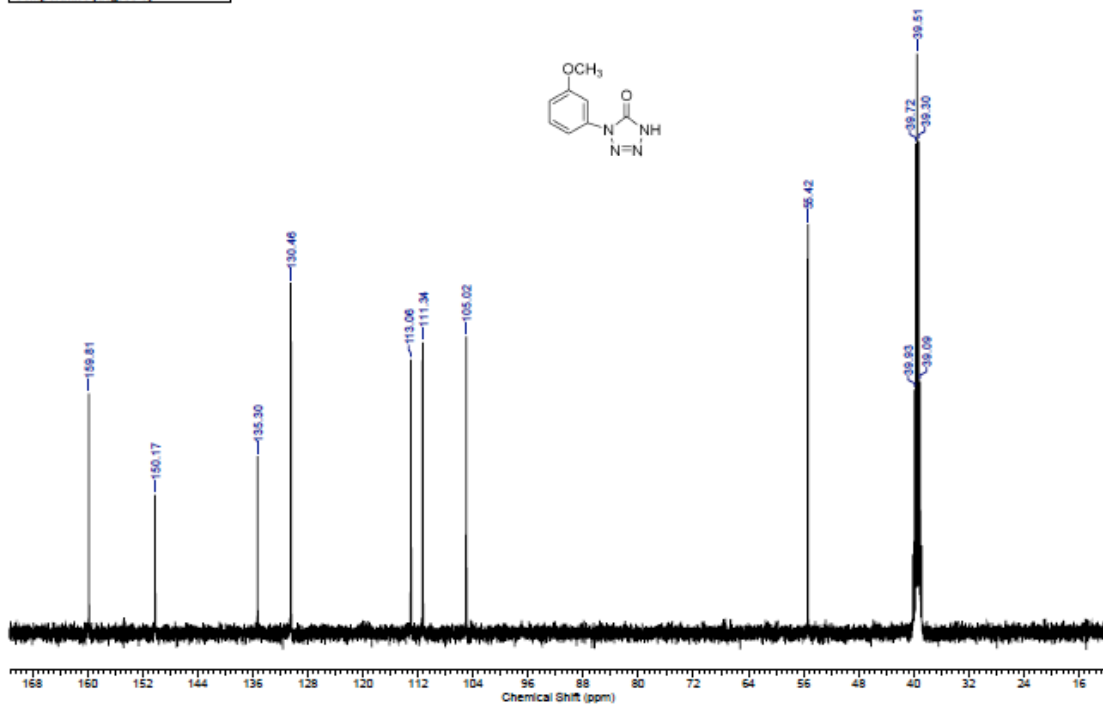
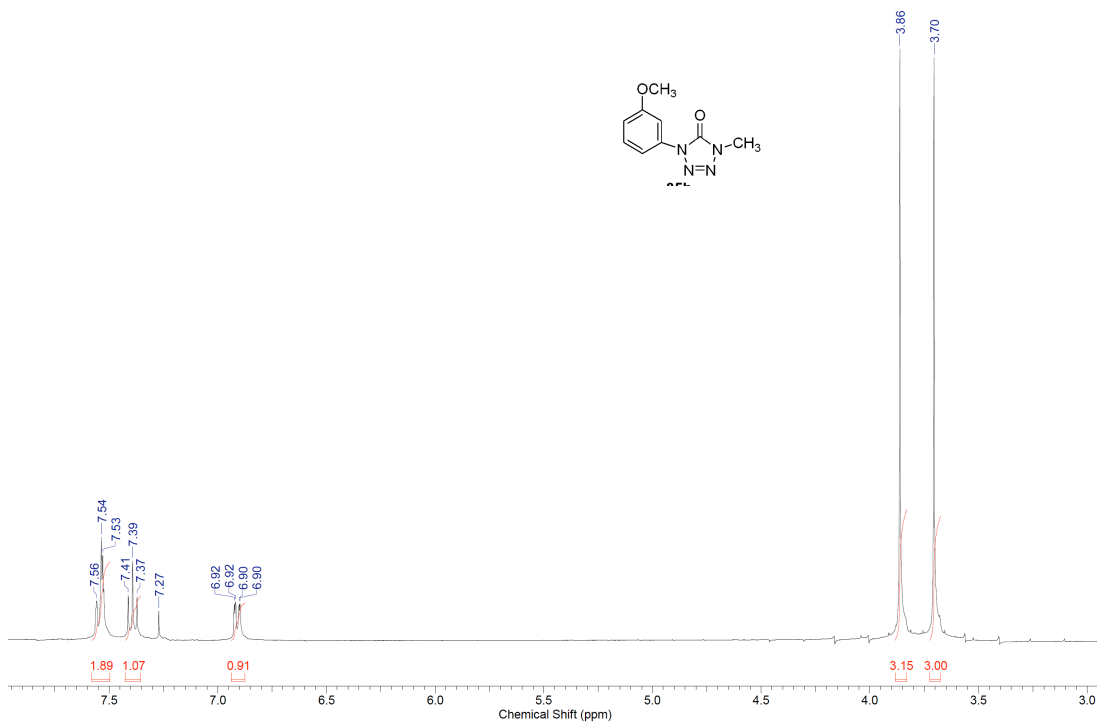


Figure A.3: ¹H and ¹³C NMR of 83b

| | | | | | | | |
|------------------------|---------------------------------|----------------------|------------|------------------|------------|------------------------|------------|
| Acquisition Time (sec) | 2.0487 | Comment | Std proton | Date | Apr 2 2012 | Date Stamp | Apr 2 2012 |
| File Name | G:\UNTITLED FOLDER\D-MMPMT-HSTD | Frequency (MHz) | 399.72 | Nucleus | 1H | Number of Transients | 4 |
| Original Points Count | 13102 | Points Count | 16384 | Pulse Sequence | s2pul | Receiver Gain | 44.00 |
| Solvent | CHLOROFORM-d | Spectrum Offset (Hz) | 2407.8904 | Sweep Width (Hz) | 6395.40 | Temperature (degree C) | 25.000 |



| | | | | | | | |
|------------------------|--------------------------------|----------------------|------------|------------------|------------|------------------------|------------|
| Acquisition Time (sec) | 1.3005 | Comment | Std proton | Date | Apr 2 2012 | Date Stamp | Apr 2 2012 |
| File Name | G:\UNTITLED FOLDER\D-MMPMT-13C | Frequency (MHz) | 100.52 | Nucleus | 13C | Number of Transients | 1000 |
| Original Points Count | 31375 | Points Count | 32768 | Pulse Sequence | s2pul | Receiver Gain | 30.00 |
| Solvent | CHLOROFORM-d | Spectrum Offset (Hz) | 10551.0859 | Sweep Width (Hz) | 24125.45 | Temperature (degree C) | 25.000 |

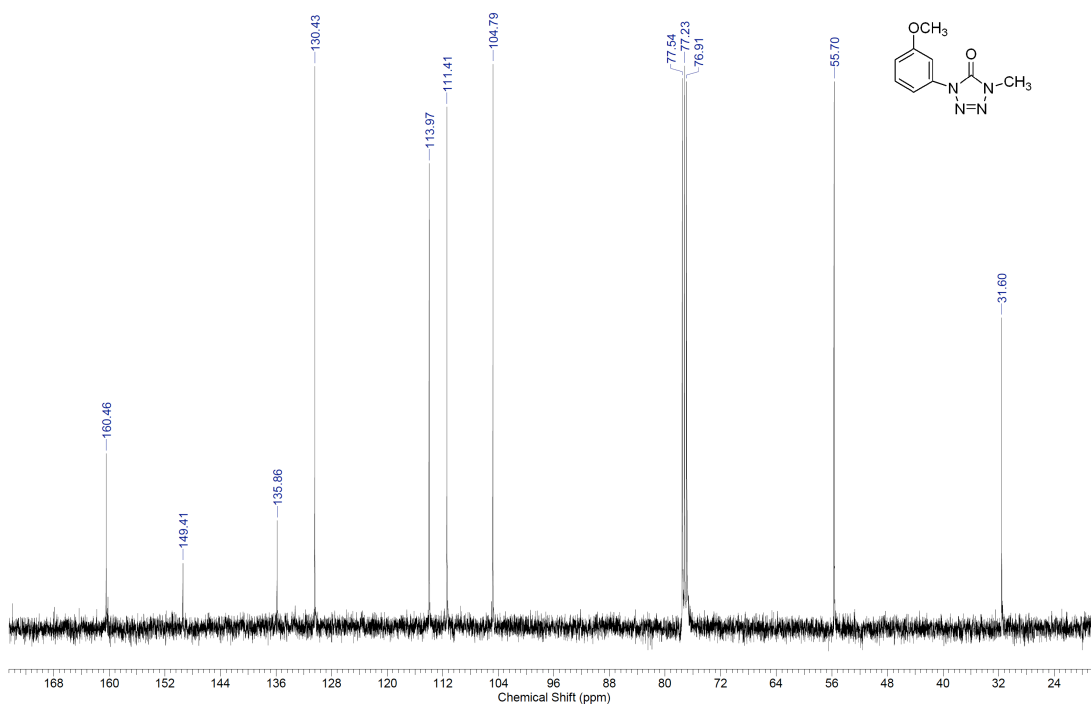
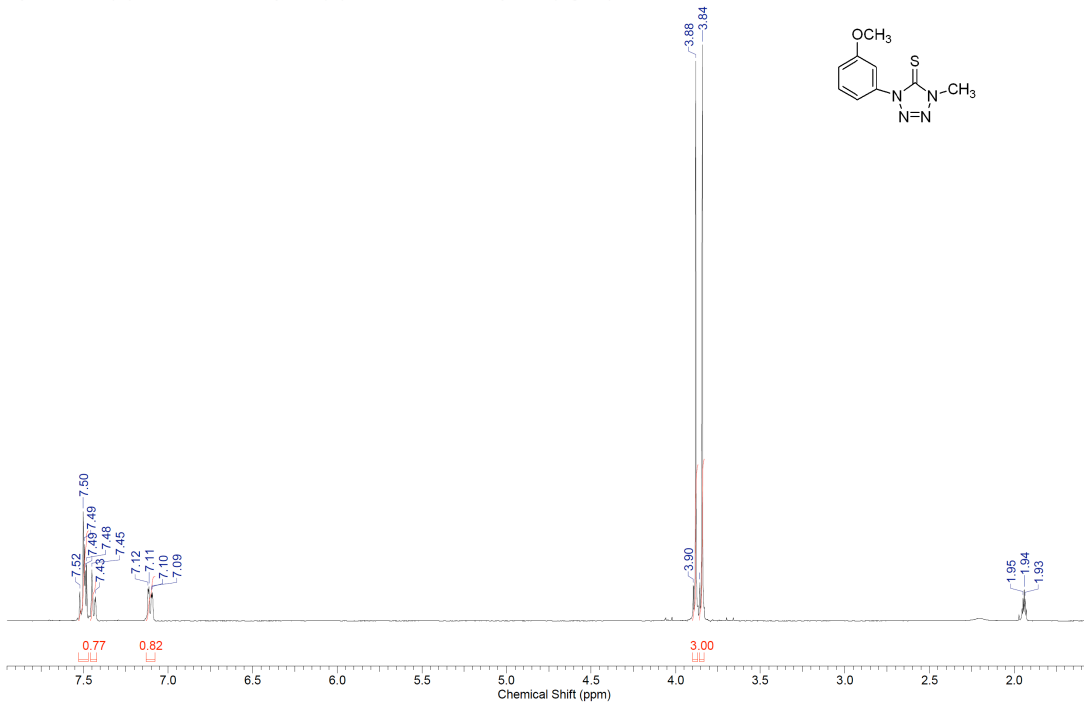


Figure A.4: ¹H and ¹³C NMR of 84b

| | | | | | | | |
|------------------------|--|----------------------|------------|------------------------|-----------------|--------------|------------|
| Acquisition Time (sec) | 2.0487 | Comment | Std proton | Date | Aug 3 2010 | Date Stamp | Aug 3 2010 |
| File Name | C:\DOCUMENTS AND SETTINGS\VGZ\DESKTOP\HG6X-MMPTT-CD3CN-H | | | Frequency (MHz) | 399.74 | Points Count | 16384 |
| Nucleus | ¹ H | Number of Transients | 16 | Original Points Count | 13103 | | |
| Pulse Sequence | s2pul | Receiver Gain | 36.00 | Solvent | ACETONITRILE-d3 | | |
| Spectrum Offset (Hz) | 2402.3823 | Sweep Width (Hz) | 6395.91 | Temperature (degree C) | 25.000 | | |



| | | | | | | | |
|------------------------|---|----------------------|------------|------------------------|-----------------|--------------|------------|
| Acquisition Time (sec) | 1.3005 | Comment | Std proton | Date | Aug 3 2010 | Date Stamp | Aug 3 2010 |
| File Name | C:\DOCUMENTS AND SETTINGS\VGZ\DESKTOP\HG6X-MMPTT-CD3CN-C13-2ATT | | | Frequency (MHz) | 100.53 | Points Count | 32768 |
| Nucleus | ¹³ C | Number of Transients | 3000 | Original Points Count | 31375 | | |
| Pulse Sequence | s2pul | Receiver Gain | 30.00 | Solvent | ACETONITRILE-d3 | | |
| Spectrum Offset (Hz) | 10632.7227 | Sweep Width (Hz) | 24125.45 | Temperature (degree C) | 25.000 | | |

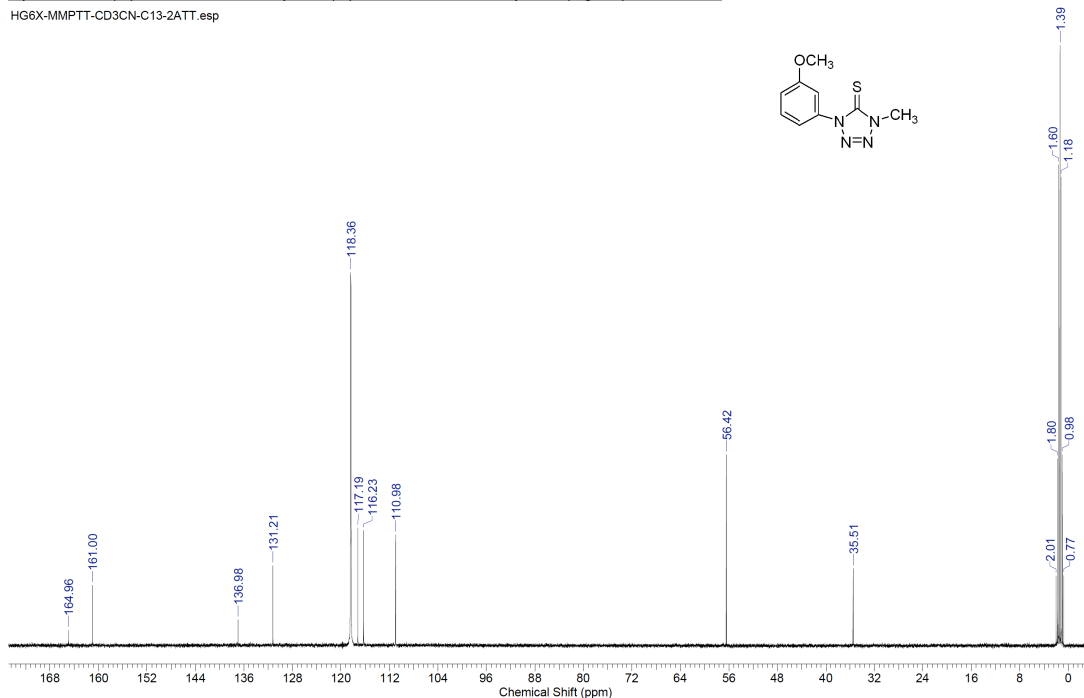
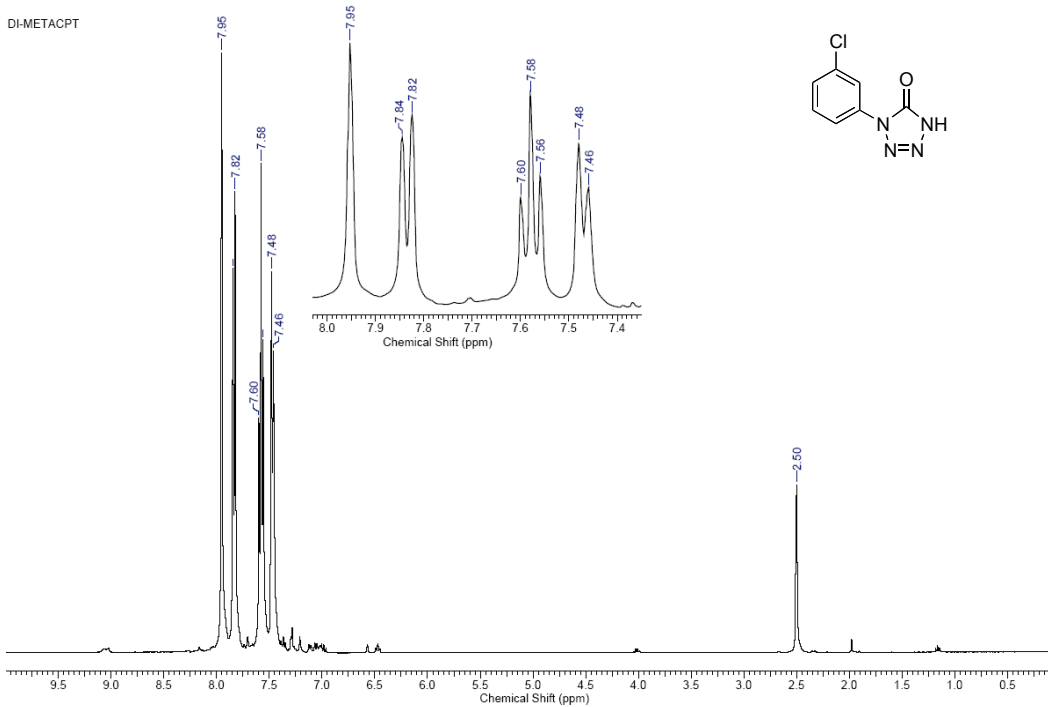


Figure A.5: ¹H and ¹³C NMR of 79b

| | | | | | | | |
|------------------------|-----------------------------------|------------------|------------|------------------------|------------|----------------------|------------|
| Acquisition Time (sec) | 2.0487 | Comment | Std proton | Date | Dec 7 2011 | Date Stamp | Dec 7 2011 |
| File Name | F:\NMR\UNTITLED FOLDER\DI-METACPT | Frequency (MHz) | 399.72 | Nucleus | 1H | Number of Transients | 16 |
| Original Points Count | 13102 | Points Count | 16384 | Pulse Sequence | s2pul | Receiver Gain | 42.00 |
| Spectrum Offset (Hz) | 2410.9854 | Sweep Width (Hz) | 6395.40 | Temperature (degree C) | 25.000 | Solvent | DMSO-d6 |

DI-METACPT



| | | | | | |
|------------------------|------------|------------------------|--|-----------------------|------------|
| Acquisition Time (sec) | 1.3005 | Comment | Std Carbon experiment | Date | Dec 7 2011 |
| Date Stamp | Dec 7 2011 | File Name | F:\NMR\UNTITLED FOLDER\DI-MCPT-C13-STD | Frequency (MHz) | 100.58 |
| Nucleus | 13C | Number of Transients | 1500 | Original Points Count | 31413 |
| Pulse Sequence | s2pul | Receiver Gain | 20.00 | Points Count | 32768 |
| Sweep Width (Hz) | 24154.59 | Temperature (degree C) | 25.000 | Solvent | DMSO-d6 |
| | | | | Spectrum Offset (Hz) | 10490.5908 |

DI-MCPT-C13-STD

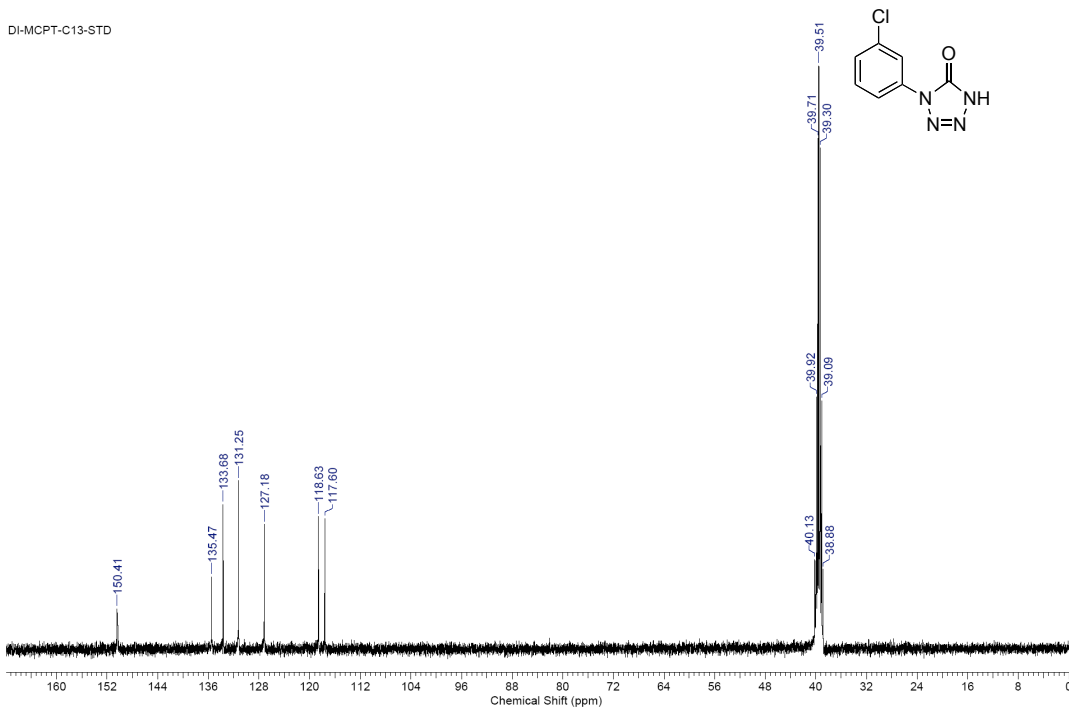
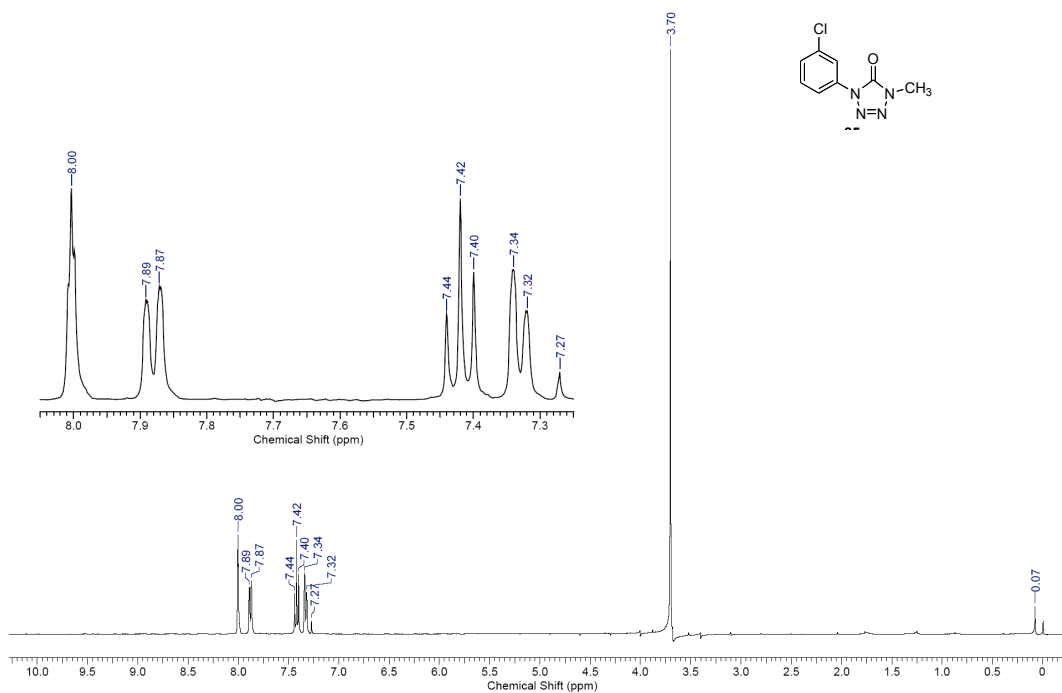


Figure A.6: ^1H and ^{13}C NMR of 83c

| | | | | | | | |
|------------------------|--|------------------------|--------------|----------------------|------------|----------------|------------|
| Acquisition Time (sec) | 2.0487 | Comment | Std proton | Date | Dec 7 2011 | Date Stamp | Dec 7 2011 |
| File Name | F:\NMR\UNTITLED FOLDER\DI-MCPTMT-H-2ATT-GD | Frequency (MHz) | 399.72 | Nucleus | 1H | | |
| Number of Transients | 16 | Original Points Count | 13102 | Points Count | 16384 | Pulse Sequence | s2pul |
| Receiver Gain | 42.00 | Solvent | CHLOROFORM-d | Spectrum Offset (Hz) | 2419.2104 | | |
| Sweep Width (Hz) | 6395.40 | Temperature (degree C) | 30.000 | | | | |



| | | | | | | | |
|------------------------|--------------------------------------|------------------------|--------------|----------------------|------------|----------------|------------|
| Acquisition Time (sec) | 1.3005 | Comment | Std proton | Date | Dec 7 2011 | Date Stamp | Dec 7 2011 |
| File Name | F:\NMR\UNTITLED FOLDER\DI-MCPTMT-C13 | Frequency (MHz) | 100.52 | Nucleus | 13C | | |
| Number of Transients | 2000 | Original Points Count | 31375 | Points Count | 32768 | Pulse Sequence | s2pul |
| Receiver Gain | 30.00 | Solvent | CHLOROFORM-d | Spectrum Offset (Hz) | 10550.3496 | | |
| Sweep Width (Hz) | 24125.45 | Temperature (degree C) | 3.000 | | | | |

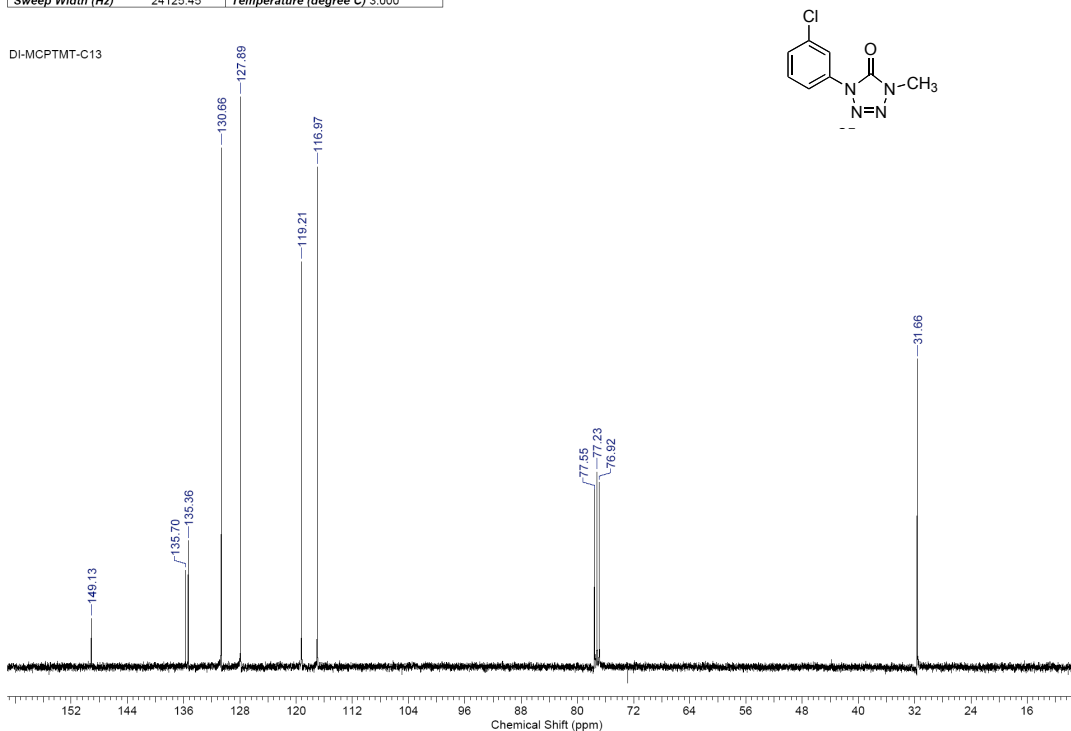
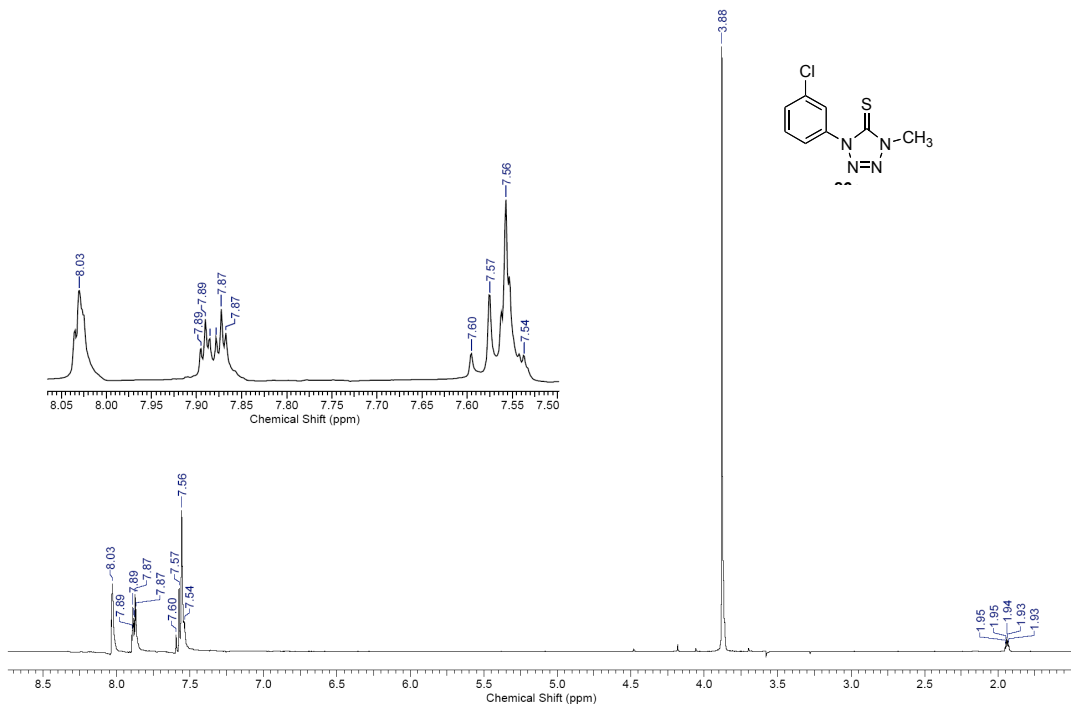


Figure A.7: ^1H and ^{13}C NMR of 84c

| | | | | | | | |
|------------------------|-----------------------------------|----------------------|------------|------------------|------------|------------------------|------------|
| Acquisition Time (sec) | 2.0487 | Comment | Std proton | Date | Dec 7 2011 | Date Stamp | Dec 7 2011 |
| File Name | F:\NMR\UNTITLED FOLDER\DI-MCPTT-H | Frequency (MHz) | 399.73 | Nucleus | 1H | Number of Transients | 4 |
| Original Points Count | 13102 | Points Count | 16384 | Pulse Sequence | s2pul | Receiver Gain | 38.00 |
| Solvent | ACETONITRILE-d3 | Spectrum Offset (Hz) | 2394.8042 | Sweep Width (Hz) | 6395.40 | Temperature (degree C) | 25.000 |



| | | | | | | | |
|------------------------|-------------------------------------|----------------------|------------|------------------|------------|------------------------|------------|
| Acquisition Time (sec) | 1.3005 | Comment | Std proton | Date | Dec 7 2011 | Date Stamp | Dec 7 2011 |
| File Name | F:\NMR\UNTITLED FOLDER\DI-MCPTT-C13 | Frequency (MHz) | 100.52 | Nucleus | 13C | Number of Transients | 3000 |
| Original Points Count | 31375 | Points Count | 32768 | Pulse Sequence | s2pul | Receiver Gain | 30.00 |
| Solvent | ACETONITRILE-d3 | Spectrum Offset (Hz) | 10629.8047 | Sweep Width (Hz) | 24125.45 | Temperature (degree C) | 25.000 |

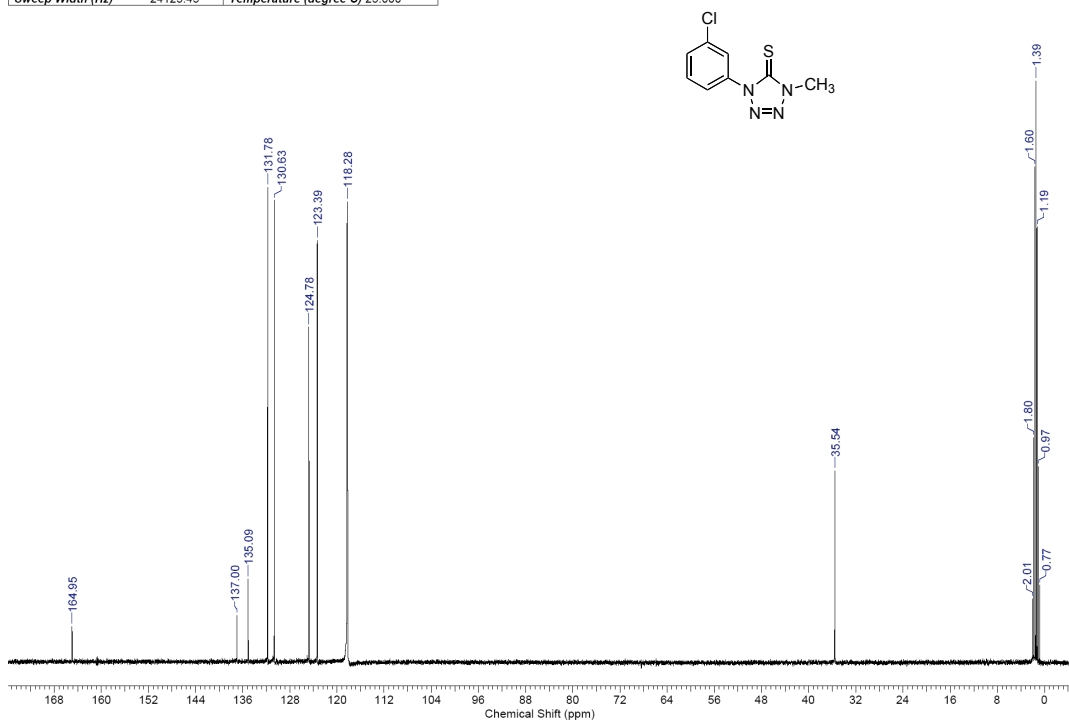
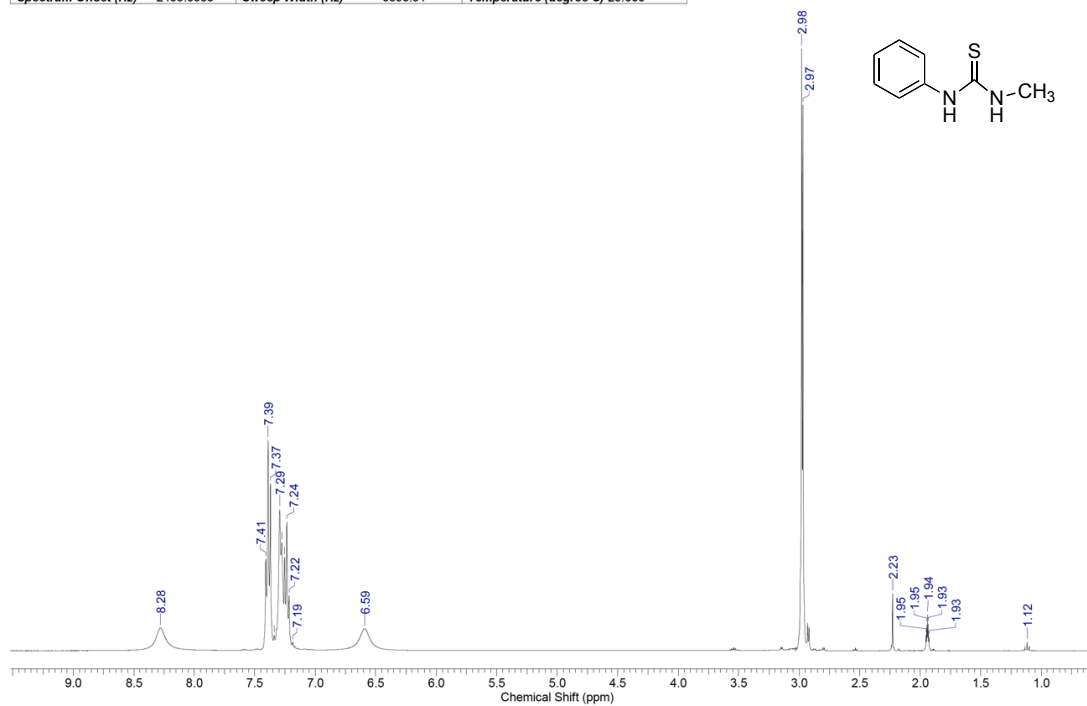


Figure A.8: ¹H and ¹³C NMR of 79c

| | | | | | | | |
|------------------------|---|----------------------|------------|------------------------|-----------------|-----------------|-------------|
| Acquisition Time (sec) | 2.0487 | Comment | Std proton | Date | Mar 18 2010 | Date Stamp | Mar 18 2010 |
| File Name | E:\OLAJIDE-NMR DATA\2010 NMR-OLAJIDE\HG-STD-PTU-H | | | | | Frequency (MHz) | 399.74 |
| Nucleus | ¹ H | Number of Transients | 8 | Original Points Count | 13103 | Points Count | 16384 |
| Pulse Sequence | s2pul | Receiver Gain | 38.00 | Solvent | ACETONITRILE-d3 | | |
| Spectrum Offset (Hz) | 2403.5535 | Sweep Width (Hz) | 6395.91 | Temperature (degree C) | 25.000 | | |



| | | | | | | | |
|------------------------|---|----------------------|------------|------------------------|-----------------|-----------------|-------------|
| Acquisition Time (sec) | 1.3005 | Comment | Std proton | Date | Mar 18 2010 | Date Stamp | Mar 18 2010 |
| File Name | E:\OLAJIDE-NMR DATA\2010 NMR-OLAJIDE\HG-STD-PTU-C13 | | | | | Frequency (MHz) | 100.52 |
| Nucleus | ¹³ C | Number of Transients | 5000 | Original Points Count | 31375 | Points Count | 32768 |
| Pulse Sequence | s2pul | Receiver Gain | 30.00 | Solvent | ACETONITRILE-d3 | | |
| Spectrum Offset (Hz) | 10517.8643 | Sweep Width (Hz) | 24125.45 | Temperature (degree C) | 25.000 | | |

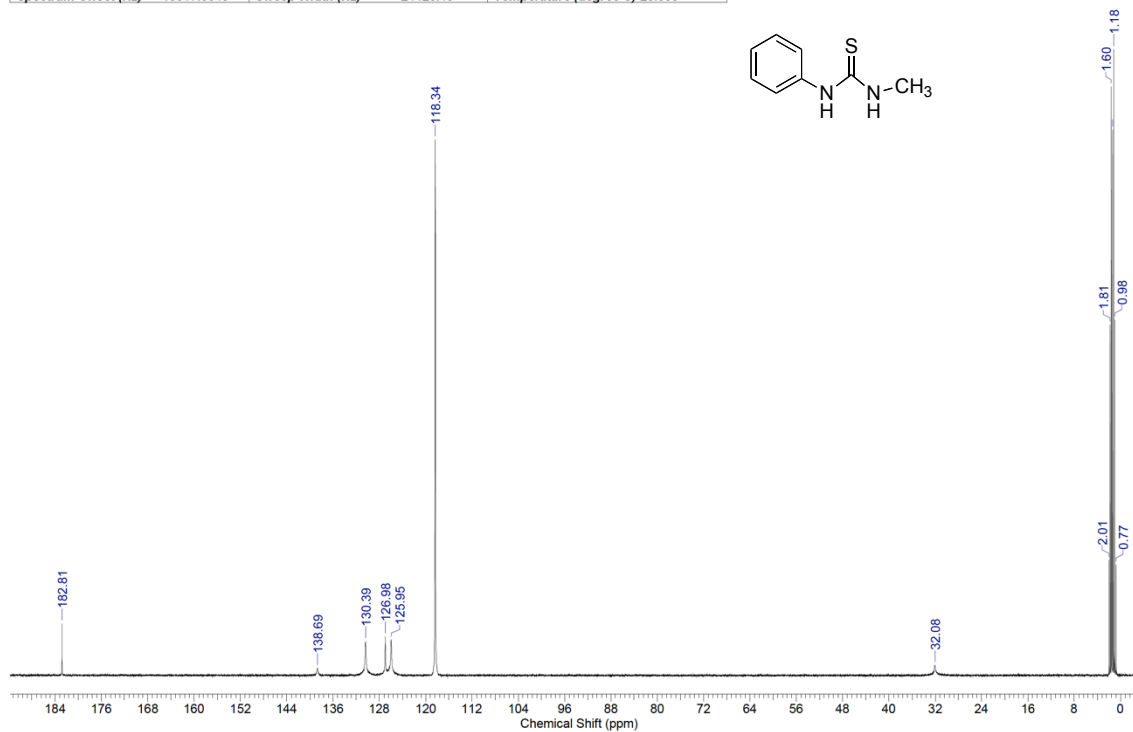


Figure A.9: ¹H and ¹³C NMR of 93a

| | | | | | | | |
|------------------------|---|----------------------|------------|------------------------|-----------------|--------------|-------------|
| Acquisition Time (sec) | 2.0487 | Comment | Std proton | Date | Mar 14 2010 | Date Stamp | Mar 14 2010 |
| File Name | E:\OLA\JIDE-NMR DATA\2010 NMR-OLA\JIDE\STD-MMP-TU-H | | | Frequency (MHz) | 399.74 | | |
| Nucleus | 1H | Number of Transients | 8 | Original Points Count | 13103 | Points Count | 16384 |
| Pulse Sequence | s2pul | Receiver Gain | 54.00 | Solvent | ACETONITRILE-d3 | | |
| Spectrum Offset (Hz) | 2403.3584 | Sweep Width (Hz) | 6395.91 | Temperature (degree C) | 25.000 | | |

STD-MMP-TU-H.ESP

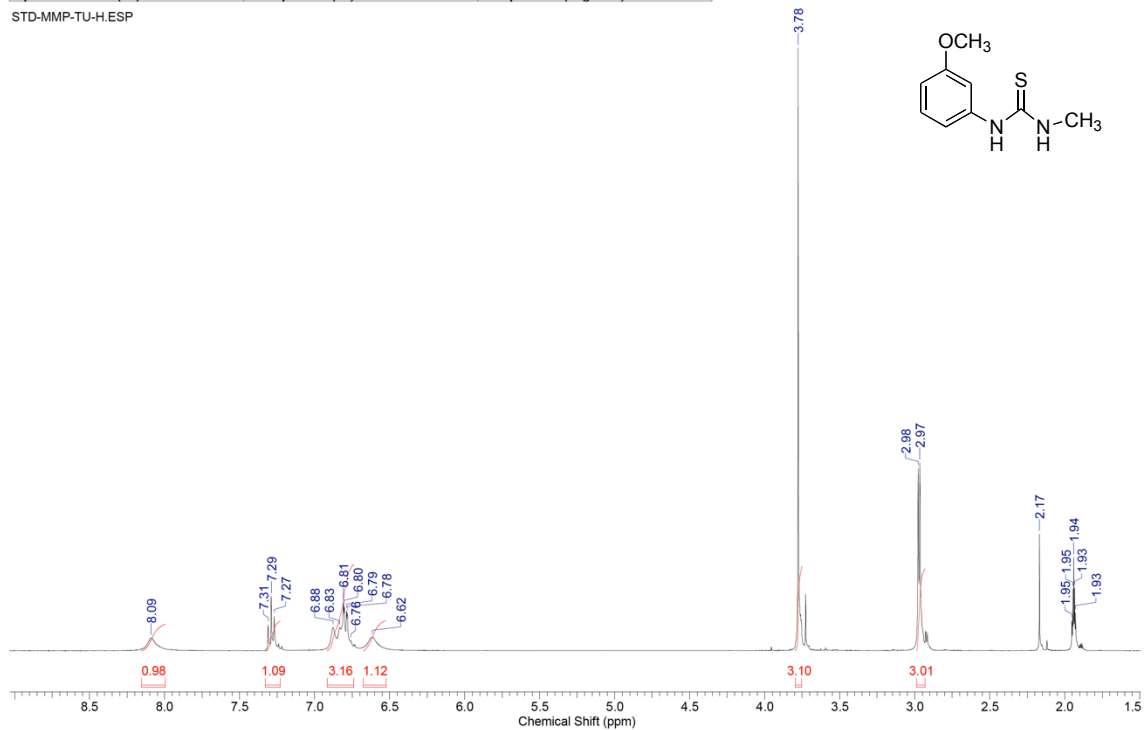
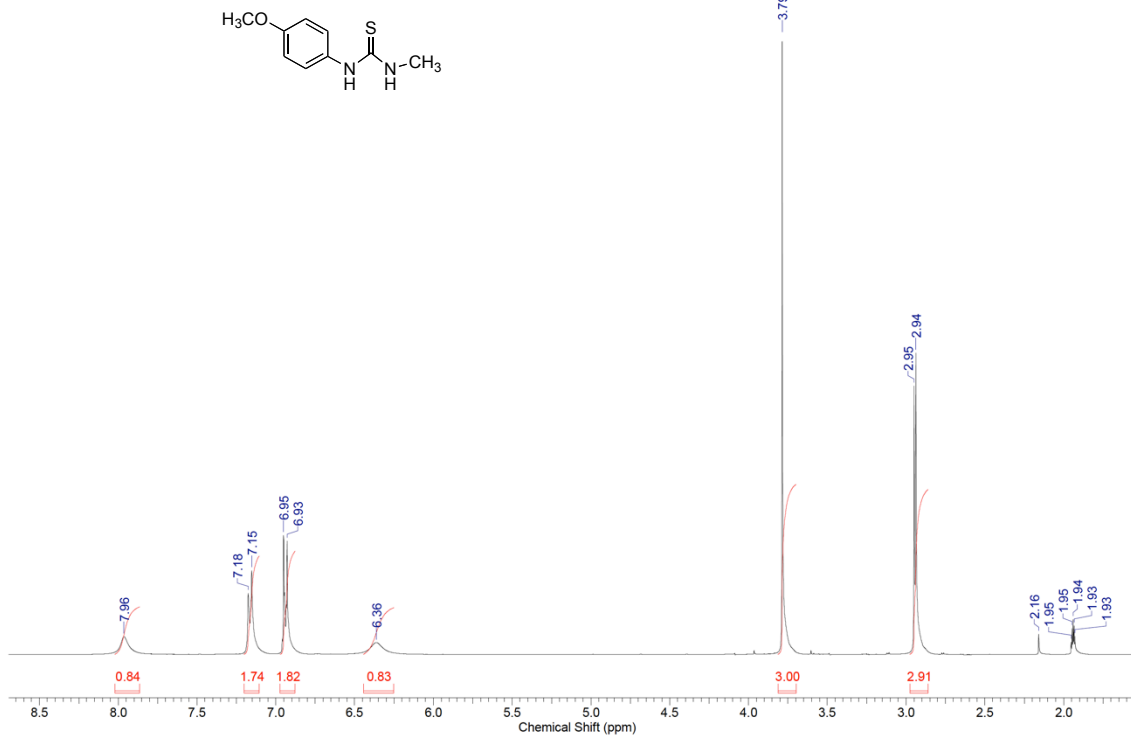


Figure A.10: ^1H NMR of 93b

| | | | | | | | |
|------------------------|---------------------------------|--------------|------------|----------------------|-------------|------------------------|-------------|
| Acquisition Time (sec) | 2.0487 | Comment | Std proton | Date | Dec 10 2011 | Date Stamp | Dec 10 2011 |
| File Name | G:\XXNMR0222\DI-POCH3THIOUREA-H | | | Frequency (MHz) | 399.73 | Nucleus | 1H |
| Original Points Count | 13102 | Points Count | 16384 | Pulse Sequence | s2pul | Receiver Gain | 42.00 |
| Solvent | ACETONITRILE-d3 | | | Spectrum Offset (Hz) | 2395.1946 | Sweep Width (Hz) | 6395.40 |
| | | | | | | Temperature (degree C) | 25.000 |



| | | | | | | | |
|------------------------|-----------------------------------|------------------------|-----------------|----------------------|-------------|----------------|-------------|
| Acquisition Time (sec) | 1.3005 | Comment | Std proton | Date | Dec 10 2011 | Date Stamp | Dec 10 2011 |
| File Name | G:\XXNMR0222\DI-POCH3THIOUREA-C13 | | | Frequency (MHz) | 100.52 | Nucleus | 13C |
| Number of Transients | 5000 | Original Points Count | 31375 | Points Count | 32768 | Pulse Sequence | s2pul |
| Receiver Gain | 30.00 | Solvent | ACETONITRILE-d3 | Spectrum Offset (Hz) | 10635.6953 | | |
| Sweep Width (Hz) | 24125.45 | Temperature (degree C) | 25.000 | | | | |

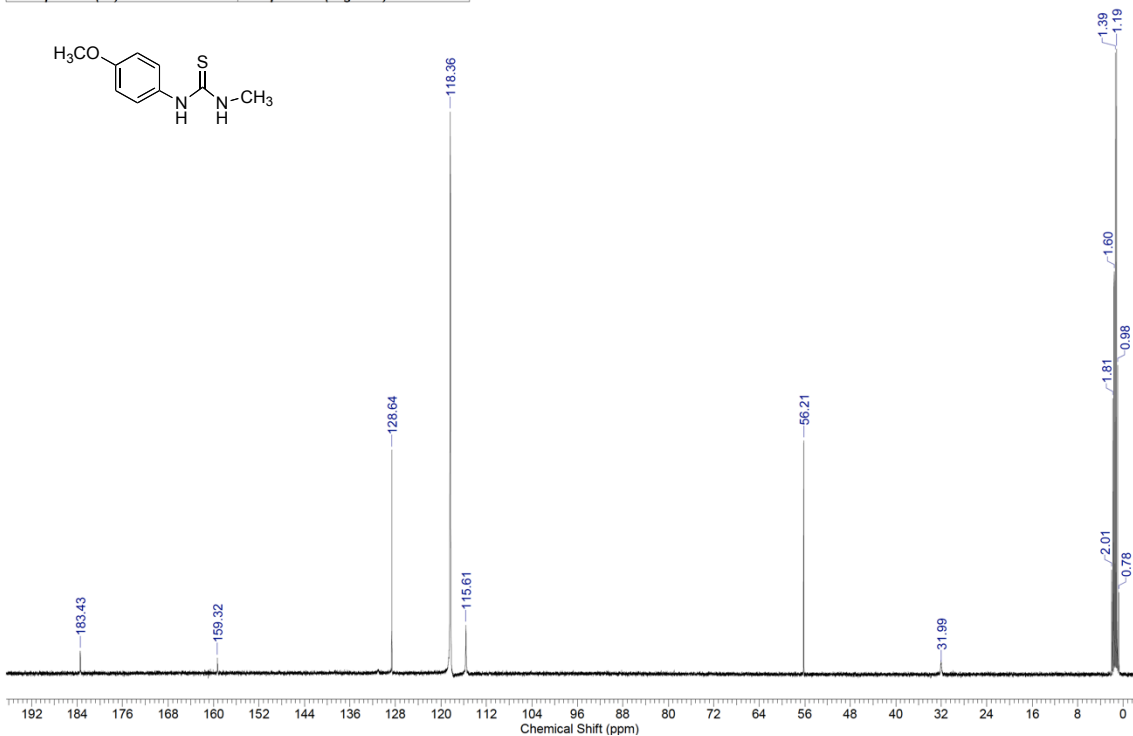
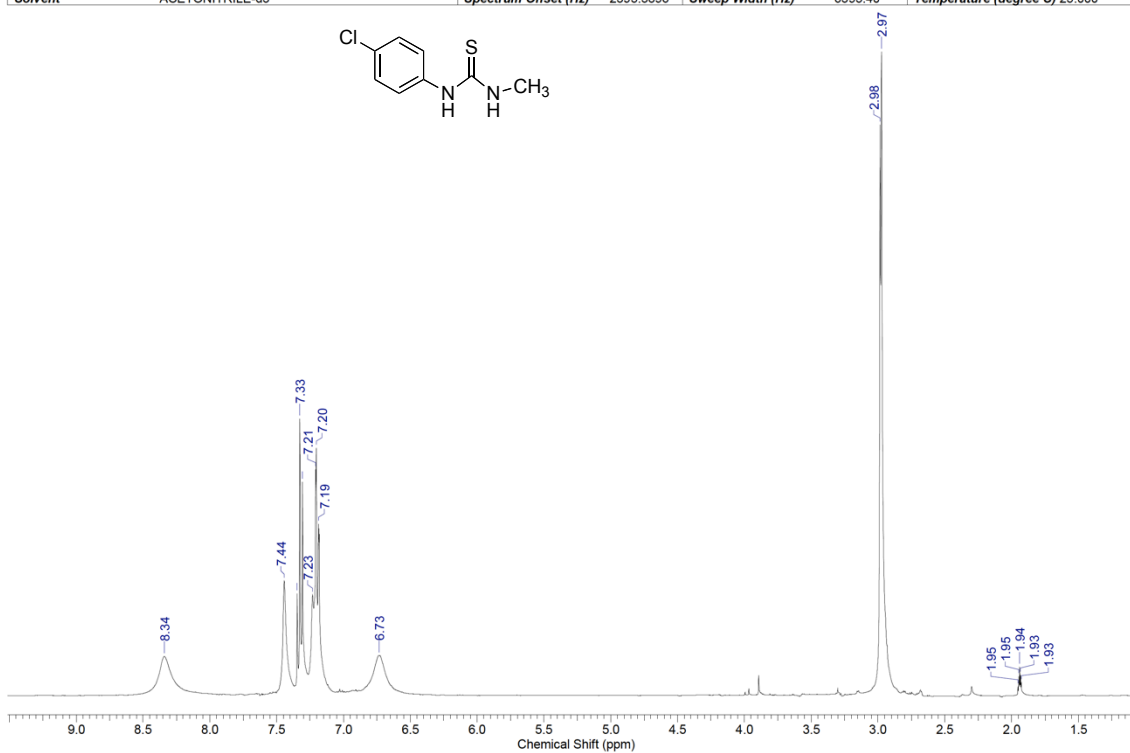


Figure A.11: ¹H and ¹³C NMR of 93c

| | | | | | | | |
|------------------------|-------------------------------|----------------------|------------|------------------|-------------|------------------------|-------------|
| Acquisition Time (sec) | 2.0487 | Comment | Std proton | Date | Dec 12 2011 | Date Stamp | Dec 12 2011 |
| File Name | G:\XXNMR0222\DI-MCLTHIOUREA-H | Frequency (MHz) | 399.73 | Nucleus | 1H | Number of Transients | 16 |
| Original Points Count | 13102 | Points Count | 16384 | Pulse Sequence | s2pul | Receiver Gain | 30.00 |
| Solvent | ACETONITRILE-d3 | Spectrum Offset (Hz) | 2395.3896 | Sweep Width (Hz) | 6395.40 | Temperature (degree C) | 25.000 |



| | | | | | | | |
|------------------------|---------------------------------|----------------------|------------|------------------|-------------|------------------------|-------------|
| Acquisition Time (sec) | 1.3005 | Comment | Std proton | Date | Dec 12 2011 | Date Stamp | Dec 12 2011 |
| File Name | G:\XXNMR0222\DI-MCLTHIOUREA-C13 | Frequency (MHz) | 100.52 | Nucleus | 13C | Number of Transients | 2000 |
| Original Points Count | 31375 | Points Count | 32768 | Pulse Sequence | s2pul | Receiver Gain | 30.00 |
| Solvent | ACETONITRILE-d3 | Spectrum Offset (Hz) | 10624.6514 | Sweep Width (Hz) | 24125.45 | Temperature (degree C) | 25.000 |

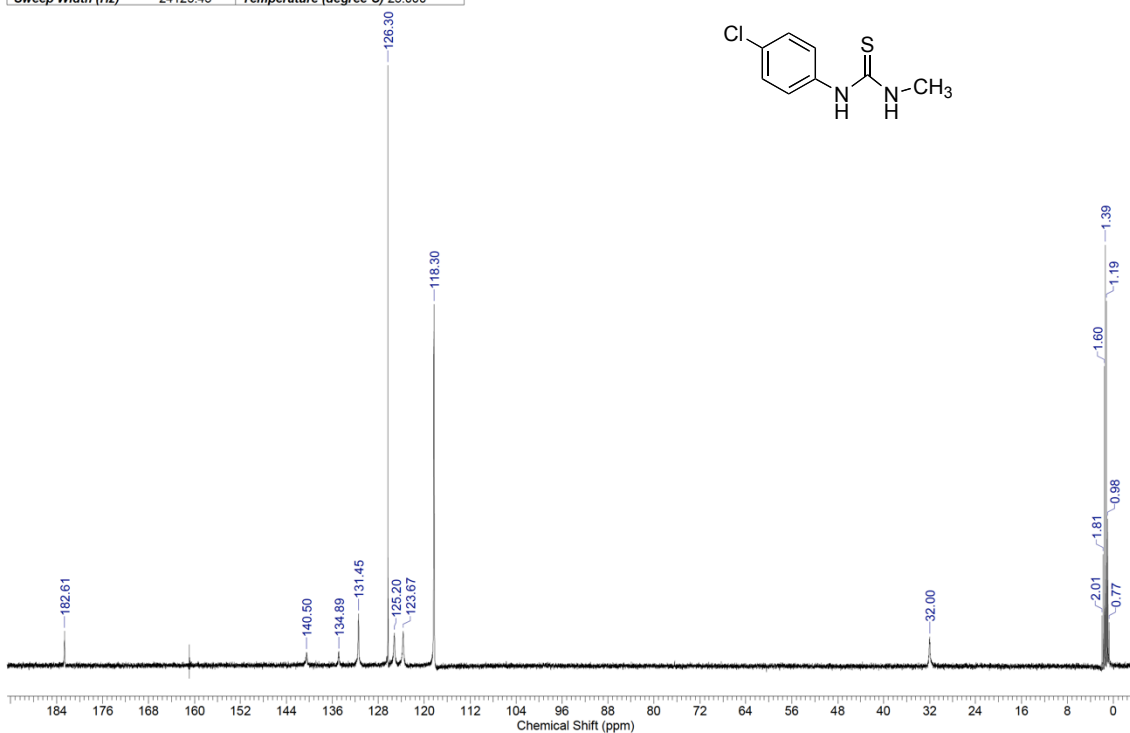


Figure A.12: ¹H and ¹³C NMR of 93d

| | | | | | | | |
|------------------------|--------------------------------|--------------|------------|----------------------|-------------|------------------------|-------------|
| Acquisition Time (sec) | 2.0487 | Comment | Std proton | Date | Dec 12 2011 | Date Stamp | Dec 12 2011 |
| File Name | G:\XXNMR0222\DI-PNO2THIOUREA-H | | | Frequency (MHz) | 399.73 | Nucleus | 1H |
| Original Points Count | 13102 | Points Count | 16384 | Pulse Sequence | s2pul | Receiver Gain | 48.00 |
| Solvent | ACETONITRILE-d3 | | | Spectrum Offset (Hz) | 2396.1704 | Sweep Width (Hz) | 6395.40 |
| | | | | | | Temperature (degree C) | 25.000 |

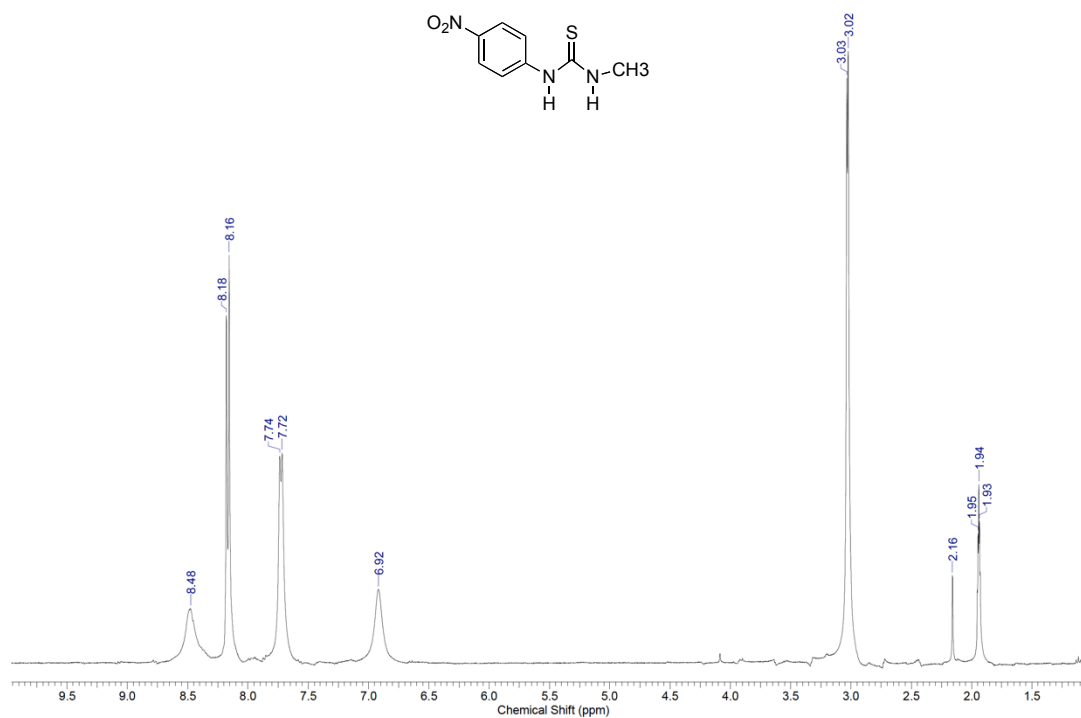
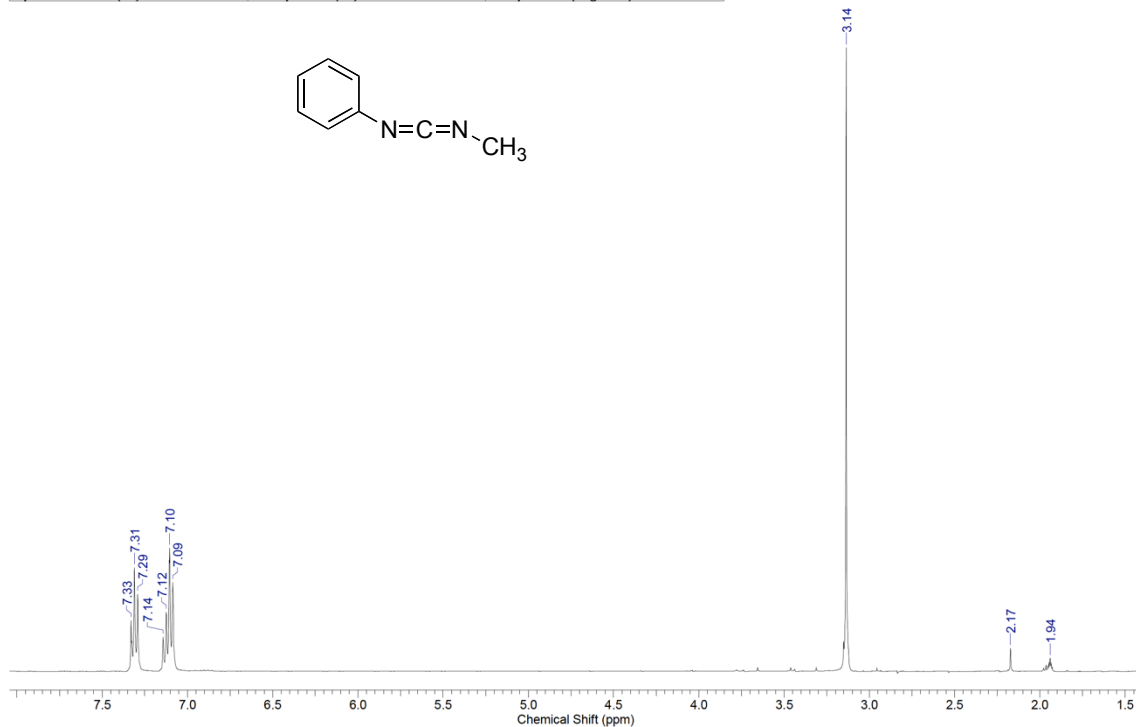


Figure A.13: ¹H NMR of 93e

| | | | | | | | |
|------------------------|---|----------------------|------------|------------------------|-----------------|--------------|------------|
| Acquisition Time (sec) | 2.0487 | Comment | Std proton | Date | Aug 5 2010 | Date Stamp | Aug 5 2010 |
| File Name | C:\DOCUMENTS AND SETTINGS\VGZ\DESKTOP\IS4C2\HG6-43PCD-H | | | Frequency (MHz) | 399.74 | | |
| Nucleus | ¹ H | Number of Transients | 16 | Original Points Count | 13103 | Points Count | 16384 |
| Pulse Sequence | s2pul | Receiver Gain | 30.00 | Solvent | ACETONITRILE-d3 | | |
| Spectrum Offset (Hz) | 2403.5535 | Sweep Width (Hz) | 6395.91 | Temperature (degree C) | 25.000 | | |



| | | | | | | | |
|------------------------|--|----------------------|------------|------------------------|-----------------|--------------|------------|
| Acquisition Time (sec) | 1.3005 | Comment | Std proton | Date | Aug 5 2010 | Date Stamp | Aug 5 2010 |
| File Name | E:\OLAJIDE-NMR DATA\2010 NMR-OLAJIDE\HG6-43PCD-C13 | | | Frequency (MHz) | 100.53 | | |
| Nucleus | ¹³ C | Number of Transients | 15000 | Original Points Count | 31375 | Points Count | 32768 |
| Pulse Sequence | s2pul | Receiver Gain | 30.00 | Solvent | ACETONITRILE-d3 | | |
| Spectrum Offset (Hz) | 10635.6680 | Sweep Width (Hz) | 24125.45 | Temperature (degree C) | 25.000 | | |

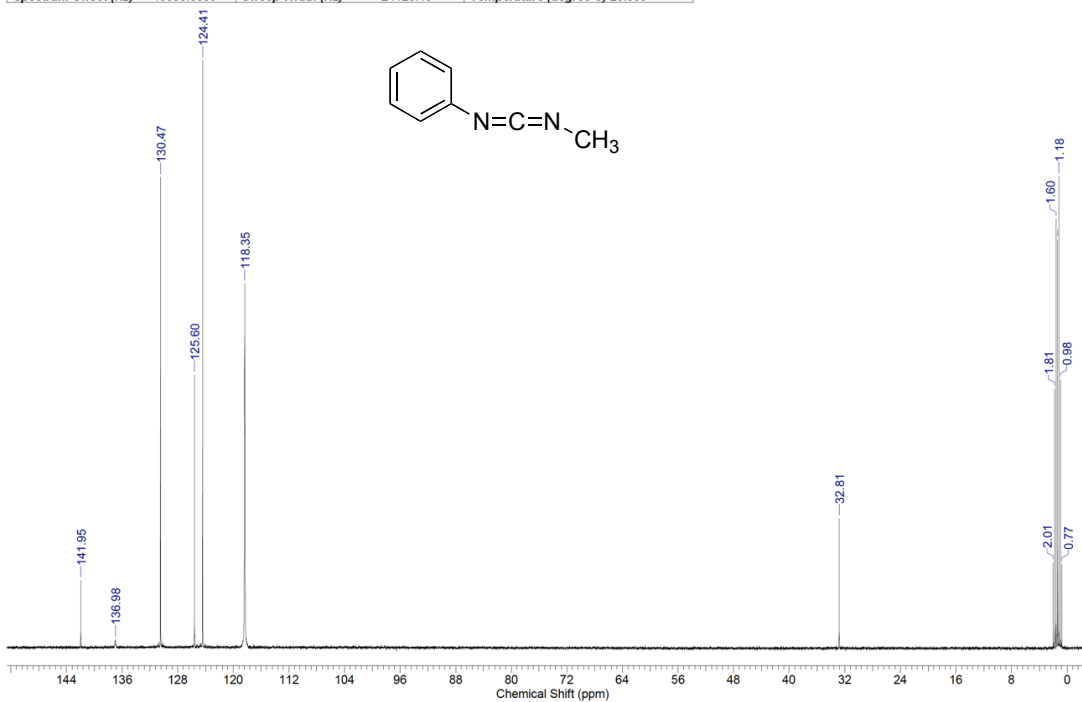
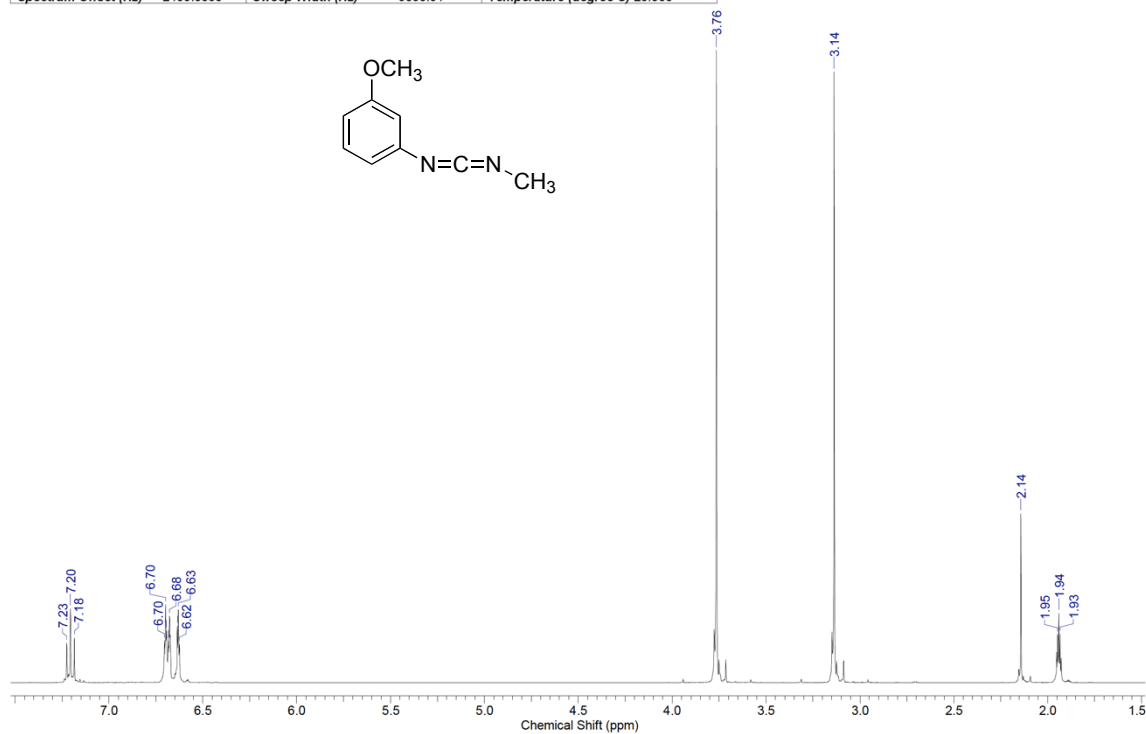


Figure A.14: ¹H and ¹³C NMR of 80a

| | | | | | | | |
|------------------------|---|----------------------|------------|------------------------|-----------------|--------------|-------------|
| Acquisition Time (sec) | 2.0487 | Comment | Std proton | Date | Mar 17 2010 | Date Stamp | Mar 17 2010 |
| File Name | E:\OLAJIDE-NMR DATA\2010 NMR-OLAJIDE\STD-MMP-CD-H | | | Frequency (MHz) | 399.74 | | |
| Nucleus | 1H | Number of Transients | 16 | Original Points Count | 13103 | Points Count | 16384 |
| Pulse Sequence | s2pul | Receiver Gain | 54.00 | Solvent | ACETONITRILE-d3 | | |
| Spectrum Offset (Hz) | 2403.5535 | Sweep Width (Hz) | 6395.91 | Temperature (degree C) | 25.000 | | |



| | | | | | | | |
|------------------------|---|----------------------|------------|------------------------|-----------------|--------------|-------------|
| Acquisition Time (sec) | 1.3005 | Comment | Std proton | Date | Mar 17 2010 | Date Stamp | Mar 17 2010 |
| File Name | E:\OLAJIDE-NMR DATA\2010 NMR-OLAJIDE\STD-MMP-CD-C13 | | | Frequency (MHz) | 100.53 | | |
| Nucleus | 13C | Number of Transients | 8000 | Original Points Count | 31375 | Points Count | 32768 |
| Pulse Sequence | s2pul | Receiver Gain | 30.00 | Solvent | ACETONITRILE-d3 | | |
| Spectrum Offset (Hz) | 10639.3486 | Sweep Width (Hz) | 24125.45 | Temperature (degree C) | 25.000 | | |

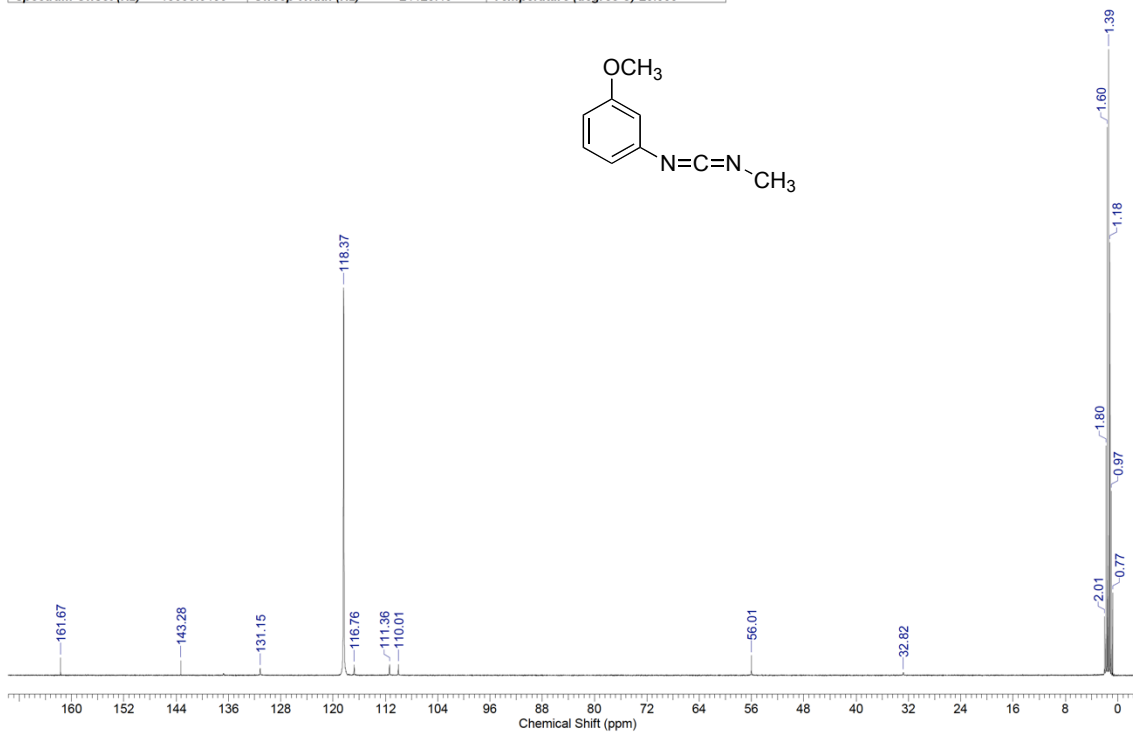
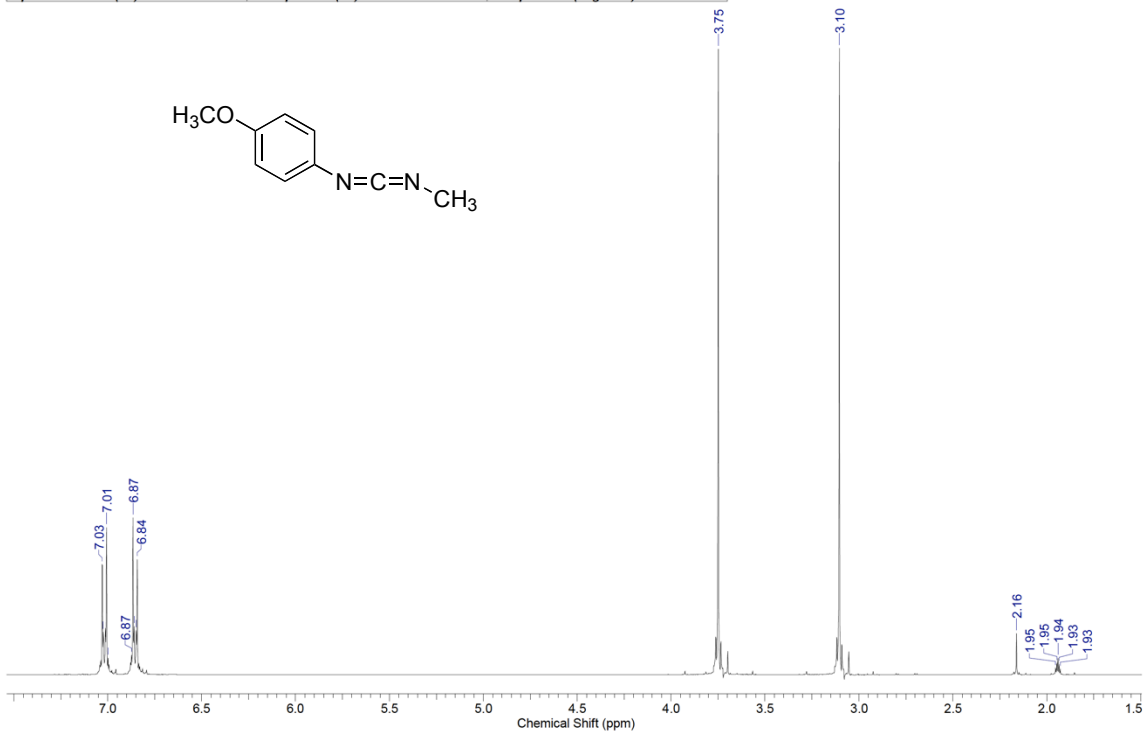


Figure A.15: ¹H and ¹³C NMR of 80b

| | | | | | | | |
|------------------------|--|----------------------|------------|------------------------|-----------------|--------------|-------------|
| Acquisition Time (sec) | 2.0487 | Comment | Std proton | Date | Mar 18 2010 | Date Stamp | Mar 18 2010 |
| File Name | C:\DOCUMENTS AND SETTINGS\VGZ\DESKTOP\IS4C2\STD-PMP-CD-H | | | Frequency (MHz) | 399.74 | | |
| Nucleus | ¹ H | Number of Transients | 16 | Original Points Count | 13103 | Points Count | 16384 |
| Pulse Sequence | s2pul | Receiver Gain | 38.00 | Solvent | ACETONITRILE-d3 | | |
| Spectrum Offset (Hz) | 2403.6575 | Sweep Width (Hz) | 6395.91 | Temperature (degree C) | 25.000 | | |



| | | | | | | | |
|------------------------|--|----------------------|------------|------------------------|-----------------|--------------|-------------|
| Acquisition Time (sec) | 1.3005 | Comment | Std proton | Date | Mar 18 2010 | Date Stamp | Mar 18 2010 |
| File Name | C:\DOCUMENTS AND SETTINGS\VGZ\DESKTOP\IS4C2\STD-PMP-CD-C13 | | | Frequency (MHz) | 100.53 | | |
| Nucleus | ¹³ C | Number of Transients | 2000 | Original Points Count | 31375 | Points Count | 32768 |
| Pulse Sequence | s2pul | Receiver Gain | 30.00 | Solvent | ACETONITRILE-d3 | | |
| Spectrum Offset (Hz) | 10638.6123 | Sweep Width (Hz) | 24125.45 | Temperature (degree C) | 25.000 | | |

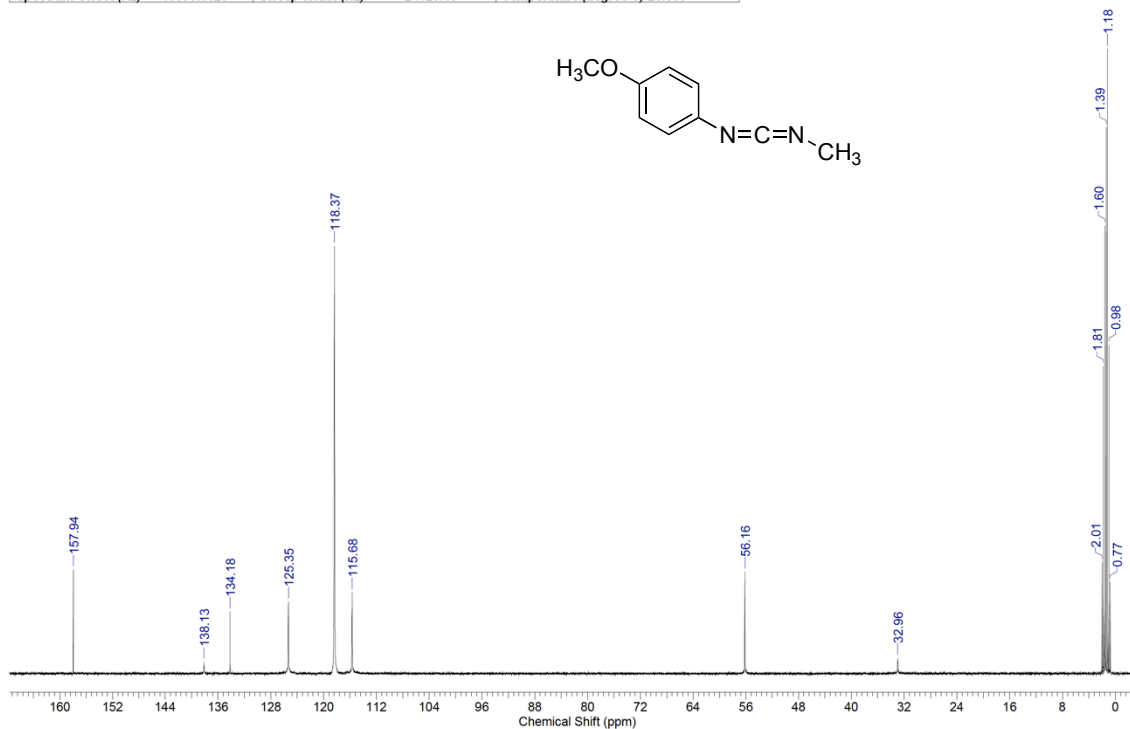
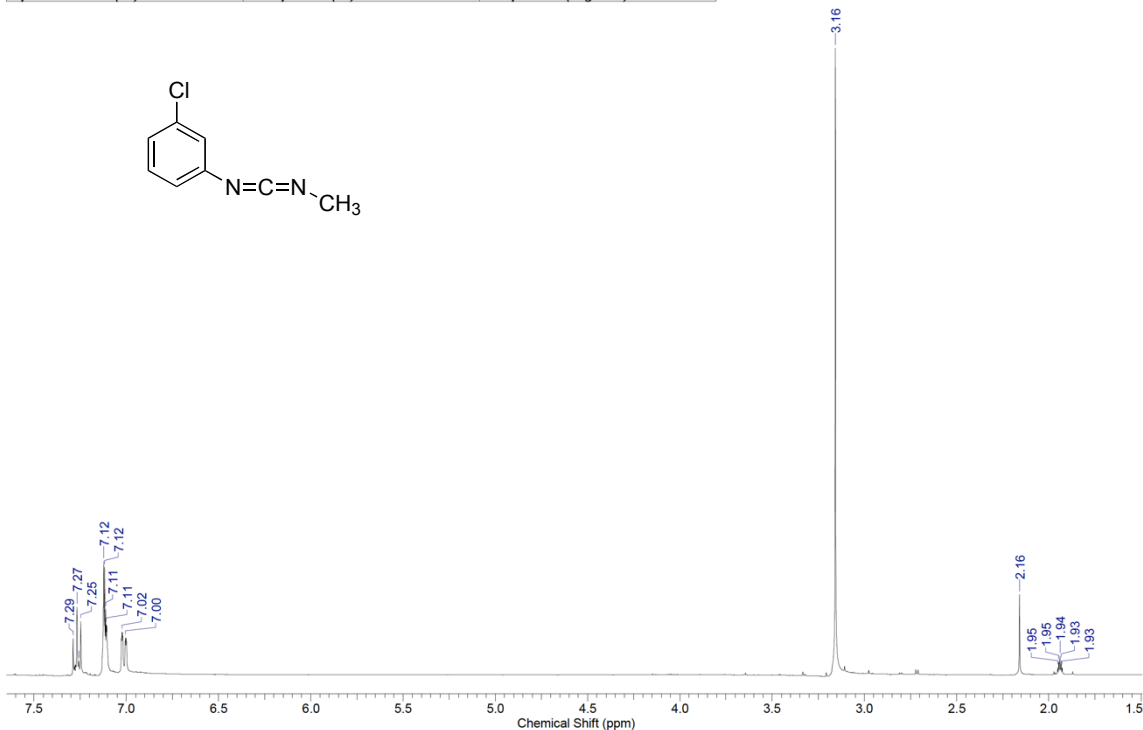


Figure A.16: ¹H and ¹³C NMR of **80c**

| | | | | | | | |
|------------------------|--|----------------------|------------|------------------------|-----------------|-----------------|-------------|
| Acquisition Time (sec) | 2.0487 | Comment | Std proton | Date | Sep 22 2010 | Date Stamp | Sep 22 2010 |
| File Name | E:\OLAJIDE-NMR DATA\2010 NMR-OLAJIDE\HG646-MCPCD-H | | | | | Frequency (MHz) | 399.74 |
| Nucleus | ¹ H | Number of Transients | 16 | Original Points Count | 13103 | Points Count | 16384 |
| Pulse Sequence | s2pul | Receiver Gain | 32.00 | Solvent | ACETONITRILE-d3 | | |
| Spectrum Offset (Hz) | 2403.6575 | Sweep Width (Hz) | 6395.91 | Temperature (degree C) | 25.000 | | |



| | | | | | | | |
|------------------------|--|----------------------|------------|------------------------|-----------------|-----------------|-------------|
| Acquisition Time (sec) | 1.3005 | Comment | Std proton | Date | Sep 22 2010 | Date Stamp | Sep 22 2010 |
| File Name | C:\DOCUMENTS AND SETTINGS\IVGZ\DESKTOP\IS4C2\HG646-MCPCD-C13 | | | | | Frequency (MHz) | 100.53 |
| Nucleus | ¹³ C | Number of Transients | 7000 | Original Points Count | 31375 | Points Count | 32768 |
| Pulse Sequence | s2pul | Receiver Gain | 30.00 | Solvent | ACETONITRILE-d3 | | |
| Spectrum Offset (Hz) | 10637.8770 | Sweep Width (Hz) | 24125.45 | Temperature (degree C) | 25.000 | | |

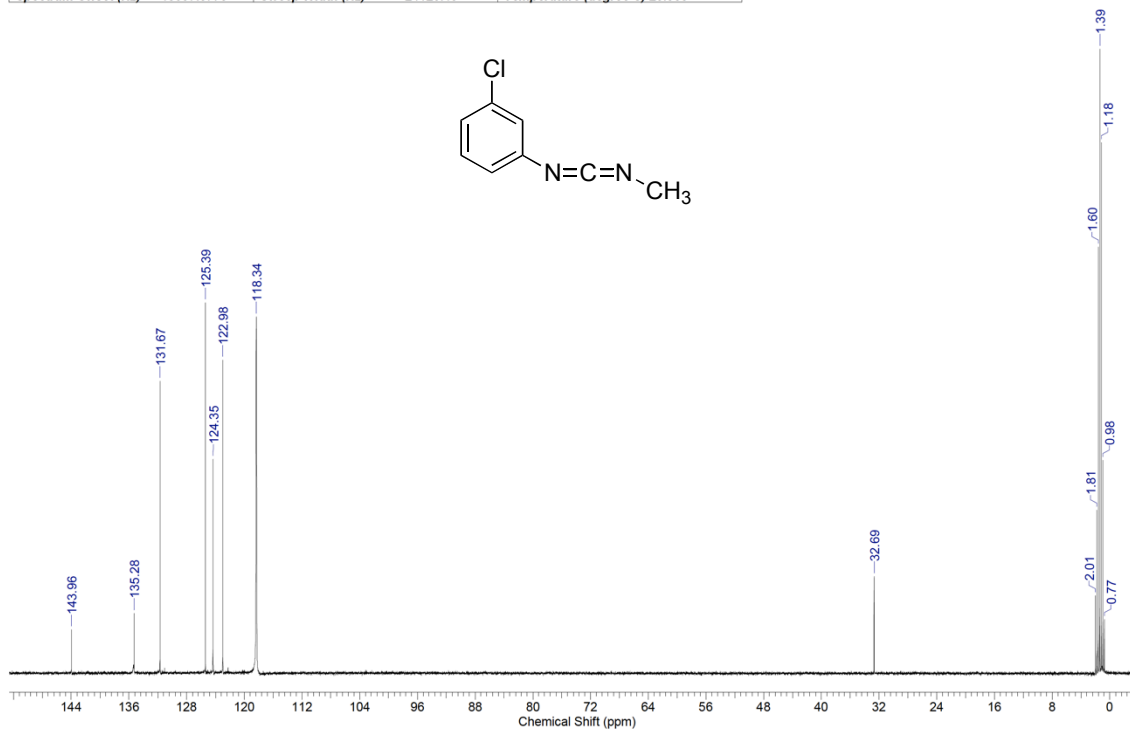
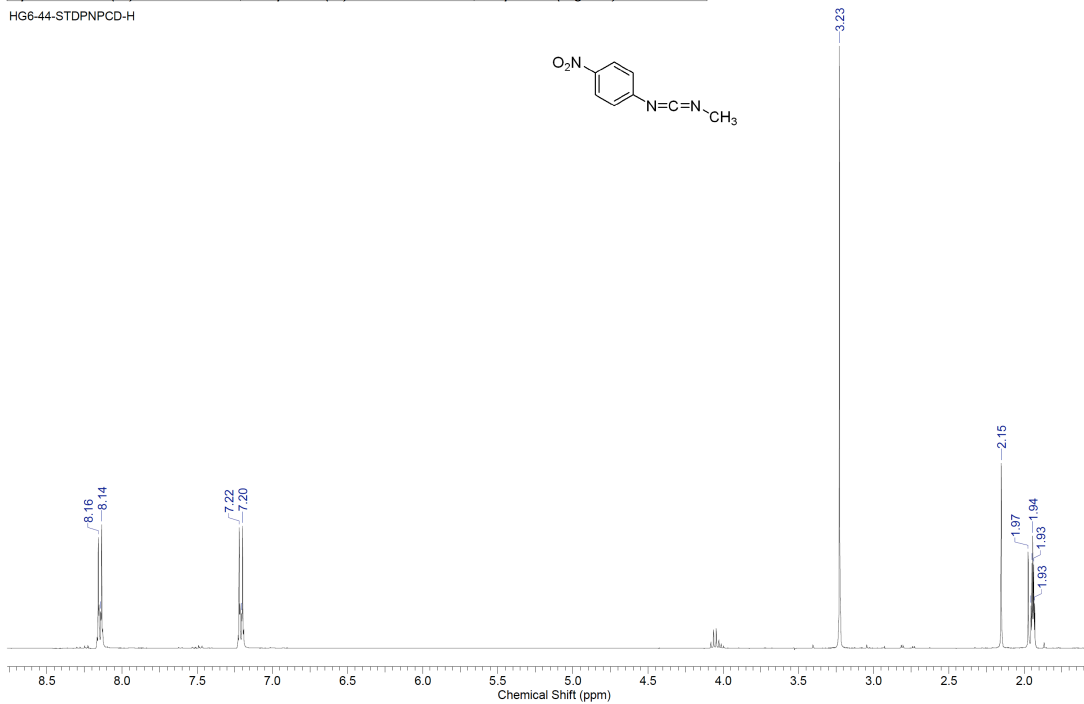


Figure A.17: ¹H and ¹³C NMR of **80d**

| | | | | | | | |
|------------------------|---|----------------------|------------|------------------------|-----------------|--------------|------------|
| Acquisition Time (sec) | 2.0487 | Comment | Std proton | Date | Aug 6 2010 | Date Stamp | Aug 6 2010 |
| File Name | C:\DOCUMENTS AND SETTINGS\VGZ\DESKTOP\PI\S4C2\HG6-44-STDPNPCD-H | | | Frequency (MHz) | 399.74 | | |
| Nucleus | ¹ H | Number of Transients | 16 | Original Points Count | 13103 | Points Count | 16384 |
| Pulse Sequence | s2pul | Receiver Gain | 48.00 | Solvent | ACETONITRILE-d3 | | |
| Spectrum Offset (Hz) | 2403.5535 | Sweep Width (Hz) | 6395.91 | Temperature (degree C) | 25.000 | | |

HG6-44-STDPNPCD-H



| | | | | | | | |
|------------------------|--|----------------------|------------|------------------------|-----------------|--------------|------------|
| Acquisition Time (sec) | 1.3005 | Comment | Std proton | Date | Aug 6 2010 | Date Stamp | Aug 6 2010 |
| File Name | C:\DOCUMENTS AND SETTINGS\VGZ\DESKTOP\PI\S4C2\HG6-44-PNPCD-C13 | | | Frequency (MHz) | 100.53 | | |
| Nucleus | ¹³ C | Number of Transients | 20000 | Original Points Count | 31375 | Points Count | 32768 |
| Pulse Sequence | s2pul | Receiver Gain | 30.00 | Solvent | ACETONITRILE-d3 | | |
| Spectrum Offset (Hz) | 10636.4375 | Sweep Width (Hz) | 24125.45 | Temperature (degree C) | 25.000 | | |

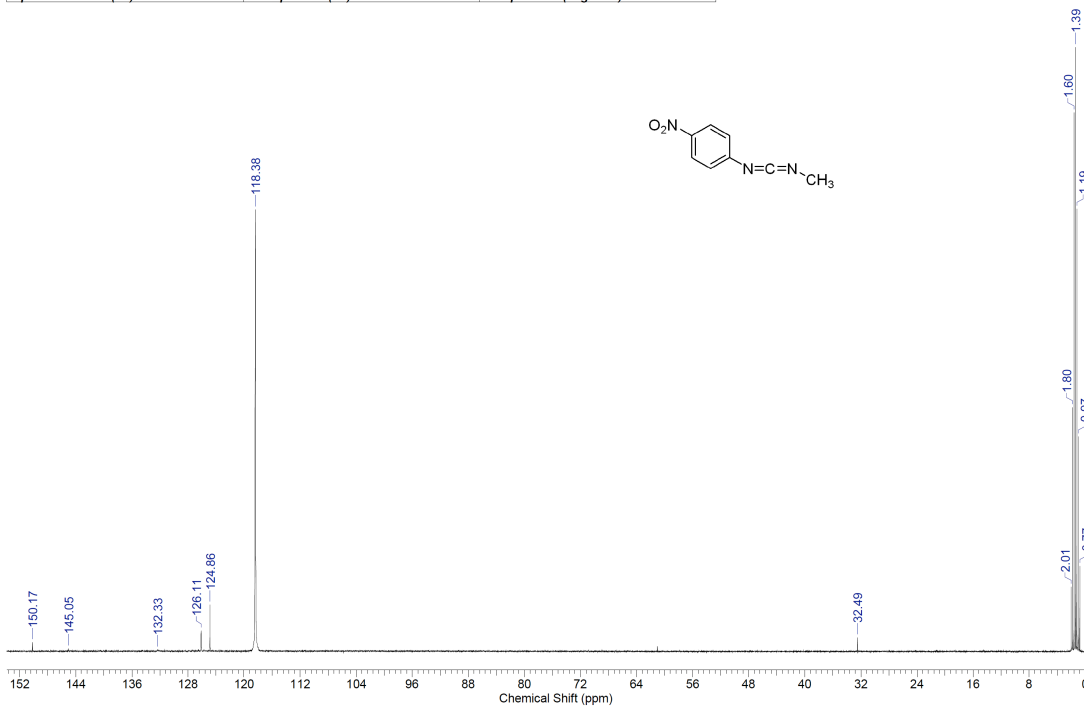


Figure A.18: ¹H and ¹³C NMR of **80e**

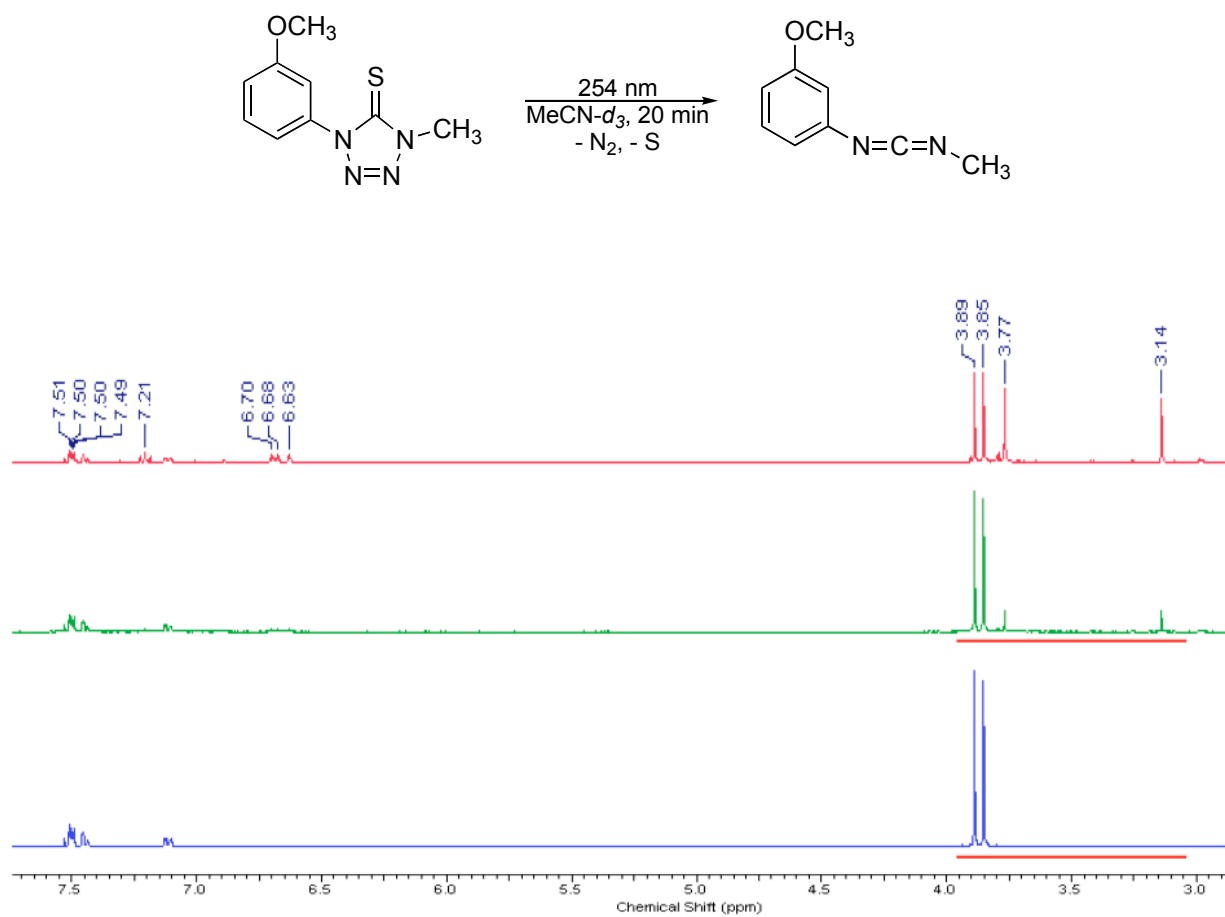


Figure A.19: ^1H NMR spectra of **79b** in acetonitrile- d_3 taken at 0 (bottom), 10 (middle) and 20 (top) min of UV-irradiation at 254 nm, respectively.

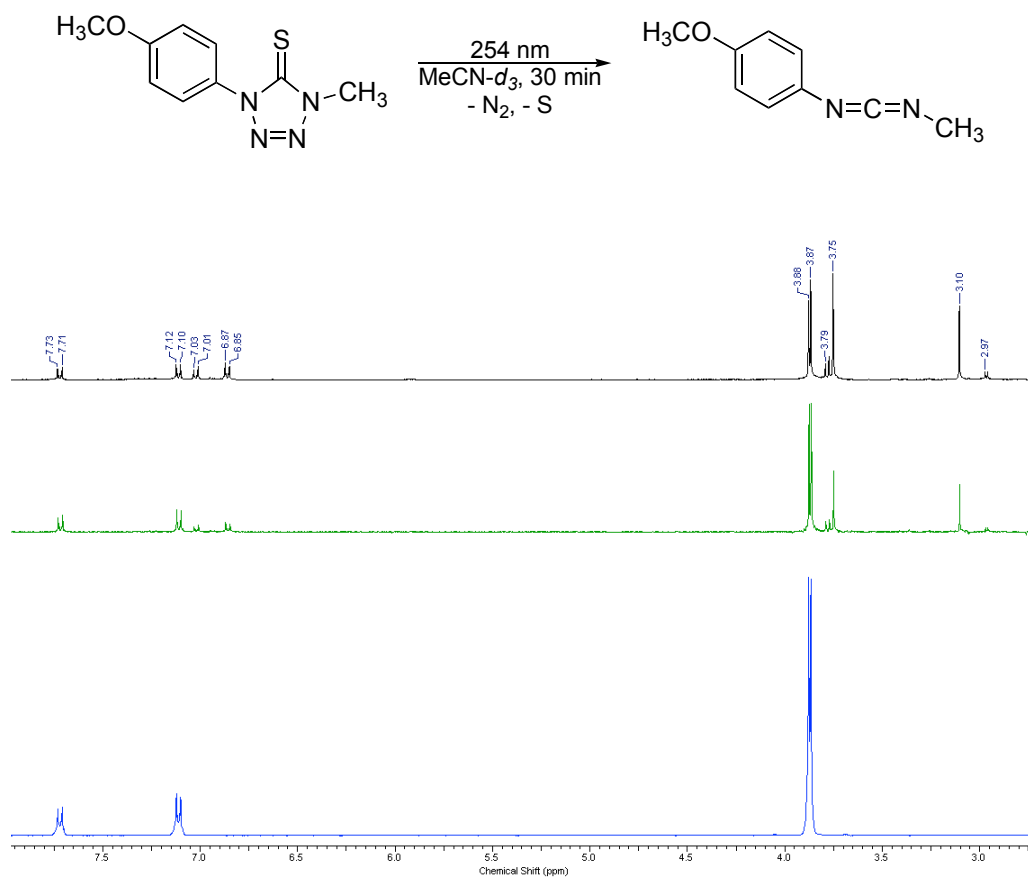


Figure A.20: ^1H NMR spectra of **79c** in acetonitrile- d_3 taken at 0 (bottom), 15 (middle) and 30 (top) min of UV-irradiation at 254 nm, respectively.

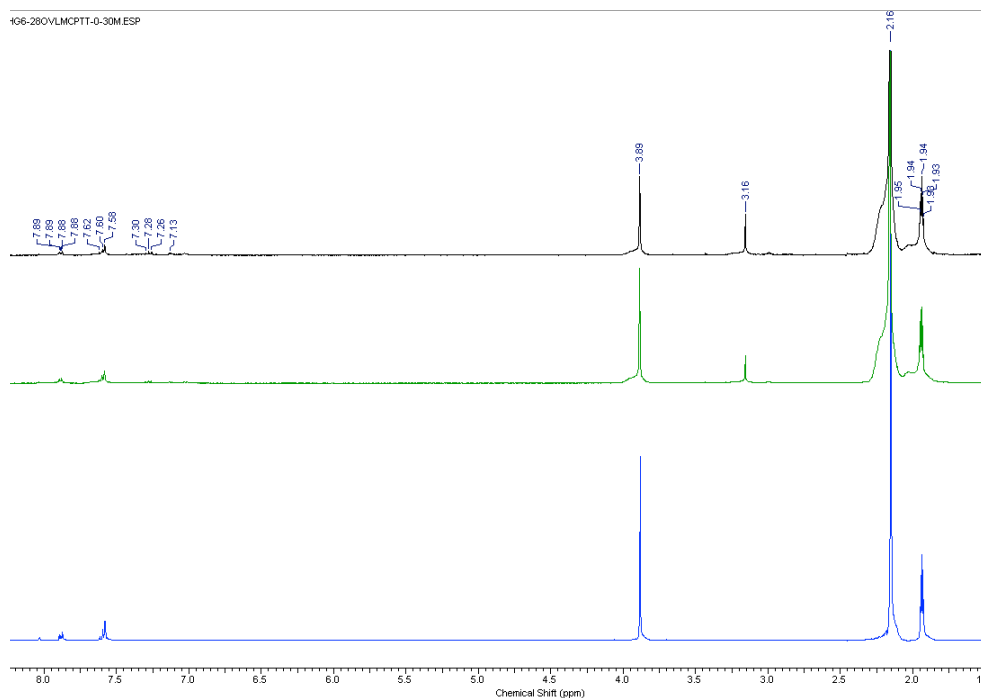
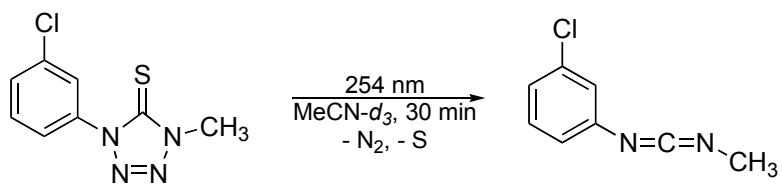


Figure A.21: ^1H NMR spectra of **79d** in acetonitril- d_3 taken at 0 (bottom), 15 (middle) and 30 (top) min of UV-irradiation at 254 nm, respectively.

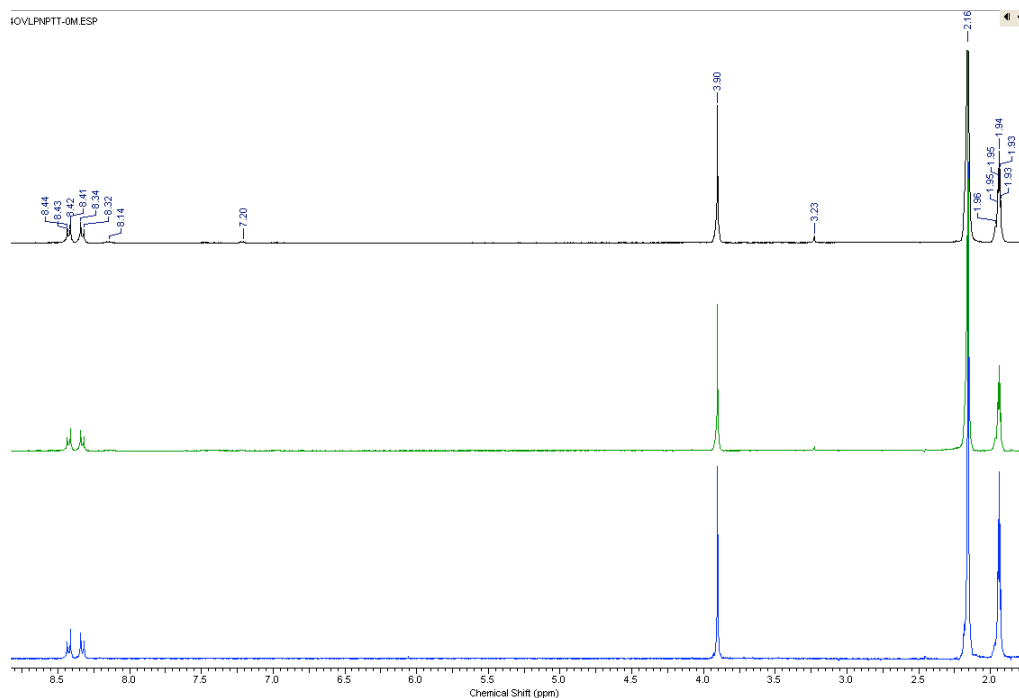
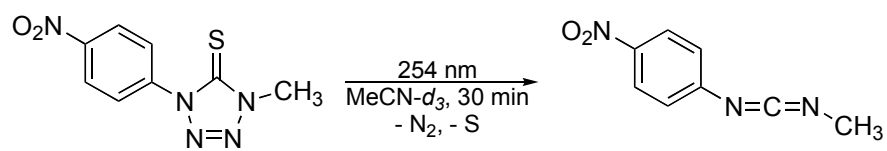


Figure A.22: ¹H NMR spectra of **79e** in acetonitrile-*d*₃ taken at 0 (bottom), 15 (middle) and 30 (top) minute of UV-irradiation at 254 nm, respectively.

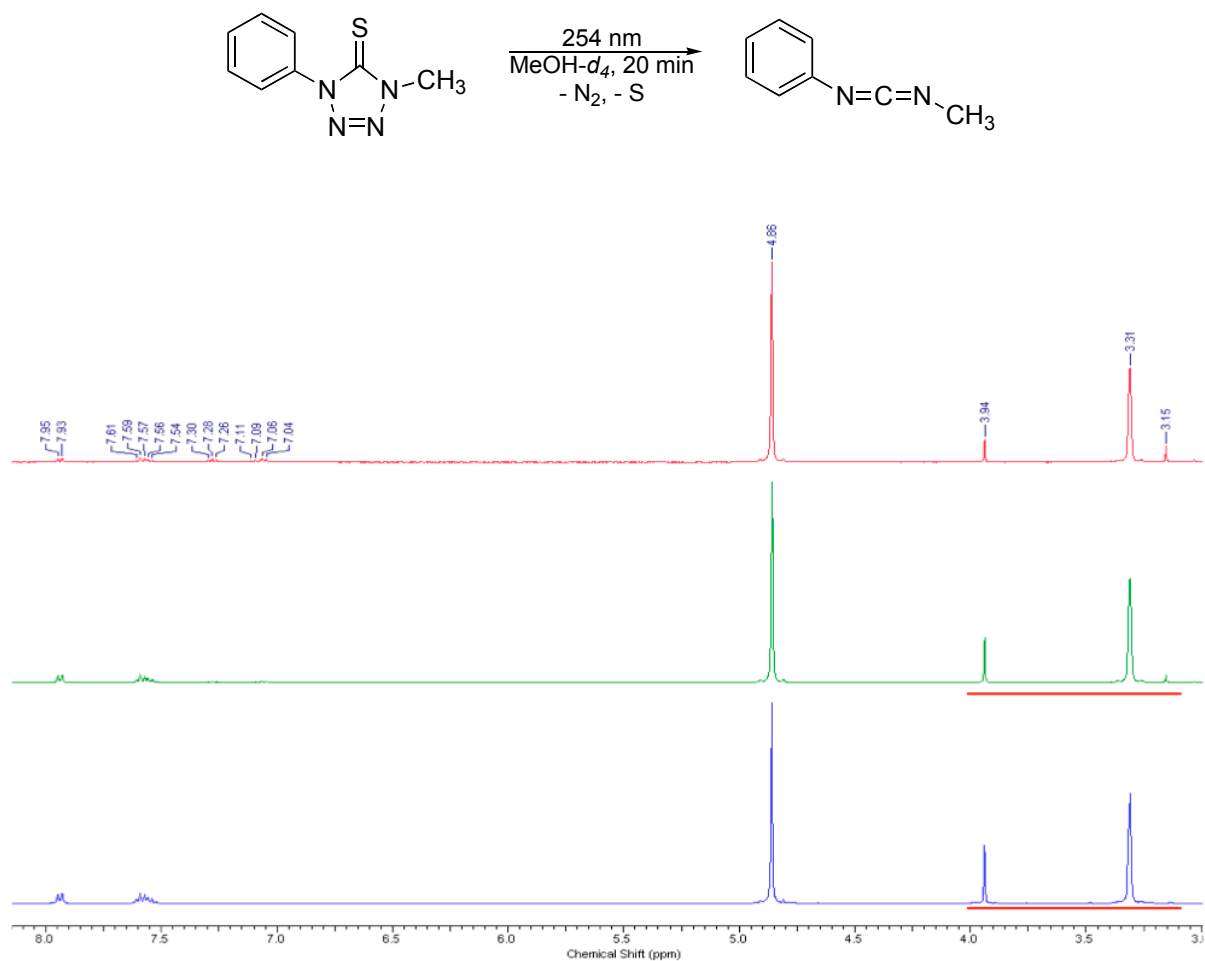


Figure A.23: 1H NMR spectra of **79a** in methanol- d_4 taken at 0 (bottom), 10 (middle) and 20 (top) min of UV-irradiation at 254 nm, respectively.

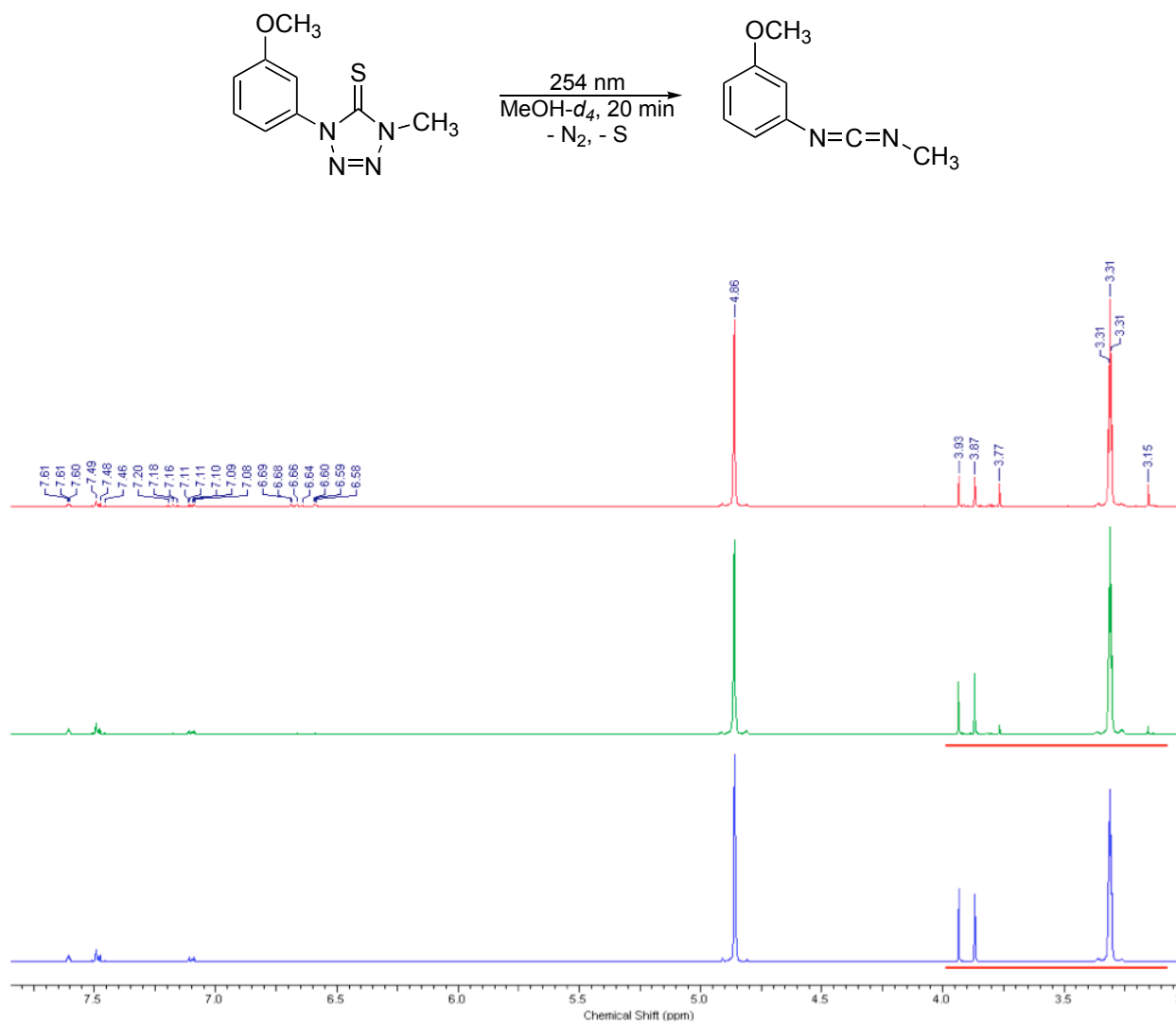


Figure A.24: ^1H NMR spectra of **79b** in methanol- d_4 taken at 0 (bottom), 10 (middle) and 20 (top) min UV-irradiation in 254 nm, respectively.

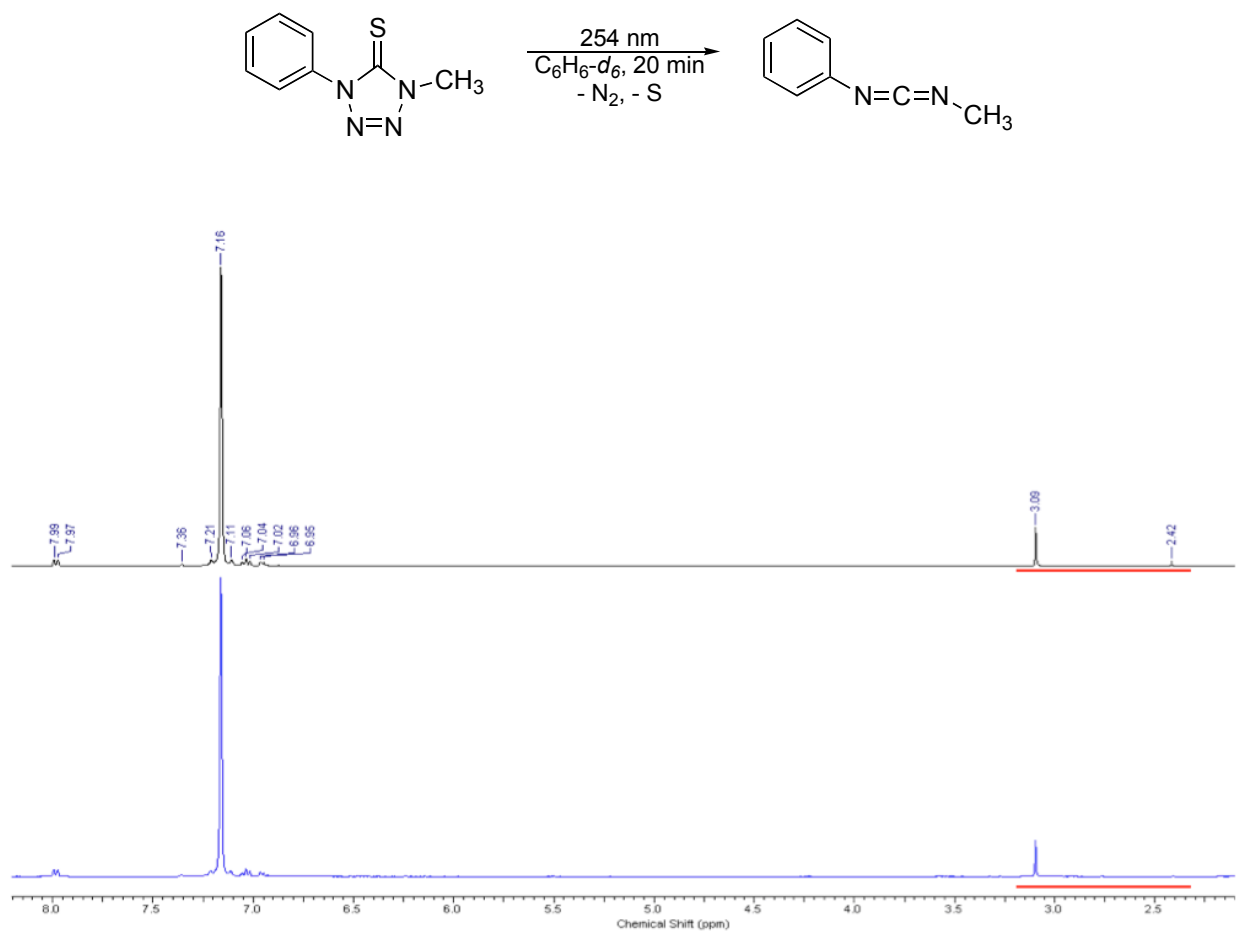


Figure A.25: ^1H NMR spectra of **79a** in benzene- d_6 taken at 0 (bottom) and 20 (top) min of UV-irradiation at 254 nm, respectively.

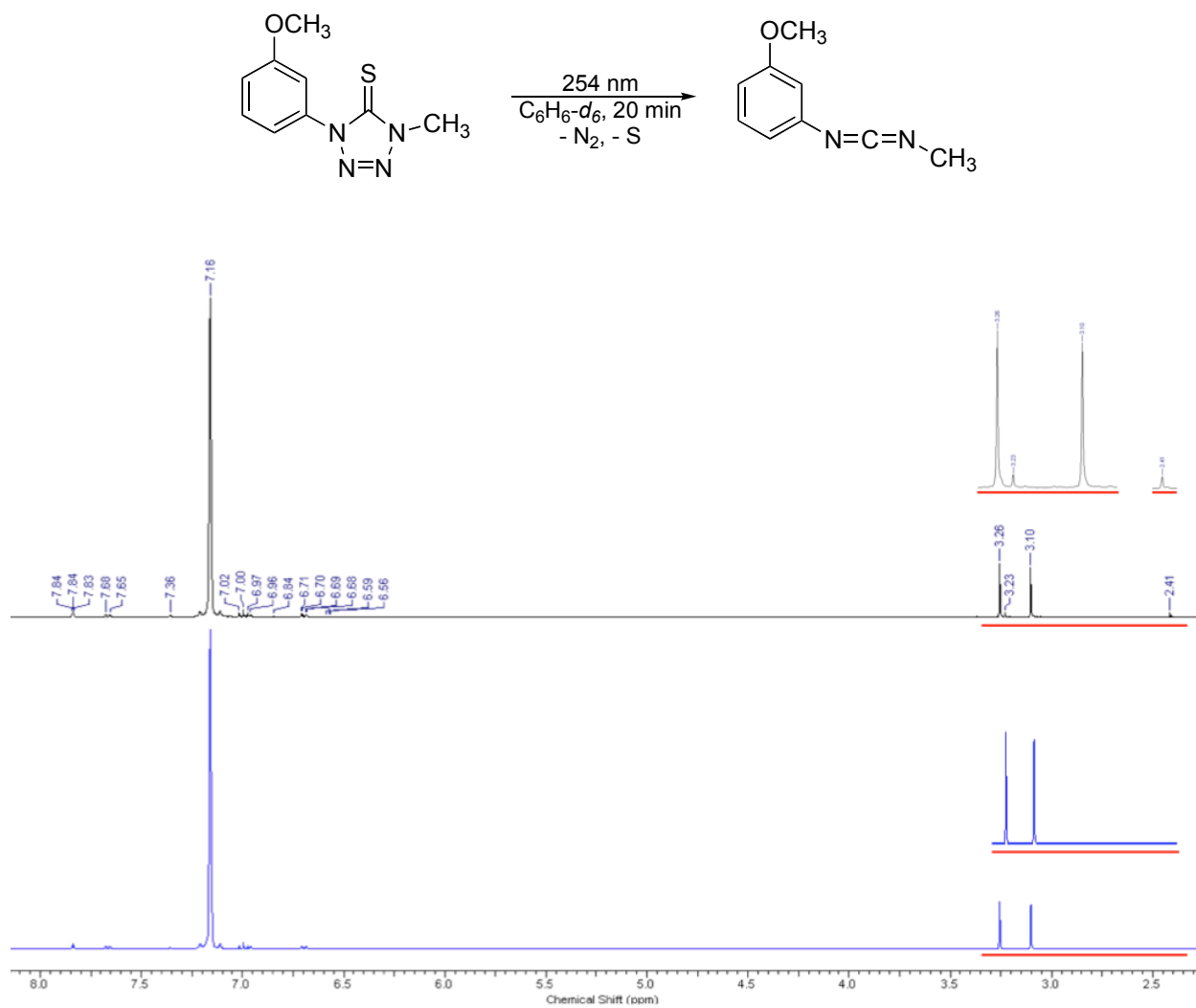


Figure A.26: ^1H NMR spectra of **79b** in benzene- d_6 taken at 0 (bottom) and 20 (top) min of UV-irradiation at 254 nm, respectively.

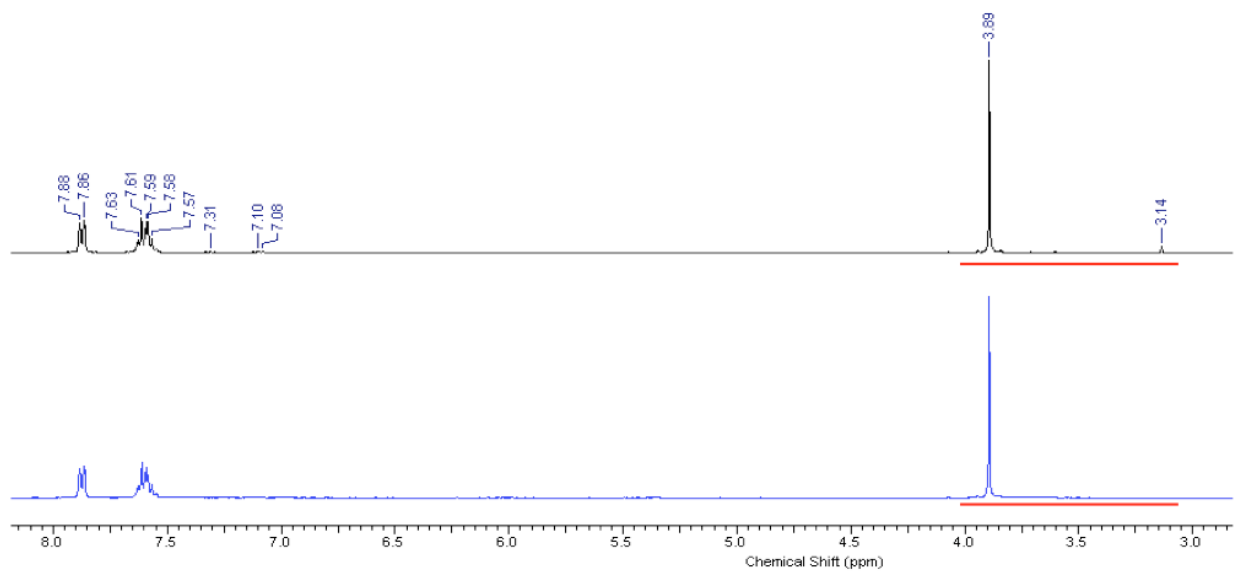
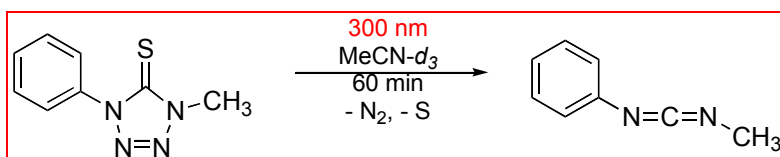


Figure A.27: ¹H NMR spectra of **79a** in acetonitrile-*d*₃ taken at 0 (bottom) and 60 (top) min of UV-irradiation at 300 nm at 300 nm, respectively.

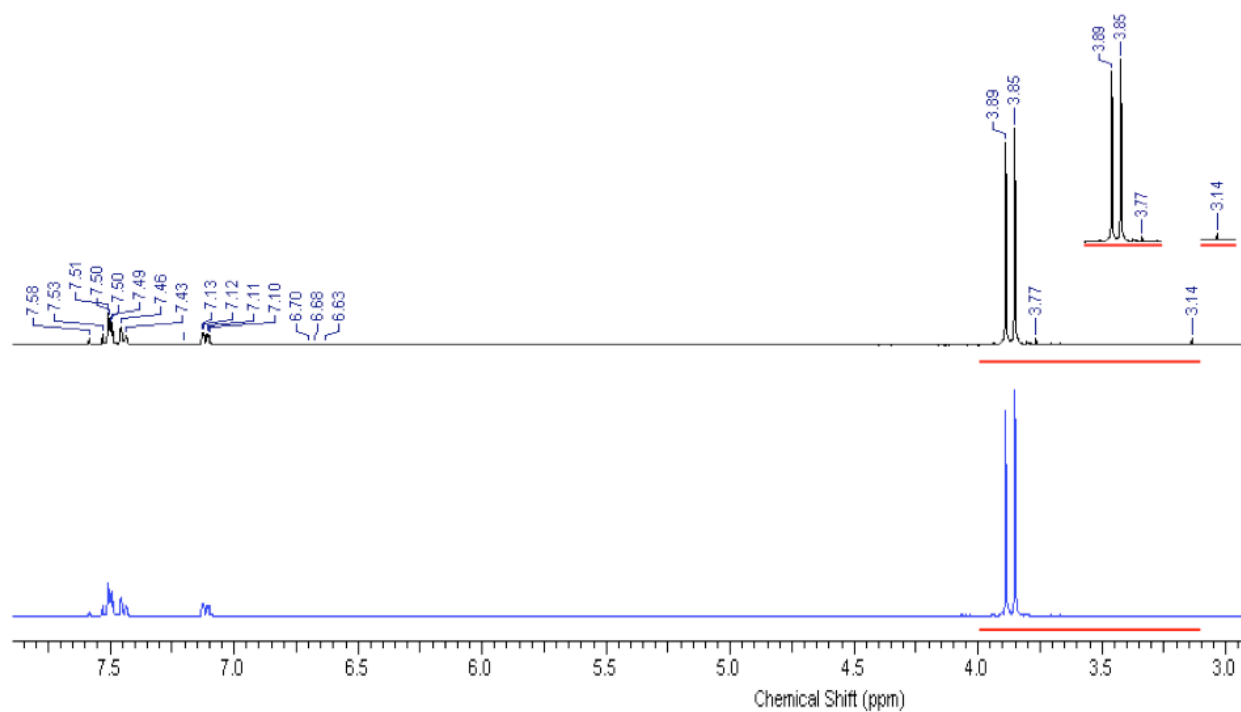
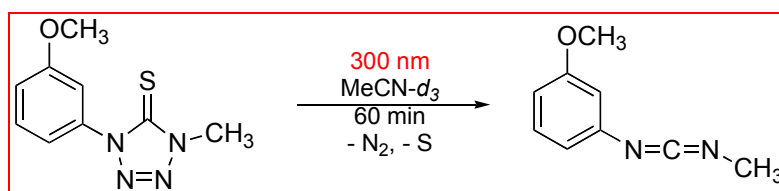


Figure A.28: ¹H NMR spectra of **79b** in acetonitrile-*d*₃ taken at 0 (bottom) and 60 (top) min of UV-irradiation at 300 nm, respectively.

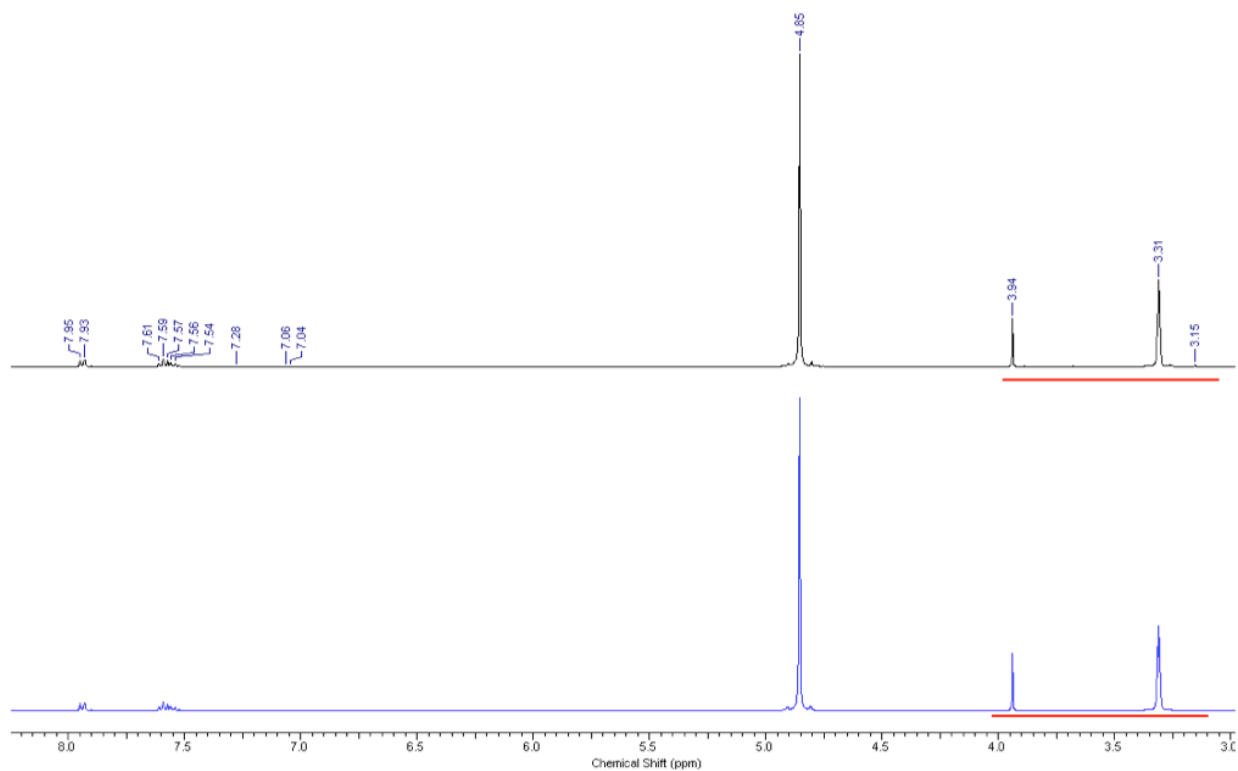
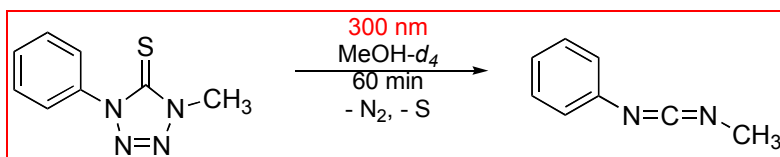


Figure A.29: ^1H NMR spectra of **79a** in methanol- d_4 taken at 0 (bottom) and 60 (top) min of UV-irradiation at 300 nm, respectively.

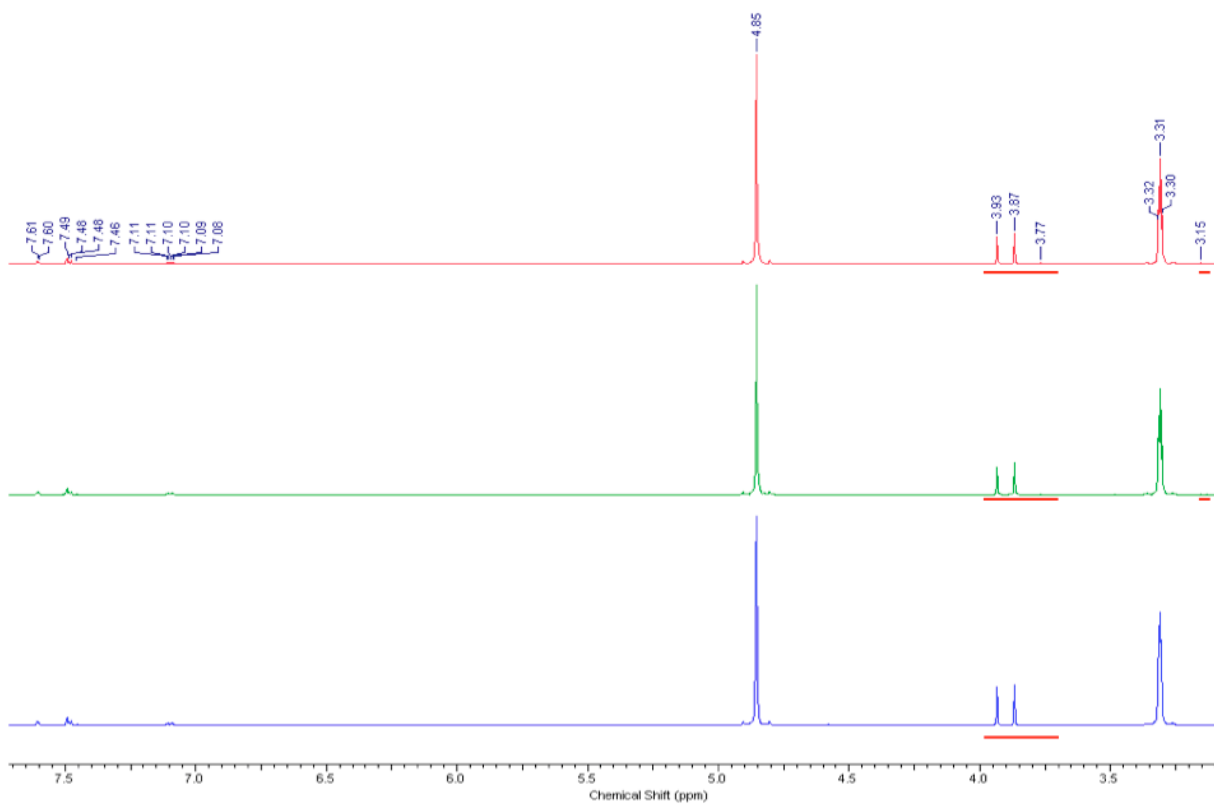
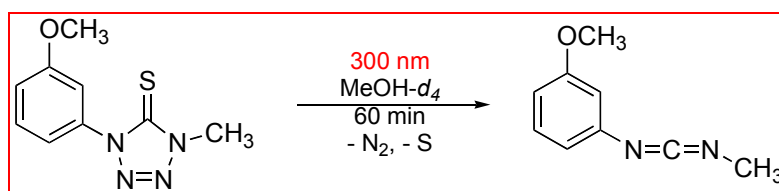


Figure A.30: ^1H NMR spectra of **79b** in methanol- d_4 taken at 0 (bottom), 30 (middle) and 60 (top) min of UV-irradiation at 300 nm, respectively.

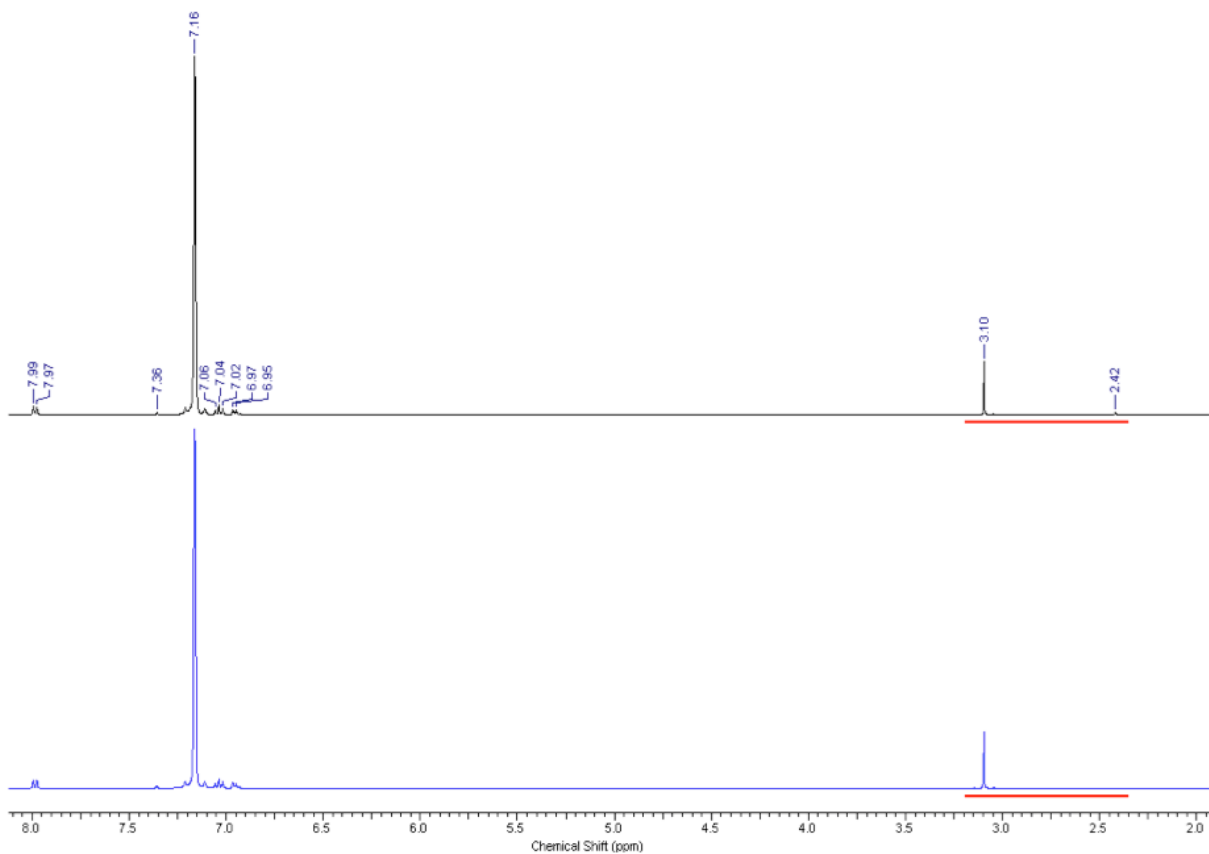
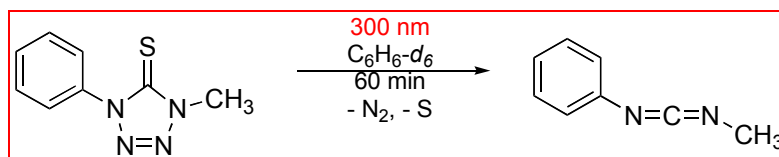


Figure A.31: ¹H NMR spectra of **79a** in benzene-*d*₆ taken at 0 (bottom) and 60 (top) minutes of UV-irradiation at 300 nm, respectively.

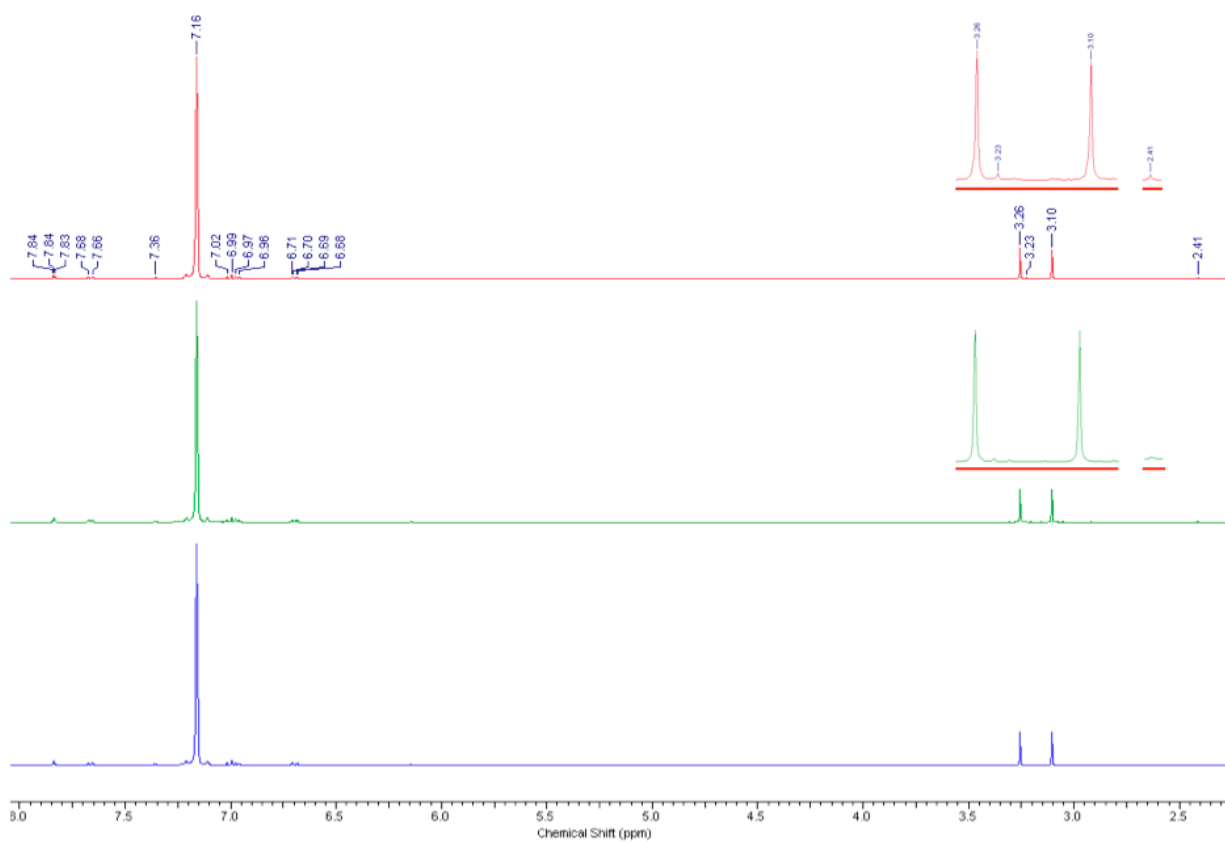
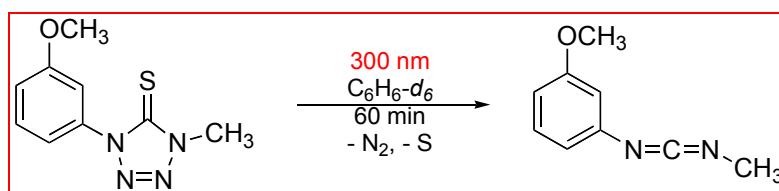


Figure A.32: ^1H NMR spectra of **79b** in benzene- d_6 taken at 0 (bottom) and 60 (top) min of UV-irradiation at 300 nm, respectively.

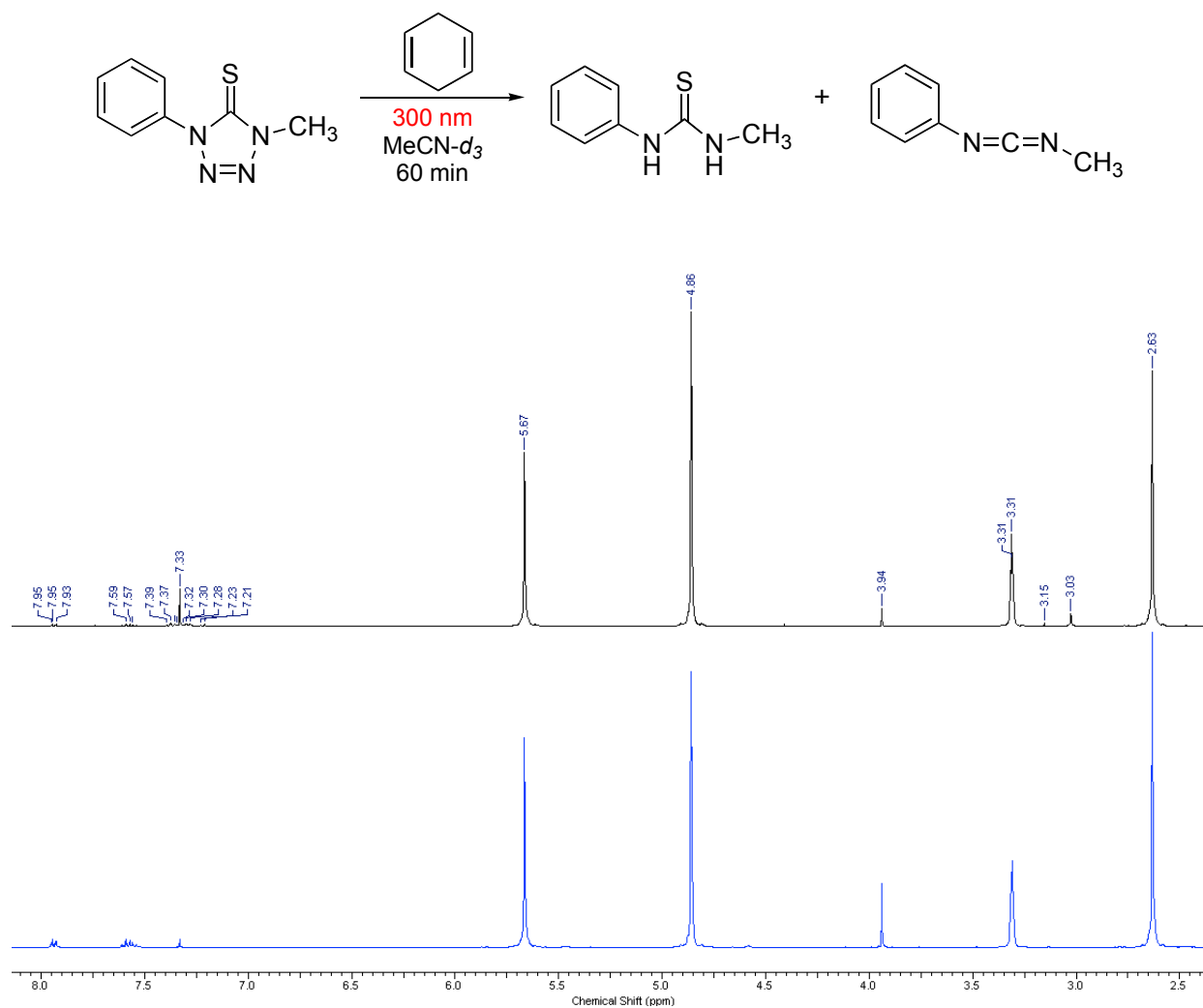


Figure A.33: ^1H NMR spectra of **79a** and 1,4-CHD in acetonitrile- d_6 taken at 0 (bottom) and 60 (top) min of UV-irradiation at 300 nm, respectively.

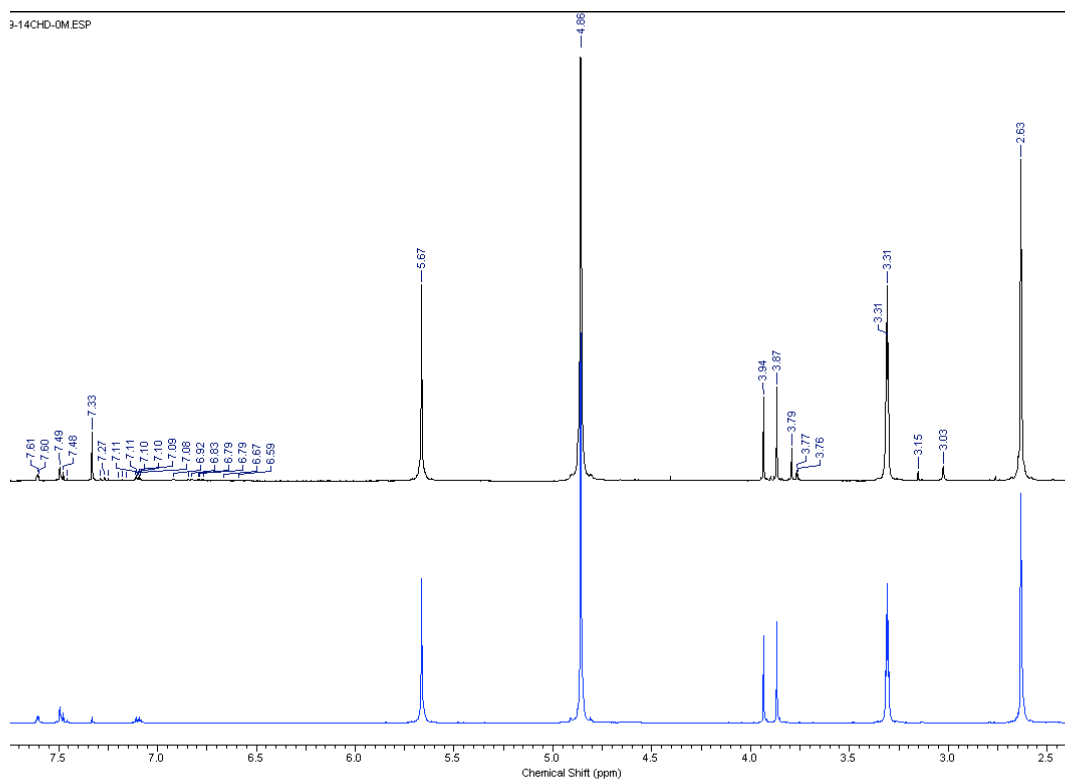
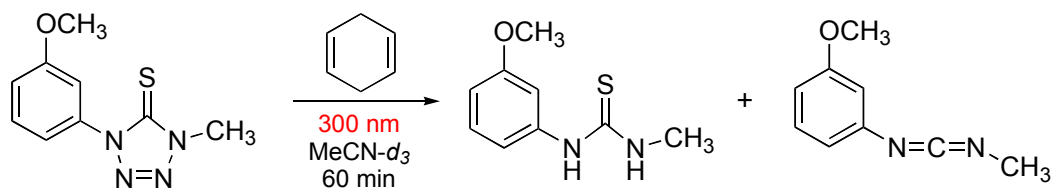
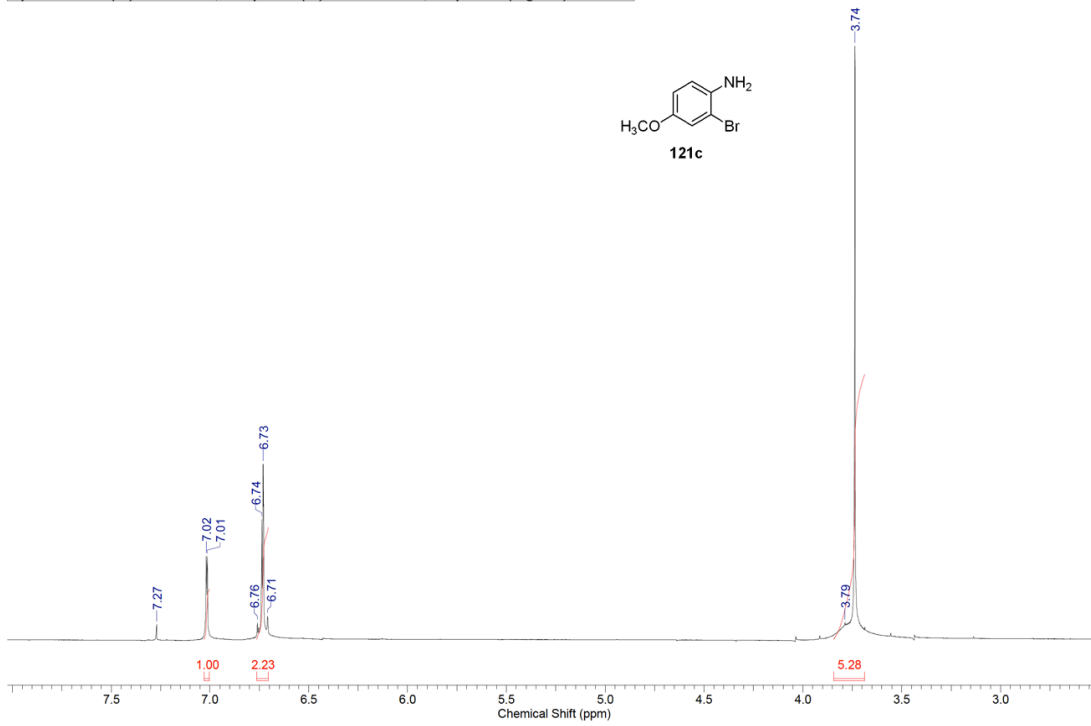


Figure A.34: ¹H NMR spectra of **79b** and 1,4-CHD in acetonitrile-*d*₆ taken at 0 (bottom) and 60 (top) min of UV-irradiation at 300 nm, respectively.

**Appendix B - NMR Spectra for 2-bromo-4-methoxyaniline,
substituted biphenyl amines, biphenyl isocyanates, 2-
((biphenylimino)methyleneamino)benzotrile, 2-halo-3-biphenyl
quinazolininium halides and phenanthridine-fused
quinazolininium salts**

| | | | | | | | |
|------------------------|-------------------|------------------|------------|------------------------|-------------|---------------|--------------|
| Acquisition Time (sec) | 2.0487 | Comment | Std proton | Date | Aug 23 2011 | Date Stamp | Aug 23 2011 |
| File Name | F:\2AMINO\HG932-H | | | Frequency (MHz) | 399.73 | Nucleus | 1H |
| Original Points Count | 13102 | Points Count | 16384 | Pulse Sequence | s2pul | Receiver Gain | 44.00 |
| Spectrum Offset (Hz) | 2415.5496 | Sweep Width (Hz) | 6395.40 | Temperature (degree C) | 25.000 | Solvent | CHLOROFORM-d |



| | | | | | | | |
|------------------------|-------------------------|--------------|------------|----------------------|-------------|------------------|-------------|
| Acquisition Time (sec) | 1.3005 | Comment | Std proton | Date | Aug 23 2011 | Date Stamp | Aug 23 2011 |
| File Name | F:\2AMINO\HG932-C13-STD | | | Frequency (MHz) | 100.52 | Nucleus | 13C |
| Original Points Count | 31375 | Points Count | 32768 | Pulse Sequence | s2pul | Receiver Gain | 30.00 |
| Solvent | CHLOROFORM-d | | | Spectrum Offset (Hz) | 10550.4766 | Sweep Width (Hz) | 24125.45 |
| Temperature (degree C) | 25.000 | | | | | | |

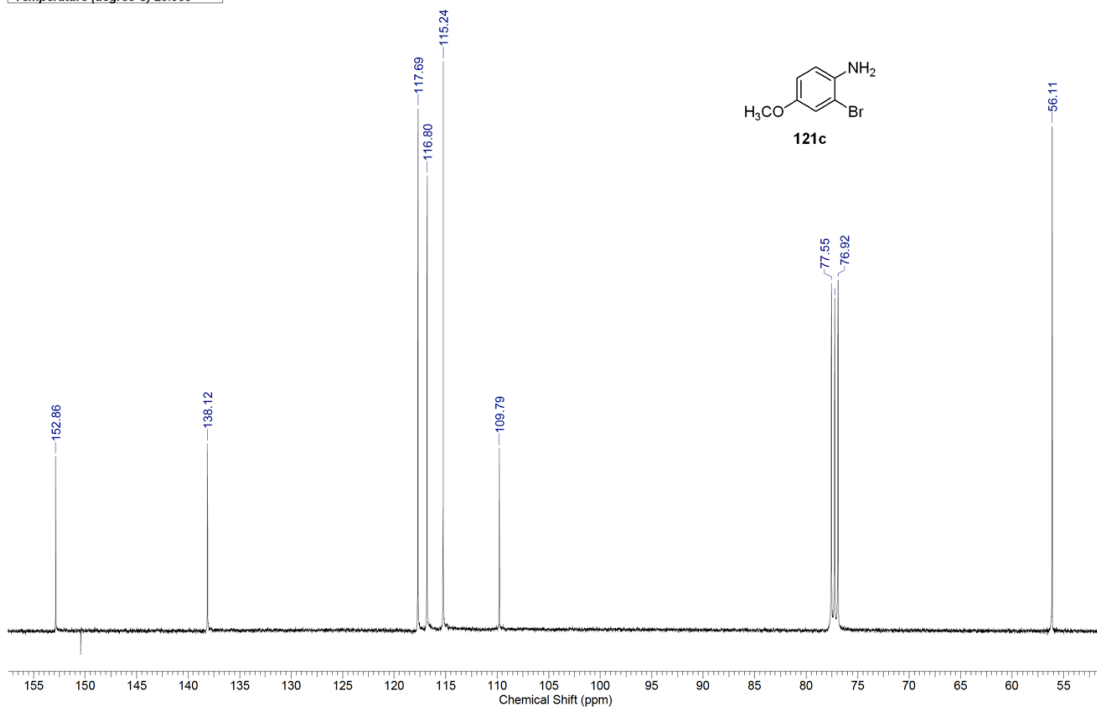
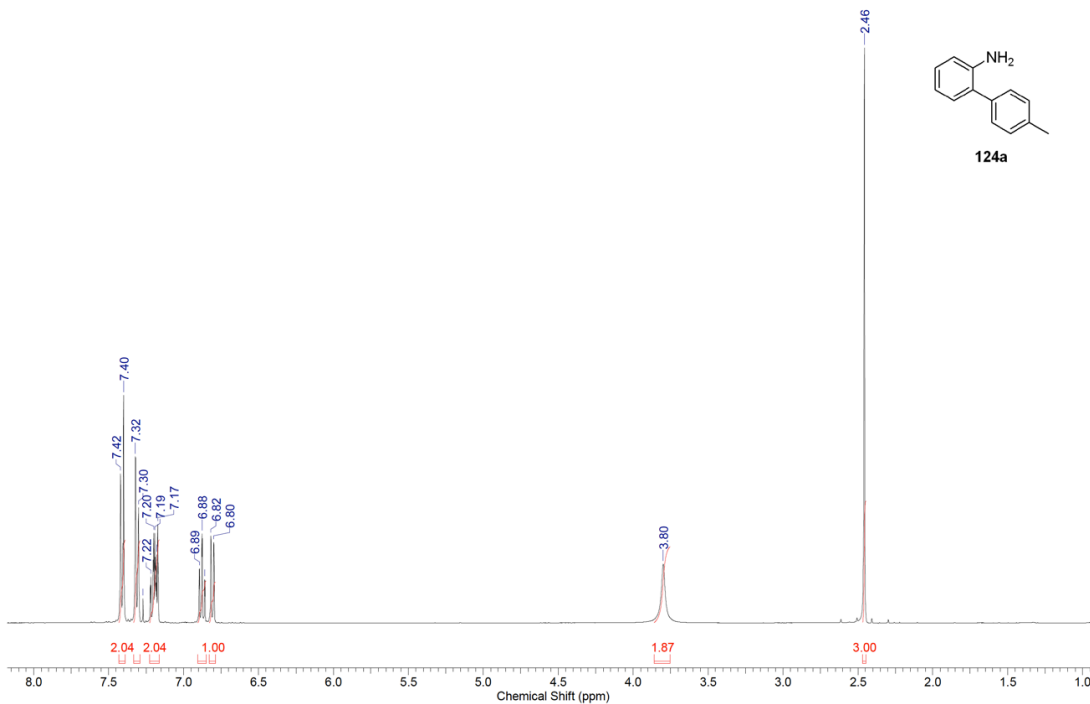


Figure B.1: ¹H and ¹³C NMR of 121j

| | | | | | | | |
|------------------------|--|----------------------|------------|------------------------|--------------|--------------|------------|
| Acquisition Time (sec) | 2.0487 | Comment | Std proton | Date | Feb 1 2011 | Date Stamp | Feb 1 2011 |
| File Name | C:\DOCUMENTS AND SETTINGS\VGZ\DESKTOP\2AMINO\HG7X-2PTOSYLANILINE-H | | | Frequency (MHz) | 399.73 | Points Count | 16384 |
| Nucleus | ¹ H | Number of Transients | 16 | Original Points Count | 13102 | Points Count | 16384 |
| Pulse Sequence | s2pul | Receiver Gain | 30.00 | Solvent | CHLOROFORM-d | | |
| Spectrum Offset (Hz) | 2415.1592 | Sweep Width (Hz) | 6395.40 | Temperature (degree C) | 25.000 | | |



| | | | | | | | |
|------------------------|--|----------------------|------------|------------------------|--------------|--------------|------------|
| Acquisition Time (sec) | 1.3005 | Comment | Std proton | Date | Feb 1 2011 | Date Stamp | Feb 1 2011 |
| File Name | C:\DOCUMENTS AND SETTINGS\VGZ\DESKTOP\2AMINO\HG7X-2PTOSYLANILINE-C13 | | | Frequency (MHz) | 100.52 | Points Count | 32788 |
| Nucleus | ¹³ C | Number of Transients | 4500 | Original Points Count | 31375 | Points Count | 32788 |
| Pulse Sequence | s2pul | Receiver Gain | 30.00 | Solvent | CHLOROFORM-d | | |
| Spectrum Offset (Hz) | 10544.5859 | Sweep Width (Hz) | 24125.45 | Temperature (degree C) | 25.000 | | |

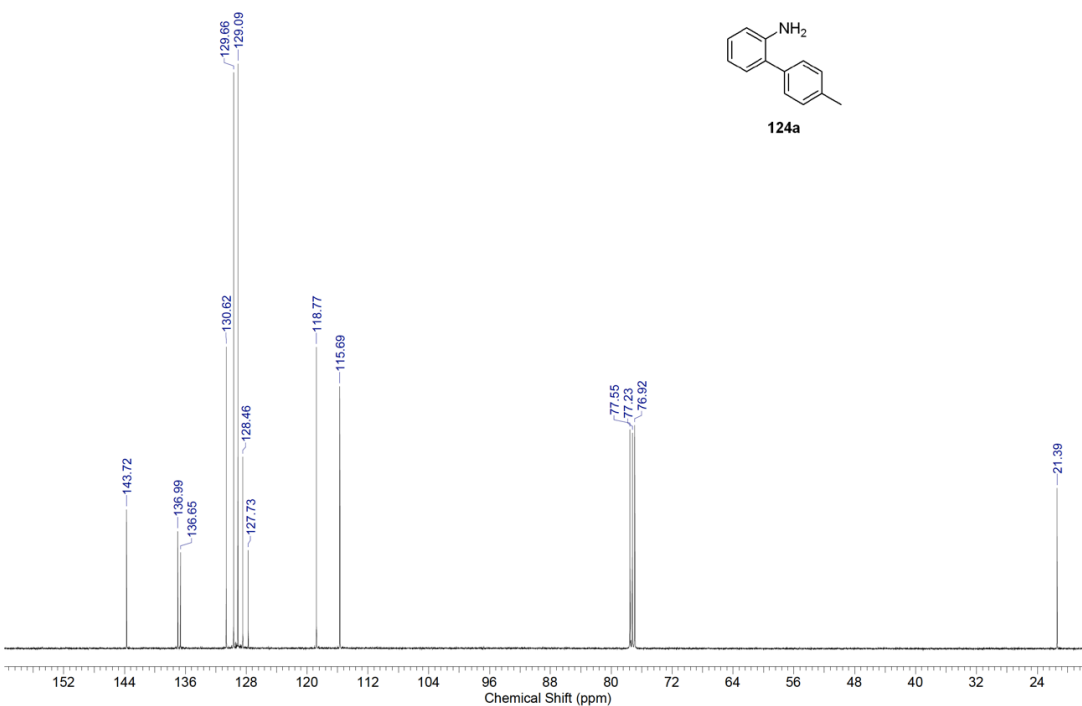
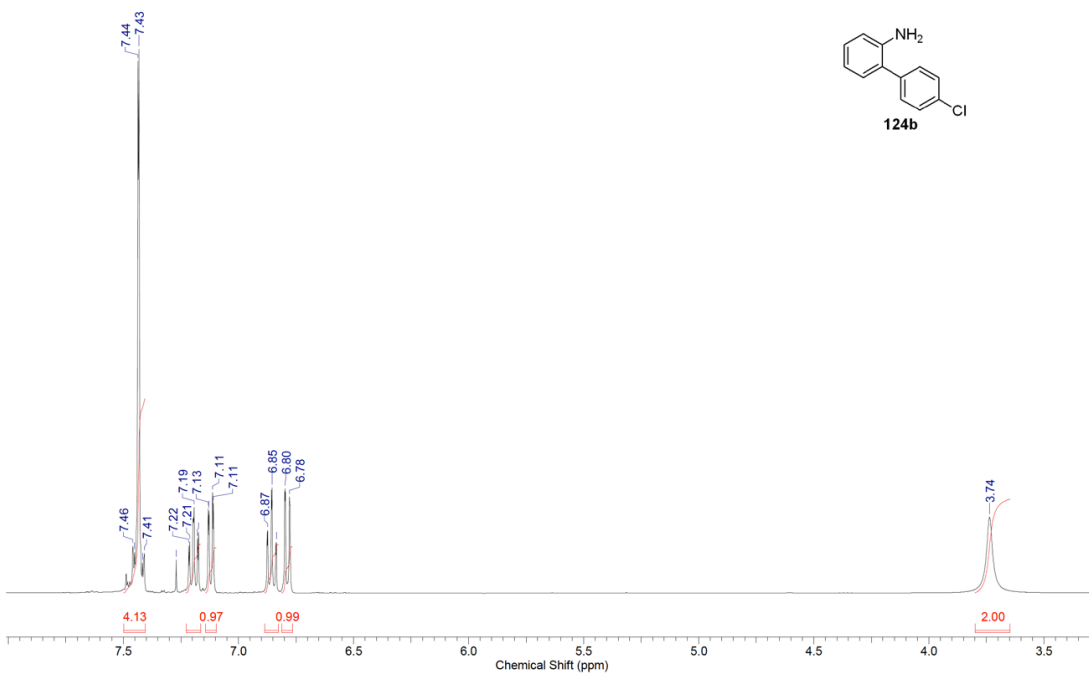


Figure B.2: ¹H and ¹³C NMR of 124a

| | | | | | | | |
|------------------------|-----------------------|------------------|------------|------------------------|-------------|---------------|----------------|
| Acquisition Time (sec) | 2.0487 | Comment | Std proton | Date | Apr 17 2011 | Date Stamp | Apr 17 2011 |
| File Name | F:\2AMINO\HG805-H-STD | Points Count | 16384 | Frequency (MHz) | 399.73 | Nucleus | ¹ H |
| Original Points Count | 13102 | Points Count | 16384 | Pulse Sequence | s2pul | Receiver Gain | 30.00 |
| Spectrum Offset (Hz) | 2414.5737 | Sweep Width (Hz) | 6395.40 | Temperature (degree C) | 25.000 | Solvent | CHLOROFORM-d |

HG805-H-STD.esp



| | | | | | | | |
|------------------------|---------------------|----------------------|------------|------------------------|-------------|------------------|-----------------|
| Acquisition Time (sec) | 1.3005 | Comment | Std proton | Date | Apr 17 2011 | Date Stamp | Apr 17 2011 |
| File Name | F:\2AMINO\HG805-C13 | Points Count | 32768 | Frequency (MHz) | 100.52 | Nucleus | ¹³ C |
| Original Points Count | 31375 | Points Count | 32768 | Pulse Sequence | s2pul | Receiver Gain | 30.00 |
| Solvent | CHLOROFORM-d | Spectrum Offset (Hz) | 10549.7402 | Temperature (degree C) | 25.000 | Sweep Width (Hz) | 24125.45 |

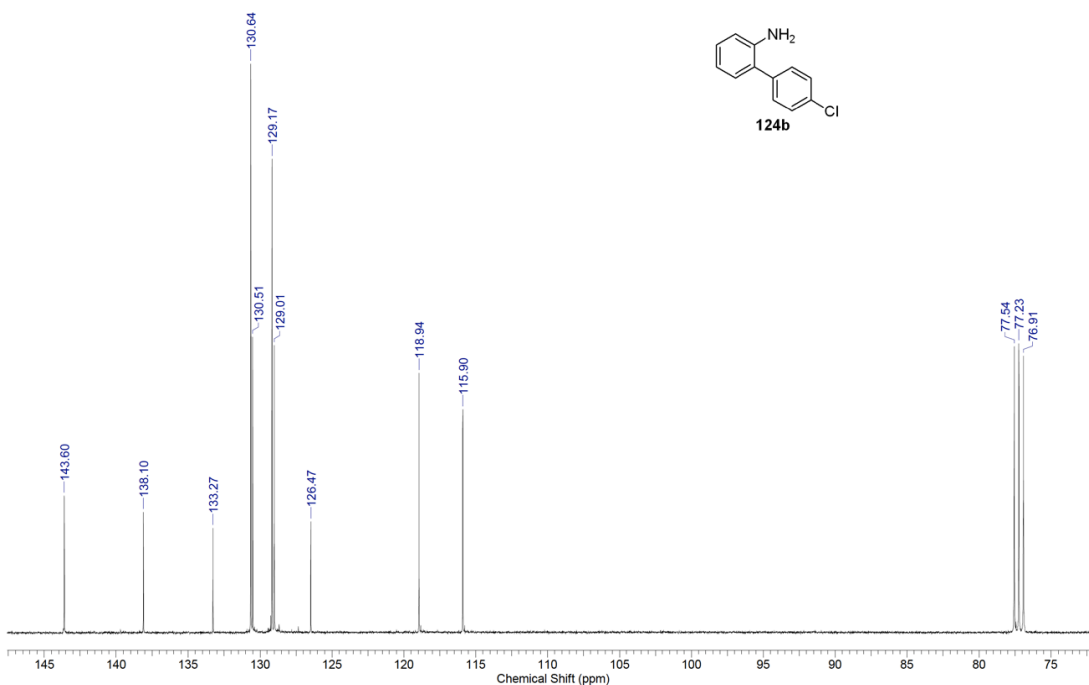
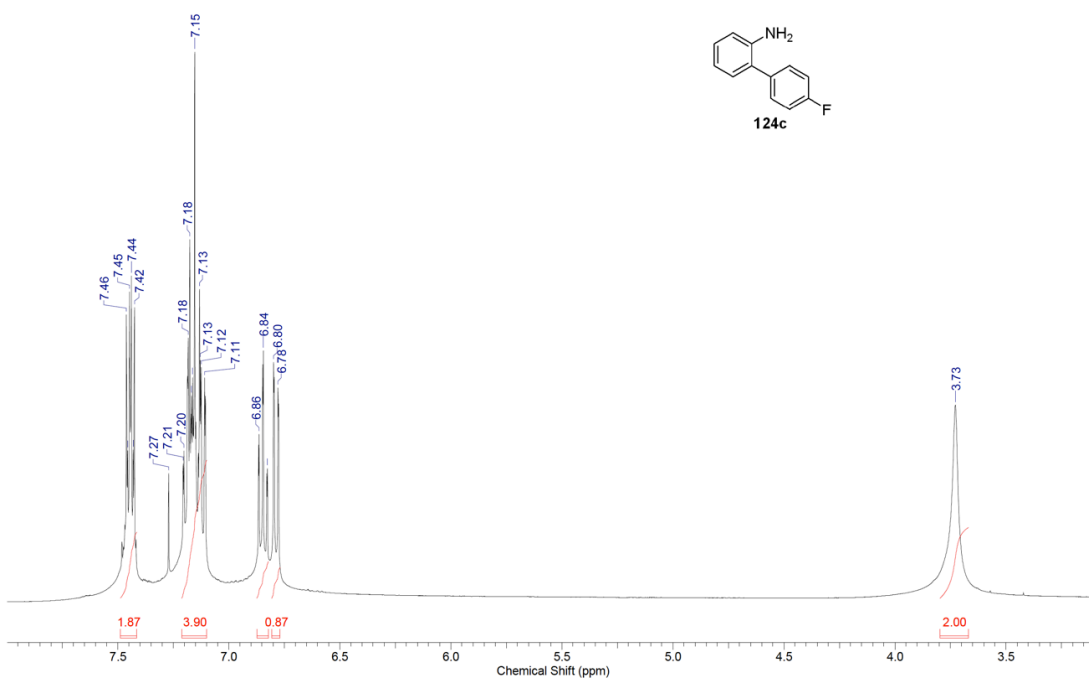


Figure B.3: ¹H and ¹³C NMR of 124b

| | | | | | | | |
|------------------------|----------------------|------------------|------------|------------------------|-------------|---------------|--------------|
| Acquisition Time (sec) | 2.0487 | Comment | Std proton | Date | May 31 2011 | Date Stamp | May 31 2011 |
| File Name | F:\2AMINO\HG852H-STD | Points Count | 16384 | Frequency (MHz) | 399.73 | Nucleus | 1H |
| Original Points Count | 13102 | Points Count | 16384 | Pulse Sequence | s2pul | Receiver Gain | 36.00 |
| Spectrum Offset (Hz) | 2414.5737 | Sweep Width (Hz) | 6395.40 | Temperature (degree C) | 25.000 | Solvent | CHLOROFORM-d |



| | | | | | | | |
|------------------------|------------------------|----------------------|------------|------------------------|-------------|------------------|-------------|
| Acquisition Time (sec) | 1.3005 | Comment | Std proton | Date | May 31 2011 | Date Stamp | May 31 2011 |
| File Name | F:\2AMINO\HG852-C13STD | Points Count | 32768 | Frequency (MHz) | 100.52 | Nucleus | 13C |
| Original Points Count | 31375 | Points Count | 32768 | Pulse Sequence | s2pul | Receiver Gain | 30.00 |
| Solvent | CHLOROFORM-d | Spectrum Offset (Hz) | 10551.9482 | Temperature (degree C) | 25.000 | Sweep Width (Hz) | 24125.45 |

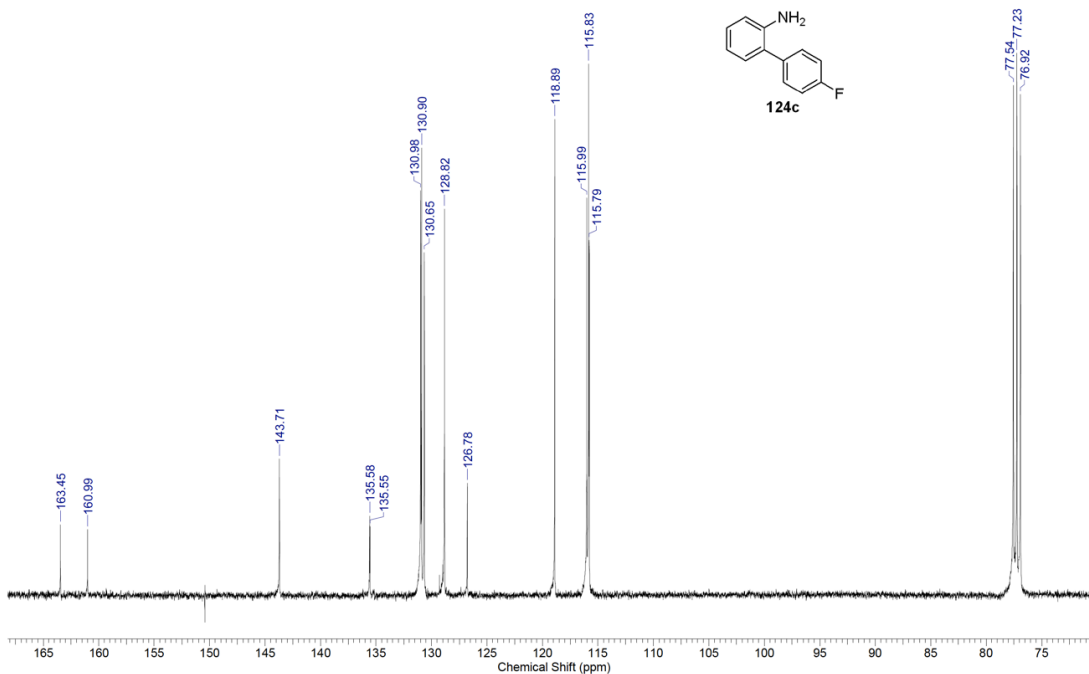
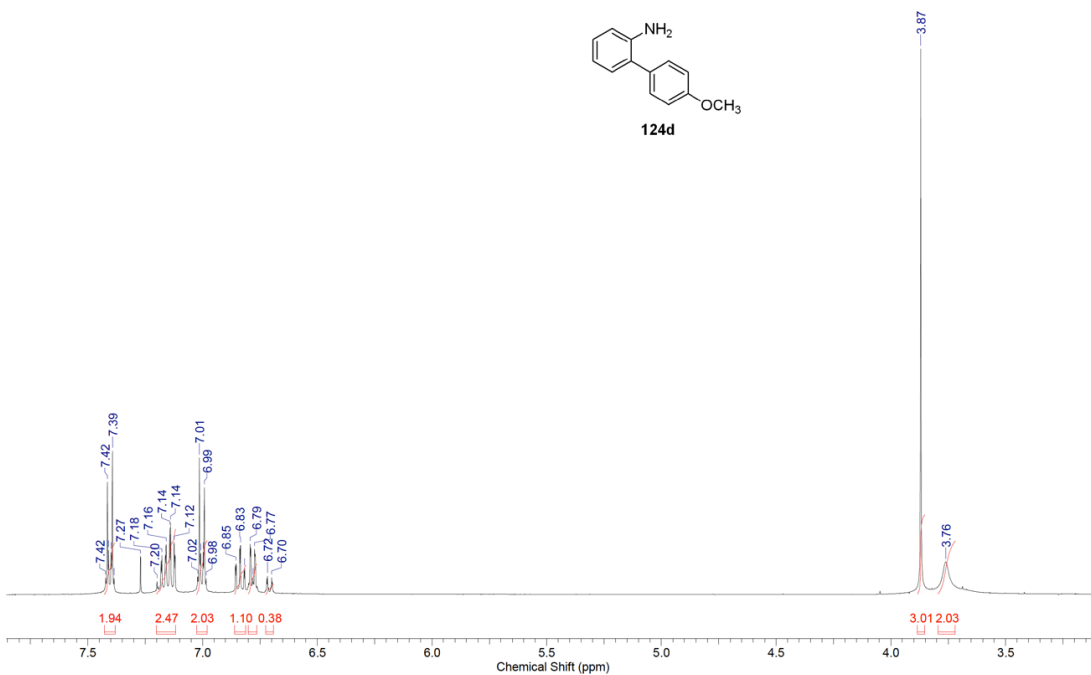
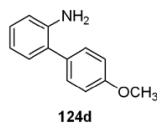


Figure B.4: ¹H and ¹³C NMR of 124c

| | | | | | | | |
|------------------------|----------------------|------------------|------------|------------------------|-------------|---------------|--------------|
| Acquisition Time (sec) | 2.0487 | Comment | Std proton | Date | May 23 2011 | Date Stamp | May 23 2011 |
| File Name | F:\2AMINO\HG848H-STD | | | Frequency (MHz) | 399.73 | Nucleus | 1H |
| Original Points Count | 13102 | Points Count | 16384 | Pulse Sequence | s2pul | Receiver Gain | 34.00 |
| Spectrum Offset (Hz) | 2415.9399 | Sweep Width (Hz) | 6395.40 | Temperature (degree C) | 25.000 | Solvent | CHLOROFORM-d |



| | | | | | | | |
|------------------------|-------------------------|--------------|------------|----------------------|-------------|------------------|-------------|
| Acquisition Time (sec) | 1.3005 | Comment | Std proton | Date | May 23 2011 | Date Stamp | May 23 2011 |
| File Name | F:\2AMINO\HG848-C13-STD | | | Frequency (MHz) | 100.52 | Nucleus | 13C |
| Original Points Count | 31375 | Points Count | 32768 | Pulse Sequence | s2pul | Receiver Gain | 30.00 |
| Solvent | CHLOROFORM-d | | | Spectrum Offset (Hz) | 10550.4766 | Sweep Width (Hz) | 24125.45 |
| Temperature (degree C) | 25.000 | | | | | | |

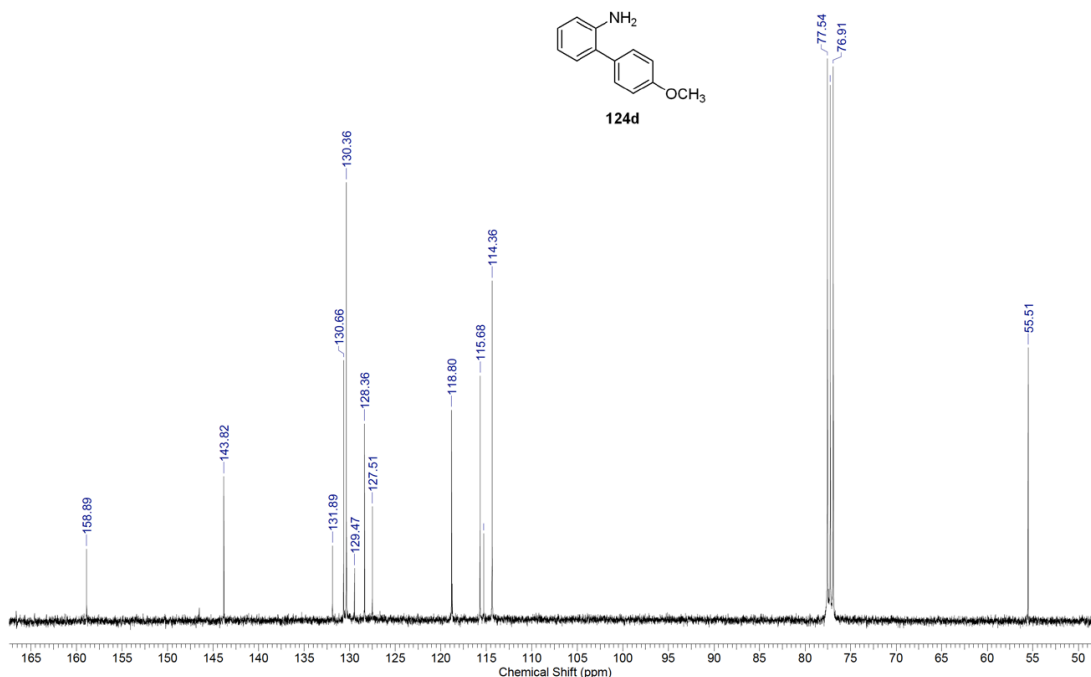
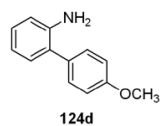
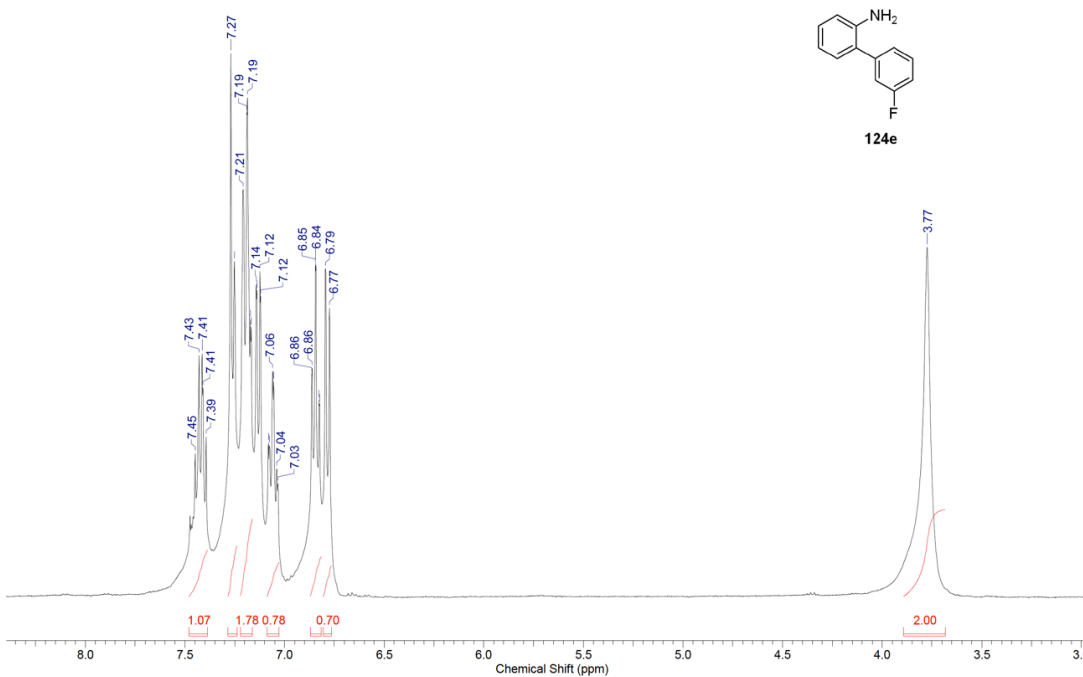


Figure B.5: ^1H and ^{13}C NMR of **124d**

| | | | | | | | |
|------------------------|---|----------------------|------------|------------------------|--------------|--------------|-------------|
| Acquisition Time (sec) | 2.0487 | Comment | Std proton | Date | Aug 25 2011 | Date Stamp | Aug 25 2011 |
| File Name | \PSFEXCHANGEID-PN012-AMINO BIPHENYLHG933H-STD.FID\FID | | | Frequency (MHz) | 399.73 | Points Count | 16384 |
| Nucleus | ¹ H | Number of Transients | 16 | Original Points Count | 13102 | Points Count | 16384 |
| Pulse Sequence | s2pul | Receiver Gain | 48.00 | Solvent | CHLOROFORM-d | | |
| Spectrum Offset (Hz) | 2414.3657 | Sweep Width (Hz) | 6395.40 | Temperature (degree C) | 25.000 | | |



| | | | | | | | |
|------------------------|---|----------------------|------------|------------------------|--------------|--------------|-------------|
| Acquisition Time (sec) | 1.3005 | Comment | Std proton | Date | Aug 25 2011 | Date Stamp | Aug 25 2011 |
| File Name | \PSFEXCHANGEID-NMR\NMR 03102011\HG933-C13.FID\FID | | | Frequency (MHz) | 100.52 | Points Count | 32768 |
| Nucleus | ¹³ C | Number of Transients | 7339 | Original Points Count | 31375 | Points Count | 32768 |
| Pulse Sequence | s2pul | Receiver Gain | 30.00 | Solvent | CHLOROFORM-d | | |
| Spectrum Offset (Hz) | 10554.1572 | Sweep Width (Hz) | 24125.45 | Temperature (degree C) | 25.000 | | |

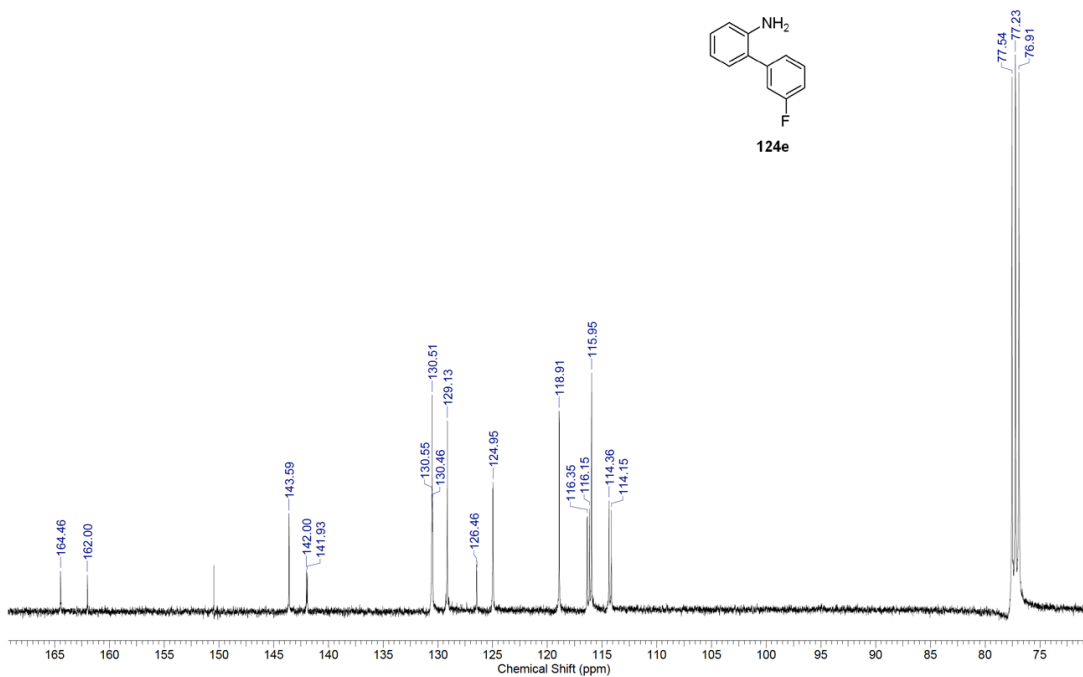
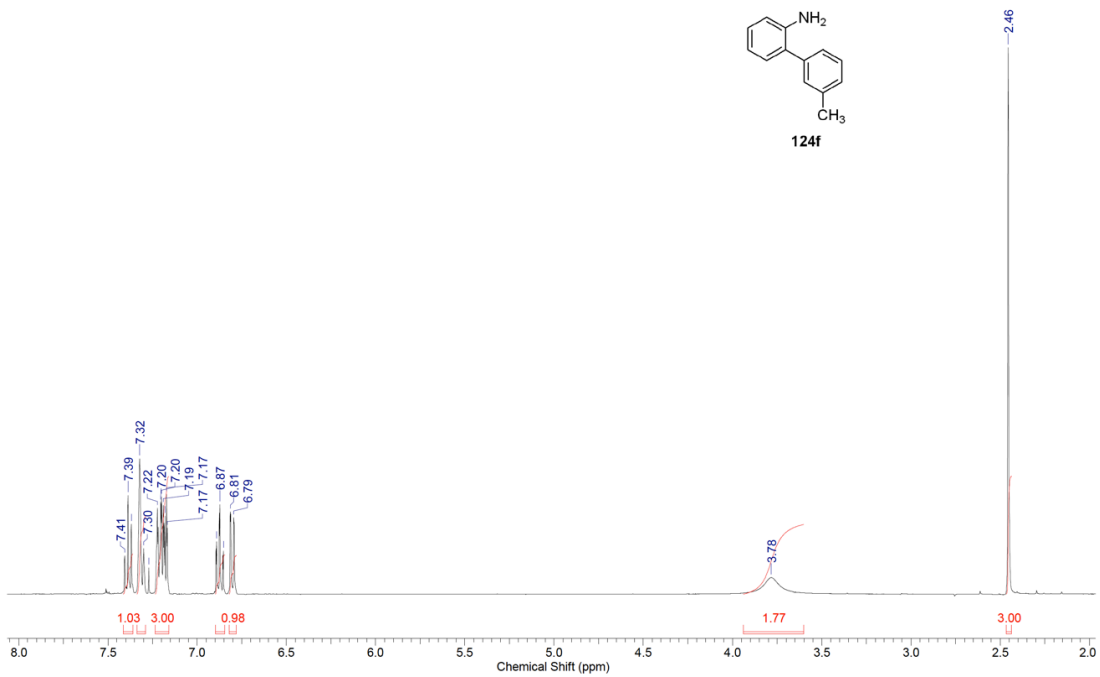


Figure B.6: ¹H and ¹³C NMR of 124e

| | | | | | | | |
|------------------------|---------------------|------------------|------------|------------------------|-------------|---------------|----------------|
| Acquisition Time (sec) | 2.0487 | Comment | Std proton | Date | Aug 21 2011 | Date Stamp | Aug 21 2011 |
| File Name | F:\2AMINO\HG927H-GD | | | Frequency (MHz) | 399.73 | Nucleus | ¹ H |
| Original Points Count | 13102 | Points Count | 16384 | Pulse Sequence | s2pul | Receiver Gain | 42.00 |
| Spectrum Offset (Hz) | 2414.5737 | Sweep Width (Hz) | 6395.40 | Temperature (degree C) | 25.000 | Solvent | CHLOROFORM-d |



| | | | | | | | |
|------------------------|-----------------------|--------------|------------|----------------------|-------------|------------------|-----------------|
| Acquisition Time (sec) | 1.3005 | Comment | Std proton | Date | Aug 21 2011 | Date Stamp | Aug 21 2011 |
| File Name | F:\2AMINO\HG927C13-GD | | | Frequency (MHz) | 100.52 | Nucleus | ¹³ C |
| Original Points Count | 31375 | Points Count | 32768 | Pulse Sequence | s2pul | Receiver Gain | 30.00 |
| Solvent | CHLOROFORM-d | | | Spectrum Offset (Hz) | 10546.0576 | Sweep Width (Hz) | 24125.45 |
| Temperature (degree C) | 25.000 | | | | | | |

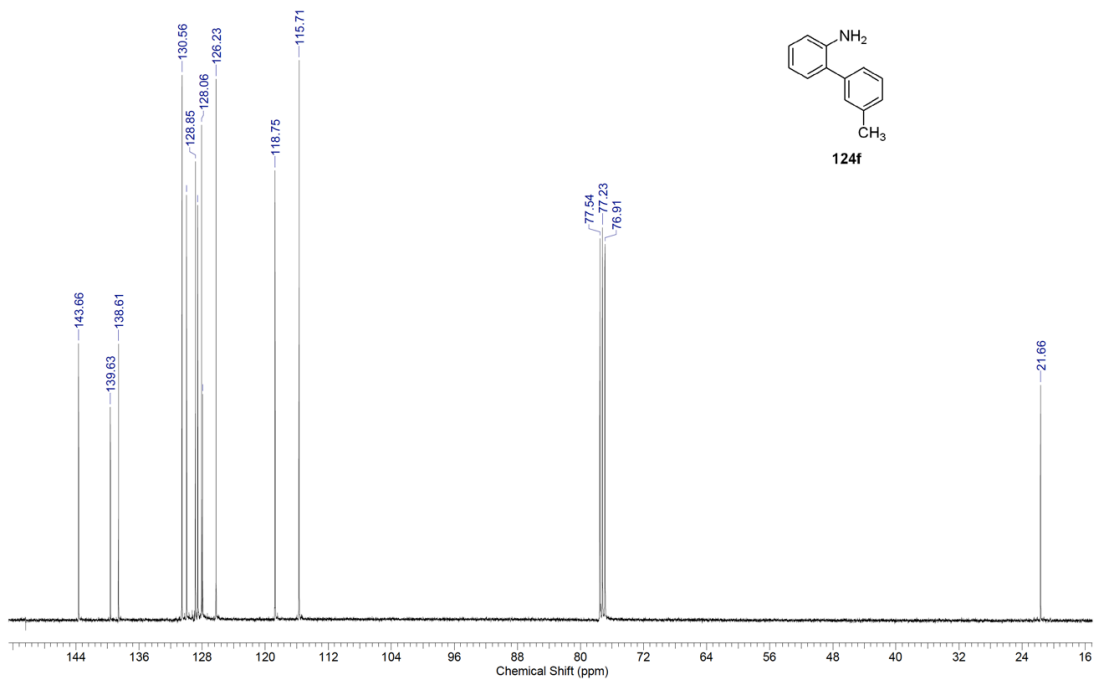
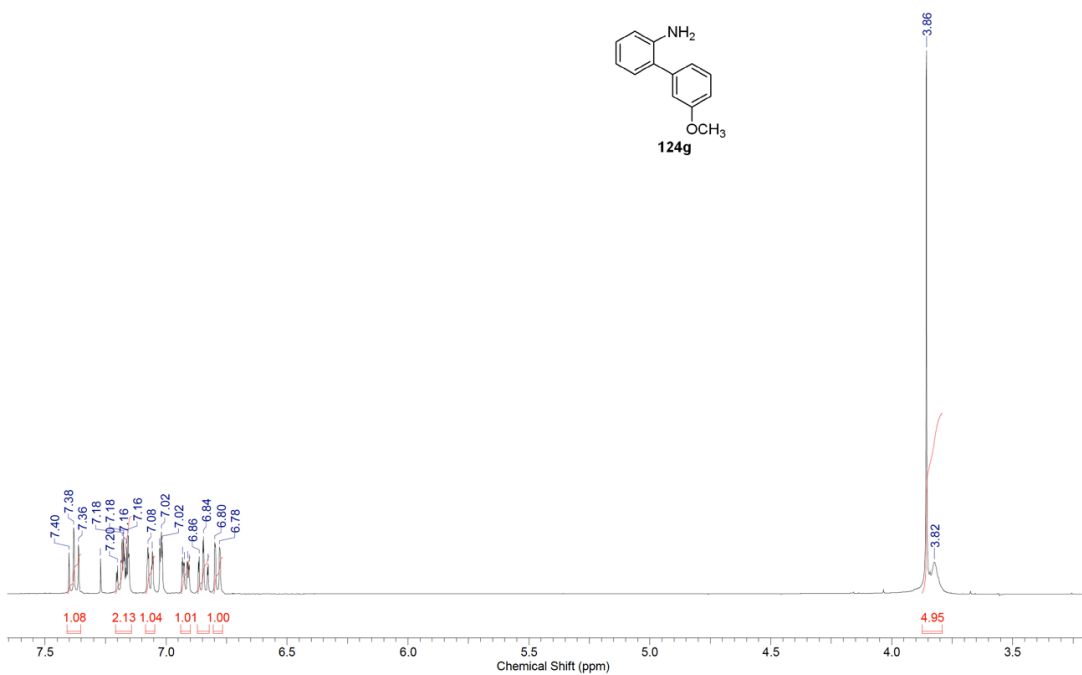
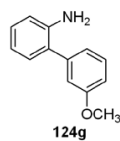


Figure B.7: ¹H and ¹³C NMR of 124f

| | | | | | | | |
|------------------------|--|----------------------|------------|------------------------|--------------|-----------------|-------------|
| Acquisition Time (sec) | 2.0487 | Comment | Std proton | Date | Oct 31 2010 | Date Stamp | Oct 31 2010 |
| File Name | E:\OLAJIDE-NMR DATA\2011 NMR-MARCH BACKUP\HG710-H-3-METHOXYPHENYLANILINE-STDGD | | | | | Frequency (MHz) | 399.74 |
| Nucleus | ¹ H | Number of Transients | 16 | Original Points Count | 13103 | Points Count | 16384 |
| Pulse Sequence | s2pul | Receiver Gain | 32.00 | Solvent | CHLOROFORM-d | | |
| Spectrum Offset (Hz) | 2418.8994 | Sweep Width (Hz) | 6395.91 | Temperature (degree C) | 25.000 | | |



| | | | | | | | |
|------------------------|--|----------------------|------------|------------------------|--------------|-----------------|-------------|
| Acquisition Time (sec) | 1.3005 | Comment | Std proton | Date | Oct 31 2010 | Date Stamp | Oct 31 2010 |
| File Name | E:\OLAJIDE-NMR DATA\2011 NMR-MARCH BACKUP\HG710-3-METHOXYPHENYLANILINE-C13 | | | | | Frequency (MHz) | 100.52 |
| Nucleus | ¹³ C | Number of Transients | 7000 | Original Points Count | 31375 | Points Count | 32768 |
| Pulse Sequence | s2pul | Receiver Gain | 30.00 | Solvent | CHLOROFORM-d | | |
| Spectrum Offset (Hz) | 10551.4023 | Sweep Width (Hz) | 24125.45 | Temperature (degree C) | 25.000 | | |

HG710-3-METHOXYPHENYLANILINE-C13.ESP

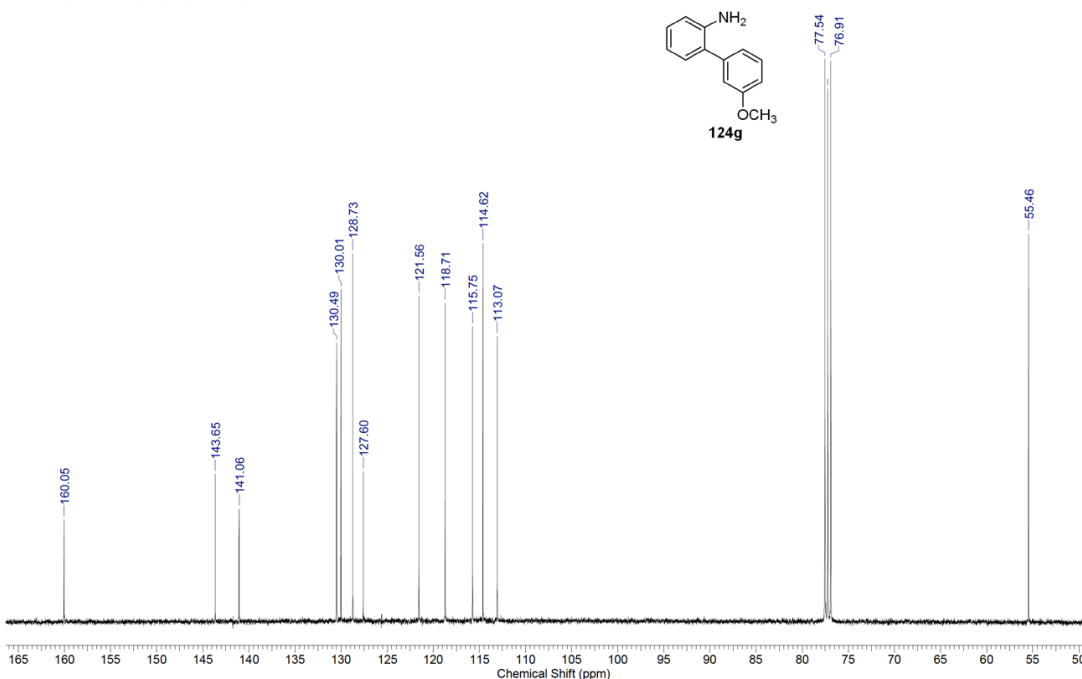
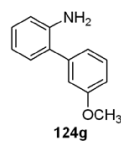
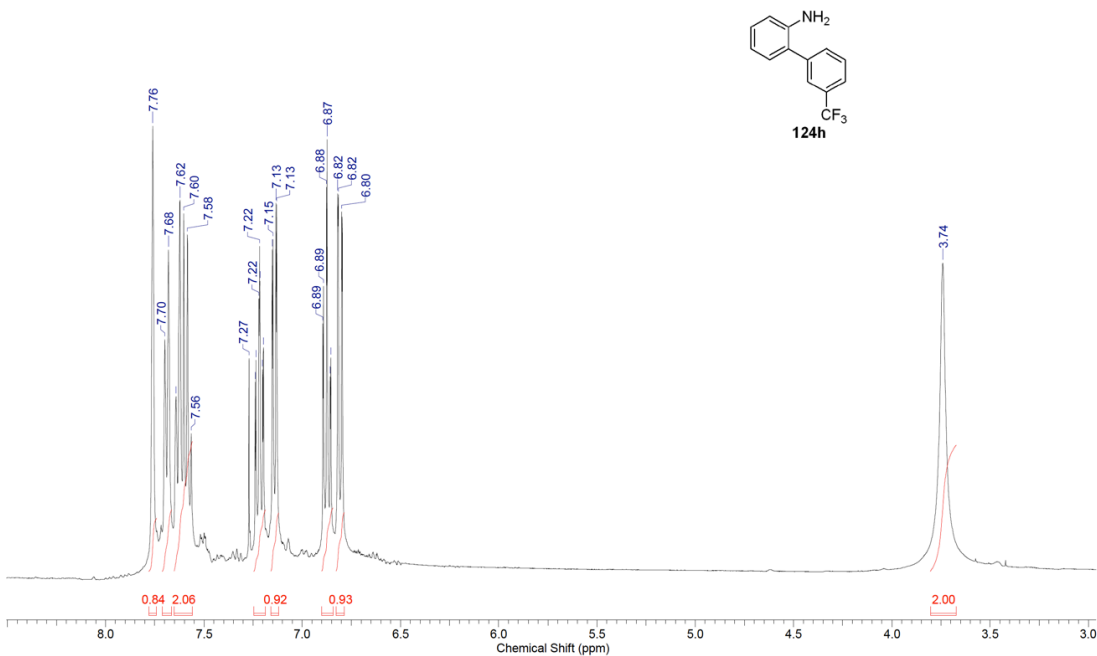


Figure B.8: ¹H and ¹³C NMR of 124g

| | | | | | | | |
|------------------------|---|----------------------|------------|------------------------|--------------|--------------|-------------|
| Acquisition Time (sec) | 2.0487 | Comment | Std proton | Date | May 20 2011 | Date Stamp | May 20 2011 |
| File Name | \PSPREXCHANGE\NMR\NMR 03102011\HG733H-STD.FID\FID | | | Frequency (MHz) | 399.73 | Points Count | 16384 |
| Nucleus | ¹ H | Number of Transients | 16 | Original Points Count | 13102 | Points Count | 16384 |
| Pulse Sequence | s2pul | Receiver Gain | 32.00 | Solvent | CHLOROFORM-d | | |
| Spectrum Offset (Hz) | 2413.4026 | Sweep Width (Hz) | 6395.40 | Temperature (degree C) | 25.000 | | |



| | | | | | | | |
|------------------------|--|----------------------|------------|------------------------|--------------|--------------|-------------|
| Acquisition Time (sec) | 1.3005 | Comment | Std proton | Date | May 18 2011 | Date Stamp | May 18 2011 |
| File Name | \PSPREXCHANGE\NMR\NMR 03102011\HG733-C13.FID\FID | | | Frequency (MHz) | 100.52 | Points Count | 32768 |
| Nucleus | ¹³ C | Number of Transients | 6264 | Original Points Count | 31375 | Points Count | 32768 |
| Pulse Sequence | s2pul | Receiver Gain | 30.00 | Solvent | CHLOROFORM-d | | |
| Spectrum Offset (Hz) | 10551.2129 | Sweep Width (Hz) | 24125.45 | Temperature (degree C) | 25.000 | | |

HG733-C13.ESP

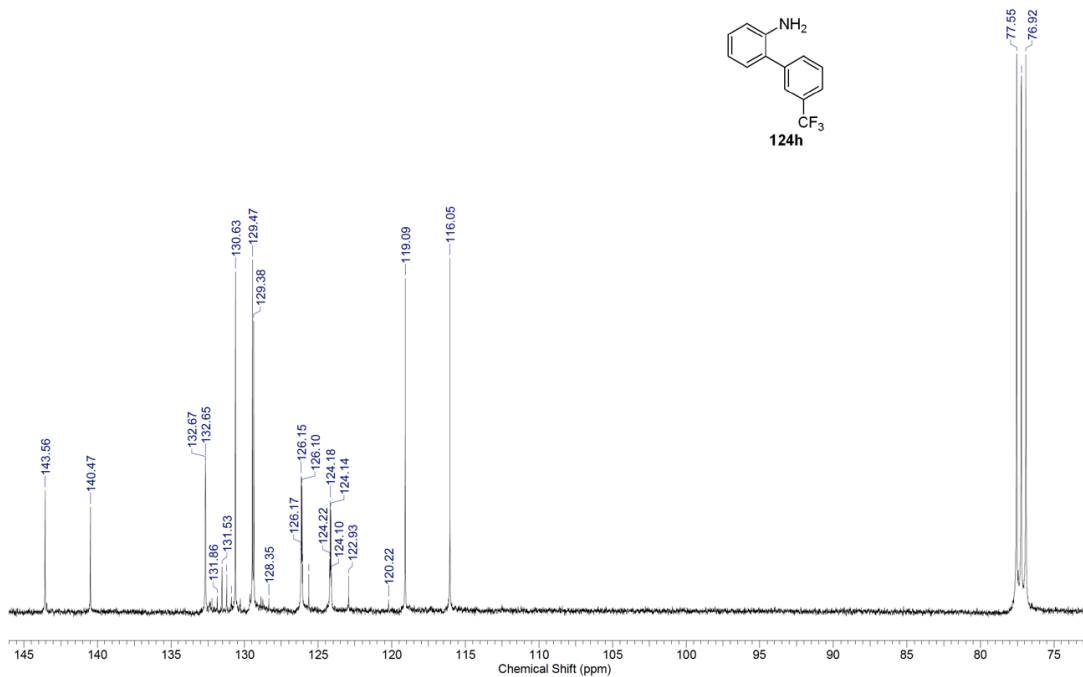
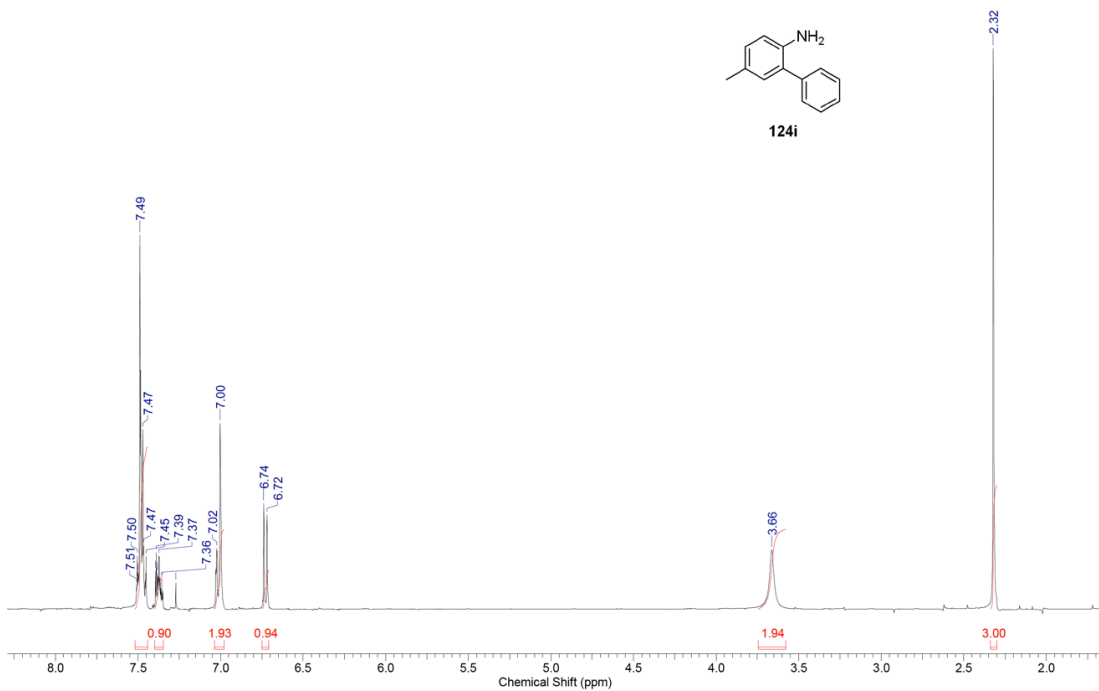


Figure B.9: ¹H and ¹³C NMR of 124h

| | | | | | | | |
|------------------------|----------------------|------------------|------------|------------------------|-------------|---------------|----------------|
| Acquisition Time (sec) | 2.0487 | Comment | Std proton | Date | Jul 18 2011 | Date Stamp | Jul 18 2011 |
| File Name | F:\2AMINO\HG883H-STD | | | Frequency (MHz) | 399.73 | Nucleus | ¹ H |
| Original Points Count | 13102 | Points Count | 16384 | Pulse Sequence | s2pul | Receiver Gain | 30.00 |
| Spectrum Offset (Hz) | 2416.3303 | Sweep Width (Hz) | 6395.40 | Temperature (degree C) | 25.000 | Solvent | CHLOROFORM-d |



| | | | | | | | |
|------------------------|------------------------|--------------|------------|----------------------|-------------|------------------|-----------------|
| Acquisition Time (sec) | 1.3005 | Comment | Std proton | Date | Jul 18 2011 | Date Stamp | Jul 18 2011 |
| File Name | F:\2AMINO\HG883C13-STD | | | Frequency (MHz) | 100.52 | Nucleus | ¹³ C |
| Original Points Count | 31375 | Points Count | 32768 | Pulse Sequence | s2pul | Receiver Gain | 30.00 |
| Solvent | CHLOROFORM-d | | | Spectrum Offset (Hz) | 10550.4766 | Sweep Width (Hz) | 24125.45 |
| Temperature (degree C) | 25.000 | | | | | | |

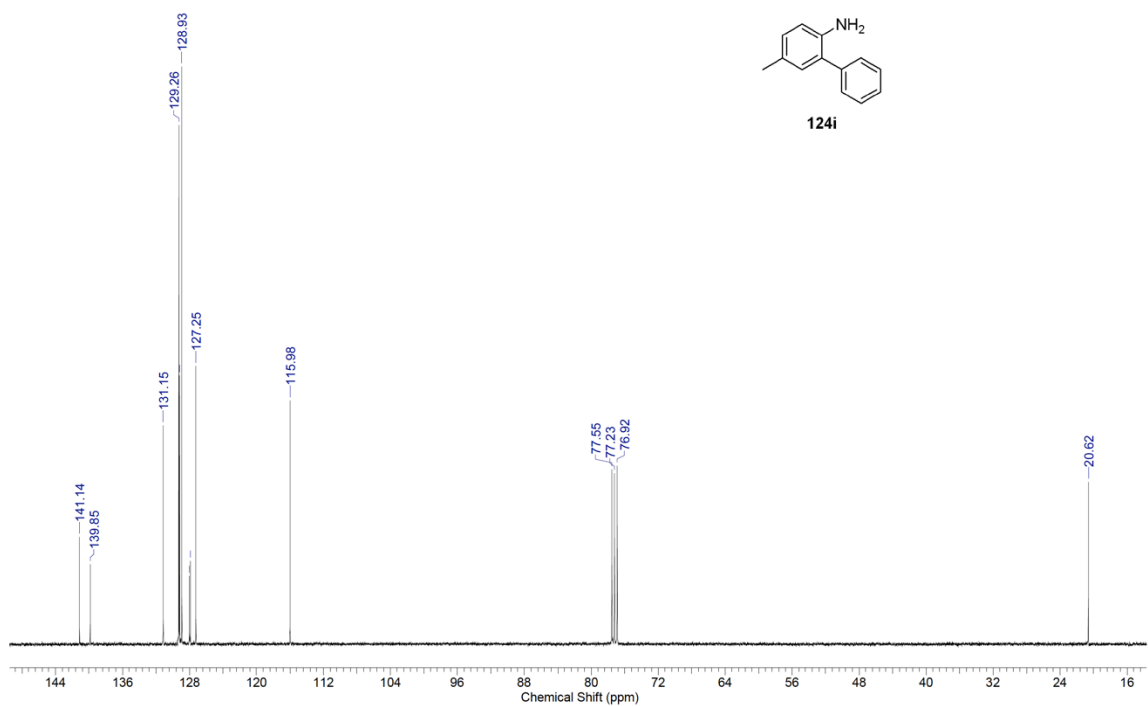
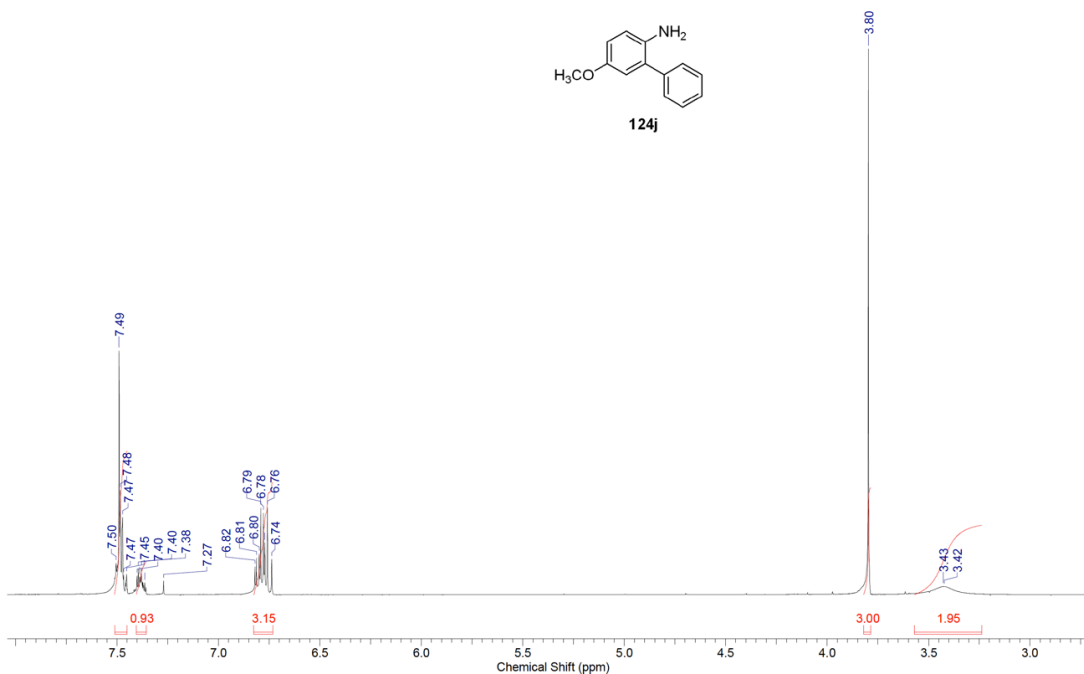


Figure B.10: ¹H and ¹³C NMR of 124i

| | | | | | | | |
|------------------------|---------------------|------------------|------------|------------------------|-------------|---------------|--------------|
| Acquisition Time (sec) | 2.0487 | Comment | Std proton | Date | Sep 26 2011 | Date Stamp | Sep 26 2011 |
| File Name | F:\2AMINO\HG936H-GD | | | Frequency (MHz) | 399.73 | Nucleus | 1H |
| Original Points Count | 13102 | Points Count | 16384 | Pulse Sequence | s2pul | Receiver Gain | 38.00 |
| Spectrum Offset (Hz) | 2416.3303 | Sweep Width (Hz) | 6395.40 | Temperature (degree C) | 25.000 | Solvent | CHLOROFORM-d |



| | | | | | | | |
|------------------------|-----------------------|--------------|------------|----------------------|-------------|------------------|-------------|
| Acquisition Time (sec) | 1.3005 | Comment | Std proton | Date | Sep 26 2011 | Date Stamp | Sep 26 2011 |
| File Name | F:\2AMINO\HG936C13-GD | | | Frequency (MHz) | 100.52 | Nucleus | 13C |
| Original Points Count | 31375 | Points Count | 32768 | Pulse Sequence | s2pul | Receiver Gain | 30.00 |
| Solvent | CHLOROFORM-d | | | Spectrum Offset (Hz) | 10548.2666 | Sweep Width (Hz) | 24125.45 |
| Temperature (degree C) | 25.000 | | | | | | |

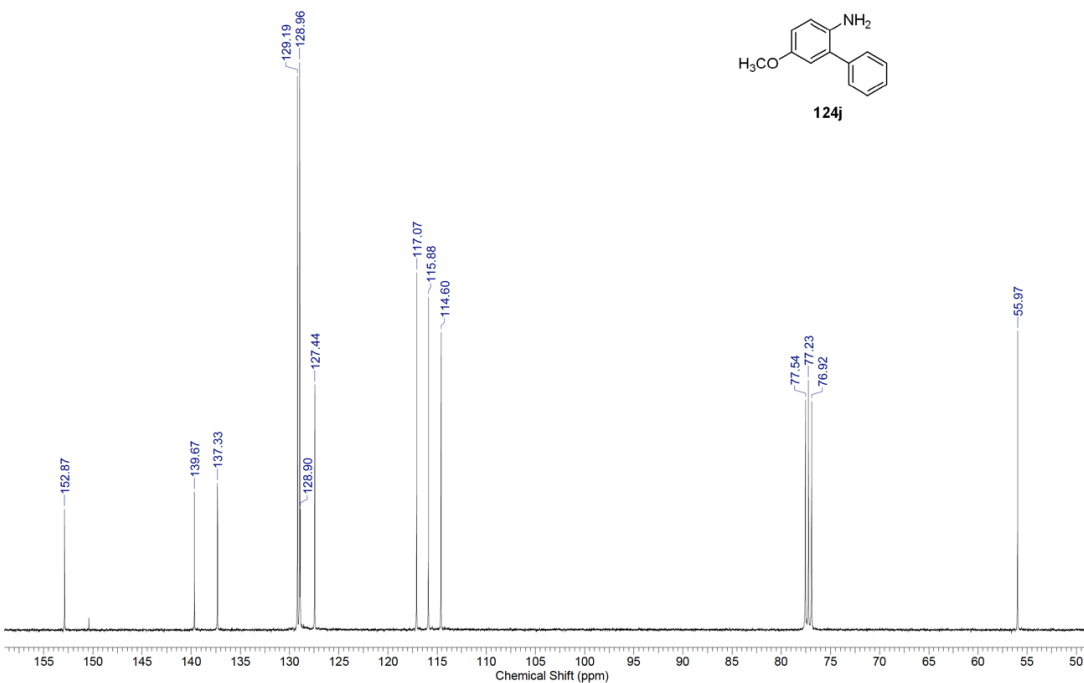
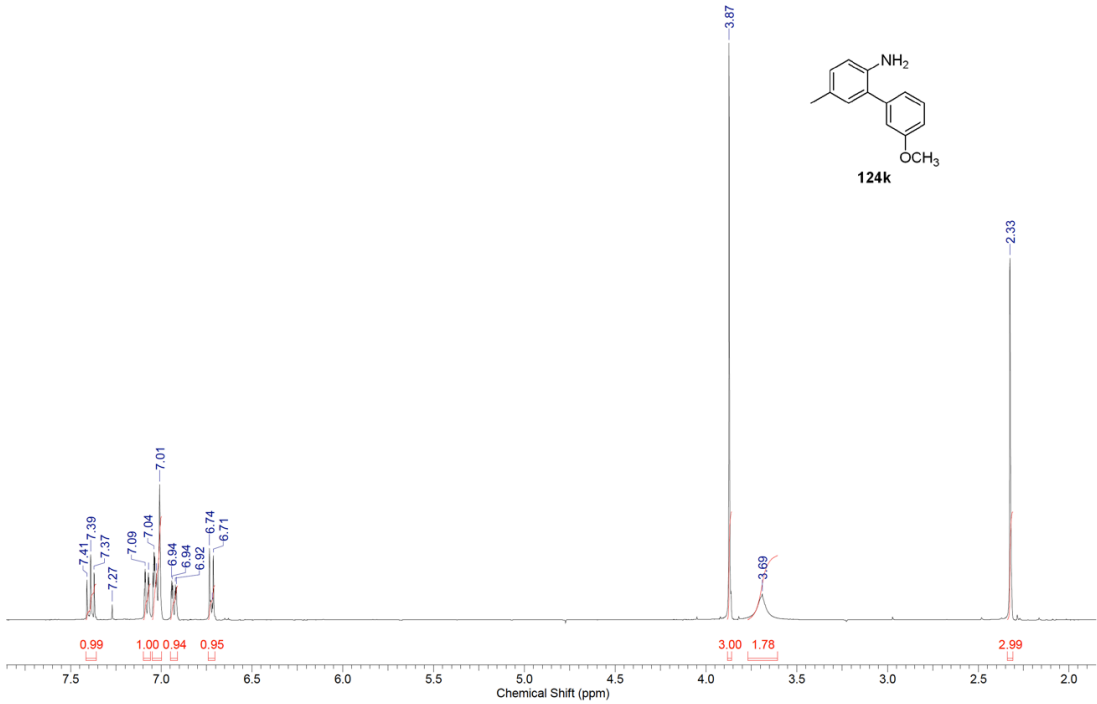


Figure B.11: ^1H and ^{13}C NMR of **124j**

| | | | | | | | |
|------------------------|----------------------|------------------|------------|------------------------|-------------|---------------|----------------|
| Acquisition Time (sec) | 2.0487 | Comment | Std proton | Date | Feb 22 2012 | Date Stamp | Feb 22 2012 |
| File Name | G:\XXNMR0222\HG937-H | | | Frequency (MHz) | 399.72 | Nucleus | ¹ H |
| Original Points Count | 13102 | Points Count | 16384 | Pulse Sequence | s2pul | Receiver Gain | 32.00 |
| Spectrum Offset (Hz) | 2407.5000 | Sweep Width (Hz) | 6395.40 | Temperature (degree C) | 25.000 | Solvent | CHLOROFORM-d |



| | | | | | | | |
|------------------------|------------------------|----------------------|------------|------------------------|-------------|------------------|-----------------|
| Acquisition Time (sec) | 1.3005 | Comment | Std proton | Date | Feb 22 2012 | Date Stamp | Feb 22 2012 |
| File Name | G:\XXNMR0222\HG937-C13 | | | Frequency (MHz) | 100.52 | Nucleus | ¹³ C |
| Original Points Count | 31375 | Points Count | 32768 | Pulse Sequence | s2pul | Receiver Gain | 30.00 |
| Solvent | CHLOROFORM-d | Spectrum Offset (Hz) | 10545.1953 | Temperature (degree C) | 25.000 | Sweep Width (Hz) | 24125.45 |

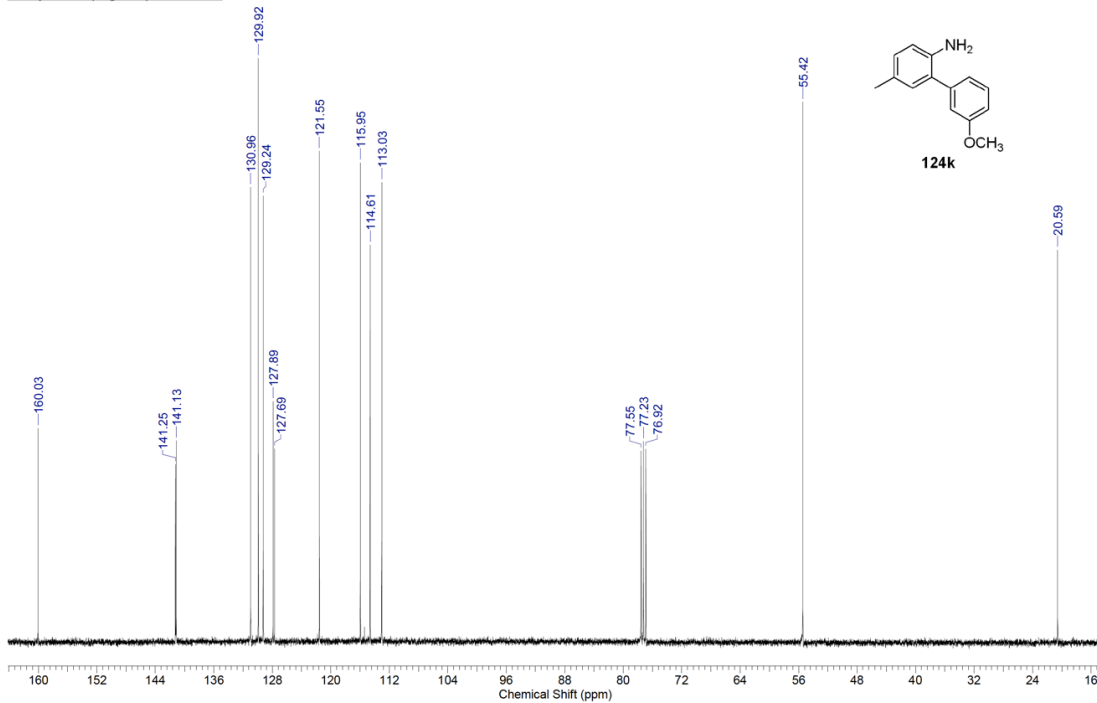
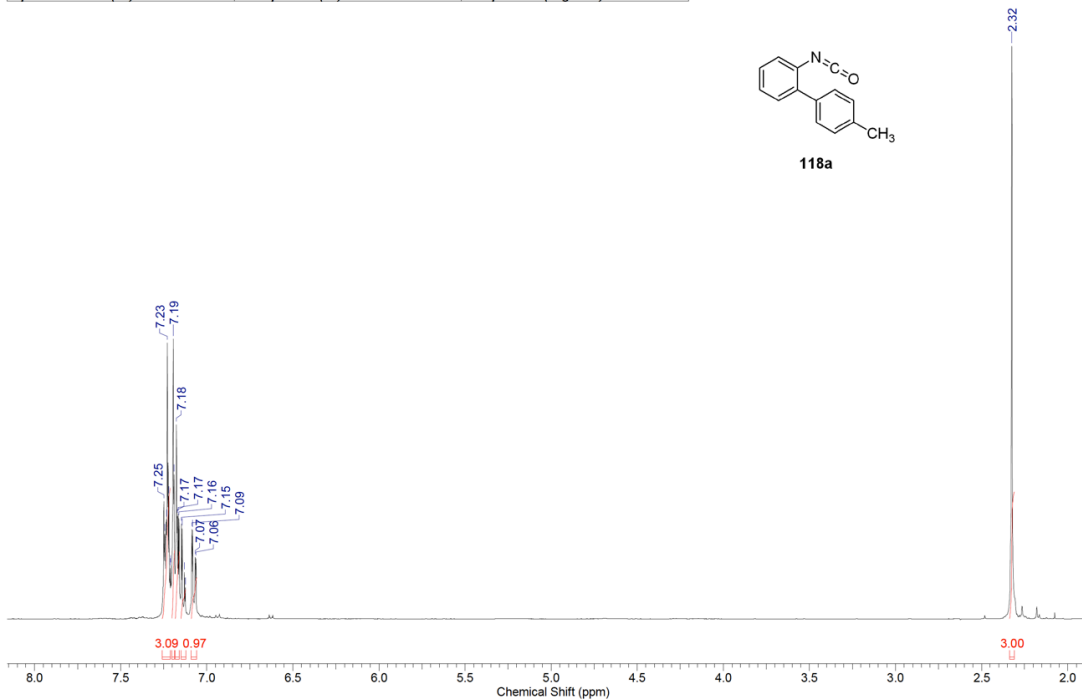


Figure B.12: ¹H and ¹³C NMR of 124k

| | | | | | | | |
|------------------------|--|----------------------|------------|------------------------|--------------|-----------------|------------|
| Acquisition Time (sec) | 2.0487 | Comment | Std proton | Date | Feb 5 2011 | Date Stamp | Feb 5 2011 |
| File Name | E:\OLAJIDE-NMR DATA\2011 NMR-MARCH BACKUP\HG790SP1-H | | | | | Frequency (MHz) | 399.73 |
| Nucleus | ¹ H | Number of Transients | 32 | Original Points Count | 13102 | Points Count | 16384 |
| Pulse Sequence | s2pul | Receiver Gain | 30.00 | Solvent | CHLOROFORM-d | | |
| Spectrum Offset (Hz) | 2358.0679 | Sweep Width (Hz) | 6395.40 | Temperature (degree C) | 25.000 | | |



| | | | | | | | |
|------------------------|--|----------------------|------------|------------------------|--------------|-----------------|------------|
| Acquisition Time (sec) | 1.3005 | Comment | Std proton | Date | Feb 5 2011 | Date Stamp | Feb 5 2011 |
| File Name | E:\OLAJIDE-NMR DATA\2011 NMR-MARCH BACKUP\HG790SP1-C13 | | | | | Frequency (MHz) | 100.52 |
| Nucleus | ¹³ C | Number of Transients | 4000 | Original Points Count | 31375 | Points Count | 32768 |
| Pulse Sequence | s2pul | Receiver Gain | 30.00 | Solvent | CHLOROFORM-d | | |
| Spectrum Offset (Hz) | 10546.7939 | Sweep Width (Hz) | 24125.45 | Temperature (degree C) | 25.000 | | |

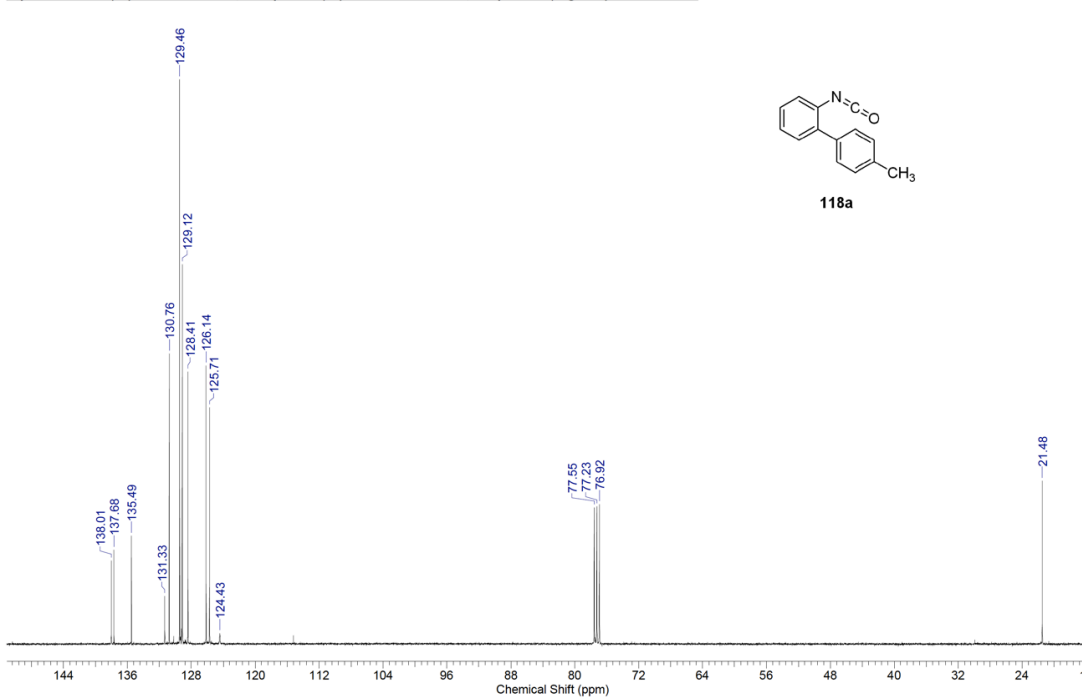
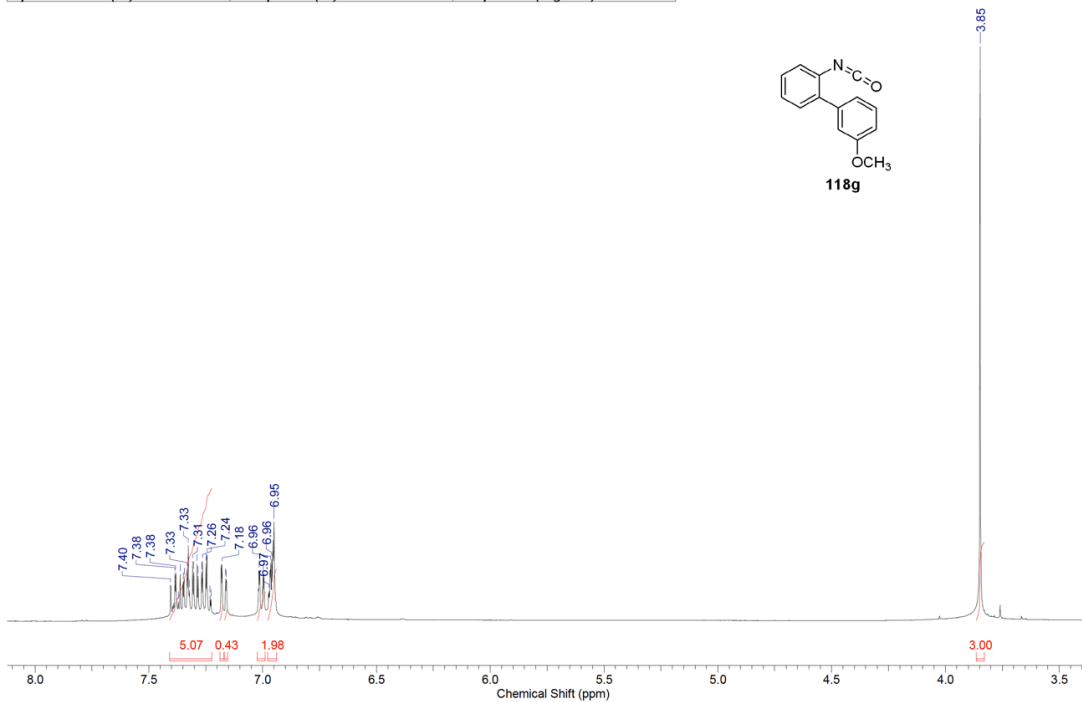


Figure B.13: ¹H and ¹³C NMR of 115a

| | | | | | | | |
|------------------------|---|----------------------|------------|------------------------|--------------|-----------------|-------------|
| Acquisition Time (sec) | 2.0487 | Comment | Std proton | Date | Jan 24 2011 | Date Stamp | Jan 24 2011 |
| File Name | E:\OLAJIDE-NMR DATA\2011NMR-MARCH\HG799CC-H | | | | | Frequency (MHz) | 399.73 |
| Nucleus | ¹ H | Number of Transients | 16 | Original Points Count | 13102 | Points Count | 16384 |
| Pulse Sequence | s2pul | Receiver Gain | 32.00 | Solvent | CHLOROFORM-d | | |
| Spectrum Offset (Hz) | 2404.4705 | Sweep Width (Hz) | 6395.40 | Temperature (degree C) | 25.000 | | |



| | | | | | | | |
|------------------------|---|----------------------|------------|------------------------|--------------|-----------------|-------------|
| Acquisition Time (sec) | 1.3005 | Comment | Std proton | Date | Jan 24 2011 | Date Stamp | Jan 24 2011 |
| File Name | E:\OLAJIDE-NMR DATA\2011NMR-MARCH\HG799CC-C13 | | | | | Frequency (MHz) | 100.52 |
| Nucleus | ¹³ C | Number of Transients | 5000 | Original Points Count | 31375 | Points Count | 32768 |
| Pulse Sequence | s2pul | Receiver Gain | 30.00 | Solvent | CHLOROFORM-d | | |
| Spectrum Offset (Hz) | 10551.2129 | Sweep Width (Hz) | 24125.45 | Temperature (degree C) | 25.000 | | |

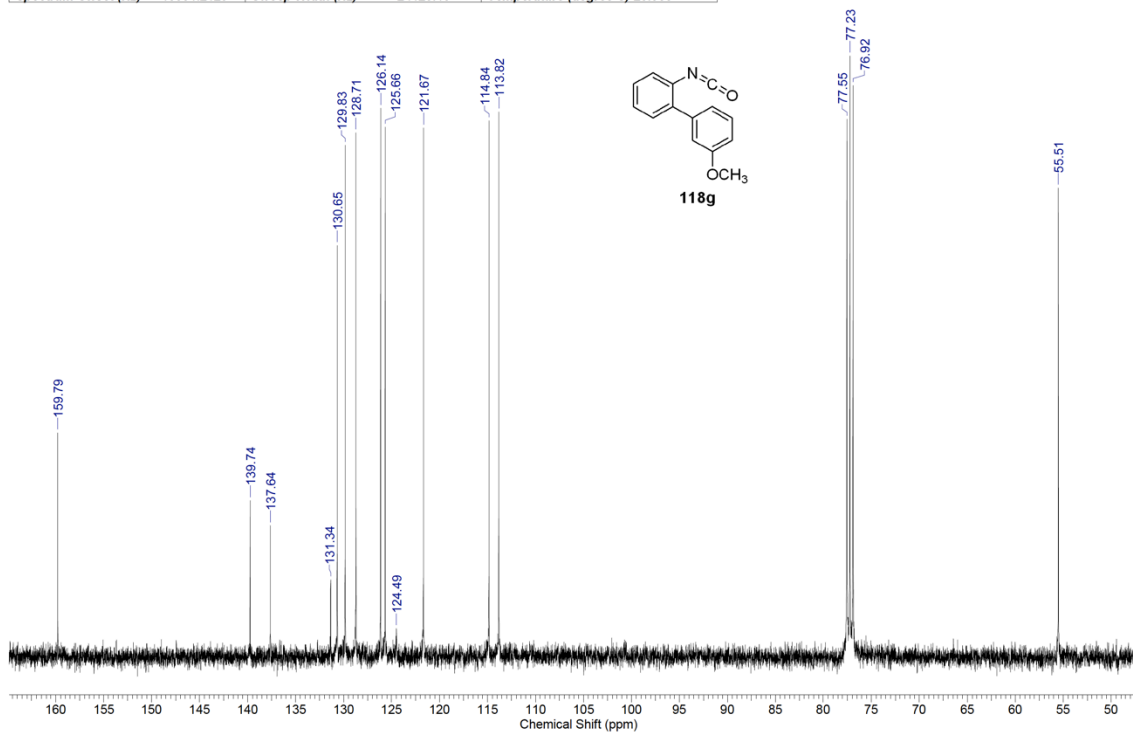
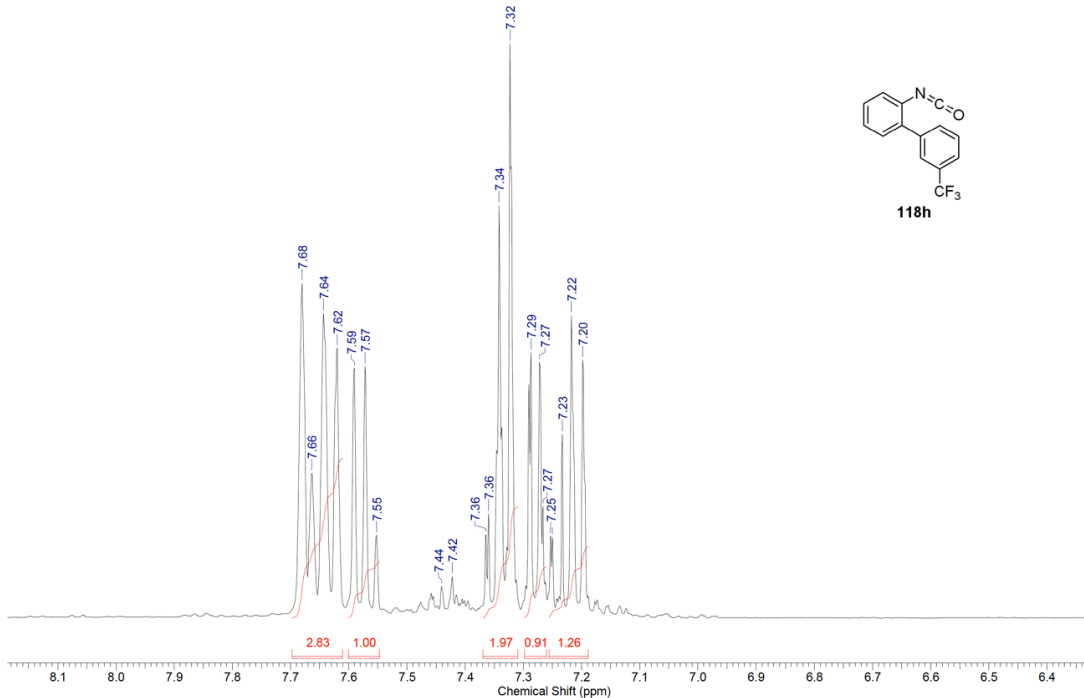


Figure B.14: ¹H and ¹³C NMR of 115g

| | | | | | | | |
|------------------------|---|----------------------|------------|------------------------|--------------|-----------------|------------|
| Acquisition Time (sec) | 2.0487 | Comment | Std proton | Date | Dec 1 2010 | Date Stamp | Dec 1 2010 |
| File Name | E:\OLAJIDE-NMR DATA\2011NMR-MARCH\2-3CF3ARYL-PHENYLISOCYANATE-H | | | | | Frequency (MHz) | 399.73 |
| Nucleus | ¹ H | Number of Transients | 8 | Original Points Count | 13102 | Points Count | 16384 |
| Pulse Sequence | s2pul | Receiver Gain | 36.00 | Solvent | CHLOROFORM-d | | |
| Spectrum Offset (Hz) | 2398.4280 | Sweep Width (Hz) | 6395.40 | Temperature (degree C) | 30.000 | | |



| | | | | | | | |
|------------------------|---|----------------------|------------|------------------------|--------------|-----------------|------------|
| Acquisition Time (sec) | 1.3005 | Comment | Std proton | Date | Dec 1 2010 | Date Stamp | Dec 1 2010 |
| File Name | E:\OLAJIDE-NMR DATA\2011NMR-MARCH\2-3CF3ARYL-PHENYLISOCYANATE-C13 | | | | | Frequency (MHz) | 100.52 |
| Nucleus | ¹³ C | Number of Transients | 7000 | Original Points Count | 31375 | Points Count | 32768 |
| Pulse Sequence | s2pul | Receiver Gain | 30.00 | Solvent | CHLOROFORM-d | | |
| Spectrum Offset (Hz) | 10551.9482 | Sweep Width (Hz) | 24125.45 | Temperature (degree C) | 30.000 | | |

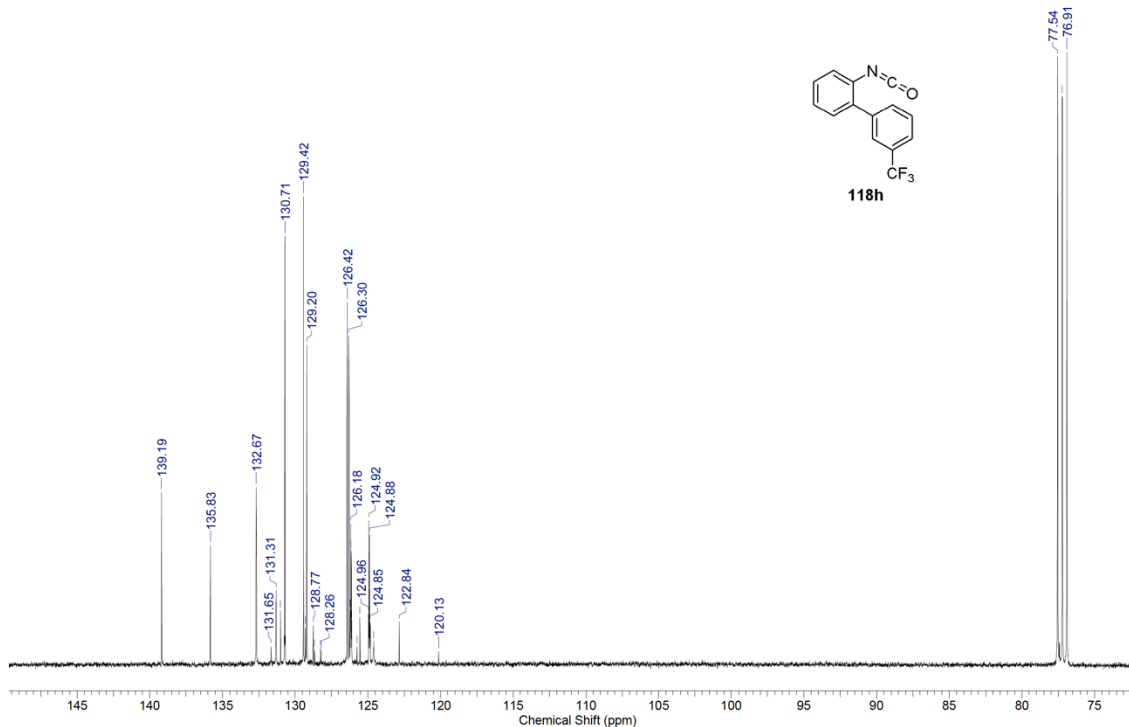
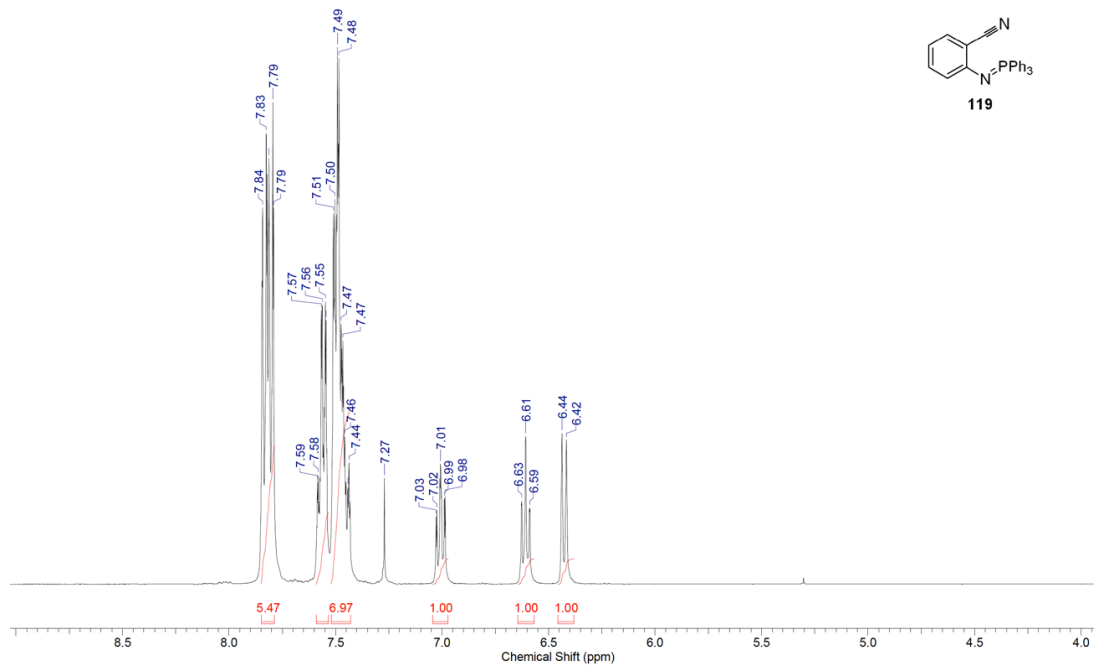


Figure B.15: ¹H and ¹³C NMR of **115h**

| Acquisition Time (sec) | 2.0487 | Comment | Std proton | Date | Dec 15 2010 | Date Stamp | Dec 15 2010 |
|------------------------|--|----------------------|------------|------------------------|--------------|-----------------|-------------|
| File Name | E:\OLAJIDE-NMR DATA\2011 NMR-MARCH BACKUP\HG692-IMINOPHOSPHORANE-RCY-H | | | | | Frequency (MHz) | 399.73 |
| Nucleus | ¹ H | Number of Transients | 16 | Original Points Count | 13102 | Points Count | 16384 |
| Pulse Sequence | s2pul | Receiver Gain | 32.00 | Solvent | CHLOROFORM-d | | |
| Spectrum Offset (Hz) | 2412.0364 | Sweep Width (Hz) | 6395.40 | Temperature (degree C) | 25.000 | | |



| Acquisition Time (sec) | 1.3005 | Comment | Std proton | Date | Dec 15 2010 | Date Stamp | Dec 15 2010 |
|------------------------|--|----------------------|------------|------------------------|--------------|-----------------|-------------|
| File Name | E:\OLAJIDE-NMR DATA\2011 NMR-MARCH BACKUP\HG692-IMINOPHOSPHORANE-RCY-C13-STD | | | | | Frequency (MHz) | 100.52 |
| Nucleus | ¹³ C | Number of Transients | 6700 | Original Points Count | 31375 | Points Count | 32768 |
| Pulse Sequence | s2pul | Receiver Gain | 30.00 | Solvent | CHLOROFORM-d | | |
| Spectrum Offset (Hz) | 10549.0029 | Sweep Width (Hz) | 24125.45 | Temperature (degree C) | 25.000 | | |

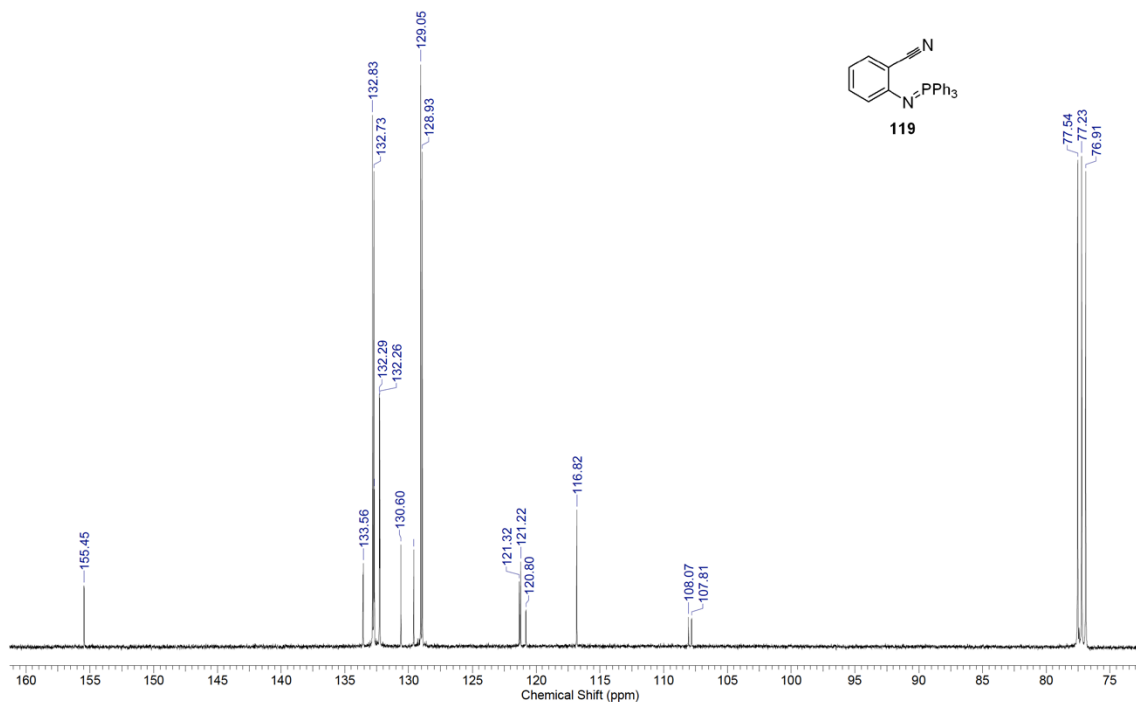
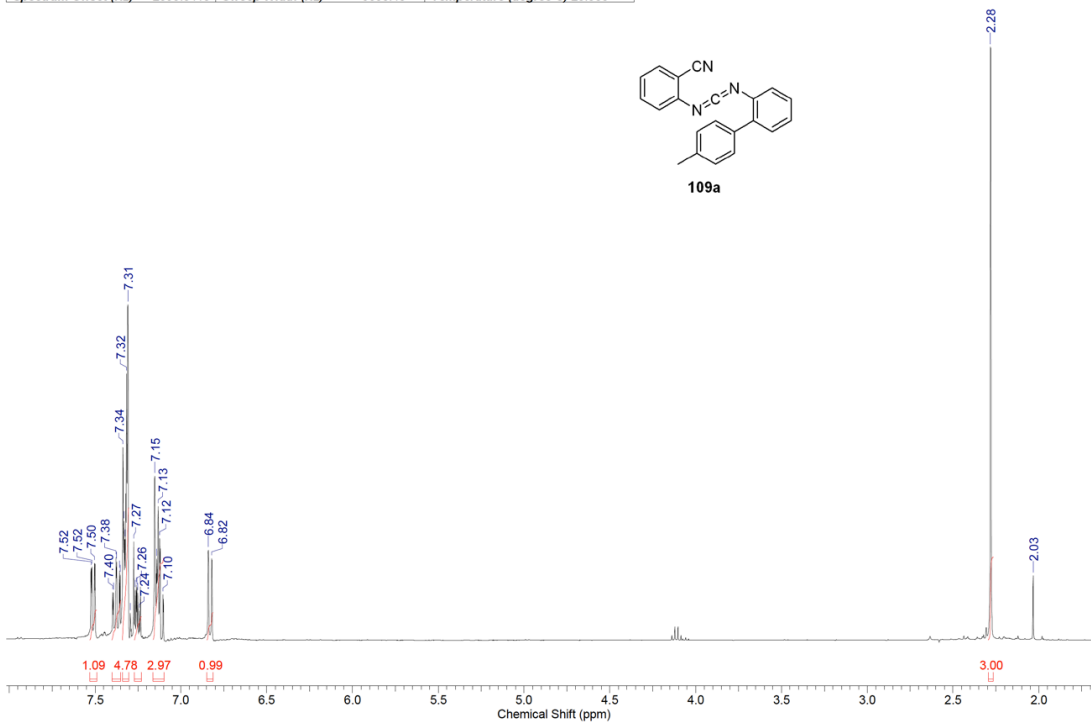


Figure B.16: ¹H and ¹³C NMR of 119

| | | | | | | | |
|------------------------|-------------------|------------------|------------|------------------------|-------------|---------------|--------------|
| Acquisition Time (sec) | 2.0487 | Comment | Std proton | Date | Dec 12 2011 | Date Stamp | Dec 12 2011 |
| File Name | F:\CD\HG884-H-STD | | | Frequency (MHz) | 399.72 | Nucleus | 1H |
| Original Points Count | 13102 | Points Count | 16384 | Pulse Sequence | s2pul | Receiver Gain | 36.00 |
| Spectrum Offset (Hz) | 2395.5410 | Sweep Width (Hz) | 6395.40 | Temperature (degree C) | 25.000 | Solvent | CHLOROFORM-d |



| | | | | | | | |
|------------------------|---------------------|--------------|------------|----------------------|-------------|------------------|-------------|
| Acquisition Time (sec) | 1.3005 | Comment | Std proton | Date | Dec 12 2011 | Date Stamp | Dec 12 2011 |
| File Name | F:\CD\HG884-C13-STD | | | Frequency (MHz) | 100.52 | Nucleus | 13C |
| Original Points Count | 31375 | Points Count | 32768 | Pulse Sequence | s2pul | Receiver Gain | 30.00 |
| Solvent | CHLOROFORM-d | | | Spectrum Offset (Hz) | 10545.1953 | Sweep Width (Hz) | 24125.45 |
| Temperature (degree C) | 25.000 | | | | | | |

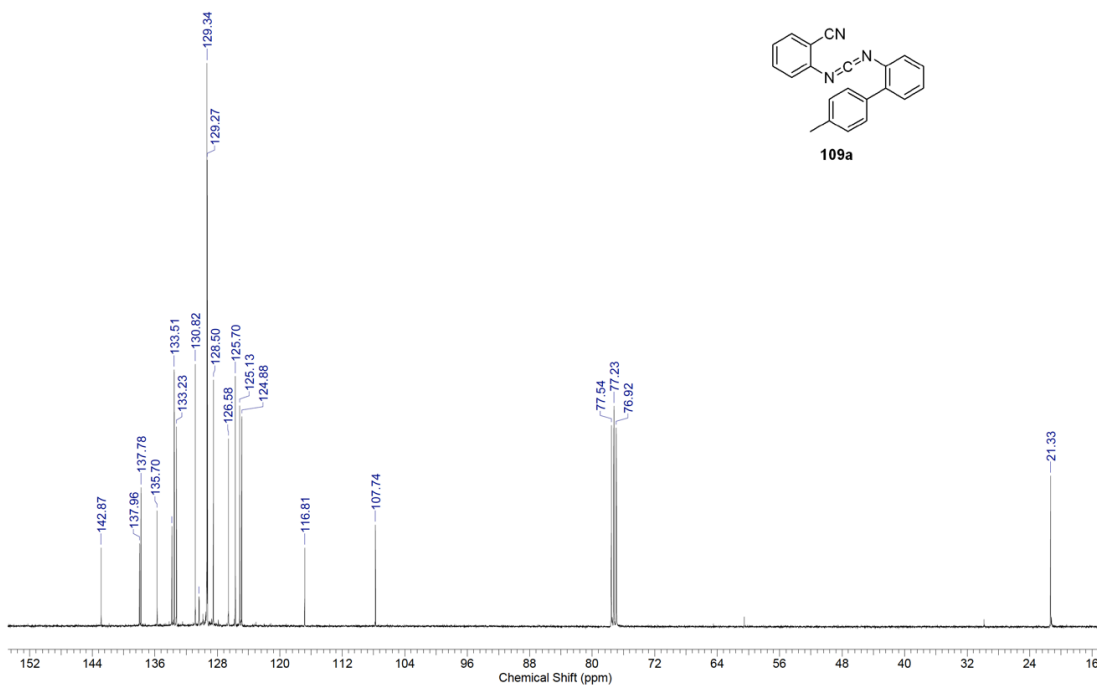
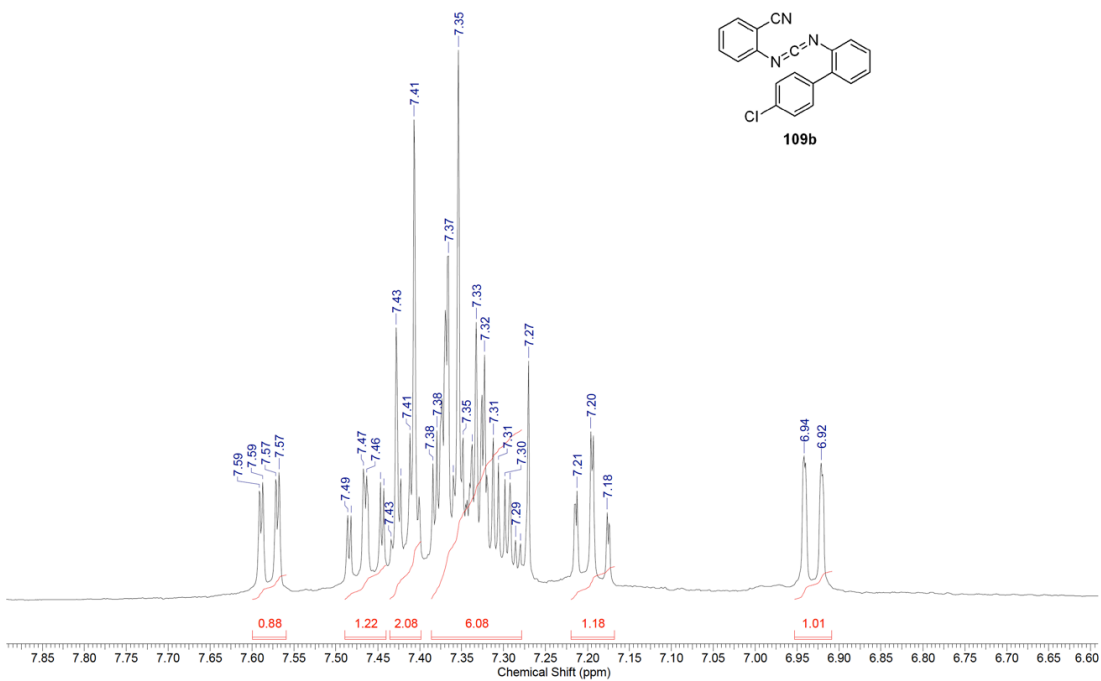


Figure B.17: ¹H and ¹³C NMR of 109a

| | | | | | | | |
|------------------------|--------------------|------------------|------------|------------------------|-------------|---------------|----------------|
| Acquisition Time (sec) | 2.0487 | Comment | Std proton | Date | May 20 2011 | Date Stamp | May 20 2011 |
| File Name | F:\CD\HG844S2H-STD | Points Count | 16384 | Frequency (MHz) | 399.73 | Nucleus | ¹ H |
| Original Points Count | 13102 | Points Count | 16384 | Pulse Sequence | s2pul | Receiver Gain | 38.00 |
| Spectrum Offset (Hz) | 2413.5979 | Sweep Width (Hz) | 6395.40 | Temperature (degree C) | 25.000 | Solvent | CHLOROFORM-d |



| | | | | | | | |
|------------------------|----------------------|----------------------|------------|------------------------|-------------|------------------|-----------------|
| Acquisition Time (sec) | 1.3005 | Comment | Std proton | Date | May 20 2011 | Date Stamp | May 20 2011 |
| File Name | F:\CD\HG844S2C13-STD | Points Count | 32768 | Frequency (MHz) | 100.52 | Nucleus | ¹³ C |
| Original Points Count | 31375 | Points Count | 32768 | Pulse Sequence | s2pul | Receiver Gain | 30.00 |
| Solvent | CHLOROFORM-d | Spectrum Offset (Hz) | 10551.2129 | Temperature (degree C) | 25.000 | Sweep Width (Hz) | 24125.45 |

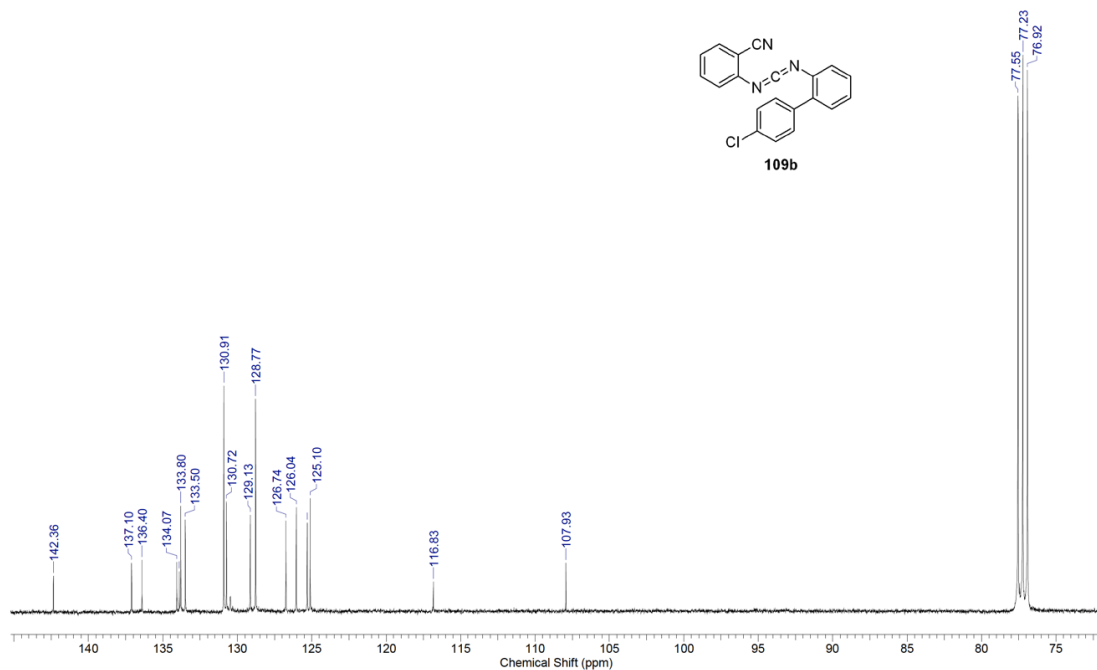
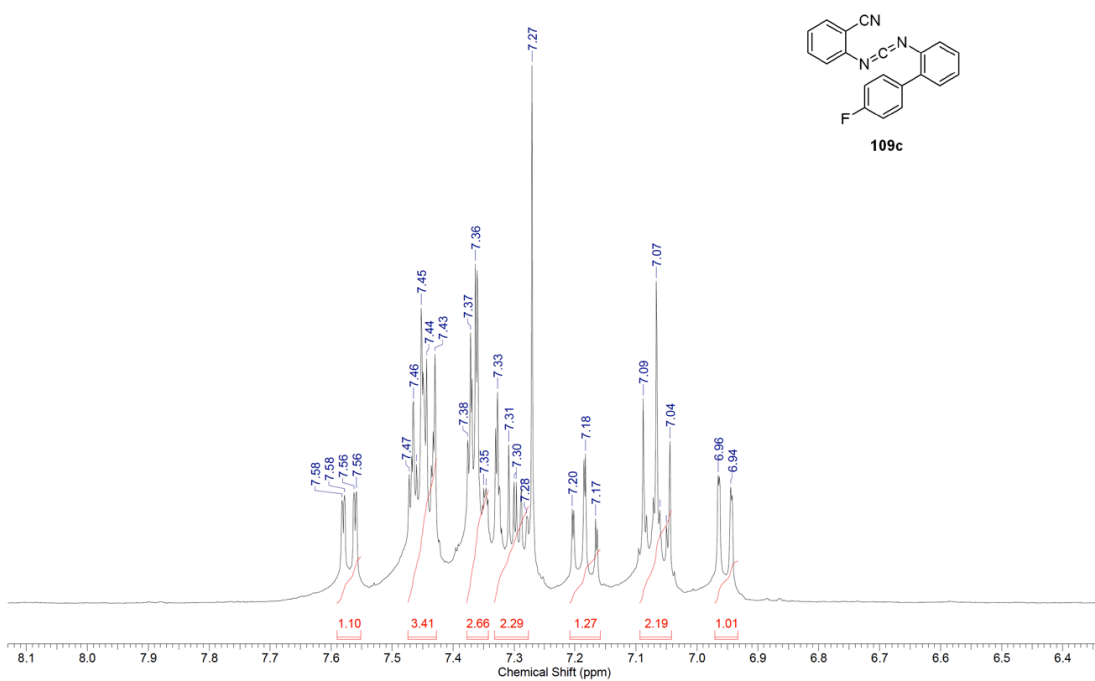


Figure B.18: ¹H and ¹³C NMR of 109b

| | | | | | | | |
|------------------------|-----------------|------------------|------------|------------------------|-------------|----------------------|--------------|
| Acquisition Time (sec) | 2.0487 | Comment | Std proton | Date | Jun 15 2011 | Date Stamp | Jun 15 2011 |
| File Name | F:\CD\HG869S2-H | Frequency (MHz) | 399.73 | Nucleus | 1H | Number of Transients | 16 |
| Original Points Count | 13102 | Points Count | 16384 | Pulse Sequence | s2pul | Receiver Gain | 46.00 |
| Spectrum Offset (Hz) | 2413.4026 | Sweep Width (Hz) | 6395.40 | Temperature (degree C) | 25.000 | Solvent | CHLOROFORM-D |



| | | | | | | | |
|------------------------|-------------------------|----------------------|------------|------------------|-------------|------------------------|-------------|
| Acquisition Time (sec) | 1.3005 | Comment | Std proton | Date | Jun 15 2011 | Date Stamp | Jun 15 2011 |
| File Name | F:\CD\HG869S2-C13DILUTE | Frequency (MHz) | 100.52 | Nucleus | 13C | Number of Transients | 7000 |
| Original Points Count | 31375 | Points Count | 32768 | Pulse Sequence | s2pul | Receiver Gain | 30.00 |
| Solvent | CHLOROFORM-D | Spectrum Offset (Hz) | 10554.8936 | Sweep Width (Hz) | 24125.45 | Temperature (degree C) | 25.000 |

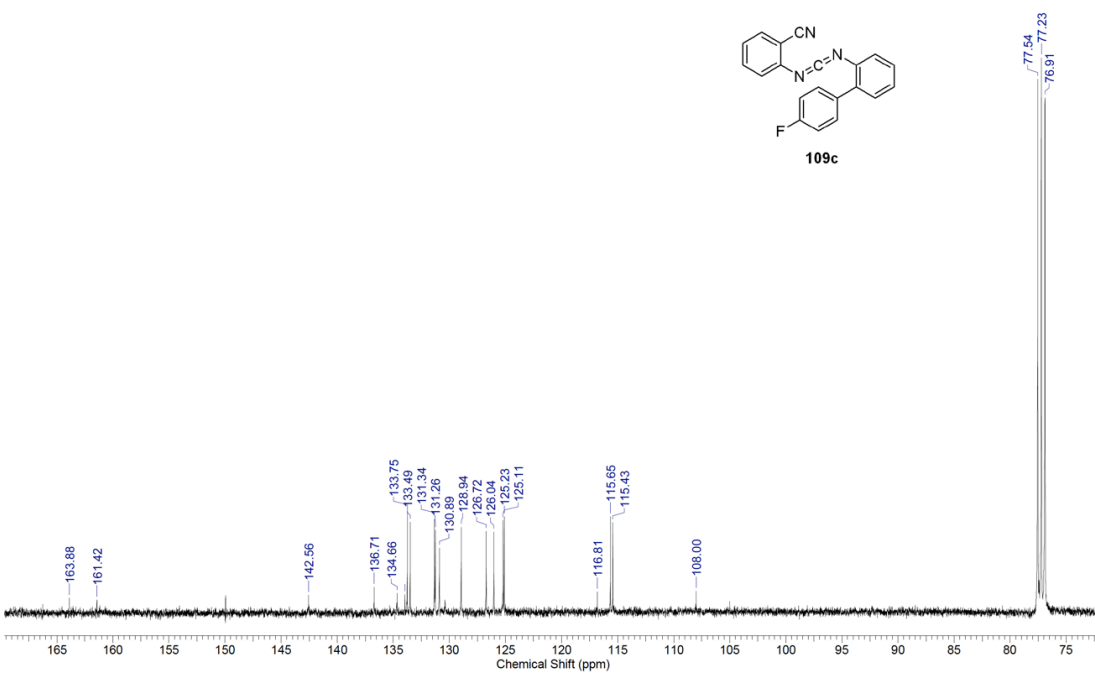
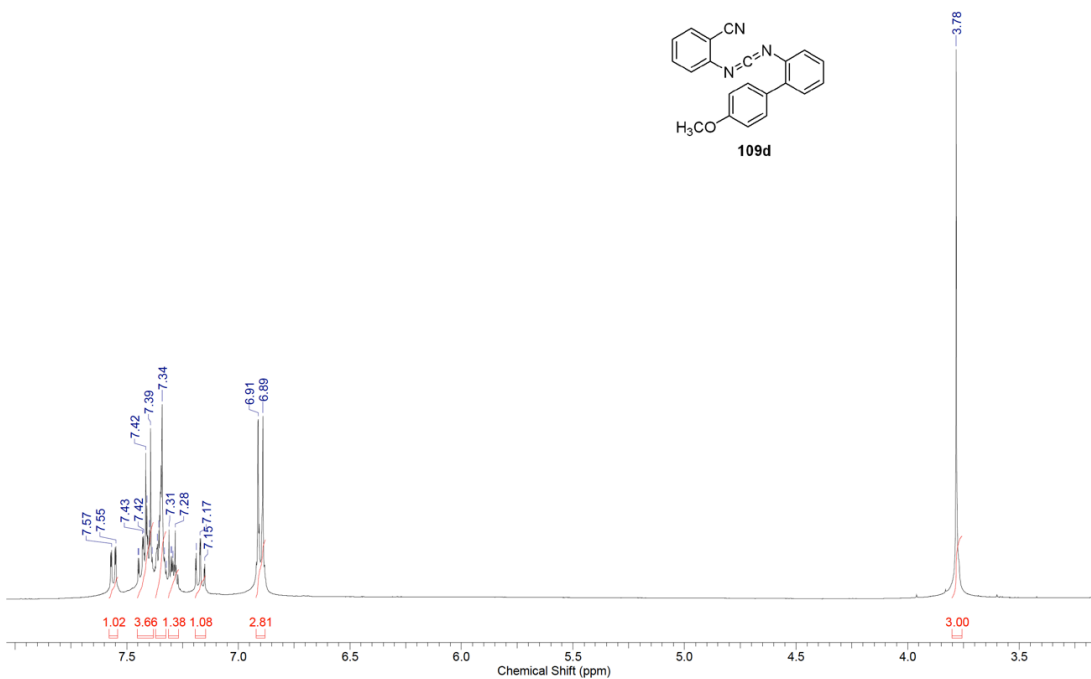


Figure B.19: ¹H and ¹³C NMR of 109c

| | | | | | | | |
|------------------------|--------------------|------------------|------------|------------------------|-------------|---------------|----------------|
| Acquisition Time (sec) | 2.0487 | Comment | Std proton | Date | May 30 2011 | Date Stamp | May 30 2011 |
| File Name | F:\CD\HG853S2H-STD | | | Frequency (MHz) | 399.73 | Nucleus | ¹ H |
| Original Points Count | 13102 | Points Count | 16384 | Pulse Sequence | s2pul | Receiver Gain | 40.00 |
| Spectrum Offset (Hz) | 2421.2095 | Sweep Width (Hz) | 6395.40 | Temperature (degree C) | 25.000 | Solvent | CHLOROFORM-d |



| | | | | | | | |
|------------------------|----------------------|--------------|------------|----------------------|-------------|------------------|-----------------|
| Acquisition Time (sec) | 1.3005 | Comment | Std proton | Date | May 30 2011 | Date Stamp | May 30 2011 |
| File Name | F:\CD\HG853S2C13-STD | | | Frequency (MHz) | 100.52 | Nucleus | ¹³ C |
| Original Points Count | 31375 | Points Count | 32768 | Pulse Sequence | s2pul | Receiver Gain | 30.00 |
| Solvent | CHLOROFORM-d | | | Spectrum Offset (Hz) | 10550.4766 | Sweep Width (Hz) | 24125.45 |
| Temperature (degree C) | 25.000 | | | | | | |

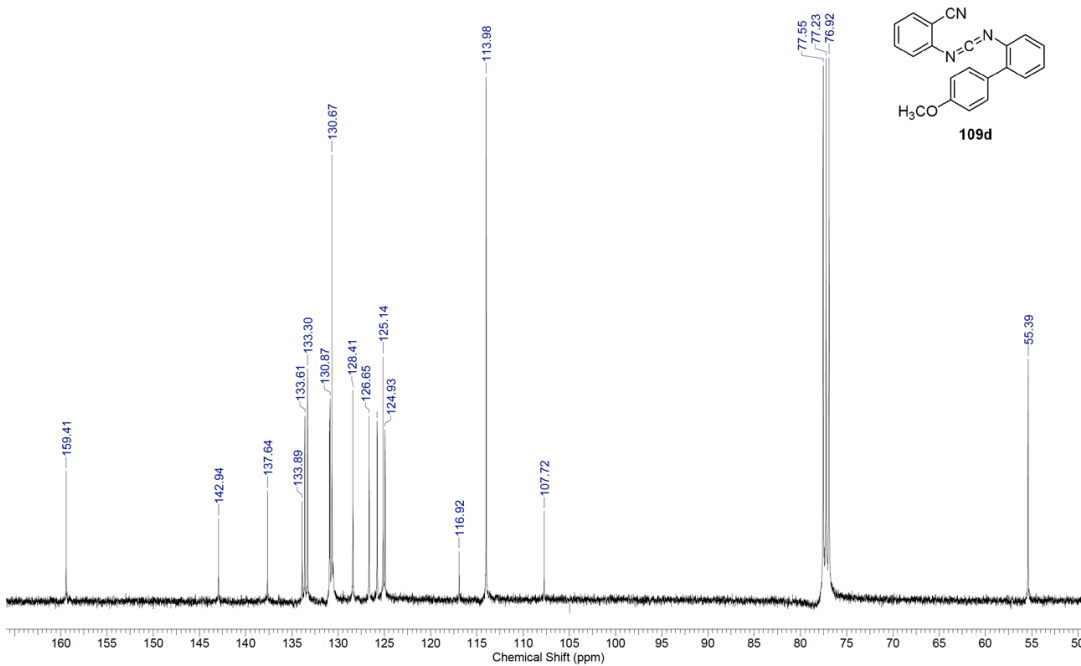
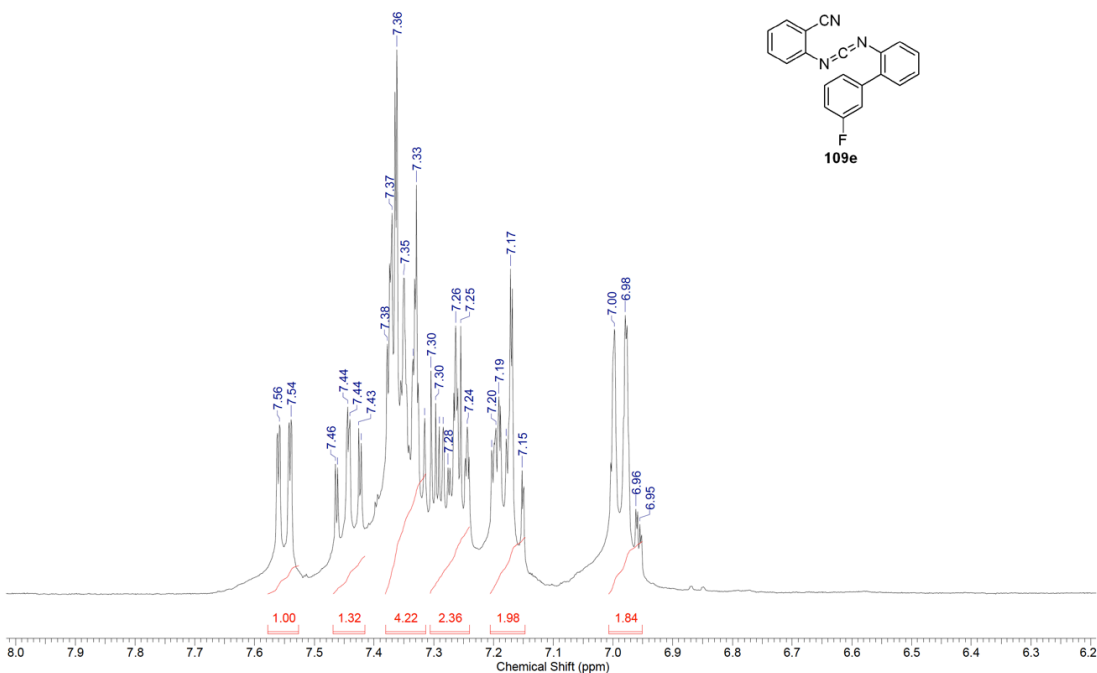


Figure B.20: ¹H and ¹³C NMR of **109d**

| | | | | | | | |
|------------------------|--|----------------------|------------|------------------------|--------------|-----------------|-------------|
| Acquisition Time (sec) | 2.0487 | Comment | Std proton | Date | Sep 10 2011 | Date Stamp | Sep 10 2011 |
| File Name | F:\OL-2 SUPPORTING.FINAL\OL_SICDIIMIDES\HG943H-GD-3F | | | | | Frequency (MHz) | 399.73 |
| Nucleus | ¹ H | Number of Transients | 16 | Original Points Count | 13102 | Points Count | 16384 |
| Pulse Sequence | s2pul | Receiver Gain | 48.00 | Solvent | CHLOROFORM-d | | |
| Spectrum Offset (Hz) | 2408.6174 | Sweep Width (Hz) | 6395.40 | Temperature (degree C) | 25.000 | | |



| | | | | | | | |
|------------------------|----------------------|--------------|------------|----------------------|-------------|----------------------|-----------------|
| Acquisition Time (sec) | 1.3005 | Comment | Std proton | Date | Sep 10 2011 | Date Stamp | Sep 10 2011 |
| File Name | F:\CD\HG943S2-C13-3F | | | | | Frequency (MHz) | 100.52 |
| Original Points Count | 31375 | Points Count | 32768 | Pulse Sequence | s2pul | Nucleus | ¹³ C |
| Solvent | CHLOROFORM-d | | | Receiver Gain | 30.00 | Number of Transients | 7500 |
| Temperature (degree C) | 25.000 | | | Spectrum Offset (Hz) | 10552.6846 | Sweep Width (Hz) | 24125.45 |

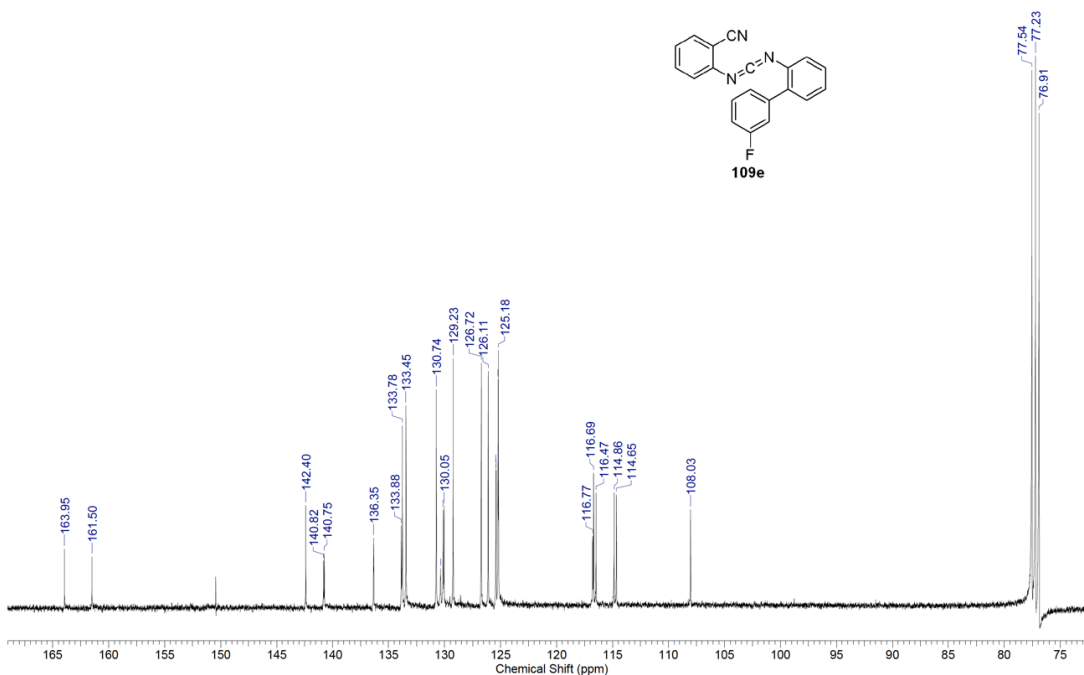
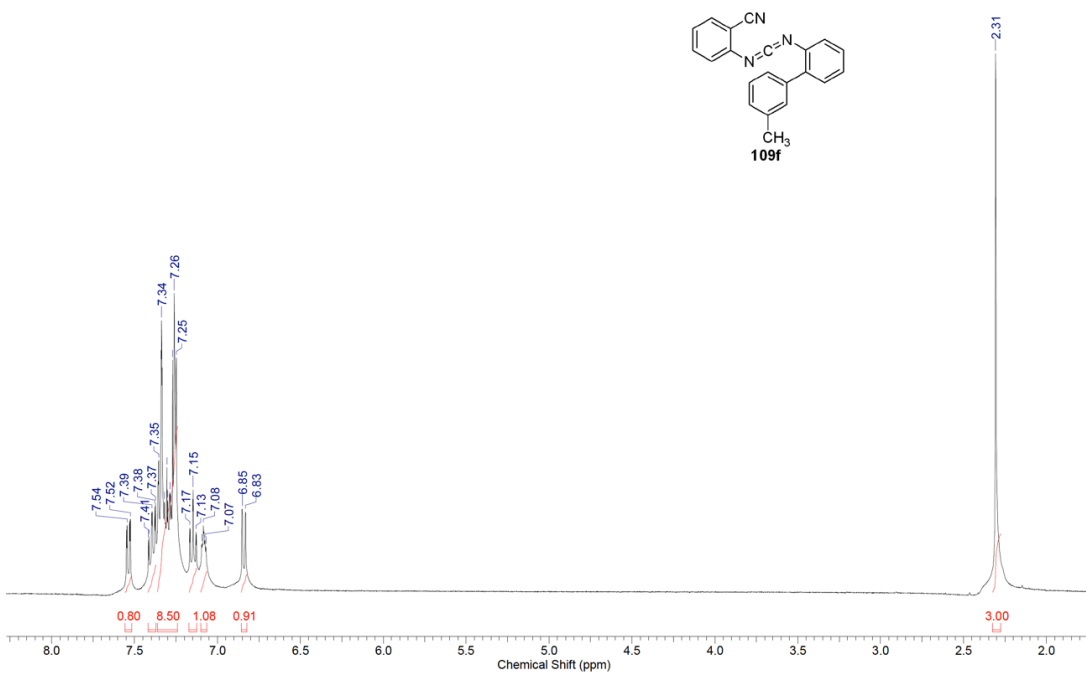


Figure B.21: ¹H and ¹³C NMR of 109e

| | | | | | | | |
|------------------------|--|----------------------|------------|------------------------|--------------|-----------------|------------|
| Acquisition Time (sec) | 2.0487 | Comment | Std proton | Date | Sep 2 2011 | Date Stamp | Sep 2 2011 |
| File Name | F:\OL-2 SUPPORTING FINAL\OL SI\CDIIMIDES\HG938S2-H-GD-3G | | | | | Frequency (MHz) | 399.73 |
| Nucleus | ¹ H | Number of Transients | 16 | Original Points Count | 13102 | Points Count | 16384 |
| Pulse Sequence | s2pul | Receiver Gain | 54.00 | Solvent | CHLOROFORM-d | | |
| Spectrum Offset (Hz) | 2414.7688 | Sweep Width (Hz) | 6395.40 | Temperature (degree C) | 25.000 | | |



| | | | | | | | |
|------------------------|--|----------------------|------------|------------------------|--------------|-----------------|------------|
| Acquisition Time (sec) | 1.3005 | Comment | Std proton | Date | Sep 2 2011 | Date Stamp | Sep 2 2011 |
| File Name | F:\OL-2 SUPPORTING FINAL\OL SI\CDIIMIDES\HG938S2-C13-GD-3G | | | | | Frequency (MHz) | 100.52 |
| Nucleus | ¹³ C | Number of Transients | 7400 | Original Points Count | 31375 | Points Count | 32768 |
| Pulse Sequence | s2pul | Receiver Gain | 30.00 | Solvent | CHLOROFORM-d | | |
| Spectrum Offset (Hz) | 10554.8936 | Sweep Width (Hz) | 24125.45 | Temperature (degree C) | 25.000 | | |

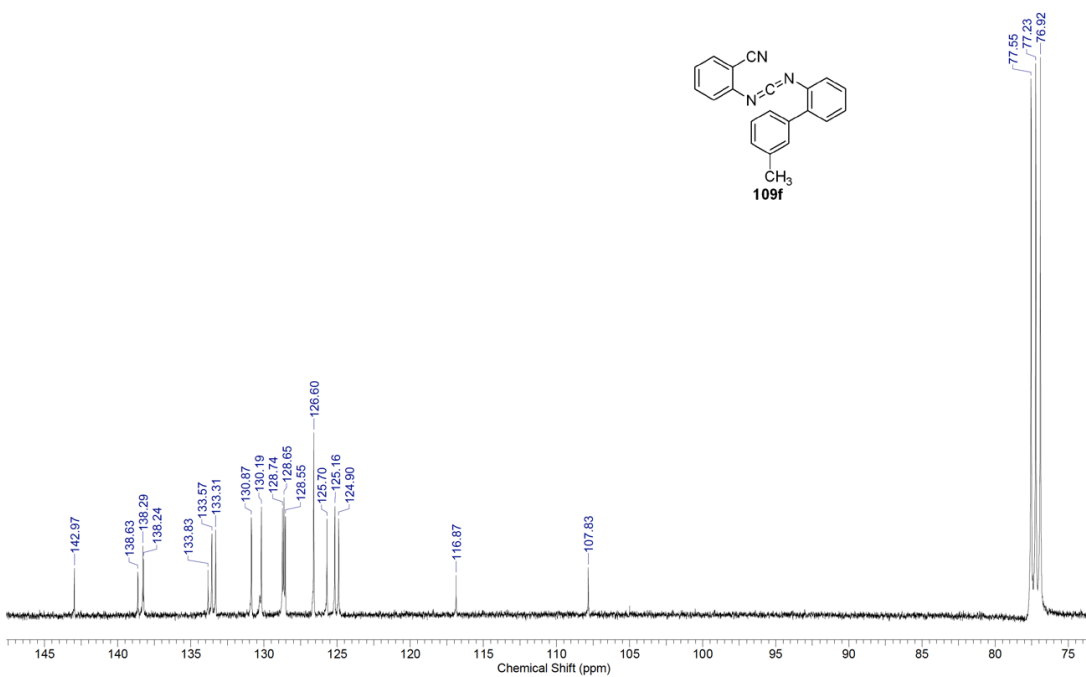
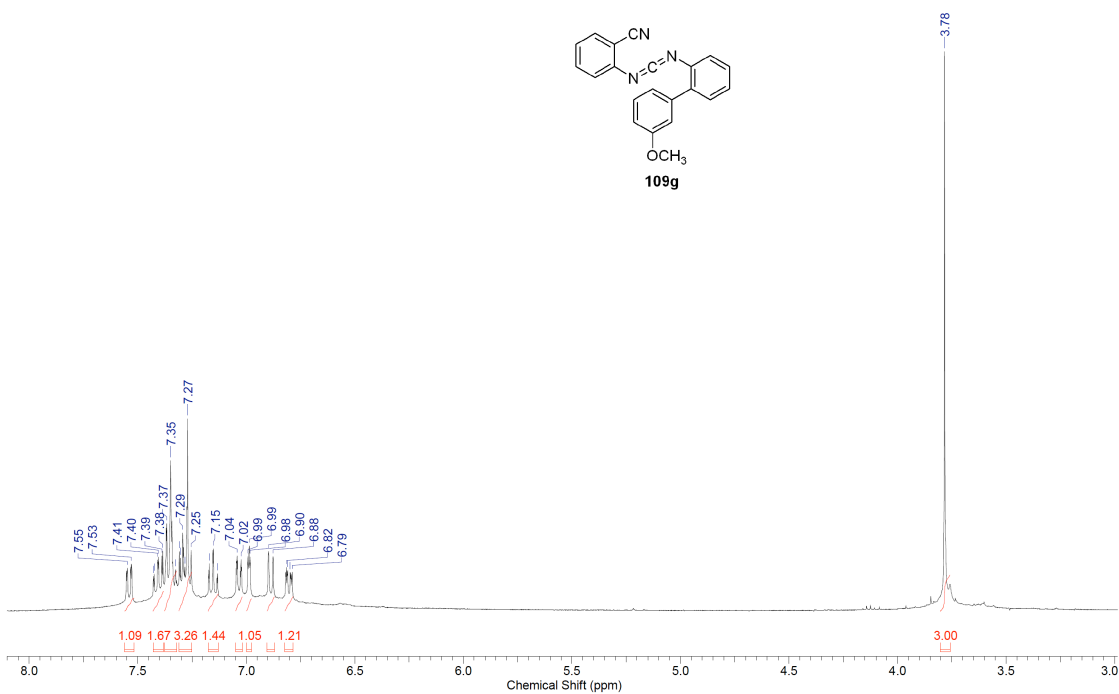
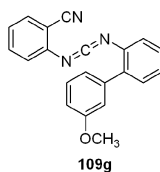


Figure B.22: ¹H and ¹³C NMR of 109f

| | | | | | | | |
|------------------------|-----------------------|------------------|------------|------------------------|-------------|---------------|--------------|
| Acquisition Time (sec) | 2.0487 | Comment | Std proton | Date | Dec 13 2011 | Date Stamp | Dec 13 2011 |
| File Name | F:\CD III\HG971-H-STD | | | Frequency (MHz) | 399.72 | Nucleus | 1H |
| Original Points Count | 13102 | Points Count | 16384 | Pulse Sequence | s2pul | Receiver Gain | 52.00 |
| Spectrum Offset (Hz) | 2406.9146 | Sweep Width (Hz) | 6395.40 | Temperature (degree C) | 25.000 | Solvent | CHLOROFORM-d |



| | | | | | | | |
|------------------------|---|------------------|------------|------------------------|-------------|---------------|--------------|
| Acquisition Time (sec) | 1.3005 | Comment | Std proton | Date | Jan 30 2011 | Date Stamp | Jan 30 2011 |
| File Name | C:\DOCUMENTS AND SETTINGS\W\GZ\DESKTOP\PIHG796-S2S2 | | | Frequency (MHz) | 100.52 | Nucleus | 13C |
| Original Points Count | 31375 | Points Count | 32768 | Pulse Sequence | s2pul | Receiver Gain | 30.00 |
| Spectrum Offset (Hz) | 10546.0586 | Sweep Width (Hz) | 24125.45 | Temperature (degree C) | 25.000 | Solvent | CHLOROFORM-d |

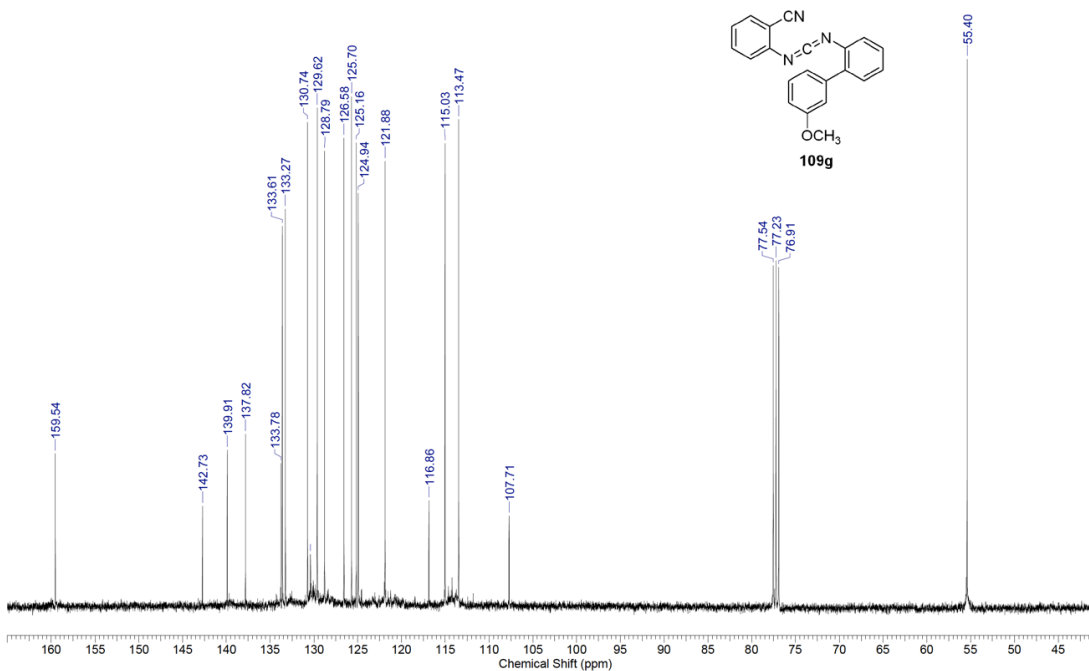
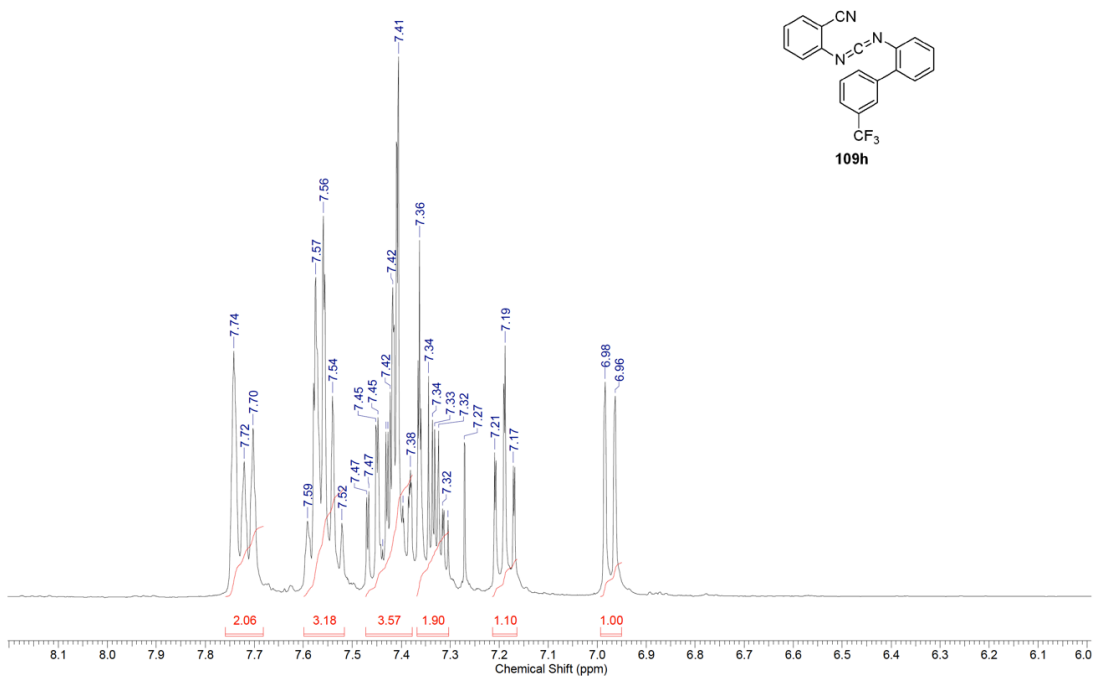


Figure B.23: ^1H and ^{13}C NMR of **109g**

| | | | | | | | |
|------------------------|----------------------|------------------|------------|------------------------|-------------|---------------|----------------|
| Acquisition Time (sec) | 2.0487 | Comment | Std proton | Date | May 17 2011 | Date Stamp | May 17 2011 |
| File Name | G:\XXNMR0222\HG841-H | Points Count | 16384 | Frequency (MHz) | 399.73 | Nucleus | ¹ H |
| Original Points Count | 13102 | Points Count | 16384 | Pulse Sequence | s2pul | Receiver Gain | 32.00 |
| Spectrum Offset (Hz) | 2413.9880 | Sweep Width (Hz) | 6395.40 | Temperature (degree C) | 25.000 | Solvent | CHLOROFORM-d |



| | | | | | | | |
|------------------------|------------------------|----------------------|------------|------------------------|-------------|------------------|-----------------|
| Acquisition Time (sec) | 1.3005 | Comment | Std proton | Date | May 17 2011 | Date Stamp | May 17 2011 |
| File Name | G:\XXNMR0222\HG841-C13 | Points Count | 32768 | Frequency (MHz) | 100.52 | Nucleus | ¹³ C |
| Original Points Count | 31375 | Points Count | 32768 | Pulse Sequence | s2pul | Receiver Gain | 30.00 |
| Solvent | CHLOROFORM-d | Spectrum Offset (Hz) | 10549.7393 | Temperature (degree C) | 25.000 | Sweep Width (Hz) | 24125.45 |

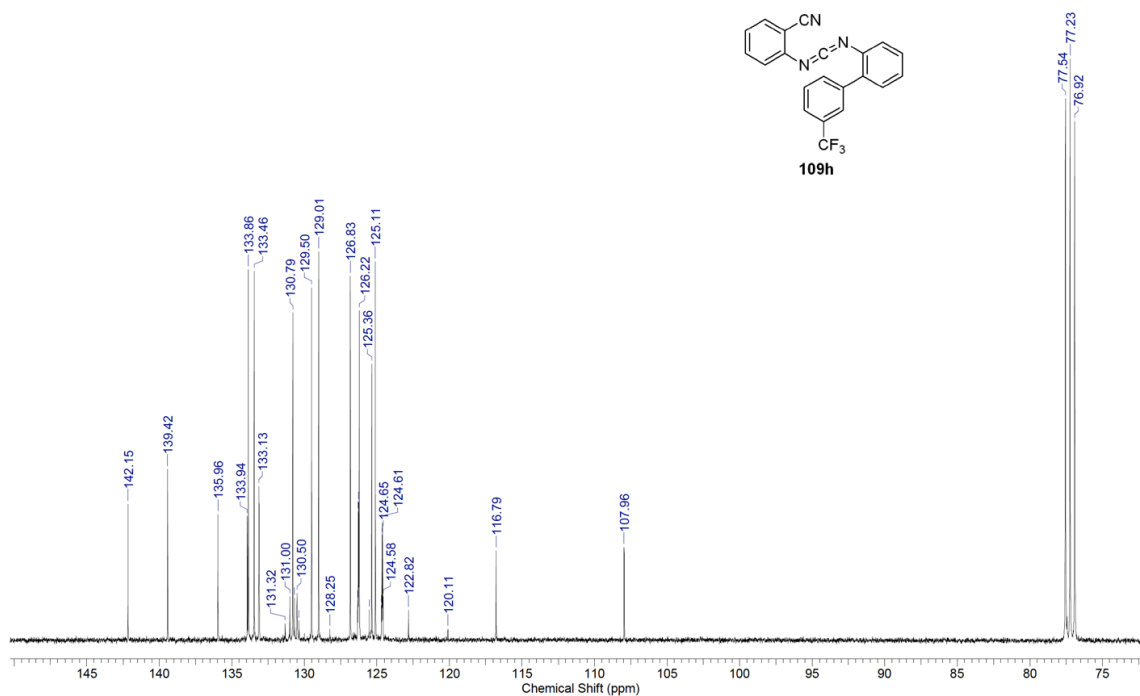
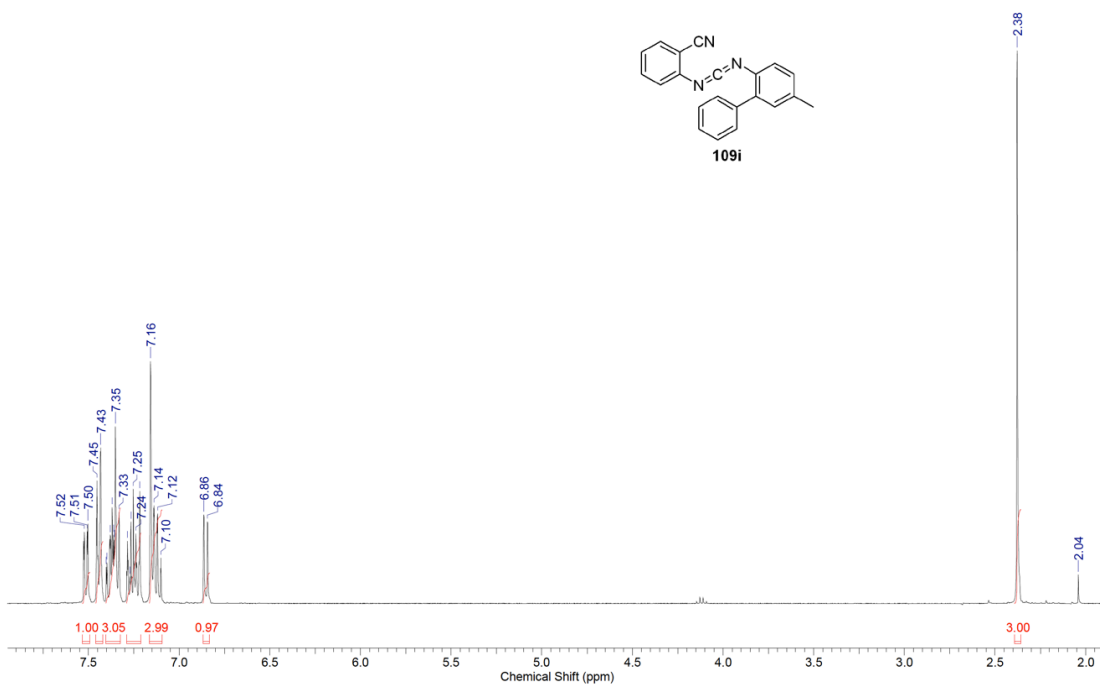


Figure B.24: ¹H and ¹³C NMR of 109h

| | | | | | | | |
|------------------------|-----------------|--------------|------------|------------------|-------------|------------------------|----------------|
| Acquisition Time (sec) | 2.0487 | Comment | Std proton | Date | Aug 22 2011 | Date Stamp | Aug 22 2011 |
| File Name | F:\CD\HG915H-GD | | | Frequency (MHz) | 399.73 | Nucleus | ¹ H |
| Original Points Count | 13102 | Points Count | 16384 | Pulse Sequence | s2pul | Receiver Gain | 52.00 |
| Spectrum Offset (Hz) | 2406.0801 | | | Sweep Width (Hz) | 6395.40 | Temperature (degree C) | 25.000 |



| | | | | | | | |
|------------------------|---------------------------------------|------------------------|--------------|-----------------|------------|----------------------|-----------------|
| Acquisition Time (sec) | 1.3005 | Comment | Std proton | Date | Dec 7 2011 | Date Stamp | Dec 7 2011 |
| File Name | F:\NMR\UNTITLED FOLDER\HG941-C13-XATT | | | Frequency (MHz) | 100.52 | Nucleus | ¹³ C |
| Number of Transients | 9000 | Original Points Count | 31375 | Points Count | 32768 | Pulse Sequence | s2pul |
| Receiver Gain | 30.00 | Solvent | CHLOROFORM-d | | | Spectrum Offset (Hz) | 10546.6680 |
| Sweep Width (Hz) | 24125.45 | Temperature (degree C) | 25.000 | | | | |

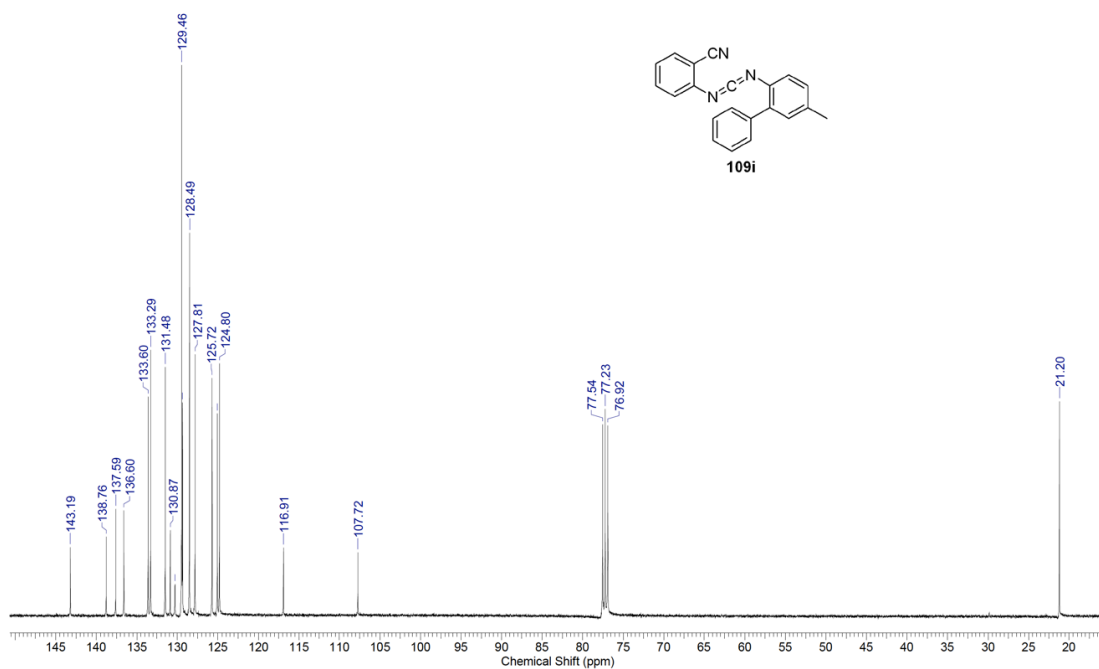
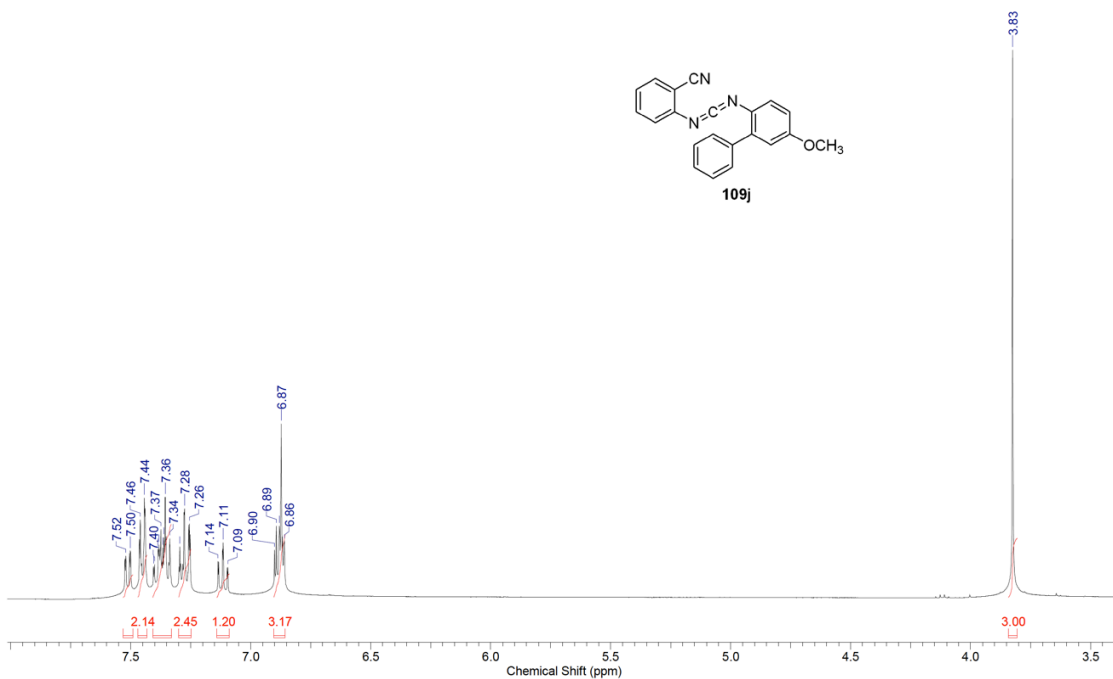


Figure B.25: ¹H and ¹³C NMR of **109i**

| | | | | | | | |
|------------------------|-----------------|--------------|------------|------------------|-------------|------------------------|-------------|
| Acquisition Time (sec) | 2.0487 | Comment | Std proton | Date | Sep 27 2011 | Date Stamp | Sep 27 2011 |
| File Name | F:\CD\HG948S2-H | | | Frequency (MHz) | 399.73 | Nucleus | 1H |
| Original Points Count | 13102 | Points Count | 16384 | Pulse Sequence | s2pul | Receiver Gain | 46.00 |
| Spectrum Offset (Hz) | 2407.2512 | | | Sweep Width (Hz) | 6395.40 | Temperature (degree C) | 25.000 |



| | | | | | | | |
|------------------------|----------------------|--------------|------------|----------------------|-------------|------------------|-------------|
| Acquisition Time (sec) | 1.3005 | Comment | Std proton | Date | Sep 27 2011 | Date Stamp | Sep 27 2011 |
| File Name | F:\CD\HG948S2-C13-GD | | | Frequency (MHz) | 100.52 | Nucleus | 13C |
| Original Points Count | 31375 | Points Count | 32768 | Pulse Sequence | s2pul | Receiver Gain | 30.00 |
| Solvent | CHLOROFORM-d | | | Spectrum Offset (Hz) | 10551.2129 | Sweep Width (Hz) | 24125.45 |
| Temperature (degree C) | 25.000 | | | | | | |

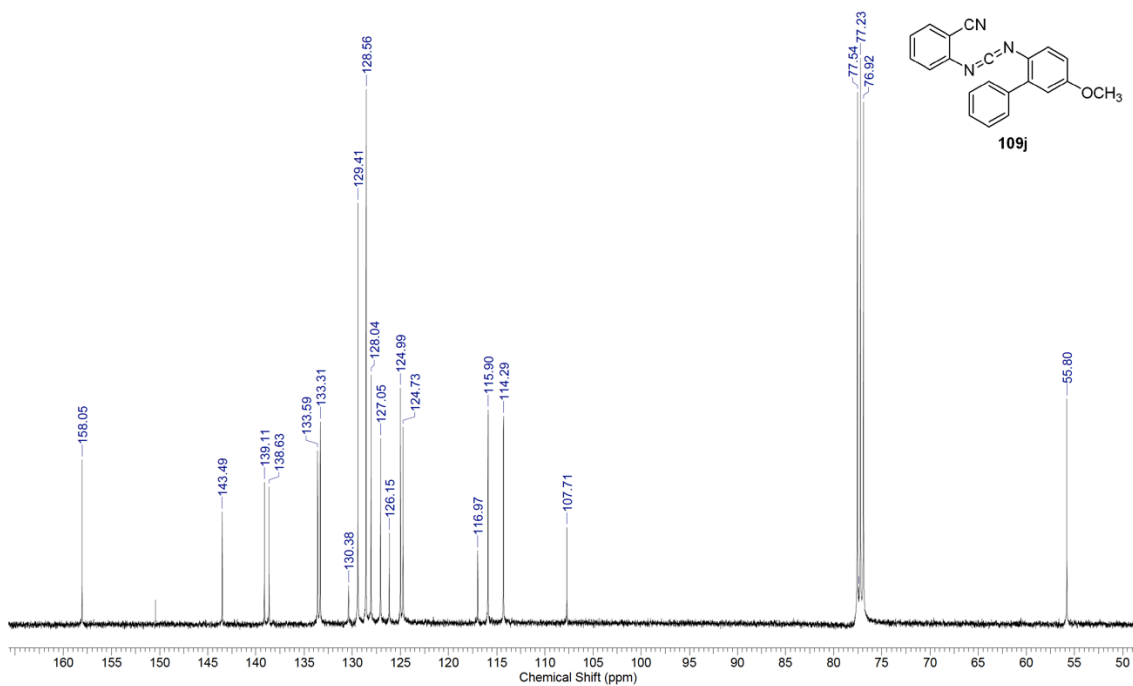
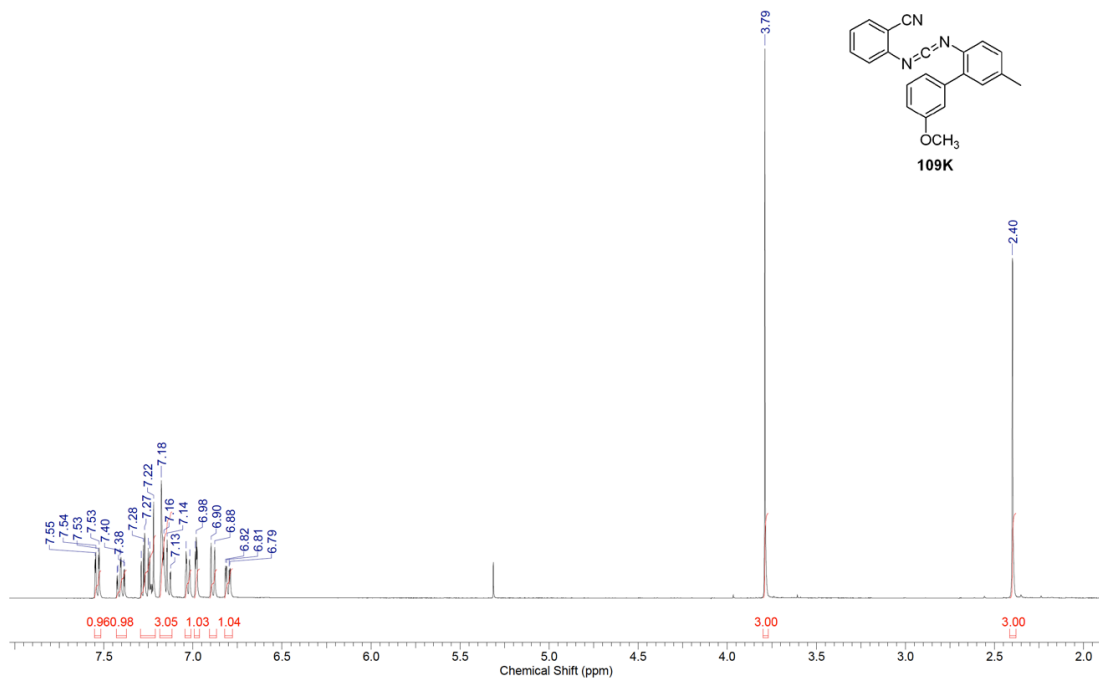


Figure B.26: ^1H and ^{13}C NMR of 109j

| | | | | | | | |
|------------------------|------------------|------------------|------------|------------------------|-------------|---------------|----------------|
| Acquisition Time (sec) | 2.0487 | Comment | Std proton | Date | Aug 18 2011 | Date Stamp | Aug 18 2011 |
| File Name | F:\CD\HG926H-STD | | | Frequency (MHz) | 399.73 | Nucleus | ¹ H |
| Original Points Count | 13102 | Points Count | 16384 | Pulse Sequence | s2pul | Receiver Gain | 48.00 |
| Spectrum Offset (Hz) | 2417.3062 | Sweep Width (Hz) | 6395.40 | Temperature (degree C) | 25.000 | Solvent | CHLOROFORM-d |



| | | | | | | | |
|------------------------|--------------------|--------------|------------|----------------------|-------------|------------------|-----------------|
| Acquisition Time (sec) | 1.3005 | Comment | Std proton | Date | Aug 19 2011 | Date Stamp | Aug 19 2011 |
| File Name | F:\CD\HG926-C13-GD | | | Frequency (MHz) | 100.52 | Nucleus | ¹³ C |
| Original Points Count | 31375 | Points Count | 32768 | Pulse Sequence | s2pul | Receiver Gain | 30.00 |
| Solvent | CHLOROFORM-d | | | Spectrum Offset (Hz) | 10548.2666 | Sweep Width (Hz) | 24125.45 |
| Temperature (degree C) | 25.000 | | | | | | |

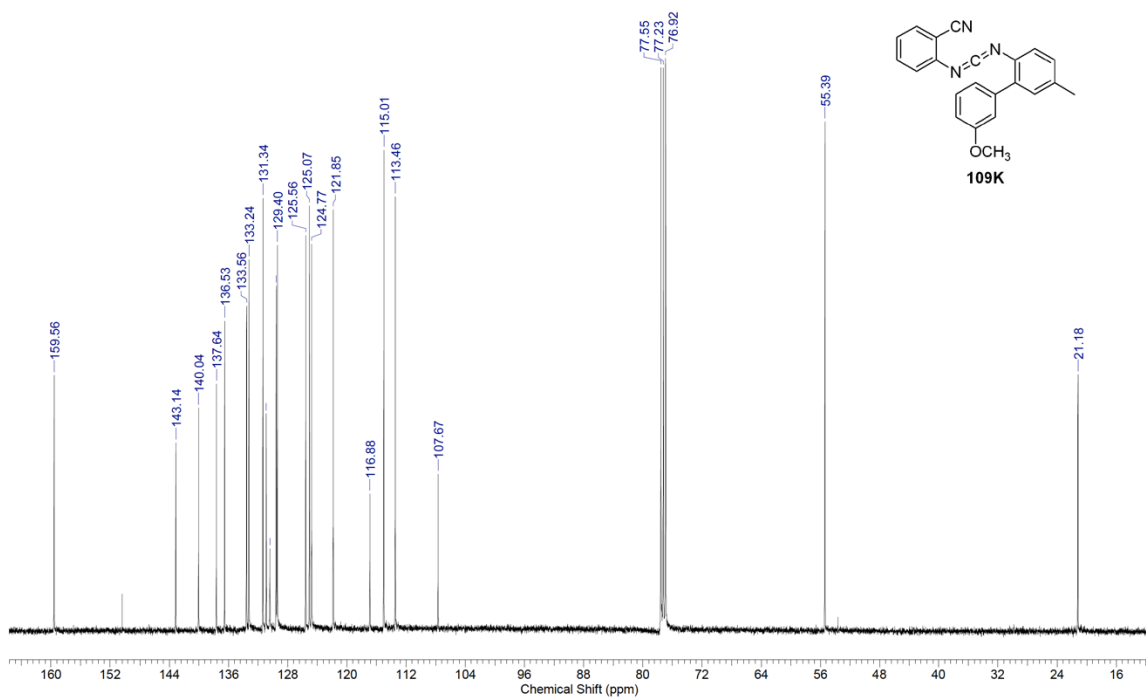
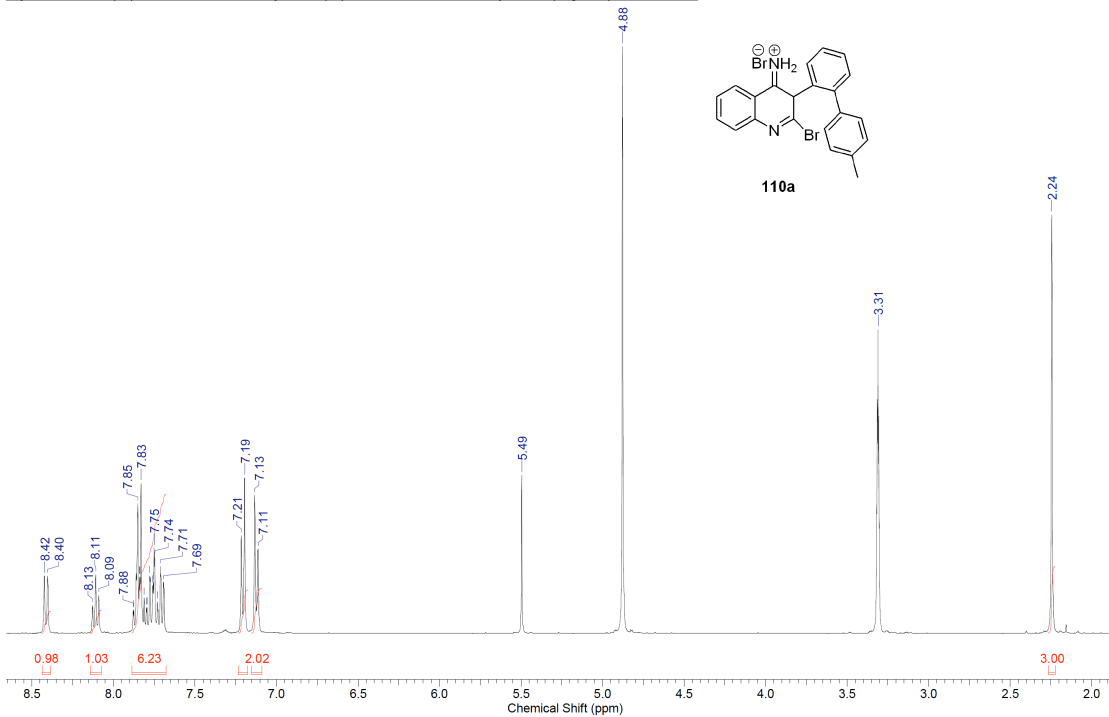


Figure B.27: ¹H and ¹³C NMR of **109k**

| | | | | | | | |
|------------------------|--|----------------------|------------|------------------------|-------------|--------------|-------------|
| Acquisition Time (sec) | 2.0487 | Comment | Std proton | Date | Feb 23 2011 | Date Stamp | Feb 23 2011 |
| File Name | C:\DOCUMENTS AND SETTINGS\VGZ\DESKTOP\PIHG7789R2-H | | | Frequency (MHz) | 399.73 | Points Count | 16384 |
| Nucleus | ¹ H | Number of Transients | 16 | Original Points Count | 13102 | Points Count | 16384 |
| Pulse Sequence | s2pul | Receiver Gain | 40.00 | Solvent | METHANOL-d4 | | |
| Spectrum Offset (Hz) | 2412.9424 | Sweep Width (Hz) | 6395.40 | Temperature (degree C) | 25.000 | | |



| | | | | | | | |
|------------------------|---|----------------------|------------|------------------------|-------------|--------------|-------------|
| Acquisition Time (sec) | 1.3005 | Comment | Std proton | Date | Feb 23 2011 | Date Stamp | Feb 23 2011 |
| File Name | C:\DOCUMENTS AND SETTINGS\VGZ\DESKTOP\PIHG789R2-C13 | | | Frequency (MHz) | 100.52 | Points Count | 32768 |
| Nucleus | ¹³ C | Number of Transients | 4800 | Original Points Count | 31375 | Points Count | 32768 |
| Pulse Sequence | s2pul | Receiver Gain | 30.00 | Solvent | METHANOL-d4 | | |
| Spectrum Offset (Hz) | 10690.2666 | Sweep Width (Hz) | 24125.45 | Temperature (degree C) | 25.000 | | |

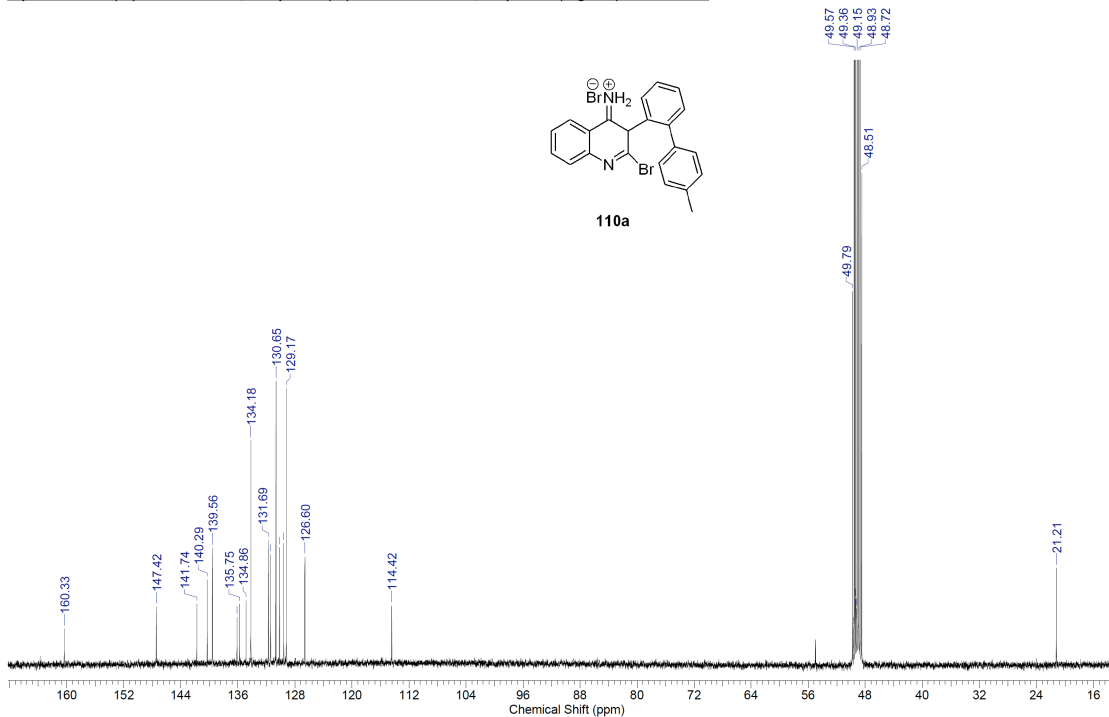
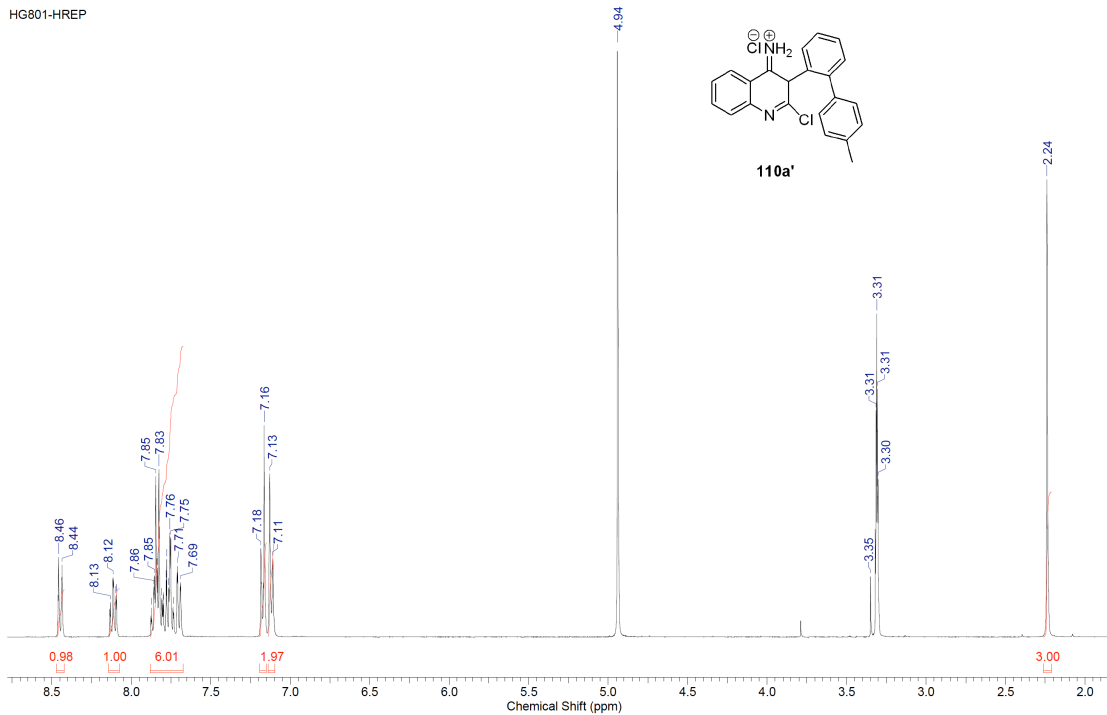


Figure B.28: ¹H and ¹³C NMR of 110a

| | | | | | |
|------------------------|----------------|------------------------|---------------|-----------------------|-------------|
| Acquisition Time (sec) | 2.0487 | Comment | Std proton | Date | Apr 16 2011 |
| Date Stamp | Apr 16 2011 | File Name | G:\HG801-HREP | Frequency (MHz) | 399.73 |
| Nucleus | ¹ H | Number of Transients | 16 | Original Points Count | 13102 |
| Receiver Gain | 42.00 | Solvent | METHANOL-d4 | Points Count | 16384 |
| Sweep Width (Hz) | 6395.40 | Temperature (degree C) | 25.000 | Spectrum Offset (Hz) | 2412.7476 |

HG801-HREP



| | | | | | | | |
|------------------------|---------------|------------------|------------|------------------------|-----------------|----------------------|-------------|
| Acquisition Time (sec) | 1.3005 | Comment | Std proton | Date | Apr 16 2011 | Date Stamp | Apr 16 2011 |
| File Name | G:\HG-801-C13 | Frequency (MHz) | 100.52 | Nucleus | ¹³ C | Number of Transients | 5000 |
| Original Points Count | 31375 | Points Count | 32768 | Pulse Sequence | s2pul | Receiver Gain | 30.00 |
| Spectrum Offset (Hz) | 10689.8633 | Sweep Width (Hz) | 24125.45 | Temperature (degree C) | 25.000 | Solvent | METHANOL-d4 |

HG-801-C13

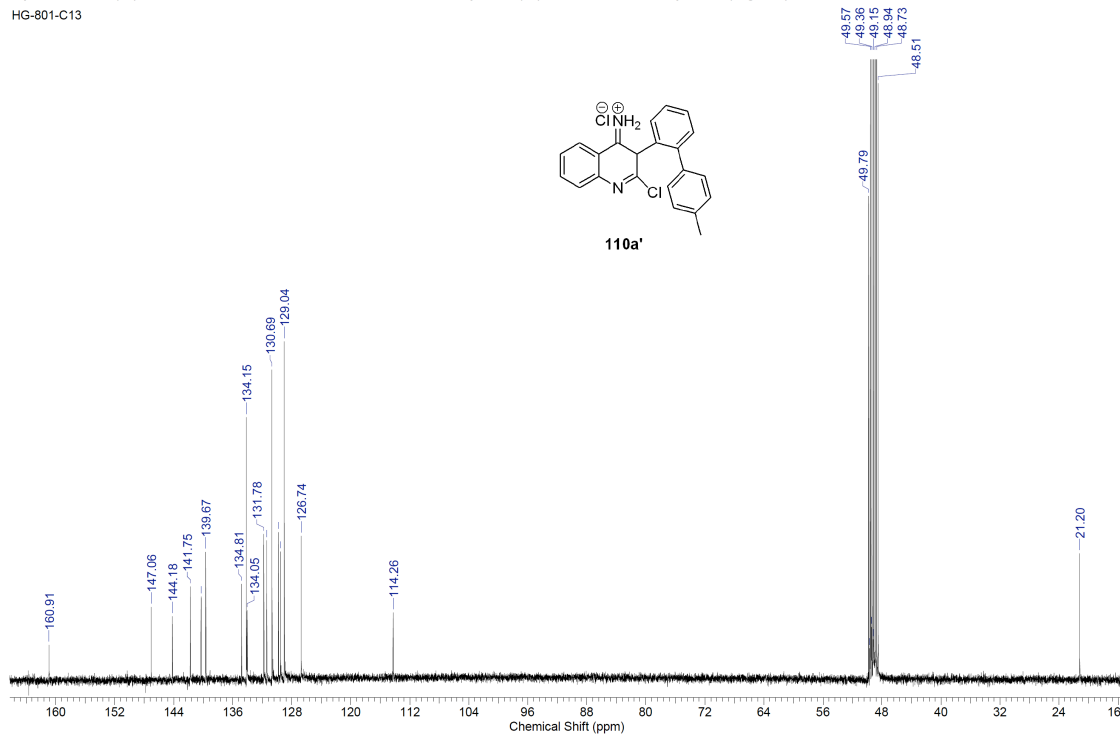
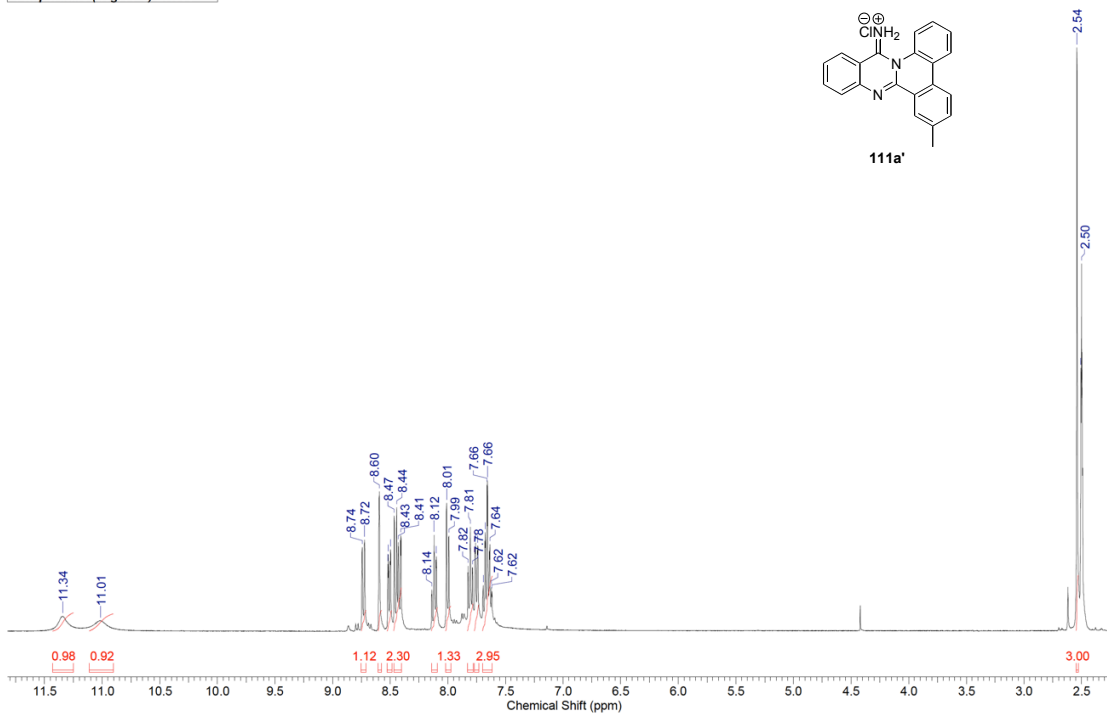


Figure B.29: ¹H and ¹³C NMR of **110a'**

| | | | | | |
|------------------------|----------------|----------------------|---------------------|-----------------------|-------------|
| Acquisition Time (sec) | 2.0487 | Comment | Std proton | Date | Jul 13 2011 |
| Date Stamp | Jul 13 2011 | File Name | G:\XXNMR0222\HG878H | Frequency (MHz) | 399.73 |
| Nucleus | ¹ H | Number of Transients | 16 | Original Points Count | 13102 |
| Receiver Gain | 44.00 | Solvent | DMSO-d6 | Points Count | 16384 |
| Temperature (degree C) | 25.000 | Spectrum Offset (Hz) | 2415.1003 | Pulse Sequence | s2pul |
| | | | | Sweep Width (Hz) | 6395.40 |



| | | | | | |
|------------------------|-----------------|------------------|------------|------------------------|-----------------|
| Acquisition Time (sec) | 1.3005 | Comment | Std proton | Date | Jul 16 2011 |
| File Name | F:\PNQ\HG878C13 | Frequency (MHz) | 100.52 | Nucleus | ¹³ C |
| Original Points Count | 31375 | Points Count | 32768 | Pulse Sequence | s2pul |
| Spectrum Offset (Hz) | 10488.0264 | Sweep Width (Hz) | 24125.45 | Receiver Gain | 30.00 |
| | | | | Number of Transients | 10000 |
| | | | | Solvent | DMSO-d6 |
| | | | | Temperature (degree C) | 25.000 |

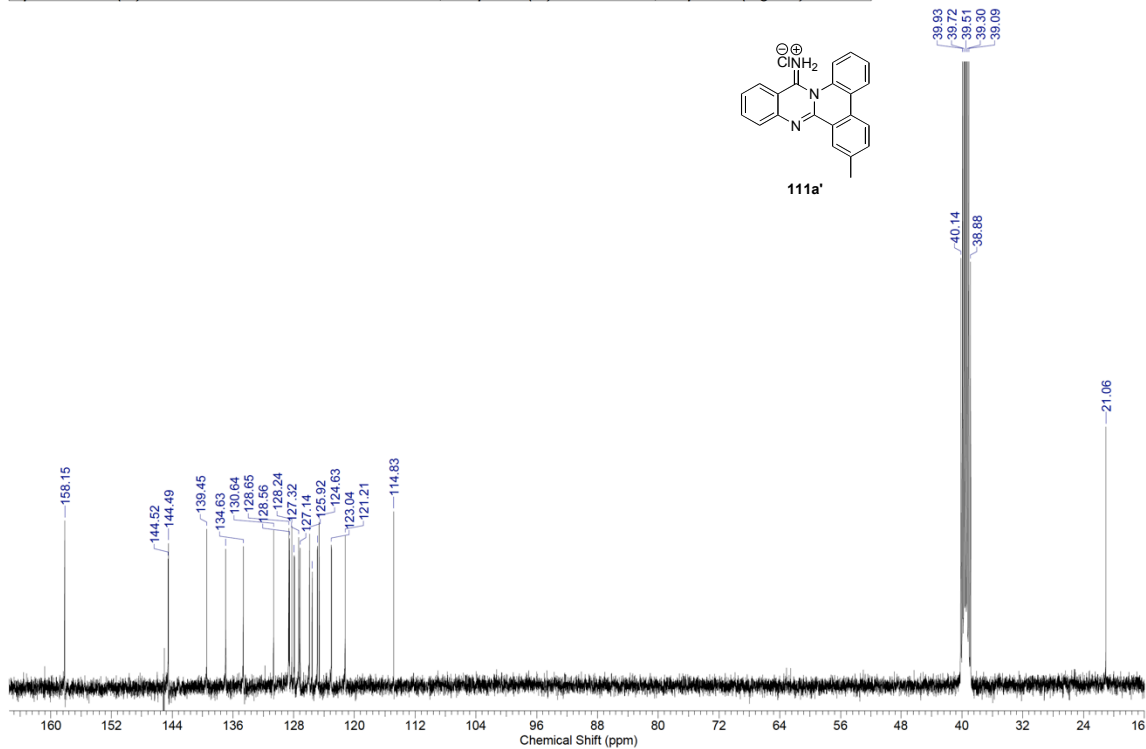
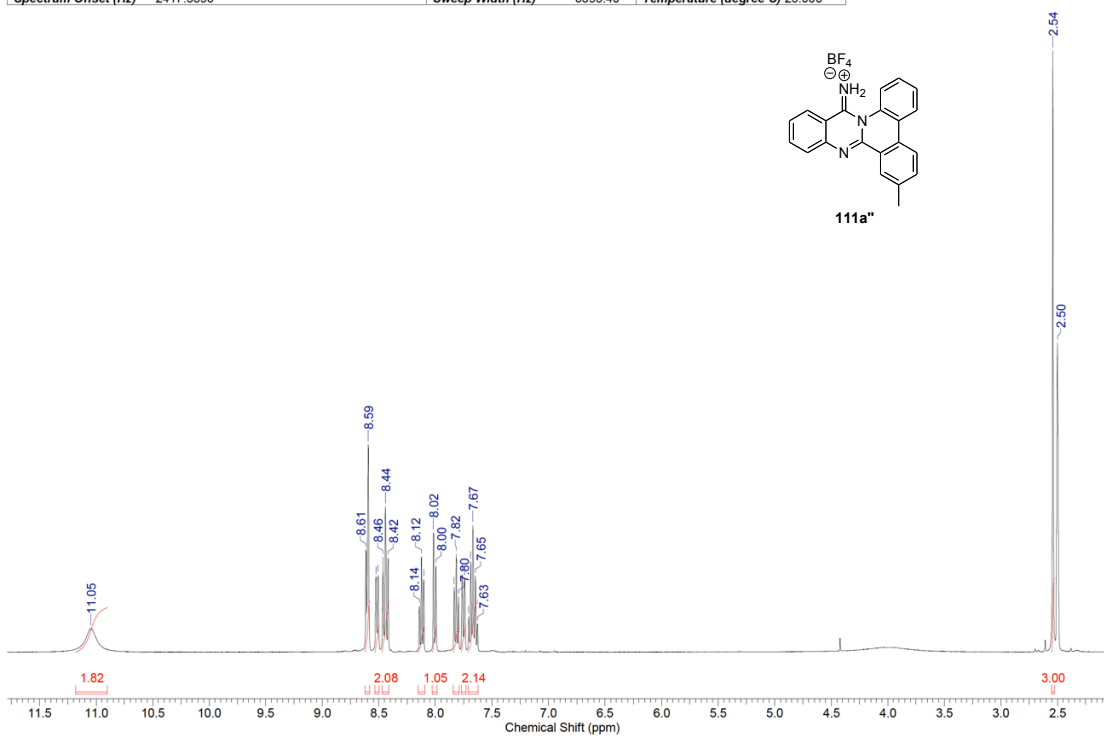


Figure B.30: ¹H and ¹³C NMR of 111a'

| | | | | | | | |
|------------------------|--------------------|--------------|------------|------------------|-------------|------------------------|----------------|
| Acquisition Time (sec) | 2.0487 | Comment | Std proton | Date | Apr 15 2011 | Date Stamp | Apr 15 2011 |
| File Name | F:\PNO\HG820H-DMSO | | | Frequency (MHz) | 399.73 | Nucleus | ¹ H |
| Original Points Count | 13102 | Points Count | 16384 | Pulse Sequence | s2pul | Receiver Gain | 40.00 |
| Spectrum Offset (Hz) | 2417.3396 | | | Sweep Width (Hz) | 6395.40 | Temperature (degree C) | 25.000 |
| | | | | | | Solvent | DMSO-d6 |



| | | | | | | | |
|------------------------|------------------------|--------------|------------|------------------|-------------|------------------------|-----------------|
| Acquisition Time (sec) | 1.3005 | Comment | Std proton | Date | Apr 15 2011 | Date Stamp | Apr 15 2011 |
| File Name | F:\PNO\HG820H-DMSO-C13 | | | Frequency (MHz) | 100.52 | Nucleus | ¹³ C |
| Original Points Count | 31375 | Points Count | 32768 | Pulse Sequence | s2pul | Receiver Gain | 30.00 |
| Spectrum Offset (Hz) | 10487.0459 | | | Sweep Width (Hz) | 24125.45 | Temperature (degree C) | 25.000 |
| | | | | | | Solvent | DMSO-d6 |

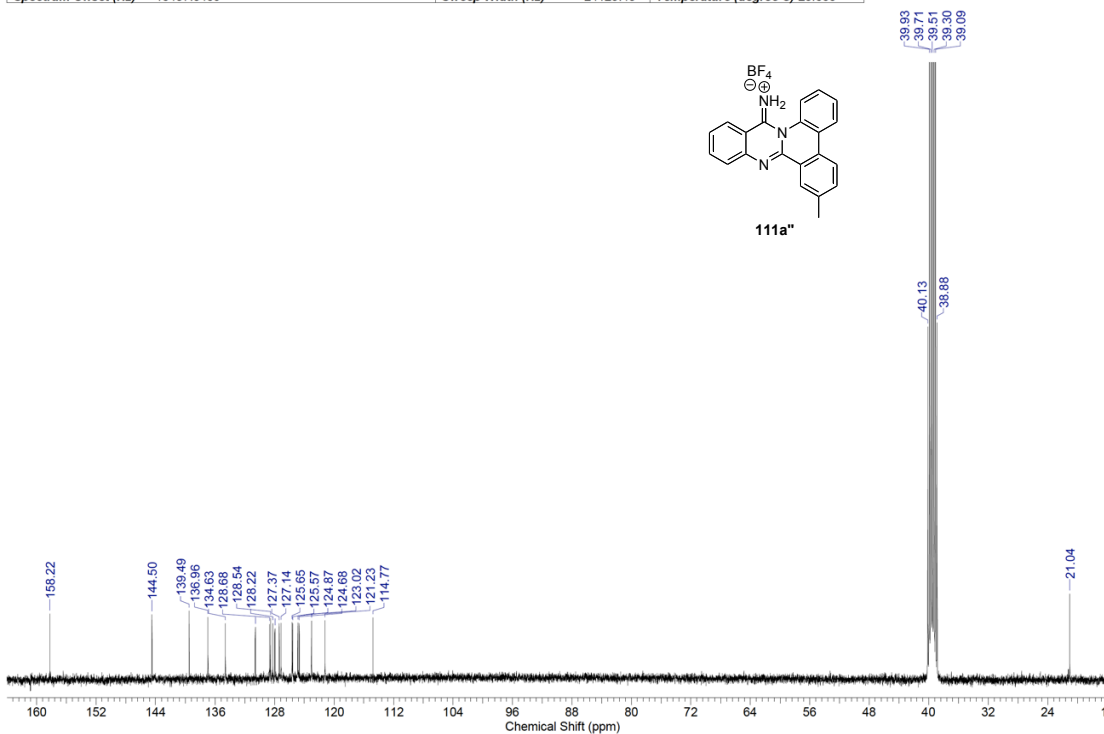
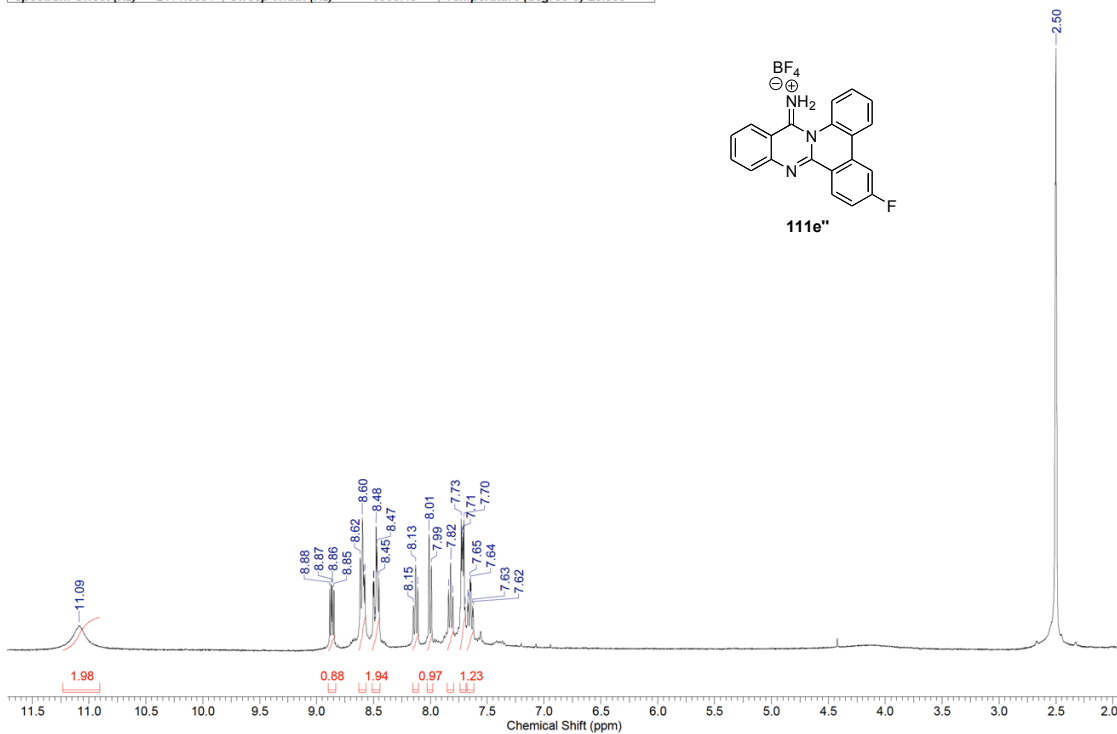


Figure B.31: ¹H and ¹³C NMR of **111a''**

| | | | | | | | |
|------------------------|------------------------------|------------------|------------|------------------------|-------------|---------------|-------------|
| Acquisition Time (sec) | 2.0487 | Comment | Std proton | Date | Dec 12 2011 | Date Stamp | Dec 12 2011 |
| File Name | G:\XXNMR0222\HG9XX-PNQ-C3F-H | | | Frequency (MHz) | 399.72 | Nucleus | 1H |
| Original Points Count | 13102 | Points Count | 16384 | Pulse Sequence | s2pul | Receiver Gain | 58.00 |
| Spectrum Offset (Hz) | 2411.8584 | Sweep Width (Hz) | 6395.40 | Temperature (degree C) | 25.000 | Solvent | DMSO-d6 |



| | | | | | | | |
|------------------------|------------------------|------------------|------------|------------------------|------------|---------------|------------|
| Acquisition Time (sec) | 1.3005 | Comment | Std proton | Date | Dec 5 2011 | Date Stamp | Dec 5 2011 |
| File Name | G:\XXNMR0222\HG956C13X | | | Frequency (MHz) | 100.52 | Nucleus | 13C |
| Original Points Count | 31375 | Points Count | 32768 | Pulse Sequence | s2pul | Receiver Gain | 30.00 |
| Spectrum Offset (Hz) | 10488.4531 | Sweep Width (Hz) | 24125.45 | Temperature (degree C) | 25.000 | Solvent | DMSO-d6 |

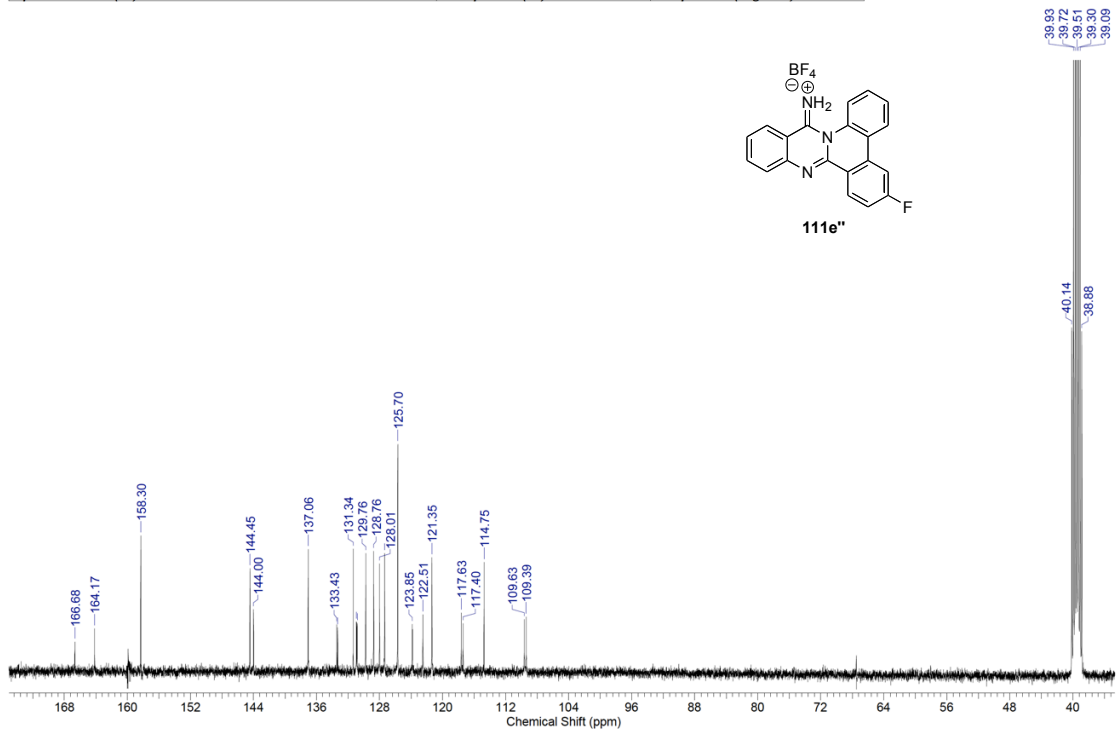
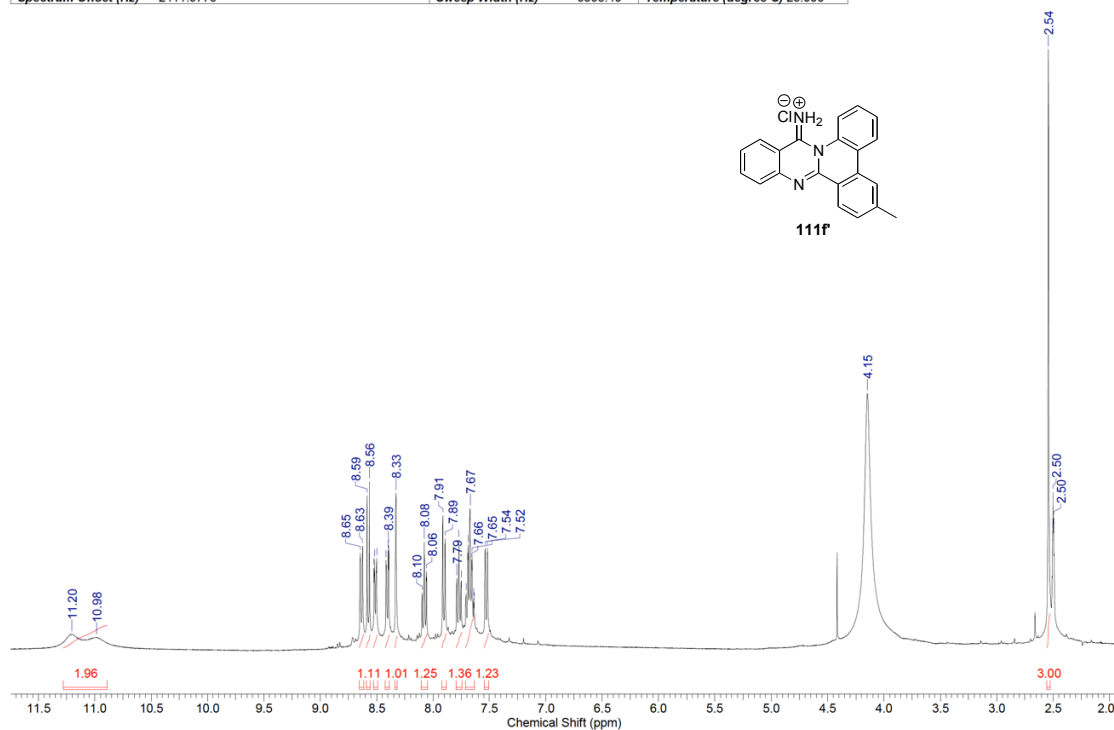


Figure B.32: ¹H and ¹³C NMR of **111e''**

| | | | | | | | |
|------------------------|--------------------|--------------|------------|------------------|-------------|------------------------|----------------|
| Acquisition Time (sec) | 2.0487 | Comment | Std proton | Date | Sep 28 2011 | Date Stamp | Sep 28 2011 |
| File Name | F:\PNQ\HG942H-CONC | | | Frequency (MHz) | 399.73 | Nucleus | ¹ H |
| Original Points Count | 13102 | Points Count | 16384 | Pulse Sequence | s2pul | Receiver Gain | 42.00 |
| Spectrum Offset (Hz) | 2411.9775 | | | Sweep Width (Hz) | 6395.40 | Temperature (degree C) | 25.000 |



| | | | | | | | |
|------------------------|-----------------------|--------------|------------|------------------|-------------|------------------------|-----------------|
| Acquisition Time (sec) | 1.3005 | Comment | Std proton | Date | Sep 29 2011 | Date Stamp | Sep 29 2011 |
| File Name | F:\PNQ\HG942-C13-CONC | | | Frequency (MHz) | 100.52 | Nucleus | ¹³ C |
| Original Points Count | 31375 | Points Count | 32768 | Pulse Sequence | s2pul | Receiver Gain | 30.00 |
| Spectrum Offset (Hz) | 10489.2539 | | | Sweep Width (Hz) | 24125.45 | Temperature (degree C) | 25.000 |

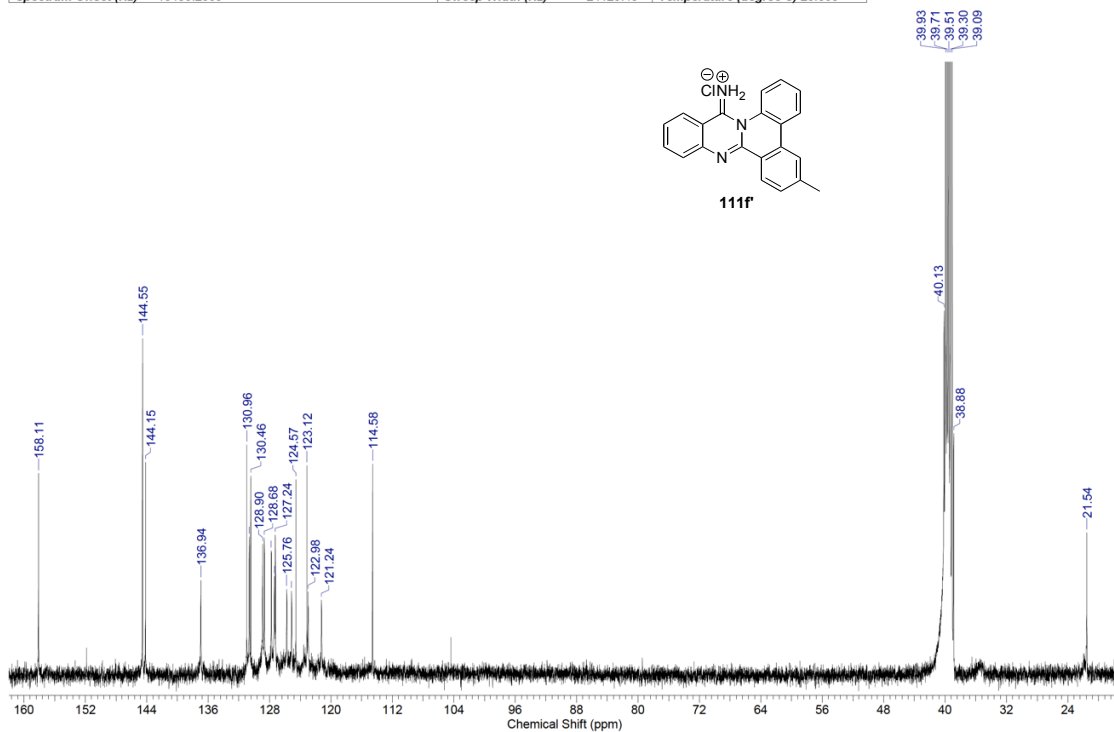
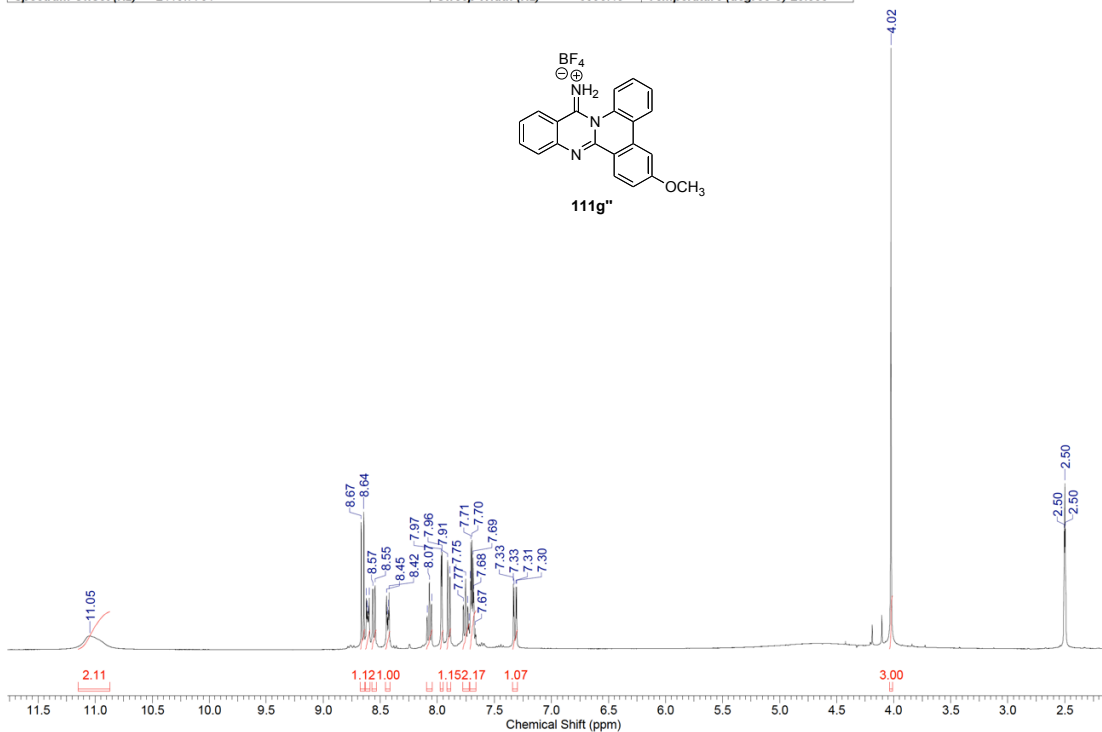


Figure B.33: ¹H and ¹³C NMR of **111f**

| Acquisition Time (sec) | 2.0487 | Comment | Std proton | Date | May 28 2011 | Date Stamp | May 28 2011 |
|------------------------|----------------------|--------------|------------|------------------|-------------|------------------------|----------------|
| File Name | G:\XXNMR0222\HGR840H | | | Frequency (MHz) | 399.73 | Nucleus | ¹ H |
| Original Points Count | 13102 | Points Count | 16384 | Pulse Sequence | s2pul | Receiver Gain | 42.00 |
| Spectrum Offset (Hz) | 2415.7781 | | | Sweep Width (Hz) | 6395.40 | Temperature (degree C) | 25.000 |



| Acquisition Time (sec) | 1.3005 | Comment | Std proton | Date | May 29 2011 | Date Stamp | May 29 2011 |
|------------------------|------------------------|--------------|------------|------------------|-------------|------------------------|-----------------|
| File Name | G:\XXNMR0222\HGR840C13 | | | Frequency (MHz) | 100.52 | Nucleus | ¹³ C |
| Original Points Count | 31375 | Points Count | 32768 | Pulse Sequence | s2pul | Receiver Gain | 30.00 |
| Spectrum Offset (Hz) | 10494.4082 | | | Sweep Width (Hz) | 24125.45 | Temperature (degree C) | 25.000 |

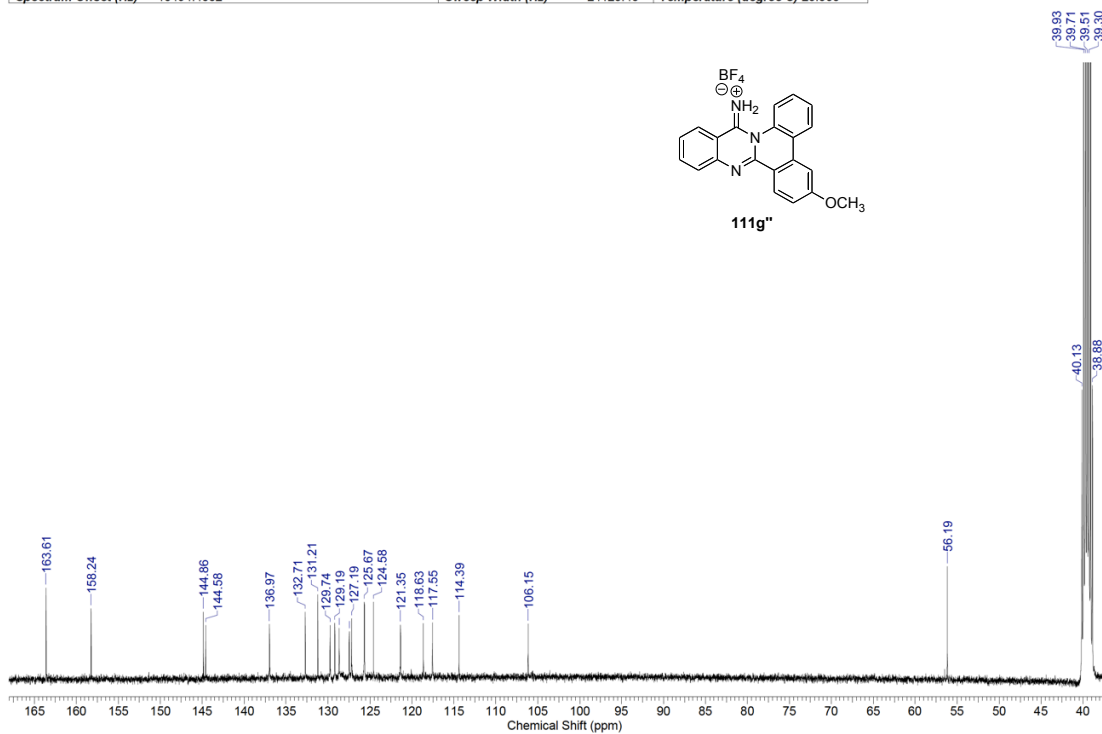
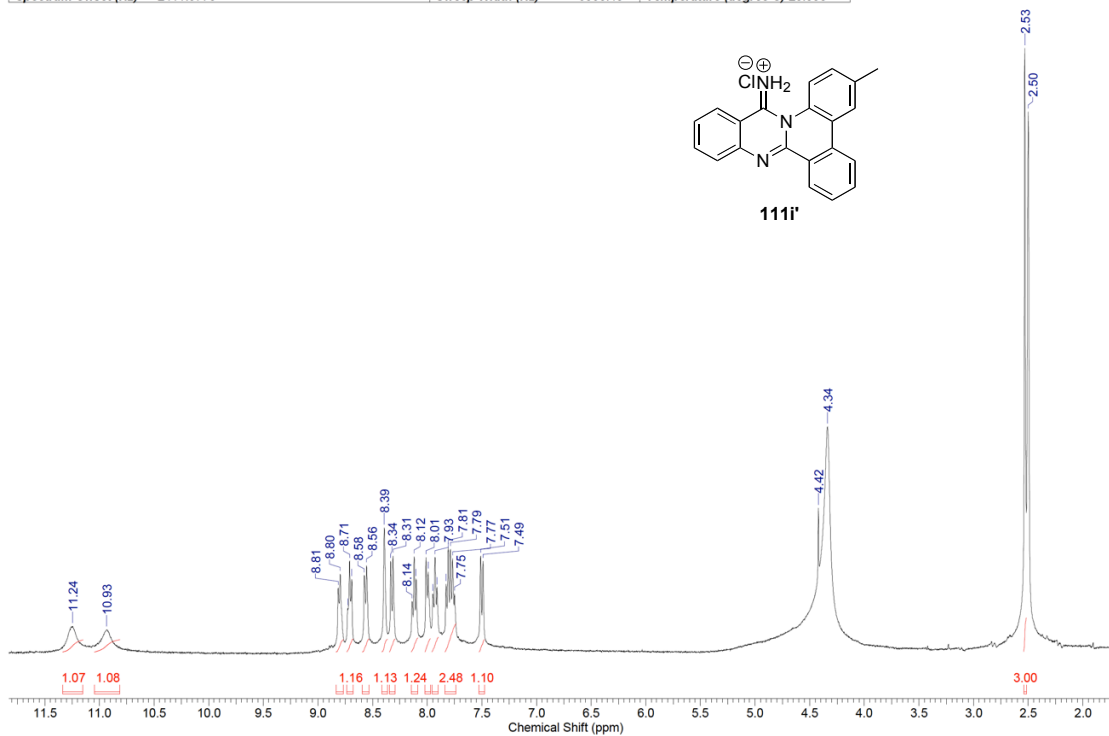


Figure B.34: ¹H and ¹³C NMR of **111g''**

| | | | | | | | |
|------------------------|--------------------|--------------|------------|------------------|-------------|------------------------|----------------|
| Acquisition Time (sec) | 2.0487 | Comment | Std proton | Date | Sep 19 2011 | Date Stamp | Sep 19 2011 |
| File Name | G:\XXNMR0222\HG945 | | | Frequency (MHz) | 399.73 | Nucleus | ¹ H |
| Original Points Count | 13102 | Points Count | 16384 | Pulse Sequence | s2pul | Receiver Gain | 58.00 |
| Spectrum Offset (Hz) | 2411.9775 | | | Sweep Width (Hz) | 6395.40 | Temperature (degree C) | 25.000 |



| | | | | | | | |
|------------------------|----------------------------|--------------|------------|------------------|-------------|------------------------|-----------------|
| Acquisition Time (sec) | 1.3005 | Comment | Std proton | Date | Nov 29 2011 | Date Stamp | Nov 29 2011 |
| File Name | G:\XXNMR0222\HG953C13-XSTD | | | Frequency (MHz) | 100.52 | Nucleus | ¹³ C |
| Original Points Count | 31375 | Points Count | 32768 | Pulse Sequence | s2pul | Receiver Gain | 30.00 |
| Spectrum Offset (Hz) | 10485.7529 | | | Sweep Width (Hz) | 24125.45 | Temperature (degree C) | 25.000 |

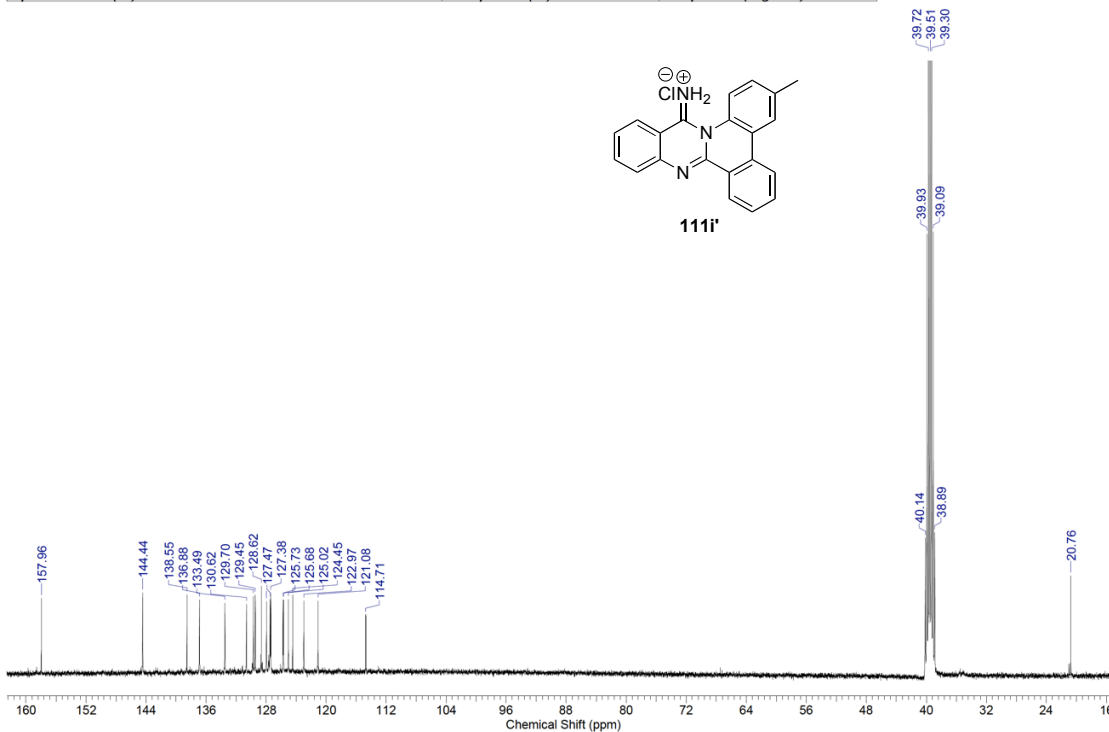
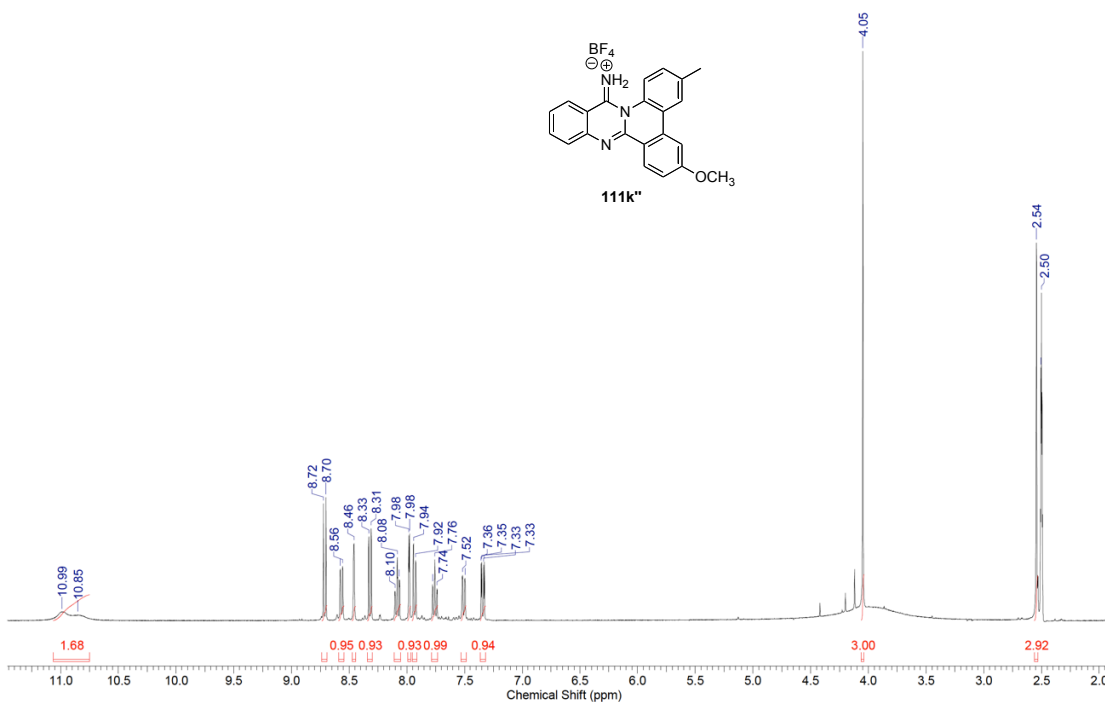


Figure B.35: ¹H and ¹³C NMR of **111i'**

| | | | | | | | |
|------------------------|--------------------|--------------|------------|------------------|-------------|------------------------|-------------|
| Acquisition Time (sec) | 2.0487 | Comment | Std proton | Date | Aug 22 2011 | Date Stamp | Aug 22 2011 |
| File Name | G:\XNMR0222\HG989H | | | Frequency (MHz) | 399.73 | Nucleus | 1H |
| Original Points Count | 13102 | Points Count | 16384 | Pulse Sequence | s2pul | Receiver Gain | 52.00 |
| Spectrum Offset (Hz) | 2415.2954 | | | Sweep Width (Hz) | 6395.40 | Temperature (degree C) | 25.000 |



| | | | | | | | |
|------------------------|-------------------------|--------------|------------|------------------|-------------|------------------------|-------------|
| Acquisition Time (sec) | 1.3005 | Comment | Std proton | Date | Aug 22 2011 | Date Stamp | Aug 22 2011 |
| File Name | G:\XNMR0222\HG989C13-OK | | | Frequency (MHz) | 100.52 | Nucleus | 13C |
| Original Points Count | 31375 | Points Count | 32768 | Pulse Sequence | s2pul | Receiver Gain | 30.00 |
| Spectrum Offset (Hz) | 10487.2900 | | | Sweep Width (Hz) | 24125.45 | Temperature (degree C) | 25.000 |

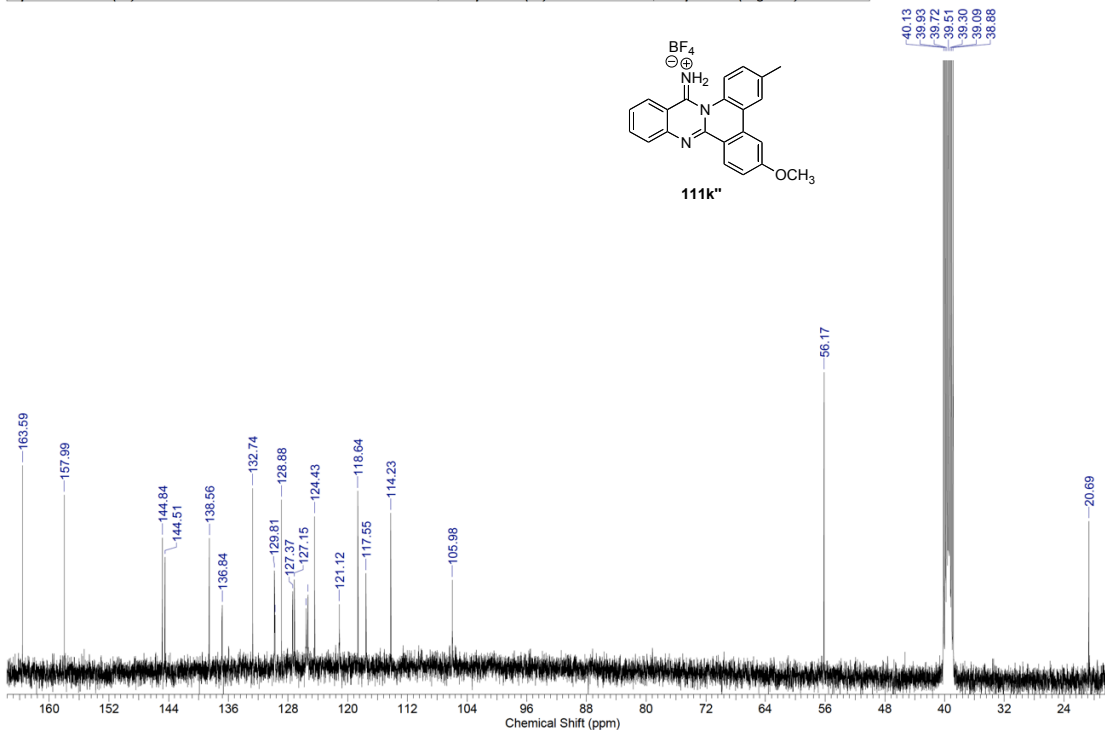
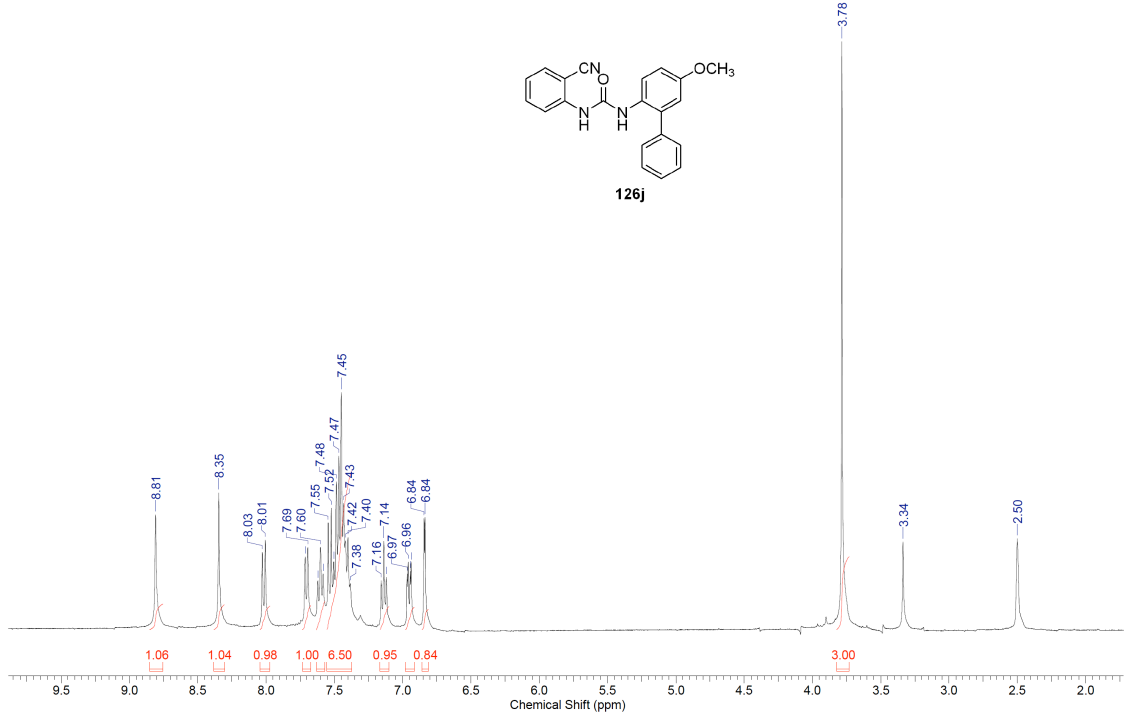


Figure B.36: ^1H and ^{13}C NMR of **111k''**

| | | | | | | | |
|------------------------|----------------|-----------------------------|------------|-----------------------|------------|----------------------|------------|
| Acquisition Time (sec) | 2.0487 | Comment | Std proton | Date | Apr 2 2012 | Date Stamp | Apr 2 2012 |
| File Name | G:\UNTITLED | FOLDERID-PARTLYCYCLIZEDCOMP | POCH3-H | | | Frequency (MHz) | 399.72 |
| Nucleus | ¹ H | Number of Transients | 8 | Original Points Count | 13102 | Points Count | 16384 |
| Pulse Sequence | s2pul | Receiver Gain | 48.00 | Solvent | DMSO-d6 | Spectrum Offset (Hz) | 2411.5708 |
| Sweep Width (Hz) | 6395.40 | Temperature (degree C) | 25.000 | | | | |



| | | | | | | | |
|------------------------|-----------------|-----------------------------|--------------|-----------------------|------------|----------------------|------------|
| Acquisition Time (sec) | 1.3005 | Comment | Std proton | Date | Apr 2 2012 | Date Stamp | Apr 2 2012 |
| File Name | G:\UNTITLED | FOLDERID-PARTLYCYCLIZEDCOMP | POCH3-C13FID | | | Frequency (MHz) | 100.52 |
| Nucleus | ¹³ C | Number of Transients | 2000 | Original Points Count | 31375 | Points Count | 32768 |
| Pulse Sequence | s2pul | Receiver Gain | 30.00 | Solvent | DMSO-d6 | Spectrum Offset (Hz) | 10487.2256 |
| Sweep Width (Hz) | 24125.45 | Temperature (degree C) | 25.000 | | | | |

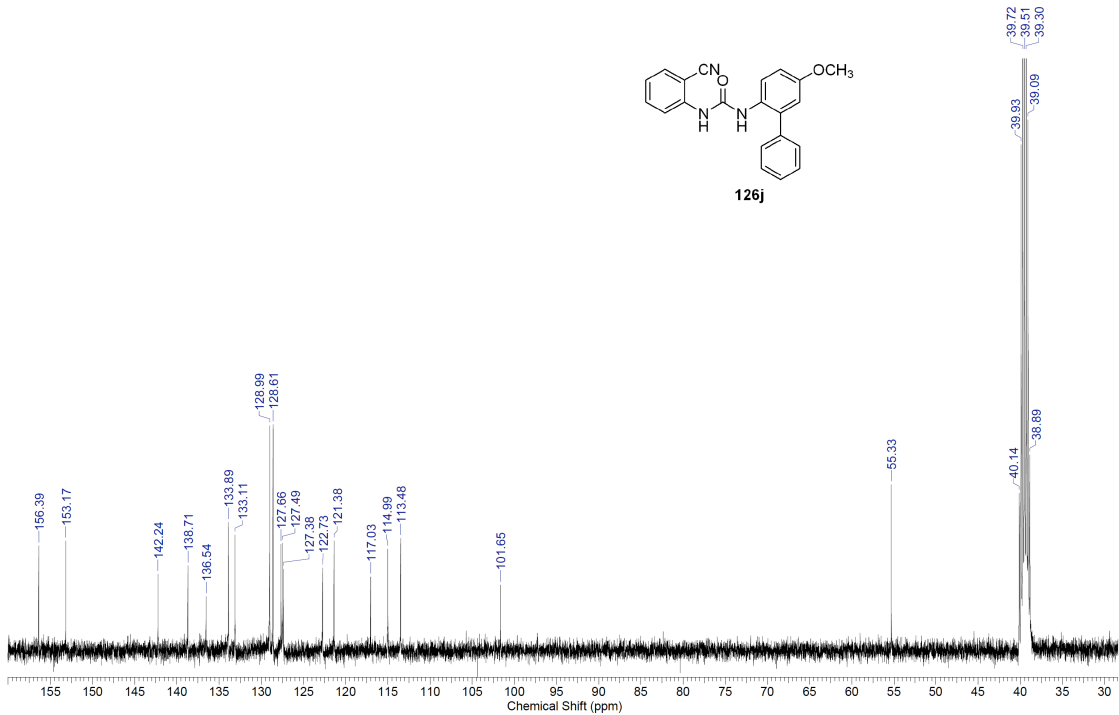
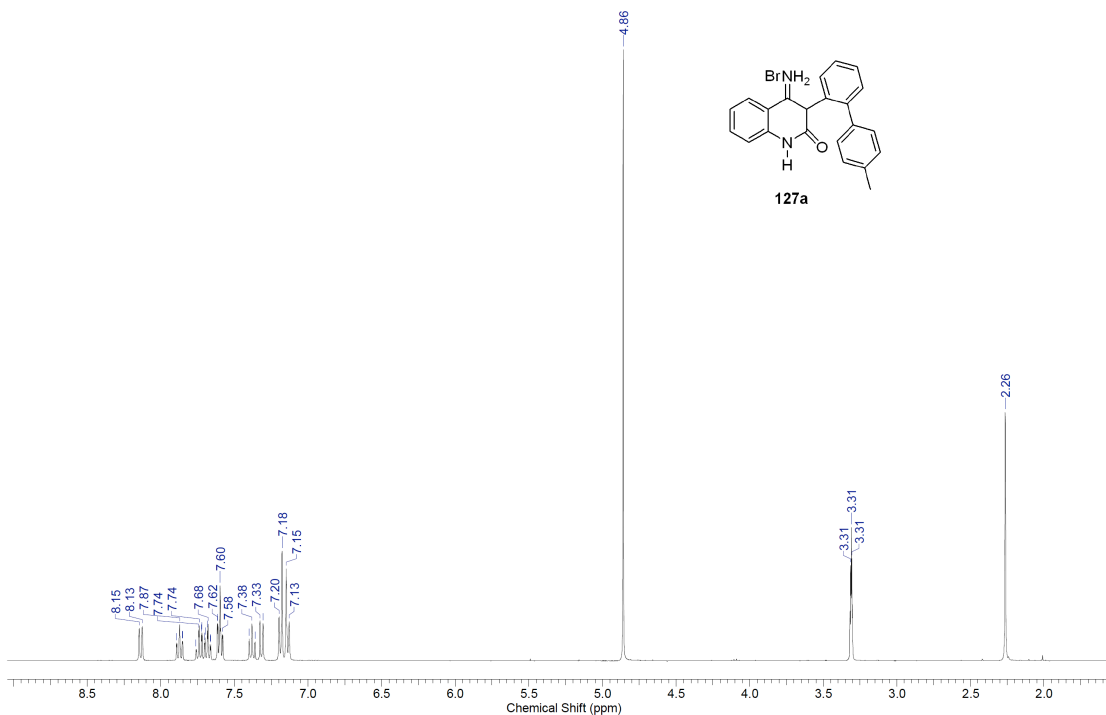


Figure B.37: ¹H and ¹³C NMR of 126j

| | | | | | | | |
|------------------------|-------------|------------------|------------|------------------------|-------------------------------------|-----------------------|-------------|
| Acquisition Time (sec) | 2.0487 | Comment | Std proton | Date | Feb 25 2011 | Std proton | |
| Date Stamp | Feb 25 2011 | | | File Name | G:\NNMRC3\HG7789R2-H-FPPT2-STANDARD | | |
| Frequency (MHz) | 399.73 | Nucleus | 1H | Number of Transients | 16 | Original Points Count | 13102 |
| Points Count | 16384 | Pulse Sequence | s2pul | Receiver Gain | 38.00 | Solvent | METHANOL-d4 |
| Spectrum Offset (Hz) | 2412.7476 | Sweep Width (Hz) | 6395.40 | Temperature (degree C) | 25.000 | | |



| | | | | | | | |
|------------------------|------------------------------|--------------|------------|----------------------|-------------|------------------------|-------------|
| Acquisition Time (sec) | 1.3005 | Comment | Std proton | Date | Feb 25 2011 | Date Stamp | Feb 25 2011 |
| File Name | G:\NNMRC3\HG7789R2-C13-FPPT2 | | | Frequency (MHz) | 100.52 | Nucleus | 13C |
| Original Points Count | 31375 | Points Count | 32768 | Pulse Sequence | s2pul | Receiver Gain | 30.00 |
| Solvent | METHANOL-d4 | | | Spectrum Offset (Hz) | 10689.5303 | Sweep Width (Hz) | 24125.45 |
| | | | | | | Temperature (degree C) | 25.000 |

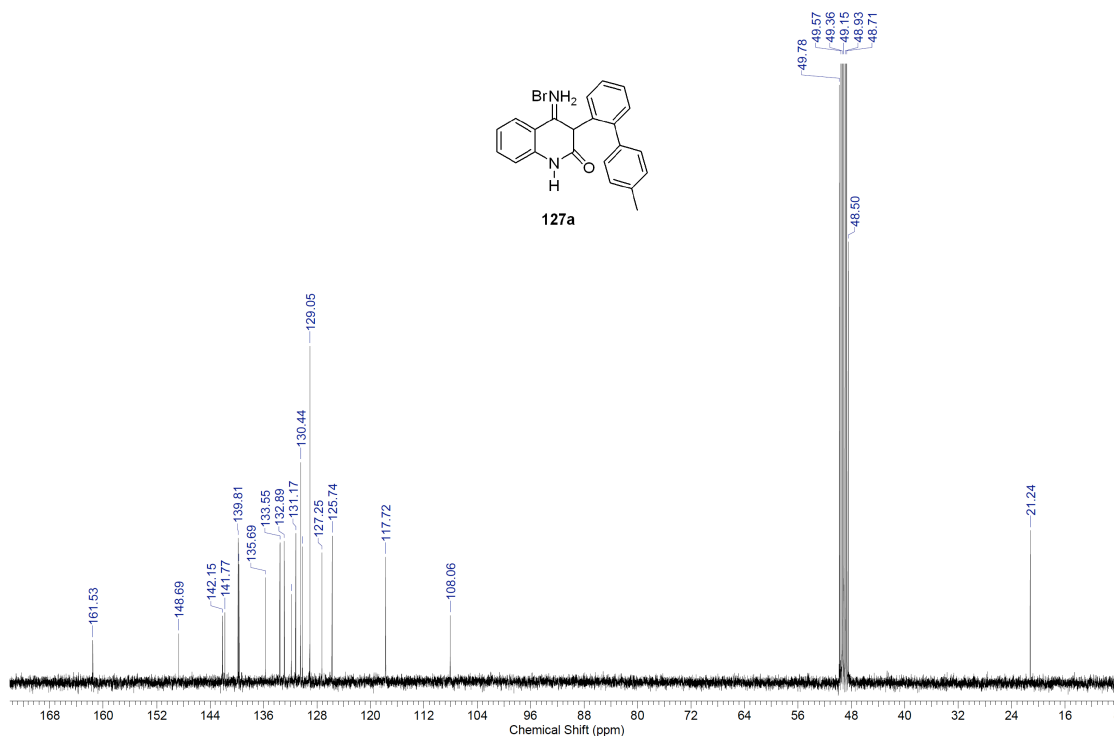


Figure B.38: ^1H and ^{13}C NMR of **127a**